UNIVERSITEIT VAN PRETORIA
UNIVERSITY OF PRETORIA
YUNIBESITHI YA PRETORIA

Synthesis and structural studies of N- and P-donor ligands in Chromium(III) complexes

by

Nicholas Frederick Brennan

Submitted in partial fulfilment of the requirements for the degree

Philosophiae Doctor

in Chemistry

In the Faculty of Natural and Agricultural Sciences

University of Pretoria

Pretoria

June 2009

TABLE OF CONTENTS

Abstract i
Acknowledgements iii
Common abbreviations iv
Complex abbreviations v
Structural drawings vi
List of Figures viii
List of Tables xvi

CHAPTER 1

INTRODUCTION 1

1.1 IMPORTANCE OF CATALYSIS 1

1.2 HOMOGENEOUS AND HETEROGENEOUS CATALYSIS 1

1.3 CATALYSIS AND TRANSITION METALS 2

1.4 CATALYTIC STEPS 2

1.5 OVERVIEW OF CATALYTIC DESIGN 3

1.6 ETHYLENE OLIGOMERISATIONS 4
1.6.1 1-Hexene 4
1.6.2 1-Octene 8

1.7 PROJECT OUTLINE 9
1.7.1 Monomeric and Dimeric States 10
1.7.2 Ligands 11
1.7.3 Characterisation and Analysis 13
1.7.3.1 X-ray Crystallography 13
1.7.3.2 Infrared and Raman Spectroscopy 14

1.7.3.3 NMR Spectroscopy 15
1.7.3.4 Computational Studies 17
1.7.3.5 Mass Spectrometry 18

1.8 EXPERIMENTAL 18
1.8.1 Safety Remarks 18
1.8.2 General Remarks 19
1.8.3 Standard Colour Changes 19
1.8.4 Synthesis of the Starting Material [$CrCl_3(thf)_3$] 20
1.8.5 General Procedure and Instrument Data:
Infrared and Raman Spectroscopy 20
1.8.6 General Procedure and Instrument Data:
X-ray Crystallography 21
1.8.7 General Procedure and Instrument Data:
^{1}H NMR Scale Experiments 22
1.8.8 General Procedure and Instrument Data:
Computational Studies 22
1.8.9 General Procedure and Instrument Data:
Mass Spectrometry 23

CHAPTER 2

CHROMIUM(III) MONODENTATE NITROGEN LIGAND CHEMISTRY 24

2.1 INTRODUCTION 24

2.2 CATEGORY ONE: SEQUENTIAL ADDITION OF PYRIDINE ... 25
2.2.1 Visual Analysis 27
2.2.2 Infrared and Raman Spectroscopy 27
2.2.3 Computational Study 33
2.2.4 NMR Spectroscopy 36
2.2.5 X-ray Crystallography 40
2.2.5.1 [$CrCl_3(py)_3$] 40

2.2.5.2 [Hpy][$CrCl_4(py)_2$] 45
2.2.6 Mass Spectrometry 53

2.3 CATEGORY TWO: BULKY SUBSTITUENTS 54
2.3.1 Infrared Spectroscopy 56
2.3.1.1 Region 3114–2804 cm^{-1} 56
2.3.1.2 Region 1660–1247 cm^{-1} 57
2.3.1.3 Region 1219–448 cm^{-1} 58
2.3.1.4 Region 415–214 cm^{-1} 59
2.3.2 X-ray Crystallography 60

2.4 CATEGORY THREE: PARA–SUBSTITUTED PYRIDINES 64
2.4.1 Infrared and Raman Spectroscopy 65
2.4.1.1 Region 3321–2869 cm^{-1} 66
2.4.1.2 Region 1638–1045 cm^{-1} 68
2.4.1.3 Region 1030–499 cm^{-1} 71
2.4.1.4 Ligand substituents 74
2.4.1.5 Bond Strength 74
2.4.1.6 Region 488–213 cm^{-1} 78
2.4.1.7 Concluding remarks 79
2.4.2 Computational Studies 84
2.4.3 NMR of [$CrCl_3(thf)_3$] and three equivalents of pyphenyl 90
2.4.4 Mass Spectrometry 90
2.4.5 X-ray Crystallography 92
2.4.5.1 [$CrCl_3(pytb)_3$] 92

2.5 EXPERIMENTAL 97
2.5.1 Synthesis of [$CrCl_3(py)(thf)_2$] **(1)** and [$CrCl_3(py)_2(thf)$] **(2)** 97
2.5.2 Synthesis of [$CrCl_3(py)_3$] **(3)** 98
2.5.3 Synthesis of [$CrCl_3$(2,6-dibromopy)$_3$] and [$CrCl_3(py)_2$(DMF)] **(5)** ... 98
2.5.4 Synthesis of [$CrCl_3(pyNH_2)_3$] **(6)** 99
2.5.5 Synthesis of [$CrCl_3(pytb)_3$] **(7)** 99
2.5.6 Synthesis of [$CrCl_3(pyphenyl)_3$] **(8)** 100
2.5.7 Synthesis of [$CrCl_3(pyOH)_3$] 100

CHAPTER 3

CHROMIUM(III) BIDENTATE NITROGEN LIGAND CHEMISTRY 101

3.1 INTRODUCTION 101

3.2 SYNTHESIS 102

3.3 SYNTHETIC ROUTE TO PRODUCT FORMATION 102

3.4 INFRARED AND RAMAN SPECTROSCOPY 103
3.4.1 Region 3329–2291 cm^{-1} 104
3.4.2 Region 1652–1104 cm^{-1} 108
3.4.3 Region 1104–522 cm^{-1} 111
3.4.3.1 Pyridine Specific 112
3.4.3.2 Bipyridine Specific 115
3.4.3.3 Thf Specific 115
3.4.3.4 Pyridinium Specific 117
3.4.4 Region 451–221 cm^{-1} 118

3.5 COMPUTATIONAL STUDIES 132
3.5.1 $[CrCl_3(bipy)(thf)]$ 132
3.5.2 $[CrCl_3(bipy)(H_2O)]$ 135
3.5.3 $[CrCl_3(bipy)(CH_3CN)]$ 137
3.5.4 $[CrCl_3(bipy)(py)]$ 140
3.5.5 $[CrCl_3(bipy)(pyphenyl)]$ 143
3.5.6 $[HpyNH_2][CrCl_4(bipy)]$ 146
3.5.7 HOMO and LUMO orbitals of the calculated complexes 149

3.6 NMR SPECTROSCOPY 152

3.7 MASS SPECTROMETRY 158

3.8 X-RAY CRYSTALLOGRAPHY 160
3.8.1 Solubility and Crystal Synthesis 160

3.8.2 [$CrCl_3$(bipy)(H_2O)] 161
3.8.3 [$HpyNH_2$][$CrCl_4$(bipy)] 167
3.8.4 [$CrCl_2$(bipy)$_2$][Cl]·H_2O 171

3.9 SYNTHETIC ROUTE CONCLUSIONS 176

3.10 EXPERIMENTAL 177
3.10.1 Synthesis of [$CrCl_3$(bipy)(thf)] **(9)** 177
3.10.2 Synthesis of [$CrCl_3$(bipy)(CH_3CN)] **(10)** 178
3.10.3 Synthesis of [$CrCl_3$(bipy)(py)] **(11)** 178
3.10.4 Synthesis of [$CrCl_3$(bipy)($pyNH_2$)] **(12)** 178
3.10.5 Synthesis of [$CrCl_3$(bipy)(pytb)] **(13)** 178
3.10.6 Synthesis of [$CrCl_3$(bipy)(pyphenyl)] **(14)** 179
3.10.7 Synthesis of [$CrCl_3$(bipy)(H_2O)] **(16)** 179
3.10.8 Synthesis of [$CrCl_2$(bipy)$_2$][Cl]·H_2O **(17)** 179

CHAPTER 4

CHROMIUM(III) BIDENTATE PHOSPHORUS CHEMISTRY 180

4.1 INTRODUCTION 180

4.2 SYNTHESIS 181

4.3 SYNTHETIC ROUTE TO PRODUCT FORMATION 182

4.4 INFRARED AND RAMAN SPECTROSCOPY 183
4.4.1 Region 3313–2863 cm^{-1} 184
4.4.2 Region 1651–1045 cm^{-1} 188
4.4.3 Region 1026–519 cm^{-1} 191
4.4.4 Region 495–215 cm^{-1} 198

4.5 COMPUTATIONAL STUDY 210

4.6 NMR SPECTROSCOPY 214

4.7 MASS SPECTROMETRY 216

4.8 X-RAY CRYSTALLOGRAPHY 218
4.8.1 [Hpyphenyl][$CrCl_4$(dppe)] 218

4.9 EXPERIMENTAL 222
4.9.1 Synthesis of [$CrCl_3$(dppe)(thf)] / [Cr(dppe)Cl_2(μ-Cl)]$_2$ **(18)** 222
4.9.2 Synthesis of [$CrCl_3$(dppe)(py)] **(19)** 223
4.9.3 Synthesis of [$CrCl_3$(dppe)($pyNH_2$)] **(20)** 223
4.9.4 Synthesis of [$CrCl_3$(dppe)(pytb)] **(21)** 223
4.9.5 Synthesis of [$CrCl_3$(dppe)(pyphenyl)] **(22)** 224

CHAPTER 5
CHROMIUM(III) BIDENTATE NITROGEN / PHOSPHORUS MIXED LIGAND CHEMISTRY 225

5.1 INTRODUCTION 225

5.2 2-PYRIDYLDIPHENYLPHOSPHINE AND [$CrCl_3(thf)_3$] 226
5.2.1 Synthesis 227

5.3 2-DIPHENYLPHOSPHINOETHYLAMINE AND [$CrCl_3(thf)_3$] 227
5.3.1 Synthesis 228
5.3.2 Infrared and Raman Spectroscopy 228
5.3.2.1 Region 3380–2867 cm^{-1} 229
5.3.2.2 Region 1652–1117 cm^{-1} 232
5.3.2.3 Region 1117–500 cm^{-1} 237
5.3.2.4 Region 500–200 cm^{-1} 243
5.3.3 Computational Study 250
5.3.4 Mass Spectrometry 253

5.4 EXPERIMENTAL 255
5.4.1 Synthesis of $[CrCl_3(dppea)(thf)]$ / $[Cr(dppea)Cl_2(\mu\text{-}Cl)]_2$ **(24)** 255
5.4.2 Synthesis of $[CrCl_3(dppea)(py)]$ **(25)** 255
5.4.3 Synthesis of $[CrCl_3(dppea)(pyNH_2)]$ **(26)** 255
5.4.4 Synthesis of $[CrCl_3(dppea)(pytb)]$ **(27)** 256
5.4.5 Synthesis of $[CrCl_3(dppea)(pyhenyl)]$ **(28)** 256

CHAPTER 6

FUTURE WORK AND CONCLUSIONS 257

6.1 FUTURE WORK 257

6.2 CONCLUSION 258

REFERENCES 261

.....

APPENDIX ..... CD

ABSTRACT

Synthesis and structural studies of N- and P-donor ligands in Chromium(III) complexes

by

Nicholas Frederick Brennan

Supervisor: Prof. P. H. van Rooyen

Co-supervisor: Prof. S. Lotz

Submitted in partial fulfilment of the requirements for the degree Philosophiae Doctor

Department of Chemistry, University of Pretoria

The fundamental knowledge of Cr(III) chemistry has been enhanced via detailed structural and spectroscopic studies of largely novel compounds that may potentially be active tri- and tetramerisation precursors.

The compounds are based on various monodentate and bidentate nitrogen and phosphorus ligands which have been coordinated to $[CrCl_3(thf)_3]$. The few compounds that have been synthesised previously have in this study been made via novel synthetic routes and incorporate a combination of new and more detailed analysis than was carried out previously.

The eight structures determined, in addition to offering novel crystallographic data, also provided insights into the synthetic pathways leading to compound formation. The isolation of monomeric structures suggests direct ligand substitution, while the cationic-anionic structures suggest the presence of dimeric intermediates which have been cleaved asymmetrically.

Infrared and Raman spectra of these structures were able to add weight to these pathway proposals and, by means of vibrational comparisons, assisted in the general band assignments of the compounds' spectra where structures were not available.

Vibrational shifts relative to the free ligands, as well as metal–ligand vibrations in the far infrared region, were also of significant value in terms of ligand coordination and geometry.

Closely associated with the infrared and Raman spectra analysis was the generation of theoretical spectra using Density Functional Theory calculations. The excellent agreement between the calculated and experimental spectra confirmed the vibrational assignments.

Also generated by computational means were the highest occupied and lowest unoccupied molecular orbitals (HOMO and LUMO) of the compounds which indicated the sites of potential nucleophilic and electrophilic attack.

^{1}H NMR spectroscopy is a technique normally avoided when studying paramagnetic materials. However, by employing a largely novel approach, information pertaining to both ligand coordination and reaction times was obtained.

FAB-MS assisted in the confirmation that the single crystal determinations did indeed reflect the composition of the bulk precipitated samples. It also provided additional structural information through the identification of fragmentation patterns which could not be gained by techniques such as elemental analysis.

ACKNOWLEDGEMENTS

I would very much like to thank my supervisors, Prof. P. H. van Rooyen and Prof. S. Lotz for all their help and guidance throughout the course of this project.

To Mike Green and SASOL – a sincere thank you for all the valued input as well as financial support.

Thank you to Eric Palmer, Dave Liles and Marilé Landman – your assistance was very much appreciated.

To my parents, Anne and John – thank you for your continuous love and support. I hope I've made you proud.

To my beautiful wife Cassandra who has been with me every step of the way and never once doubted me: I love you.

COMMON ABBREVIATIONS

• Acetyl acetonate	acac
• 4–amino pyridine	pyNH_2
• 2, 2'–bipyridine	bipy
• Bis-diphenylphosphinoethane	dppe
• 4–Bu^t pyridine	pytb
• Density Functional Theory	DFT
• Dichloromethane	DCM
• Dimethylformamide	DMF
• Dimethylsulphoxide	DMSO
• 2–(diphenylphosphino)ethylamine	dppea
• 2–pyridyldiphenylphosphine	dpp
• Far–infrared	FIR
• Fast Atom Bombardment Mass Spectrometry	FAB-MS
• Highest Occupied Molecular Orbital	HOMO
• Infrared	IR
• Linear Alpha Olefins	LAOs
• Lowest Unoccupied Molecular Orbital	LUMO
• Mid–infrared	MIR
• Nuclear Magnetic Resonance	NMR
• Nuclear Overhauser Effect	NOE
• 4–phenyl pyridine	pyphenyl
• Pyridine	py
• Pyridinium ion	pyH
• Tetrahydrofuran	thf

COMPLEX ABBREVIATIONS

$[CrCl_3(py)(thf)_2]$	**1**
$[CrCl_3(py)_2(thf)]$	**2**
$[CrCl_3(py)_3]$	**3**
$[Hpy][CrCl_4(py)_2]$	**4**
$[CrCl_3(py)_2(DMF)]$	**5**
$[CrCl_3(pyNH_2)_3]$	**6**
$[CrCl_3(pytb)_3]$	**7**
$[CrCl_3(pyphenyl)_3]$	**8**
$[CrCl_3(bipy)(thf)]$	**9**
$[CrCl_3(bipy)(CH_3CN)]$	**10**
$[CrCl_3(bipy)(py)]$	**11**
$[CrCl_3(bipy)(pyNH_2)]$	**12**
$[CrCl_3(bipy)(pytb)]$	**13**
$[CrCl_3(bipy)(pyphenyl)]$	**14**
$[HpyNH_2][CrCl_4(bipy)]$	**15**
$[CrCl_3(bipy)(H_2O)]$	**16**
$[CrCl_2(bipy)_2][Cl]\cdot H_2O$	**17**
$[CrCl_3(dppe)(thf)]/ [Cr(dppe)Cl_2(\mu\text{-}Cl)]_2$	**18**
$[CrCl_3(dppe)(py)]$	**19**
$[CrCl_3(dppe)(pyNH_2)]$	**20**
$[CrCl_3(dppe)(pytb)]$	**21**
$[CrCl_3(dppe)(pyphenyl)]$	**22**
$[Hpyphenyl][CrCl_4(dppe)]$	**23**
$[CrCl_3(dppea)(thf)]/ [Cr(dppea)Cl_2(\mu\text{-}Cl)]_2$	**24**
$[CrCl_3(dppea)(py)]$	**25**
$[CrCl_3(dppea)(pyNH_2)]$	**26**
$[CrCl_3(dppea)(pytb)]$	**27**
$[CrCl_3(dppea)(pyphenyl)]$	**28**

STRUCTURAL DRAWINGS

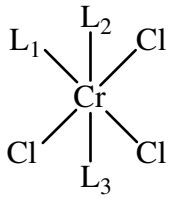

1 L^1 = py, L^2,L^3 = thf
2 L^1,L^2 = py, L^3 = thf
3 L^1,L^2,L^3 = py
5 L^1,L^2 = py, L^3 = DMF

6 L^1,L^2,L^3 = $pyNH_2$
7 L^1,L^2,L^3 = pytb
8 L^1,L^2,L^3 = pyphenyl

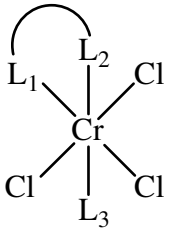

9 L^1L^2 = bipy, L^3 = thf
10 L^1L^2 = bipy, L^3 = CH_3CN
11 L^1L^2 = bipy, L^3 = py
12 L^1L^2 = bipy, L^3 = $pyNH_2$

13 L^1L^2 = bipy, L^3 = pytb
14 L^1L^2 = bipy, L^3 = pyphenyl
16 L^1L^2 = bipy, L^3 = H_2O
18 L^1L^2 = dppe, L^3 = thf *
19 L^1L^2 = dppe, L^3 = py
20 L^1L^2 = dppe, L^3 = $pyNH_2$
21 L^1L^2 = dppe, L^3 = pytb
22 L^1L^2 = dppe, L^3 = pyphenyl
24 L^1L^2 = dppea, L^3 = thf *
25 L^1L^2 = dppea, L^3 = py
26 L^1L^2 = dppea, L^3 = $pyNH_2$
27 L^1L^2 = dppea, L^3 = pytb

28 L^1L^2 = dppea, L^3 = pyphenyl

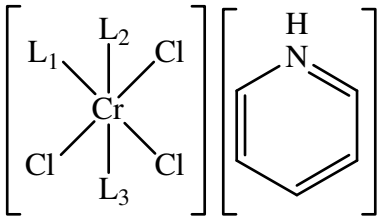

4 L^1,L^2 = py

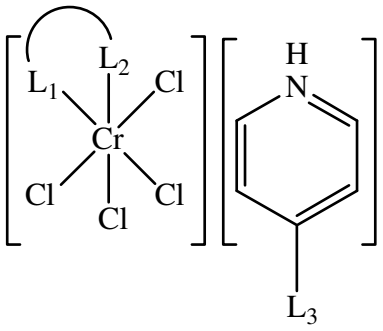

15 L^1L^2 = bipy, $L^3 = NH_2$

23 L^1L^2 = dppe, L^3 = phenyl

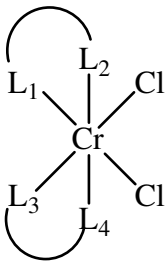

17 L^1L^2, L^3L^4 = bipy

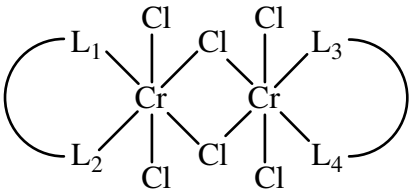

18 L^1L^2, L^3L^4 = dppe *

24 L^1L^2, L^3L^4 = dppea *

LIST OF FIGURES

Figure 1.1 Typical key steps in the study of many catalytic systems [3] 3
Figure 1.2 Formation of 1-hexene via a metallacycle 4
Figure 1.3 The Kohn catalyst 6
Figure 1.4 The Wass catalyst 6
Figure 1.5 Variations of the Wass catalyst by McGuinness [31] 7
Figure 1.6 Formation of the SNS complex 7
Figure 1.7 Variation in spacer length of tridentate ligands 8
Figure 1.8 The first tetramerisation catalyst 8
Figure 1.9 Pathways to 1-octene formation 9
Figure 1.10 Symmetrically (A) and asymmetrically (B) cleaved chloro dimers [100] 11
Figure 1.11 Direct ligand substitution and symmetrical dimeric cleavage pathways [100] 11
Figure 1.12 Ligands incorporated in this study 12
Figure 2.1 Sequential addition of pyridine to the chromium precursor 26
Figure 2.2 Olive green precipitate 27
Figure 2.3 Comparisons of the IR spectra of free pyridine (blue) and $[CrCl_3(py)_3]$ (red) 28
Figure 2.4 Raman spectrum of $[CrCl_3(py)_3]$ 28
Figure 2.5 Shifting of the free pyridine band (blue) in the IR spectrum at 992 cm^{-1} upon coordination (red) 29
Figure 2.6 Comparison between $[CrCl_3(thf)_3]$ (blue) and $[CrCl_3(py)_3]$ (red) IR spectra 30
Figure 2.7 FIR comparison between $[CrCl_3(thf)_3]$ (blue) and $[CrCl_3(py)_3]$ (red) spectra 31
Figure 2.8 Experimental (red) and calculated (blue) MIR spectra of $[CrCl_3(py)_3]$ 33
Figure 2.9 Experimental (red) and calculated (blue) Raman spectra of $[CrCl_3(py)_3]$ 34
Figure 2.10 Experimental (red) and calculated (blue) FIR spectra of $[CrCl_3(py)_3]$ .. 34
Figure 2.11 HOMO and LUMO orbitals of $[CrCl_3(py)_3]$ 36

Figure 2.12 ^{1}H NMR spectrum of free thf in acetone-d_6 37
Figure 2.13 ^{1}H NMR spectrum of $[CrCl_3(thf)_3]$ in acetone-d_6 38
Figure 2.14 Stacked ^{1}H NMR spectra for the reaction of pyridne with $[CrCl_3(thf)_3]$ over time. 1 = py, 2 = thf, 3 = water peak in acetone, 4 = acetone-d_6, 5 = thf 38
Figure 2.15 ^{1}H NMR spectrum of $[CrCl_3(py)_3]$ in acetone-d_6 after a further hour ... 39
Figure 2.16 ^{13}C NMR spectrum of $[CrCl_3(py)_3]$ precipitate formed after removal of above reaction from NMR instrument 40
Figure 2.17 A = Perspective drawing of $[CrCl_3(py)_3]$ structure determined in this study, B = Perspective drawing of $[CrCl_3(py)_3]$ structure determined by Howard [83] 41
Figure 2.18 The ring twists observed for $[CrCl_3(py)_3]$ of this study (grey) and that of Howard [83] (red) 43
Figure 2.19 Short contacts observed in the packing arrangement of $[CrCl_3(py)_3]$ of this study 44
Figure 2.20 Packing arrangement of $[CrCl_3(py)_3]$ of this study which includes space fill arrangement 44
Figure 2.21 Possible pathways to product formation 47
Figure 2.22 The planarity of the pyridine rings as well as the tilting of the pyridinium ion 48
Figure 2.23 Hydrogen bonding observed in $[Hpy][CrCl_4(py)_2]$ 50
Figure 2.24 Packing arrangement of $[Hpy][CrCl_4(py)_2]$ 50
Figure 2.25 Alternative view of the packing arrangement of $[Hpy][CrCl_4(py)_2]$ 51
Figure 2.26 Packing and space fill of $[Hpy][CrCl_4(py)_2]$ 51
Figure 2.27 Alternative view of the packing and space fill of $[Hpy][CrCl_4(py)_2]$ 51
Figure 2.28 FAB-MS spectrum of $[CrCl_3(py)_3]$ 53
Figure 2.29 Bulky substituent reactions that were carried out 55
Figure 2.30 IR spectrum of the region 3114 - 2804 cm^{-1} 57
Figure 2.31 IR spectrum of the region 1660 - 1247 cm^{-1} 58
Figure 2.32 IR spectrum of the region 1219 - 448 cm^{-1} 59
Figure 2.33 IR spectrum of the region 415 - 214 cm^{-1} 60
Figure 2.34 A = Perspective drawing of $[CrCl_3(py)_2(DMF)]$ structure determined in this study, B = Perspective drawing of $[CrCl_3(py)_2(DMF)]$ structure determined by Broomhead [88] 61

Figure 2.35 Non-planarity of the *trans* pyridine ligands in $[CrCl_3(py)_2(DMF)]$ 61
Figure 2.36 Packing and space fill arrangement of $[CrCl_3(py)_2(DMF)]$.....63
Figure 2.37 Para-substituted pyridine ligands 65
Figure 2.38 IR and Raman spectra of $[CrCl_3(pyNH_2)_3]$ (red), $[CrCl_3(pytb)_3]$ (blue) $[CrCl_3(pyphenyl)_3]$ (green) in the region 3321 - 2869 cm^{-1}.....67
Figure 2.39 IR and Raman spectra of $[CrCl_3(pyNH_2)_3]$ in the region 1638 - 1045 cm^{-1} 69
Figure 2.40 IR and Raman spectra of $[CrCl_3(pytb)_3]$ in the region 1638 - 1045 cm^{-1} 70
Figure 2.41 IR and Raman spectra of $[CrCl_3(pyphenyl)_3]$ in the region 1638 - 1045 cm^{-1}.....71
Figure 2.42 IR and Raman spectra of $[CrCl_3(pyNH_2)_3]$ in the region 1030 - 499 cm^{-1} 72
Figure 2.43 IR and Raman spectra of $[CrCl_3(pytb)_3]$ in the region 1030 - 499 cm^{-1}.....73
Figure 2.44 IR and Raman spectra of $[CrCl_3(pyphenyl)_3]$ in the region 1030 - 499 cm^{-1} 74
Figure 2.45 Shifting of the characteristic ring breathing vibration in the IR spectra of $[CrCl_3(pyNH_2)_3]$, $[CrCl_3(pytb)_3]$ and $[CrCl_3(pyphenyl)_3]$, relative to free ligand positions (blue). Raman spectra of $[CrCl_3(pyNH_2)_3]$, $[CrCl_3(pytb)_3]$ and $[CrCl_3(pyphenyl)_3]$.....77
Figure 2.46 Experimental (red) and calculated (blue) MIR spectra of $[CrCl_3(pyNH_2)_3]$ 84
Figure 2.47 Experimental (red) and calculated (blue) Raman spectra of $[CrCl_3(pyNH_2)_3]$ 85
Figure 2.48 HOMO and LUMO orbitals of $[CrCl_3(pyNH_2)_3]$ 87
Figure 2.49 Experimental (red) and calculated (blue) MIR spectra of $[CrCl_3(pytb)_3]$ 87
Figure 2.50 Experimental (red) and calculated (blue) Raman spectra of $[CrCl_3(pytb)_3]$ 88
Figure 2.51 HOMO and LUMO orbitals of $[CrCl_3(pytb)_3]$ 89
Figure 2.52 Stacked ^1H NMR spectrum for the reaction of pyphenyl with $[CrCl_3(thf)_3]$ over time. 1 = pyphenyl, 2 = thf, 3 = acetone-d_6, 4 = thf.....90

Figure 2.53 .....FAB-MS spectrum of [$CrCl_3$(pyphenyl)$_3$]……91

Figure 2.54 FAB-MS spectrum of [$CrCl_3$(pyphenyl)$_3$]……...91

Figure 2.55 Perspective drawing of [$CrCl_3$(pytb)$_3$] structure determined 92

Figure 2.56 Twisting of the aromatic systems relative to the axial chlorine atoms in [$CrCl_3$(pytb)$_3$] 93

Figure 2.57 Packing arrangement of [$CrCl_3$(pytb)$_3$] 96

Figure 2.58 Space fill representation of the packing arrangements 96

Figure 3.1 IR spectra of [$CrCl_3$(bipy)($pyNH_2$)] (blue), [$HpyNH_2$][$CrCl_4$(bipy)] (red) and [$CrCl_3$(bipy)(H_2O)] (green) in the region 3329 – 2291 cm^{-1} 105

Figure 3.2 IR spectra showing the presence of thf C–Hs in [$CrCl_3$(bipy)(thf)] (blue) and their absence in [$CrCl_3$(bipy)(H_2O)] (red).....106

Figure 3.3 Comparison of the IR spectra of [$CrCl_3$(thf)$_3$] (blue) and [$CrCl_3$(bipy)(pyphenyl)] (red) 106

Figure 3.4 Characteristic IR and Raman vibrations in [$CrCl_3$(bipy)(CH_3CN)] (red) and [$CrCl_3$(bipy)(pytb)] (blue).....107

Figure 3.5 IR and Raman vibrations in [$CrCl_3$(bipy)(thf)] (blue), [$CrCl_3$(bipy)(py)] (red) and [$HpyNH_2$][$CrCl_4$(bipy)] (purple) 109

Figure 3.6 Bipyridine specific IR vibrations present in all complexes represented by the comparison between [$CrCl_3$(bipy)(thf)] (red) and [$CrCl_3$(py)$_3$] (blue).....110

Figure 3.7 IR and Raman vibrations of tertiary butyl-specific vibrations in the region 1652 – 1104 cm^{-1} 111

Figure 3.8 Spectra showing the shifting of the characteristic ring breathing vibration in the IR of [$CrCl_3$(bipy)(py)], [$CrCl_3$(bipy)($pyNH_2$)], [$CrCl_3$(bipy)(pytb)] and [$CrCl_3$(bipy)(pyphenyl)] from free ligand positions. Raman spectra of [$CrCl_3$(bipy)(py)], [$CrCl_3$(bipy)(pytb)] and [$CrCl_3$(bipy)(pyphenyl)] 113

Figure 3.9 Evidence of coordinated pyridine in the IR spectra of [$CrCl_3$(bipy)(py)] (red), [$CrCl_3$(bipy)($pyNH_2$)] (blue), [$CrCl_3$(bipy)(pytb)] (purple) and [$CrCl_3$(bipy)(pyphenyl)] (green).....114

Figure 3.10 thf / unassigned / pyridinium vibration in IR and Raman spectra of [$CrCl_3$(bipy)(thf)] (red), [$CrCl_3$(bipy)(pytb)] (blue) and[$HpyNH_2$][$CrCl_4$(bipy)] (green) 116
Figure 3.11 IR spectrum of [$CrCl_3$(bipy)(thf)] (red), [$CrCl_3$(bipy)($pyNH_2$)] (blue), [$CrCl_3$(bipy)(pyphenyl)] (green) and[$HpyNH_2$][$CrCl_4$(bipy)] (purple). Raman spectrum of [$HpyNH_2$][$CrCl_4$(bipy)] 117
Figure 3.12 IR and Raman bands associated with [$HpyNH_2$][$CrCl_4$(bipy)] 118
Figure 3.13 FIR vibrations represented by spectra of [$CrCl_3$(bipy)(H_2O)] (red), [$CrCl_3$(bipy)(py)] (blue) and [$HpyNH_2$][$CrCl_4$(bipy)] (green) 120
Figure 3.14 Experimental (red) and calculated (blue) MIR spectra of [$CrCl_3$(bipy)(thf)] 133
Figure 3.15 Experimental (red) and calculated (blue) Raman spectra of [$CrCl_3$(bipy)(thf)] 133
Figure 3.16 Experimental (red) and calculated (blue) MIR spectra of [$CrCl_3$(bipy)(H_2O)] 135
Figure 3.17 Experimental (red) and calculated (blue) MIR spectra of [$CrCl_3$(bipy)(CH_3CN)] 137
Figure 3.18 Experimental (red) and calculated (blue) Raman spectra of [$CrCl_3$(bipy)(CH_3CN)] 138
Figure 3.19 Experimental (red) and calculated (blue) MIR spectra of [$CrCl_3$(bipy)(py)] 140
Figure 3.20 Experimental (red) and calculated (blue) Raman spectra of [$CrCl_3$(bipy)(py)] 141
Figure 3.21 Experimental (red) and calculated (blue) MIR spectra of [$CrCl_3$(bipy)(pyphenyl)] 143
Figure 3.22 Experimental (red) and calculated (blue) Raman spectra of [$CrCl_3$(bipy)(pyphenyl)] 144
Figure 3.23 Experimental (red) and calculated (blue) Raman spectra of [$HpyNH_2$][$CrCl_4$(bipy)] 147
Figure 3.24 Experimental (red) and calculated (blue) Raman spectra of [$HpyNH_2$][$CrCl_4$(bipy)] 147
Figure 3.25 HOMO and LUMO orbitals of [$CrCl_3$(bipy)(thf)] 149
Figure 3.26 HOMO (left) and LUMO (right) orbitals of [$CrCl_3$(bipy)(H_2O)] 150
Figure 3.27 HOMO and LUMO orbitals of [$CrCl_3$(bipy)(MeCN)] 150

Figure 3.28 HOMO and LUMO orbitals of [$CrCl_3$(bipy)(py)] 151
Figure 3.29 HOMO and LUMO orbitals of [$CrCl_3$(bipy)(pyphenyl)] 151
Figure 3.30 HOMO and LUMO orbitals of [$HpyNH_2$][$CrCl_4$(bipy)] 152
Figure 3.31 Stacked ^{1}H NMR spectra for the reaction of bipy with [$CrCl_3(thf)_3$] over time. 1 = bipy, 2 = thf, 3 = water peak in acetone, 4 = acetone d_6 , 5 = thf 153
Figure 3.32 Plot of integration of bipy:thf resonances over time 153
Figure 3.33 ^{1}H NMR spectrum of [$CrCl_3$(bipy)(thf)] final product in acetone-d_6 .. 154
Figure 3.34 ^{13}C NMR spectrum of [$CrCl_3$(bipy)(thf)] final product in DMSO-d_6 . 155
Figure 3.35 ^{1}H NMR spectrum of [$CrCl_3$(bipy)(CH_3CN)] in acetone-d_6 156
Figure 3.36 ^{1}H NMR spectrum of [$CrCl_3$(bipy)(py)] in acetone-d_6 157
Figure 3.37 ^{1}H NMR spectrum of [$CrCl_3$(bipy)(H_2O)] in DMSO-d_6 157
Figure 3.38 FAB-MS spectrum of [$CrCl_3$(bipy)(thf)]..... 158
Figure 3.39 FAB-MS spectrum of [$CrCl_3$(bipy)(H_2O)]..... 159
Figure 3.40 FAB-MS spectrum of [$CrCl_3$(bipy)(CH_3CN)]..... 159
Figure 3.41 FAB-MS spectrum of [$CrCl_3$(bipy)(pyphenyl)]..... 160
Figure 3.42 A = Perspective drawing of [$CrCl_3$(bipy)(H_2O)] structure determined in this study, B = Perspective drawing of the structure determined by Namba [108] 162
Figure 3.43 Hydrogen bond interactions 164
Figure 3.44 Short contacts between aromatic ring layers 165
Figure 3.45 Comparison of the experimental and theoretically obtained X-ray diffraction powder patterns of [$CrCl_3$(bipy)(H_2O)] 165
Figure 3.46 Hydrogen bond interactions 169
Figure 3.47 Staggered π–π interactions in the packing arrangement of [$HpyNH_2$][$CrCl_4$(bipy)] 169
Figure 3.48 Packing and space fill of [$HpyNH_2$][$CrCl_4$(bipy)] 170
Figure 3.49 Perspective drawing showing the two formula units of [$CrCl_2(bipy)_2$][Cl]·H_2O in the asymmetric unit 172
Figure 3.50 Packing arrangements for [$CrCl_2(bipy)_2$][Cl]·H_2O 173

Figure 3.51 Packing and space fill arrangements for $[CrCl_2(bipy)_2][Cl]\cdot H_2O$ 174
Figure 3.52 Summary of routes to complex formation 177
Figure 4.1 Proposed routes to complex formation 183
Figure 4.2 IR spectra showing band shifts in $[CrCl_3(dppe)(thf)]$ (red) relative to free dppe (blue) 185
Figure 4.3 IR spectra of $[CrCl_3(dppe)(pytb)]$ (red) and free dppe (blue) 186
Figure 4.4 N–H vibrations observed in the IR spectrum of $[CrCl_3(dppe)(pyNH_2)]$ (blue) 187
Figure 4.5 Comparisons between IR spectra of$[CrCl_3(dppe)(thf)]$ (red), [Hpyphenyl][$CrCl_4$(dppe)] (blue) and free dppe (green). Raman spectrum of $[CrCl_3(dppe)(thf)]$ 188
Figure 4.6 Band intensity comparison between the IR spectra of $[CrCl_3(dppe)(py)]$ (red) and [Hpyphenyl][$CrCl_4$(dppe)] (blue) 189
Figure 4.7 IR spectrum of $[CrCl_3(dppe)(pytb)]$-specific vibrations 191
Figure 4.8 IR and Raman spectra of $[CrCl_3(dppe)(thf)]$ (red) with the IR highlighting the lack of shifting relative to free dppe (blue) 192
Figure 4.9 Ring breathing shift in IR bands of $[CrCl_3(dppe)(py)]$ (red) 193
Figure 4.10 IR and Raman spectra of $[CrCl_3(dppe)(pyNH_2)]$ (green) and $[CrCl_3(dppe)(pytb)]$ (red) 194
Figure 4.11 Comparisons between IR spectra of $[CrCl_3(dppe)(pyphenyl)]$ (red), [Hpyphenyl][$CrCl_4$(dppe)] (blue) and free dppe (green) 195
Figure 4.12 IR spectra showing pyH-specific vibration in [Hpyphenyl][$CrCl_4$(dppe)] (blue) which is absent in $[CrCl_3(dppe)(pyphenyl)]$ (red) 196
Figure 4.13 IR spectra of $[CrCl_3(dppe)(py)]$ (red), $[CrCl_3(dppe)(pytb)]$ (blue), $[CrCl_3(dppe)(thf)]$ (purple) and free dppe (green) 197
Figure 4.14 FIR spectra of $[CrCl_3(dppe)(thf)]$ (red), $[CrCl_3(dppe)(py)]$ (blue) and $[CrCl_3(dppe)(pytb)]$ (green) 200
Figure 4.15 FIR spectra of $[CrCl_3(dppe)(pyphenyl)]$ (red) and [Hpyphenyl][$CrCl_4$(dppe)] (blue) 201
Figure 4.16 Experimental (red) and calculated (blue) MIR spectra of $[CrCl_3(dppe)(pytb)]$ 211
Figure 4.17 Experimental (red) and calculated (blue) Raman spectra of $[CrCl_3(dppe)(pytb)]$ 211

Figure 4.18 Experimental (red) and calculated (blue) FIR spectra of [$CrCl_3$(dppe)(pytb)] 212
Figure 4.19 HOMO and LUMO orbitals of [$CrCl_3$(dppe)(pytb)] 214
Figure 4.20 ^{1}H NMR spectrum of [$CrCl_3$(dppe)(thf)] final product in DMSO-d_6 .. 215
Figure 4.21 ^{31}P NMR spectrum free dppe in DMSO-d_6 215
Figure 4.22 ^{31}P NMR spectrum of [$CrCl_3$(dppe)(thf)] in DMSO-d_6 216
Figure 4.23 FAB-MS spectum showing paeks present in [$CrCl_3$(dppe)(thf)], [$CrCl_3$(dppe)($pyNH_2$)] and [$CrCl_3$(dppe)(pyphenyl)]..... 217
Figure 4.24 FAB-MS spectrum of [$CrCl_3$(dppe)(pyphenyl)]..... 217
Figure 4.25 Perspective drawing showing the asymmetric unit of [Hpyphenyl][$CrCl_4$(dppe)] showing hydrogen bond interactions 218
Figure 4.26 P–C–C–P torsion angle comparison between [Hpyphenyl][$CrCl_4$(dppe)]and the Gray structure 219
Figure 4.27 Packing arrangement with space-filled component of [Hpyphenyl][$CrCl_4$(dppe)] 221
Figure 5.1 Results of structural framework searches using Cambridge Database [117] 226
Figure 5.2 IR spectra of N–H bands in [$CrCl_3$dppea($pyNH_2$)] (red) and [$CrCl_3(pyNH_2)_3$] (blue) 230
Figure 5.3 IR and Raman spectra of [$CrCl_3$(dppea)(pytb)] 231
Figure 5.4 IR and Raman spectra of [$CrCl_3$(dppea)(py)] 233
Figure 5.5 Pyridine-specific vibration absent in [$CrCl_3$(dppea)(thf)] (green) and free dppea (blue) 234
Figure 5.6 IR spectrum of $pyNH_2$ vibrations observed in [$CrCl_3$(dppea)($pyNH_2$)] 236
Figure 5.7 IR spectra of free pyridine (blue), free dppe (green) and free dppea (red) 238
Figure 5.8 IR spectra comparison between [$CrCl_3$(dppea)(py)] (red) and free pyridine (blue) 239
Figure 5.9 IR spectra comparison between [$CrCl_3$(dppea)(pytb)] (red) and free pytb (blue) 240

Figure 5.10 IR spectra comparison between [$CrCl_3$(dppea)(pyphenyl)] (red) and free pyphenyl (green).....241
Figure 5.11 IR and Raman spectra of [$CrCl_3$(dppeay)(py)] (red), [$CrCl_3$(dppea)($pyNH_2$)] (blue), [$CrCl_3$(dppea)(pytb)] (green) and [$CrCl_3$(dppea)(pyphenyl)] (purple) showing shifting of the characteristic ring breathing vibration.....242
Figure 5.12 FIR and Raman spectra of [$CrCl_3$(dppea)(py)].....245
Figure 5.13 Experimental (red) and calculated (blue) MIR spectra of [$CrCl_3$(dppea)(pytb)] 251
Figure 5.14 Experimental (red) and calculated (blue) Raman spectra of [$CrCl_3$(dppea)(pytb)] 251
Figure 5.15 HOMO and LUMO orbitals of [$CrCl_3$(dppea)(pytb)]].....253
Figure 5.16 FAB-MS spectrum of [$CrCl_3$(dppea)(pytb)]……..254
Figure 5.17 FAB-MS spectrum of [$CrCl_3$(dppea)(pyphenyl)]……254
Figure 6.1 ((RP)–1–[(1S)–1–aminoethyl)–2–(diphenylphosphino)ferrocene).....258

LIST OF TABLES

Table 2.1 Characteristic pyridine shifts in the IR spectrum**Error! Bookmark not defined.**
Table 2.2 Vibrational assignments of [$CrCl_3$(py)($thf)_2$] (1), [$CrCl_3(py)_2$(thf)] (2), [$CrCl_3(py)_3$] (3) 32
Table 2.3 Selected experimental and calculated IR and Raman band assignments for [$CrCl_3(py)_3$] ..... **Error! Bookmark not defined.**
Table 2.4 Scaling factors determined for [$CrCl_3(py)_3$]**Error! Bookmark not defined.**
Table 2.5 Selected bond lengths [Å] and angles [°] for [$CrCl_3(py)_3$]**Error! Bookmark not define**
Table 2.6 Selected torsion angles [°] for [$CrCl_3(py)_3$]**Error! Bookmark not defined.**
Table 2.7 Differences in crystal data between [$CrCl_3(py)_3$] of this study and that of Howard [83] ..... **Error! Bookmark not defined.**
Table 2.8 Crystal data and structure refinement for [$CrCl_3(py)_3$] of this study**Error! Bookmark n**
Table 2.9 Selected bond lengths [Å], bond angles [°] and torsion angles [°] for [Hpy][$CrCl_4(py)_2$]..... **Error! Bookmark not defined.**

Table 2.10 Hydrogen bonds for [Hpy][$CrCl_4(py)_2$] [Å and °] 50
Table 2.11 Crystal data and structure refinement for [Hpy][$CrCl_4(py)_2$] 52
Table 2.12 Selected bond lengths [Å], bond angles [°] and torsion angles [°] for [$CrCl_3(py)_2(DMF)$] 62
Table 2.13 Crystal data and structure refinement for [$CrCl_3(py)_2(DMF)$] 63
Table 2.14 Infrared and Raman band shifts in the region 1 638 – 1 045 cm^{-1} [$CrCl_3(pyNH_2)_3$] 68
Table 2.15 IR and Raman band shifts in the region 1638 to 1045 cm^{-1}[$CrCl_3(pytb)_3$] 69
Table 2.16 IR and Raman band shifts in the region 1030 – 499 cm^{-1} [$CrCl_3(pyNH_2)_3$] 71
Table 2.17 IR and Raman band shifts in the region 1030 – 499 cm^{-1} [$CrCl_3(pytb)_3$] 72
Table 2.18 IR and Raman band shifts in the region 1030 – 499 cm^{-1} [$CrCl_3(pyphenyl)_3$] 73
Table 2.19 Shifting of the characteristic ring breathing vibration in [$CrCl_3py_3$], [$CrCl_3(pyNH_2)_3$], [$CrCl_3(pytb)_3$] and [$CrCl_3(pyphenyl)_3$] 75
Table 2.20 Vibrational assignments of [$CrCl_3(py)_2$DMF] (5), [$CrCl_3(pyNH_2)_3$] (6), [$CrCl_3(pytb)_3$] (7) and [$CrCl_3(pyphenyl)_3$] (8) 80
Table 2.21 Selected experimental and calculated IR and Raman band assignments for [$CrCl_3(pyNH_2)_3$] 86
Table 2.22 Scaling factors determined for [$CrCl_3(pyNH_2)_3$] 86
Table 2.23 Selected experimental and calculated IR and Raman band assignments for [$CrCl_3(pytb)_3$] 88
Table 2.24 Scaling factors determined for [$CrCl_3(pytb)_3$] 89
Table 2.25 Selected bond lengths [Å], bond angles [°] and torsion angles [°] for [$CrCl_3(pytb)_3$] 94
Table 2.26 Crystal data and structure refinement for [$CrCl_3(pytb)_3$] 94
Table 3.1 Bipyridine-specific vibrations present in the spectra of all complexes 109
Table 3.2 Pyridine specific vibrations 110
Table 3.3 Shifting of the characteristic ring breathing vibration in [$CrCl_3(bipy)(py)$], [$CrCl_3(bipy)(pyNH_2)$], [$CrCl_3(bipy)(pytb)$] and [$CrCl_3(bipy)(pyphenyl)$] 112

Table 3.4 Vibrational assignments of [$CrCl_3$(bipy)(thf)] (9), [$CrCl_3$(bipy)(CH_3CN)] (10), [$CrCl_3$(bipy)(py)] (11), [$CrCl_3$(bipy)($pyNH_2$)] (12), [$CrCl_3$(bipy)(pytb)] (13), [$CrCl_3$(bipy)(pyphenyl)] (14), [$HpyNH_2$][$CrCl_4$(bipy)] (15), [$CrCl_3$(bipy)(H_2O)] (16) and [$CrCl_2$(bipy)$_2$][Cl]·H_2O (17) 121
Table 3.5 Selected experimental and calculated IR and Raman band assignments for [$CrCl_3$(bipy)(thf)] 134
Table 3.6 Scaling factors determined for [$CrCl_3$(bipy)(thf)] 134
Table 3.7 Selected experimental and calculated IR band assignments for [$CrCl_3$(bipy)(H_2O)] 136
Table 3.8 Scaling factors determined for [$CrCl_3$(bipy)(H_2O)] 136
Table 3.9 Selected experimental and calculated IR and Raman band assignments for [$CrCl_3$(bipy)(CH_3CN)] 139
Table 3.10 Scaling factors determined for [$CrCl_3$(bipy)(CH_3CN)] 140
Table 3.11 Selected experimental and calculated IR and Raman band assignments for [$CrCl_3$(bipy)(py)] 142
Table 3.12 Scaling factors determined for [$CrCl_3$(bipy)(py)] 143
Table 3.13 Selected experimental and calculated IR and Raman band assignments for [$CrCl_3$(bipy)(pyphenyl)] 145
Table 3.14 Scaling factors determined for [$CrCl_3$(bipy)(pyphenyl)] 146
Table 3.15 Selected experimental and calculated IR and Raman band assignments for [$HpyNH_2$][$CrCl_4$(bipy)] 148
Table 3.16 Scaling factors determined for [$HpyNH_2$][$CrCl_4$(bipy)] 149
Table 3.17 Selected bond lengths [Å], bond angles [°] and torsion angles [°] for [$CrCl_3$(bipy)(H_2O)] 163
Table 3.18 Crystallographic differences between the two structures 163
Table 3.19 Hydrogen bonds for [$CrCl_3$(bipy)(H_2O)] [Å and °] 164
Table 3.20 Crystal data and structure refinement for [$CrCl_3$(bipy)(H_2O)]. 166
Table 3.21 Selected bond lengths [Å] and angles [°] for [$HpyNH_2$][$CrCl_4$(bipy)] 167
Table 3.22 Hydrogen bonds for [$HpyNH_2$][$CrCl_4$(bipy)] [Å and º] 168
Table 3.23 Crystal data and structure refinement for [$HpyNH_2$][$CrCl_4$(bipy)] 170
Table 3.24 Crystallographic differences between the two structures 173
Table 3.25 Bond lengths [Å] and angles [°] for [$CrCl_2$(bipy)$_2$][Cl]·H_2O 174
Table 3.26 Crystal data and structure refinement for [$CrCl_2$(bipy)$_2$][Cl]·H_2O 175

Table 4.1 pytb-specific vibrations 190
Table 4.2 Shifting of the characteristic ring breathing vibration in [$CrCl_3$(dppe)(py)], [$CrCl_3$(dppe)($pyNH_2$)], [$CrCl_3$(dppe)(pytb)] and [$CrCl_3$(dppe)(pyphenyl)] 195
Table 4.3 pytb specific vibrations 198
Table 4.4 Vibrational assignments of [$CrCl_3$(dppe)(thf)] (19), [$CrCl_3$(dppe)(py)] (20), [$CrCl_3$(dppe)($pyNH_2$)] (21), [$CrCl_3$(dppe)(pytb)] (22), [$CrCl_3$(dppe)(pyphenyl)] (23) and [Hpyphenyl][$CrCl_4$(dppe)] (24) 202
Table 4.5 Selected experimental and calculated IR and Raman band assignments for [$CrCl_3$(dppe)(pytb)] 212
Table 4.6 Scaling factors determined for [$CrCl_3$(dppe)(pytb)] 213
Table 4.7 Bond lengths [Å] and angles [°] for [Hpyphenyl][$CrCl_4$(dppe)] 219
Table 4.8 Hydrogen bonds for [Hpyphenyl][$CrCl_4$(dppe)] [Å and °] 220
Table 4.9 Crystal data and structure refinement for [Hpyphenyl][$CrCl_4$(dppe)]. 221
Table 5.1 IR vibrations associated with coordinated pyridine 233
Table 5.2 IR vibrations associated with coordinated $pyNH_2$ 235
Table 5.3 IR vibrations associated with coordinated pyridine 239
Table 5.4 IR vibrations associated with coordinated pytb 240
Table 5.5 IR vibrations associated with coordinated pyphenyl 241
Table 5.6 Shifting of the characteristic ring breathing vibration in [$CrCl_3$(dppea)(py)], [$CrCl_3$(dppea)($pyNH_2$)], [$CrCl_3$(dppea)(pytb)] and [$CrCl_3$(dppea)(pyphenyl)] 242
Table 5.7 Vibrational assignments of [$CrCl_3$(dppea)(thf)] (26), [$CrCl_3$(dppea)(py)] (27), [$CrCl_3$(dppea)($pyNH_2$)] (28), [$CrCl_3$(dppea)(pytb)] (29) and [$CrCl_3$(dppea)(pyphenyl)] (30) 246
Table 5.8 Selected experimental and calculated IR and Raman band assignments for [$CrCl_3$(dppea)(pytb)] 252
Table 5.9 Scaling factors determined for [$CrCl_3$(dppea)(pytb)] 253

Chapter 1

Introduction

1.1 IMPORTANCE OF CATALYSIS

The global chemical industry of today is driven by catalysis to such an extent that one cannot underestimate the importance of catalytic processes to the wealth creation of any country. For example, it has been estimated that around 20% of the entire US Gross National Product is generated through the use of catalytic processes. These are instrumental in fields that include, but are not limited to, the production of fuels, petrochemicals, pharmaceuticals, polymers and agrichemicals, as well as environmentally favourable technologies such as catalytic converters [1].

1.2 HOMOGENEOUS AND HETEROGENEOUS CATALYSIS

Within catalytic research there are two main different types of catalytic processes that are utilised and investigated, namely homogeneous and heterogeneous catalysis.

In homogeneous catalysis the reactions occur at metal centres and the metal complex catalysts, promoters, reagents and products are all soluble in the reaction medium. Conversely, heterogeneous catalytic reactions occur on a surface with many metal centres and the reagents (normally in the liquid or gas phase) are led over or through the catalyst, which in fact aids the separation of products from the reaction process [2].

Both processes have various advantages and disadvantages depending on what product or process is required. For instance, it has been said that the first response of an industrialist is to heterogenise a catalyst since this leads to a potentially simpler process, but that the academic often makes the case for the homogeneous catalyst since it is potentially easier to study and is more easily modified [1]. This is of course to some extent a generalisation as many industrial catalytic processes are in fact homogeneous, but is remains a fact that to a large degree these are easier to study than their heterogeneous counterparts. This particular study is based on

homogeneity as the potential catalytic reactions involved in this project are of a homogeneous nature.

1.3 CATALYSIS AND TRANSITION METALS

Transition metals and homogeneous catalysis go hand in hand. This is due to certain favourable properties that transition metals possess [2]:

1. Bonding ability – Ability to form both sigma and pi bonds which is an essential factor in imparting catalytic properties to the transition metals and their complexes.
2. Extensive choice of ligands – Transition metals readily form linkages with the majority of other elements in the periodic table and with almost any organic molecule. It is this property that results in transition metals having such rich coordination chemistry relevant to their role as catalysts.
3. Ligand effects – The ability of transition metal catalysts to accommodate both participative and non-participative ligands within their coordination sphere offers us the possibility of being able to direct the course of the reaction between participative ligands by modifying the structural/electronic properties of the non–participative ligands.
4. Variability of oxidation states – Having access to a wide range of oxidation states helps transition metals to form complexes with a wide range of other elements and compounds. More important than access is the ability to interchange readily between oxidation states during the course of a catalytic cycle.
5. Variability of coordination number – The dissociation of ligands to create vacant coordination sites is associated with changes in the molecular structure of the catalyst.

1.4 CATALYTIC STEPS

All catalytic processes proceed via a number of interlinked steps [1]:

1. activation of the metal centre or generation of the active catalyst
2. movement of the reactants to the active centre and their binding and activation
3. making and breaking of the reactant bonds to generate new intermediate species
4. liberation of these intermediate species as products, with the return of the catalyst to a state where it is ready to begin the cycle again.

Incorporated within these standard catalytic steps are a number of key reactions. Each catalytic process makes use of some, and at times all, of these reactions:

1. Ligand substitution
2. Oxidative addition
3. Migratory insertion
4. Nucleophilic attack
5. Reductive elimination
6. β–elimination
7. α–elimination

1.5 OVERVIEW OF CATALYTIC DESIGN

Before detailing and discussing specific catalytic processes, it is important for one to appreciate that the study of any catalyst is driven by a number of key elements than can be traced back to a specific market need. This is illustrated in the Figure 1.1.

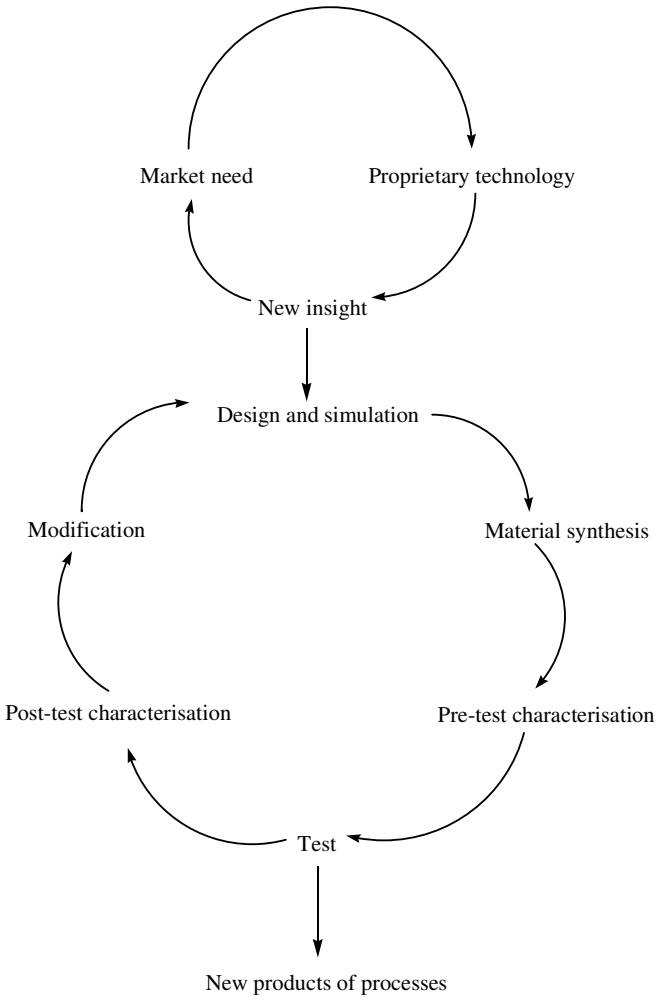

Figure 1.1 Typical key steps in the study of many catalytic systems [3]

Prime examples of where these steps would have been considered are given in the following section which provides a summary of the chemistry that has led to the fundamental catalytic precursor investigations undertaken in this study.

1.6 ETHYLENE OLIGOMERISATIONS

Selective trimerisation and tetramerisation of ethylene are the preferred on-purpose routes to the formation of the LAOs, namely 1–hexene and 1–octene respectively. They are useful intermediates in the production of co–polymers, detergents, synthetic lubricants and plasticiser alcohols [4].

1.6.1 1–HEXENE

It is widely agreed that the formation of both 1–hexene and 1–octene takes place via reactive metallacycles. Figure 1.2 shows the formation of 1-hexene [5]; the formation of 1–octene will be discussed with Figure 1.9. The formation of a five–membered metal ring system (metallocyclopentane) is achieved via the coordination of two ethene molecules, followed by oxidative coupling. Coordination of a further ethene molecule, along with olefin insertion, leads to a metallacycloheptane system. At this stage β–hydrogen elimination and then reductive elimination lead to the production of 1–hexene [5].

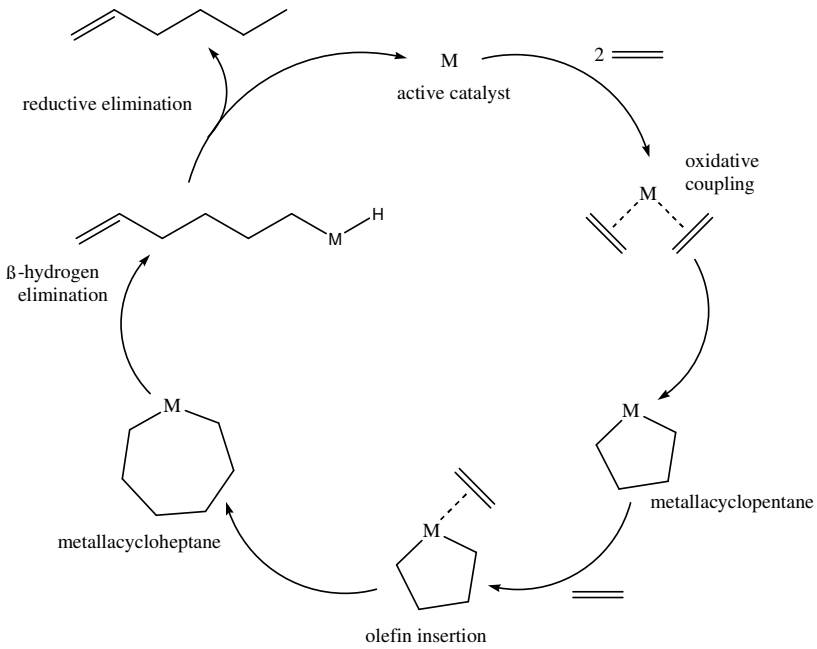

Figure 1.2 Formation of 1-hexene via a metallacycle

The first commercially productive trimerisation system was created in the late 1980s; this was the Phillips petroleum catalyst system based on chromium pyrrolyl compounds [6, 7]. However, it must be noted that this work was based on earlier research carried out by Manyik [8, 9].

Since the success of the Phillips system, a great deal of research has gone into modifying the pre–catalytic compounds and the catalytic conditions (i.e. activators, pressure, temperature, etc). While of course varying the catalytic conditions plays a significant role in optimising the production of 1–hexene and 1–octene, this can be done only once a good catalytic precursor has been designed.

Variations in the pre–catalytic compounds can be achieved by varying both the metal centre and the coordinated ligands. The search for metals other than chromium (Phillips system) revolved around environmental concerns, as well as the aim of enhancing catalytic performance. The metals studied included zirconium [10, 11], vanadium [12], tantalum [13, 14] and titanium [15, 16]. However, due to a combination of low activity, high costs and other practical problems, these metals have not been as successful as chromium [4]. The ligands studied included pyrrolyl derivatives with common steric and electronic properties.

The following discussion gives a brief insight into some of the major core ligand frameworks that have evolved in the search for more active and selective ethylene catalytic systems. Although not specifically mentioned, the frameworks have included various substituents with different steric and electronic properties. In 1997 the Tosoh Corporation developed a catalyst based on chromium and maleimidyl ligands. [17]. However, the 1–hexene selectivity was 12 to 15% lower than that of the Phillips catalyst and therefore not an economically viable option. Other similar ligands over the years have included cyclopentadienyl [18, 19], boratabenzenyl [20] and aryloxide [21, 22, 23, 24] ligands, all with varying degrees of success. Although these catalysts were noteworthy equivalents to the Phillips system, their lower selectivity towards 1-hexene made them less desirable from an economic viewpoint. Further ligand development began to focus on multidentate heteroatomic ligands, namely bidentate and tridentate ligands associated with nitrogen, phosphorous, sulphur and mixtures thereof.

With this in mind an advance worthy of mention was the Kohn system (Figure 1.3) which was originally developed as a homogeneous analogue of the Phillips CrO_3/SiO_2 polymerisation catalyst [25]. It entailed a tridentate nitrogen–based donor ligand (N–alkyl triazocyclohexane) that complexed with $[CrCl_3(thf)_3]$ to yield 1–hexene (as well as higher olefins). The selectivity towards 1–hexene under certain conditions was impressive, with >90% conversion. [26]. In fact this system was also used in the selective trimerisation of 1–decene and 1–dodecene [27].

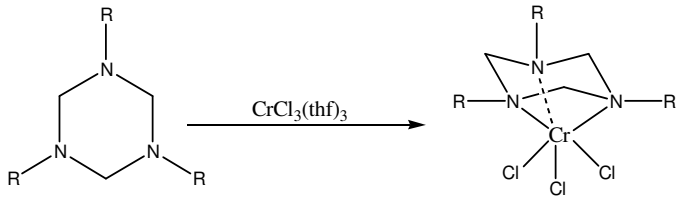

Figure 1.3 The Kohn catalyst

The Wass system (Figure 1.4) was built on the tridentate theme of Kohn but incorporated a combination of both nitrogen and phosphorous donor atoms in the ligand. More specifically, the system was based on bis(diarylphosphino)amine ligands coordinated with pendant methoxy groups that were thought to stabilise the coordinatively unsaturated intermediates proposed during the catalytic cycle, and were crucial to obtaining active systems [28]. This linked with work carried out by Bercaw and co–workers in which PNP ligands with ortho–methoxyaryl and ortho–thiomethoxy substituents were investigated [29, 30]. The selectivity of the Wass system was around 90%.

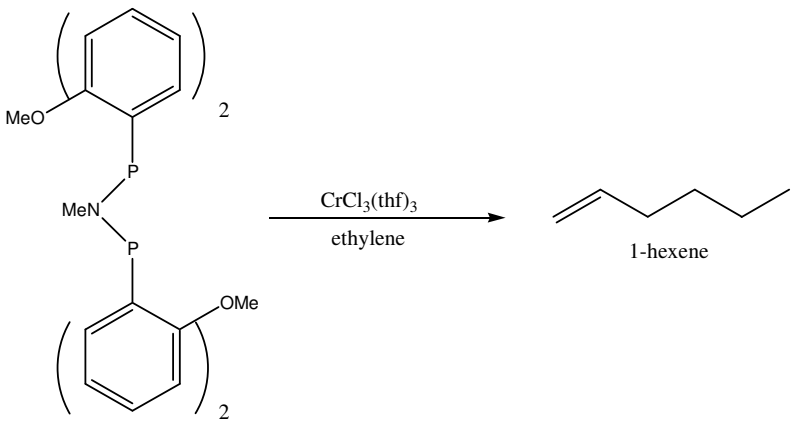

Figure 1.4 The Wass catalyst

In 2003 McGuinness and co–workers varied the Wass ligand system, as illustrated in Figure 1.5, and obtained a highly active system that was selective to 1–hexene. Of particular interest was that a crystal structure was obtained of the catalytic precursor and an octahedral geometry with a *mer* arrangement of ligands was seen [31]. Also to be noted is that, compared with the Wass system, it was more selective to 1–hexene but less active and stable.

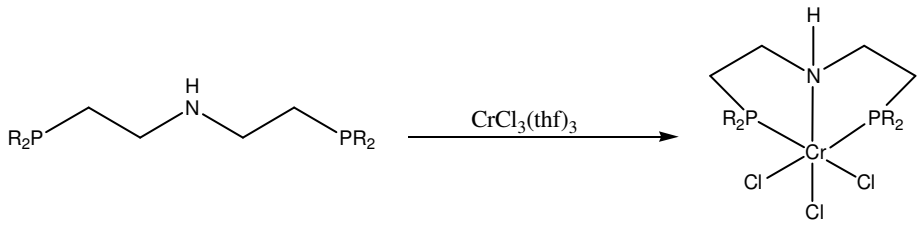

Figure 1.5 Variation of the Wass catalyst by McGuinness [31]

Although the PNP tridentate catalyst was highly selective towards 1–hexene, there were certain drawbacks. The toxicity of phosphines, their sensitivity to oxidation and the high cost of secondary alkyl phosphine precursors all contributed to the search for other catalysts that possessed the positive attributes of PNP but without the drawbacks. As a result the analogous SNS tridentate system, using both sulphur- and nitrogen-containing ligands came about [32].

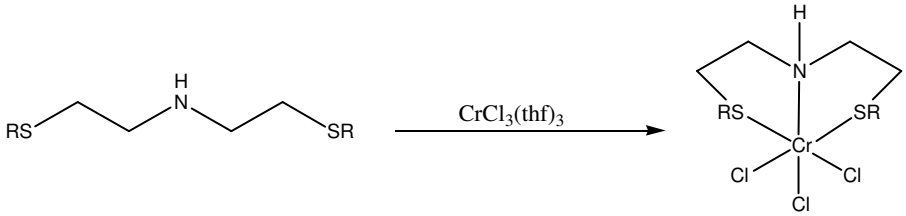

Figure 1.6 Formation of the SNS complex

Its attractiveness lay in its low cost, ease of synthesis and similar donor properties to PNP, while maintaining high activity and 1–hexene selectivity.

Due to the success of both the PNP and SNS systems, it was logical then to develop mixed-donor ligands which include SPS, PSP and PPP combinations. Also varied was the length of the N–S spacer to give asymmetrical SNS ligands. However, results have shown that these manipulations did not give the same high levels of activity or selectivity towards 1–hexene formation [33].

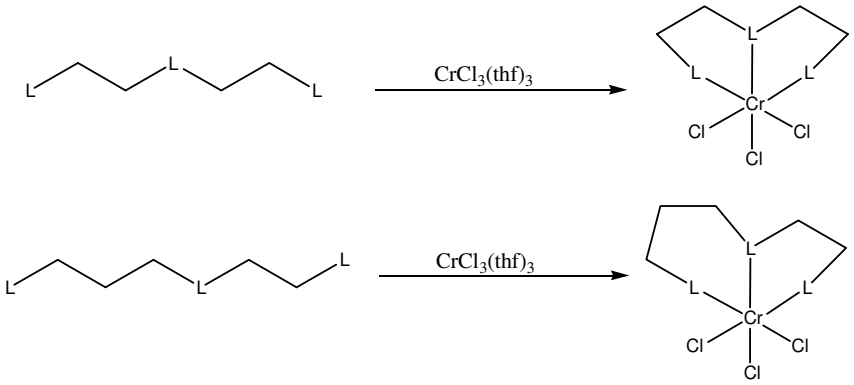

Figure 1.7 **Variation in spacer length of tridentate ligands**

1.6.2 1-OCTENE

All of the above systems have to a greater or lesser extent been useful as ethylene trimerisation catalysts. However, although the production of 1–octene via tetramerisation was also desirable, it had long been thought that this would be improbable as the metallocycle depicted in Figure 1.2 would have to extend to a nine–membered ring. This was said to be unlikely as the further ethylene insertion to give the metallanonane would compete with 1-hexene elimination. However, this was indeed achieved by the South African chemical company SASOL with essentially a modified bis(diarylphosphinoamine) Wass-type catalyst [34].

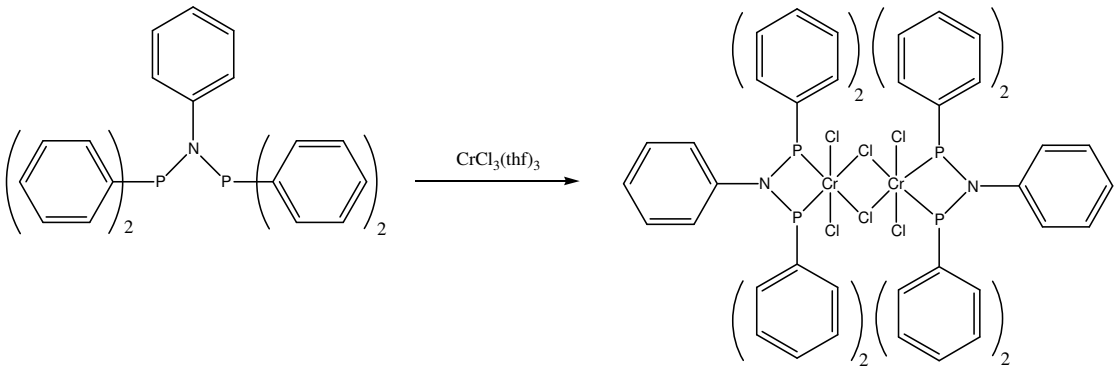

Figure 1.8 **The first tetramerisation catalyst**

As can be seen from Figure 1.8, this system was found to be based on a dimeric form for the active catalyst. As a result of the success of this catalyst, the metallacycle was studied in depth and it is now suggested that the production of 1–octene can occur via one of two pathways, as depicted in Figure 1.9 [5].

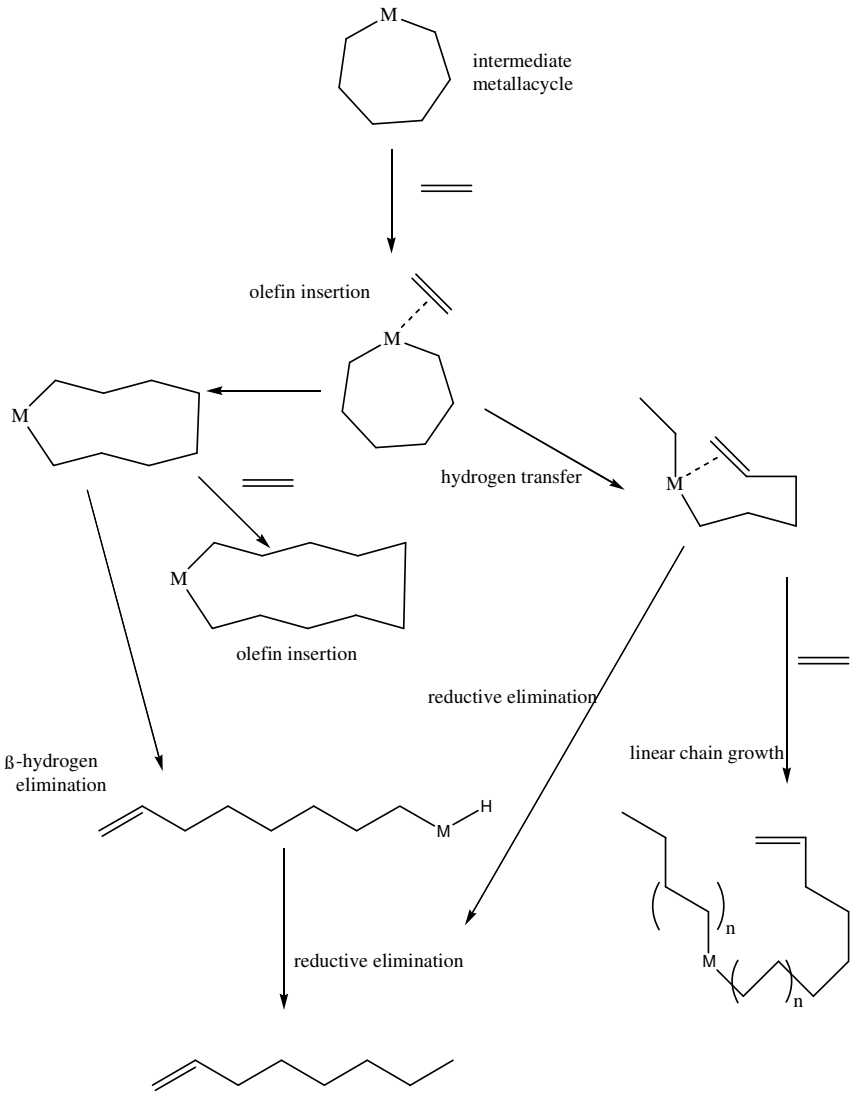

Figure 1.9 Pathways to 1–octene formation

1.7 PROJECT OUTLINE

Even with the great deal of research carried out to date on ethylene tri- and tetramerisation reactions, there remain a number of outstanding issues. One such issue is that of identifying the catalytically active species. This involves the complex composition, the mode of activation and the metal redox couple responsible for the olefin coordination and carbon–carbon coupling reactions during the chain growth [4, 35, 36].

With this in mind the aim of this project was to identify and study the fundamental chemistry behind potentially active novel chromium-based systems as these concepts can be applied to the chemistry of existing successful systems. This was to be achieved by making use of a variety of spectroscopic and structural techniques. Of these techniques, IR and Raman spectroscopy, in particular, have to an extent been underutilised as a means of investigating

catalytic precursor chemistry. Emphasis is placed on the comparisons that can be drawn between the techniques, which results in well-characterised compounds in addition to a number of novel and interesting insights. Such insights refer to, among others, the monomeric and dimeric state of these systems. The following subsections (1.7.1 to 1.7.3.5) discuss the details of the project and include: the relevance of the monomeric and dimeric states, the selection of ligands and the characterisation techniques used.

1.7.1 MONOMERIC AND DIMERIC STATES

The conditions under which monomeric and dimeric states are formed are of interest. The catalytic precursors were synthesised via straightforward ligand substitution reactions to yield the monomer. However, it is generally believed that the co–catalyst acts upon the chromium precursor to give a cationic catalytically active intermediate [29, 25, 35, 36]. Also generally accepted is the role of dimeric chloro–bridged intermediates, the existence of which has been postulated or indicated by solid–state structures (as mentioned above) [34, 37, 38]. Isolated dimers show catalytic activity [38] and recently Jabri, Duchateau and co–workers isolated a dinuclear chloro-bridged chromium(III) complex after activation with excess $AlEt_2Cl$ [39, 40]. The stabilisation of vacant coordination sites is essential in a pre–catalytic stage to facilitate the coordination of ethylene at a later stage. Displacement of the weakly coordinated thf by bridging chloro ligands is assumed to be a way of reserving vacant coordination sites for attack by the co–catalyst, and eventual reaction with ethylene. In this study the focus was on the formation and cleaving of some dichromium(III) compounds containing bridging chloro ligands. The formation of such a dimer after the thermal decomposition of $[Cr(bipy)Cl_4]^-$ has been postulated and reported [41].

Figure1.10 shows that these dimers could be cleaved in a symmetrical (**A**) or asymmetrical (**B**) fashion with the choice of ligands discussed in detail in Subsection 1.8.3. The latter lead to the formation of cationic and anionic intermediates. This is, according to current thinking, more appropriate for the situation pertaining to the generation of the active catalyst for the tri– and tetramerisation of ethylene.

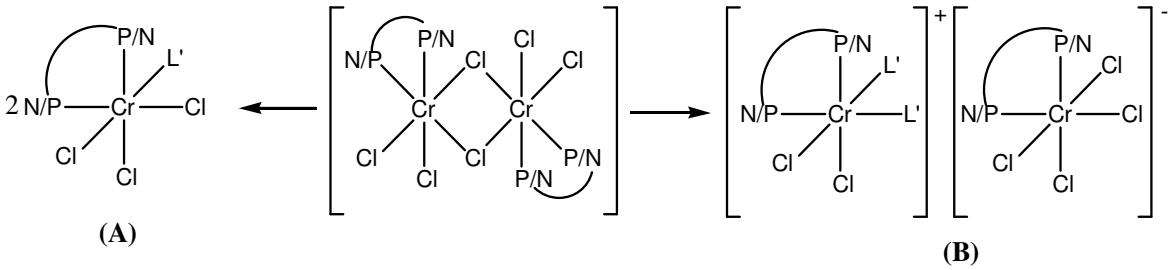

Figure 1.10 **Symmetrically (A) and asymmetrically (B) cleaved chloro dimers [100]**

Figure 1.11 shows both the substitution of the remaining thf ligand after the addition of the respective bidentate ligands and the breaking of a bridging chloro bond by the secondary amine ligands.

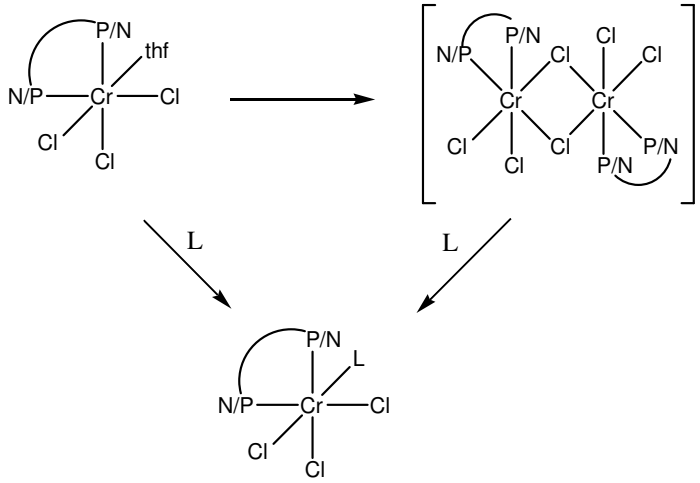

Figure 1.11 **Direct ligand substitution and symmetrical dimeric cleavage pathways [100]**

It is of interest to note that McGuinness et al. recently published work on chromium(III) complexes of bis(carbene)pyridine ligands with their focus on insights into the extended metallocycle mechanism of chain growth [42]. With respect to the bidentate pyridyl–carbene addition to $[CrCl_3(thf)_3]$, they also discuss the formation of monomeric and dimeric species.

1.7.2 LIGANDS

The choice of classes of compounds investigated in this study has stemmed from the fact that ligands containing phosphorus and nitrogen donor atoms are for the most part the cornerstone of the successful catalytic precursors of ethylene tri– and tetramerisation. Thus, in an attempt to gain further insight into structural and reactivity properties, various monodentate and bidentate P and N ligands were coordinated to Cr(III) to produce largely novel compounds. Although some of these compounds have been synthesised previously, novel synthetic routes

were used, and new structural and new spectroscopic insights (through extensive use of, inter alia, IR and Raman spectroscopy) were gained.

The choice of ligands can be divided into distinct ligand categories, the addition of pyridine and sterically and electronically differing para–substituted derivatives thereof being the common thread throughout. At the start of each chapter the reasoning behind the particular ligand choices is presented. There was a logical progression from N-monodentate ligands to mixed P–N bidentate ligands. Figure 1.12 outlines all the ligands investigated, with arrows indicating the progression to the next ligand.

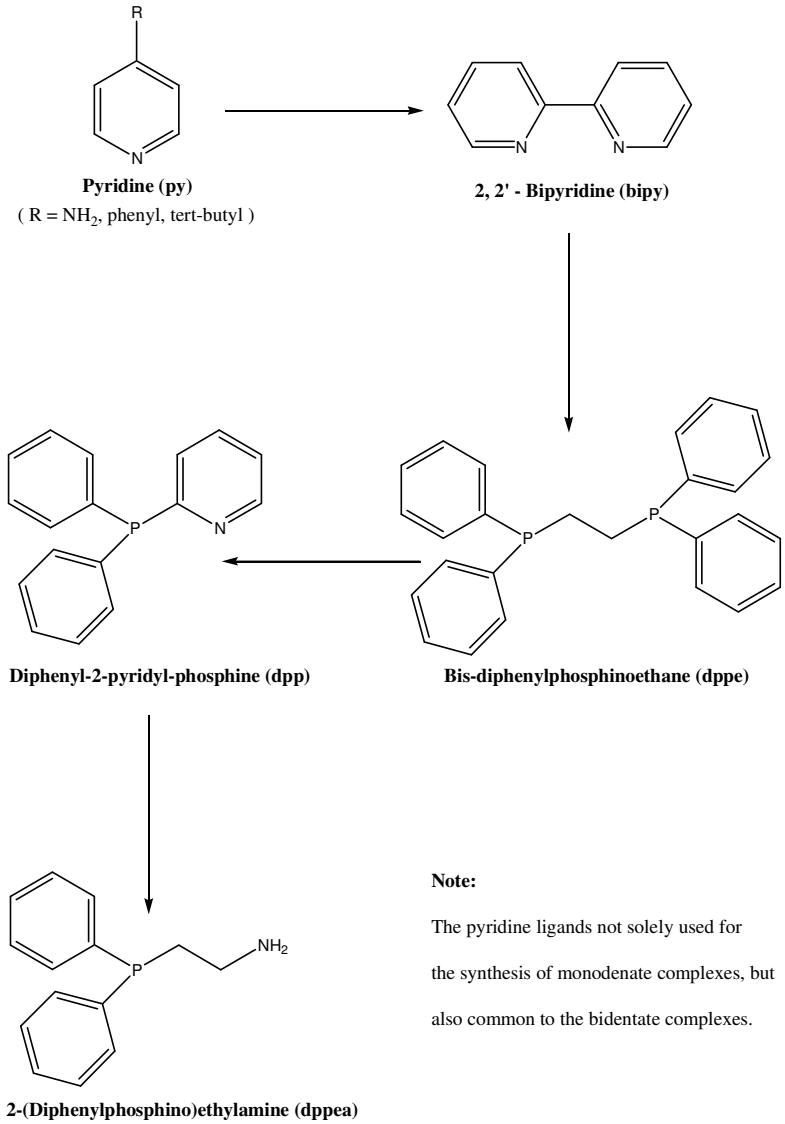

Figure 1.12 Ligands incorporated in this study

1.7.3 CHARACTERISATION AND ANALYSIS

The characterisation and study of these compounds involved a number of analytical techniques, each of which when studied independently is a source of valuable information. However, the full potential of these techniques is only realised when one combines and integrates all the various results as in fact all the techniques utilised in this study complement each other.

1.7.3.1 X–ray Crystallography

X–ray crystallography is the most favoured technique for characterising and studying novel compounds and thus a great deal of emphasis was placed on the pursuit of crystals of a sufficient size for the single–crystal diffractometer. However, as is widely recognised in the scientific community, this can be a difficult and, at times, frustrating practice which requires a combination of patience, perseverance and luck.

A number of crystal–growing techniques were employed and a total of eight structures were solved. The biggest problem encountered was that most of the compounds in this study were generally insoluble and only dissolved in a small number of solvents. These included and were limited to DMSO, DMF, CH_3CN and $ClCH_2CN$. The problem was confounded by the fact that both DMSO and DMF have high vapour pressures and are thus not conducive to evaporation. Nevertheless, all compounds underwent solubility tests in a large number of solvents, both polar and non–polar. Also varied was the type of vessel, which ranged from glass polytops and NMR tubes to Schlenk tubes, all with varying degrees of success.

It should be noted that the solutions for which these techniques were used came not only from dissolving the synthesised precipitates in appropriate solvents, but also directly from the reaction medium, as well as from the supernatant produced when the solution was washed with ether as part of the work–up.

The actual process of growing the crystals took the form of slow evaporation, slow cooling, vapour diffusion and the Hanging Drop Method.

The slow evaporation was carried out at room temperature, as well as at 4 and -30 °C. The second method of slow cooling was based on sound theory as the slower crystals grow, the lower the levels of entropy induced defects to its perfection [43]. The compounds were

dissolved in solvents and heated. They were then placed in beakers of water which had been heated to temperatures of 40, 60 and 80 °C.

Vapour diffusion, otherwise known as "isothermal distillation" was the third method used and is based on the concept of polarity. The compounds were dissolved in suitable solvents and placed in test tubes. A less polar solvent than that used for dissolving the samples is placed in beakers. The test tubes are then placed in the beakers and sealed. The theory is that the less polar solvent diffuses through the vapour phase into a solution of a compound in the more polar solvent and hence reduces the solubility. This slow diffusion should stimulate crystals to form.

A variation of vapour diffusion is the Hanging Drop Method which is a technique normally reserved for the crystallisation of macromolecules such as proteins. A drop of compound dissolved in solvent is placed in vapour equilibrium with a liquid reservoir of solvents. For equilibrium to be achieved, vapour must begin to leave the drop and reach the reservoir. The sample increases in supersaturation. The concentration of both the compound and the solvent increases as solvent leaves the drop for the reservoir. Therefore when both the drop and the reservoir have equal concentrations, equilibrium is reached [44].

1.7.3.2 Infrared and Raman Spectroscopy

With respect to these specific types of compound, IR and Raman spectroscopy have to an extent been under–utilised. MIR spectra are able to confirm the presence or indeed absence of the respective ligands while, perhaps more importantly, FIR spectra can indicate metal–ligand vibrations that will give a real indication of complexation (note that the Raman spectra incorporate both regions). In addition such metal-ligand vibrations may assist in the differentiation of monomeric and dimeric species with the presence of bridging and terminal chlorine atoms. The shifting of bands can also indicate that the complexes have been formed through comparison of the respective ligand spectra with those of the complexes.

IR and Raman are spectroscopic techniques that go hand in hand when analysing the vibrational modes of compounds.

The fundamental difference between these techniques is that vibrations that are IR active cause a change in the dipole moment of the molecule, whereas Raman active vibrations change the molecular polarisability [45].

Interestingly, the particular vibrational values (measured in wavenumbers) of both IR and Raman spectra are dependent on both the masses of the atoms (whereby heavier atoms vibrate at lower frequencies than lighter ones) and the relative strength of the bonds. A further influential factor is the environment of the molecule, i.e. the molecular substituents and molecular geometry which affect the vibrational force constant and in turn affect the vibrational energy (band position) [46].

The study of the Raman and IR activities of the fundamental vibrations of these compounds can be summarised by the Rule of Mutual Exclusion. This states that if a molecule has a centre of symmetry, then Raman active vibrations are IR inactive, and vice versa. If there is no centre of symmetry, then some (but not necessarily all) vibrations may be both Raman and IR active. However, one must be cautious in comparing the presence and absence of bands in these two spectroscopic techniques as a vibration may be Raman or IR active but either too weak to be observed [47] or involved in band overlapping.

Unfortunately, not all the compounds in this study gave good Raman spectra. The problem was that of fluorescence and this can be correlated to the electronic nature of the samples. Fluorescence occurs when an electronically excited molecule decays back to the ground state spontaneously, emitting radiation at a frequency characteristic of the transition between the excited and ground states. As a result such radiation engulfs the weak Raman signal [47].

No such problems were encountered in the IR spectra of the compounds. Although it is discussed in detail in Chapter 2, special mention must be made here of the favourable characteristics of pyridine–IR, stemming from their simplicity, as this played a large role in the decision to incorporate pyridine ligands into all the complexes in this study.

1.7.3.3 NMR Spectroscopy

Unfortunately, the identification and characterisation of these types of species by NMR spectroscopy is complicated by the paramagnetic nature of the chromium in solution, with the problem stemming from the presence of unpaired electrons. This causes the relaxation times

of the nuclei to shorten and gives rise to severe line broadening, which makes interpretation of the spectra rather difficult [48].

However, paramagnetic effects are not always undesirable as in certain instances they are required or are advantageous in helping to shorten interpulse times or increase pulse angles. This is achieved via the addition of trace amounts of compounds such as $Cr(acac)_3$. $Cr(acac)_3$ is a preferred choice as it is coordinatively saturated and kinetically inert, yet no more than 0.03 M conc. can be added as any more results in unwanted line broadening [48]. Paramagnetic substances can also cause the shifting of signals that can aid in spectral analysis. This has, however, proved to be a successful technique only with the lanthanides as most other ions suffer from severe line broadening which outweighs the benefits of the shift effects [49]. Paramagnetic usefulness also stems to ^{13}C NMR spectroscopy as interactions with paramagnetic chelate complexes sometimes serves a useful purpose by suppressing the NOE [50].

This particular study incorporated a novel approach with respect to paramagnetic species of this type and NMR spectroscopy, whereby insights into ligand coordination and reaction progress were identified. What is indicated by the findings is that upon coordination to the Cr(III) metal centre, the free ligand resonances disappear as a direct result of their proximity to the paramagnetic centre. This phenomenon is observed only where the donor atoms themselves are either conjugated or aromatic as ligands such as thf and dppe are all visible in their respective spectra.

For the aromatic ligands, the appearance of new ligand signals was expected upon coordination but in the range δ = -4 to 16 ppm, no such resonances were identified. It follows that the signals are NMR silent in this range due to paramagnetic effects. The range was broadened from -30 to 30 ppm, but still no new resonances were observed.

These intriguing observations led to the development of a series of novel ^1H NMR experiments, whereby the substitution of thf in $[CrCl_3(thf)_3]$ with the respective nitrogen and phosphorus donor ligands was followed by proton NMR spectroscopy. This took place via the slow addition of stoichiometric amounts of the ligands in acetone-d_6 to $[CrCl_3(thf)_3]$ in an NMR tube. By obtaining a series of spectra in rapid succession (approximately every four minutes), the substitution reactions that took place could be closely followed and, in addition,

the time required for reaction completion was indicated by the complete disappearance of the ligand resonances.

Where applicable, ^{13}C NMR and ^{31}P NMR were also utilised in this study and the resulting spectra were largely unaffected by paramagnetic effects.

It must be noted that no kinetic studies were undertaken from the resulting spectra. This was due largely to the problems with integration described above, as well as to the fact that the ratio of signals (integrals) does not depend on the concentration of the sample alone. For instance, the dilution of an NMR sample by 50% would give the same ratio of signals (integrals) irrespective of the initial concentration and in order to study kinetics, exact concentrations are important.

1.7.3.4 Computational Studies

In today's scientific era computational chemistry continues to gain momentum as an important source of information. At the forefront of quantum mechanical methodology is the now well–established DFT; this prominence is understandable considering its accuracy and computational speed [51]. One of the many capabilities involves the calculating of vibrational frequencies which can then be compared with those obtained experimentally and thus assist in molecular identification. With regard to the compounds in this study, in which IR and Raman spectroscopy were utilised extensively, such a comparative study is of benefit. One must, however, note that the calculated vibrational frequencies usually overestimate the experimental fundamentals for a variety of reasons. These include neglect of anharmonicity and the inaccurate description of the electron–electron interaction. The need for a scaling factor that will correct the calculated values to match the experimental observables is thus evident. This factor was computed by dividing the experimental values by those that were calculated.

DFT was also used to generate the frontier orbitals of a number of the complexes as such investigations reveal information pertaining to reaction behaviour. These HOMO and LUMO shed light on the regions of the complexes that are susceptible to electrophilic and nucleophilic attack respectively.

1.7.3.5 Mass Spectrometry

The need to confirm that any single crystal determinations did indeed reflect the composition of the bulk precipitated samples is of importance for this study. Precipitates were studied by physical (microscope, etc.) and spectroscopic methods (IR and Raman). In addition, the use of FAB-MS allowed for such information to be attained and provided additional structural information through the identification of fragmentation patterns which could not be gained by techniques such as elemental analysis. The presence of chlorine atoms in all the compounds was also a factor in the decision to use mass spectrometry. The isotopic distribution patterns could be studied and compared to theoretically generated patterns via the use of an isotopic distribution calculator. All FAB-MS spectral data are included in the supportive material section.

1.8 EXPERIMENTAL

1.8.1 SAFETY REMARKS

As in any scientific study involving the use of chemicals, awareness of the safety precautions that must be taken is of paramount importance. All the chemicals used in synthesising the compounds carried safety symbols indicating their harmful and toxic nature.

To eliminate or at least minimise the risks involved in handling these chemicals, a number of standard safety precautions must be adhered to. These include the wearing of safety glasses, lab coats and latex gloves, as well as carrying out all operations within a functional fume cupboard.

As well as the chemical precautions, there are also the apparatus–based precautions which include the proper management of the distillations used to dry the solvents. Both the daily running and the disposal of the solvent distillations need careful attention. In terms of daily running, the stills must be carefully monitored. Equally important is the disposal of the still residues. As all solvents differ in terms of the appropriate method of disposal, it is important to adhere to the respective solvent's method.

All solvents in this study were dried via the addition of metal sodium, with benzophenone utilised as an indicator. The disposal of such a still involved the removal of remnant thf,

followed by the slow addition of isopropanol over a period of three days as a means of ensuring that all sodium was inactive and thus safe.

1.8.2 GENERAL REMARKS

All reactions and manipulations were performed under an inert atmosphere using standard Schlenk tube techniques. Ligands were purchased from Sigma Aldrich and used without further purification.

The synthetic pathway for these reactions was modelled on the similar tridentate ligand substitution reactions, whereby the thf molecules of $[CrCl_3(thf)_3]$ were displaced by the respective ligands [32, 34]. The ease with which the thf molecules are substituted allows for mild reaction conditions.

Arriving at these conditions was achieved via a process of essentially trial and error, whereby various solvents, temperatures and time scales were tested. In the end the solvents of choice were thf (reaction medium) and diethyl ether (work–up). As a direct consequence of the high solubility of the chromium precursor and ligands in thf, elevated temperatures were unnecessary and thus most reactions were carried out at room temperature. Although some of the reactions appeared to be immediate due to colour changes and in some cases the formation of precipitates, others, such as the bipyridine experiments, took substantially longer. Furthermore, the addition of the secondary ligands did not always yield an obvious recognisable change. As a result all reactions were allowed to stir overnight to ensure completion.

A positive attribute of the majority of the formed precipitates was their stability in air, heat and light. These characteristics are certainly attractive to a practising catalytic chemist as any further manipulations are straightforward.

1.8.3 STANDARD COLOUR CHANGES

The addition of the pure amine ligands resulted in dark green solutions with precipitates of a slightly lighter green. In contrast, the phosphorus ligand, dppe, yielded a dark and light blue solution and precipitate respectively. It was therefore not unexpected to find that the addition of the ‘green’ pyridine ligands to the ‘blue’ dppe compound resulted in blue/green solutions and precipitates. The same was true for the mixed P–N ligands.

Although the colour changes that were indicative of ligand substitution were immediate in most cases, the slower coordination speed of the bipyridine ligand was of benefit as it allowed the observation of an intermediate light blue colour which is, according to our interpretation, associated with dimer formation.

1.8.4 SYNTHESIS OF THE STARTING MATERIAL [$CrCl_3(thf)_3$]

According to literature, there are various ways of preparing [$CrCl_3(thf)_3$]. For comparison, two of these methods were carried out [77, 78]. The resulting products of both methods were identical in colour and gave identical IR spectra with the characteristic thf bands present. However, while some initial test reactions were being carried out, the addition of bipyridine yielded the crystal structure [$CrCl_3(bipy)(H_2O)$]. This result cast a certain amount of doubt on the purity of the synthesised [$CrCl_3(thf)_3$] as it was plausible that unreacted water from the chromium hexahydrate starting material was still present. Therefore, to alleviate all doubts concerning purity, all reactions were carried out using the [$CrCl_3(thf)_3$] that was purchased from Sigma Aldrich.

1.8.5 GENERAL PROCEDURE AND INSTRUMENT DATA: INFRARED AND RAMAN SPECTROSCOPY

The instrumentation used to collect the required MIR vibrational data was a Perkin Elmer Spectrum RX-1, FT–IR System. The analysis of all the compounds was carried out in the solid state. A quantity of 2 mg of each complex and ~100 mg of KBr powder were ground together using a pestle and mortar until a fine homogeneous powder remained. The KBr is used as a diluting agent as it does not absorb above 250 cm^{-1} [52], which means that all bands seen in the spectra relate to the complexes. The fine powder was then pressed using a hydraulic press until a clear pellet was produced for analysis. In each interferogram 32 scans were signal averaged, with a spectral resolution of 2 cm^{-1}.

As some of the ligands were in the liquid state, sample preparation was not as straightforward as with the standard KBr pellets used in the solid state MIR. A number of sample preparation methods were tried in order to obtain spectra of a high quality.

The first method was the dissolution of the ligands in thf. Unfortunately, the spectra obtained were of poor quality because concentration problems led to background subtraction

abnormalities, which in turn did not allow clear band resolution as was seen from solvent–sample superposition. As thf by its very nature has many vibrations, it was thought that this superposition could be minimised by using a vibrationally simpler solvent such as CCl_4. This attempt was, however, unsuccessful as both ligands were found to be insoluble in CCl_4.

The expense of these ligands, coupled within the small amounts available, did not allow further solubility tests and so another method was tried. This proved to be very successful indeed as it avoided the use of solvents and required minimal amounts of the ligands. A drop of ligand was placed between two KBr pellets. The resulting spectrum was well defined with no background interference.

The FIR data was collected using a Bruker IFS113V spectrometer. The sample preparation was slightly different from that above as polyethylene was used in place of KBr. A quantity of 2 mg of sample was shaken vigorously in ~200 mg of polyethylene. The resulting mixture was pressed into a clear pellet for analysis using a hydraulic press. In each interferogram 32 scans were signal–averaged, with a spectral resolution of 2 cm^{-1}.

In order to reduce the extreme fluorescence experienced with the initially tested 514.5 nm laser excitation, an FT–Raman Spectrometer was used which contained an Nd:YAG laser to excite the Raman effect. The Nd:YAG laser has a wavelength of 1 064 nm and at this wavelength there are fewer electronic transitions, which in many instances are responsible for a high fluorescence background. The laser power was 250 mW and 256 scans were accumulated with a resolution of 4 cm^{-1}. As with the majority of the IR experiments, the analysis was carried out in the solid state but, unlike the IR studies, very little sample preparation was required. A small amount of each complex was placed in an aluminium holder and loaded into the sample compartment. The only necessary and important factor to be considered is that the sample must be in the foci of the laser beam and collection lens [53].

1.8.6 GENERAL PROCEDURE AND INSTRUMENT DATA: X-RAY CRYSTALLOGRAPHY

All data sets were collected at 20 ºC on a Siemens P4 diffractometer fitted with a Bruker 1K CCD detector and SMART control software [54] using graphite–monochromated, Mo Ka radiation by means of a combination of phi and omega scans. Data reduction was performed using SAINT+ [54] and the intensities were corrected for absorption using SADABS [54].

The structures were solved by direct methods using SHELXTS [54] and refined by full–matrix least squares using SHELXTL [54] and SHELXL–97 [55]. Drawings of the structure were produced using Ortep–3 for Windows [56], Mercury [57] and POV–Ray for Windows [58].

1.8.7 GENERAL PROCEDURE AND INSTRUMENT DATA: ^{1}H NMR SCALE EXPERIMENTS

A dry degassed NMR tube was charged with small amounts of $[CrCl_3(thf)_3]$ (*ca* 4 mg) and placed under vacuum on the Schlenk line, after which it was purged with argon by three purge cycles. Stoichiometric amounts of the respective ligands were weighed out into sample vials. Acetone-d_6 was added to the ligands and injected into the NMR tube via a rubber septum (after ensuring complete dissolution). The tube was immediately placed in the NMR spectrometer, where a lock signal had already been obtained using an acetone-d_6 reference standard. A ^{1}H spectrum was obtained every few minutes to track the progress of the reaction.

Acetone-d_6 was the solvent of choice where the readily soluble ligands were added together, while for spectra of the insoluble final products, DMSO-d_6 was used. Comparisons between the different solvent spectra revealed that the chemical shifts were identical and not affected by the change in solvent. This was advantageous as the spectra were therefore comparable. The instrument was a Bruker Avance 500 with the spectra measured at 500.13 MHz.

1.8.8 GENERAL PROCEDURE AND INSTRUMENT DATA: COMPUTATIONAL STUDIES

A *quantum-chemical ab-initio calculation* of the total molecular energy *E* at the ground state of the potential-minimum configuration of a molecule, called the "fully optimised geometrical structure", yields the sum total of the two effects: those caused by *short-range forces* and *long-range forces*. These are calculated for the isolated molecules in the gas phase, and exclude specific intermolecular interactions such as packing forces The molecular structure of each molecule was optimised using the molecular symmetry point group C_1, and no further enforcement of higher symmetry was attempted due to the lack of any obvious additional point group symmetry operators in the molecules for which solid–state structures were available.

Ab-initio quantum-chemical computations were carried out on an IBM–cluster with a pre–compiled set of Gaussian-03 molecular orbital programs [59] configured for parallel computing under LINUX [60]. Default computational settings for Gaussian-03 *ab-initio* DFT/B3LYP calculations were implemented, while a 6-311G (p, d) basis set was used as described in the Gaussian manual [61]. This basis set was chosen instead of the more elaborate 6-311++G(3df,3pd) basis set to represent a balance between computational level and computational economy. More details about the background of the computational methodology can be found in the books by Hirst [62], Kohanoff [63], and Foresman and Frisch [64], as well as in the original references cited in the Gaussian Manual [59].

In order to determine whether the optimised geometry, where the slope approaches ($\partial E/\partial X$) $\rightarrow 0$, where X is the structural parameter being subjected to refinement, occurs at a potential minimum and not at a saddle point, the harmonic molecular vibrational modes and their associated frequencies were calculated at the optimised geometric configuration [65]. It was established that all the optimised geometries of the molecules studied yielded only positive vibrational frequencies, i.e. all the optimised geometries were thus determined at *potential energy minimum positions*. The energies and other computed physical properties may, therefore, be compared and contrasted with confidence. Due to the nature of the calculations, the absolute energy values are not of significance and thus are not reported.

All calculations were carried out using the spin quartet ground state. In addition to previous Cr(III) computational literature [66, 67, 68], this selection was confirmed by the excellent agreement between the calculated and experimental vibrational spectra of this study.

1.8.9 GENERAL PROCEDURE AND INSTRUMENT DATA: MASS SPECTROMETRY

Mass spectroscopy data was collected by means of Fast Atom Bombardment using a VG70SE with xenon atom gun. This was operated at 8Kv using a 3-nba matrix.

Chapter 2

Chromium(III) Monodentate Nitrogen Ligand Chemistry

2.1 INTRODUCTION

The classes of compounds synthesised in this study belong predominantly to the chemistry of bidentate metal coordinated ligands which serve as a variation on the known successful catalytically active tridentate systems [32].

However, common to these classes of compounds is the addition of monodentate pyridine and derivatives thereof; these are expected to occupy the one remaining thf site around the metal centre of which the precursor molecule is $[CrCl_3(thf)_3]$.

Since its discovery in 1846 by Anderson [69], pyridine chemistry has played an important role in a wide array of chemical disciplines. This heterocyclic planar hexagonal framework is widely recognised for its stability and coordination capabilities. The former is a result of the delocalised π–electron cloud formed via sp^2 hybridisation, while the latter stems from the lone pair of electrons on the endocyclic nitrogen atom which aligns perpendicular to the ring system and is available for bonding to transition metals [70]. These factors, coupled with the ability to alter both the steric and electronic properties of the system via the addition of various substituents at the 2, 3 and 4 ring positions, were important in the selection of pyridine for this particular study. The recent work by McGuinness [42] on Cr(III) pyridyl–carbene complexes only served to confirm this selection as it illustrates that chromium(III)–pyridine chemistry is still very relevant.

It was therefore decided that it would be of benefit first to study the coordination of these monodentate ligands to the chromium metal centre. This resulted in novel crystallographic,

spectroscopic and computational insights which provided the perfect backdrop to the analysis of the bidentate systems that follow.

Although $[CrCl_3(py)_3]$ **(3)** and $[CrCl_3(pyphenyl)_3]$ **(8)** had been synthesised previously [71, 72], their synthetic routes differed and the studies lacked the additional characterisation and analytical insights provided by this study.

It is worth mentioning that pyridine chemistry and IR spectroscopy in particular are well suited since assignments are both straightforward and uncomplicated for a number of reasons. Firstly, the assignments of the vibrational modes of the free pyridine ligand have long since been known and so comparisons with complexes can be made in terms of the shifting of bands. This leads to a second simplifying feature. Only a small number of the internal vibrations of pyridine shift upon coordination to a metal centre, while the majority recur virtually band for band, with a few minor exceptions [73]. The bands that are affected shift by varying degrees relative to a number of factors, which include ligand substituents, type of metal, geometrical arrangements, etc. [74, 75].

Thirdly, the assignment of many metal–ligand vibrations in the IR region is complicated by the presence of ligand modes. This, however, is not the case in pyridine complexes as below 400 cm^{-1} no pyridine bands are visible, thus aiding M–L assignments [73].

Within this study there are three distinct categories. The first focused on the ability to control the sequential addition of the pyridine ligand to the precursor. The second involved an investigation based on steric hindrance and whether substituents at the ortho position of the pyridine would allow coordination via the endocyclic nitrogen to take place. The third category was the addition of three molar equivalents of the respective substituted pyridine ligands to the metal centre.

2.2 CATEGORY ONE: SEQUENTIAL ADDITION OF PYRIDINE

The ability to coordinate different monodentate ligands selectively and sequentially to the same $[CrCl_3(thf)_3]$ precursor would provide a wide array of monomeric compounds with different steric and electronic properties. This was investigated through the addition of pyridine to

$[CrCl_3(thf)_3]$ in thf in 1, 2 and 3 molar equivalents (see Figure 2.1) with the hope of extending the study to incorporate various substituted pyridines. A further reaction was carried out whereby pyridine was added to the chromium precursor in a large excess and, in fact, the pyridine acted as both ligand and solvent. Upon immediate addition of the ligands (regardless of the molar quantity), a dark green solution accompanied by an olive green precipitate was observed. The reactions were stirred overnight at room temperature to ensure completion.

On addition of the varying amounts of ligand, all four reactions turned green via a grey/blue intermediatory colour which was visible only for a matter of seconds and therefore was unable to be isolated. This is of importance as Elowe [38] discussed the relationship between dimers and such colours. In fact, the dimeric existence was indirectly proved for this category by one of the crystal structures that was determined during this investigation.

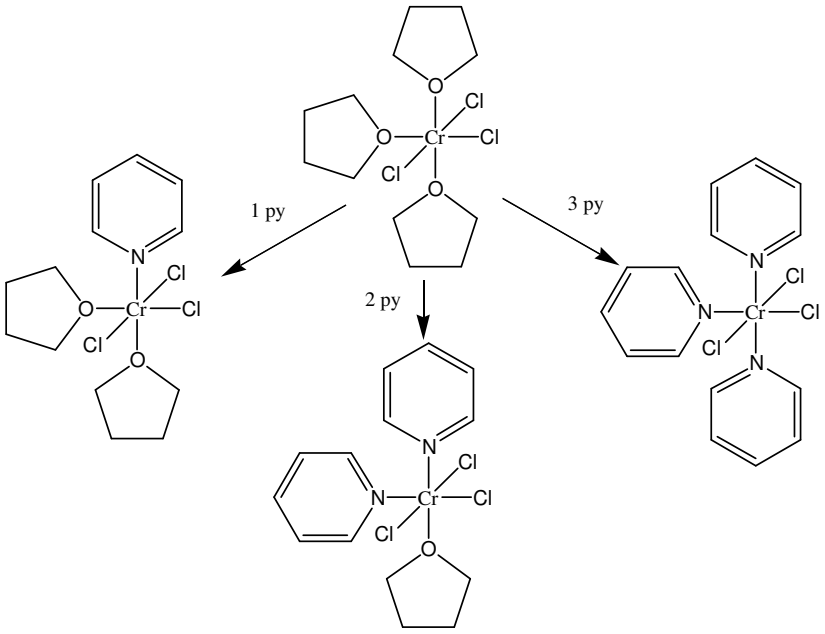

Figure 2.1 **Sequential addition of pyridine to the chromium precursor**

2.2.1 VISUAL ANALYSIS

This was the first technique to suggest similarities in the four complexes as all precipitates had the same olive green colour (Figure 2.2).

Figure 2.2 Olive green precipitate

2.2.2 INFRARED AND RAMAN SPECTROSCOPY

The results added further weight to the initial visual analysis and correlated well with the crystallographic structures of $[CrCl_3(py)_2(thf)]$ **(2)** and $[CrCl_3(py)_3]$ that follow, as the spectra of the different molar equivalents were virtually identical. In these spectral comparisons it is worth highlighting that the IR spectrum of the single crystal material was identical to the precipitate spectra. This indicates that the determined structure is representative of the bulk material.

They all possess the expected vibrations associated with a pyridine ligand with respect to C–H and ring vibrations [73, 74]. A number of characteristic shifts relative to the free pyridine were also observed, which are recognised as being indicative of coordination to a metal centre [73, 74]. These are documented in Table 2.1 with the spectra of free pyridine and $[CrCl_3(py)_3]$ shown in Figure 2.3.

Table 2.1 Characteristic pyridine shifts in the IR spectrum

Free pyridine IR / cm^{-1}	$[CrCl_3(py)_3]$ IR / cm^{-1}	Shift / cm^{-1}
1582	1609	27
1438	1447	9
1029	1046	17
992	1014	22
746	763/754	17/8
604	640	36
404	445	41

Note that the values in the table are taken from the spectrum of $[CrCl_3(py)_3]$.

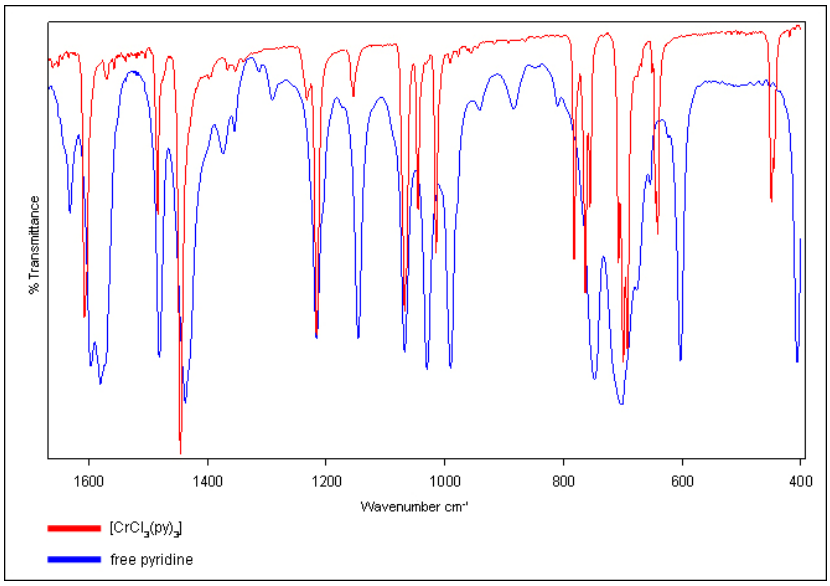

Figure 2.3 **Comparisons of the IR spectra of free pyridine (blue) and $[CrCl_3(py)_3]$ (red)**

Although the Raman spectrum of $[CrCl_3(py)_3]$ was virtually identical to the IR spectrum, as illustrated in Figure 2.4 the intensities of the vibrations were noticeably different. One should be aware that although this is not entirely clear from the figure presented, there are in fact very weak vibrations at 783, 768 and 704 cm^{-1} which correspond to those exhibited in the IR spectrum.

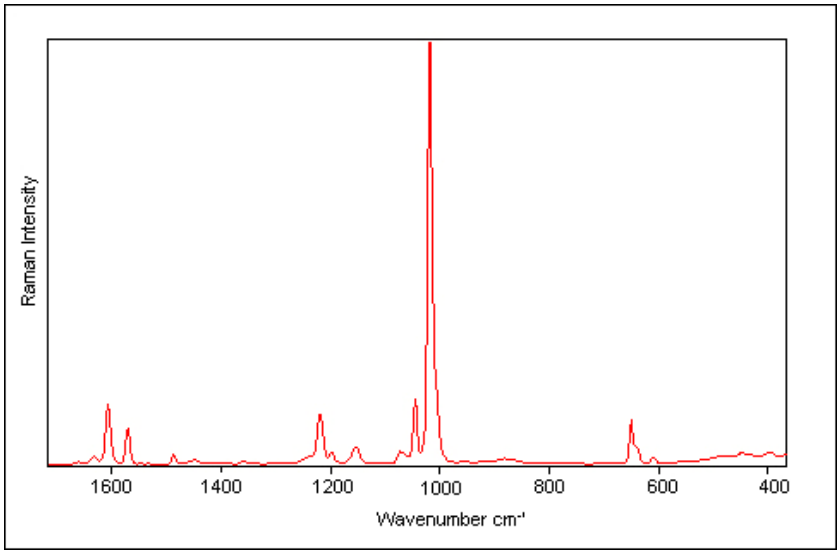

Figure 2.4 **Raman spectrum of $[CrCl_3(py)_3]$**

Worthy of particular mention is the shifting of the band at 992 cm^{-1} in free pyridine to 1014 cm^{-1} in the complex, as has been specifically highlighted in Figure 2.5. This is widely recognised as an indication of both bond strength and coordination, and is of particular interest in the study of the substituted pyridines as the degree of shifting is substituent dependent [75].

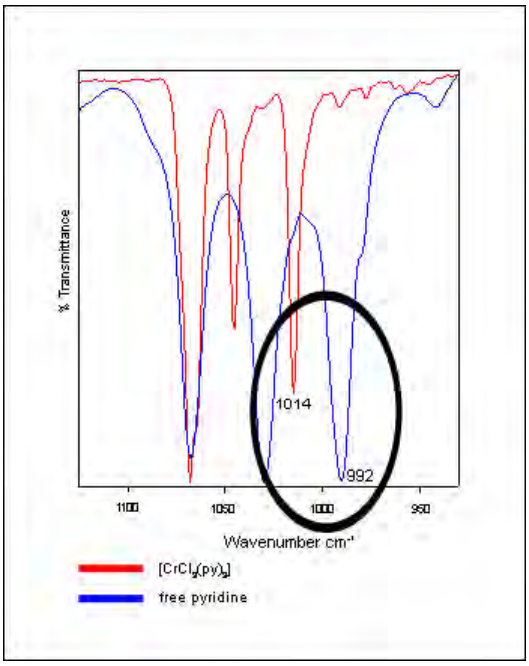

Figure 2.5 **Shifting of the free pyridine band (blue) in the IR spectrum at 992 cm^{-1} upon coordination (red)**

Relevant to this investigation is the absence of thf vibrations as it will aid the verification of tri-pyridine coordination. C–H vibrations of thf would have been expected around 2962-2925 cm^{-1} (lower than pyridine C–Hs [76]), while one of the most characteristic vibrations associated with coordinated thf (C–O–C) should have been observed as a strong IR vibration at ~856 cm^{-1} [77, 78]**.**

The fact that none of these vibrations were observed in any of the compounds further confirmed the tri–pyridine coordination and thus the inability to control pyridine addition under these conditions.

Figure 2.6 highlights the presence of the characteristic thf–related vibrations in the $[CrCl_3(thf)_3]$ precursor and their absence in $[CrCl_3(py)_3]$.

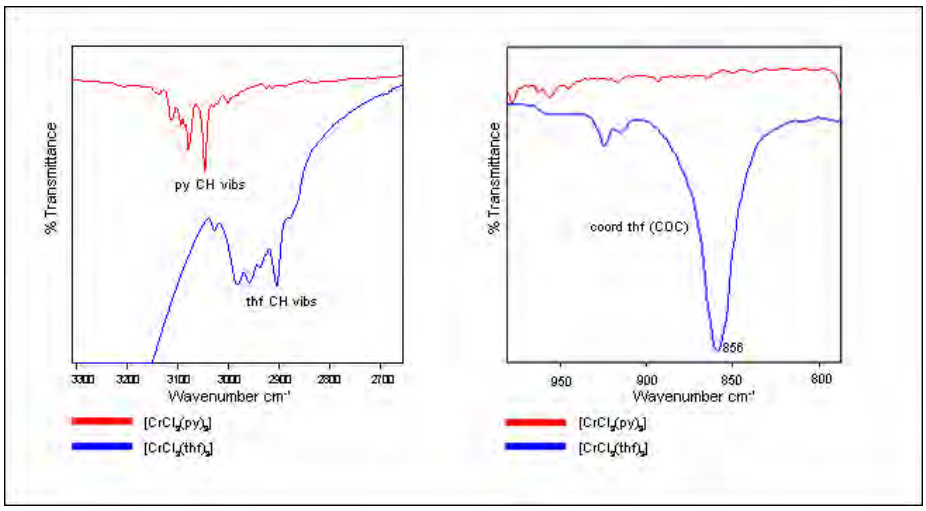

Figure 2.6 Comparison between $[CrCl_3(thf)_3]$ (blue) and $[CrCl_3(py)_3]$ (red) IR spectra

Furthermore, the molecular geometry observed in the crystallographic results was supported by the presence of three Cr–Cl vibrations which are indicative of the *mer* orientation [79]. They are visible between 390 and 310 cm^{-1} in all four compounds.

Perhaps most important is the assignment of the metal–ligand vibrations (Table 2.2). Clearly visible in $[CrCl_3(py)_3]$ is the band at 221 cm^{-1} which corresponds to Cr–N of pyridine [41, 80, 81]. Unfortunately, the Cr–O of thf vibration is not as easy to assign but according to Fowles it may be the band observed at 284 cm^{-1} [82] and, as seen in Figure 2.7, this is absent in the spectrum of $[CrCl_3(py)_3]$.

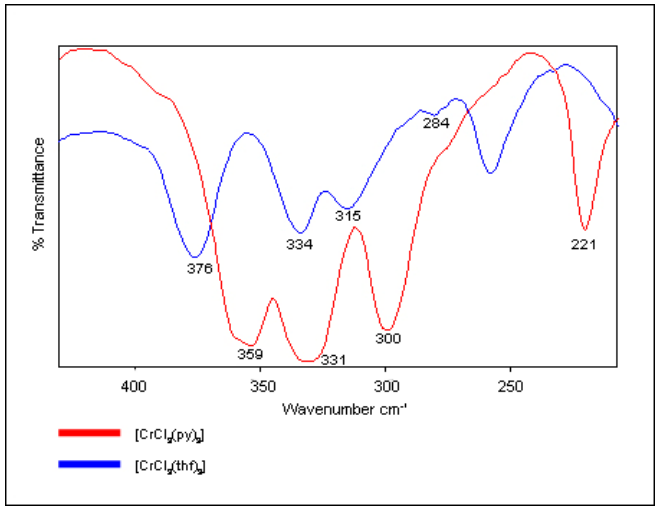

Figure 2.7 **FIR comparison between $[CrCl_3(thf)_3]$ (blue) and $[CrCl_3(py)_3]$ (red) spectra**

Table 2.2 Vibrational assignments of $[CrCl_3(py)(thf)_2]$ (1), $[CrCl_3(py)_2(thf)]$ (2), $[CrCl_3(py)_3]$ (3)

1 IR / cm^{-1}	2 IR / cm^{-1}	3 IR / cm^{-1}	3 RAMAN / cm^{-1}	Assignment
3130m	3112m	3111w	3142w	ν (CH)
-	3078m	3079m	3079s	ν (CH)
3059m	3049m	3046m	3049m	ν (CH)
3030m	3028m	3030w	3030w	ν (CH)
1631m	-	-	1631w	ν_{ring}
1607s	1605s	1609s	1607m	ν_{ring}
1568m	1568w	1573w	1571m	ν_{ring}
1484s	1486m	1483m	1487w	ν_{ring}
1447s	1443s	1447s	1449w	ν_{ring}
1217s	1218s	1217s	1218m	δ (CH)
-	1148m	1153w	1152w	δ (CH)
1072s	1066s	1068s	1072w	δ (CH)
1045s	1045s	1046m	1046m	ν_{ring}
1015s	1014s	1014s	1018vs	Ring breathing (py)
-	-	781s	783vw	unassigned
756s	763s	763s 754m	768vw	γ (CH)
690s	698s	707s 699s 691s	704vw	γ (CH)
643s	642s	640s	650m 641sh	δ_{ring}
447s	449s	445s	448w	γ_{ring}
359s	364s	363s	-	Cr-Cl
331s	342s	339s	340m	Cr-Cl
300s	306s	306s	329m	Cr-Cl
221s	221s	221s	230m 205m	Cr-N(py)

ν = stretching, δ = in plane bending, γ = out of plane bending, vs = very strong, s = strong, m= medium, w = weak, vw = very weak

2.2.3 COMPUTATIONAL STUDY

In order to complement or verify the above vibrational assignments, DFT calculations were carried out on $[CrCl_3(py)_3]$ to allow the generation of the theoretical IR and Raman spectra in the minimised conformation. Comparisons between these and the spectra obtained experimentally showed that the frequencies correlate extremely well. These comparisons are illustrated in Figure 2.8 (MIR) and Figure 2.9 (full Raman). Figure 2.10 highlights the FIR region (but is also the case in the far Raman region) whereby only one Cr–Cl vibration appears to be visible in the calculated spectrum. This is a direct result of the solid state effects which result from the fact that the computed spectrum reflects the vibrations of an isolated gas–phase molecule, thus ignoring any intermediate perturbations. With the aid of computational software, the other Cr–Cl modes were identified.

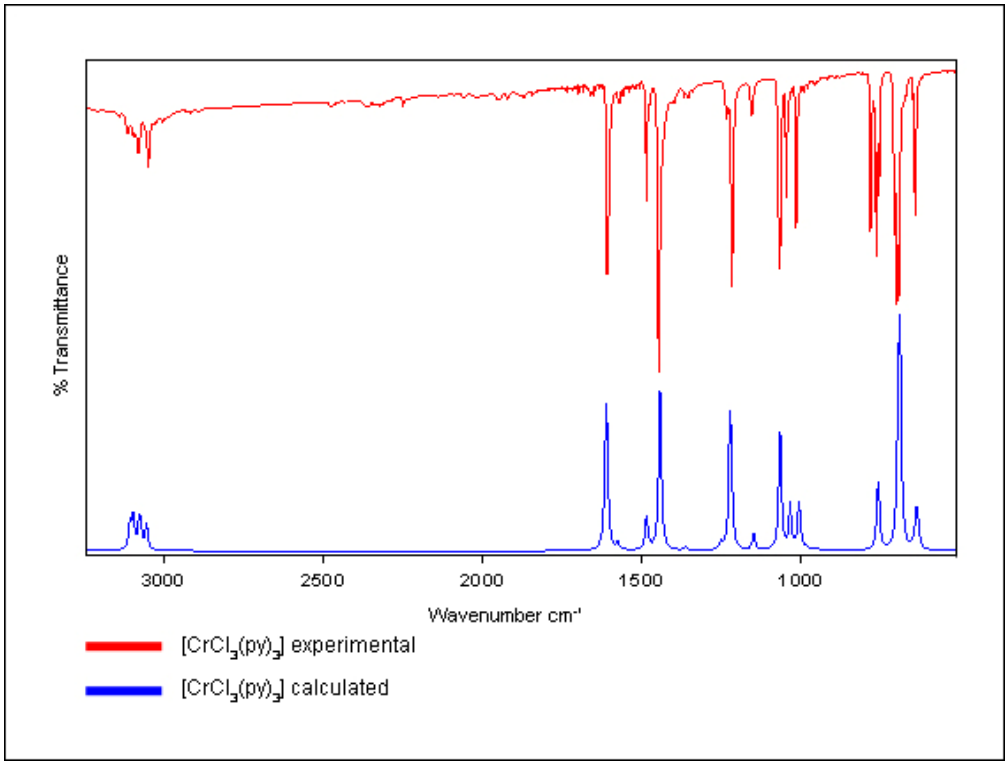

Figure 2.8 Experimental (red) and calculated (blue) MIR spectra of $[CrCl_3(py)_3]$

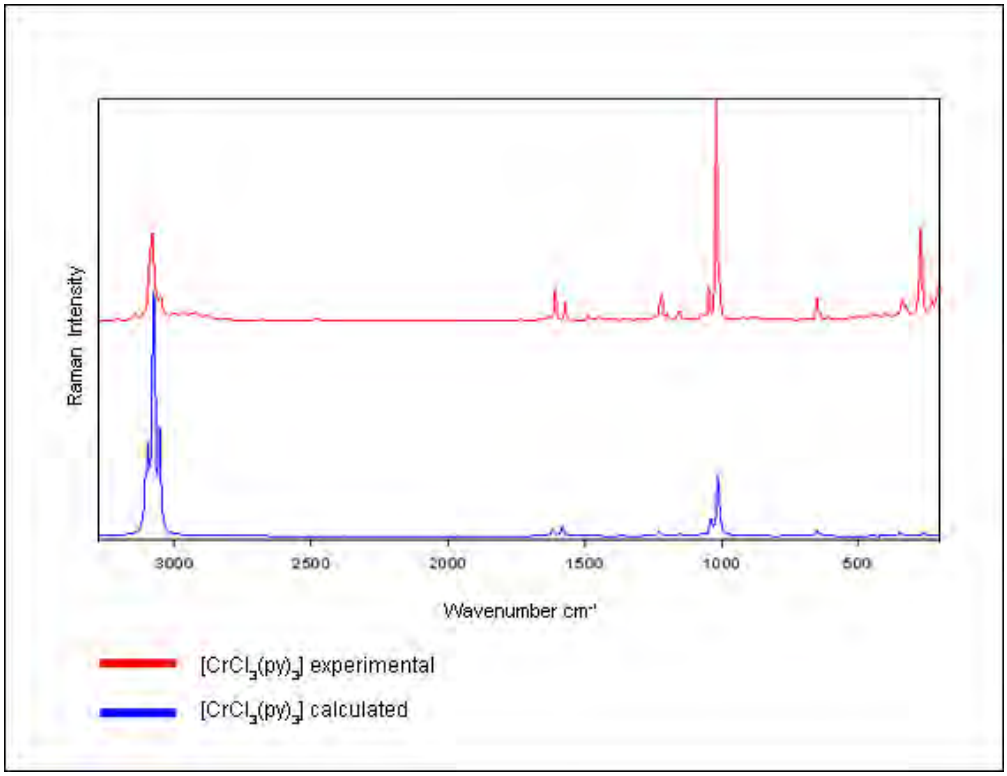

Figure 2.9 **Experimental (red) and calculated (blue) Raman spectra of $[CrCl_3(py)_3]$**

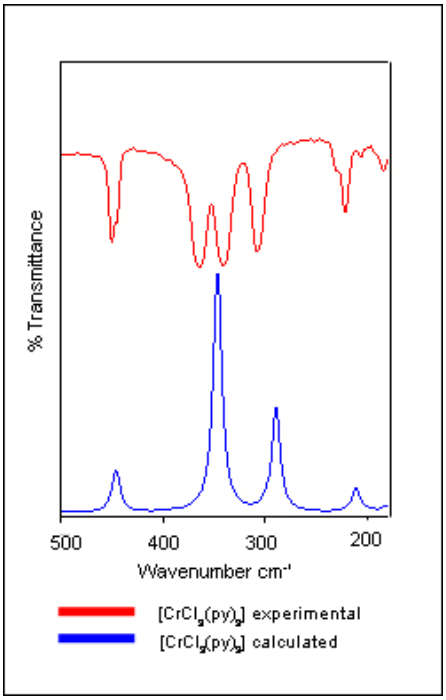

Figure 2.10 **Experimental (red) and calculated (blue) FIR spectra of $[CrCl_3(py)_3]$**

Table 2.3 highlights a number of the important vibrations that are indicative of pyridine coordination, which include ring vibrations and metal–ligand vibrations. With regard to the latter, there are some discrepancies with the lower than expected Cr–Cl vibration at 255 cm^{-1} and the higher than expected Cr–N vibration at 290 cm^{-1}. Another observation that is worthy of mention is the absence of the characteristic C–O–C coordinated thf vibration at ~856 cm^{-1} in the calculated IR spectrum. This is thus an indirect reiteration of its assignment. Table 2.4 presents the scaling factors determined for $[CrCl_3(py)_3]$.

Table 2.3 Selected experimental and calculated IR and Raman band assignments for $[CrCl_3(py)_3]$

$[CrCl_3(py)_3]$ IR / cm^{-1}		$[CrCl_3(py)_3]$ Raman / cm^{-1}		Assignment	
Experimental	**Calculated**	**Experimental**	**Calculated**	**Experimental**	**Calculated**
1609	1611	1607	1617	ν_{ring}	ν_{ring}
1447	1444	1449	-	ν_{ring}	ν_{ring}
1046	1035	1046	1038	ν_{ring}	ν_{ring}
1014	1006	1018	1014	Ring breathing (py)	Ring breathing (py)
763/754	759	768	761	γ (CH)	γ (CH)
640	638	650/641(sh)	650/640 (sh)	δ_{ring}	δ_{ring}
445	446	448	447	γ_{ring}	γ_{ring}
363, 339, 306	346, 344, 255	340, 329	348, 346, 256	Cr-Cl	Cr-Cl
221	290	230	289	Cr-N	Cr-N

ν = stretching, δ = in plane bending, γ = out of plane bending

Table 2.4 Scaling factors determined for $[CrCl_3(py)_3]$

Region / cm^{-1}	IR	Raman
0 – 1854	0.978141	0.974252
2980 – 3434	0.960063	0.960354

In addition to the vibrational data, the HOMO and LUMO orbitals were generated for $[CrCl_3(py)_3]$. From Figure 2.11 it is clear that the chlorine atoms are nucleophilic sites of high electron density which are susceptible to electrophilic attack, while nucleophilic attack will only occur at the pyridine ring system that is *trans* to a chlorine atom. Such electron deficiency is assumed to result from the fact that it is found on a polarisable axis where electrons will be

drawn to the more electronegative chlorine atom. It could also be argued that this high electron density on the chlorine atoms facilitates the formation of bridging chloro ligands for dimeric intermediates.

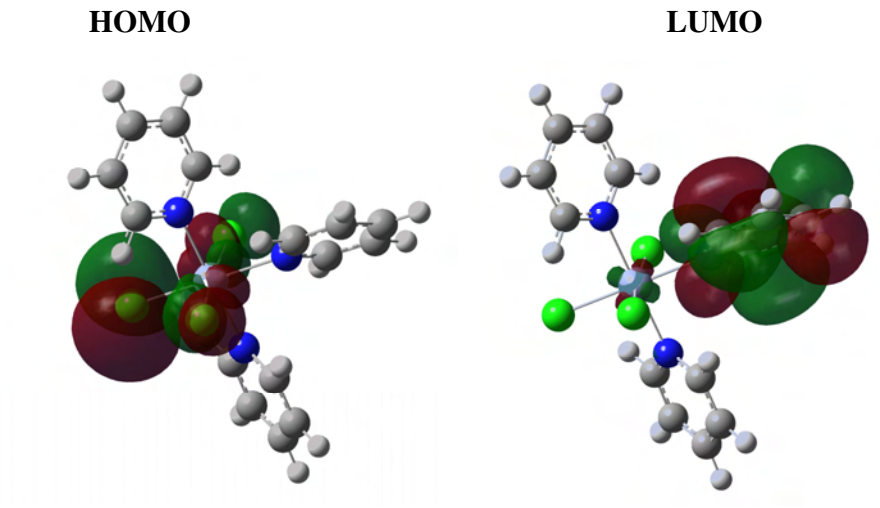

Figure 2.11 HOMO and LUMO orbitals of $[CrCl_3(py)_3]$

2.2.4 NMR SPECTROSCOPY

Although this is normally avoided as a plausible means of analysis when investigating paramagnetic Cr(III) metal compounds, a novel ^1H NMR experiment was devised which used the paramagnetic effects of the compound as a means of gaining information on ligand coordination and reaction time.

The substitution of thf with three equivalents of pyridine in $[CrCl_3(thf)_3]$ was followed by proton NMR spectroscopy through slow addition of stoichiometric amounts of pyridine in acetone–d_6 to $[CrCl_3(thf)_3]$ in an NMR tube. Initial attempts to follow the reaction resulted in excessive line broadening and complete loss of the lock signal after *ca.* 10 minutes of the reaction. This problem was solved by adding minimal quantities of the chromium starting material $[CrCl_3(thf)_3]$, *ca.* 5 mg, and then following the reaction in the spectrometer. Initially at t_0 (the start of the experiment), a mixture of thf starting material ($\delta = 1.79–3.63$ ppm) and free, uncoordinated pyridine ($\delta = 7.30–8.57$ ppm) is observed in the spectrum. It must be noted that due to the poor resolution of the spectra, the chemical shift values given are not completely accurate. The coordinated thf ligands in the starting material have resonances that are similar to

those of free thf, which makes differentiation between free and coordinated thf difficult. Due to the ease of obtaining a lock signal for proton NMR spectroscopy using acetone–d_6, it was possible to obtain spectra in rapid succession (approximately every four minutes). In so doing the course and progress of the reaction were followed. As the pyridine coordinates to the Cr centre, thus displacing the thf ligands, line broadening is observed in the thf resonance region, while the free pyridine resonances disappear as they coordinate to the chromium centre. After *ca*. 180 minutes the reaction is complete as the free pyridine resonances disappear. This is an important observation because to the naked eye the immediate colour change upon the addition of the three pyridine equivalents initially suggested that the reaction completion time was a matter of minutes, whereas in reality it is ~3 hours.

Figures 2.12 and 2.13 illustrate the similarities in the ^{1}H NMR spectra resonances of both free thf and coordinated thf as observed in the spectrum of the precursor [$CrCl_3(thf)_3$].

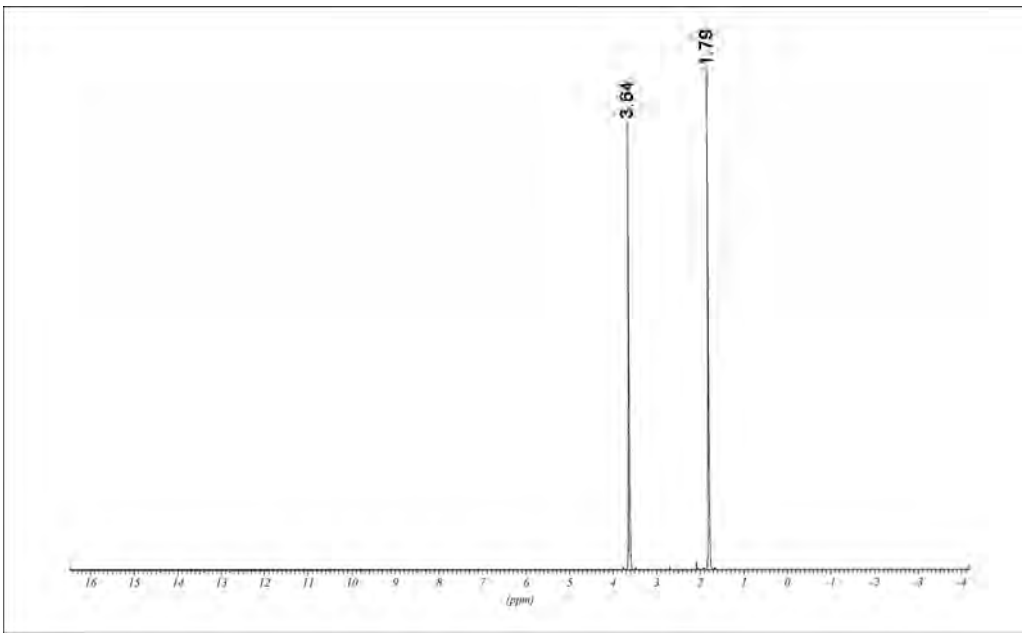

Figure 2.12 **^{1}H NMR spectrum of free thf in acetone-d_6**

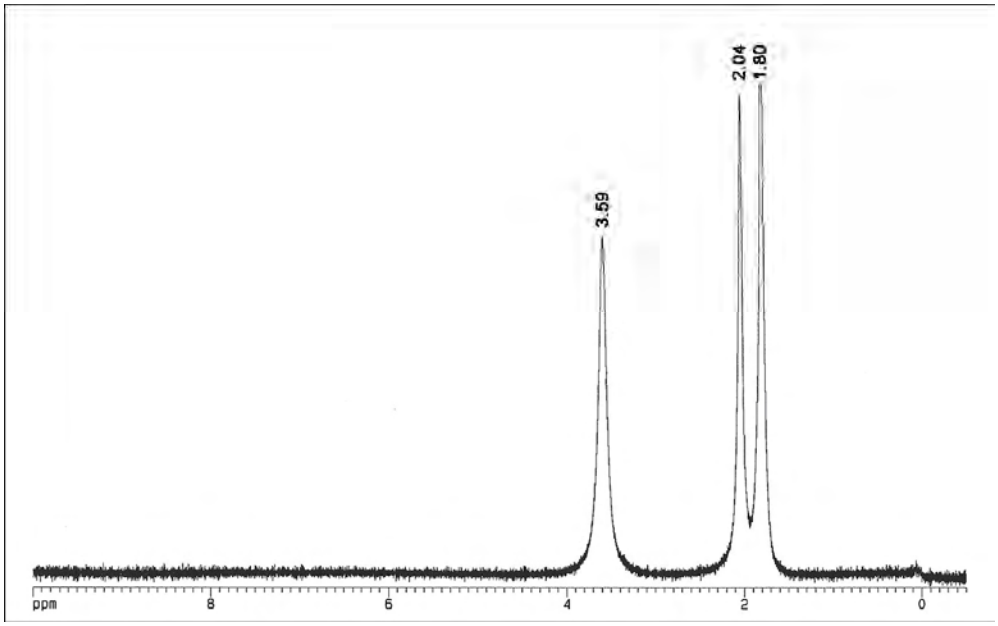

Figure 2.13 **^{1}H NMR spectrum of $[CrCl_3(thf)_3]$ in acetone-d_6**

The stacked spectra in Figure 2.14 clearly show how the free pyridine resonances disappear and broaden over time upon coordination to the Cr(III) centre. As expected, there is also an increased amount of free thf (4) as the substitution reaction proceeds.

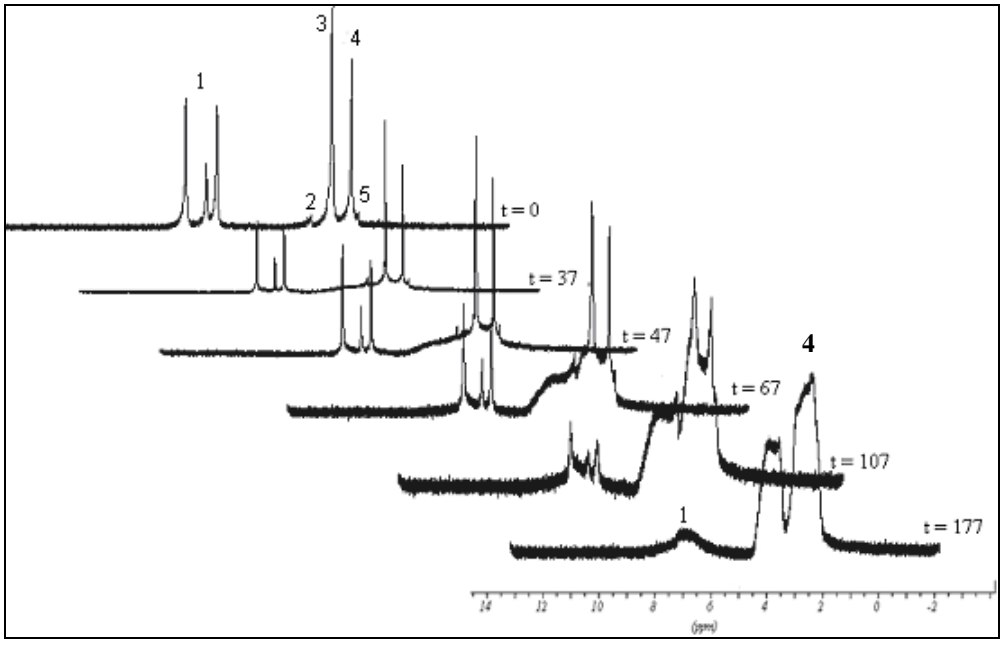

Figure 2.14 **Stacked ^{1}H NMR spectra for the reaction of pyridine with $[CrCl_3(thf)_3]$ over time. 1 = py, 2 = thf, 3 = water peak in acetone, 4 = acetone-d_6, 5 = thf**

Although one cannot use this data for kinetic investigations (rate determination, etc.), as was mentioned in Chapter 1 it does give valuable insights into the reaction profile and progress.

The sample was left in the instrument and after a further hour had elapsed, another spectrum was recorded. Although the result was the same, the resonance quality of the later spectrum was noticeably higher as can be seen in Figure 2.15.

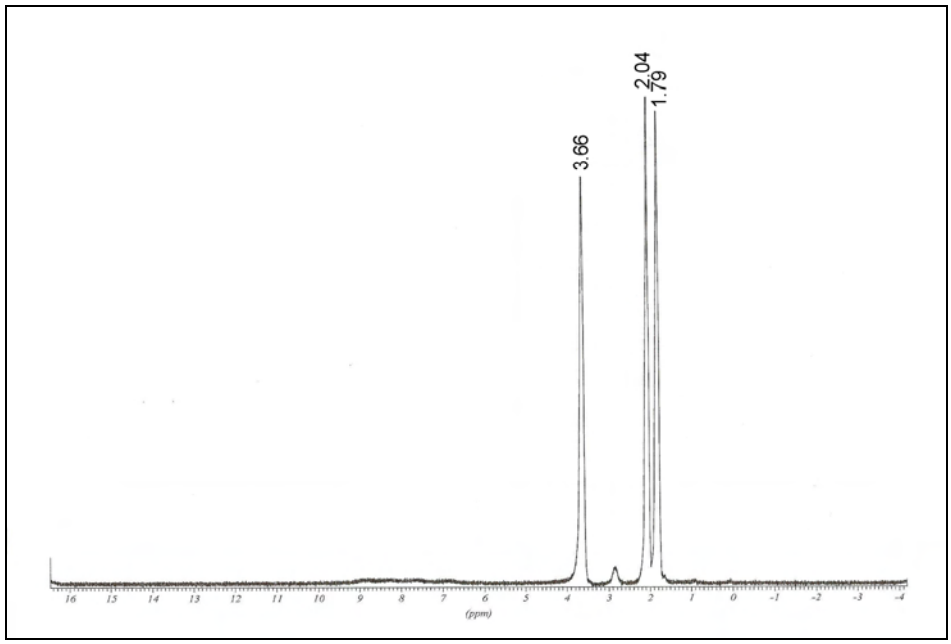

Figure 2.15 **^{1}H NMR spectrum of $[CrCl_3(py)_3]$ in acetone-d_6 after a further hour**

Upon removal of the sample from the instrument, a small amount of the expected olive green precipitate was present. This acetone-insoluble product was dried, then dissolved in DMSO–d_6 and a subsequent ^{13}C NMR spectrum recorded. As mentioned in the experimental section of Chapter 1, the acetone–d_6 and DMSO–d_6 spectra are comparable due to no differing solvent-induced shifts and the resulting ^{13}C NMR spectrum.

The absence of any ligand resonances (pyridine and thf) in the resulting ^{13}C NMR spectrum (Figure 2.16) is a notable result for two reasons. Firstly, it is a strong indication of pyridine coordination and secondly, it suggests that the thf resonances observed in the final ^{1}H NMR reaction spectra above are associated with free thf (Figures 2.14 and 2.15).

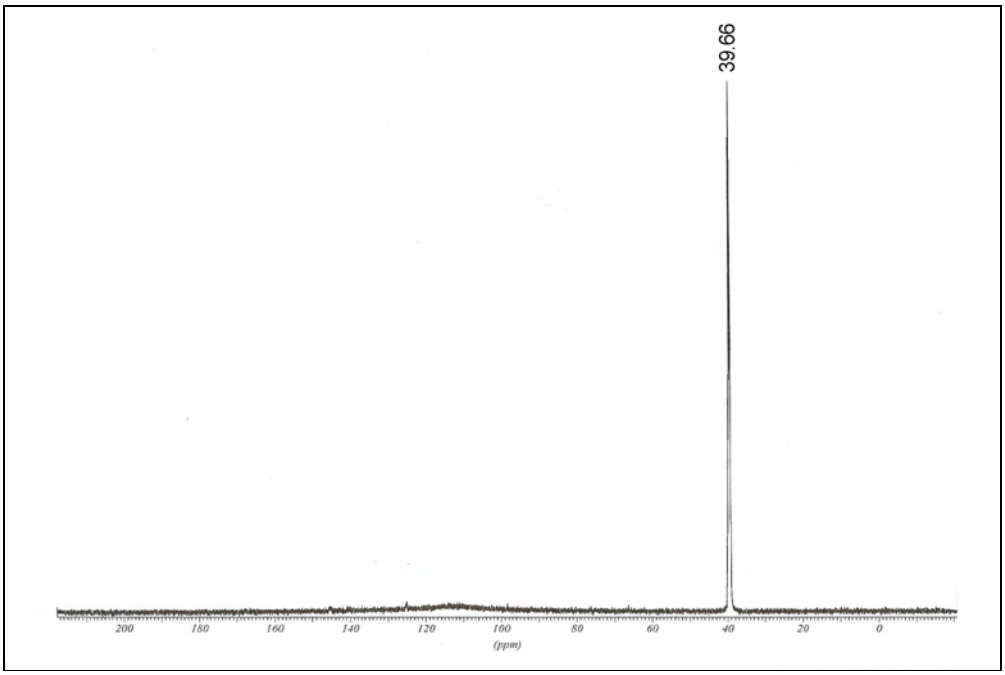

Figure 2.16 **^{13}C NMR spectrum of [$CrCl_3(py)_3$] precipitate formed after removal of above reaction from NMR instrument**

2.2.5 X-RAY CRYSTALLOGRAPHY

2.2.5.1 [$CrCl_3(py)_3$]

A wide range of solvents and crystallisation techniques were utilised in attempts to obtain and isolate single crystals of these compounds that could be analysed on the single crystal diffractometer. Note that a further hint that [$CrCl_3(py)_3$] was formed in all four experiments was given by their similar solubilities. As was stated in Chapter 1, the insoluble nature of these types of compound proved in general to be troublesome.

However, with regard to this category three single crystals of sufficiently good quality were isolated. The first two (crystals of the addition of two and three molar equivalents of pyridine) were grown from CH_3CN and, perhaps unsurprisingly, were identical in structure. Along with the visual and IR analysis, this was a further, and in fact stronger, indication of the inability to control the addition of individual monodentate ligands. What is implied is that the addition of one or two pyridine ligands suffices to activate and increase the lability of the remaining thf

molecules. From a mechanistic point of view this is an important result as it is an indication that compound formation could take place via direct ligand substitution or indeed via symmetrical cleavage of a dimeric species. Although the structure had previously been determined by Howard [83], structural differences were observed as a result of the encaptured CH_3CN solvent molecule found within the unit cell of this study's structure. Figure 2.17 compares perspective drawings of both the structure determined in this study and that of Howard [83].

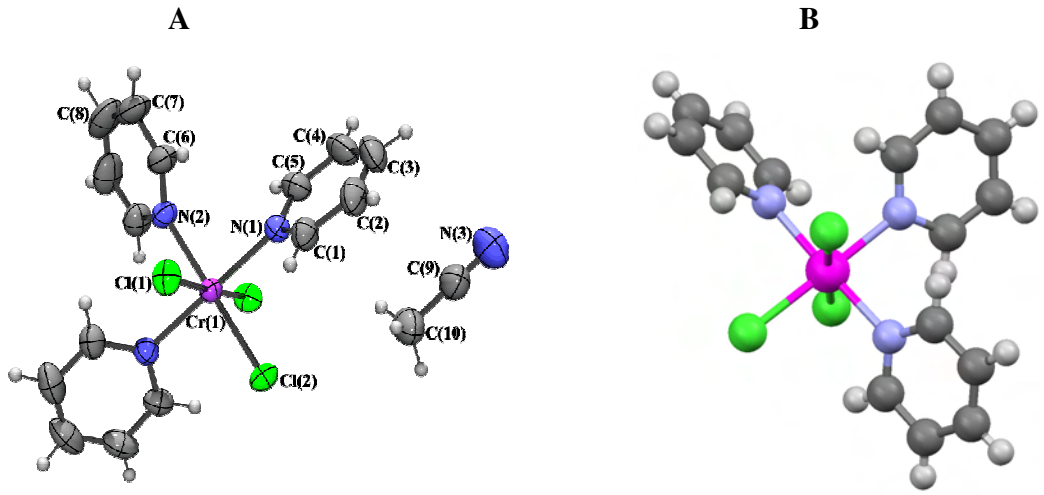

Figure 2.17 **A = Perspective drawing of $[CrCl_3(py)_3]$ structure determined in this study, B = Perspective drawing of $[CrCl_3(py)_3]$ structure determined by Howard [83]**

In both instances, the chromium atom is coordinated to three chlorine atoms and three nitrogen atoms of the individual pyridine molecules in a clear *mer* fashion. The coordination is approximately octahedral, with the Howard structure [83] exhibiting the greatest deviation of 2.14° which relates to the Cl(2)–Cr(1)–Cl(1) angle. The corresponding angle in addition to N(2)–Cr(1)–Cl(1) both exhibit the largest deviation from this study's structure of 1.61°. All the other angles of this structure fall within the range 89.36(4)–90.64(4)°, which is similar to the range of Howard [83] between 88.4(1) and 91.8(1)°.

With regard to bond lengths, the focus has centred on the metal–ligand bonds. As expected, these are virtually identical for both structures as the pyridine ligands are sterically and electronically identical. Table 2.5 highlights these bond lengths and also includes the bond angles that indicate the approximate octahedral geometry.

Table 2.5 **Selected bond lengths [Å] and angles [°] for $[CrCl_3(py)_3]$**

Cr(1)-N(2)	2.1037(17)	Cr(1)-Cl(2)	2.3196(6)
Cr(1)-N(1)#1	2.1040(13)	Cr(1)-Cl(1)#1	2.3304(4)
Cr(1)-N(1)	2.1040(13)	Cr(1)-Cl(1)	2.3304(4)
N(2)-Cr(1)-N(1)#1	90.06(3)	N(1)-Cr(1)-Cl(1)#1	89.36(4)
N(2)-Cr(1)-N(1)	90.06(3)	Cl(2)-Cr(1)-Cl(1)#1	91.614(11)
N(1)#1-Cr(1)-Cl(2)	89.94(3)	N(2)-Cr(1)-Cl(1)	88.386(11)
N(1)-Cr(1)-Cl(2)	89.94(3)	N(1)#1-Cr(1)-Cl(1)	89.36(4)
N(2)-Cr(1)-Cl(1)#1	88.386(11)	N(1)-Cr(1)-Cl(1)	90.64(4)
N(1)#1-Cr(1)-Cl(1)#1	90.64(4)	Cl(2)-Cr(1)-Cl(1)	91.614(11)

Symmetry transformations used to generate equivalent atoms:
#1 -x,y,-z+1/2

One of the differences between the two structures is seen in the analysis of the torsion angles involving the coordination of the pyridine molecules to the metal centre. Figure 2.18 shows that the pyridine ring systems of the two structures twist in opposite directions to each other relative to one of the axial chlorines. A look at the actual angles reveals notable differences, which indicate that these oppositely twisted rings are not enantiomers of each other. The comparisons of torsion angles in Table 2.6 below are limited to the twisting relative to the axial chlorine atoms.

Table 2.6 **Selected torsion angles [°] for $[CrCl_3(py)_3]$**

Cl(1)#1-Cr(1)-N(1)-C(1)	-137.42(11)	Cl(1)#1-Cr(1)-N(2)-C(6)	-130.63(9)
Cl(1)-Cr(1)-N(1)-C(1)	45.81(11)	Cl(1)-Cr(1)-N(2)-C(6)	49.37(9)
Cl(1)#1-Cr(1)-N(1)-C(5)	38.36(12)	Cl(1)#1-Cr(1)-N(2)-C(6)#1	49.37(9)
Cl(1)-Cr(1)-N(1)-C(5)	-138.41(12)	Cl(1)-Cr(1)-N(2)-C(6)#1	-130.63(9)

Symmetry transformations used to generate equivalent atoms:
#1 -x,y,-z+1/2

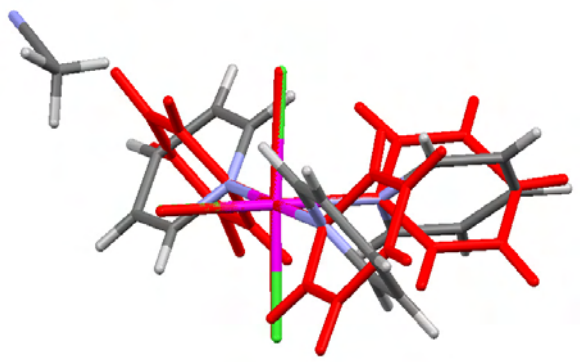

Figure 2.18 **The ring twists observed for $[CrCl_3(py)_3]$ of this study (grey) and that of Howard [83] (red)**

Even though both structures are monoclinic, differences are observed in the crystal data, including the space group, cell dimensions, volume and R–factor.

Table 2.7 **Differences in crystal data between $[CrCl_3(py)_3]$ of this study and that of Howard [83]**

Crystal data	$[CrCl_3(py)_3]$ – This study	$[CrCl_3(py)_3]$ – Howard [83]
Space group	C 2/c	P 2_1/n
Cell dimensions	a = 19.3355(12) Å α= 90° b = 10.8197(7) Å β= 116.5860(10)° c = 11.9758(8) Å γ = 90°	a = 9.088 Å α = 90° b = 12.42 Å β = 91.33° c = 15.557 Å γ = 90°
Volume	2 240.5(3) $Å^3$	1 758.598 $Å^3$
Volume/non-H atoms	20.0 $Å^3$	19.9 $Å^3$
R-factor	2.99%	5.2%

More details of the crystal and structure refinement of this study's structure are given in Table 2.7, while a full set of crystallographic tables is to be found in the appendix.

From the differences observed in Table 2.7 above it is the notably lower R–factor for the complex solved in this study that deserves particular mention.

Note that no hydrogen bond interactions were observed between the CH_3CN and the Cr compound, a finding that is reiterated by the very similar volumes/non-hydrogen atoms calculated for both structures. However, within the packing arrangement (Figures 2.19 and 2.20) there are short contacts that may be defined as weak hydrogen bond interactions as they exist between a chlorine atom and the hydrogen of the pyridine ring at distances of 2.948 Å.

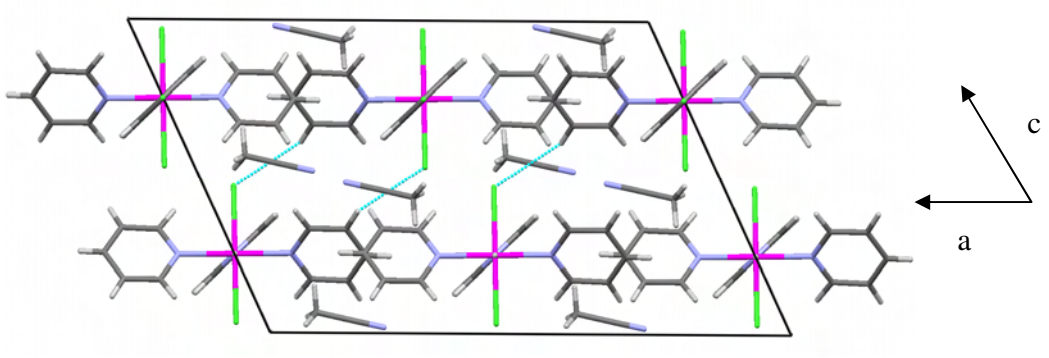

Figure 2.19 **Short contacts observed in the packing arrangement of $[CrCl_3(py)_3]$ of this study**

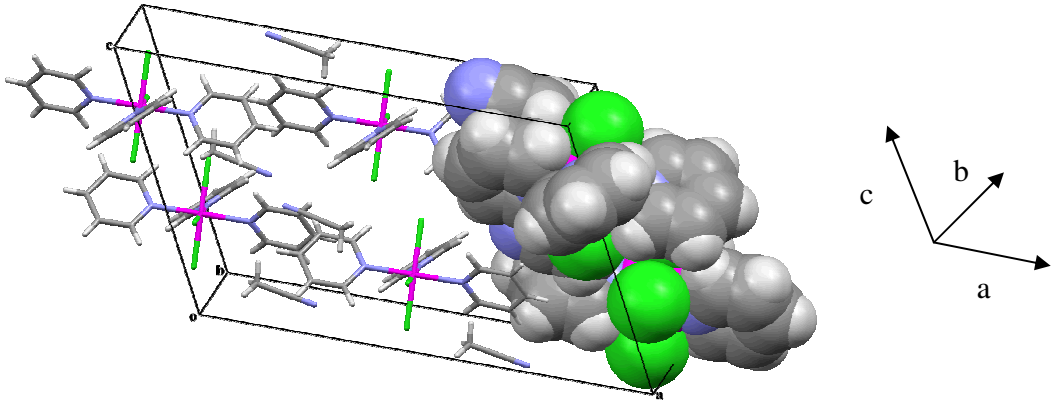

Figure 2.20 **Packing arrangement of $[CrCl_3(py)_3]$ of this study which includes space fill arrangement**

The crystal data and structure refinement for $[CrCl_3(py)_3]$ is presented in Table 2.8.

Table 2.8 **Crystal data and structure refinement for $[CrCl_3(py)_3]$ of this study**

Empirical formula	$C_{19}\ H_{21}\ Cl_3\ Cr\ N_5$	
Formula weight	477.76	
Temperature	293(2) K	
Wavelength	0.71073 Å	
Crystal system	Monoclinic	
Space group	C 2/c	
Unit cell dimensions	a = 19.3355(12) Å	α = 90°
	b = 10.8197(7) Å	β = 116.5860(10)°
	c = 11.9758(8) Å	γ = 90°

Volume	2 240.5(3) $Å^3$
Z	4
Density (calculated)	1.416 Mg/m^3
Absorption coefficient	0.883 mm^{-1}
F(000)	980
Crystal size	0.42 x 0.24 x 0.22 mm^3
Theta range for data collection	3.25 to 26.48°
Index ranges	-22<=h<=19, -13<=k<=8, -9<=l<=14
Reflections collected	5 912
Independent reflections	2 128 [R(int) = 0.0237]
Completeness to theta = 25.00°	99.5%
Absorption correction	Semi-empirical from equivalents
Max. and min. transmission	0.823 and 0.681
Refinement method	Full-matrix least-squares on F^2
Data / restraints / parameters	2 128 / 0 / 171
Goodness-of-fit on F^2	1.059
Final R indices [I>2σ(I)]	R1 = 0.0299, wR2 = 0.0828
R indices (all data)	R1 = 0.0323, wR2 = 0.0860
Extinction coefficient	0
Largest diff. peak and hole	0.281 and -0.251 $e.Å^{-3}$

2.2.5.2 [Hpy][$CrCl_4(py)_2$] (4)

The second structure was unexpected and most interesting in nature as it posed questions regarding the synthetic pathway via which compounds of this nature form. The light green diamond-shaped crystals were grown from the NMR solution of [$CrCl_3(thf)_3$] and three pyridine equivalents in acetone–d_6 that had been used in the above NMR study. The growth period was five days.

This anionic chromium species with a cationic counter-ion has in fact been synthesised previously but, importantly, no crystal structure was ever obtained.

One of the first mentions of $[Hpy][CrCl_4(py)_2]$ in the literature was in 1973 when Brown and Richardson carried out thermal decomposition studies on it and related Cr(III) compounds, including $[CrCl_3(py)_3]$ [41]. It should be noted that the synthetic route to produce $[Hpy][CrCl_4(py)_2]$ was a most awkward procedure which involved $[CrCl_3.6H_2O]$, pyridine, thionyl chloride and benzene. Their analysis led them to the conclusion that $[CrCl_3(py)_3]$ decomposes upon heating to give the dimeric species $[Cr_2Cl_6(py)_4]$, while the thermal decomposition of $[Hpy][CrCl_4(py)_2]$ led to the same dimer via the loss of pyHCl [41].

Interest in $[Hpy][CrCl_4(py)_2]$ resurfaced again in 1990 when Brenčič [84] were able to remake the compound via a simpler and more straightforward method involving the addition of pyHCl to $[CrCl_3(py)_3]$. Their particular interest lay not in any mechanistic details but in the adopted configuration of the $[Hpy][CrCl_4(py)_2]$ compound. In addition to evidence from other similar compounds, they concluded that it adopts the *trans* configuration due largely to the fact that when pyridine is added to $[Hpy][CrCl_4(py)_2]$, the trans $[CrCl_3(py)_3]$ forms.

1. $[CrCl_3(py)_3] + pyHCl \longrightarrow [Hpy][CrCl_4(py)_2] + py$
2. $[Hpy][CrCl_4(py)_2] \longrightarrow [CrCl_3(py)_3] + HCl$

The determination of this crystal as part of this study was able to confirm Brenčič's predictions of *trans* conformer formation. Also, more weight was added to the dimeric link proposed by Brown and Richardson [41] as in relation to this study $[Hpy][CrCl_4(py)_2]$ had to have formed from an asymmetrically cleaved dimeric intermediate. This correlates well with the grey/blue intermediatory colour seen in these compounds that Elowe [38] associated with dimeric species, as mentioned earlier. Thus, what is implied is that perhaps more than one mechanism is plausible. The first is direct ligand substitution as suggested previously. However, in the light of this anionic chromium-type structure, one must certainly entertain the possibility of dimer formation.

This can be cleaved either symmetrically or asymmetrically, resulting in the neutral monomer or the anionic chromium species $[Hpy][CrCl_4(py)_2]$ incorporating the pyridinium counter-ion. The asymmetrical cleavage would also have resulted in the other portion of the dimer, which would possess a cationic chromium species. Interestingly with regard to previous studies in this field, it is the cationic chromium species that is assigned as the catalytically active species, as mentioned in Chapter 1. It was unfortunate that this species could not be isolated. The possible pathways to product formation are presented in Figure 2.21.

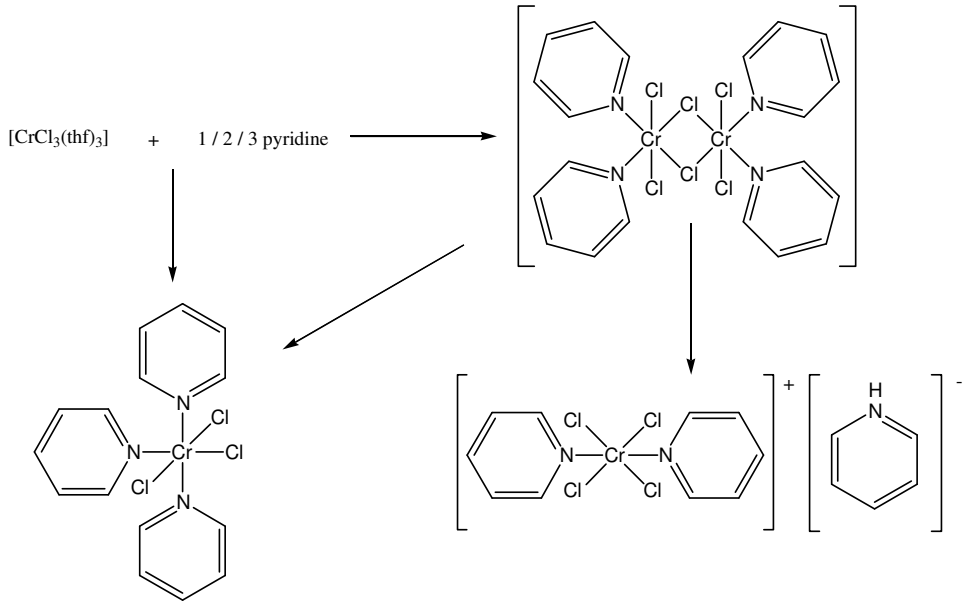

Figure 2.21 Possible pathways to product formation

The next logical question concerns the driving force behind symmetrical and asymmetrical cleavage. The only difference in how the $[CrCl_3(py)_3]$ and $[Hpy][CrCl_4(py)_2]$ compounds were formed was that their solvents of crystallisation differed ($[CrCl_3(py)_3] = CH_3CN$, $[Hpy][CrCl_4(py)_2]$ = acetone–d_6).

Of the limited number of $CrCl_4L_2$ (L = donor ligands) crystal structures that have been solved throughout the literature, only two structures (excluding the structure $[Hpy][CrCl_4(py)_2]$) possess unlinked monodentate donor ligands that are coordinated to the chromium centre via single bonds. They are:

- Trimethylphosphoniumtrans–tetrachloro–bis–(trimethylphosphine)–chromium(III) [85].
- Quinolinium tetrachloro–bis(acetonitrile) chromium (III) acetonitrile solvate [86].

Of these two, 3D coordinates were available only for the former. In this novel $[Hpy][CrCl_4(py)_2]$ compound the chromium atom is coordinated to four chlorine atoms and two nitrogen atoms of the pyridine ligands, while that in literature has the chromium atom coordinated to four chlorine atoms and two trimethylphosphine ligands. In both cases similar donor ligands are *trans* to each other. The coordination of this novel pyridine-based compound is approximately octahedral with the largest deviation being the Cl(3)–Cr(1)–Cl(4) bond angle (88.28(3))°. All other *cis* X–Cr–Y bond angles are in the range 89.17(7) to 91.12(3)°. The metal–ligand bond lengths were, unsurprisingly, of very similar magnitudes to those of $[CrCl_3(py)_3]$.

The torsion angles for both pyridine ligands are virtually identical (difference of 1.5° between C(1)–N(1)–Cr(1)–Cl(1) and C(10)–N(2)–Cr(1)–Cl(1)) as they are observed in the same plane. This aromatic planarity is presented in Figure 2.22. The observed tilting of the pyridinium ion is discussed under the paragraph that highlights hydrogen bonding.

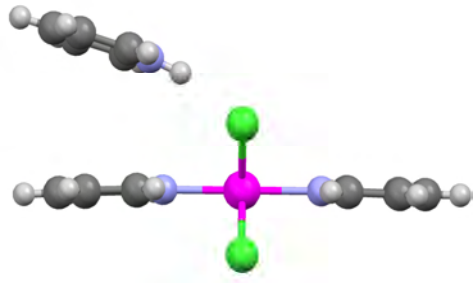

Figure 2.22 The planarity of the pyridine rings as well as the tilting of the pyridinium ion

Table 2.9 presents a combination of metal–ligand bond lengths, bond angles associated with the octahedral geometry and torsion angles relative to the axial chlorine atoms.

Unlike the phosphine-based structure in the literature, hydrogen bonding is observed between the pyridinium cation and the anionic chromium species. The pyridinium N(3)–H(3N) group is hydrogen bonded to Cl(3) and Cl(4). A consequence of these interactions is the tilting of the pyridinium ion towards the respective chlorine atoms. This phenomenon can be seen clearly in both Figures 2.22 and 2.23, while Table 2.10 details the interactions.

Table 2.9 **Selected bond lengths [Å], bond angles [°] and torsion angles [°] for [Hpy][$CrCl_4(py)_2$]**

Cr(1)-N(1)	2.097(2)	Cr(1)-Cl(1)	2.3398(8)
Cr(1)-N(2)	2.109(2)	Cr(1)-Cl(3)	2.3451(8)
Cr(1)-Cl(2)	2.3387(8)	Cr(1)-Cl(4)	2.3490(8)
N(1)-Cr(1)-Cl(2)	90.36(6)	N(2)-Cr(1)-Cl(3)	90.41(7)
N(2)-Cr(1)-Cl(2)	89.95(6)	Cl(2)-Cr(1)-Cl(3)	91.12(3)
N(1)-Cr(1)-Cl(1)	90.43(6)	N(1)-Cr(1)-Cl(4)	90.23(6)
N(2)-Cr(1)-Cl(1)	89.17(7)	N(2)-Cr(1)-Cl(4)	89.46(6)
Cl(2)-Cr(1)-Cl(1)	90.05(3)	Cl(1)-Cr(1)-Cl(4)	90.54(3)
N(1)-Cr(1)-Cl(3)	89.99(6)	Cl(3)-Cr(1)-Cl(4)	88.28(3)
Cl(2)-Cr(1)-N(1)-C(1)	-133.5(2)	Cl(2)-Cr(1)-N(2)-C(10)	135.0(2)
Cl(1)-Cr(1)-N(1)-C(1)	-43.4(2)	Cl(1)-Cr(1)-N(2)-C(10)	44.9(2)
Cl(3)-Cr(1)-N(1)-C(1)	135.4(2)	Cl(3)-Cr(1)-N(2)-C(10)	-133.9(2)
Cl(4)-Cr(1)-N(1)-C(1)	47.1(2)	Cl(4)-Cr(1)-N(2)-C(10)	-45.6(2)
Cl(2)-Cr(1)-N(1)-C(5)	44.9(2)	Cl(2)-Cr(1)-N(2)-C(6)	-43.4(2)
Cl(1)-Cr(1)-N(1)-C(5)	134.9(2)	Cl(1)-Cr(1)-N(2)-C(6)	-133.5(2)
Cl(3)-Cr(1)-N(1)-C(5)	-46.3(2)	Cl(3)-Cr(1)-N(2)-C(6)	47.7(2)
Cl(4)-Cr(1)-N(1)-C(5)	-134.5(2)	Cl(4)-Cr(1)-N(2)-C(6)	136.0(2)

Table 2.10 **Hydrogen bonds for [Hpy][$CrCl_4(py)_2$] [Å and °]**

D-H...A	d(D-H)	d(H...A)	d(D...A)	<(DHA)
N(3)-H(3N)...Cl(4)	0.89(5)	2.43(5)	3.235(4)	150(5)
N(3)-H(3N)...Cl(3)	0.89(5)	2.94(5)	3.586(4)	131(4)

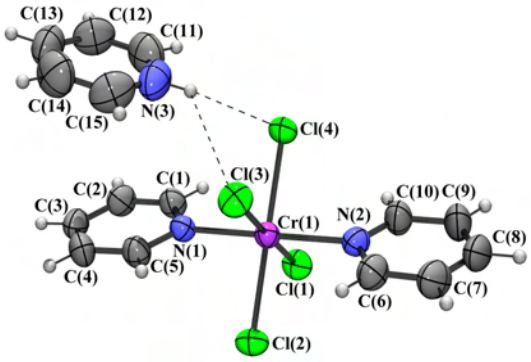

Figure 2.23 **Hydrogen bonding observed in [Hpy][$CrCl_4(py)_2$]**

Figures 2.24 to 2.27 illustrate the packing arrangement and space filling adopted by the structure with no short contacts of importance visible between the layers.

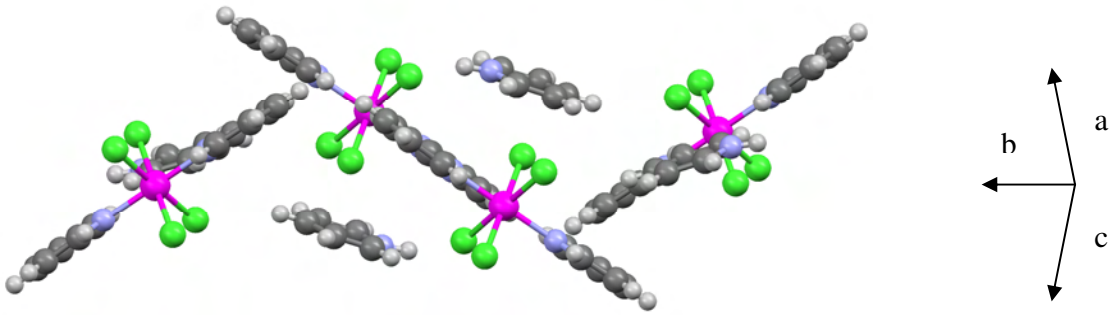

Figure 2.24 **Packing arrangement of [Hpy][$CrCl_4(py)_2$]**

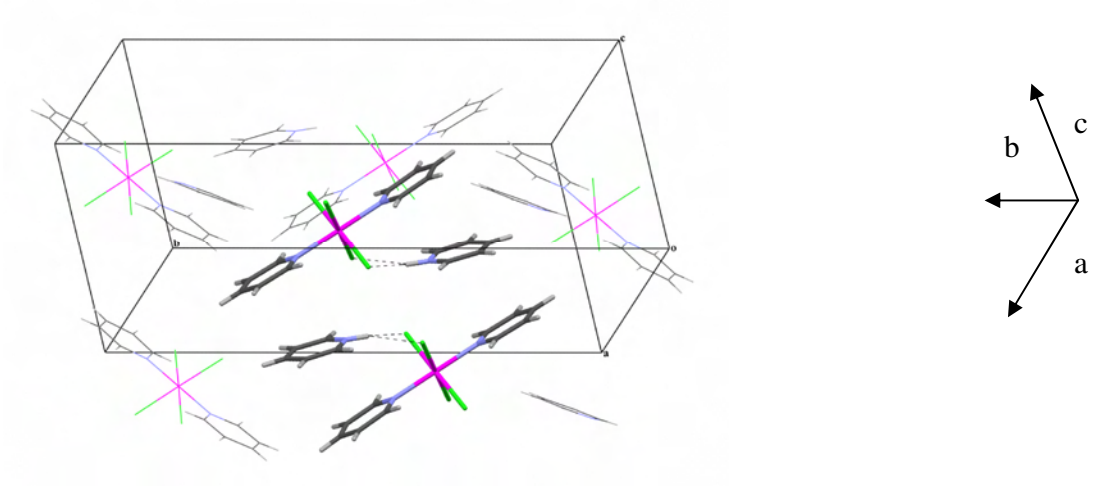

Figure 2.25 Alternative view of the packing arrangement of [Hpy][$CrCl_4(py)_2$]

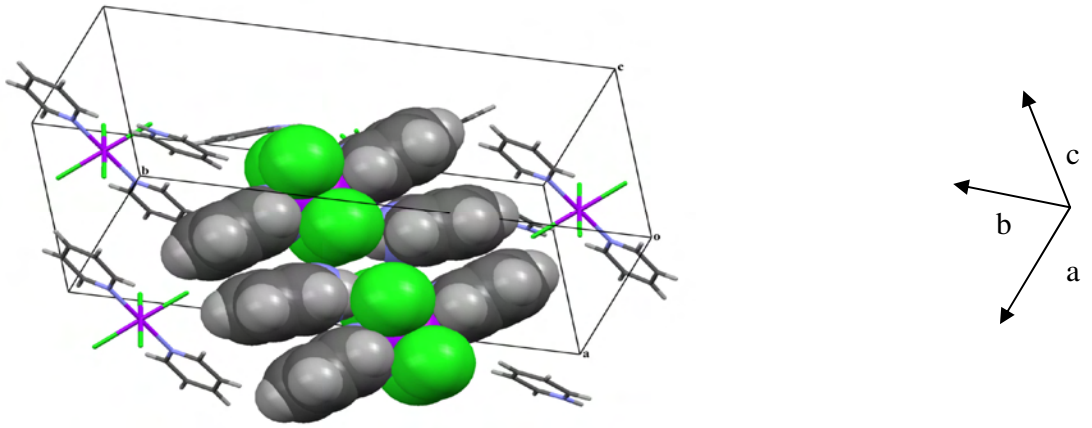

Figure 2.26 Packing and space fill of [Hpy][$CrCl_4(py)_2$]

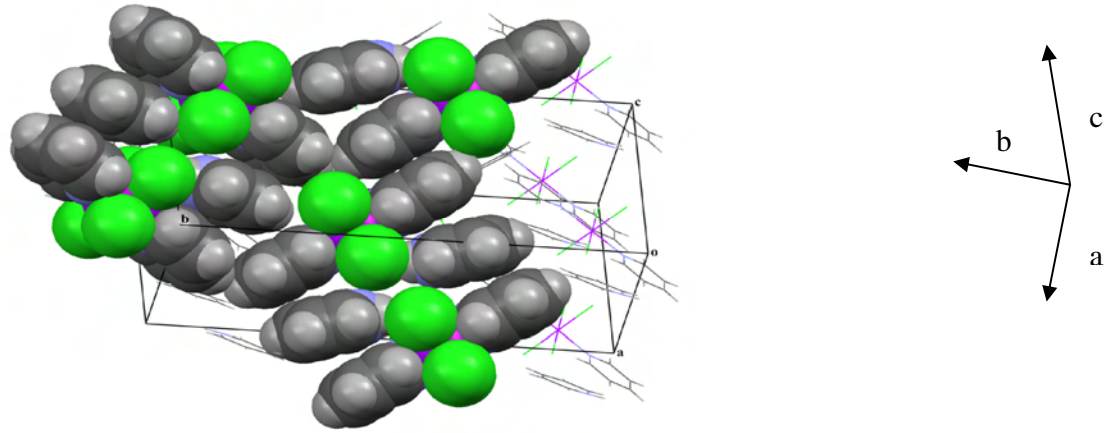

Figure 2.27 Alternative view of the packing and space fill of [Hpy][$CrCl_4(py)_2$]

Crystal data and details of structure refinement are shown in Table 2.11, while the complete set of crystallographic data is given in the appendix.

Table 2.11 Crystal data and structure refinement for [Hpy][$CrCl_4(py)_2$]

Empirical formula	$C_{15}\ H_{16}\ Cl_4\ Cr\ N_3$	
Formula weight	432.11	
Temperature	298(2) K	
Wavelength	0.71073 Å	
Crystal system	Monoclinic	
Space group	P 2_1/n	
Unit cell dimensions	a = 8.1070(7) Å	α = 90°
	b = 22.5413(18) Å	β = 92.9970(10)°
	c = 10.1760(8) Å	γ = 90°
Volume	1857.0(3) $Å^3$	
Z	4	
Density (calculated)	1.546 Mg/m^3	
Absorption coefficient	1.192 mm^{-1}	
F(000)	876	
Crystal size	0.22 x 0.14 x 0.12 mm^3	
Theta range for data collection	2.67 to 26.51°.	
Index ranges	-10<=h<=10, -12<=k<=28, -10<=l<=12	
Reflections collected	10 038	
Independent reflections	3 531 [R(int) = 0.0345]	
Completeness to theta = 25.00°	99.7%	
Absorption correction	Semi-empirical from equivalents	
Max. and min. transmission	0.867 and 0.724	
Refinement method	Full-matrix least-squares on F^2	
Data / restraints / parameters	3 531 / 0 / 211	
Goodness-of-fit on F^2	1.087	
Final R indices [I>2sigma(I)]	R1 = 0.0351, wR2 = 0.0828	

R indices (all data)	R1 = 0.0538, wR2 = 0.0950
Extinction coefficient	0
Largest diff. peak and hole	0.344 and -0.257 e.Å^{-3}

2.2.6 MASS SPECTROMETRY

The FAB-MS spectrum of the $[CrCl_3(py)_3]$ precipitate shows the isotopic distribution pattern associated with $[M–HCl]^+$ (m/z = 358). This assignment is possible because a crystal structure determination excluded the formation of the dimeric structure, $[(\mu\text{-}Cl)_2\{CrCl_2(py)_3\}_2]$, in the solid state. This pattern correlates strongly with the expected pattern generated by the isotopic distribution calculator. As the $[M–3Cl]^+$ peak (m/z = 289) is also observed it is evident that the chlorine atoms are more readily removed than the pyridine ligands. These findings which are presented in Figure 2.28 verify the already discussed spectroscopic and crystallographic data and provide further evidence that the single crystal determination of $[CrCl_3(py)_3]$ represents the bulk material.

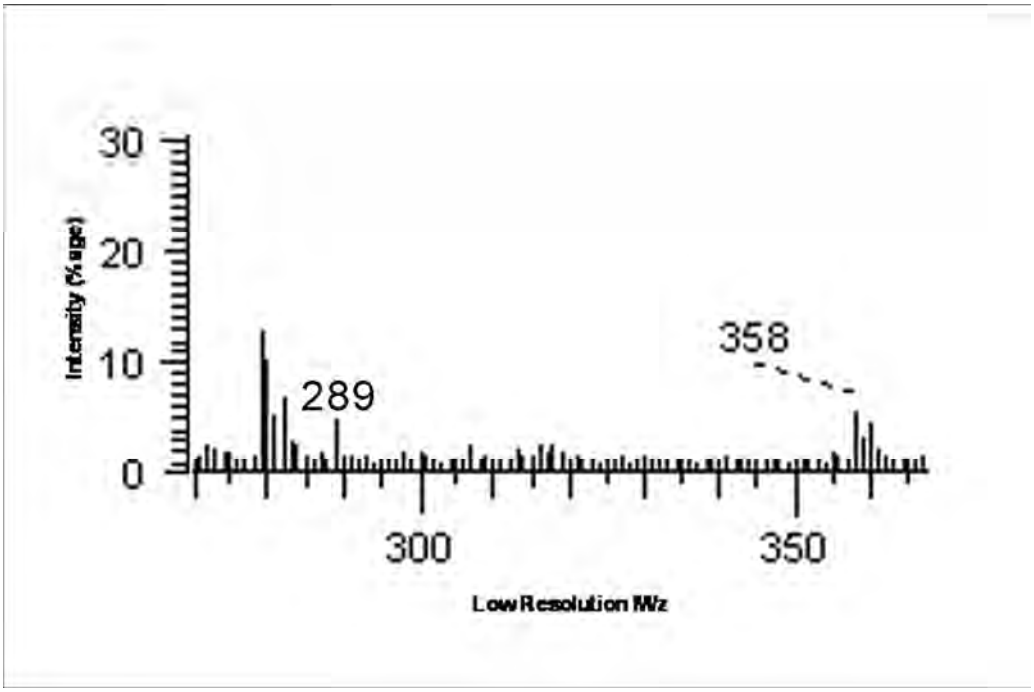

Figure 2.28 FAB-MS spectrum of $[CrCl_3(py)_3]$

2.3 CATEGORY TWO: BULKY SUBSTITUENTS

One is always aware of selecting ligands that are sterically capable of coordination to the metal centre as bulkiness at a particular position of the ligand may prohibit such coordination. With respect to the addition of pyridines to $[CrCl_3(thf)_3]$, the following question was posed: Would substituents at the ortho position of pyridine prohibit coordination or could the ligands in fact orientate themselves in such a way as to allow coordination to take place? Two reactions were carried out simultaneously (Figure 2.29).

In the first reaction three equivalents of 2,6-dibromopyridine were added to $[CrCl_3(thf)_3]$ in thf, with the interest lying in whether or not the large bromine substituents would allow the endocyclic nitrogen donor atoms of the pyridines to coordinate to the chromium. On immediate addition of the ligand no reaction was visible as the deep colour of $[CrCl_3(thf)_3]$ dissolved in thf remained unchanged. The reaction was then stirred at room temperature and closely monitored. After 12 hours the reaction was stopped as no reaction had yet occurred. The solution was then refluxed at 80°C for a further 12 hours with no change evident.

In the second reaction, to one equivalent of $[CrCl_3(thf)_3]$ was added one molar equivalents of 2,6–dibromopyridine, 2,6–dimethylpyridine and unsubstituted pyridine. All three ligands were added simultaneously to ensure equal competition for sites.

The resulting green precipitate was sparingly soluble in most solvents but dissolved particularly well in DMF. This solution was placed in a fridge and left to crystallise. After a period of four weeks dark green plate-like crystals formed, which were large enough and of sufficiently good quality for analysis on the single crystal diffractometer. The resulting structure was somewhat surprising. All three thf molecules of the chromium precursor had been displaced, but by two equivalents of pyridine and one DMF solvent molecule which had coordinated through the oxygen atom.

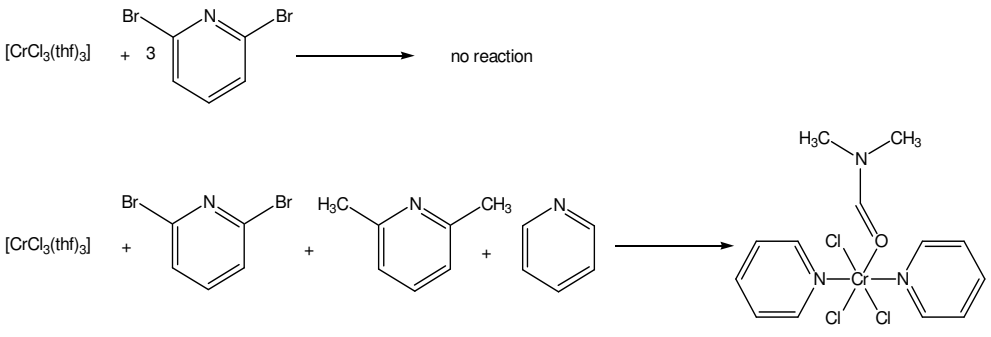

Figure 2.29 Bulky substituent reactions that were carried out

This meant that the question concerning the coordination of ortho substituted pyridines was answered conclusively in the negative. Furthermore, the fact that although only one equivalent of pyridine was added, two such molecules coordinated to the metal centre added weight to the idea discussed in the previous section that only one pyridine would suffice to activate the other available sites. However, with this in mind one would have expected all three available thf sites to have been substituted by pyridines. Instead one of the sites was occupied by a DMF molecule. This is of interest because as a result of the relatively low concentration of pyridine and the labilisation of the thf ligands, one may have expected the formation of a chloro-bridged dimer, which was not observed. It was therefore perceived that DMF was a very good ligand under these conditions.

This finding is yet more evidence supporting the plausibility of direct ligand substitution as a synthetic pathway to compound formation.

As a direct consequence of this resulting structure, it seemed logical to attempt a further reaction whereby all three thf molecules of the precursor could potentially be displaced by three equivalents of the coordinating DMF molecule, thus resulting in a novel structure determination. The reaction involved using DMF as both solvent and ligand. This excess also gave the best possible chance for the DMF to coordinate at the three available sites. On immediate addition of excess DMF to $[CrCl_3(thf)_3]$ a dark green supernatant was observed. The reaction was stirred overnight at room temperature. In order to mimic the conditions that allowed the formation of $[CrCl_3(py)_2(DMF)]$ **(5),** the solution was then placed in a fridge. Unfortunately, no crystals were ever formed and

because of the nature of this particular solvent it was not ideal to take the reaction further by reducing the solvent and trying to force out a precipitate. Hence no further attempts were made with regard to this reaction.

2.3.1 INFRARED SPECTROSCOPY

The yield of crystals grown was sufficient for an IR spectrum to be run, but not for the corresponding Raman spectrum. Nonetheless, the IR spectrum was important as the resulting bands could be used as a reference for comparison with those IR spectra of similar compounds where crystals were unobtainable.

Relatively straightforward assignment of bands is possible as the two ligand environments (pyridine and DMF) are very different and thus immune to band overlap.

This result actually serves to reaffirm the conclusion drawn regarding the sequential addition (control of ligand addition) of ligands to $[CrCl_3(thf)_3]$ – it is not possible via this route.

2.3.1.1 Region 3114–2804 cm^{-1}

This region plays host to three different C–H environments, which include the aromatic heterocycle of pyridine and the methyl and carbonyl functionalities of DMF.

Between 3114 and 3032 cm^{-1} are those vibrations associated with pyridine and they are unshifted relative to the free ligand position, as expected [73, 74, 76]. The methyl frequencies are visible at 3000 and 2940 cm^{-1}, while the carbonyl-specific vibrations are in among them at 2877 and 2804 cm^{-1}[87]. Figure 2.30 highlights these vibrations.

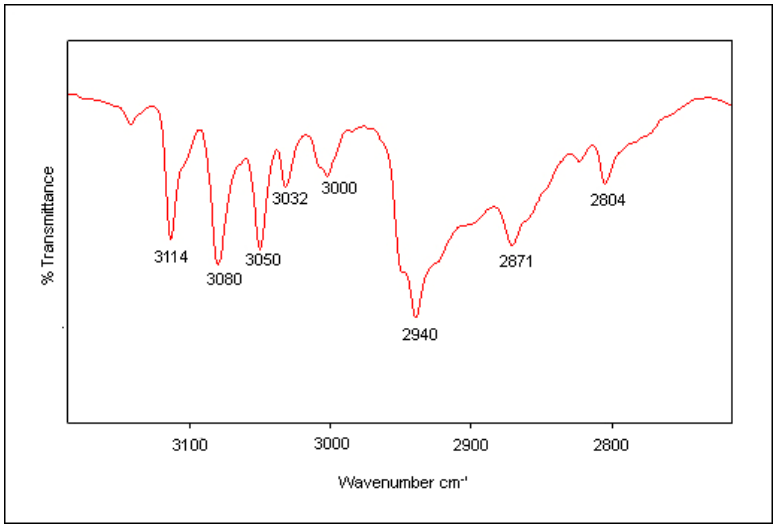

Figure 2.30 IR spectrum of the region 3114 – 2804 cm^{-1}

2.3.1.2 Region 1660–1247 cm^{-1}

An informative region with characteristic ligand vibrations is found between 1660–1247 cm^{-1} (see Figure 2.31). The strongest and probably most recognisable vibrations of the entire spectrum are the two vibrations at 1660 and 1649 cm^{-1} which are characteristic of C=O carbonyl stretches of DMF [88]. A band found very close to these modes is the expected pyridine vibration at 1606 cm^{-1} which has shifted from either 1599 cm^{-1} or 1580 cm^{-1} upon coordination [73, 74]. Other pyridine-assignable bands are those at 1572, 1485 and 1446 cm^{-1}, with only that at 1446 cm^{-1} shifting upon coordination from a free pyridine ring vibration of 1438 cm^{-1} [73, 74]. The remaining bands relate to DMF [87] and include:

1433 cm^{-1} δ(sym) CH_3

1391 cm^{-1} δ N–C–H in plane carbonyl

1247 cm^{-1} ν(asym) C–N of $N(CH_3)_2$

(δ(sym) = symmetrical bending, ν(asym) = asymmetrical stretching)

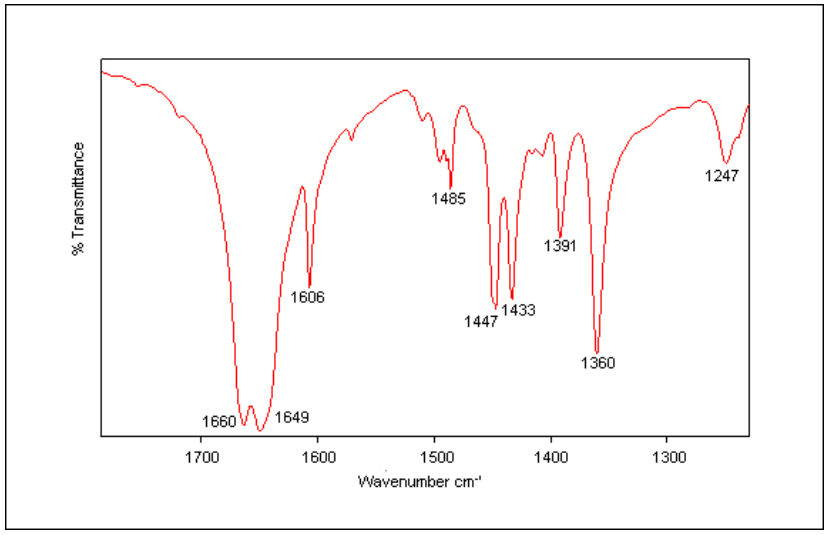

Figure 2.31 **IR spectrum of the region 1660 – 1247 cm^{-1}**

2.3.1.3 Region 1219– 448 cm^{-1}

Very few bands corresponding to the DMF molecule are found in this region with only that at 1095 cm^{-1} being assignable solely to DMF with any level of surety [89].

The remaining bands are pyridine vibrations, three of which exhibit characteristic shifts indicative of coordination. They are found at 1015, 644 and 448 cm^{-1}and have shifted from their free ligand positions of 991, 605 and 405 cm^{-1} respectively. All three shifts are in accordance with those observed for $[CrCl_3(py)_3]$ [73, 74]. All important vibrations are presented in Figure 2.32.

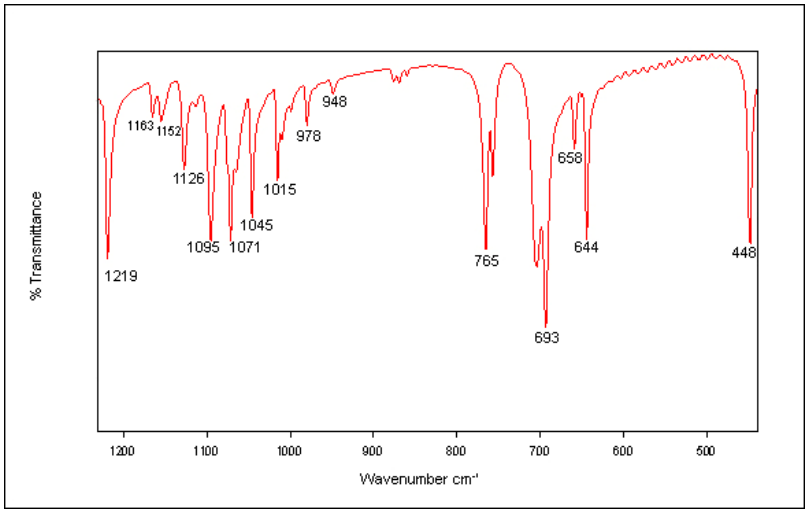

Figure 2.32 **IR spectrum of the region 1219 – 448 cm^{-1}**

2.3.1.4 Region 415–214 cm^{-1}

More evidence of pyridine coordination by way of characteristic shifts is observed with the vibrations at 644 and 448 cm^{-1}. Their shifting from the free ligand positions of 605 and 405 cm^{-1} is widely accepted [73, 74].

DMF vibrations in the form of C–N–C deformations are also observed at 397 and 390 cm^{-1} [90, 91], although they do overlap with the assignment of a tertiary butyl C–C–C deformation [92].

Relatively distinguishable are the expected three Cr–Cl bands at 358, 324 and 302 cm^{-1} and they are in accordance with the observed *mer* orientation witnessed in the crystal structure [80].

Although the literature asserts that the Cr–N of pyridine band is at 221 cm^{-1} [41, 80, 81], it is plausible that because of its novel ligand environment (the proximity of coordinated DMF), it is now present at 214 cm^{-1}. This then allows for the Cr–O of DMF vibration to be the band at 230 cm^{-1}. It is, however, assigned with a certain amount of caution due to the lack of evidence in the literature.

The IR bands have been tabulated alongside the substituted pyridine compounds which are discussed in the following section due to the coordination of pyridine derivatives in all. Figure 2.33 highlights the vibrations found in this region.

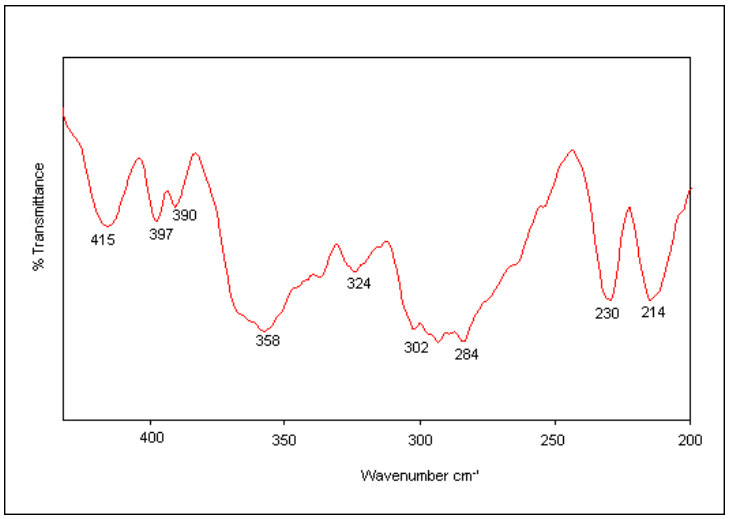

Figure 2.33 IR spectrum of the region 415 – 214 cm^{-1}

2.3.2 X-RAY CRYSTALLOGRAPHY

In 1977 Broomhead [88] solved the crystal structure for the compound *mer*-trichloro(dimethylformamide)(1, 10-phenanthroline)chromium(III) which, until the results of this study, was the only known structure of a chromium–DMF complex. Interesting comparisons can be drawn between the two structures although differences are certainly expected as [$CrCl_3(py)_2(DMF)$] is essentially the first structure determination in which the nitrogen donor ligands are of a monodentate nature. Figure 2.34 shows the two structures.

In [$CrCl_3(py)_2(DMF)$] the central chromium atom is coordinated to three chlorine atoms, two nitrogen atoms of pyridine molecules and an oxygen atom of a DMF molecule. The pyridine ligands are *trans* to each other and unlike the 'Broomhead structure' the DMF is *trans* to a chlorine atom. The coordination is approximately octahedral with the largest deviation being the N(1)–Cr(1)–O(1) bond angle (86.98(10)°). All the other *cis* X–Cr–Y bond angles are in the range 87.90(7)–92.93(7)°.

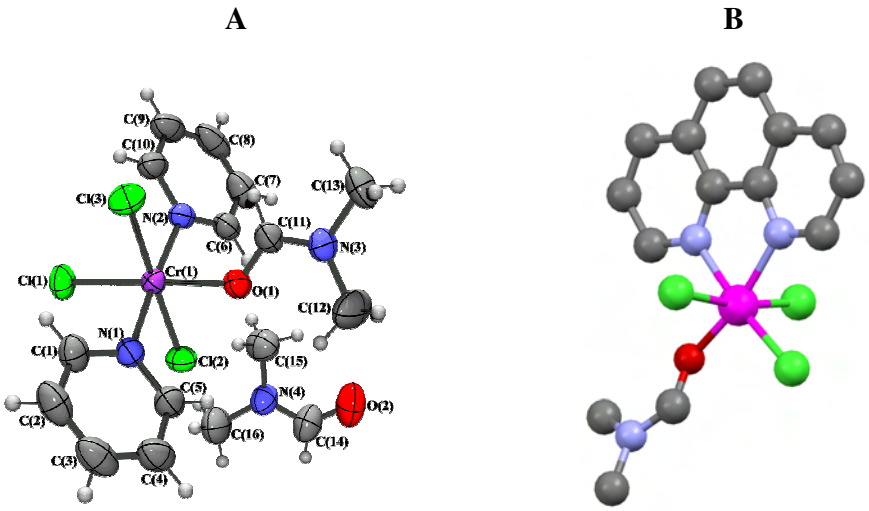

Figure 2.34 **A = Perspective drawing of $[CrCl_3(py)_2(DMF)]$ structure determined in this study, B = Perspective drawing of $[CrCl_3(py)_2(DMF)]$ structure determined by Broomhead [88]**

The pyridine rings are non-planar relative to each other with a difference in corresponding torsion angles of 8.9° (as shown in Figure 2.35) where C(1)–N(1)–Cr(1)–Cl(3) is 50.9(2)° and C(10)– N(2)–Cr(1)–Cl(3) is 42.0(2)°. This twist is noticeably larger than the 1.5° difference observed between the *trans* pyridine ligands in $[Hpy][CrCl_4(py)_2]$.

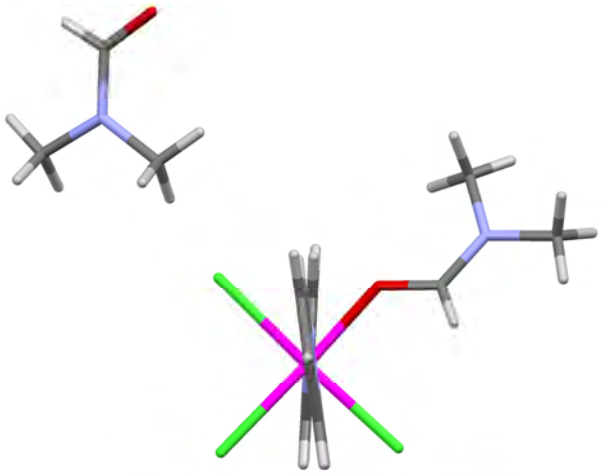

Figure 2.35 **Non-planarity of the *trans* pyridine ligands in $[CrCl_3(py)_2(DMF)]$**

A closer look at the metal–ligand bond lengths shows the Cr–Cl and Cr–N bonds correspond well with those of the two structures above. Favourable comparisons are also made with the 'Broomhead structure', with the only noticeable deviation being the shortening and thus strengthening of the equatorial Cr–Cl in the 'Broomhead structure'. This is not observed in the structure of this study and can be explained by the fact that a different ligand environment is *trans* to this particular Cr–Cl bond. This observation highlights the effects that different ligands in different structural orientations have on the properties of other bonds in a complex. To a lesser extent this also had an effect on the bond length of the Cr–O bonds as again that of the 'Broomhead structure' is slightly shorter.

As in the $[CrCl_3(py)_3]$ complex with an encapsulated solvent molecule, no obvious hydrogen bond interactions were observed between the DMF solvate and the metal complex. However, a weak contact (2.795 Å) between a chlorine atom of the complex and a hydrogen atom of the CH_3CN solvent molecule is observed, which may be construed as a weak hydrogen bond.

Table 2.12 highlights all the important metal–ligand bond lengths, as well as those bond angles that infer an octahedral geometry. As in the structures above, the selected torsion angles are relative to the axial chlorine atoms.

Table 2.13 offers details on crystal data and structural refinement, but a full set of crystallographic data is found in the appendix.

Table 2.12 **Selected bond lengths [Å], bond angles [°] and torsion angles [°] for $[CrCl_3(py)_2(DMF)]$**

Cr(1)-O(1)	2.003(2)	Cr(1)-Cl(1)	2.3120(9)
Cr(1)-N(1)	2.102(3)	Cr(1)-Cl(3)	2.3268(9)
Cr(1)-N(2)	2.106(3)	Cr(1)-Cl(2)	2.3277(9)
O(1)-Cr(1)-N(1)	86.98(10)	N(2)-Cr(1)-Cl(3)	90.36(8)

O(1)-Cr(1)-N(2)	88.77(10)	Cl(1)-Cr(1)-Cl(3)	92.12(4)
N(1)-Cr(1)-Cl(1)	92.93(7)	O(1)-Cr(1)-Cl(2)	87.90(7)
N(2)-Cr(1)-Cl(1)	91.33(7)	N(1)-Cr(1)-Cl(2)	89.34(8)
O(1)-Cr(1)-Cl(3)	89.91(7)	N(2)-Cr(1)-Cl(2)	90.83(8)
N(1)-Cr(1)-Cl(3)	89.32(8)	Cl(1)-Cr(1)-Cl(2)	90.06(3)

Cl(3)-Cr(1)-N(1)-C(1)	50.9(2)	Cl(2)-Cr(1)-N(2)-C(10)	140.2(2)
Cl(2)-Cr(1)-N(1)-C(1)	-131.3(2)	Cl(3)-Cr(1)-N(2)-C(6)	141.7(2)
Cl(3)-Cr(1)-N(1)-C(5)	-129.7(2)	Cl(2)-Cr(1)-N(2)-C(6)	-36.1(2)
Cl(2)-Cr(1)-N(1)-C(5)	48.2(2)	Cl(3)-Cr(1)-O(1)-C(11)	-32.2(3)
Cl(3)-Cr(1)-N(2)-C(10)	-42.0(2)	Cl(2)-Cr(1)-O(1)-C(11)	149.0(3)

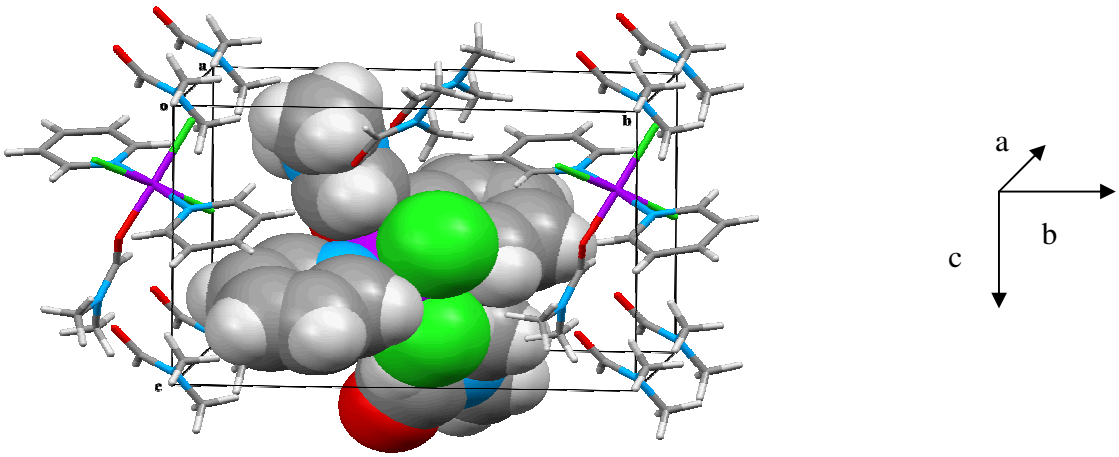

Figure 2.36 **Packing and space fill arrangement of [$CrCl_3(py)_2(DMF)$]**

Table 2.13 **Crystal data and structure refinement for [$CrCl_3(py)_2(DMF)$]**

Empirical formula	$C_{16}\ H_{24}\ Cl_3\ Cr\ N_4\ O_2$
Formula weight	462.74
Temperature	293(2) K
Wavelength	0.71073 Å
Crystal system	Monoclinic
Space group	P 2_1

Unit cell dimensions	a = 8.8882(7) Å	α = 90°
	b = 13.3255(10) Å	β = 94.2880(10)°
	c = 9.0420(7) Å	γ = 90°
Volume	1067.93(14) $Å^3$	
Z	2	
Density (calculated)	1.439 Mg/m^3	
Absorption coefficient	0.928 mm^{-1}	
F(000)	478	
Crystal size	0.26 x 0.18 x 0.06 mm^3	
Theta range for data collection	2.73 to 26.54°.	
Index ranges	-9<=h<=10, -16<=k<=15, -4<=l<=11	
Reflections collected	5 833	
Independent reflections	3 703 [R(int) = 0.0288]	
Completeness to theta = 25.00°	99.6%	
Absorption correction	Semi-empirical from equivalents	
Max. and min. transmission	0.946 and 0.793	
Refinement method	Full-matrix least-squares on F^2	
Data / restraints / parameters	3703 / 1 / 239	
Goodness-of-fit on F^2	1.071	
Final R indices [I>2σ(I)]	R1 = 0.0339, wR2 = 0.0835	
R indices (all data)	R1 = 0.0384, wR2 = 0.0867	
Absolute structure parameter	0.02(2)	
Extinction coefficient	0	
Largest diff. peak and hole	0.247 and -0.218 $e.Å^{-3}$	

2.4 CATEGORY THREE: PARA–SUBSTITUTED PYRIDINES

The coordination of a variety of electronically and sterically different para-substituent pyridine ligands to the Cr(III) precursor was undertaken with the aim of investigating novel structure–reactivity insights.

In light of the investigations above, three molar equivalents of each ligand were added and only para–substituted pyridine derivatives were used as steric interactions with other ligands / substituents are minimised at this position.

Figure 2.37 highlights the pyridine derivatives that were investigated.

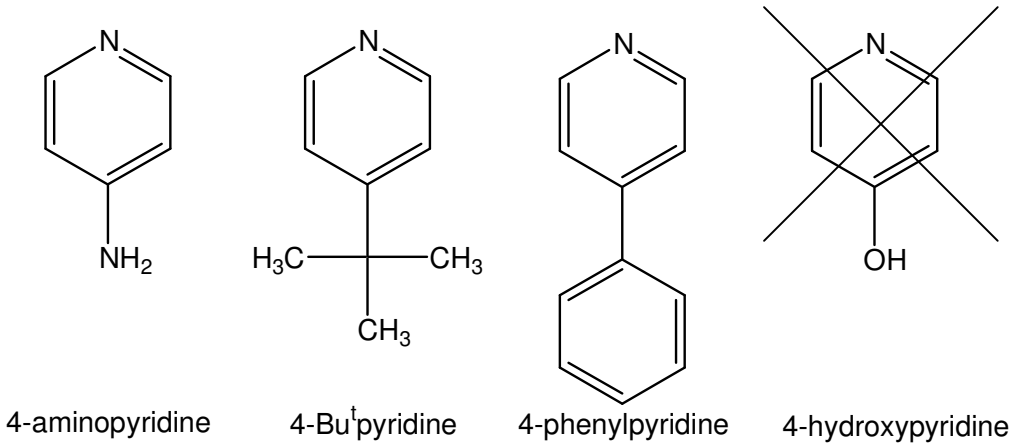

Figure 2.37 Para-substituted pyridine ligands

Only the hydroxy derivative did not yield results as it was insoluble in all workable solvents. The coordination chemistry of the 4–aminopyridine was also of interest as it possesses two nitrogen donor atoms that could coordinate equally through their lone pairs to the metal.

2.4.1 INFRARED AND RAMAN SPECTROSCOPY

The importance of at least one single crystal determination for a class of compounds is clearly illustrated in these pyridine complexes whereby the IR and Raman spectral assignments of precipitates can be made with a degree of confidence.

Detailed vibrational comparisons can be made between the spectra of $[CrCl_3(py)_3]$, $[CrCl_3(py)_2(DMF)]$ and $[CrCl_3(pytb)_3]$ **(7)**, with known crystal structures, and the precipitates of $[CrCl_3(pyNH_2)_3]$ **(6)** and $[CrCl_3(pyphenyl)_3]$. Note that as was the case for $[CrCl_3(py)_3]$, spectra were taken of both the single crystal material and the precipitate of $[CrCl_3(pytb)_3]$. The fact that these spectra were identical infers that the single crystal

determination is representative of the bulk precipitate. Of course vibrational differences are expected due to the substituents but there should also be notable similarities.

Furthermore, in the light of the structural determination of [Hpy][$CrCl_4(py)_2$] which asks questions about the synthetic route to product formation, IR and Raman spectra are of value.

Evidence of dimeric species in addition to pyridinium–type vibrations is of interest. Although no spectrum of [Hpy][$CrCl_4(py)_2$] was obtained due to lack of sample, the presence and absence of bands in these compounds can be compared with the findings of previous literature studies [93, 94, 95] and with the pyH compounds synthesised from the bidentate systems that follow for which spectra were obtained.

With regard to the two spectroscopic techniques themselves, as there is no centre of symmetry in any of the compounds it is expected that all vibrations will be both IR and Raman active [47]. One must be aware, however, that the intensities of the vibrations may differ and a vibration that may seem inactive in either of the two techniques is more than likely simply too weak to be observed. In the following compounds there is a definite trend for the IR vibrations to be stronger than the Raman equivalents.

2.4.1.1 Region 3321–2869 cm^{-1}

Common to all three compounds is the presence of C–H pyridine vibrations. In addition, N–H and C–H bands of the respective substituents are also observed.

[$CrCl_3(pyNH_2)_3$] is the only compound in which bands at 3321 and 3203 cm^{-1} are observed. They are strong vibrations in the IR spectrum but noticeably weaker in intensity in the Raman equivalent. That at 3321 cm^{-1} is confidently assigned to a NH_2 asymmetrical stretch vibration which has shifted from its free ligand position of 3300 cm^{-1} [76, 96], thus being an early indication of coordination to the metal. Furthermore, its moderate shift is also an indication that coordination has taken place via the endocyclic pyridine nitrogen and not the nitrogen of the amino group (as both are valid donor

atoms). If that had indeed been the case, a drastic red shift of between 150 and 200 cm^{-1} would have been observed [96]. The other band at 3203 cm^{-1} is assigned the symmetrical NH_2 stretching mode [76]. Note also that it is absent in all the other complexes. It is, however, worth mentioning that a pyridinium vibration is expected at this same value [94]. Notably, though, this and one other band are the only evidence, suggesting pyridinium ion formation in the entire spectrum as will be seen in the coming regions.

In the case of the $[CrCl_3(pytb)_3]$, strong bands in both the IR and Raman spectra at 2965, 2906 cm^{-1} (visible only in the Raman spectrum as in the literature [92]) and 2870 cm^{-1} infer symmetrical and asymmetrical CH_3 stretching vibrations [92]. A further symmetrical CH_3 stretch is observed only in the Raman spectrum at 2930 cm^{-1}. This is in accordance with the literature [92]. It is more difficult to assign bands specifically to the phenyl substituent of $[CrCl_3(pyphenyl)_3]$ as the vibrations are very similar to those of pyridine. Note that the opposite of the pytb compound is seen as there is a band at 3013 cm^{-1} visible only in the IR spectrum [97]. Figure 2.38 highlights the important vibrations.

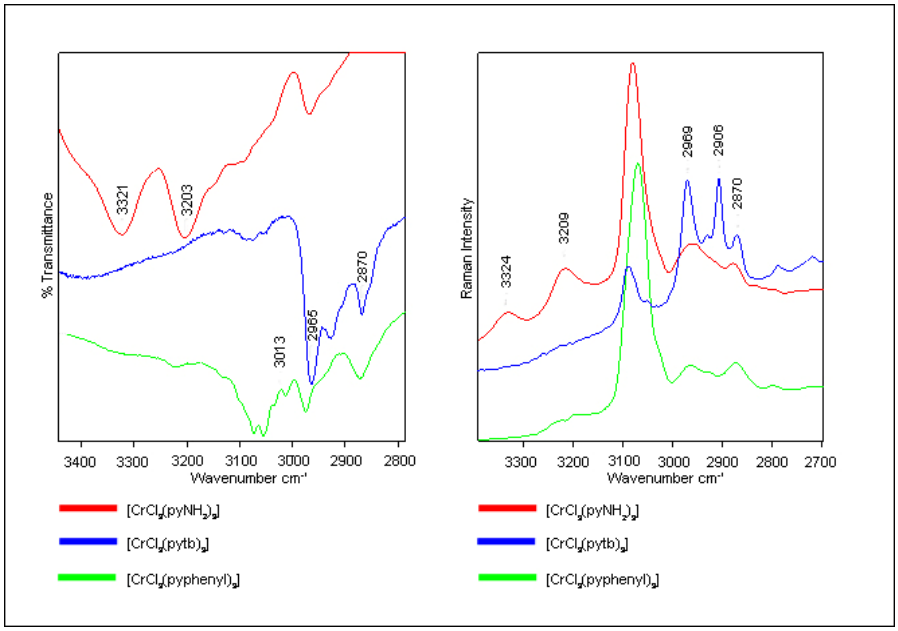

Figure 2.38 **IR and Raman spectra of $[CrCl_3(pyNH_2)_3]$ (red), $[CrCl_3(pytb)_3]$ (blue), $[CrCl_3(pyphenyl)_3]$ (green) in the region 3321 – 2869 cm^{-1}**

2.4.1.2 Region 1638–1045 cm^{-1}

This is an interesting region which possesses a combination of ring and C–H vibrations pertaining to the different pyridine derivatives. In all cases there is a strong correlation with the literature in terms of those bands that experience shifts and those that do not, as a consequence of coordination.

$[CrCl_3(pyNH_2)_3]$

Two amino-specific vibrations are observed at 1638 (δNH_2) and 1285 cm^{-1} (ν C–NH_2), where their free ligand positions are 1648 and 1268 cm^{-1} respectively. Both shifts indicate coordination to the metal centre, backed by the literature, even though a downward shift for the δNH_2 mode is perhaps surprising as most coordinating shifts are in the opposite direction. The remaining bands, with the exception of 1196 cm^{-1}, are associated with $pyNH_2$ vibrations, with more than half shifting to higher frequencies [96]. Note the comparison between IR and Raman band intensities – IR being predominantly stronger. The vibrational shifts are presented in Table 2.14 while the spectrum is highlighted in Figure 2.39).

Table 2.14 Infrared and Raman band shifts in the region 1638 – 1045 cm^{-1}

Free $pyNH_2$ IR/RAMAN /cm^{-1}	**$[CrCl_3(pyNH_2)_3]$ IR / cm^{-1}**	**RAMAN / cm^{-1}**	**Shift / cm^{-1} IR/RAMAN**
1602	1616sh	1617m	14/15
1556	1556m	1556vw	0
1506	1520s	1523w	14/17
1440	1459m	1461w	19/21
1333	1354m	1350w	21/17
1268	1285m	1285w	17/17
1213	1213s	1218w	0/5
1055	1055s	1059m	0/4

1196 cm^{-1} is more than likely a C–H vibration associated with the pyridine ring, with no shifting observed [92].

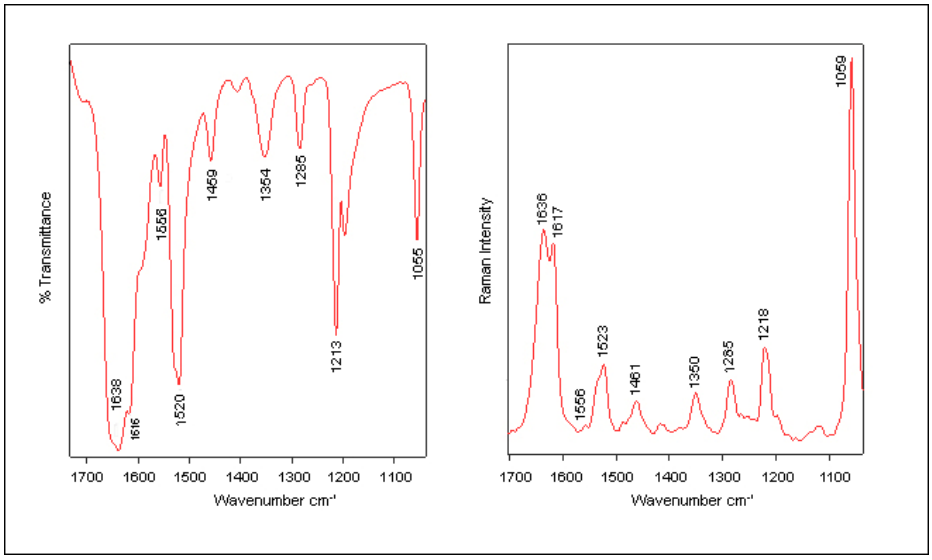

Figure 2.39 IR and Raman spectra of $[CrCl_3(pyNH_2)_3]$ in the region 1638 – 1045 cm^{-1}

$[CrCl_3(pytb)_3]$

All expected ligand vibrations are clearly visible and easily assignable. The five tertiary butyl-specific vibrations exhibit a degree of shifting indicative of metal–ligand coordination and can be assigned to symmetrical (1421 cm^{-1}) and asymmetrical (1475, 1463, 1368 cm^{-1}) CH_3 deformations, as well as C–C stretching modes (1128 cm^{-1}).

The remainder are a combination of ring and C–H pyridine vibrations and, as in the amino compound, more than half are shifted to higher frequencies With respect to IR and Raman band intensity, all vibrations correspond well with the literature [92]. The band shifts as well as the spectra are presented in Table 2.15 and Figure 2.40 respectively.

Table 2.15 IR and Raman band shifts in the region 1638 – 1045 cm^{-1}

Free pytb IR/RAMAN /cm^{-1}	$[CrCl_3(pytb)_3]$ IR / cm^{-1}	$[CrCl_3(pytb)_3]$ RAMAN / cm^{-1}	Shift / cm^{-1} IR/RAMAN
1596/1596	1617s	1618m	21/22
1544/1543	1556m	1556vw	12/12
1494/1495	1501s	1501w	7/6
1274/1274	1274s	1275m	0/1
1224/1224	1230s	1234m	6/10
1203/1202	1203m	1202m	0/0
1074/1074	1068s	1072s	-4/-2

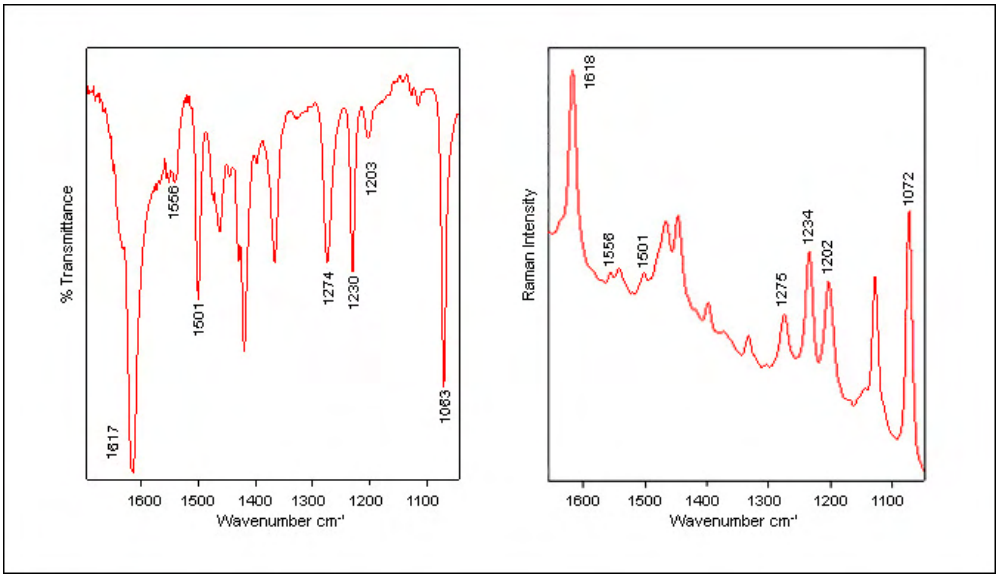

Figure 2.40 IR and Raman spectra of $[CrCl_3(pytb)_3]$ in the region 1638 – 1045 cm^{-1}

$[CrCl_3(pyphenyl)_3]$

As in the region 3321 to 2869 cm^{-1}, there is difficulty in differentiating between the heterocyclic pyridine and the phenyl vibrations, and a large amount of band superposition is expected. However, it is observed that neither free pyridine nor coordinated pyridine possesses bands at 1514, 1289 and 1045 cm^{-1}, and these are therefore tentatively assigned as phenyl-specific modes. Interestingly, the two former (of three) vibrations are considerably stronger in the Raman spectrum than in the IR spectrum, while the latter band at 1045 cm^{-1} is too weak in the Raman spectrum to be observed.

The only evidence of shifting is observed with the band at 1612 cm^{-1} in the complex that is assignable to coordinated pyridine and has shifted from 1600 cm^{-1} [97]. Both the IR and Raman spectra are presented in Figure 2.41.

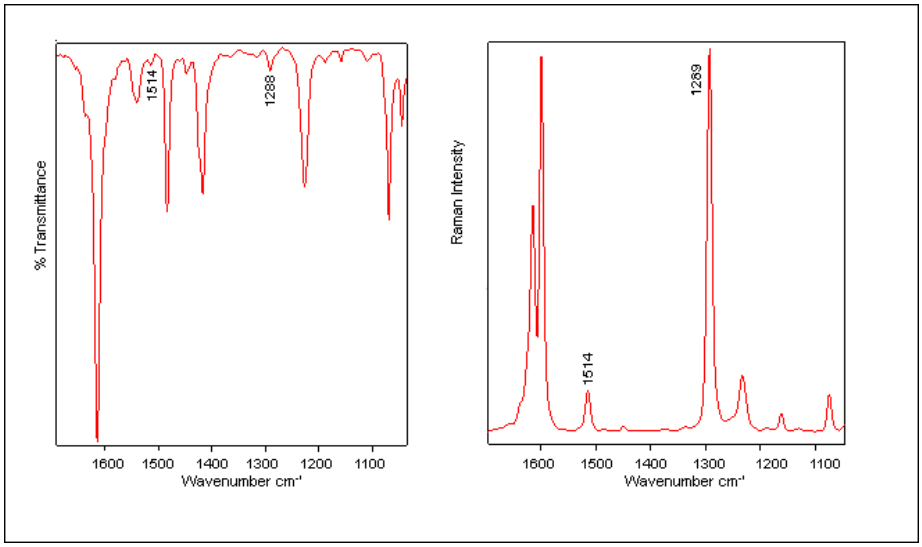

Figure 2.41 **IR and Raman spectra of $[CrCl_3(pyphenyl)_3]$ in the region 1638 – 1045 cm^{-1}**

2.4.1.3 Region 1030–499 cm^{-1}

This is a region with yet more vibrational evidence associated with both pyridine and the respective para–substituents. In addition, there is also valuable information pertaining to both ligand substitution and the strength of specific bonds.

$[CrCl_3(pyNH_2)_3]$

Bands associated with both $pyNH_2$ ring and C–H vibrations in accordance with the literature are present. A number of these bands have shifted from the free ligand positions [96] (see Table 2.16). The spectra are presented in Figure 2.42.

Table 2.16 **IR and Raman band shifts in the region 1030 – 499 cm^{-1}**

Free $pyNH_2$	**$[CrCl_3(pyNH_2)_3]$**		**Shift / cm^{-1}**
IR / cm^{-1}	**IR / cm^{-1}**	**RAMAN / cm^{-1}**	**IR/RAMAN**
991	1022s	1022m	31/31
842	855w	858vs	13/16
824	827s	not visible	3/-
661	667vw	667m	6/-
536	571s	569w	35/33
522	528s	528w	6/-

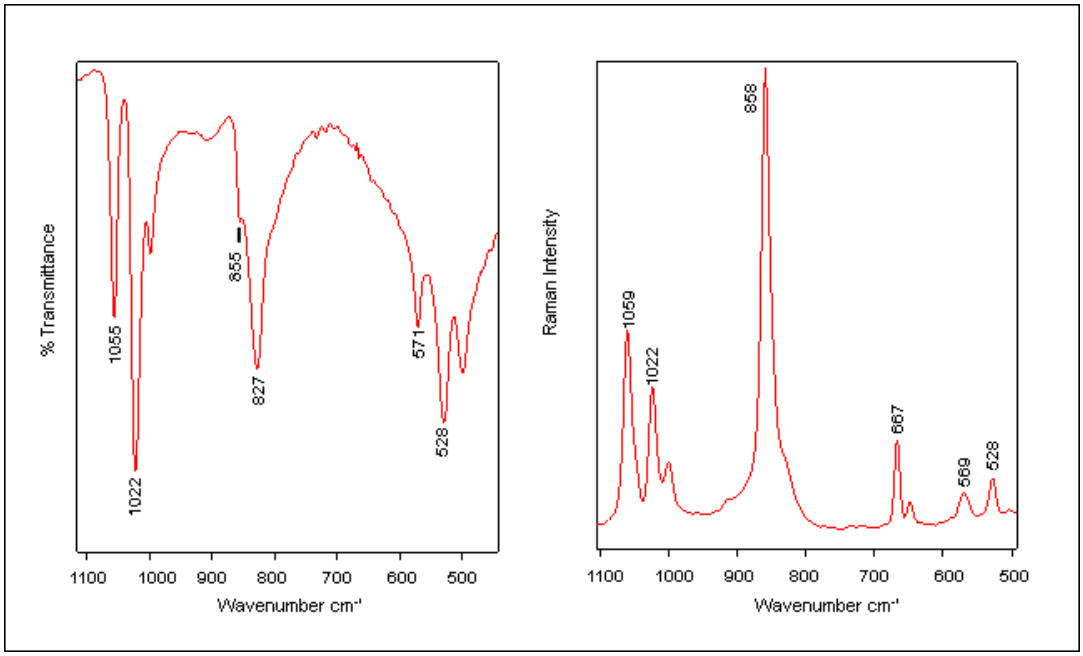

Figure 2.42 IR and Raman spectra of $[CrCl_3(pyNH_2)_3]$ in the region 1030 – 499 cm^{-1}

$[CrCl_3(pytb)_3]$

As well as the expected pytb ring and C–H vibrations, substituent specific bands at 928 (CH_3 rock), (tertiary butyl skeletal stretch) and 548 cm^{-1} (tertiary butyl rock) are present [92]. Vibrational shifts are visible in Table 2.17 while the spectra of $[CrCl_3(pytb)_3]$ is presented in Figure 2.43.

.

Table 2.17 IR and Raman band shifts in the region 1030 – 499 cm^{-1}

Free pytb	$[CrCl_3(pytb)_3]$		Shift / cm^{-1}
IR / cm^{-1}	IR / cm^{-1}	RAMAN / cm^{-1}	IR/RAMAN
991	1028s	1028s	37/37
927	928w	931w	1/4
842	844m	844w	2/2
821	831s	not visible	10
711	729m	730s	18/19
669	665w	668m	-4/-1
569	573s	575w	4/6
534	548w	549w	14/15

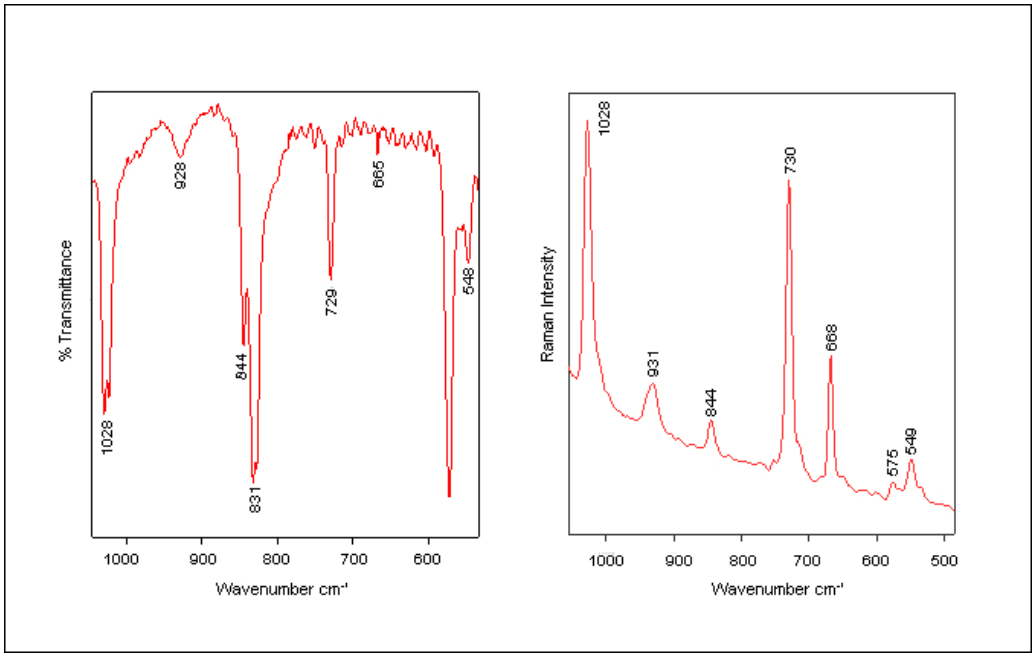

Figure 2.43 **IR and Raman spectra of $[CrCl_3(pytb)_3]$ in the region 1030 – 499 cm^{-1}**

$[CrCl_3(pyphenyl)_3]$

As in the previous region, comparative studies allow tentative differentiations between the pyridine and phenyl modes. The bands at 839, 769, 731 and 565 cm^{-1} are assigned to phenyl while the remainder are associated with pyridine [97]. Band shifts and spectra are presented in Table 2.18 and Figure 2.44 respectively.

Table 2.18 **IR and Raman band shifts in the region 1030 – 499 cm^{-1}**

Free pyphenyl	**$[CrCl_3(pyphenyl)_3]$**		**Shift / cm^{-1}**
IR / cm^{-1}	**IR / cm^{-1}**	**RAMAN / cm^{-1}**	**IR/RAMAN**
1017	1032m	1032s	15/15
991	1012m	1014m	21/23
832	839m	841w	7/9
762	769s	760m	7/-2
731	731m	not visible	0
687	694m	not visible	7
608	625s	617w	17/9
561	565m	564w	4/3

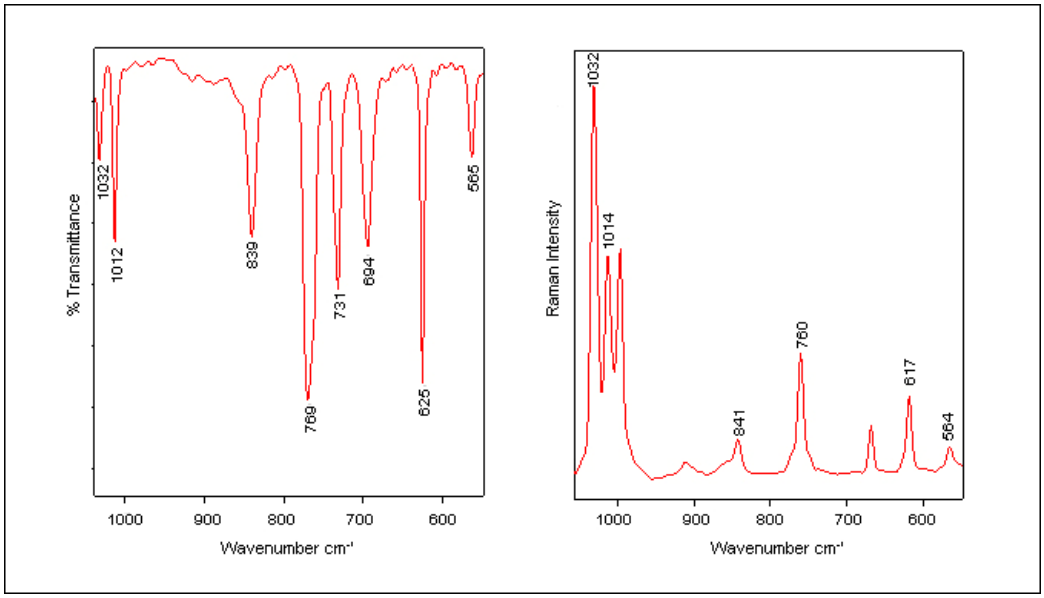

Figure 2.44 IR and Raman spectra of $[CrCl_3(pyphenyl)_3]$ in the region 1030 – 499 cm^{-1}

2.4.1.4 Ligand substituents

Here the importance of analysing a compound of known crystal structure is exemplified, in this case $[CrCl_3(pytb)_3]$. One of the strongest indications of coordinated thf from the $[CrCl_3(thf)_3]$ precursor is a strong band at around 856 cm^{-1} and its presence in these compounds would be indicative of partial substitution of thf ligands. All three compounds possess a band in and around this region at 855 ($pyNH_2$), 844 (pytb) and 839 cm^{-1} (pyphenyl), yet they can be confidently assigned to respective ligand vibrations [92, 96, 97, 98].

What the spectrum of a known crystal structure does is rule out ambiguity in assignments. Note that the amino complex is the only one of the three where the Raman vibration is stronger than the IR.

2.4.1.5 Bond strength

According to Topacli and Bayari [75] there is much information to be gained from the shifting of pyridine ring vibrations to higher frequencies upon coordination to the chromium centre. The extent to which the pyridine vibrations shift once coordinated to the metal can be correlated to the mass, nature, number and position of the various

pyridine substituents and can be explained as the coupling of the internal modes of the aromatic molecule with the metal–nitrogen (M–N) vibrations [75]. The data to date show that the majority of the ring vibrations are indeed shifted to higher frequencies upon coordination. The band in and around 990 cm^{-1} is a characteristic pyridine ring breathing band. It is also present in the para–substituted derivatives. If one considers the mass of the substituents, one notices the correlation between increasing mass and shifting of this band. The smallest substituent by mass is the amino group, which has bands at 997 and 1022 cm^{-1}. When compared with the free $pyNH_2$ ligand, it is clear that the former is a $pyNH_2$-specific band shifted from 949 cm^{-1}, while the latter at 1022 cm^{-1} is the characteristic ring breathing mode. The next largest is the tertiary butyl group with a band at 1028 cm^{-1} and the largest is the phenyl group with a band at 1030 cm^{-1}. The phenyl also has a band at 1012 cm^{-1}, but this was initially assigned to a C–H band associated with the para-positioning [97]. Once again, the value of crystal structural data combined with spectroscopy is highlighted as studies discussed in Chapter 4 will reveal that in fact 1011 cm^{-1} has shifted from 991 and 1030 cm^{-1} is a C–H vibration of the pyphenyl ligand, probably shifted from 1017 cm^{-1}. The band at 997 cm^{-1} in the Raman spectrum is assigned to a trigonal ring breathing mode of the phenyl ring [113]. These shifts are highlighted in Table 2.19 and Figure 2.45.

Table 2.19 **Shifting of the characteristic ring breathing vibration in $[CrCl_3py_3]$, $[CrCl_3(pyNH_2)_3]$, $[CrCl_3(pytb)_3]$ and $[CrCl_3(pyphenyl)_3]$**

Pyridine / cm^{-1}	**$[CrCl_3py_3]$ / cm^{-1}**	**Shift / cm^{-1}**
990s	1014m	24

$pyNH_2$ / cm^{-1}	**$[CrCl_3(pyNH_2)_3]$ / cm^{-1}**	**Shift / cm^{-1}**
991s	1022	31

pytb / cm^{-1}	**$[CrCl_3(pytb)_3]$ / cm^{-1}**	**Shift / cm^{-1}**
995vs	1028	33

pyphenyl / cm^{-1}	**$[CrCl_3(pyphenyl)_3]$ / cm^{-1}**	**Shift / cm^{-1}**
1001s	1011	10

The substituents also have an effect on the strength of the metal–nitrogen bonds. In fact, the order of the M–N ligand stretching vibrations reflects the increasing strength of the M–N bond. Therefore, as well as the mass effects, the increase in charge density on the pyridine ring brought about by the various electronic effects of the substituents is also influential. The concept of releasing charge density into the ring and thereby increasing the electron density on the nitrogen atom has the effect of strengthening the M–N bond [75]. One would expect the amino group, as the strongest electron-donating group, to exhibit the greatest shift, followed by the phenyl and tertiary butyl groups which release similar charges into the pyridine ring, with the unsubstituted pyridine complex shifting the least. This is not entirely reflected in the recorded spectra although what is interesting is that similar results were found when investigating the three pyridine derivatives coordinating to other metal compounds [75, 92, 96, 97].

It was suggested that the small shifts in the 4–aminopyridine compound may be due to hydrogen bonding of the NH_2 group [75]. Furthermore, the fact that $[CrCl_3(pyNH_2)_3]$ in particular exhibits these shifts also allows one to conclude that it is the endocyclic nitrogen lone pair that is involved in metal coordination as opposed to the amino group nitrogen [96] (supported by the N–H stretching vibrations discussed earlier).

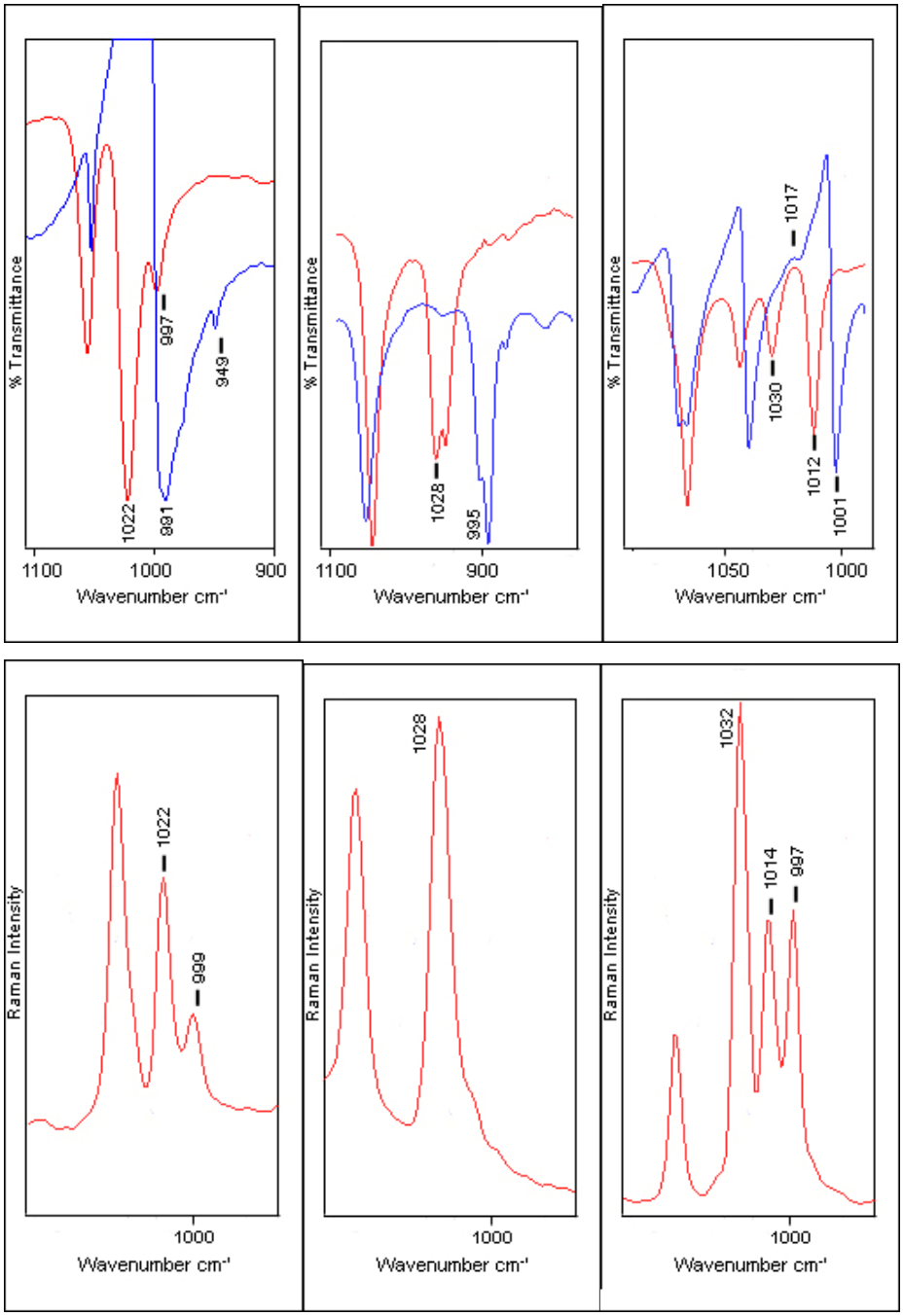

Figure 2.45 **Shifting of the characteristic ring breathing vibration in the IR spectra of $[CrCl_3(pyNH_2)_3]$, $[CrCl_3(pytb)_3]$ and $[CrCl_3(pyphenyl)_3]$, relative to free ligand positions (blue). Raman spectra of $[CrCl_3(pyNH_2)_3]$, $[CrCl_3(pytb)_3]$ and $[CrCl_3(pyphenyl)_3]$**

The effects of the substituents are not limited to the pyridine ring vibrations. The FIR spectra of metal–pyridine compounds assigns the band in and around 221 cm^{-1} to the Cr–

N stretch vibration [41, 80, 81]. Therefore the presence of this band is most certainly a strong indication that the substitution of the thf ligands has taken place and the pyridine is now coordinated to the chromium centre. It must be noted that this band is metal-sensitive and the value of 221 cm^{-1} defines Cr–N bonds specifically. The literature suggests that this band shifts to lower frequencies as the mass of the substituent on the pyridine ligand increases [81]. With respect to the pyridine compounds at hand, where expected, downward shifting has occurred. However, apart from the $[CrCl_3(py)_3]$ compound with an expected band at 221 cm^{-1}, only the pytb compound has a single decisive band in this region. This band is at 213 cm^{-1}, which conforms to the literature suggestion [81]. The amino and phenyl spectra are less clear as they both possess bands at 219 and 213 cm^{-1}. One would expect the shift of both these substituents to be of a similar if not greater (especially the bulky phenyl) magnitude than pytb, hence the value of 213 cm^{-1} is more sensible. However, when one compares these values with those in section 1 of the bipyridine compounds, it can be seen that it was in fact the phenyl that shifted the most, with the tertiary butyl and amino showing no shifting. It is therefore clear that the environment of the ligands must be taken into account and one cannot simply rely on the mass of substituents for definitive shifts.

2.4.1.6 Region 488–213 cm^{-1}

It is in the FIR spectra where a great deal of interest lies as the presence of metal–ligand vibrations confirm coordination. The three bands indicative of Cr–Cl vibrations in the *mer* arrangement are duly present in all the compounds [80]. This also implies that the precipitates are monomeric as pyridinium-type species such as $[Hpy][CrCl_4(py)_2]$ would have shown four Cr–Cl bands in accordance with both the literature [99] and the data presented in the later chapters.

An interesting band, which is unassignable in terms of the literature, is that at 268 cm^{-1}. The fact that it is present in all three substituted pyridine compounds and not in the unsubstituted pyridine compound may lead one to infer that it stems from a para–position substituent effect. Moreover, the possibility of the band being indicative of Cr–O [82] and thus coordinated thf was ruled out as the band is also present in $[CrCl_3(pytb)_3]$.The effects

of the substituents are not limited to the pyridine ring vibrations. The FIR spectra of metal–pyridine compounds assign the band in and around 221 cm^{-1} to the Cr–N stretch vibration [41, 80, 81]. Therefore the presence of this band is most certainly a strong indication that substitution of the thf ligands has taken place and the pyridine is now coordinated to the chromium centre. It must be noted that this band is metal-sensitive and the value of 221 cm^{-1} defines Cr–N bonds specifically. The literature suggests that this band shifts to lower frequencies as the mass of the substituent on the pyridine ligand increases [81]. With respect to the pyridine compounds at hand, where expected, downward shifting has occurred. However, apart from the $[CrCl_3(py)_3]$ compound with an expected band at 221 cm^{-1}, only the pytb compound has a single decisive band in this region. This band is at 213 cm^{-1}, which conforms to the suggestion in the literature [71]. The amino and phenyl spectra are less clear as they both possess bands at 219 and 213 cm^{-1}. One would expect the shift of both these substituents to be of a similar magnitude to, if not greater (especially the bulky phenyl) than, the tertiary butyl, hence the value of 213 cm^{-1} is more sensible. However, when these values are compared with those of the bipyridine compounds, it is apparent that it was in fact the phenyl that shifted the most, with the tertiary butyl and amino showing no shifting. It is therefore clear that the environment of the ligands must be taken into account and one cannot simply rely on the mass of the substituents for definitive shifts.

2.4.1.7 Concluding remarks

All of the vibrational frequencies of the pyridine and substituted pyridine compounds have been compared with the structures in this study published by Brennan [100] and are discussed later in Chapter 3, which includes one equivalent of these ligands along with bipyridine in the compounds. As expected, the relevant bands were all present except for the CH_3 rocking vibration of the pytb compound at 927 cm^{-1} [92]. The correlation between the FIR bands was also made with the confirmation of the Cr–Cl bands and the Cr–N bands (see Section 2.4 for Cr–N detail).

Table 2.20 Vibrational assignments of $[CrCl_3(py)_2DMF]$ (5), $[CrCl_3(pyNH_2)_3]$ (6), $[CrCl_3(pytb)_3]$ (7) and $[CrCl_3(pyphenyl)_3]$ (8)

5	6		7		8		Assignment
IR / cm^{-1}	IR / cm^{-1}	RAMAN / cm^{-1}	IR / cm^{-1}	RAMAN / cm^{-1}	IR / cm^{-1}	RAMAN / cm^{-1}	
-	3321s	3324w	-	-	-	-	$\nu(NH_2)$ asym (76, 96)
-	3203s	3209w	-	-	-	-	$\nu(NH_2)$ sym (76, 96)
3114w, 3080w, 3050w, 3032w	3092s	3082m	3081m	3088m	3072m	3073m	ν(CH) (97, 73, 74, 96, 92)
-	-		-	-	3013m	-	ν(CH) (97)
3000w, 2940w	-	-	-	-	-	-	ν(CH of CH_3 - DMF) (87)
2804w, 2871w	-	-	-	-	-	-	ν(CH) of carbonyl - DMF (87)
-	-	-	-	-	2977m	2982vw	unassigned
-	-	-	2965vs	2969s	-	-	ν (CH_3) asym (92)
-	-	-	-	2930w	-	-	ν (CH_3) sym (92)
-	2966s	2961w	-	-	-	-	unassigned
-	-	-	-	2906m	-	-	ν (CH_3) sym (92)
-	-	-	2870s	2870m	-	-	ν (CH_3) sym (92)
-	-	-	-	-	2873m	2873w	unassigned
1660vs, 1649vs	-	-	-	-	-	-	ν(C=O) of carbonyl (88)
-	1638s	1636m	-	-	-	-	$\delta(NH_2)$ (26)
1606s	1616sh	1617m	1617vs	1618vs	1612vs	1614m,1600vs	ν_{ring} (97, 73, 74, 96, 92)
-	1556m	1556vw	1556w	1556w	1539m	-	ν_{ring} (97, 73, 74, 96, 92)
-	1520s	1523w	1501m	1501w	1514vw	1514m	ν_{ring} (97, 96, 92)
1485m	-	-	-	-	1483s	1483vw	ν_{ring} (97, 73, 74)

5	6		7		8		Assignment
-	-	-	1475m	-	-	-	(CH_3) asym def (92)
-	1459m	1461w	1463m	1466m	-		ν_{ring} (97, 96)
1447s	-	-	1446w	1446m	-	-	(CH_3) asym def (92) / ν_{ring} (73, 74)
1433s	-	-	-	-	-	-	$\delta(CH_3)$ - DMF (87)
-	-	-	1421s	1420vw	-	-	(CH_3) sym def (92)
-	-	-	-	-	1417s	1407vw	δ(CH) (97)
1391m	-	-	-	-	-	-	δ(NCH) carbonyl (87)
-	-	-	1368m	1371vw	-	-	(CH_3) asym def (92)
1360s	1354m	1350w	-	-	-	-	ν_{ring} (96)
-	-	-	-	-	1288w	1289vs	ν_{ring} + δ(CH) (97)
-	1285m	1285w	-	-	-	-	$\nu(C\text{-}NH_2)$ (96)
-	-	-	1274m	1275m	-	-	δ(CH) (92)
1247m	-	-	-	-	-	-	ν(C-N) asym of $N(CH_3)_2$ (87)
-	-	-	1230m	1234m	1227s	1232m	δ(CH) (97, 82)
1219s	1213s	1218w	-	-	-	-	δ(CH) (96)
-	1196m	1197w	1203w	1202m	-	-	δ(CH) / ν (CC) (97, 96)
1163w, 1152w	-	-	-	-	1160vw	1160m	δ(CH) (97, 73, 74)
1126m	-	-	1128w	1128m	-	-	ν (CC) (92) / CH_3 def – DMF (91)
1095m	-	-	-	-	-	-	$\gamma(CH_3)$ - DMF (89)
1071m	-	-	1068s	1072s	1070s	1074m	δ(CH) (96) / ν_{ring} (97)
-	1055s	1059m	-	-	-	-	δ_{ring} (96)

5	6		7		8		Assignment
1045m	-	-	-	-	1045m	-	ν_{ring} (97) / γ (CH_3) - DMF (89)
-	-	-		-	1030m	1032s	δ(CH) (97)
1015m	1022s	1022m	1028m	1028s	1012m	1014m	Ring breathing (pyX) (97, 73, 74, 96, 92)
-	997m	999m	-	-	998vw	997m	Trigonal ring breathing (phenyl ring) (114) / pyNH_2 vib (96)
978w, 948w	-	-	-	-	-	-	γ(CHO) op - DMF (87)
-	-	-	928w	931w	-	-	(CH_3) rock (92)
-	855w	858vs	-	-	-	-	X-sens (96, 98)
-	827s	-	844m, 831s	844w	839m	841w	py breathing (92)
765s	-	-	-	-	769s	760m	$\delta_{ring} + \nu_{ring}$ (97)
-	-	-	729m	730s	731m	-	γ_{ring} def (92) / γ(CH) (97)
693s	-	-	-	-	694m	-	γ_{ring} (97)
658m	667vw	667m	665w	668m	-	-	δ_{ring} (96) / ν (CC) (92)
644s	-	-	-	-	-		δ_{ring} (73, 74)
-	-	-	-	-	625s	617w	δ_{ring} (97)
-	571s	569w	573s	575w	565m	564w	skeletal str (92)
-	-	-	548w	548w	-	-	rock (tb) (92)
-	528s	528w	-	-	-	-	X-sens (96)
-	499s	501vw	-	-	-	-	unassigned
448m	-	-	-	-	488m	-	δ_{ring} (97, 73, 74)
415m	414vw	412m	-	-	-	-	γ_{ring} (96)
-	-	-	-	-	406w	404m	γ_{ring} (96)

5	6		7		8		Assignment
397m, 390s	-	-	399w	399w	-	-	CCC def (tb) (92) / (CNC) def - DMF (91, 92)
358m	352m	-	371s	369w	366s	365m	Cr – Cl (80)
324m	334m	332w	353m	352w	355s	-	Cr – Cl (80)
302m	312m	-	326m	327w	331s	331w	Cr – Cl (80)
-	-	-	-	-	301w	305w	unassigned
284m, 230m	-	-	-	-	-	-	Cr - O
-	268w	270m	268m	265s	266s	263m	para - py
-	219w	216sh	-	-	219w	-	Cr – N (py) (41, 80, 81)
214	213w	-	213w	-	214w	213w	Cr – N (py) (41, 80, 81)

ν = stretching, δ = in plane bending, γ = out of plane bending, def = deformation, asym = asymmetric, sym = symmetric vs = very strong, s = strong, m = medium, w = weak, vw = very weak

2.4.2 COMPUTATIONAL STUDIES

Of the three substituent pyridine complexes, $[CrCl_3(pyNH_2)_3]$ and $[CrCl_3(pytb)_3]$ were selected as representative examples for computational study. This decision was reached on the basis of the more distinctive substituent vibrations, coupled with the fact that pyphenyl compounds have been selected for computational studies in the later chapters. A further reason for choosing $[CrCl_3(pytb)_3]$ was that its crystal structure has been determined.

For the most part, the experimental spectra correlate very well with their calculated equivalents in both complexes. Note that as a result of the same solid-state effects that were highlighted for the calculated IR spectrum of $[CrCl_3(py)_3]$ in Figure 2.10, the FIR spectra of these two complexes are not shown.

$[CrCl_3(pyNH_2)_3]$

With respect to the characteristic N–H and C–H stretching vibrations expected above 3000 cm^{-1}, the strongest correlation between experimental and calculated frequencies is seen in the IR spectra. However, as can be seen in Figures 2.46 and 2.47, the rest of the mid–vibrational region shows good frequency matches in both the IR and Raman spectra.

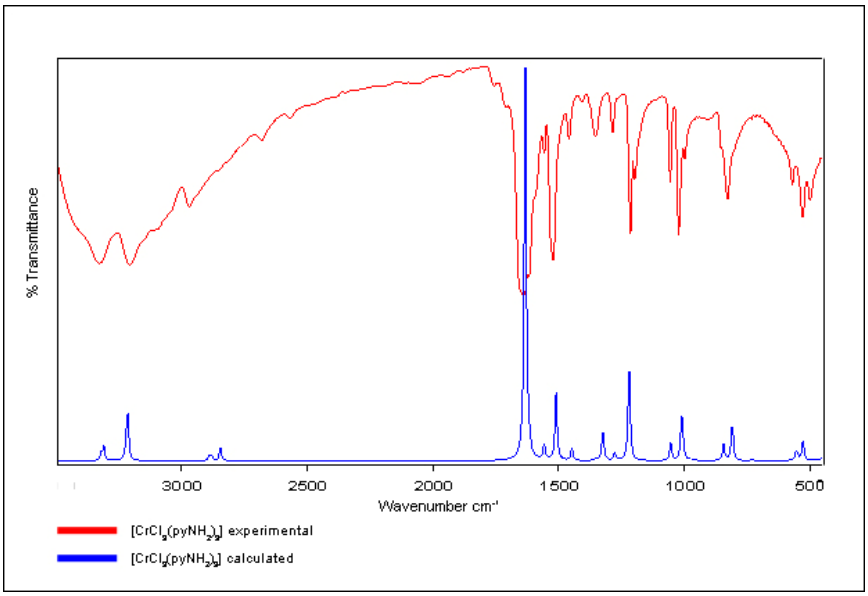

Figure 2.46 Experimental (red) and calculated (blue) MIR spectra of $[CrCl_3(pyNH_2)_3]$

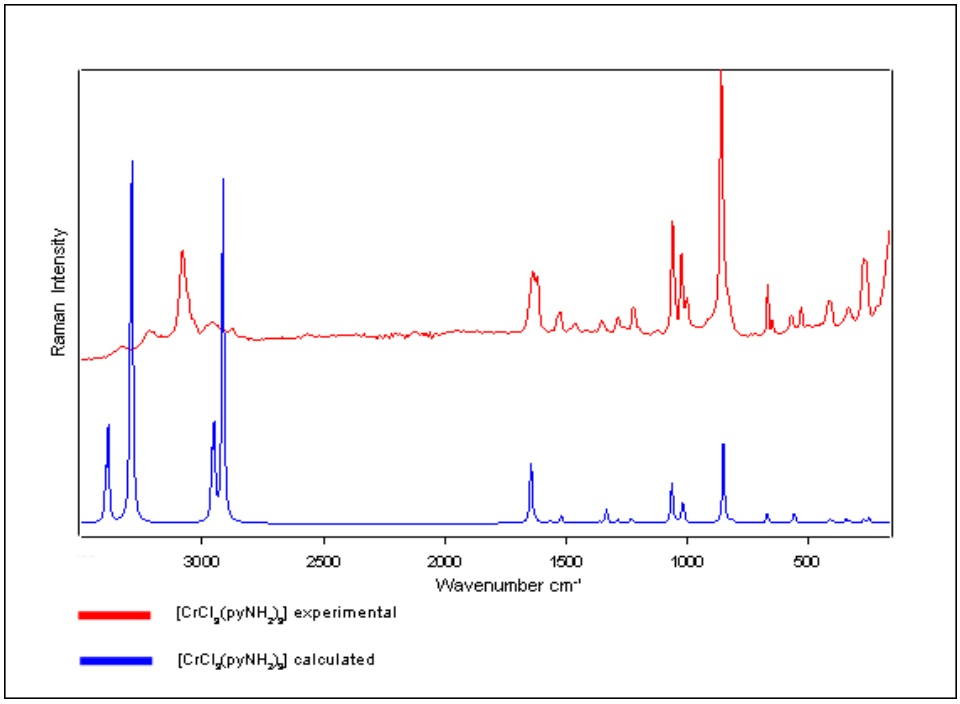

Figure 2.47 Experimental (red) and calculated (blue) Raman spectra of $[CrCl_3(pyNH_2)_3]$

Selected vibrations of importance have been documented in Table 2.21. The N–H vibrations are of interest as the literature assignments of asymmetrical and symmetrical stretching modes are confirmed by the computational data. The much-discussed ring breathing mode of pyridine is also of importance as the calculated values help to confirm that this has resulted from the shifting of the free pyridine vibration at ~992 cm^{-1}.

The FIR spectra metal–ligand vibrations correspond reasonably well, bearing in mind the expected solid state effects. Interestingly, the calculated Cr–N vibration is found at approximately the same value as in $[CrCl_3(py)_3]$, which is higher than that found in the literature [41, 80, 81].

Table 2.21 **Selected experimental and calculated IR and Raman band assignments for $[CrCl_3(pyNH_2)_3]$**

$[CrCl_3(pyNH_2)_3]$ IR / cm^{-1}		$[CrCl_3(pyNH_2)_3]$ Raman / cm^{-1}		Assignment	
Experimental	**Calculated**	**Experimental**	**Calculated**	**Experimental**	**Calculated**
3321	3310	3324	3391	$\nu(NH_2)$ asym	$\nu(NH_2)$ asym
3203	3214	3209	3292	$\nu(NH_2)$ sym	$\nu(NH_2)$ sym
1638	1637	1636	1643	$\delta(NH_2)$	$\delta(NH_2) + \nu_{ring}$
1285	1278	1285	1286	ν(C-NH_2)	C-NH_2 rock + ν_{ring}
1022	1011	1022	1018	Ring breathing ($pyNH_2$)	Ring breathing ($pyNH_2$)
352, 334, 312	343, 337	332	345, 339, 247	Cr-Cl	Cr-Cl
	327	-	329	-	NH wag
219, 213	295	216	297	Cr-N	Cr-N

ν = stretching, $\delta(NH_2)$ = scissoring

Table 2.22 **Scaling factors determined for $[CrCl_3(pyNH_2)_3]$**

Region / cm^{-1}	IR	Raman
0 – 1878	0.974597	0.980275
2980 – 3909	0.894264	0.916082

Unlike the unsubstituted tri–pyridine complex, both the HOMO and LUMO orbitals that were generated are centred on the chlorine atoms (Figure 2.48), which is a direct result of the resonance effects associated with amino-substituted delocalised systems.

HOMO **LUMO**

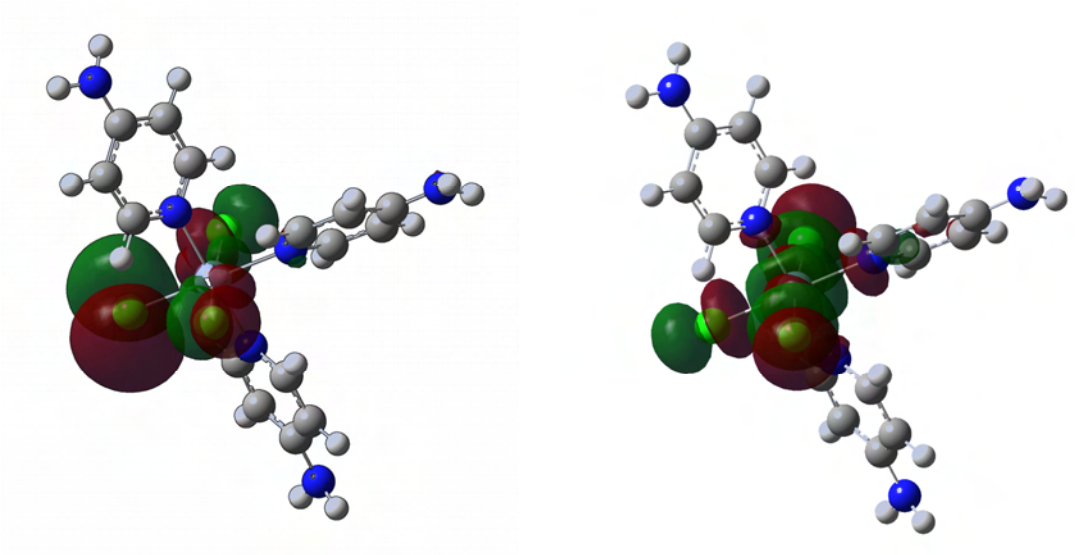

Figure 2.48 **HOMO and LUMO orbitals of $[CrCl_3(pyNH_2)_3]$**

$[CrCl_3(pytb)_3]$

As illustrated in Figures 2.49 and 2.50, there is an excellent agreement between the experimental and calculated spectra.

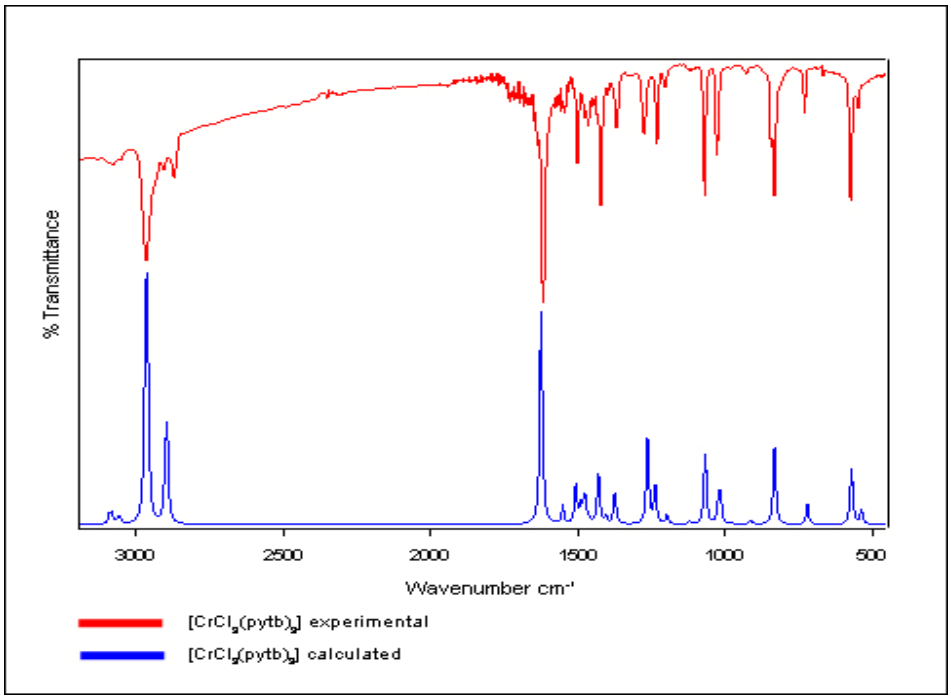

Figure 2.49 **Experimental (red) and calculated (blue) MIR spectra of $[CrCl_3(pytb)_3]$**

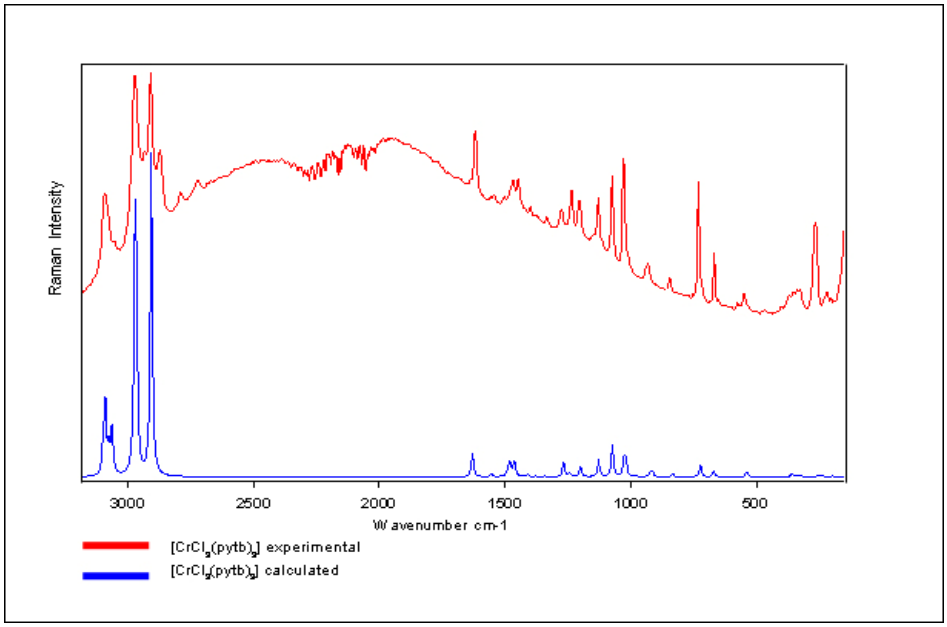

Figure 2.50 **Experimental (red) and calculated (blue) Raman spectra of $[CrCl_3(pytb)_3]$**

Characteristic substituent, ring and metal–ligand vibrations indicative of coordination are highlighted in Table 2.23. Of these, the calculated metal–ligand modes are the hardest to identify as many of the frequencies are a combination of modes.

Table 2.23 **Selected experimental and calculated IR and Raman band assignments for $[CrCl_3(pytb)_3]$**

$[CrCl_3(pytb)_3]$ IR / cm^{-1}		$[CrCl_3(pytb)_3]$ Raman / cm^{-1}		Assignment	
Experimental	Calculated	Experimental	Calculated	Experimental	Calculated
2965	2965	2969	2968	ν (CH_3) asym	ν (CH_3) asym
2870	2895	-	-	ν (CH_3) sym	ν (CH_3) sym
1617	1624	1618	1628	ν_{ring}	ν_{ring}
1368	1374	1371	1376	CH_3 asym def	CH_3 sym def
1029, 1023	1020	1028	1024	Ring breathing (pytb)	Ring breathing (pytb) + CH_3 wag
371, 353, 326	360, 352, 344	369, 352, 327	360, 354, 343	Cr-Cl	Cr-Cl + pytb rock + Cr-N
-	-	-	325	-	Pytb rock

-	322	-	325	-	Cr-Cl + CH_3 twist
268	276	265	276	Para py	Cr-N + CH_3 twist
213	262	-	-	Cr-N	Cr-N + CH_3 twist

Table 2.24 Scaling factors determined for $[CrCl_3(pytb)_3]$

Region / cm^{-1}	IR	Raman
0 - 1861	0.978328	0.980529
2826 - 3433	0.956048	0.957495

The nature of the tertiary butyl substituents reveals, as expected, HOMO and LUMO orbitals similar to those found in $[CrCl_3(py)_3]$, with the chlorine atoms being rich in electron density and thus susceptible to electrophilic attack. Likewise, the *trans* chlorine ring system is electron-deficient due to being found on a polarised axis and is thus open to attack by nucleophilic species. See Figure 2.51.

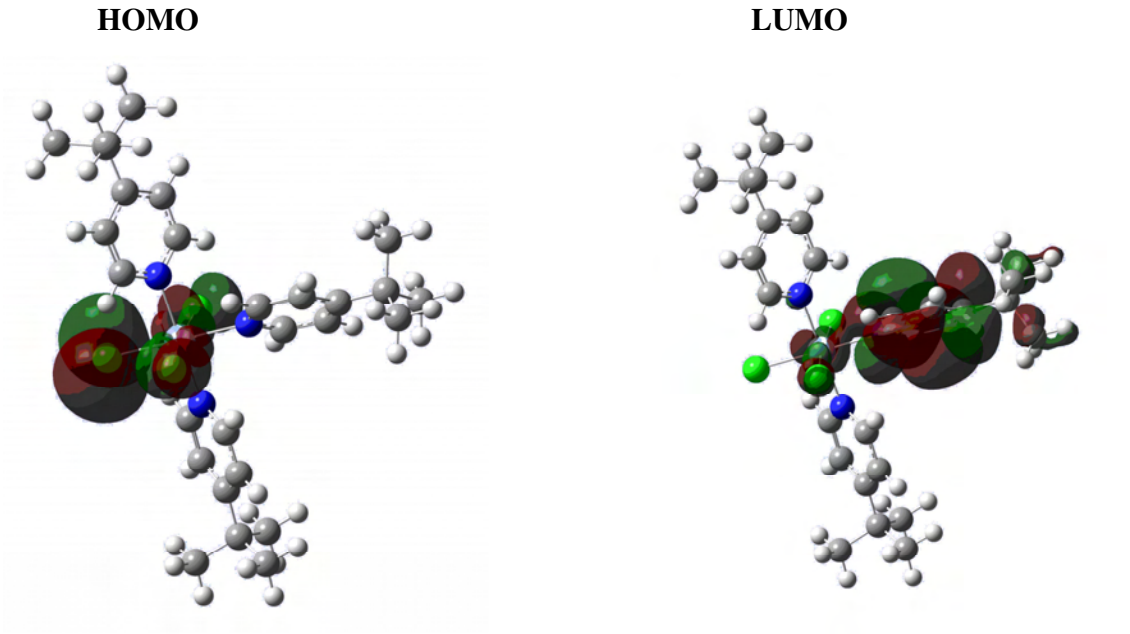

Figure 2.51 HOMO and LUMO orbitals of $[CrCl_3(pytb)_3]$

2.4.3 ^{1}H NMR OF [$CrCl_3(thf)_3$] AND THREE EQUIVALENTS OF PYPHENYL

The in situ ^{1}H NMR reaction study that followed the addition of three equivalents of unsubstituted pyridine to [$CrCl_3(thf)_3$] to yield [$CrCl_3(py)_3$] was repeated for the tri–para substituted para–phenylpyridine complex. The method and reaction conditions were unchanged, with acetone–d_6 remaining the solvent of choice. The resulting spectra are depicted in Figure 2.52 and show that after 173 minutes all pyphenyl resonances have disappeared, which infers complete coordination to the paramagnetic metal centre.

One had perhaps expected phenyl vibrations to remain present upon completion of the reaction on the basis that they are sufficiently far away from the paramagnetic centre, but this was not the case.

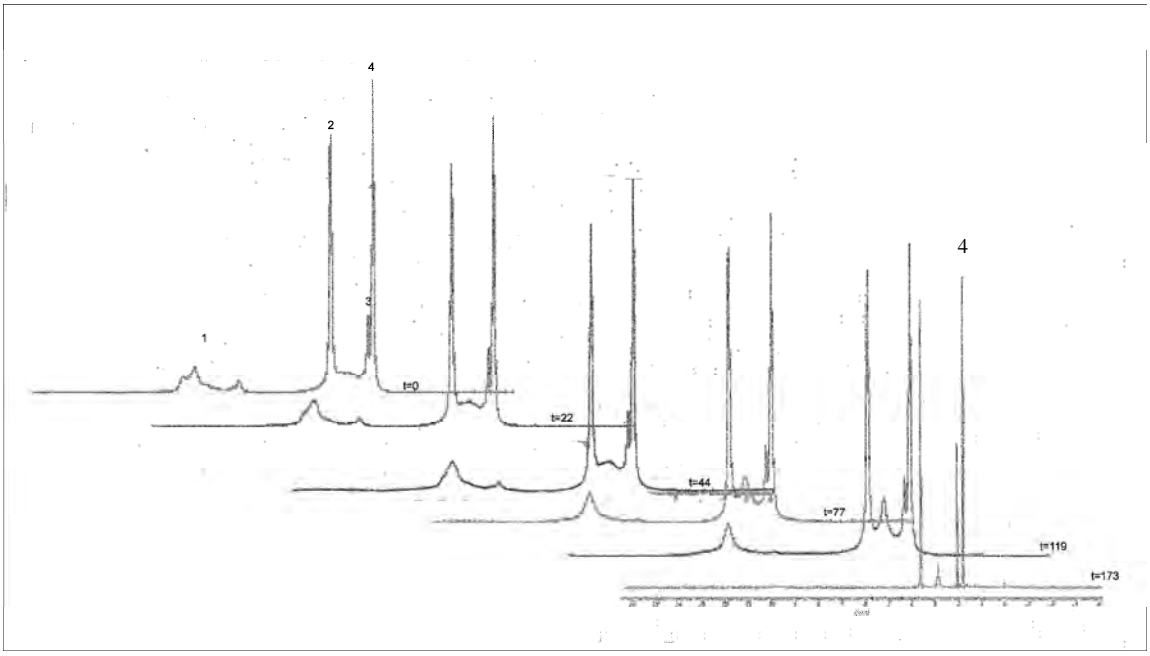

Figure 2.52 **Stacked ^{1}H NMR spectra for the reaction of pyphenyl with [$CrCl_3(thf)_3$] over time. 1 = pyphenyl, 2 = thf, 3 = acetone-d_6, 4 = thf**

2.4.4 MASS SPECTROMETRY

The FAB-MS of the [$CrCl_3$(pyphenyl)$_3$] precipitate is shown in Figures 2.53 and 2.54 and discussed as a representative example of the three substituted pyridine complexes. The isotopic distribution patterns of a number of fragments associated with the precipitate

sample of $[CrCl_3(pyphenyl)_3]$ were observed. These included the molecular ion, $[M]^+$ (m/z = 625), in addition to $[M–Cl]^+$ (m/z = 587), $[M–pyphenylCl]^+$ (m/z = 432) and $[M–pyphenylCl_2]^+$ (m/z = 397). All patterns were in agreement with the theoretically generated equivalents.

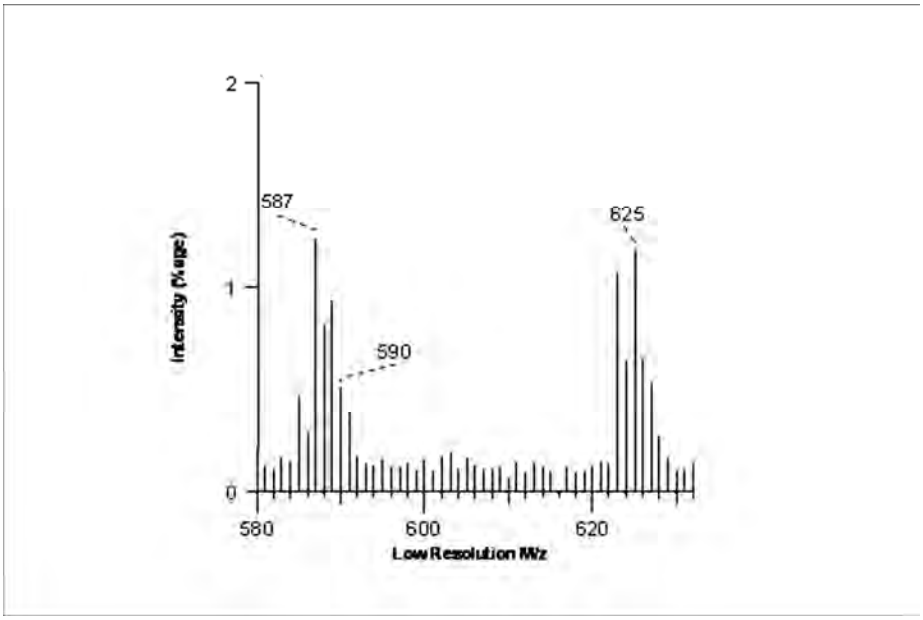

Figure 2.53 FAB-MS spectrum of $[CrCl_3(pyphenyl)_3]$

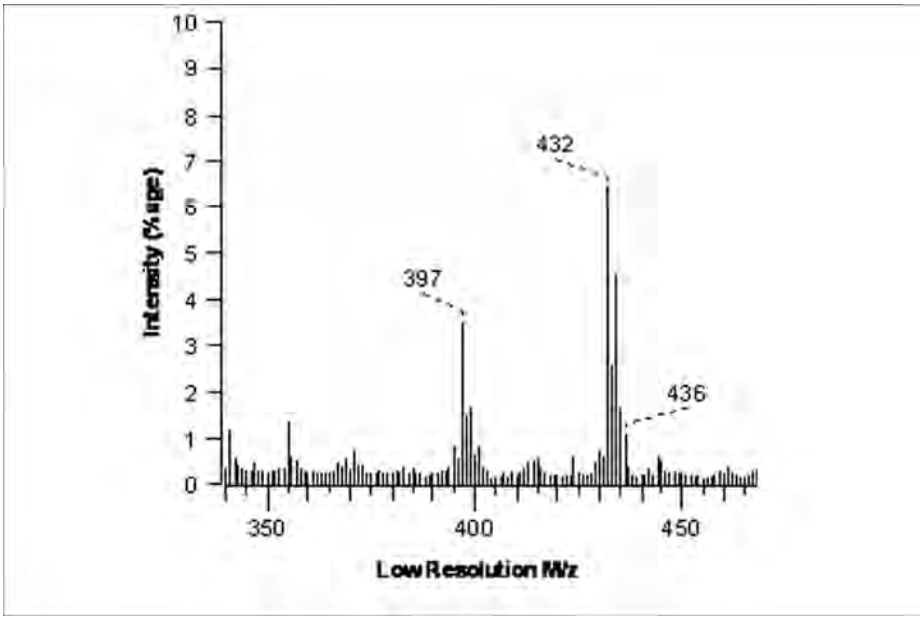

Figure 2.54 FAB-MS spectrum of $[CrCl_3(pyphenyl)_3]$

2.4.5 X-RAY CRYSTALLOGRAPHY

2.4.5.1 $[CrCl_3(pytb)_3]$

The single crystals of $[CrCl_3(pytb)_3]$ were isolated from the reaction mixture of the three equivalents of pytb added to $[CrCl_3(thf)_3]$ in thf that had been allowed to stir at room temperature overnight. The resulting dark green supernatant was left to stand and after 3 days dark green plate–like crystals were observed. Crystallographic data was then able to reveal the novel structural determination of $[CrCl_3(pytb)_3]$. A perspective drawing of the determined structured is shown in Figure 2.55.

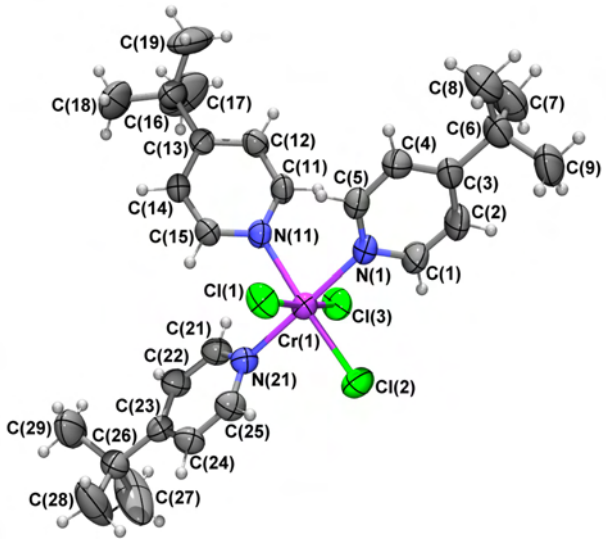

Figure 2.55 Perspective drawing of $[CrCl_3(pytb)_3]$ structure determined

The molecular structure of $[CrCl_3(pytb)_3]$ is an interesting variant on both the unsubstituted equivalent $[CrCl_3(py)_3]$ ([83] and this study) and the ethyl equivalent reported by Modec [101] known as *mer*–trichloro–tris(4–ethylpyridine)chromium(III), $[CrCl_3(pyEt)_3]$. Comparisons in terms of bond lengths, bond angles and torsion angles are of interest in order to gauge the effect of increasing the steric bulk of the ligand. In addition, a particularly interesting feature observed solely in the lattice packing arrangement of $[CrCl_3(pytb)_3]$ will also be discussed.

The chromium atom is coordinated to three chlorine atoms and three nitrogen atoms of the pytb ligands in a *mer* arrangement. What appear to be two disordered hexane and thf molecules are also found within the unit cell.

The coordination is approximately octahedral, with the largest deviation being the Cl(1)-Cr(1)–Cl(2) bond angle (93.73(4)°). All the other *cis* X–Cr–Y bond angles are in the range 86.58(7)–92.41(4)°.

As in all the analogous structures the ring systems are non–planar. However, it is observed that the $[CrCl_3(py)_3]$ structure determined in this study is the only structure in which the pyridine ligands twist anti–clockwise relative to the axial chlorine atoms. A clockwise twist is seen in the other structures, including this novel $[CrCl_3(pytb)_3]$ structure. Figure 2.56 clearly shows the clockwise twisting of the aromatic systems relative to the axial chlorine atoms.

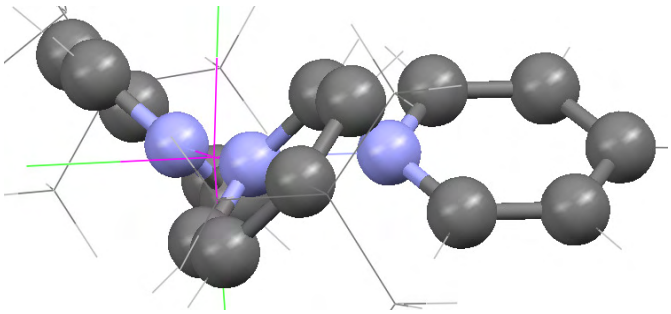

Figure 2.56 **Twisting of the aromatic systems relative to the axial chlorine atoms in $[CrCl_3(pytb)_3]$**

A comparison between the metal–ligand bond lengths of unsubstituted ethyl and tertiary butyl pyridines showed very little variation. It should also be noted that the disordered solvent molecules did not interact via hydrogen bonding with the complex. Table 2.25 gives the equivalent bond length, bond angle and torsion angle data highlighted in the three structures above while Table 2.26 gives the crystal and structural refinement data.

Table 2.25 **Selected bond lengths [Å], bond angles [°] and torsion angles [°] for [$CrCl_3(pytb)_3$]**

Cr(1)-N(1)	2.105(2)	Cr(1)-Cl(2)	2.3056(9)
Cr(1)-N(21)	2.105(2)	Cr(1)-Cl(1)	2.3248(9)
Cr(1)-N(11)	2.130(2)	Cr(1)-Cl(3)	2.3263(9)
N(1)-Cr(1)-N(11)	88.03(9)	N(11)-Cr(1)-Cl(1)	87.32(7)
N(21)-Cr(1)-N(11)	92.08(9)	Cl(2)-Cr(1)-Cl(1)	93.73(4)
N(1)-Cr(1)-Cl(2)	89.49(7)	N(1)-Cr(1)-Cl(3)	91.18(7)
N(21)-Cr(1)-Cl(2)	90.44(7)	N(21)-Cr(1)-Cl(3)	90.55(7)
N(1)-Cr(1)-Cl(1)	89.70(7)	N(11)-Cr(1)-Cl(3)	86.58(7)
N(21)-Cr(1)-Cl(1)	88.57(7)	Cl(2)-Cr(1)-Cl(3)	92.41(4)
Cl(1)-Cr(1)-N(1)-C(5)	-39.8(2)	Cl(1)-Cr(1)-N(11)-C(11)	126.7(2)
Cl(3)-Cr(1)-N(1)-C(5)	134.1(2)	Cl(3)-Cr(1)-N(11)-C(11)	-54.4(2)
Cl(1)-Cr(1)-N(1)-C(1)	141.9(3)	Cl(1)-Cr(1)-N(21)-C(25)	-49.2(2)
Cl(3)-Cr(1)-N(1)-C(1)	-44.3(3)	Cl(3)-Cr(1)-N(21)-C(25)	136.9(2)
Cl(1)-Cr(1)-N(11)-C(15)	-53.7(2)	Cl(1)-Cr(1)-N(21)-C(21)	126.3(2)
Cl(3)-Cr(1)-N(11)-C(15)	125.2(2)	Cl(3)-Cr(1)-N(21)-C(21)	-47.5(2)

Symmetry transformations used to generate equivalent atoms:
#1 y+1/3,-x+y+2/3,-z+2/3 #2 x-y+1/3,x-1/3,-z+2/3

Table 2.26 **Crystal data and structure refinement for [$CrCl_3(pytb)_3$]**

Empirical formula	$C_{30}\ H_{46}\ Cl_3\ Cr\ N_3\ O_{0.5}$	
Formula weight	615.05	
Temperature	293(2) K	
Wavelength	0.71073 Å	
Crystal system	Trigonal	
Space group	R 3	
Unit cell dimensions	a = 33.3142(14) Å	α = 90°

	b = 33.3142(14) Å β = 90°
	c = 15.6483(13) Å γ = 120°
Volume	15040.3(15) $Å^3$
Z	18
Density (calculated)	1.222 Mg/m^3
Absorption coefficient	0.606 mm^{-1}
F(000)	5 832
Crystal size	0.32 x 0.18 x 0.14 mm^3
Theta range for data collection	2.45 to 26.58°
Index ranges	-41<=h<=41, -40<=k<=41, -6<=l<=19
Reflections collected	27 543
Independent reflections	6 532 [R(int) = 0.0405]
Completeness to theta = 25.00°	99.9%
Absorption correction	Semi-empirical from equivalents
Max. and min. transmission	0.919 and 0.784
Refinement method	Full-matrix least-squares on F^2
Data / restraints / parameters	6 532 / 0 / 381
Goodness-of-fit on F^2	1.064
Final R indices [I>2σ(I)]	R1 = 0.0502, wR2 = 0.1264
R indices (all data)	R1 = 0.0758, wR2 = 0.1423
Extinction coefficient	0
Largest diff. peak and hole	0.388 and -0.289 $e.Å^{-3}$

Perhaps the most interesting aspect of this novel structure was the lattice packing arrangement. As can be seen in Figures 2.57 and 2.58 there are two distinct cavities or channels, with the larger of the two accommodating a molecule of the thf solvent.

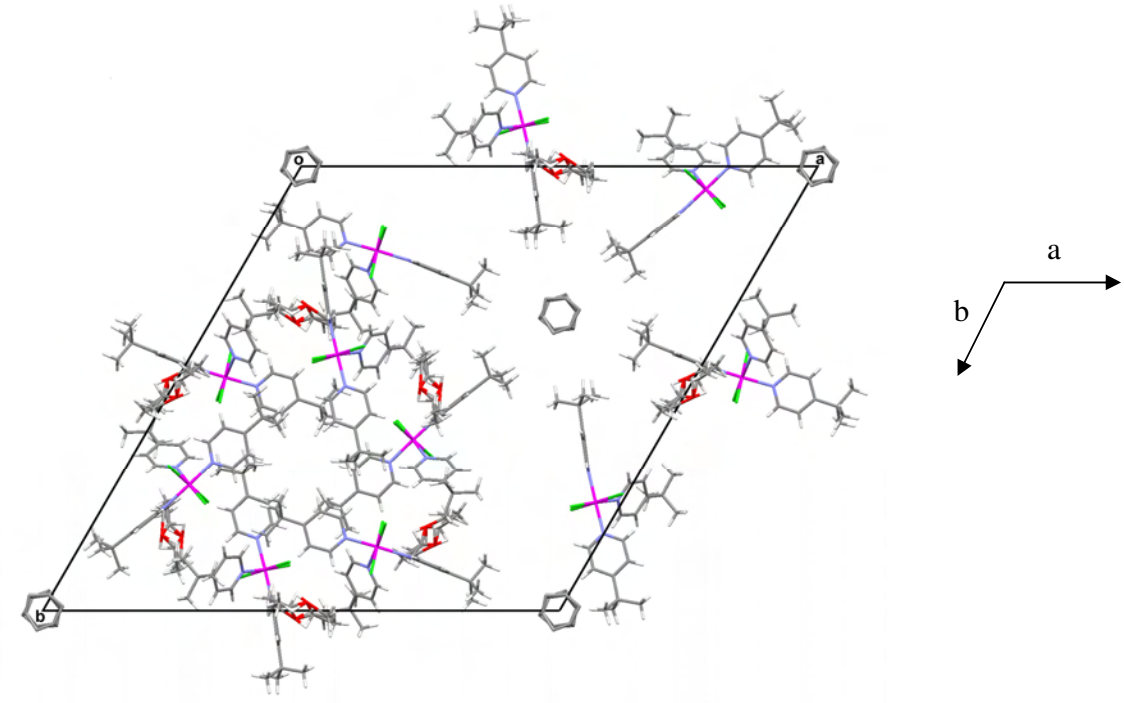

Figure 2.57 **Packing arrangement of $[CrCl_3(pytb)_3$**

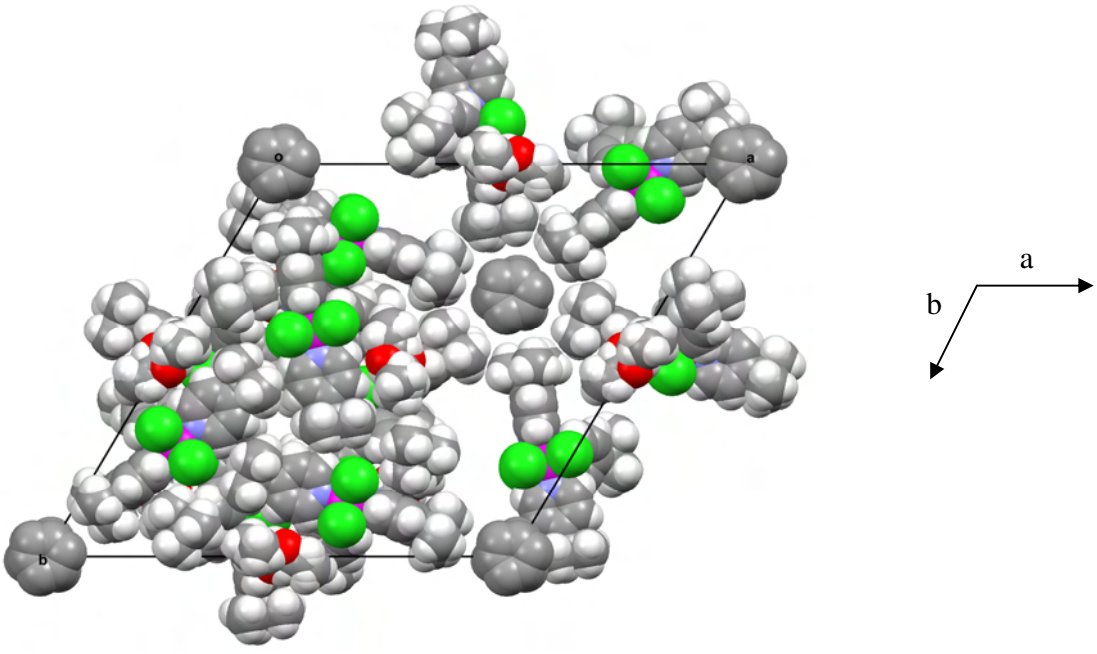

Figure 2.58 **Space fill representation of the packing arrangements**

This then opened the way for further experimentation with respect to being able to vary the encapsulated molecule by varying the reaction solvent. This, however, was not a straightforward task. The problem in choosing a solvent was that it had to solubilise the metal precursor in the reaction, as well as being of suitable size to be accommodated by the cavity. One was also wary of solvents that could potentially coordinate to the metal centre which would lead to unwanted competition for the available sites. This has already been observed in the compound $[CrCl_3(py)_2(DMF)]$ and will also be seen in later chapters.

After many different solvents had been investigated, the best choice appeared to be dioxane. As well as having the correct solubility, it is also of similar size and shape to the thf molecule. Unfortunately, the inability to grow single crystals of suitable size for structural data collection did not allow confirmation of dioxane encapsulation within the cavity.

In the light of the previous results given in this chapter, one must assume that this neutral monomeric compound was formed either from direct ligand substitution or by the symmetrical cleavage of the dimeric intermediate.

2.5 EXPERIMENTAL

2.5.1 SYNTHESIS OF $[CrCl_3(py)(thf)_2]$ (1) AND $[CrCl_3(py)_2(thf)]$ (2)

As stated above, these reactions yielded $[CrCl_3(py)_3]$ as product. Crystals supposedly of $[CrCl_3(py)_2(thf)]$ were grown in CH_3CN, with structural determination confirming the compound $[CrCl_3(py)_3]$.

Schlenk tubes were charged with $[CrCl_3(thf)_3]$ (0.19 g, 0.507 mmol and 0.17 g, 0.454 mmol respectively) and thf (20 cm^3). One and two molar equivalents of pyridine (0.04 ml and 0.07 ml) were added to the respective reaction solutions, affording immediate light green solutions and precipitates. The reactions were stirred overnight and after the same work-up as above (Et_2O 3 x 20 cm^3 and dried under reduced pressure),

yielded good yields of product (one equivalent of pyridine: 0.15 g, 75% **(1)**, two equivalents of pyridine: 0.16 g, 89% **(2)**).

2.5.2 SYNTHESIS OF $[CrCl_3(py)_3]$ (3)

A Schlenk tube was charged with $[CrCl_3(thf)_3]$ (0.23 g, 0.614 mmol) and pyridine (30 cm^3), where pyridine was both reagent and solvent. The reaction was stirred at room temperature overnight to ensure completion. The supernatant was removed and the remaining residue washed with Et_2O (3 x 20 cm^3) and dried under reduced pressure for 3 hours to afford an olive green precipitate **(3)** in good yield (0.20 g, 83%).

Crystals of **(3)** were grown from the slow evaporation of a CH_3CN solution. The reaction was repeated in a NMR tube to follow the reaction course and profile. Acetone-d_6 was the solvent used. Refer to NMR chapter for details. After a period of 5 days, dark green plate–like crystals large enough for the diffractometer were formed in the NMR tube. Structure determination gave the compound $[pyH][CrCl_4(py)_2]$ **(4)**.

2.5.3 SYNTHESIS OF $[CrCl_3(2,6\text{-dibromopy})_3]$ AND $[CrCl_3(py)_2(DMF)]$ (5)

Up to this point all substituents were at the para position of the pyridine as coordination to the metal centre was guaranteed not be affected by steric hindrance. However, test reactions were carried out using an ortho–substituted pyridine to ensure that they could not indeed be utilised as a result of their bulkiness at a position too close to the proposed Cr–N coordination site. In the case of the attempted synthesis of $[CrCl_3(thf)_3]$ plus 3 molar equivalents of 2, 6-dibromopyridine the expected result of no reaction was the case. However, a second experiment was carried out where by both pyridine and 2, 6-dibromopyridine were combined in a Schlenk tube with $[CrCl_3(thf)_3]$ resulting in an interesting crystal structure of $[CrCl_3(py)_2(DMF)]$.

A Schlenk tube was charged with $[CrCl_3(thf)_3]$ (0.23 g, 0.614 mmol) and thf (20 cm^3). Followed by the addition of one molar equivalents of 2,6-dibromopyridine (0.14 g, 0.614 mmol), 2,6-dimethylpyridine (0.06 g, 0.614 mmol) and unsubstituted pyridine (0.05 cm^3). All three ligands were added simultaneously to ensure equal competition for sites. To

ensure completion the reaction was stirred overnight at room temperature. The supernatant was removed via syringe and the residue washed with Et_2O (3 x 20 cm^3). The residue was then dried under reduced pressure for 3 hours yielding (0.21 g, 87%). The crystallisation of the recovered product was limited to DMF and DMSO as solvents due to the insolubility in all other solvents. Dark green plate–like crystals of **(5)** were formed from DMF after approximately 10 weeks.

2.5.4 SYNTHESIS OF $[CrCl_3(pyNH_2)_3]$ (6)

Varying the electronic effects of the ligands was achieved by introducing $pyNH_2$ as the ligand.

A Schlenk tube was charged with $[CrCl_3(thf)_3]$ (0.25 g, 0.667 mmol) and thf (20 cm^3). On immediate addition of the $pyNH_2$ (0.19 g, 2.001 mmol) the solution turned green and a green precipitate was visible. The reaction was stirred overnight at room temperature. The supernatant was removed after the residue had been allowed to settle. It was subsequently washed with Et_2O (3 x 20 cm^3) and dried under reduced pressure for 3 hours to afford a light green precipitate **(6)** in good yield (0.24 g, 83%).

2.5.5 SYNTHESIS OF $[CrCl_3(pytb)_3]$ (7)

With the success of the $[CrCl_3(py)_3]$ compound, the steric effects of the ligands were varied by introducing pytb in place of pyridine.

A Schlenk tube was charged with $[CrCl_3(thf)_3]$ (0.26 g, 0.0694 mmol) and thf (20 cm^3). Three equivalents of pytb (0.26 cm^3, 2.082 mmol) were then added and the reaction was monitored. It was noted that on immediate addition of the pytb, the reaction mixture turned dark green. The reaction was stirred at room temperature overnight to ensure completion. As no precipitate formed, the green supernatant was reduced under pressure to leave behind an oil–like green substance. Et_2O (10 cm^3) was then added which forced out an olive green precipitate. This ether-based supernatant was removed and after 3 days of standing at room temperature afforded dark green platelet crystals of $[CrCl_3(pytb)_3]$.

The green precipitate was washed again in Et_2O (3 x 20 cm^3) and then dried under reduced pressure to leave an olive green precipitate **(7)** in good yield (0.24 g, 62%).

2.5.6 SYNTHESIS OF $[CrCl_3(pyphenyl)_3]$ (8)

The steric bulk of the ligands was increased further with the addition of pyphenyl ligands. A Schlenk tube was charged with $[CrCl_3(thf)_3]$ (0.22 g, 0.587 mmol) and dissolved in thf (20 cm^3). Three equivalents of pyphenyl (0.27 g, 1.761 mmol) were then added, turning the supernatant green and affording a green precipitate. To ensure completion, the reaction was stirred at room temperature overnight. The green supernatant was removed via syringe and the residue washed with Et_2O (3 x 20 cm^3), followed by drying of the residue under reduced pressure. An olive green precipitate **(8)** remained in good yield (0.21 g, 58%).

2.5.7 SYNTHESIS OF $[CrCl_3(pyOH)_3]$

With the idea of continuing the theme of varying the electronic properties of the coordinating ligands, it was hoped to synthesise $[CrCl_3(pyOH)_3]$. However, this was not possible as the pyOH ligand was insoluble in all workable solvents.

Chapter 3

Chromium(III) Bidentate Nitrogen Ligand Chemistry

3.1 INTRODUCTION

Since its discovery at the end of the nineteenth century, the bipyridine ligand (commonly referred to as (bipy) has been used extensively in the complexation of metal ions. This particular aromatic nitrogen-containing heterocyclic ligand exhibits six possible region–isomeric forms – three symmetrical (2,2' , 3,3' , 4,4') and three asymmetrical (2,3' , 2,4' , 3,4'). The most common of these is the 2, 2' isomer. Due to its robust stability and ease of functionalisation, 2, 2'–bipyridine allows the formation of stable, rigid, five–membered chelate rings with the metal centre. Coordination takes place via the σ–donating nitrogen atoms [102].

As only two of the three available coordination sites are taken up, via substitution of the thf ligands in the $[CrCl_3(thf)_3]$ precursor, the addition of bipyridine allows the further addition of a monodentate ligand. For the most part, in keeping with the theme of Chapter 2, it was logical to continue coordinating N–donor ligands to the Cr(III) centre. As well as the para-substituted pyridine ligands, CH_3CN was also coordinated. Straying slightly from the N-donor trend, the coordination of water was also found to provide important results.

The choice of all the above-mentioned ligands was in keeping with the known donor atoms that have been previously coordinated to Cr(III) to yield catalytically active species successfully.

Although the complexes $[CrCl_3(bipy)(thf)]$ **(9)**, $[CrCl_3(bipy)(CH_3CN)]$ **(10)** and $[CrCl_3(bipy)(py)]$ **(11),** all of which were prepared and characterised in this study, are known complexes [79, 103], their reported synthetic routes differ from those in this study and their

characterisation lacks the detailed spectroscopic data and novel computational data provided here. The reported procedures for making these complexes involve the use of hydrated chromium chlorides, different precursors and solvents.

3.2 SYNTHESIS

Adding the bipyridine to the $[CrCl_3(thf)_3]$ (which had been dissolved in thf) afforded no immediate colour change or formation of precipitate. Over a period of approx. 2 hours the reaction solution turned from deep purple to grey/brown to grey/blue to the final colour of dark green. Once the precipitate had been washed with ether and dried under reduced pressure, a light green precipitate remained.

Owing to the fact that the secondary monodentate ligands (namely the pyridine ligands Chapter 2) coordinated at a much greater speed than the bidentate bipyridine and the fact that the $[CrCl_3(bipy)(thf)]$ compound was virtually insoluble in all solvents, the monodentate ligands were added in one of two ways:

1. $[CrCl_3(bipy)(thf)]$ was resynthesised for each new desired compound and as the green precipitate began to form, the secondary ligand was added.
2. In some cases the $[CrCl_3(bipy)(thf)]$ was soluble in the monodentate ligand and so these ligands were used as both solvent and ligand for the reactions.

3.3 SYNTHETIC ROUTE TO PRODUCT FORMATION

Once all the complexes had been synthesised, there were two key focus areas, namely the characterisation of the complexes and the determination of their synthetic pathways. These areas actually go hand in hand as both rely on the spectroscopic and structural data as tools for characterisation and analysis. The need for confirmation of compound formation is obvious. However, the pathway taken is not a straightforward case of direct ligand substitution as was illustrated in Chapter 2 with the complex $[Hpy][CrCl_4(py)_2]$. The cornerstone of information on which this study was built was the three very different crystal structures that were solved. The first was the neutral monomeric species $[CrCl_3(bipy)(H_2O)]$ **(16)**, the second was the anionic species $[HpyNH_2][CrCl_4(bipy)]$ **(15)** and the third was $[CrCl_2(bipy)_2][Cl]\cdot H_2O$ **(17)**. It is worth mentioning that with respect to $[CrCl_3(bipy)(H_2O)]$, spectra were taken of both the single crystal

material and the precipitate. The fact that these spectra are identical infers that the single crystal determination id representative of the bulk material. Apart from the respective secondary ligands, the method of synthesis for each was unchanged. This clearly leads one to believe that this class of compounds coordinates via the same potential pathways as the monodentate N–ligands.

3.4 INFRARED AND RAMAN SPECTROSCOPY

The key to a successful and comprehensive study of the vibrational spectra of these compounds lies not just in the interpretation of the spectra, but also in the comparative studies that can be undertaken with the results of the other techniques, not to mention the spectra of the other classes of compound. In particular, although there is much overlap in the bands assigned to bipyridine and pyridine, detailed analysis involving comparative studies with the compounds of Chapter 2 can clear up the ambiguity surrounding a number of these bands and in this way they can be assigned specifically to either the bipyridine or pyridine ligands. With regard to band assignment it is perhaps, above all, the comparisons with the spectra of those compounds for which single crystals were obtained that adds the most weight and thus confidence to the assignments. In addition to the presence of the respective ligand vibrations, it is the bands that have shifted to higher frequencies from the free ligand positions that are of particular interest since coordination to the metal is thus implied.

As both IR and Raman spectra of the compound $[HpyNH_2][CrCl_4(bipy)]$ were obtained, comparisons can be made with the other compounds as this will help to deduce whether the final compounds are monomeric or have in fact been cleaved asymmetrically to yield the anionic chromium–pyridinium species. According to the literature [93], important indications will be the strength of bands, as well as their presence or absence, particularly bands indicative of the pyridinium ion. These ions also have a tendency to show greater shifting of bands compared with their neutral counterparts as they possess more prominent polar and conjugation effects [104].

With regard to the results of the individual compounds, it should be noted that Raman spectra were not obtained for the compounds $[CrCl_3(bipy)(pyNH_2)]$ **(12)**, $[CrCl_3(bipy)(H_2O)]$ and $[CrCl_2(bipy)_2][Cl]\cdot H_2O$ owing to problems of fluorescence (see Chapter 1) and lack of sample in the latter case. For the same reason of sample deficiency no FIR spectrum of

$[CrCl_2(bipy)_2][Cl]\cdot H_2O$ was obtained. Note also that the isolated crystal structure, $[HpyNH_2][CrCl_4(bipy)]$, encapsulated a molecule of solvent, namely DCM. Evaporation would explain the lack of evidence of such a molecule in the corresponding IR or Raman spectra.

3.4.1 Region 3329–2291 cm^{-1}

The only complexes to exhibit bands above 3136 cm^{-1} are $[CrCl_3(bipy)(pyNH_2)]$, $[HpyNH_2][CrCl_4(bipy)]$ and $[CrCl_3(bipy)(H_2O)]$ (see Figure 3.1). Both $[CrCl_3(bipy)(pyNH_2)]$ and $[HpyNH_2][CrCl_4(bipy)]$ possess strong IR bands at 3319 and 3312 cm^{-1}, 3206 and 3211 cm^{-1}, as well as 3146 and 3153 cm^{-1} respectively which are indicative of N–H stretching vibrations [96]. $[HpyNH_2][CrCl_4(bipy)]$, in addition, possesses a further three vibrations that are absent in $[CrCl_3(bipy)(pyNH_2)]$. This is an early indication that they are not the same compound, i.e. the addition of $pyNH_2$ does not necessarily lead to the asymmetrically cleaved species. As the structure of $[HpyNH_2][CrCl_4(bipy)]$ has been solved crystallographically, these additional bands are assumed to be pyridinium-related.

While both complexes possess what would appear to be a free $pyNH_2$ ligand shift from 3300 to 3319 and 3312 cm^{-1} respectively, it is plausible that the $[CrCl_3(bipy)(pyNH_2)]$ band is indicative of coordination, while that of $[HpyNH_2][CrCl_4(bipy)]$ is a pyridinium effect. It is worth mentioning that the regions that follow include yet further evidence to suggest differences between the two compounds, in the form of additional bands in $[HpyNH_2][CrCl_4(bipy)]$ that correspond with literature assignments of pyridinium ions.

The relatively benign red shift in $[CrCl_3(bipy)(pyNH_2)]$ has further importance as it indicates that this ligand coordinates to the metal centre via the endocyclic nitrogen, as opposed to the amine substituent where one would have expected a dramatic red shift of between 150 and 200 cm^{-1} [96].

The single, broad, strong band at 3280 cm^{-1} in $[CrCl_3(bipy)(H_2O)]$ is indicative of coordinated water, i.e. characteristic O–H vibration [76, 105].
Between 3139 and 2960 cm^{-1}, all the complexes possess bands associated with the C–H vibrational modes of bipyridine and pyridine [76]. It is very difficult to differentiate between the

two due to their extreme similarities in this regard. However, this has been achieved with some success in the regions that follow.

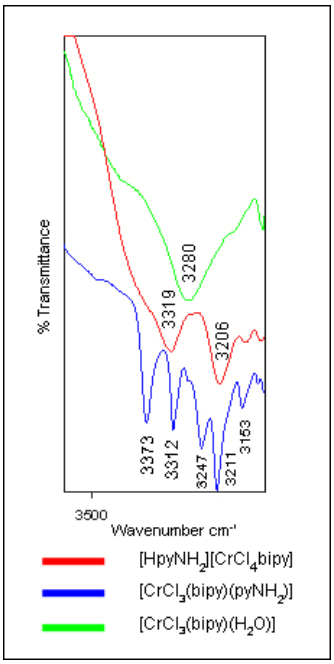

Figure 3.1 IR spectra of [$CrCl_3$(bipy)($pyNH_2$)] (blue), [$HpyNH_2$][$CrCl_4$(bipy)] (red) and [$CrCl_3$(bipy)(H_2O)] (green) in the region 3329 – 2291 cm^{-1}

It is widely recognised that bands indicative of C–H vibrations associated with thf molecules are observed at lower frequencies than those of aromatic molecules [76], and their presence or absence is of importance with respect to the precursor of this study, [$CrCl_3$(thf)$_3$]. The appearance of three such vibrations at 2948, 2929 and 2897 cm^{-1} in [$CrCl_3$(bipy)(thf)] (present as weak vibrations in the equivalent Raman spectrum) suggests that direct ligand substitution, whereby one of the thf molecules remains coordinated to the chromium, is a valid pathway to compound formation. These bands are absent in all the other compounds except for [$CrCl_3$(bipy)(pyphenyl)] **(14),** which may appear to be indicative of a mixture, however, the FAB-MS results presented later suggest otherwise. Figure 3.2 shows the presence of C-H vibrations in [$CrCl_3$(bipy)(thf)] and their absence in [$CrCl_3$(bipy)(H_2O)] while Figure 3.3 compares the spectra of [$CrCl_3$(thf)$_3$] and [$CrCl_3$(bipy)(pyphenyl)].

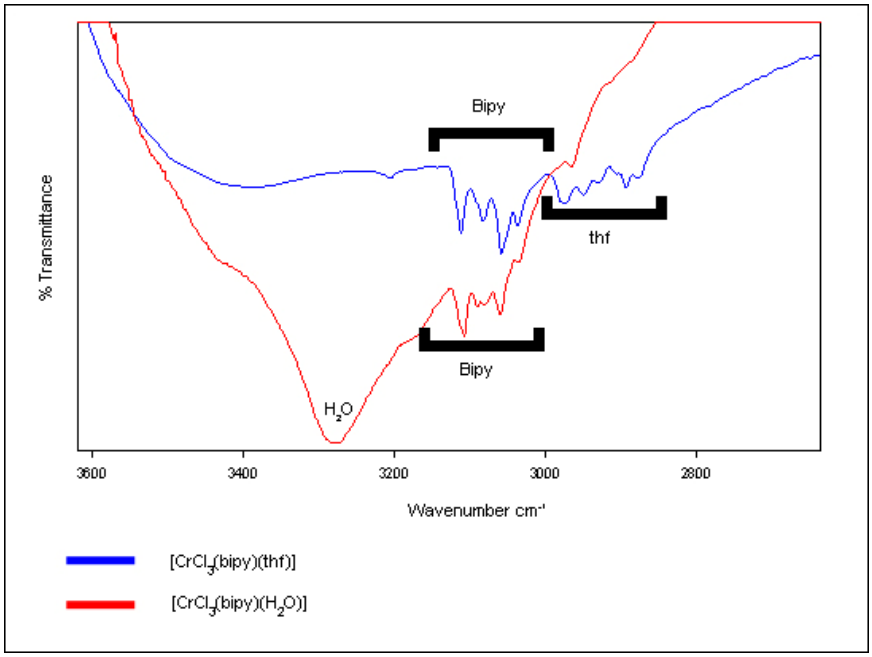

Figure 3.2 **IR spectra showing the presence of thf C–Hs in [$CrCl_3$(bipy)(thf)] (blue) and their absence in [$CrCl_3$(bipy)(H_2O)] (red)**

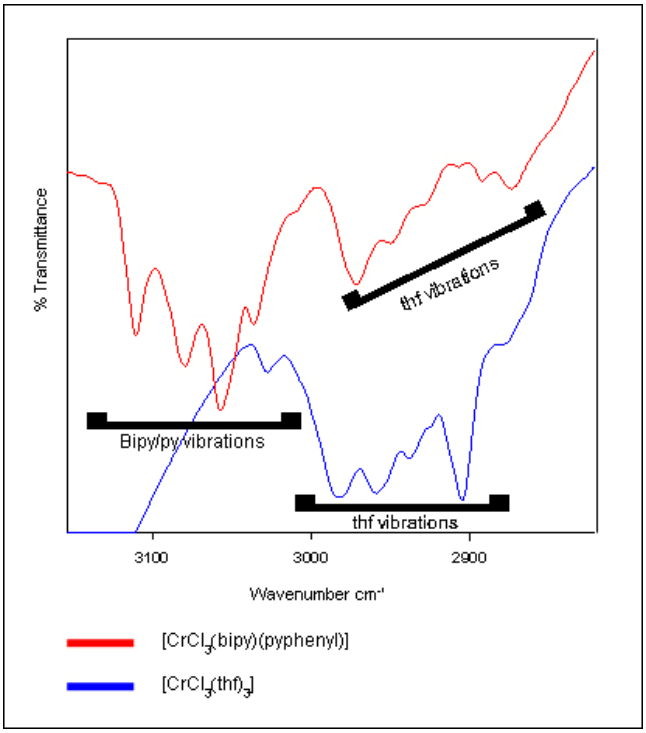

Figure 3.3 **Comparison of the IR spectra of [$CrCl_3$(thf)$_3$] (blue) and [$CrCl_3$(bipy)(pyphenyl)] (red)**

Note that this is really only an early indication as with this information alone it is very difficult to differentiate between coordinated and free thf. The study of coordinated thf is discussed further and with more confidence in the region 1104 to 522 cm^{-1} where more distinctive and conclusive bands are found.

Other bands in this overall region are those associated with the symmetrical and asymmetrical CH_3 stretch vibrations of the tertiary butyl substituent of pytb found in $[CrCl_3(bipy)(pytb)]$ **(13)** (2962 cm^{-1} IR / 2969 cm^{-1} R), (2905 cm^{-1} IR / 2906 cm^{-1} R) and (2868 cm^{-1} IR / 2870 cm^{-1} R) respectively, as well as with the CH_3 symmetrical stretch and C≡N modes of the CH_3CN ligand (2910 cm^{-1} IR / 2913 cm^{-1} R), (2318 cm^{-1} IR / 2321 cm^{-1} R) and (2291 cm^{-1} IR / 2293 cm^{-1} R) respectively. They are all observed as strong vibrations, where R indicates the Raman frequencies. The lack of shifting of the tertiary butyl modes is expected even upon coordination [92], while the CH_3CN modes undergo significant shifts relative to their free ligand positions of 2900 [92], 2289 and 2252 cm^{-1} respectively [79]. Figure 3.4 presents the spectral comparisons between $[CrCl_3(bipy)(CH_3CN)]$ and $[CrCl_3(bipy)(pytb)]$.

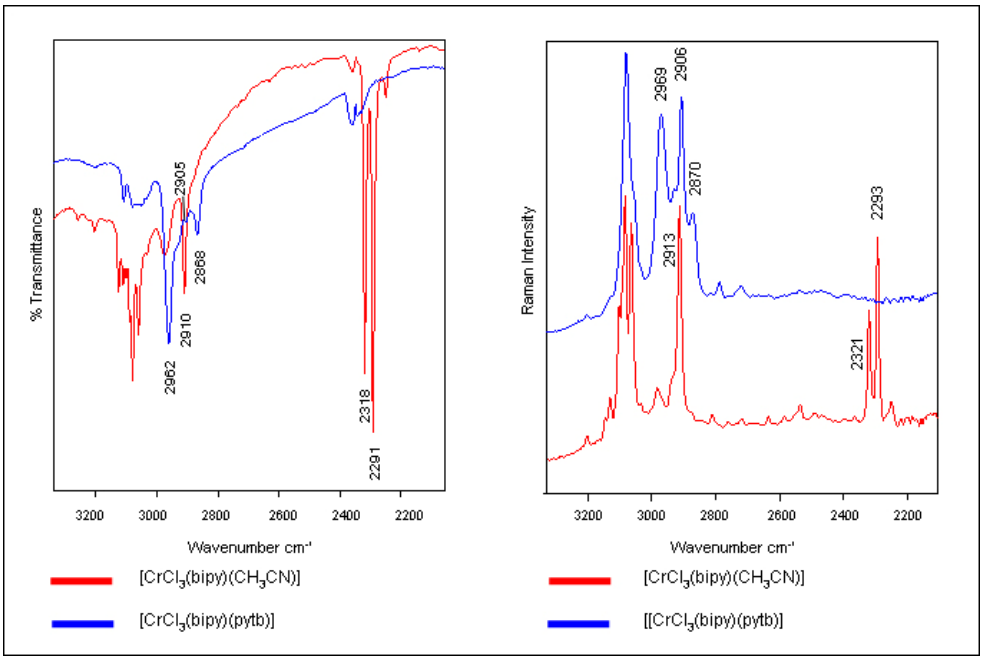

Figure 3.4 **Characteristic IR and Raman vibrations in $[CrCl_3(bipy)(CH_3CN)]$ (red) and $[CrCl_3(bipy)(pytb)]$ (blue)**

3.4.2 Region 1652–1104 cm^{-1}

This particular region possesses bands indicative of both bipyridine and pyridine ring vibrations. These include vibrations that are specifically assigned to the para–substituted pyridine substituents. In addition, pyridinium-specific vibrations associated with ring stretching, C–H bending and N^+-H are also expected. As already stated, one must expect a certain amount of band superposition when investigating compounds involving both bipyridine and pyridine. One such example is the ring vibrations observed at 1596 and 1580 cm^{-1} in free pyridine and also at 1580 cm^{-1} in free bipyridine. Upon coordination all three are expected to shift to ~1600 cm^{-1}, which therefore makes differentiating between the ligands very difficult. Attempts were made, however, by comparing the spectra of the non–pyridine compounds ($[CrCl_3(bipy)(thf)]$, $[CrCl_3(bipy)(H_2O)]$ and $[CrCl_3(bipy)(CH_3CN)]$) and those that do possesses pyridine and its derivatives. Although still no specific assignment to either bipyridine or pyridine could be made, none of the complex spectra showed the free ligand vibrations, which implies that both ligands have coordinated and thus shifted to the higher frequency. Interestingly, a look at the IR spectrum of the $[HpyNH_2][CrCl_4(bipy)]$ complex indicates that the free pyridine vibration at 1580 cm^{-1} has shifted to 1585 cm^{-1} which, in the light of both the above analysis and the confirmed structure of $[HpyNH_2][CrCl_4(bipy)]$, is a pyridinium ion effect. The fact that it is only found in this particular compound suggests that the other compounds are of a neutral, monomeric nature. Note that the same band is absent in the corresponding Raman spectrum.

Figure 3.5 shows the IR comparison of free bipyridine and pyridine with selected spectra representing both the non–pyridine and pyridine compounds, as well as the pyridinium compound. Visible in both figures is another bipyridine band shift from 1556 to 1565 cm^{-1} upon coordination, with band splitting evident in the IR spectrum.

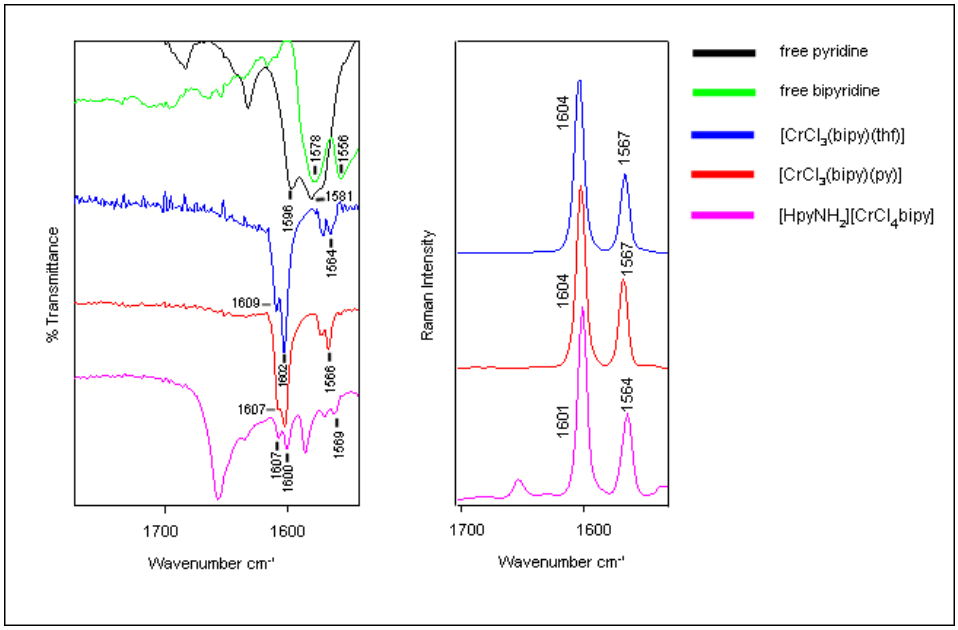

Figure 3.5 **IR and Raman vibrations in [$CrCl_3$(bipy)(thf)] (blue), [$CrCl_3$(bipy)(py)] (red) and [$HpyNH_2$][$CrCl_4$(bipy)] (purple)**

There are a number of other vibrations that are either bipyridine or pyridine-specific. Table 3.1 highlights the bipyridine ring vibrations (as well as a CN mode at 1318 cm^{-1}) that are absent in the pyridine literature [73, 74]. Figure 3.6 compares the IR spectra of [$CrCl_3$(bipy)(thf)] and [$CrCl_3(py)_3$].

Table 3.1 **Bipyridine-specific vibrations present in the spectra of all complexes**

Free bipy / cm^{-1}	Bipy complexes / cm^{-1}	Shift / cm^{-1}
1557	1564	7
1496	1496	0
1472	1472	0
1318	1318	0
1245	1245	0
1090	1104	14

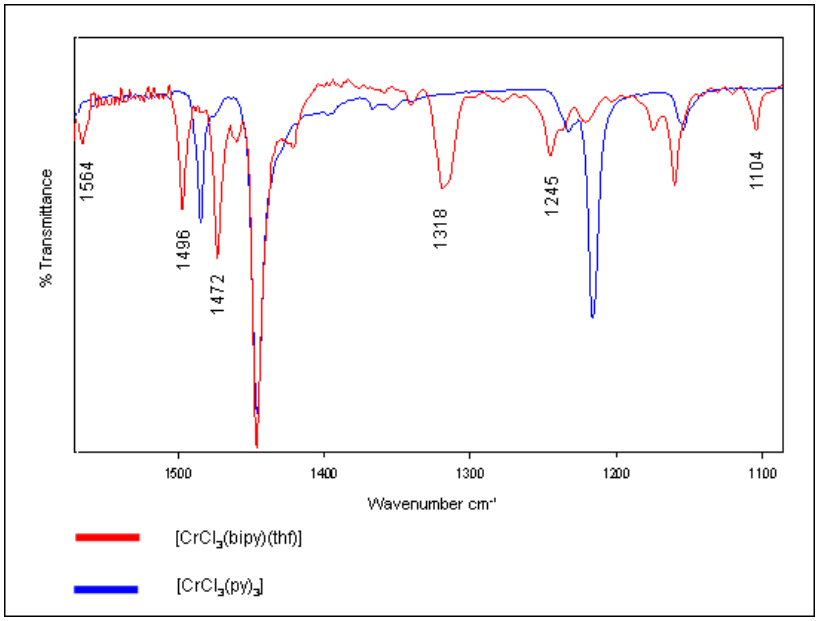

Figure 3.6 **Bipyridine specific IR vibrations present in all complexes represented by the comparison between [$CrCl_3$(bipy)(thf)] (red) and [$CrCl_3(py)_3$] (blue)**

The pyridine ring vibrations are largely influenced by their substituents, hence there is no band superposition observed (see Table 3.2).

Table 3.2 **Pyridine specific vibrations**

	Free ligand / cm^{-1}	Complex / cm^{-1}	Shift / cm^{-1}
$pyNH_2$	1506	1530	14
	-	1196	-
pytb	-	1397	-
pyphenyl	1512	1513	1
	1279	1291	12

The only substituent vibrations that are visible are those associated with the tertiary butyl group and these appear to be unshifted, which correlates to similar metal-coordinated compounds in the literature. They are observed at (1365 cm^{-1} IR / 1360 cm^{-1} R), (1202 cm^{-1} IR / 1203 cm^{-1} R) and (1120 cm^{-1} IR / 1128 cm^{-1} R); the first is assigned to a CH_3 asymmetrical deformation while the other two are C=C stretches [92]. See Figure 3.7.

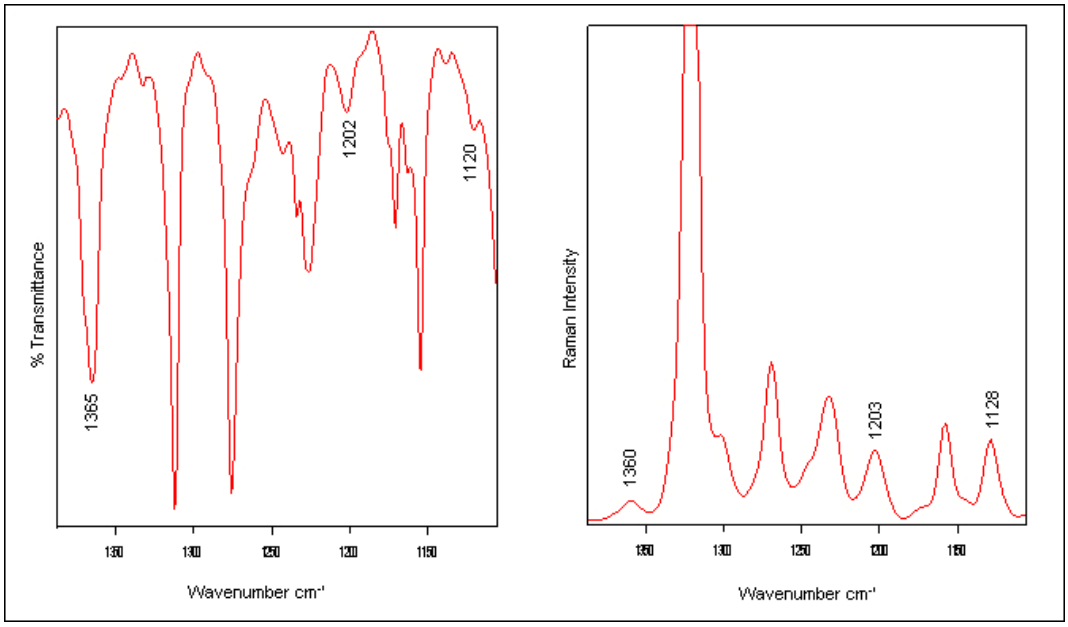

Figure 3.7 IR and Raman vibrations of tertiary butyl-specific vibrations in the region 1652 – 1104 cm^{-1}

3.4.3 Region 1104–522 cm^{-1}

This is an important region not just because there is further evidence of ligand coordination by way of free-ligand vibrational shifts, but also because of the ability to discuss some of these shifts with regard to bond strength. As this is common to Chapter 2, both experimental comparisons and literature comparisons can be made.

Evidence of coordinated thf is also visible, which helps to shed light on the synthetic route to compound formation. In the same vein, further comparisons with the spectrum of $[HpyNH_2][CrCl_4(bipy)]$ are helpful and, as expected, there are also a number of pyridine substituent vibrations.

Due to the band superposition already discussed, some of the vibrations that could equally be assigned to bipyridine or pyridine are those at ~1070, ~1060, ~1032 and ~769 cm^{-1}. Little to no shifting is observed upon complexation, except in the case of 769 cm^{-1} (shifted from 756 cm^{-1} in bipyridine or 749 cm^{-1} in pyridine).

3.4.3.1 Pyridine-specific

In the light of the vibrational assignments in Chapter 2, much emphasis is placed on the free-pyridine ring breathing mode found at ~992 cm^{-1} which shifts relative to the substituents. A number of factors are responsible for the extent of shifting, including mass, number, nature and position of substituents [75].

Interestingly, the degrees of shifting of all the ligand-specific vibrations in all the complexes correspond very well to those of Chapter 2 (see Table 3.3 and Figure 3.8) and seem unaffected by the change of complex environment (i.e. coordinated bipyridine). With regard to $pyNH_2$, this shift is yet further evidence of endocyclic nitrogen coordination as opposed to the equally plausible amino group coordination.

Table 3.3 Shifting of the characteristic ring breathing vibration in $[CrCl_3(bipy)(py)]$, $[CrCl_3(bipy)(pyNH_2)]$, $[CrCl_3(bipy)(pytb)]$ and $[CrCl_3(bipy)(pyphenyl)]$

Pyridine / cm^{-1}	$[CrCl_3(bipy)(py)]$ / cm^{-1}	Shift / cm^{-1}
990	1013	23

$pyNH_2$ / cm^{-1}	$[CrCl_3(bipy)(pyNH_2)]$ / cm^{-1}	Shift / cm^{-1}
991	1022	31

Pytb / cm^{-1}	$[CrCl_3(bipy)(pytb)]$ / cm^{-1}	Shift / cm^{-1}
995	1025	30

Pyphenyl / cm^{-1}	$[CrCl_3(bipy)(pyphenyl)]$ / cm^{-1}	Shift / cm^{-1}
1001	1011	10

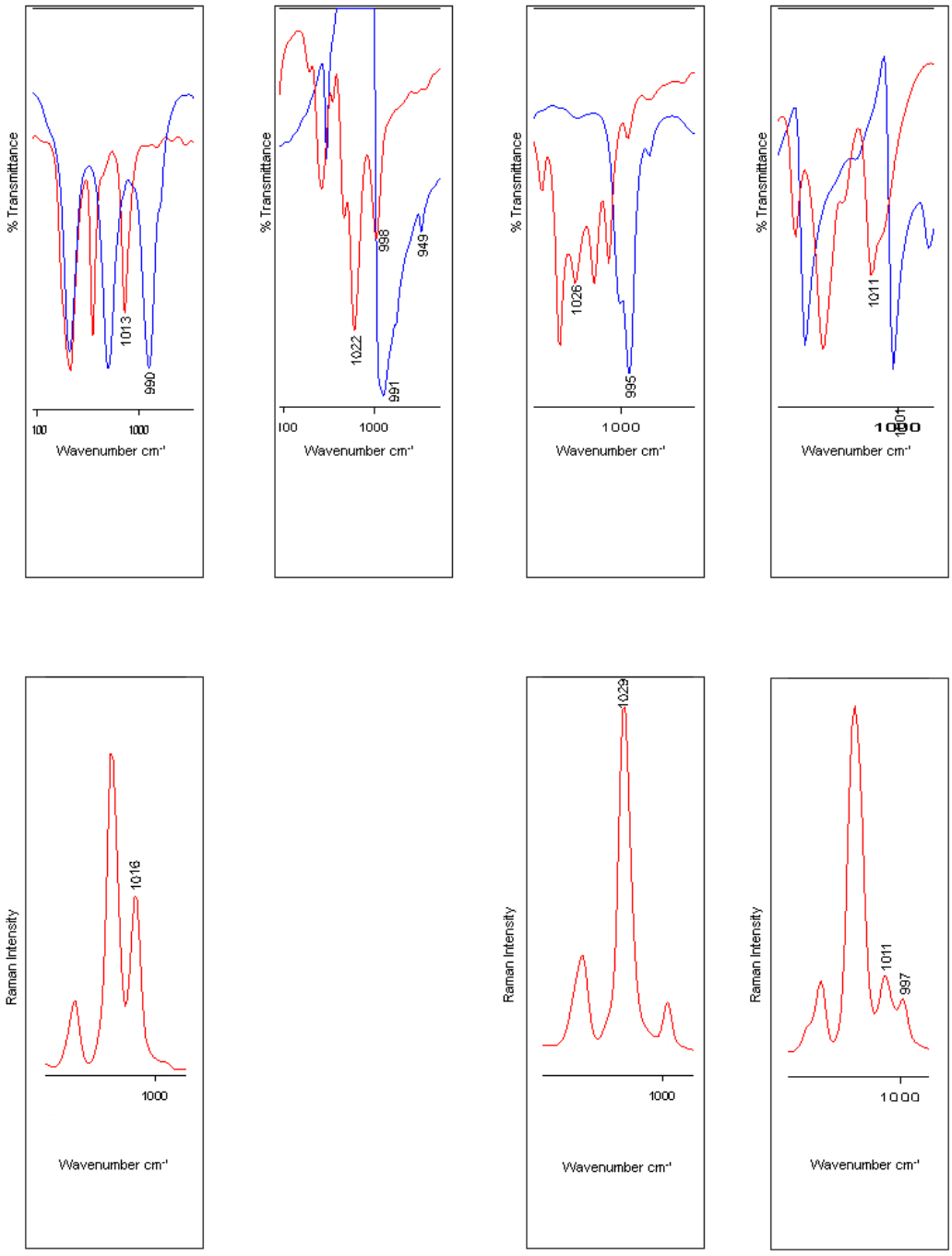

Figure 3.8 **Spectra showing the shifting of the characteristic ring breathing vibration in the IR of [$CrCl_3$(bipy)(py)], [$CrCl_3$(bipy)($pyNH_2$)], [$CrCl_3$(bipy)(pytb)] and [$CrCl_3$(bipy)(pyphenyl)] from free ligand positions. Raman spectra of [$CrCl_3$(bipy)(py)], [$CrCl_3$(bipy)(pytb)] and [$CrCl_3$(bipy)(pyphenyl)]**

Although pytb shows a second band at 1015 cm^{-1}, it is the band at 1026 cm^{-1} that corresponds with the shift observed for the similar complex, $[CrCl_3(pytb)_3]$, in Chapter 2. Indeed, in the chapters that follow the same band at 1026 cm^{-1} is also exhibited upon addition of the pytb ligand.

The presence of a band at 1022 cm^{-1} in $[HpyNH_2][CrCl_4(bipy)]$ is assignable to a pyridinium α(C–C–C) vibration [94, 95].

Another pyridine vibration that characteristically shifts upon coordination is that at 605 cm^{-1} [73, 74], which is found in the complexes at 643 cm^{-1} (see Figure 3.9). Even though it is also present in $[HpyNH_2][CrCl_4(bipy)]$, one must expect vibrational overlap and it is more than likely a pyridinium-type band. Although unshifted, a further pyridine vibration is that observed at 698 cm^{-1} [97].

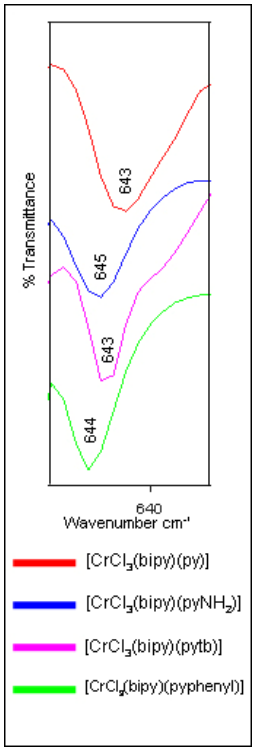

Figure 3.9 **Evidence of coordinated pyridine in the IR spectra of $[CrCl_3(bipy)(py)]$ (red), $[CrCl_3(bipy)(pyNH_2)]$ (blue), $[CrCl_3(bipy)(pytb)]$ (purple) and $[CrCl_3(bipy)(pyphenyl)]$ (green)**

There are also a number of vibrations associated with the respective pyridine substituents. The tertiary butyl bands at 930 (CH_3 rock) and 661 cm^{-1} (C–C stretch) follow the trend of similar compounds in the literature by not undergoing shifting upon coordination [92], while the lone phenyl ring mode observed at (625 cm^{-1} IR / 616 cm^{-1} R) also follows the literature and does shift from 608 cm^{-1} [97]. Amino vibrations are observed in both [$CrCl_3$(bipy)($pyNH_2$)] and [$HpyNH_2$][$CrCl_4$(bipy)] at 855 (X-sens), 527 cm^{-1} (X-sens) [96]. They undergo coordinative shifts from 842 and 522 cm^{-1} respectively. A further band at 501 cm^{-1} is not observed in the literature but is observed only in these two compounds and is thus assigned to a $pyNH_2$ vibration.

3.4.3.2 Bipyridine-specific

With regard to bipyridine-exclusive bands, it would appear that only those at ~995, 730, 665 and 651 cm^{-1} are assignable. 730 cm^{-1} is not present in free bipyridine nor in any of the other ligands and its presence is therefore assumed to be a coordination indicator, perhaps associated with the formation of the chelate ring.

3.4.3.3 Thf-specific

One of the most important assignments within this region elucidates the synthetic pathway via which these compounds are formed. Strong IR bands at 1006 and 856 cm^{-1} are indicative of coordinated thf [77, 78] and both of these vibrations are found in [$CrCl_3$(bipy)(thf)] (note that in the equivalent Raman spectrum the 1006 cm^{-1} mode is absent and that at 856 cm^{-1} is very weak). This is strong evidence to suggest that direct ligand substitution is a plausible route of synthesis resulting in the monomeric species and builds on the evidence observed in the region 3329–2291 cm^{-1}. There is a band similar to that at 1006 cm^{-1} in [$CrCl_3$(bipy)(pytb)] and [$HpyNH_2$][$CrCl_4$(bipy)]. As the crystal structure of the latter has been solved, and no thf is present, it can be assigned to a pyridinium vibration. Unlike the thf mode, this vibration is clearly visible in the equivalent Raman spectrum. Figure 3.10 shows the IR and Raman spectra of the above compounds.

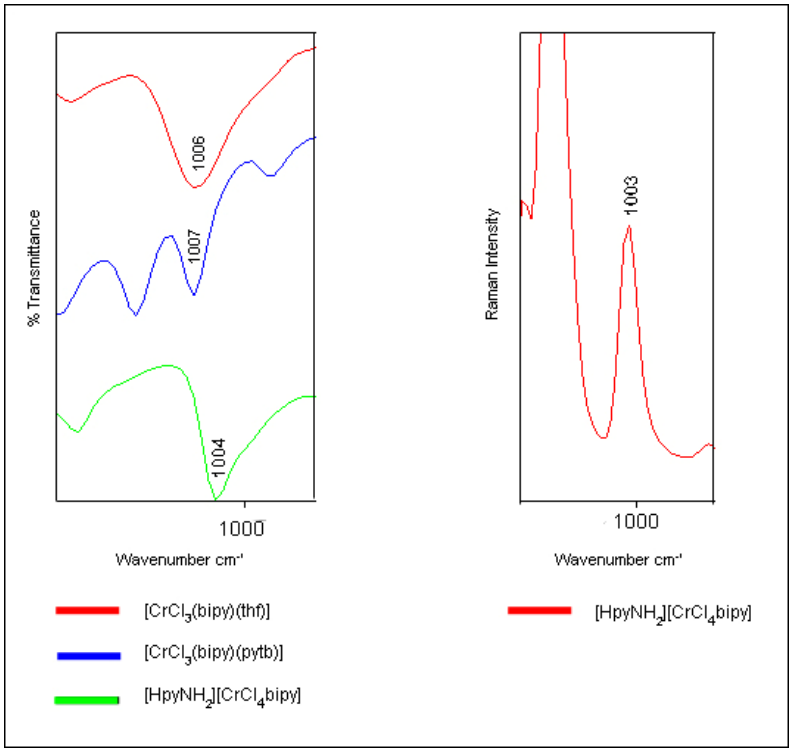

Figure 3.10 **Thf / unassigned / pyridinium vibration in IR and Raman spectra of [$CrCl_3$(bipy)(thf)] (red), [$CrCl_3$(bipy)(pytb)] (blue) and[$HpyNH_2$][$CrCl_4$(bipy)] (green)**

Regarding the 856 cm^{-1} vibration, it is also observed in [$CrCl_3$(bipy)($pyNH_2$)] (prominent shoulder), [$HpyNH_2$][$CrCl_4$(bipy)] and [$CrCl_3$(bipy)(pyphenyl)]. Its presence in the two amino compounds can be explained as a $pyNH_2$ vibration according to the literature [96, 98], but its unexpected presence in [$CrCl_3$(bipy)(pyphenyl)] may be an indication of a mixture of substituted and unsubstituted material, once again backed by the C–H (thf) bands in the region 3329–2291 cm^{-1}. In the same mould as the 1006 cm^{-1} mode, only the [$HpyNH_2$][$CrCl_4$(bipy)] Raman spectrum showed a band of worthwhile intensity. The IR spectra of [$CrCl_3$(bipy)(thf)], [$CrCl_3$(bipy)($pyNH_2$)], [$CrCl_3$(bipy)(pyphenyl)] and [$HpyNH_2$][$CrCl_4$(bipy)] in addition to the Raman spectrum of [$HpyNH_2$][$CrCl_4$(bipy)] are presented in Figure 3.11.

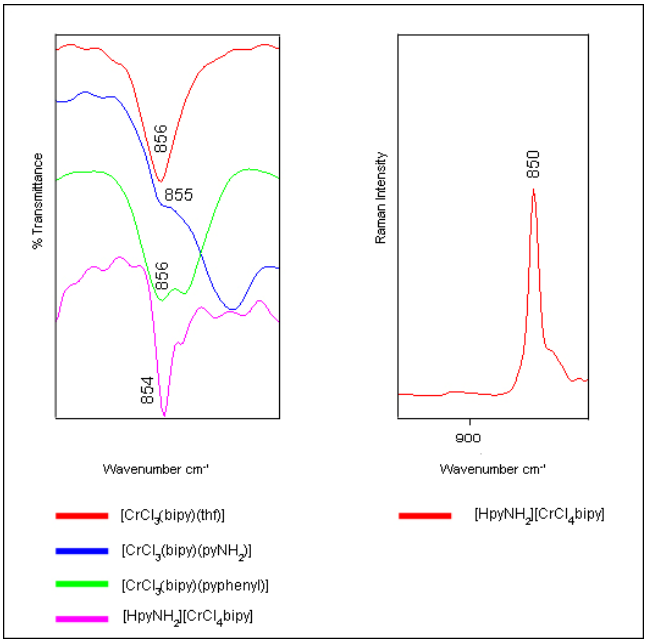

Figure 3.11 IR spectrum of [$CrCl_3$(bipy)(thf)] (red), [$CrCl_3$(bipy)($pyNH_2$)] (blue), [$CrCl_3$(bipy)(pyphenyl)] (green) and[$HpyNH_2$][$CrCl_4$(bipy)] (purple). Raman spectrum of [$HpyNH_2$][$CrCl_4$(bipy)]

.

3.4.3.4 Pyridinium-specific

Throughout the above discussions pyridinium-assignable vibrations have already been mentioned (1022, 1004 and 643 cm^{-1}). In addition, there are a further two modes that are present solely in [$HpyNH_2$][$CrCl_4$(bipy)] and are observed at 1046 and 590 cm^{-1}. Both are yet further evidence of monomeric product formation with respect to the other compounds. See Figure 3.12.

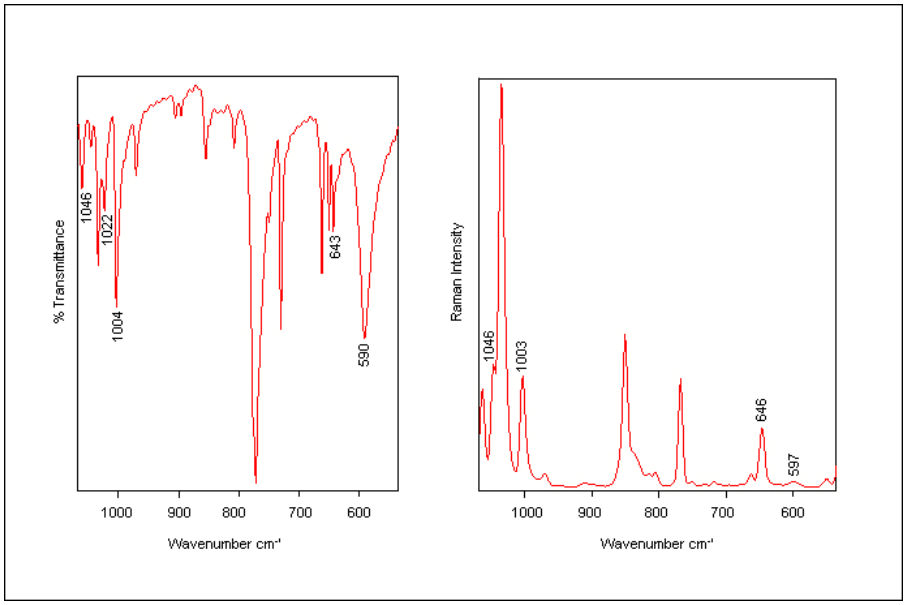

Figure 3.12 **IR and Raman bands associated with [HpyNH$_2$][CrCl$_4$(bipy)]**

3.4.4 Region 451–221 cm^{-1}

As can be seen in Table 3.4, the vibrations discussed here are present in both the IR and Raman spectra. However, the intensity of many of the Raman vibrations is a lot weaker than that of their IR counterparts. For this reason the representative spectra shown in Figure 3.13 are IR vibrations.

This is perhaps the most important region with regard to ligand coordination, and indeed compound geometry, as the bands are associated predominantly with metal–ligand vibrations. There is, however, a small number of pure ligand modes; the emphasis is on the word 'small' as their scarcity in this region is advantageous since the ambiguity that comes with band overlap as in the other regions is ruled out. The modes include bands at 428 and 402 cm^{-1} in free bipyridine which characteristically shift upon coordination to values of ~451 and ~414 cm^{-1} respectively [79]. These are common to all the compounds. The lone pyridine vibration is observed at 405 cm^{-1} and its shifting to around 442 cm^{-1} is widely accepted to be indicative of coordination [73, 74]. Note that it is solely observed in the unsubstituted pyridine compound, which is identical to what was observed in the previous chapter.

The geometry of the compounds can be linked to the number of Cr–Cl vibrations observed. The presence of two Cr–Cl bands indicates the *cis* isomer, while three Cr–Cl bands imply that the *mer* isomer has been adopted [80]. As per the crystal structure of the monomer $[CrCl_3(bipy)(H_2O)]$, whereby the *mer* configuration is adopted, three bands are visible for nearly all the compounds. In the case of $[HpyNH_2][CrCl_4(bipy)]$, which is an asymmetrically cleaved dimer, four strong Cr–Cl bands are observed and this is in agreement with literature findings on similar compounds [99].

The ability to assign specific M–N bonds is of obvious interest and indeed importance. The Cr–N bands associated with the coordination of bipyridine and pyridine are seen in the spectra between 236 and 246, and at 221 cm^{-1} respectively [41, 79, 80, 81]. The band at 209 cm^{-1} in $[CrCl_3(bipy)(pyphenyl)]$ falls outside the assigned range, but can be explained by the fact that increasing the mass of the ring by substitution lowers the metal–N value [81]. Also the 222 cm^{-1} vibration in $[HpyNH_2][CrCl_4(bipy)]$ is related to a pyH mode.

The tentative assignment of the Cr–O (thf) band at 284 cm^{-1} is based on work by Fowles [82]. The same band has also previously been assigned to other vibrations, including the skeletal stretch of H_2O [106]. It is interesting to note that this band with a slight downward shift is present in all the complexes except $[CrCl_3(bipy)(pyphenyl)]$. As this includes the known structural identity of $[HpyNH_2][CrCl_4(bipy)]$, one must assume that it is also assignable to a bipyridine/pyridine vibration common to all.

As in previous work, the assignment of Cr–N (CH_3CN) has not been made [107]. It is also notable that no Cr–O (H_2O) bands in $[CrCl_3(bipy)(H_2O)]$ are present where expected, although the crystal structure along with other IR bands (presence of sharp water band and absence of coordinated thf) suggests otherwise.
Figure 3.13 is a representation of what is seen in all the spectra with regard to:

- The absence of the unsubstituted pyridine mode that is observed solely in $[CrCl_3bipy(py)]$ at 442 cm^{-1}
- The presence of the two shifted bipyridine vibrations at ~451 and ~414 cm^{-1} respectively

- The three Cr–Cl vibrations common to all complexes except [$HpyNH_2$][$CrCl_4$(bipy)], which exhibits four
- The Cr–N (bipy) between 236 and 246 cm^{-1} and the Cr–N (py) at ~221 cm^{-1}.

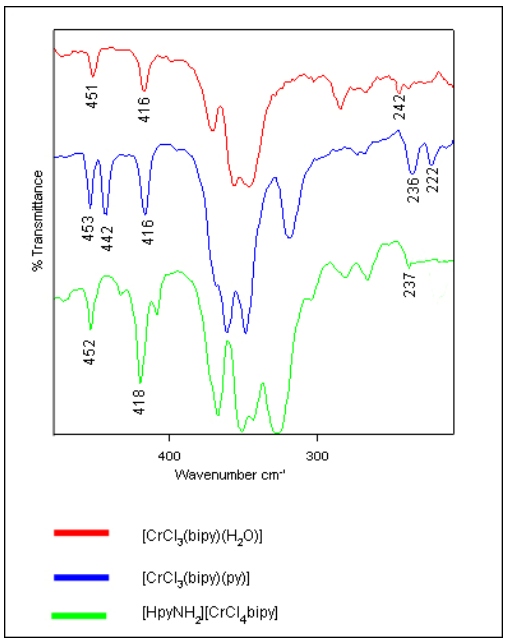

Figure 3.13 **FIR vibrations represented by spectra of [$CrCl_3$(bipy)(H_2O)] (red), [$CrCl_3$(bipy)(py)] (blue) and [$HpyNH_2$][$CrCl_4$(bipy)] (green)**

Table 3.4 Vibrational assignments of $[CrCl_3(bipy)(thf)]$ (9), $[CrCl_3(bipy)(CH_3CN)]$ (10), $[CrCl_3(bipy)(py)]$ (11), $[CrCl_3(bipy)(pyNH_2)]$ (12), $[CrCl_3(bipy)(pytb)]$ (13), $[CrCl_3(bipy)(pyphenyl)]$ (14), $[HpyNH_2][CrCl_4(bipy)]$ (15), $[CrCl_3(bipy)(H_2O)]$ (16) and $[CrCl_2(bipy)_2][Cl]\cdot H_2O$ (17)

9		10		11		12	13		14		15		16	17	assignment
IR / cm^{-1}	R / cm^{-1}	IR / cm^{-1}	R / cm^{-1}	IR / cm^{-1}	R / cm^{-1}	IR / cm^{-1}	IR / cm^{-1}	R / cm^{-1}	IR / cm^{-1}	R / cm^{-1}	IR / cm^{-1}	R / cm^{-1}	IR / cm^{-1}	IR / cm^{-1}	
-	-	-	-	-	-	-	-	-	-	-	3373s	3376w	-	-	ν (NH_2) (96)
-	-	-	-	-	-	3319s	-	-	-	-	3312s	3313w	-	-	ν (NH_2) asym (76, 96)
-	-	-	-	-	-	-	-	-	-	-	-	-	3280s	-	ν(OH) (76, 105)
-	-	-	-	-	-	-	-	-	-	-	3278w	3275w	-	-	ν (NH_2) (96)/ pyH
-	-	-	-	-	-	-	-	-	-	-	3247s	3244w	-	-	ν (NH_2) (96)/ pyH
-	-	-	-	-	-	3206s	-	-	-	-	3211s	3214w	-	-	ν (NH_2) sym (76, 96)
-	-	-	-	-	-	3146s	-	-	-	-	3153s	3142w	-	-	ν (NH_2) sym (76, 96)
-	3132w	3126m	3129w	3136vw	3139w	-	-	3126w	-	3132w	3119s	3127w	-	-	Bipy/py ν(CH) (73, 74, 76)
3107s	-	3107m	3101m	3107m	-	3111s	3109m	-	3110s	-	3104s	3104w	3106s	3112m	Bipy/py

9		10		11		12	13		14		15		16	17	assignment
															ν(CH) (73, 74, 76)
3081s	3079s	3080m	3082m	3083m	3088s	3088s	3080m	3079s	3080s	3085m	3080s	3077s	3089s 3078s	3084m 3075m	Bipy/py ν(CH) (73, 74, 76)
3057s	3062m	3061m	3064m	3063m	3065m	3060sh	3068m 3066m	-	3057s	3064sh	3060s 3053s	3071s 3056w	3059s	3060w	Bipy/py ν(CH) (73, 74, 76)
-	-	-	-	3048m	3052m	-	3056m	3056sh	-	-	-	-	-	3052w	Bipy/py ν(CH) (73, 74, 76)
3036s	3037w	-	-	-	-	3036sh	3034m	3034sh	3036s	-	3032s	3033w	3034s	3027w	Bipy/py ν(CH) (73, 74, 76)
2979s	2982w	2966m	2987w	2973m	2960w	2969s	-	-	2971m	2985vw	2972s	2979w	2964sh	2976w	Bipy/py ν(CH) (73, 74, 76)
-	-	-	-	-	-	-	2962s	2969s	-	-	-	-	-	-	ν (CH_3) asym (tb) (92)
2948s 2929s	2948vw 2932w	-	-	-	-	-	-	-	2948m	2949vw	-	-	-	-	thf ν(CH) (76)
-	-	-	-	-	-	-	2927m	2928m	-	-	-	-	-	-	ν (CH_3) sym (tb) (92)

9		10		11		12	13		14		15		16	17	assignment
-	-	2910m	2913s	-	-	-	2905m	2906s	-	-	-	-	-	-	ν (CH_3) sym (MeCN) / (pytb) (92)
2897s	Nv	-	-	-	-	-	-	-	2892m	2892vw	-	-	-	-	thf -ν(CH) (76)
2876m	2873w	-	-	-	-	-	-	-	2874m	2874vw	-	-	-	2875w	unassigned
-	-	-	-	-	-	-	2868m	2870m	-	-	-	-	-	-	ν (CH_3) sym (tb) (92)
-	-	2318m	2321m	-	-	-	-	-	-	-	-	-	-	-	δ(CH_3) sym + ν(CC) – MeCN (79)
-	--	2291m	2293m	-	-		-	-	-	-	-	-	-	-	ν(C≡N) (79)
-	-	-	-	-	-	1651s	-	-	-	-	1656s	1653m	-	-	δ(NH_2) (96)
-	-	-	-	-	-	-	-	-	-	-	-	-	1608s	-	H-O-H (105)
1609m	-	1608m	-	1607m sh	-	1610sh	1609s	-	1610s	1613sh	1607m	-	-	-	Coord ν_{ring} (bipy)/(py)/ pyH (73, 74, 104)
1602s	1604s	1600s	1600s	1602s	1604s	1601s	1601s	1602s	1602m	1600vs	1600m	1601s	1600s	1601m	Coord ν_{ring} (bipy) (76)
-	-	-	-	-	-	-	-	-	-	-	1585m	-	-	-	pyH ν(CC)

9		10		11		12	13		14		15		16	17	assignment
-	-	-	-		-	1572w	1572m	-	1572w	-	-	-	-	1578m	ν_{ring} (py) (73-76, 92-97)
1564w	1567s	1564w	1567s	1566w	1567s	1565w	1564m	1564s	1565w	1567s	1569w 1561w	- 1564s	1568w	-	ν_{ring} (bipy) (73, 74, 76)
-	-	-	-	-	-	1555w	1547m	-	-	-	-	-	-	1557m	ν_{ring} (py) (73-76, 92-97)
-	--	-	-	-	-	1528s	-	-	-	-	1530s	1533w	-	-	ν_{ring} ($pyNH_2$) (96)
-	-	-	-	-	-	-	-	-	1513vw	1513vw	-	-	-	-	ν_{ring} (pyphenyl) (97)
1496m	1497s	1494w	1497s	1495w	1497s	1496m	1495m	1498s	1496w	1496s	1495w	1497s	1497m	1497w	ν_{ring} (bipy) (76)
1472s	-	1470m	1469vw	1471w	1473vw	1471m	1471m	1483w	1472m	-	1473m	-	1472m	1470w	ν_{ring} (bipy) (76)
1446s	1440w	1440s	1436w	1445s	1437w	1444s	1445s	1448m	1445s	1440w	1443s	1443w	1445s	1447s	ν_{ring} (bipy/py) (73-76, 92-97)

9		10		11		12	13		14		15		16	17	assignment
1421w	1424w	1418 sh	1419w			1420w	1418m	1421w	1418m	1420w	1426sh	1420w	1422w	1415m	ν_{ring} (bipy/py) (73-76, 92-97)
-	-	-	-	-	-	-	1397sh	1399w	-	-	-	-	-	-	pytb
-	-	1367w	1367w	-	-	-	1365m	1360w	-	-	-	-	-	-	(CH_3) asym def (tb) (92)
1341vw	1352w	-	1350w	1347vw	1345w	1358w	1346m	-	1340vw	1352w	-	-	-	-	ν_{ring} (bipy/py) (73-76, 92-97)
1318m	1321s	1318w 1309m	1317s -	1313m	1321s	1313m	1312m	1320s	1313m	1317s	1319m	1318s	1313m	1315m	ν_{ring}(CN) (76)
-	-	-	-	-	-	-	-	-	1291w	1292s	-	-	-	-	ν_{ring} + δ(CH) (pyphenyl) (97)
1277vw	1271m	-	-	1276vw	-	1284w	1275m	1269m	1280vw	1276m	1283w	1285vw	1281vw	1278w	C-NH_2 / δ(CH) (bipy/py) (73-76, 92-97)
-	-	1261w	1269m	1261w	1268m	1263vw	-	-	-	-	-	1269	1259w	1268w	ν_{ring} (bipy/py) (73-76, 92-

9		10		11		12	13		14		15		16	17	assignment
															97)
1247m	1247w	1242w	1244w	1245w	1246w	1245w	-	-	-	-	1245m	1249m	1242w	1249m	ν_{ring} (bipy) (73-76, 92-97)
1218w	-	1220w	1220vw	1210w	1213w	1216s	1227w	1232m	1225m	-	1220w	1220m	1222w	1212w	δ(CH) (bipy/py) (73-76, 92-97)
-	-	-	-	-	-	-	1202w	1203m	-	-	-	-	-	-	ν (CC) (tb) (92)
-	-	-	-	-	-	1196s	-	-	-	-	1194m	1197w	-	-	$PyNH_2$
-	-	-	-	1175w	1178w	1174m	1163w	-	1173w	-	1174m	1174w	1167w	1177w	ν(CC/CH) (bipy/py) (73-76, 92-97)
1160m	1160m	1165w	1168w	1161w	1163w	1159m	1156m	1157m	1159m	1158w	1157m	1158m	1156m	1160w	ν(CC/CH) (bipy/py) (73-76, 92-97)
-	-	1146w	1151m	-	-	-	-	-	-	-	-	-	-	-	MeCN vib
-	-	1116w	1118vw	-	-	1121vw	1122vw	1128m	-	-	-	1118w	-	-	ν (CC) (tb) (92)
1104w	1104w	1101w	1100w	1106w	1108w	1107w	1107w	1108vw	1105w	1105w	1106w	1107w	1105m	1106w	ν_{ring} (bipy) (76)
-	-	1070w	-	-	-	1072sh	1074m	-	1070m	-	1073w	-	1072m	-	δ (CH)

9		10		11		12	13		14		15		16	17	assignment
															(py/bipy) (73-76, 92-97)
1063w	1062m	-	1064m	1064s	1066m	1058m	1058m	1064m	1062m	1063w	1060w	1063m	1060m	1064w	ν(CC/CH) (bipy/py) (73-76, 92-97)
-	-	-	-	-	-	-	-	-	-	-	1046w	1046m	-	-	pyH ν(CC) (93)
1034m	1035s	1033m	1035s	1035m	1036s	1033m	1034m	-	1033m	1038s	1033m	1035s	1035m	1039m 1031m	ν(CC/CH) (bipy/py) (73-76, 92-97)
-	-	-	-	-	-	-			-	-	1022w	-	-	-	pyH α(CCC) (94, 95)
-	-	-	-	1013w	1016s	1022s	1026m 1015m	1029s -	1011m	1011w		-	-	-	Ring breathing (pyX) (73-75)
1006m	-	-	-	-	-		1007m	-	-	-	1004m	1003m	-	-	Coord thf ν (COC) asym (77, 78) / pyH ν(CC) (95)

9		10		11		12	13		14		15		16	17	assignment
-	-	-	-	-	-	998m	998vw	996m	-	997w	-	-	-	991m	ν_{ring} (bipy) (76) / pyX-specific / ring breath (113)
-	-	-	-	-	-	-	930vw	930w	-	-	-	-	-	-	(CH_3) rock (tb) (92)
856s	854vw	-	-	-	-	855w	-	-	856s	849w	854w	850m	-	-	Coord thf ν (COC) sym (77, 78) / ($pyNH_2$) (96, 98)
-	-	-	-	-	-	-	842w	844w	847s	-	-	-	-	-	Py breathing (92)
-	-	-	-	-	-	830m	827m	-	-	-	-	816w	-	-	δ (CH) py (92, 96)
769s	766m	768s	771m	761s	768s	770s	768s	767m	768vw	768m	771s	768m	779s 772s	-	ν_{ring} / δ_{ring} (bipy/py) (73-76, 92-97)
-	-	-	-	-	-	-		-	750br	750w	-	-	754w	756s	ν_{ring} (bipy) (76)
730s	-	730m	739w	-	-	730s	731m	732m	730s	-	730m	732vw	729s	729m	ν_{ring} (bipy)

9		10		11		12	13		14		15		16	17	assignment
															(76)
-	-	-	-	698s	-	694	-	-	693m	-	-	-	-	-	ν_{ring} (py) (97)
665m	669w	664w	665w	663w	663vw	663m	667m	668m	663m	667w	661m	661vw	663m	665m	ν_{ring} (bipy) (76)
-	-	-	-	-	-	-	661m	-	-	-	-	-	-	-	N(CC) (pytb) (92)
651m	646w	649m	646w	650w	650m	652m	651m	-	-	-	650m	-	650m	654w	ν_{ring} (bipy)
-	-	-	-	643w	-	645m	643m	643w	-	646w	642m	646m	-	-	Coord δ_{ring} (py) / pyH α(CCC) (73, 74)
-	-	-	-	-	-	-	-	-	625m	616w	-	-	-	-	δ_{ring} (pyphenyl) (97)
-	-	-	-	-	-	-	-	-	-	-	590s	597vw	-	-	ν(CC) PyH
-	-	-	-	-	-	572m	568m	-	564m	565w	-	-	-	-	δ_{ring} / skeletal str (tb) (92, 97)
-	-	-	-	-	-	527s	-	-	-	-	528m	529m	-	-	X-sens ($pyNH_2$) (96)
-	-	-	-	-	-	501s	-	-	-	-	498m	501w	-	-	$PyNH_2$
451w	451w	454m	-	453m	470w	453m	451w	452vw	454m	-	452w	452w	451m	450w	Coord bipy ring def

9		10		11		12	13		14		15		16	17	assignment
															(79)
-	-	-	-	442m	442w	-	-	-	-	-	-	-	-	-	Coord py (73, 74)
414m	418br	415m	410w	416m	-	419m	417w	-	419m	424w	418m	420m	416m	416w	Coord ring def (bipy) (79)
369s	369m	365sh	369m	360s	365m	369s	366s	-	372s	369m	366s	367w	371s	-	Cr – Cl (80, 99)
355s	350m	352s	350m	348s	350m	346s	352s	355m	355s	352sh	350s	352m	355s	-	Cr – Cl (80, 99)
345s	341m	337s	336sh	319s	317vw	328ssh	323sbr	335m	323s	304w	343s	-	346s	-	Cr – Cl (80, 99)
-	-	-	-	-	-	-	-	-	-	-	327s	326vw	-	-	Cr – Cl (80, 99)
284w	271s	276w	276s	273vw	271s	279w	282m	-	-	-	280w	-	284w	-	Bip/py/Cr-O (thf)(82)/ Cr-O (H_2O) (106)
-	-	-	-		-	-	274m	-	-	-	-	-	-	-	unassigned
-	-	-	-	-	-	-	266m	267m	267vw	270m	265w	268s	-	-	unassigned
244w	234m	243w	244w	236w	236m	236w	246m	-	236m	232w	237w	235m	242vw	-	Cr – N (bipy) (79)
-	-	-	-	222w	222m	220w	220m	229m 216m	209w	213w	220w	220m	-	-	Cr – N (py) (41, 80, 81)/pyH

ν = stretching, δ = in plane bending, γ = out of plane bending, def = deformation, asym = asymmetric, sym = symmetric vs = very strong, s = strong, m= medium, w = weak, vw = very weak

3.5 COMPUTATIONAL STUDIES

In total, six of the complexes were selected for computational analysis on the basis that they were representative of most of the important vibrations found in all the complexes. The solid state effects in the FIR region that affect the number of vibrations visible in the calculated spectra are present for these complexes as they were in Chapter 2. For this reason the FIR spectra are not shown. However, all vibrations, both observed and masked, in the calculated spectra are presented in the appropriate tables.

3.5.1 [$CrCl_3$(bipy)(thf)]

This complex was selected as it was an important indicator relevant to understanding the mechanistic pathway to complex formation, particularly with regard to the experimentally assigned thf vibrations which are indicative of the monomeric species. Figures 3.14 and 3.15 highlight the very strong correlation between the experimental and calculated spectra, from which meaningful deductions can be made. The first deduction relates to the C–H vibrations associated with the thf ligand which, with respect to these types of complex, are now confirmed as being found as definitive vibrations at lower frequencies than their aromatic heterocycle counterparts (bipyridine and pyridine). The presence of not just thf but, specifically, coordinated thf, is confirmed with the correlation of the asymmetrical ν(C–O–C) vibration found exclusively in the IR of both the experimental and calculated spectra at 1006 and 995 cm^{-1} respectively. Another characteristic thf vibration is the symmetrical ν(C–O–C) which, in direct correlation with the literature, is found at 856 cm^{-1} in this complex. Interestingly, the calculated equivalent IR and Raman spectra possess three ν(C–O–C) modes, two asymmetrical stretches at 844 and 816 cm^{-1}, in addition to one symmetrical stretch at 831 cm^{-1}. Of all the vibrations, perhaps the strongest correlation between experimental and calculated relates to the bipyridine frequencies that are found at positions inferring coordination.

Unfortunately, the specific metal–ligand vibrations in the calculated spectra cannot be easily assigned to individual vibrations as the modes are mixed.

A selection of all the important vibrations discussed above is given in Table 3.5.

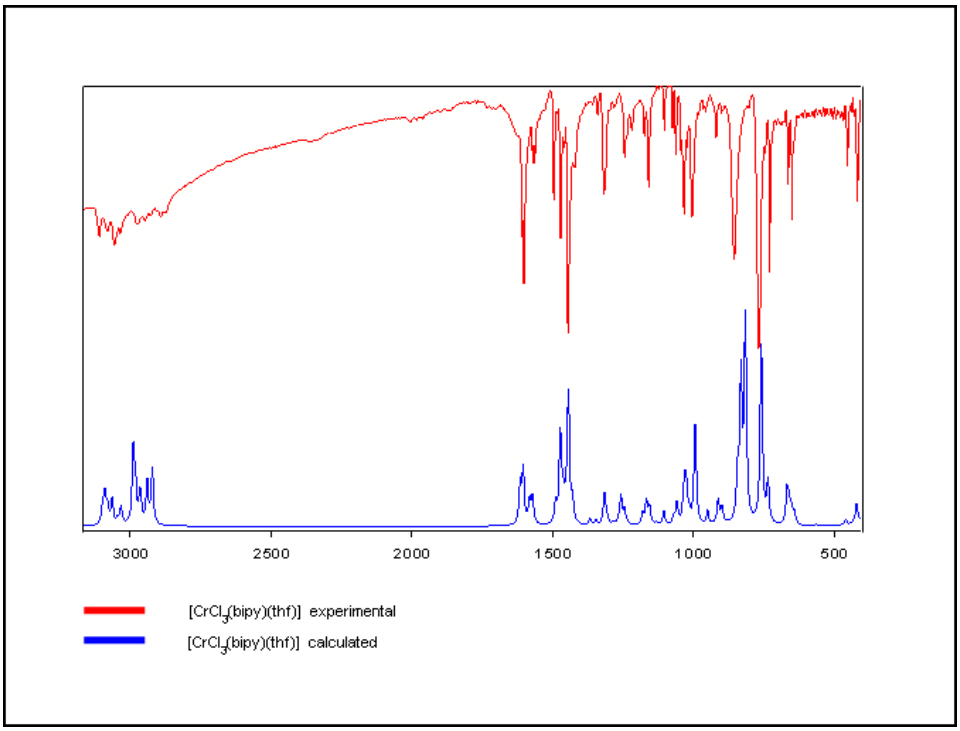

Figure 3.14 **Experimental (red) and calculated (blue) MIR spectra of $[CrCl_3(bipy)(thf)]$**

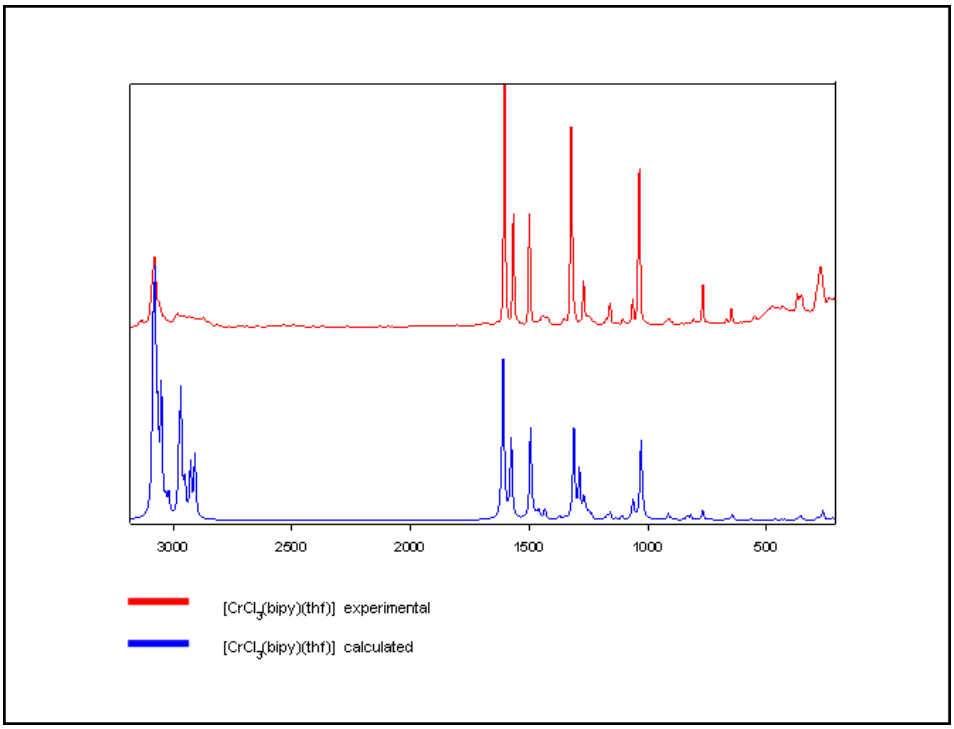

Figure 3.15 **Experimental (red) and calculated (blue) Raman spectra of $[CrCl_3(bipy)(thf)]$**

Table 3.5 **Selected experimental and calculated IR and Raman band assignments for [$CrCl_3$(bipy)(thf)]**

[$CrCl_3$(bipy)(thf)] IR / cm^{-1}		[$CrCl_3$(bipy)(thf)] Raman / cm^{-1}		Assignment	
Experimental	**Calculated**	**Experimental**	**Calculated**	**Experimental**	**Calculated**
2948	2966	2948	2968	thf ν(CH)	thf ν(CH)
2929	2941	2932	2952	thf ν(CH)	thf ν(CH)
1609, 1602	1616, 1606	1604	1606	ν_{ring} (bipy)	ν_{ring} (bipy)
1318	1317	1321	1311	ν_{ring} (CN)	ν_{ring} (CN)
1006	995	-	-	thf ν(COC) asym	thf ν(COC) asym
856	844, 831, 816	854	845, 834, 818	thf ν(COC) sym	thf ν(COC) asym, sym, asym
665	662	669	662	ν_{ring} (bipy)	ν_{ring} (bipy)
451	460	-	-	bipy ring def	bipy ring def
369, 355, 345	363, 350	369, 350, 341	364, 351	Cr-Cl	Cr-Cl + Cr-N
284	311	271	312	Cr-O	Cr-O + Cr-N
244	262	234	263	Cr-N (bipy)	Cr-Cl + thf twist

Table 3.6 **Scaling factors determined for [$CrCl_3$(bipy)(thf)]**

Region / cm^{-1}	IR	Raman
0 - 1854	0.976911	0.979130
2839 - 3422	0.961780	0.957214

3.5.2 $[CrCl_3(bipy)(H_2O)]$

The fact that this complex's crystal structure has been solved as part of this study made it an ideal choice for computational study. It is, however, unfortunate that no Raman spectrum comparisons could be made due to the sample fluorescence already discussed.

As can be seen from Figure 3.16, there is strong agreement between the experimental and calculated IR frequencies, with the one obvious exception being the O–H stretching band above 3000 cm^{-1}. Although the calculated spectrum shows two vibrations associated with the symmetrical and asymmetrical modes of O–H, it is widely accepted that a single broad band in this region is indicative of coordinated water.

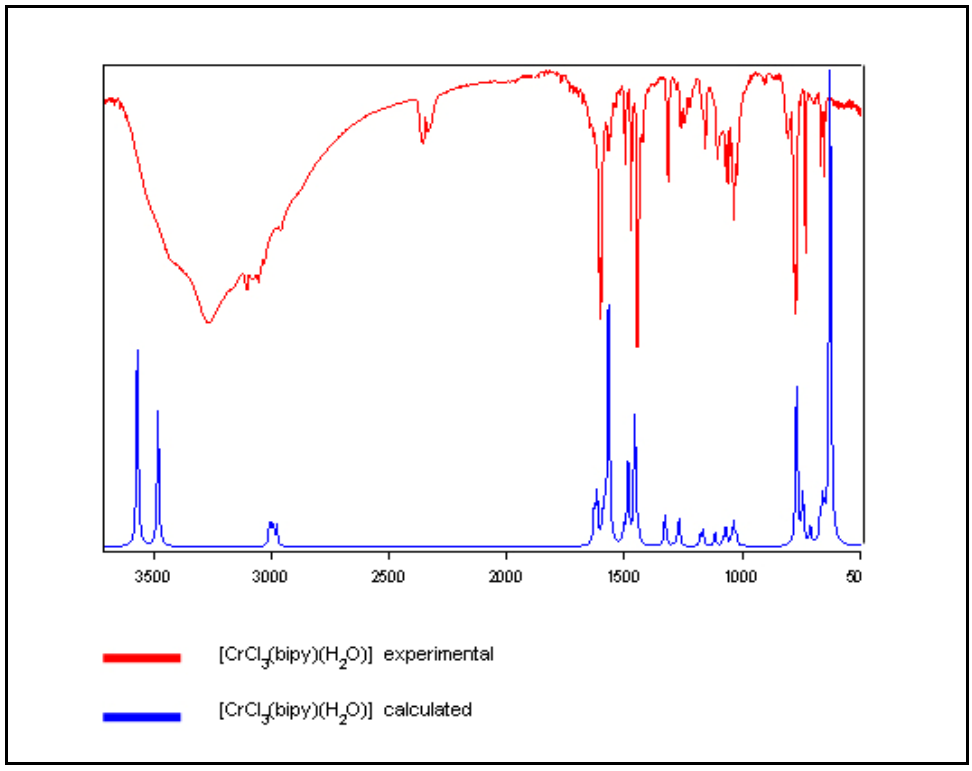

Figure 3.16 Experimental (red) and calculated (blue) MIR spectra of $[CrCl_3(bipy)(H_2O)]$

Along with a selection of other characteristic vibrations, Table 3.7 shows that the presence of coordinated water is confirmed, with the calculated data agreeing with the experimental assignment found just above 1600 cm^{-1}. The assignments of bipyridine-specific vibrations is also confirmed, which therefore indicates coordination.

Of the metal–ligand vibrations, the Cr–Cl modes show the strongest correlation, although, as with the Cr–O and Cr–N modes, the expected third vibration in the calculated spectrum was mixed with other vibrations.

Table 3.7 **Selected experimental and calculated IR band assignments for [$CrCl_3(bipy)(H_2O)$]**

[$CrCl_3(bipy)(H_2O)$] IR / cm^{-1}		**Assignment**	
Experimental	**Calculated**	**Experimental**	**Calculated**
3278	3574, 3490	ν(OH)	ν (OH) sym, asym
1608	1620	H-O-H	H-O-H + ν_{ring}
1570	1567	ν_{ring}	O-H scissors
1313	1332	ν_{ring} (CN)	ν_{ring} (CN)
451	462	bipy ring def	bipy ring def
416	424	bipy ring def	bipy ring def
-	390	-	Cr-O
371, 355, 346	360, 354	Cr-Cl	Cr-Cl
284	279	ν_{ring} / Cr-O	Cr-N + Cr-O + Cr-Cl
242	259, 232	Cr-N	Cr-N + Cr-O + Cr-Cl

Table 3.8 **Scaling factors determined for [$CrCl_3(bipy)(H_2O)$]**

Region / cm^{-1}	**Infrared**
0 – 1861	0.984833
2988 – 3422	0.935161

3.5.3 [$CrCl_3$(bipy)(CH_3CN)]

This complex was selected for computational investigation because it is the only one in this class to offer a non–pyridine-based monodentate N–type ligand and because the ligand itself possesses a number of characteristic vibrations.

The findings presented in Figures 3.17 and 3.18 show strong agreement between the experimental and computational values of the IR and Raman spectra.

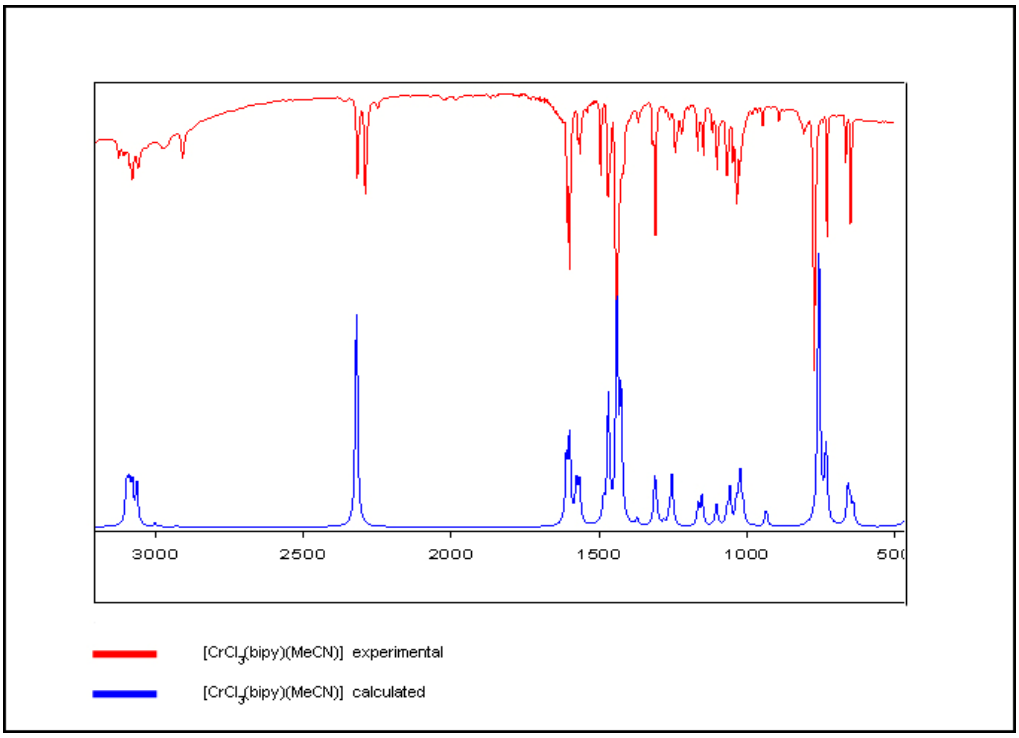

Figure 3.17 Experimental (red) and calculated (blue) MIR spectra of [$CrCl_3$(bipy)(CH_3CN)]

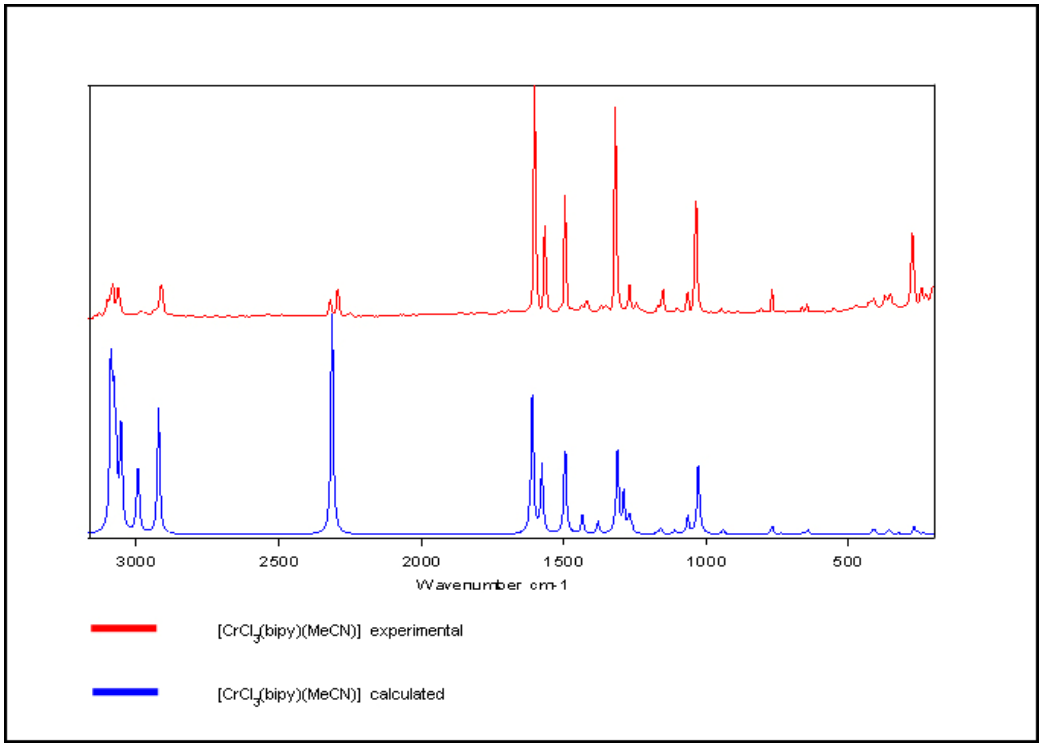

Figure 3.18 Experimental (red) and calculated (blue) Raman spectra of [$CrCl_3$(bipy)(CH_3CN)]

The only obvious difference is in the number of CH_3CN vibrations found between 2000 and 2500 cm^{-1}. Although it has already been mentioned in the vibrational discussions above, it is worth reiterating that all the previous literature on CH_3CN vibrations concurs with the two bands observed in the experimental spectra. These, along with a selection of other important ligand vibrations found in the complex, are highlighted in Table 3.9.

As in the previous complexes, the metal–ligand vibrational comparisons are again hampered by the mixing of modes in the calculated spectra to the extent that a clear distinction is not even made between the very different Cr–N (bipy) and Cr–N (CH_3CN) environments. This does to some extent, however, add weight to the conclusions drawn in the literature-based experimental assignments whereby no Cr–N (CH_3CN)-specific vibration was defined.

Table 3.9 **Selected experimental and calculated IR and Raman band assignments for [$CrCl_3$(bipy)(CH_3CN)]**

[$CrCl_3$(bipy)(CH_3CN)] IR /cm^{-1}		$CrCl_3$(bipy)(CH_3CN)] Raman/cm^{-1}		Assignment	
Experimental	**Calculated**	**Experimental**	**Calculated**	**Experimental**	**Calculated**
2910	2933	2913	2922	ν (CH_3) sym	ν (CH_3) sym
2318	-	2321	-	δ(CH_3) sym + ν(CC) (MeCN)	-
2291	2321	2293	2312	ν (C≡N)	ν (C≡N)
1608, 1600	1610, 1602	1600	1609	ν_{ring}	ν_{ring}
1367	1370	1367	1379	(CH_3) asym def	CH_3 def
1318, 1309	1311	1317	1315	ν_{ring} (CN)	ν_{ring} (CN)
664	658	665	653	ν_{ring} (bipy)	ν_{ring} (bipy)
454	459	-	-	bipy ring def	bipy ring def
365, 352, 337	357, 349	369, 350, 336	360, 350	Cr-Cl	Cr-Cl + Cr-N (bipy) + MeCN wag
-	322	-	322	-	Cr-N (bipy) + Cr-N (MeCN)
243	236	244	237	Cr-N (bipy)	Cr-Cl + Cr-N (MeCN) + bipy rock

ν = stretching, δ = in plane bending, def = deformation

Table 3.10 **Scaling factors determined for [$CrCl_3$(bipy)(CH_3CN)]**

Region / cm^{-1}	IR	Raman
0 – 1854	0.973658	0.979560
2213 – 3423	0.962099	0.958557

3.5.4 [$CrCl_3$(bipy)(py)]

Of particular interest with this compound was whether the assignments made to the experimental spectrum with regard to differentiating between bipyridine and pyridine vibrations could be supported. What aided this investigation was the extremely good match between the experimental and calculated vibrations seen in Figures 3.19 and 3.20.

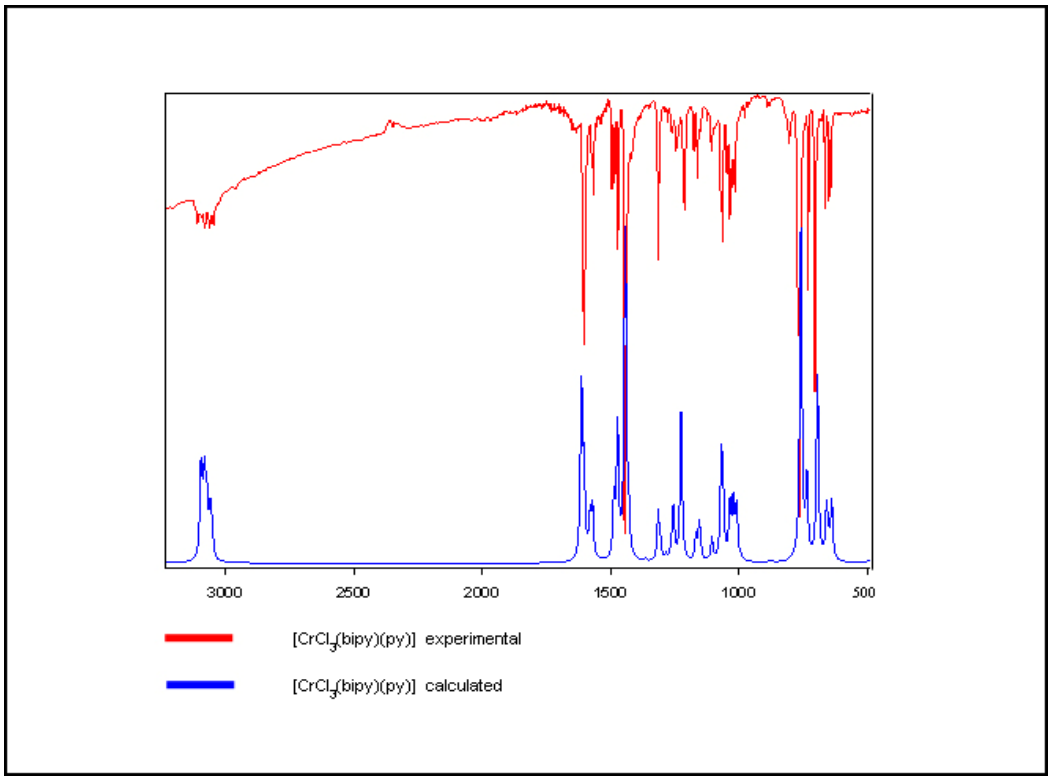

Figure 3.19 **Experimental (red) and calculated (blue) MIR spectra of [$CrCl_3$(bipy)(py)]**

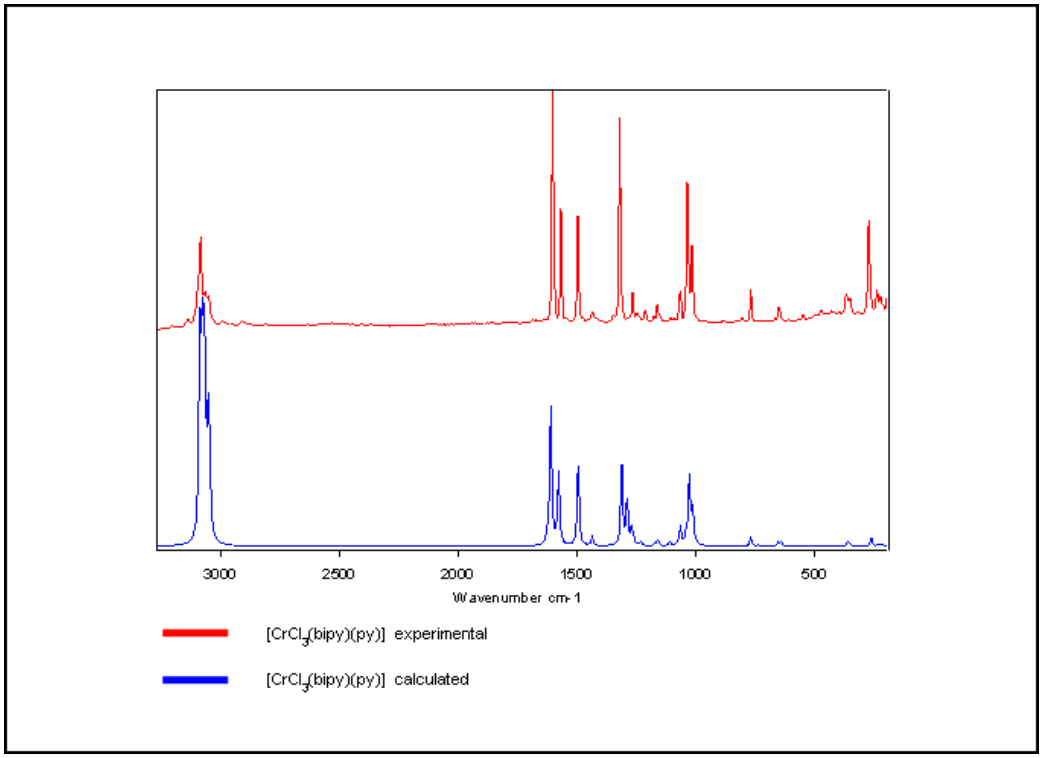

Figure 3.20 Experimental (red) and calculated (blue) Raman spectra of [$CrCl_3$(bipy)(py)]

As can been seen in Table 3.11, which highlights the important vibrations, computationally backed differences between the two heterocyclic N–ligands can be confirmed; these are all found at positions indicative of coordination.

Unfortunately, the same cannot be said for the Cr–N vibrations as, rather surprisingly, the calculated data makes no distinction between the two ligand environments and finds them both to be at ~305 cm^{-1}. As with [$CrCl_3$(bipy)(py)], the mixing of vibrations allows only two clear Cr–Cl vibrations to be observed in the calculated spectrum.

Table 3.11 **Selected experimental and calculated IR and Raman band assignments for [$CrCl_3$(bipy)(py)]**

[$CrCl_3$(bipy)(py)] IR / cm^{-1}		$CrCl_3$(bipy)(py)] Raman / cm^{-1}		Assignment	
Experimental	**Calculated**	**Experimental**	**Calculated**	**Experimental**	**Calculated**
1607	1613	-	-	ν_{ring} (py)	ν_{ring} (bipy + py)
1602	1604	1604	1610	ν_{ring} (bipy)	ν_{ring} (bipy)
1566	1570	1567	1577	ν_{ring} (bipy)	ν_{ring} (bipy)
1313	1315	1321	1312	ν_{ring} (CN)	ν_{ring} (CN)
1013	1008	1016	1012	Ring breathing (py)	Ring breathing (py)
663	657	663	652	ν_{ring} (bipy)	ν_{ring} (bipy)
643	636	-	-	δ_{ring} (py)	δ_{ring} (py)
453	459	470	462	bipy ring def	bipy ring def
442	443	442	445	ν_{ring} (py)	ν_{ring} (py) + weak ν_{ring} (bipy)
360, 348, 319	359, 345	365, 350, 317	360, 345	Cr-Cl	Cr-Cl
-	305	-	306	-	Cr-N (bipy + py)
236	231	236	231	Cr-N (bipy)	Cr-Cl + bipy rock + py rock
222	217	222	217	Cr-N (py)	Cr-Cl + bipy rock + py rock

ν = stretching, δ = in-plane bending, def = deformation

Table 3.12 Scaling factors determined for [$CrCl_3$(bipy)(py)]

Region / cm^{-1}	IR	Raman
0 - 1854	0.975740	0.980158
2980 - 3425	0.960663	0.957941

3.5.5 [$CrCl_3$(bipy)(pyphenyl)]

Computational analysis was conducted on this complex as the experimental analysis (literature) indicated that there may be coordinated thf present and that the complex may in fact be a mixture. With the strong correlation between the experimental and calculated spectra shown in Figures 3.21 and 3.22, positive deductions could be made.

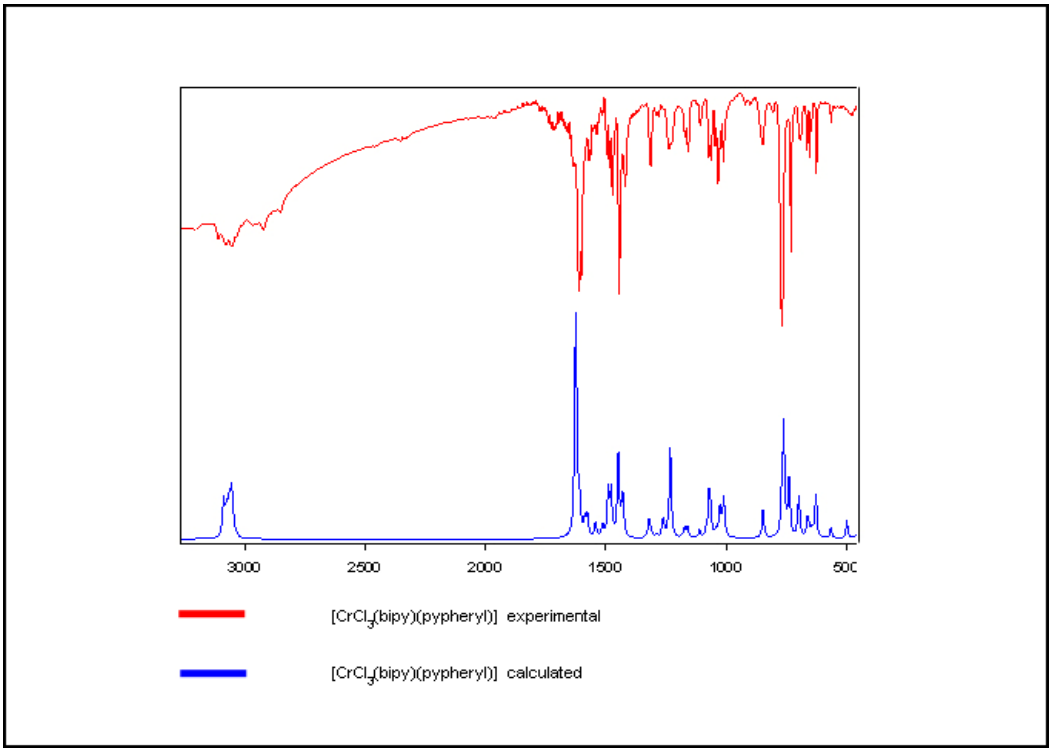

Figure 3.21 Experimental (red) and calculated (blue) MIR spectra of [$CrCl_3$(bipy)(pyphenyl)]

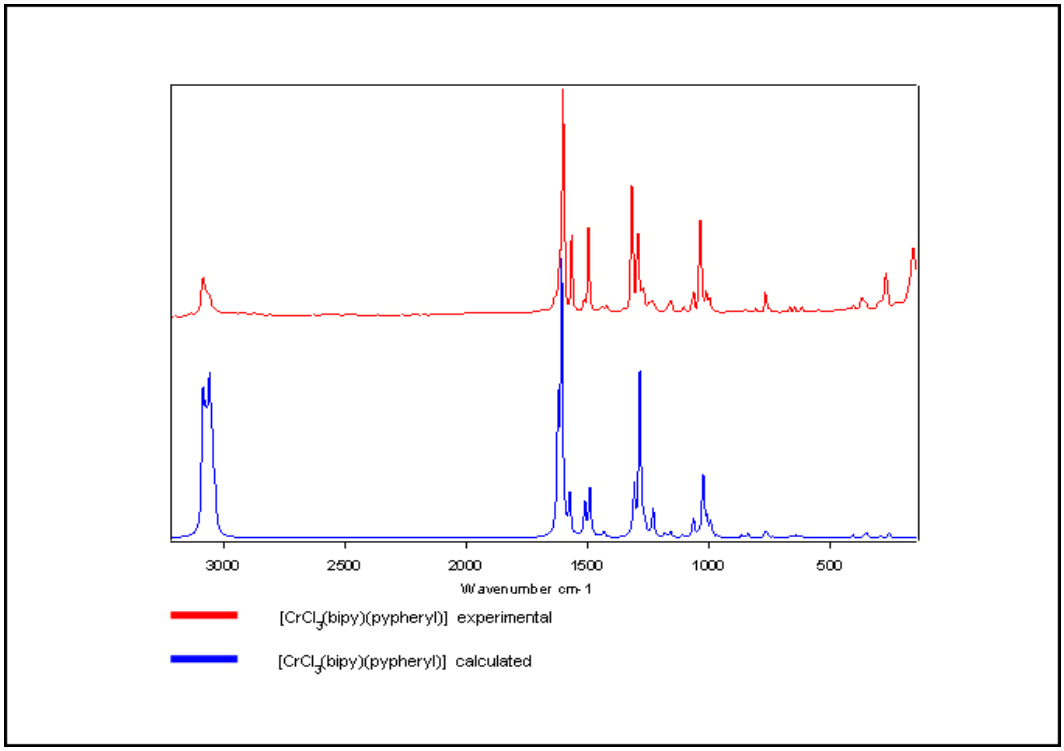

Figure 3.22 Experimental (red) and calculated (blue) Raman spectra of [$CrCl_3$(bipy)(pyphenyl)]

The reason that a mixture is suspected is due to the presence of the band at 856 cm^{-1} associated with coordinated thf (C–O–C). However, as a result of the computational data this band can now be assigned with confidence to a pyphenyl-specific vibration. If one then assumes that the C–H vibrations previously assigned to thf (2948, 2892 cm^{-1}) are associated with free thf (since a distinction between free and coordinated is most difficult), then there is sufficient evidence to suggest that this is not a mixture.

A summary of the important vibrations is given in Table 3.13 in which, in addition to the above-mentioned 856 cm^{-1} mode, one is able to see the strong agreement between the experimental and calculated assignments of both the bipyridine and pyphenyl vibrations.

With regard to the metal–ligand vibrations, the same trend is followed as with the other bipyridine complexes whereby only two distinct Cr–Cl vibrations are observed in the calculated spectra, with more observed as mixed vibrations at lower frequencies. However, unlike [$CrCl_3$(bipy)(py)], an obvious Cr–N vibration associated with the pyphenyl coordination is observed in the calculated IR spectrum at

348 cm^{-1}. Unfortunately, the same cannot be said regarding the Cr–N bipy equivalent, which is seen as a mixed mode at 293 cm^{-1}.

Table 3.13 **Selected experimental and calculated IR and Raman band assignments for [$CrCl_3$(bipy)(pyphenyl)]**

[$CrCl_3$(bipy)(pyphenyl)] IR / cm^{-1}		$CrCl_3$(bipy)(pyphenyl)] Raman / cm^{-1}		Assignment	
Experimental	**Calculated**	**Experimental**	**Calculated**	**Experimental**	**Calculated**
1610	1625	1613	1622	ν_{ring} (pyphenyl)	ν_{ring} (pyphenyl)
1602	-	1600	1606	ν_{ring} (bipy)	ν_{ring} (bipy)
1513	1513	1513	1511	ν_{ring} (pyphenyl)	ν_{ring} (pyphenyl)
1313	1320	1317	1309	ν_{ring} (CN)	ν_{ring} (CN)
1291	1292	1292	1285	ν_{ring} (bipy) + ν_{ring} pyphenyl	ν_{ring} (bipy) + ν_{ring} pyphenyl
1011	1010	1011	1008	Ring breathing (pyphenyl)	Ring breathing (pyphenyl)
856	856	849	863	Coord thf	δ_{ring} (pyphenyl)
625	627	616	620	δ_{ring} (pyphenyl)	δ_{ring} (pyphenyl)
454	462	-	-	bipy ring def	bipy ring def
419	419	424	434	bipy ring def	bipy ring def
-	389	-	-	-	δ_{ring} (pyphenyl)

372, 355, 323	364, 340	369, 352, 304	363, 340	Cr-Cl	Cr-Cl
-	348	-	-	-	Cr-N (pyphenyl)
-	293	-	292	-	Cr-N (bipy + pyphenyl)
236	229	232	229	Cr-N (bipy)	Cr-Cl + bipy rock + py rock
209	217	213	216	Cr-N (pyphenyl)	Cr-Cl + bipy rock + py rock

ν = stretching, δ = in-plane bending, def = deformation

Table 3.14 Scaling factors determined for [$CrCl_3$(bipy)(pyphenyl)]

Region / cm^{-1}	IR	Raman
0 – 1859	0.979713	0.977676
2966 – 3424	0.958930	0.957493

3.5.6 [$HpyNH_2$][$CrCl_4$(bipy)]

In contrast to the similar cationic-anionic crystal structure [Hpy][$CrCl_4(py)_2$] that was determined in Chapter 2, it was possible to collect IR and Raman data for this compound. This therefore allowed theoretical spectra to be generated and comparisons carried out with the corresponding experimental spectra. The fact that the calculations ignored the DCM molecule encaptured as part of the crystal structure was of little importance as no evidence of this molecule was found in the experimental IR or Raman spectra due to evaporation.

While Figures 3.23 and 3.24 indicate the good correlations between the respective theoretical and experimental spectra, it is the assignment comparisons of key bands presented in Table 3.15 that emphasise the true strength of these correlations.

Unfortunately, the mixing of modes in the calculated spectra inhibited the assignment of specific metal–ligand vibrations.

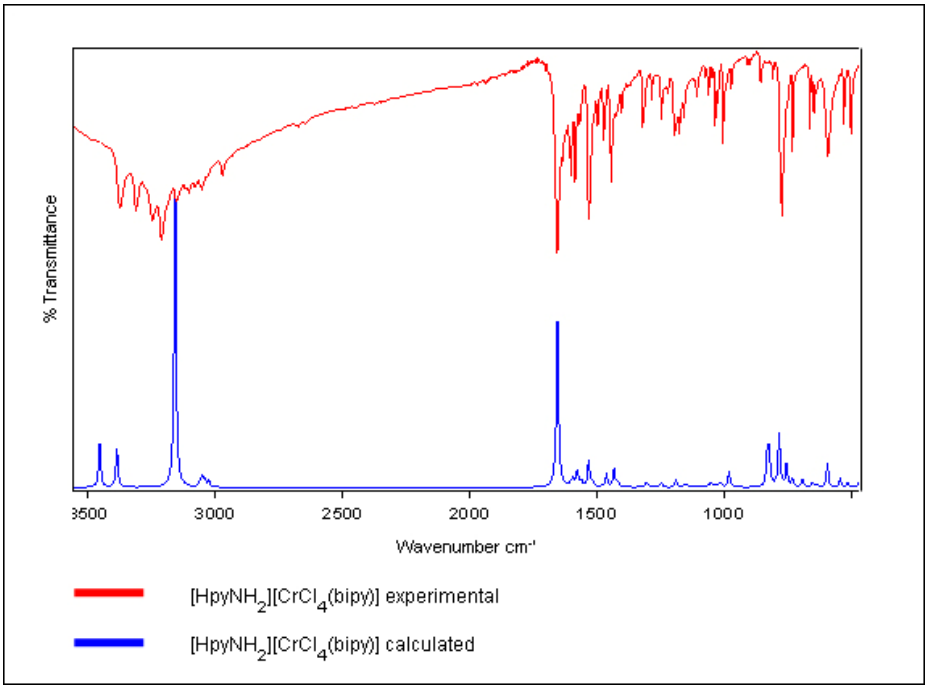

Figure 3.23 Experimental (red) and calculated (blue) Raman spectra of $[HpyNH_2][CrCl_4(bipy)]$

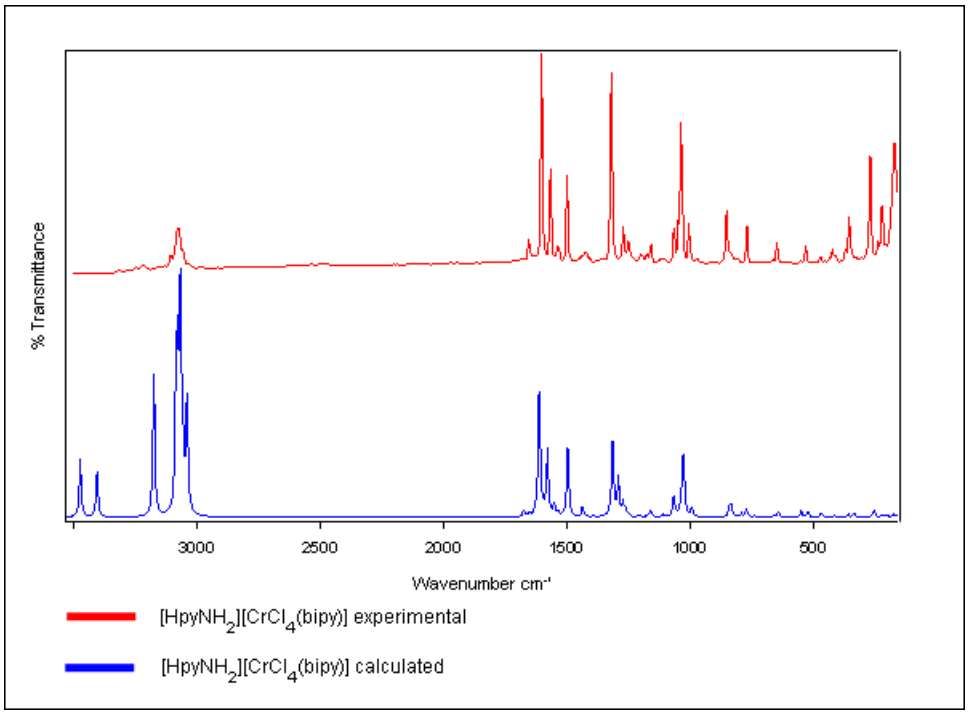

Figure 3.24 Experimental (red) and calculated (blue) Raman spectra of $[HpyNH_2][CrCl_4(bipy)]$

Table 3.15 **Selected experimental and calculated IR and Raman band assignments for $[HpyNH_2][CrCl_4(bipy)]$**

$[HpyNH_2][CrCl_4(bipy)]$ IR / cm^{-1}		$[HpyNH_2][CrCl_4(bipy)]$ Raman / cm^{-1}		Assignment	
Experimental	**Calculated**	**Experimental**	**Calculated**	**Experimental**	**Calculated**
3153	3157	3142	3173	$\nu(NH_2)$ sym	$\nu(NH_2)$ asym
1656	1655	1653	1654	$\delta(NH_2)$	$\delta(NH_2) + \nu_{ring}$
1600	1592	1601	1610	ν_{ring} (bipy)	ν_{ring} (bipy)
1585	1576	-	-	pyH (CC)	pyH (CC)
1318	1305	1318	1320	ν_{ring} (CN)	ν_{ring} (CN)
661	652	661	653	ν_{ring} (bipy)	ν_{ring} (bipy)
642	631	646	639	pyH (CCC)	pyH (CCC)
590	592	597	598	pyH (CC)	pyH (N^+H)
452	456	452	461	bipy ring def	bipy ring def
366, 350, 343, 327	330	367, 352, 326	334	Cr-Cl	Cr-Cl
-	327, 311	-	331, 314	-	Cr-Cl + Cr-N
-	248, 220	-	250, 223	-	Cr-Cl + bipy rock
237	-	235	-	Cr-N	-
220	211	220	213	pyH	pyH

ν = stretching, δ = in-plane bending, def = deformation

Table 3.16 **Scaling factors determined for $[HpyNH_2][CrCl_4(bipy)]$**

Region / cm^{-1}	IR	Raman
0 – 1854	0.969057	0.980070
2980 – 3425	0.950532	0.954942

3.5.7 HOMO AND LUMO ORBITALS OF THE CALCULATED COMPLEXES

In the case of all the complexes discussed in Chapter 2 the chlorine atoms are sites of high electron density and are susceptible to electrophilic attack. However, what is perhaps surprising is that the various monodentate ligands that differ both sterically and electronically from each other do not play a role in altering the region of nucleophilic attack, which in all cases is found to be the bipyridine ligand. The same trend holds true for $[HpyNH_2][CrCl_4(bipy)]$. Figures 3.25-3.30 depict the HOMO and LUMO orbitals of the compounds.

HOMO **LUMO**

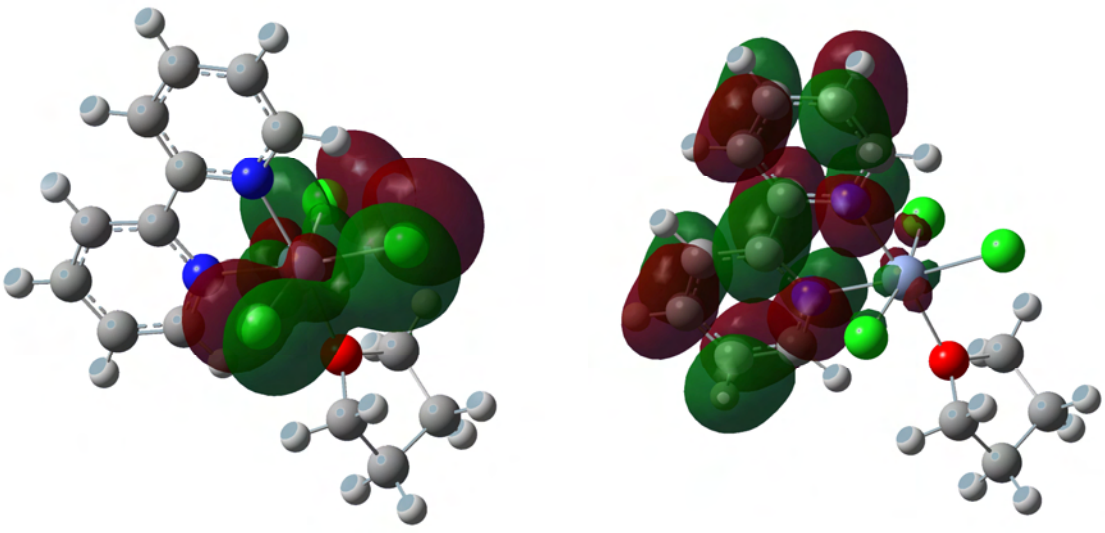

Figure 3.25 **HOMO and LUMO orbitals of $[CrCl_3(bipy)(thf)]$**

HOMO **LUMO**

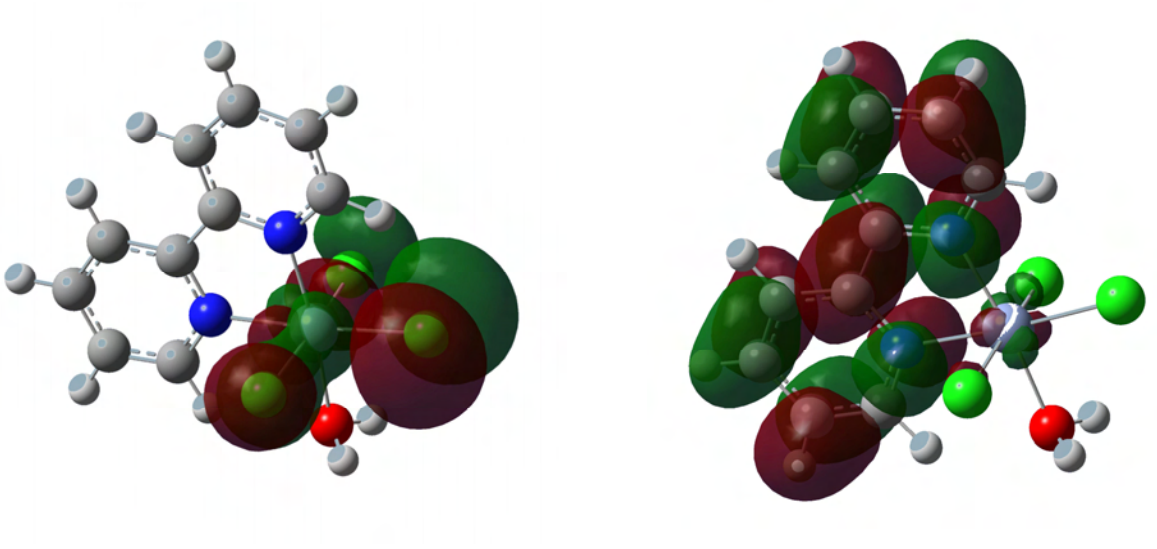

Figure 3.26 **HOMO and LUMO orbitals of [$CrCl_3$(bipy)(H_2O)]**

HOMO **LUMO**

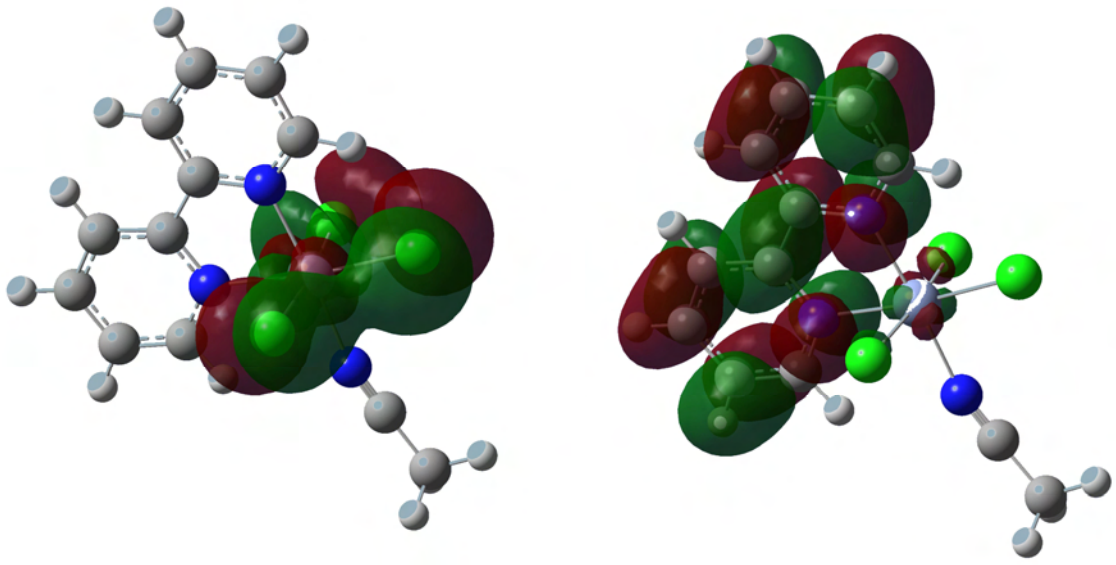

Figure 3.27 **HOMO and LUMO orbitals of [$CrCl_3$(bipy)(MeCN)]**

HOMO **LUMO**

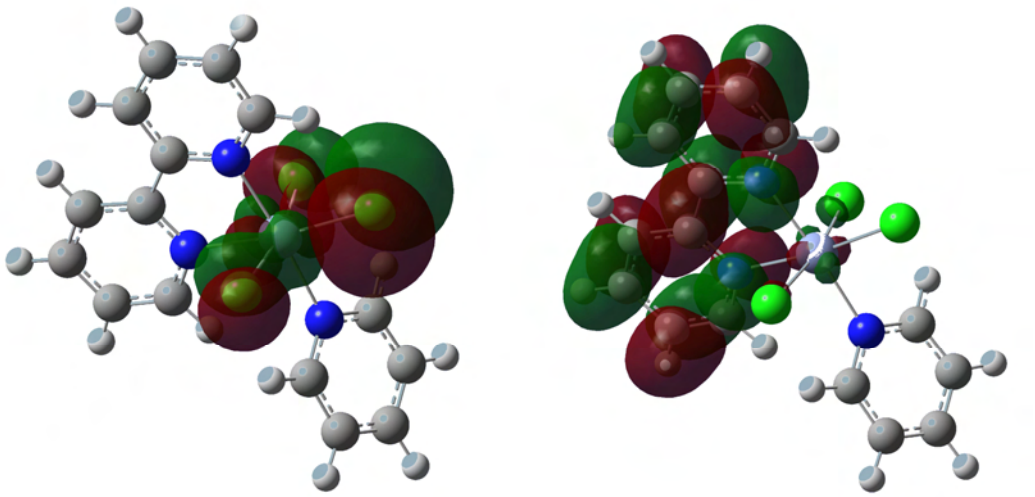

Figure 3.28 **HOMO and LUMO orbitals of [$CrCl_3$(bipy)(py)]**

HOMO **LUMO**

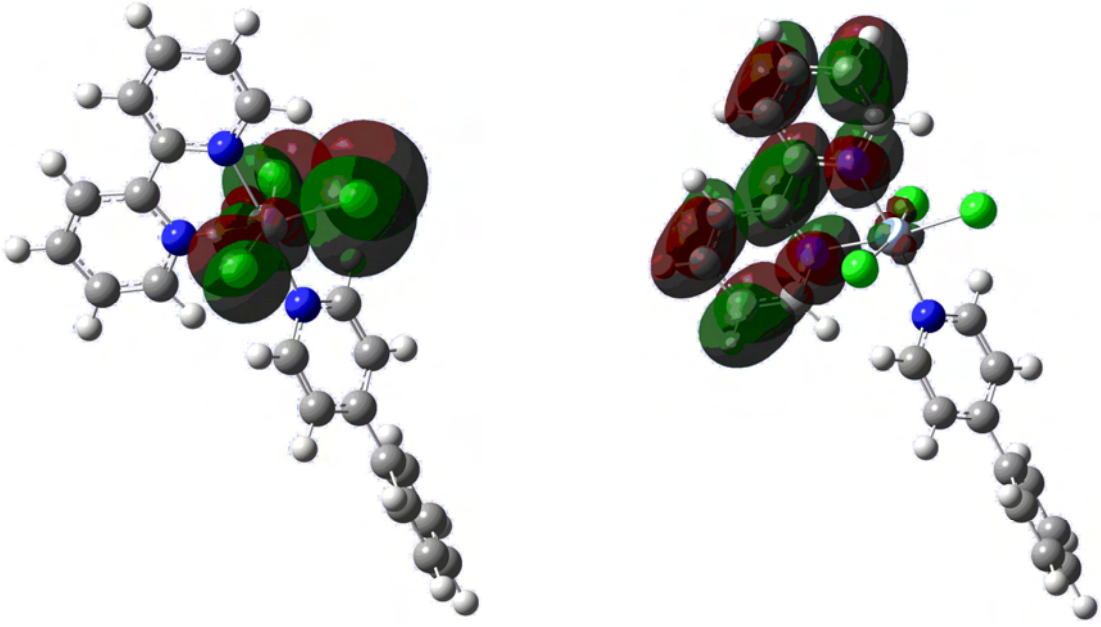

Figure 3.29 **HOMO and LUMO orbitals of [$CrCl_3$(bipy)(pyphenyl)]**

HOMO **LUMO**

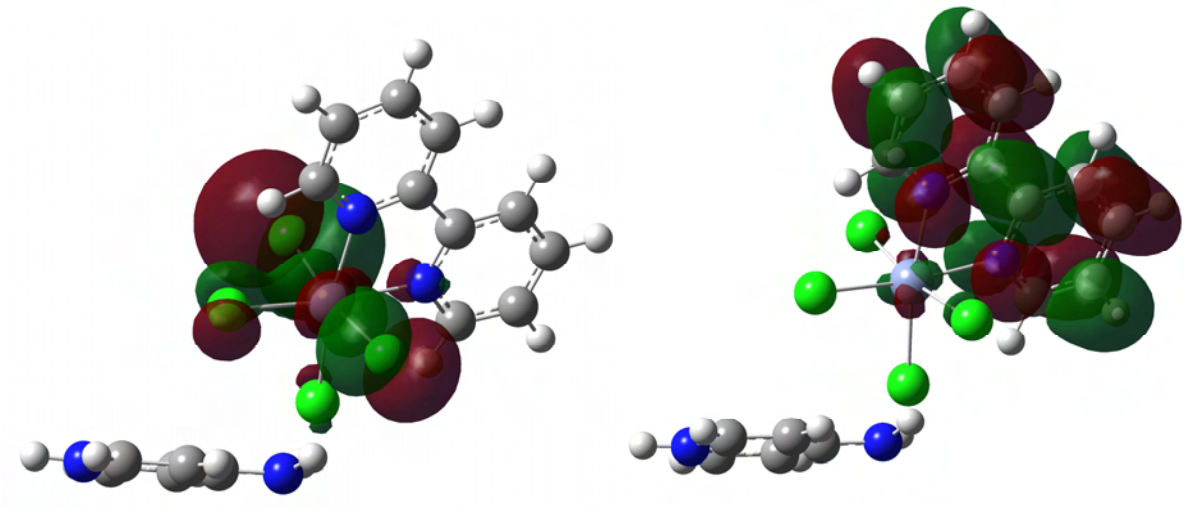

Figure 3.30 HOMO and LUMO orbitals of [HpyNH$_2$][CrCl$_4$(bipy)]

3.6 NMR SPECTROSCOPY

In the light of the success achieved in being able to follow the substitution of thf with monodentate pyridine ligands via ^{1}H NMR spectroscopy (as seen in Chapter 2), an analogous experiment was carried out whereby one equivalent of bipyridine was added to the [CrCl$_3$(thf)$_3$] precursor. The results were equally satisfactory.

The same procedure was employed, which involved the addition of stoichiometric amounts of bipyridine in acetone-d$_6$ to [CrCl$_3$(thf)$_3$] in an NMR tube. As expected, the result of collecting spectra in rapid succession was that the resonances associated with the free aromatic N–donor ligand (δ=7.49–8.62 ppm) disappeared upon coordination to the paramagnetic metal centre over time. See Figure 3.31.

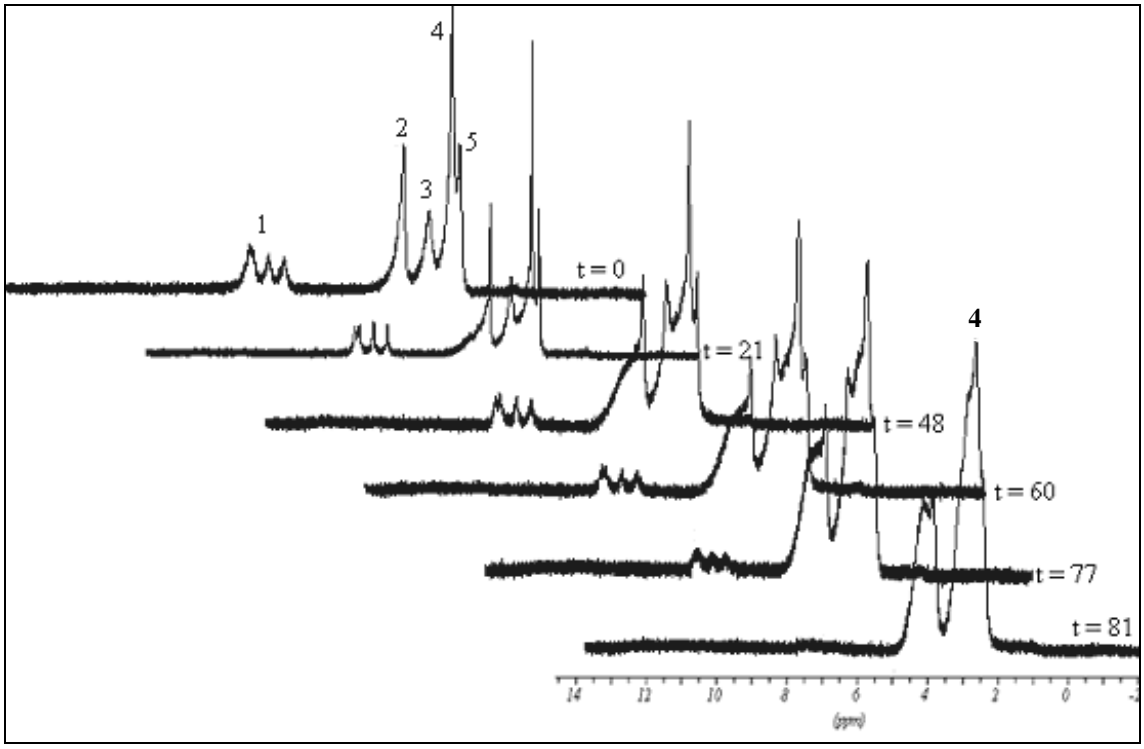

Figure 3.31 **Stacked ^{1}H NMR spectra for the reaction of bipy with $[CrCl_3(thf)_3]$ over time. 1 = bipy, 2 = thf, 3 = water peak in acetone, 4 = acetone d_6 , 5 = thf**

An integration of the resonances of uncoordinated bipyridine to the thf resonances was plotted as a ratio vs time in Figure 3.32. It can be clearly seen that the value of the ratio bipyridine:thf decreases linearly over time.

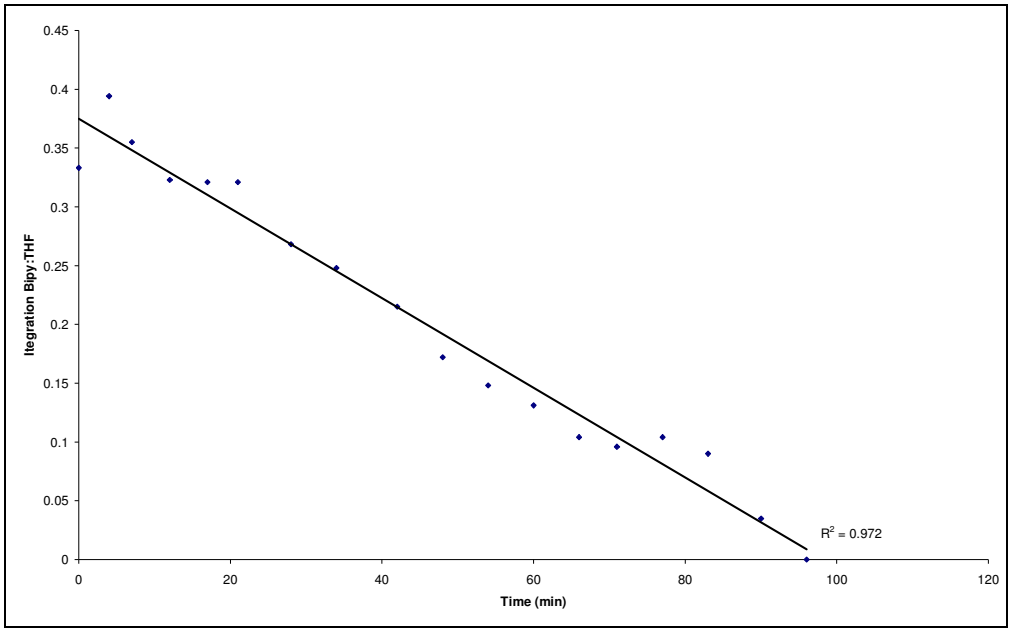

Figure 3.32 **Plot of integration of bipy:thf resonances over time**

In contrast to the pyridine results, the reaction was complete after 81 minutes and, unlike the monodentate results, this completion time coincided well with the visual observations of product formation made with the naked eye while the same reaction was being carried out under standard Schlenk conditions in the laboratory.

In keeping with the methodology of Chapter 2, the sample was left in the instrument for a further hour, after which time another spectrum was recorded (see Figure 3.33). As was the case with the analogous pyridine experiment, the spectral resonances were more defined.

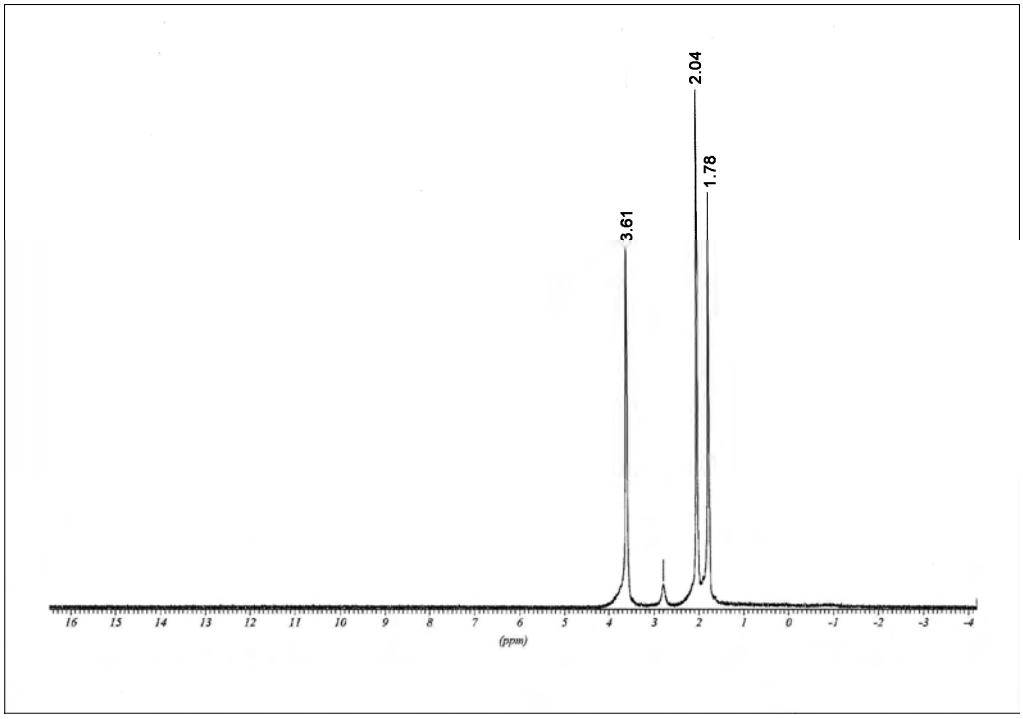

Figure 3.33 **^{1}H NMR spectra of [$CrCl_3$(bipy)(thf)] final product in acetone-d_6**

Again, the pyridine experiments were followed; a small amount of the expected olive green precipitate was dried and dissolved in DMSO-d_6 and a ^{13}C NMR spectrum recorded, Figure 3.34. The absence of bipyridine resonances suggests coordination as was the case for the monomer (pyridine) while, unlike in the previous chapter, the presence of thf resonances is indicative of coordinated thf which would be in agreement with the IR and Raman results indicating the formation of the monomer [$CrCl_3$(bipy)(thf)].

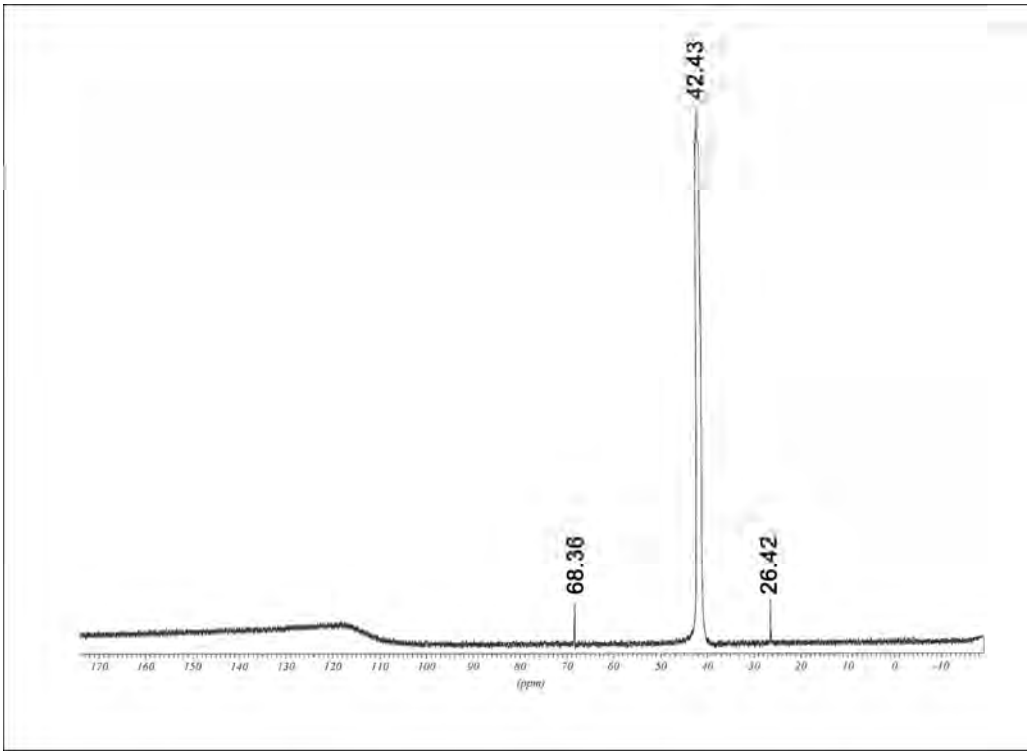

Figure 3.34 **^{13}C NMR spectrum of [$CrCl_3$(bipy)(thf)] final product in DMSO-d_6**

In an attempt to confirm that the thf resonances in the above compound were associated with the coordinated ligand, ^{1}H NMR spectra of a selection of some of the other compounds synthesised in this particular bipyridine class were studied. They included [$CrCl_3$(bipy)(CH_3CN)], [$CrCl_3$(bipy)(H_2O)] and [$CrCl_3$(bipy)(py)]. Figures 3.35 ([$CrCl_3$(bipy)(CH_3CN)]) and 3.36 ([$CrCl_3$(bipy)(py)]) are the analogous spectra to that of [$CrCl_3$(bipy)(thf)] in Figure 3.33. Figure 3.37 was recorded using DMSO-d_6 as it was the final precipitate.

Nevertheless, in all three cases bipyridine and thf resonances are absent, with the latter possibly implying coordination of the monodentate ligands. Yet further evidence of monodentate ligand coordination is observed in [$CrCl_3$(bipy)(CH_3CN)] and [$CrCl_3$(bipy)(py)] in that these monodentate ligand resonances are also absent in the respective product spectra (7.30–8.57 ppm and 1.9 ppm respectively). As the water molecule is observed at 3.3 ppm there is a suggestion that coordination to the metal has not taken place. This inability to suggest H_2O coordination via ^{1}H NMR is of no real concern as the crystal structure has been solved as part of this study.

Comparisons of these three compounds' spectra with that of $[CrCl_3(thf)_3]$ and bipyridine therefore suggest that the thf observed in the final spectrum is indicative of coordinated thf and thus the formation of $[CrCl_3(bipy)(thf)]$.

Note that the NMR deductions regarding all these compounds correlate well with the IR and Raman spectra deductions regarding the respective final products.

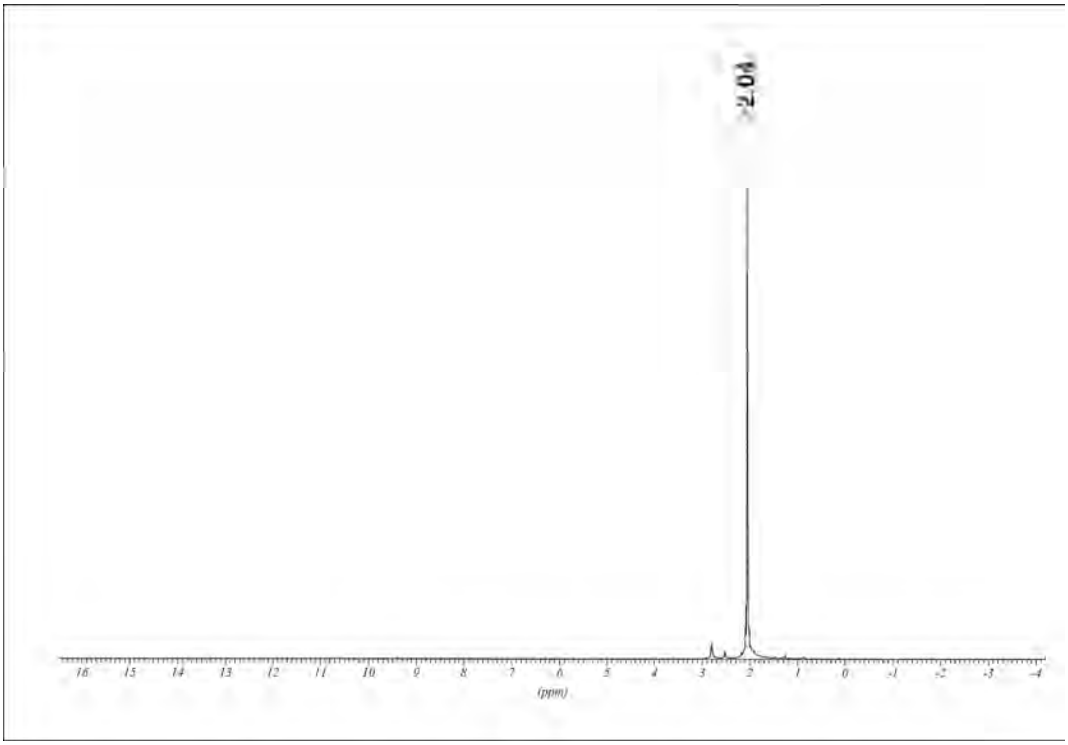

Figure 3.35 **^{1}H NMR spectrum of $[CrCl_3(bipy)(CH_3CN)]$ in acetone-d_6**

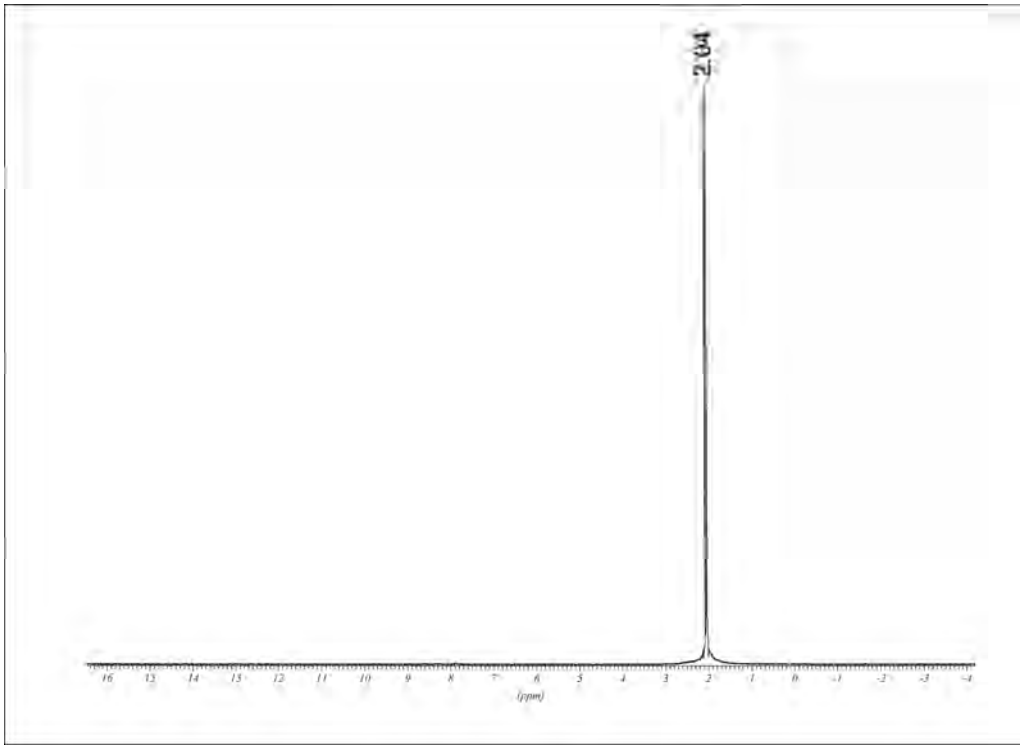

Figure 3.36 ^{1}H NMR spectrum of [$CrCl_3$(bipy)(py)] in acetone-d_6

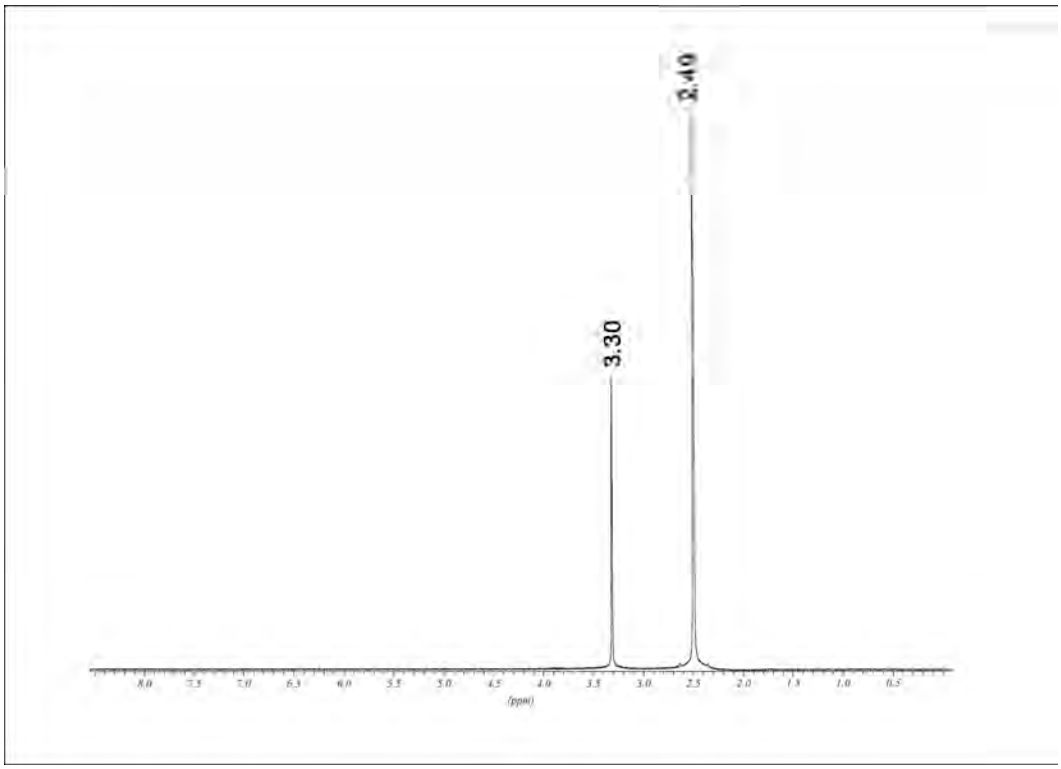

Figure 3.37 ^{1}H NMR spectrum of [$CrCl_3$(bipy)(H_2O)] in DMSO-d_6

3.7 MASS SPECTROMETRY

As was the case for the computational analysis, a representative selection of the compounds were analysed by FAB-MS. These included [$CrCl_3$(bipy)(thf)], [$CrCl_3$(bipy)(H_2O)], [$CrCl_3$(bipy)(CH_3CN)] and [$CrCl_3$(bipy)(pyphenyl)].

In conjunction with the vibrational results the FAB-MS spectrum of the [$CrCl_3$(bipy)(thf)] precipitate suggests the monomeric species. The isotopic distribution patterns for $[M–thfCl]^+$ (m/z = 278) and $[M–thfH2Cl]^+$ (m/z = 243) fragments are observed and correspond with the equivalent theoretically generated patterns. See Figure 3.38.

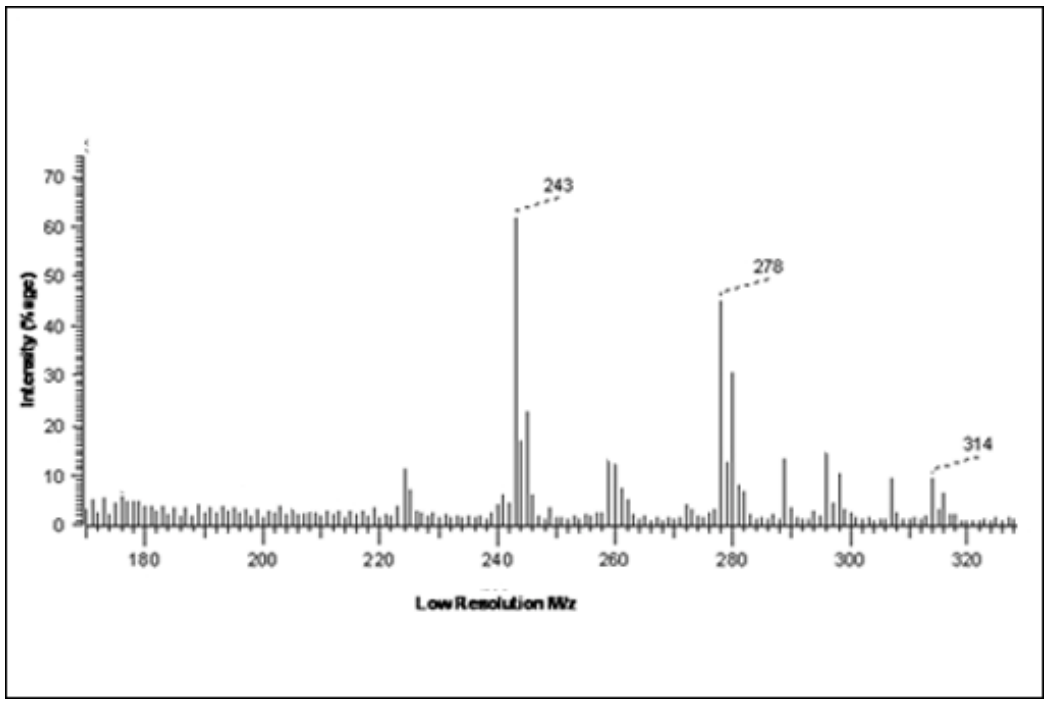

Figure 3.38 FAB-MS spectrum of [$CrCl_3$(bipy)(thf)]

The mass spectrum of the [$CrCl_3$(bipy)(H_2O)] precipitate is shown in Figure 3.39 and corresponds with the structure elucidated from the single crystal determination. Well defined isotopic distribution patterns are observed for the $[M–Cl]^+$ (m/z = 296) and $[M–H_2OCl]^+$ (m/z = 278) fragments and these are in agreement with the theoretical equivalents.

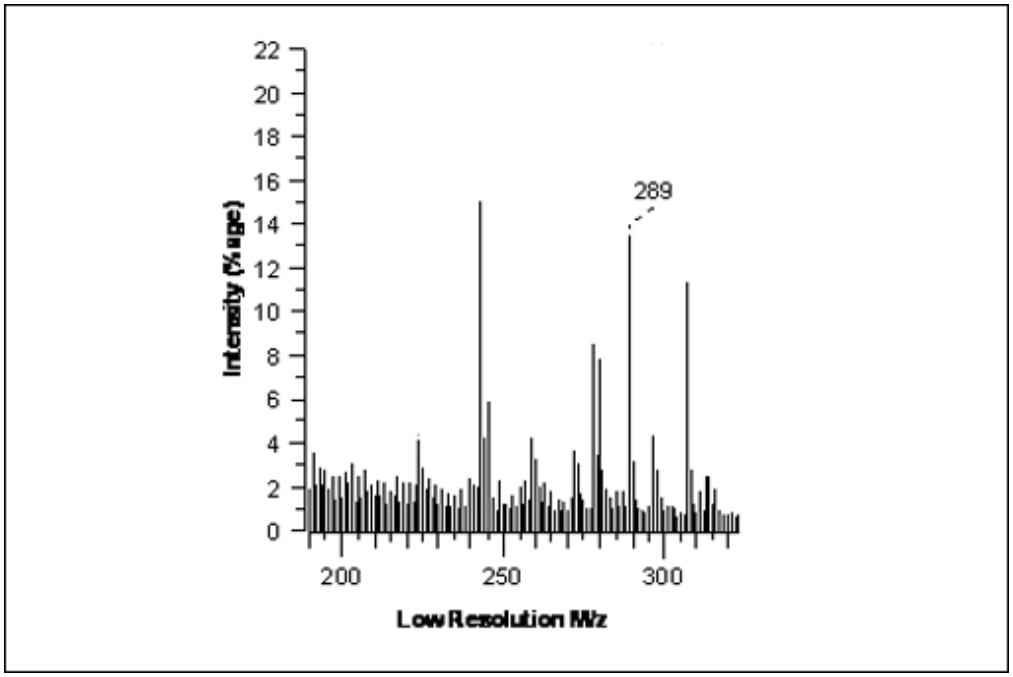

Figure 3.39 FAB-MS spectrum of [$CrCl_3$(bipy)(H_2O)]

The molecular fragments $[M–CH_3CNCl]^+$ (m/z = 278) and $[M–CH_3CN2Cl]^+$ (m/z = 243) are observed for the precipitate of [$CrCl_3$(bipy)(CH_3CN)] (see Figure 2.40) and are confirmed by good isotopic patterns which correlate with those calculated theoretically. Based on the MS results of the other compounds within this class these fragments are associated with the monomeric species.

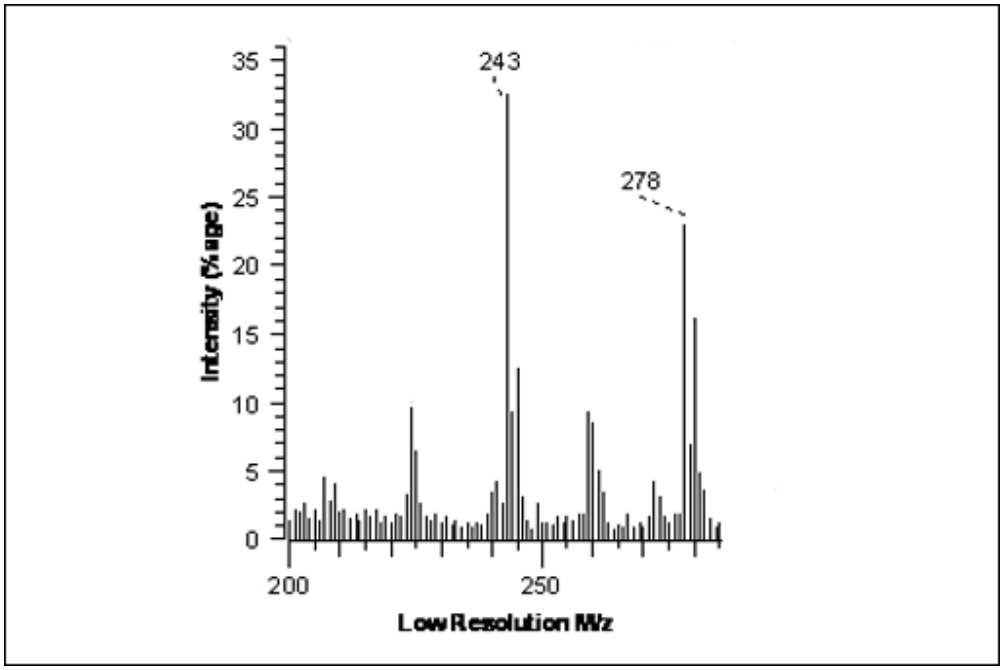

Figure 3.40 FAB-MS spectrum of [$CrCl_3$(bipy)(CH_3CN)]

Confirmation of the monomeric species as defined by the vibrational analysis is seen in the MS spectrum of the [$CrCl_3$(bipy)(pyphenyl)] precipitate in Figure 3.41. Isotopic distribution patterns that correlate to those generated by the isotopic calculator include $[M–Cl]^+$ (m/z = 433), $[M–pyphenylCl]^+$ (m/z = 278) and $[M–pyphenyl2Cl]^+$ (m/z = 243).

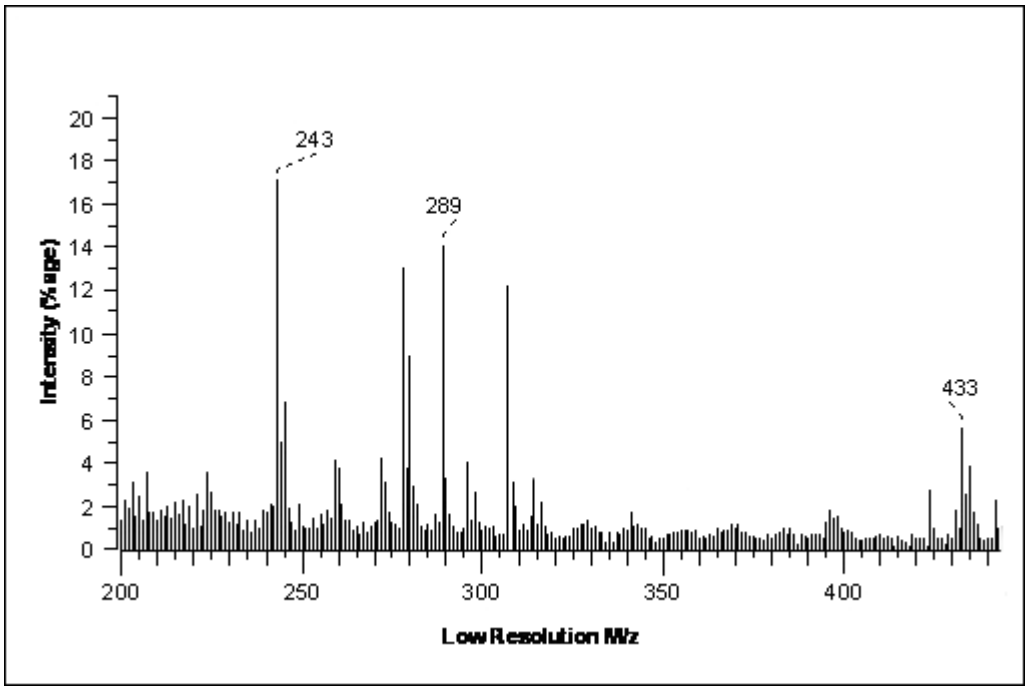

Figure 3.41 FAB-MS spectrum of [$CrCl_3$(bipy)(pyphenyl)]

3.8 X-RAY CRYSTALLOGRAPHY

3.8.1 SOLUBILITY AND CRYSTAL SYNTHESIS

As with the class of compounds discussed in the previous chapter, solubility once again proved problematic and the growing of suitably sized crystals was both a difficult and at times a frustrating practice. Of the wide array of solvents tested to carry out crystallisation, only four successfully dissolved the precipitates to a suitable degree. Perhaps unsurprisingly, these included the highly polar solvents DMSO and DMF with dielectric constants of 47.2 and 38.3 respectively. Although crystals have previously been grown from these solvents, not least the compound [$CrCl_3(py)_2$(DMF)] in the previous chapter, they are not normally regarded as the

solvents of choice for crystallisation as their high vapour pressures inhibit evaporation.

The successful crystallisations were achieved by the slow evaporation of the solvents CH_3CN (dielectric constant of 37.5) and $ClCH_2CN$ (dielectric constant of 30) to yield $[CrCl_3(bipy)(H_2O)]$ and $[HpyNH_2][CrCl_4(bipy)]$ respectively. $ClCH_2CN$ was certainly the better of the two solvents in terms of solubility. The author ascribes this to the increased polarity attributed to the addition of the chlorine atom. Although there was only sparing solubility in CH_3CN, the filtering of a saturated CH_3CN solution proved successful in yielding suitable crystals.

3.8.2 $[CrCl_3(bipy)(H_2O]$

As previously mentioned in regard to the early investigation into the synthesis of $[CrCl_3(thf)_3]$ in Chapter 1, the crystal structure of $[CrCl_3(bipy)(H_2O)]$ resulted from the reaction between bipyridine and water-contaminated $[CrCl_3(thf)_3]$. It is worth mentioning, however, that a precipitate of $[CrCl_3(bipy)(H_2O)]$ was synthesised by the addition of a few drops of water to a $[CrCl_3(bipy)(thf)]$ reaction mixture which used Sigma Aldrich grade $[CrCl_3(thf)_3]$. IR characterisation of the precipitate revealed a spectrum identical to that of the H_2O-coordinated crystal structure.

Although the molecular structure of complex $[CrCl_3(bipy)(H_2O)]$ is similar to that reported for aqua-(4,4'–t–butyl–2,2'–bipyridyl) trichlorochromium(III) tetrahydrofuran solvate by Namba [108], there are significant crystallographic differences between the two structures. Figure 3.42 shows the perspective drawings of the two structures.

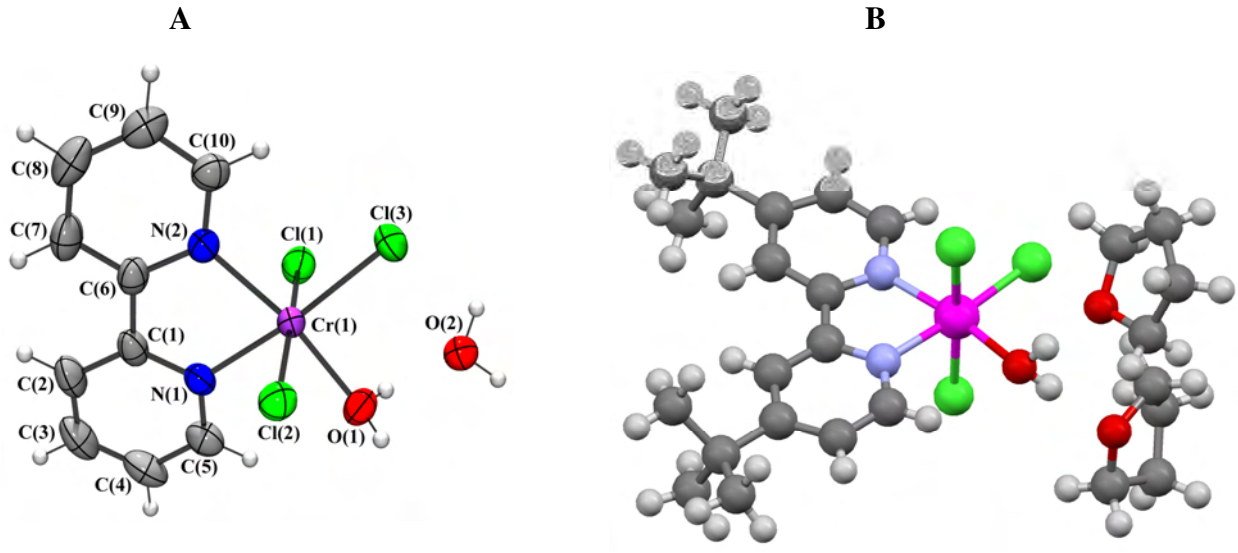

Figure 3.42 **A = Perspective drawing of [$CrCl_3(bipy)(H_2O)$] structure determined in this study, B = Perspective drawing of the structure determined by Namba [108]**

In both structures the chromium atom is coordinated to three chlorine atoms, the two nitrogen atoms of the bipyridine group and the oxygen atom of a water ligand. The water ligand is *trans* to one of the bipyridine nitrogen atoms in both structures. In [$CrCl_3(bipy)(H_2O)$] the coordination is approximately octahedral, with the largest deviation being the N–Cr–N bond angle (78.79(9)°). This is a significantly greater deviation than was observed for the pyridine structures of Chapter 2 and is a direct result of the five–membered chelate ring. Note that all the other *cis* Cr-centred bond angles are in the range 85.16(6) to 95.70(7)° (see Table 3.17). The slight shortening of the Cr–N bond lengths relative to the monodentate analogues was also observed and is also a direct consequence of the bipyridine-induced chelate ring.

To continue the comparison with the 'Namba structure', it was observed that the bipyridine ligands in both complexes are non–planar. The degree of twisting between the two ring systems is, however, greater in the unsubstituted bipyridine structure of this study and is clearly seen in the N(1)–C(5)–C(6)–N(2) torsion angle comparisons of 3.9(5)° ('Namba structure') and 9.0(3)° (this study).

Table 3.17 **Selected bond lengths [Å], bond angles [°] and torsion angles [°] for [$CrCl_3(bipy)(H_2O)$]**

Cr(1)-O(1)	2.003(2)	Cr(1)-Cl(3)	2.3083(8)
Cr(1)-N(1)	2.059(2)	Cr(1)-Cl(2)	2.3114(8)
Cr(1)-N(2)	2.066(2)	Cr(1)-Cl(1)	2.3435(8)
O(1)-Cr(1)-N(1)	92.28(9)	N(2)-Cr(1)-Cl(2)	89.74(6)
N(1)-Cr(1)-N(2)	78.79(9)	Cl(3)-Cr(1)-Cl(2)	93.26(3)
O(1)-Cr(1)-Cl(3)	93.31(7)	O(1)-Cr(1)-Cl(1)	88.28(7)
N(2)-Cr(1)-Cl(3)	95.70(7)	N(1)-Cr(1)-Cl(1)	85.16(6)
O(1)-Cr(1)-Cl(2)	87.50(7)	N(2)-Cr(1)-Cl(1)	93.46(6)
N(1)-Cr(1)-Cl(2)	88.83(6)	Cl(3)-Cr(1)-Cl(1)	93.16(3)
N(1)-C(1)-C(6)-N(2)	9.0(3)	C(2)-C(1)-C(6)-C(7)	10.8(4)

Table 3.18 highlights the differences of structural importance.

Table 3.18 **Crystallographic differences between the two structures**

Crystal data	**[$CrCl_3(bipy)(H_2O)$]**	**Namba structure[109]**
Crystal system	Monoclinic	Orthorhombic
Space group	C 2/c	P $2_12_12_1$
Volume/non-H atoms	19.1 $Å^3$	21.6 $Å^3$
R-factor	3.51%	6.97%

As both structures possess different solvent molecules within their respective unit cells, variations are also observed regarding solvent–complex interactions. In fact, a comparison between the volumes/non-H atoms of the two structures, as documented in Table 3.18, suggests that there is more efficient packing in the structure of this study as a result of stronger intermolecular interactions. The hydrogen bond interactions within the [$CrCl_3(bipy)(H_2O)$] complex will now be discussed in detail.

The oxygen atom of the non–coordinated water molecule lies on a crystallographic twofold rotation axis. Both the coordinated and non–coordinated water molecules,

together with two of the chlorine atoms (Cl(1) and Cl(3)), are involved in an extended network of hydrogen bonds (see Figure 3.43 and Table 3.19). Each non–coordinated water molecule is involved in four hydrogen bonds: two as a donor to two symmetry–related Cl(1) atoms and two as an acceptor from two symmetry–related coordinated water molecules. Each coordinated water molecule is involved in two hydrogen bonds: as a donor to both a non–coordinated water molecule and a symmetry–related Cl(3) atom.

Table 3.19 **Hydrogen bonds for [$CrCl_3(bipy)(H_2O)$] [Å and °]**

D-H...A	d(D-H)	d(H...A)	d(D...A)	<(DHA)
O(1)-H(1B)...O(2)	0.72(4)	1.98(4)	2.690(3)	173(4)
O(1)-H(1A)...Cl(3)#1	0.80(3)	2.40(4)	3.192(2)	176(3)
O(2)-H(2A)...Cl(1)#1	0.84(3)	2.39(3)	3.1671(17)	156(3)

Symmetry transformations used to generate equivalent atoms:
#1 x,-y,z-1/2

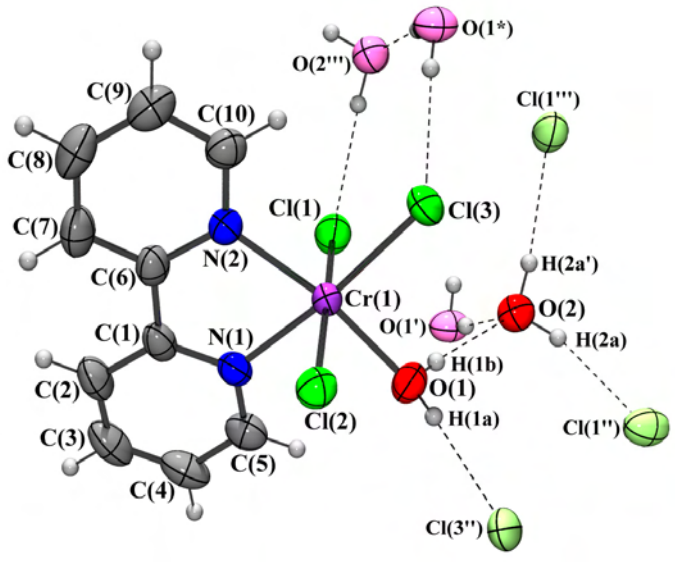

Figure 3.43 **Hydrogen bond interactions**

The final difference between the two structures is observed in their respective packing arrangements, with only [$CrCl_3(bipy)(H_2O)$] possessing short-contact interactions between the aromatic ring layers. They are best described as staggered π–π interactions with a maximum distance of 3.379 Å. See Figure 3.44.

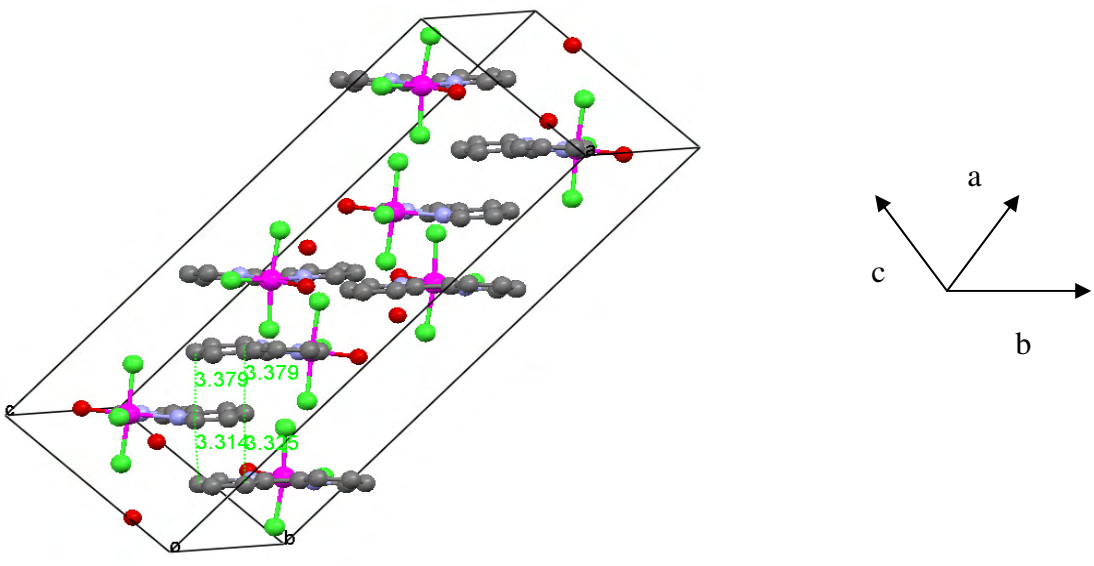

Figure 3.44 Short contacts between aromatic ring layers

In addition, the powder X–ray diffraction pattern of [$CrCl_3(bipy)(H_2O)$] calculated from the crystal structure was compared with the experimentally obtained powder X-ray diffraction pattern; the excellent agreement is shown in Figure 3.45.

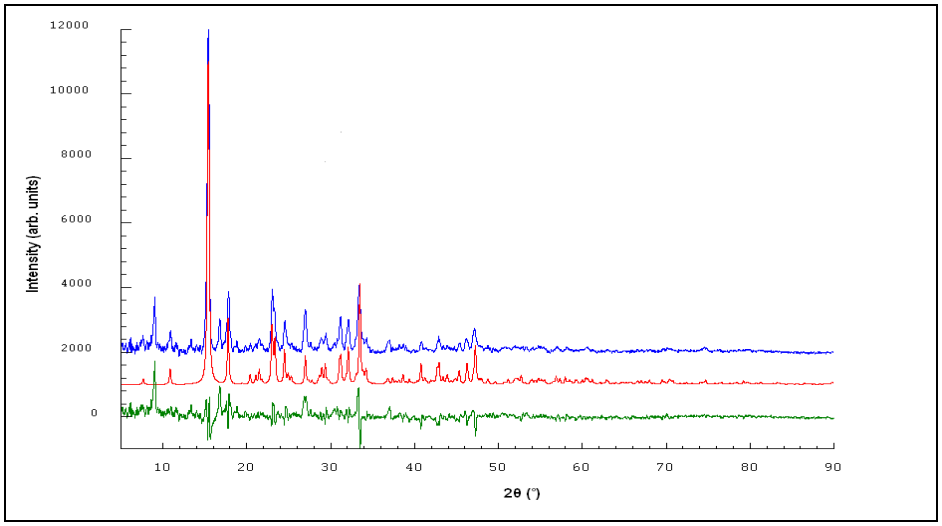

RED: Calculated BLUE: Single crystal sample GREEN: Difference

Figure 3.45 Comparison of the experimental and theoretically obtained X-ray diffraction powder patterns of [$CrCl_3(bipy)(H_2O)$]

Table 3.20 Crystal data and structure refinement for [$CrCl_3$(bipy)(H_2O)].

Empirical formula	$C_{10}\ H_{11}\ Cl_3\ Cr\ N_2\ O_{1.5}$	
Formula weight	341.56	
Temperature	293(2) K	
Wavelength	0.71073 Å	
Crystal system	Monoclinic	
Space group	C 2/c	
Unit cell dimensions	a = 27.034(3) Å	α= 90°
	b = 10.1086(12) Å	β= 97.371(2)°
	c = 9.8700(12) Å	γ = 90°
Volume	2674.9(6) $Å^3$	
Z	8	
Density (calculated)	1.696 Mg/m^3	
Absorption coefficient	1.443 mm^{-1}	
F(000)	1 376	
Crystal size	0.38 x 0.20 x 0.18 mm^3	
Theta range for data collection	2.93 to 26.37°	
Index ranges	-33<=h<=33, -9<=k<=11, -12<=l<=5	
Reflections collected	6 715	
Independent reflections	2 486 [R(int) = 0.0262]	
Completeness to theta = 25.00°	99.2%	
Absorption correction	Semi-empirical from equivalents	
Max. and min. transmission	0.771 and 0.540	
Refinement method	Full-matrix least-squares on F^2	
Data / restraints / parameters	2 486 / 0 / 168	
Goodness-of-fit on F^2	1.091	
Final R indices [I>2σ(I)]	R1 = 0.0351, wR2 = 0.0921	
R indices (all data)	R1 = 0.0437, wR2 = 0.1011	
Extinction coefficient	0	
Largest diff. peak and hole	0.478 and -0.387 e.$Å^{-3}$	

3.8.3 [$HpyNH_2$][$CrCl_4$(bipy)]

The [$HpyNH_2$][$CrCl_4$(bipy)] structure was isolated from the reaction in which bipyridine and $pyNH_2$ were both added to the chromium precursor in thf and stirred overnight. The resulting precipitate was dissolved in $ClCH_2CN$ and after a period of three days, a relatively large number of suitably sized crystals was observed.

[$HpyNH_2$][$CrCl_4$(bipy)] crystallises in an orthorhombic space group, Pnnm. The molecular structure is shown in Figure 3.46 and represents the only known structure of a bipy tetrachloro chromium complex anion. However, the coordination geometry is similar to that of the complex anion in the published structure of benzyl triphenylphosphonium tetrachloro (1,2–phenylenediamine N,N) chromium(III) dichloromethane solvate [109]. A certain degree of comparison can also be made with the previously solved Cr–bipyridine structure, [$CrCl_3$(bipy)(H_2O)].

The chromium atom is coordinated to four chlorine atoms and the two nitrogen atoms of the bipyridine ligand. The coordination is approximately octahedral with the largest deviation being the N(1)–Cr(1)–N(1)#1 bond angle (78.02(14)°) which is, as expected, very similar to other Cr–bipyridine structures. All the other *cis* X–Cr–Y bond angles are in the range 86.63(7) to 94.23(7)° (see Table 3.21). The dihedral angle between the mean planes through each of the two rings comprising the bipyridine ligand is 4.63(10)°. Unlike the novel structure above, the bipyridine ligand is observed as planar, with the N(1)–C(1)–C(10)–N(10) torsion angle constrained by symmetry to be 0°.

The metal–ligand bond lengths can be seen in Table 3.21, with both the Cr–N and Cr-Cl distances being comparable to those of [$CrCl_3$(bipy)(H_2O)].

Table 3.21 Selected bond lengths [Å] and angles [°] for [$HpyNH_2$][$CrCl_4$(bipy)]

Cr(1)-N(1)	2.088(3)	Cr(1)-Cl(3)	2.3172(9)
Cr(1)-N(1)#1	2.088(3)	Cr(1)-Cl(1)	2.3415(13)
Cr(1)-Cl(3)#1	2.3172(9)	Cr(1)-Cl(2)	2.3515(12)
N(1)-Cr(1)-N(1)#1	78.02(14)	Cl(3)#1-Cr(1)-Cl(1)	93.22(4)

N(1)#1-Cr(1)-Cl(3)#1	94.23(7)	Cl(3)-Cr(1)-Cl(1)	93.22(4)
N(1)-Cr(1)-Cl(3)	94.23(7)	N(1)-Cr(1)-Cl(2)	87.46(7)
Cl(3)#1-Cr(1)-Cl(3)	93.52(5)	N(1)#1-Cr(1)-Cl(2)	87.46(7)
N(1)-Cr(1)-Cl(1)	86.63(7)	Cl(3)#1-Cr(1)-Cl(2)	91.99(4)
N(1)#1-Cr(1)-Cl(1)	86.63(7)	Cl(3)-Cr(1)-Cl(2)	91.99(4)
N(1)-C(1)-C(2)-C(3)	0.0(5)	C(3)-C(4)-C(5)-N(1)	0.0(6)

Symmetry transformations used to generate equivalent atoms:
#1 x, y, -z+1 #2 -x+1, -y+1, z

Interestingly, the pyridinium N–H and amine groups, together with the two *trans* Cl ligands of the complex anion, are involved in an extended network of hydrogen bonds (see Figure 3.46 and Table 3.22). The pyridinium N(2)–H(2N) group is hydrogen bonded to two symmetry–related Cl(2) ligands which are, in turn, hydrogen bonded to a second, symmetry–related N(2)–H(2N) group. The pyridinium amine, N(3)–H(3N), is hydrogen bonded to Cl(1). A crystallographic twofold rotation axis generates the second amine hydrogen and the Cl(1) ligand of a second complex anion to which it is hydrogen bonded. The two Cl(1) ligands are, in turn, also hydrogen bonded to a second pyridinium amine group. There are further weak hydrogen bonds (not shown in Figure 3.46) between the amine hydrogens and the chlorine atoms of the DCM solvate molecules.

Table 3.22 Hydrogen bonds for [HpyNH$_2$][CrCl$_4$(bipy)] [Å and º]

D-H...A	d(D-H)	d(H...A)	d(D...A)	<(DHA)
N(2)-H(2N)...Cl(2)#3	0.76(7)	2.67(5)	3.250(4)	134.9(10)
N(3)-H(3N)...Cl(1)	0.96(7)	2.66(8)	3.278(3)	123(6)
N(3)-H(3N)...Cl(4)#2	0.96(7)	2.80(7)	3.605(3)	142(6)

Symmetry transformations used to generate equivalent atoms:
#1 x ,y, -z+1 #2 -x+1, -y+1, z #3 x+1/2, -y+1/2, -z+1/2

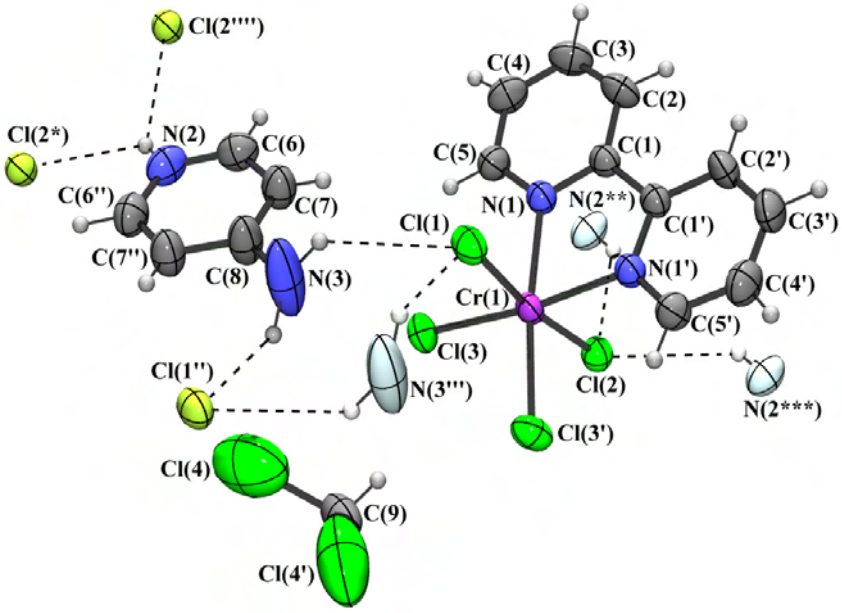

Figure 3.46 Hydrogen bond interactions

Further interactions are observed between the bipyridine and pyridinium ring systems and, as can be seen in Figure 3.47, these are best described as staggered π–π interactions. Figure 3.48 shows a packing and space fill arrangement.

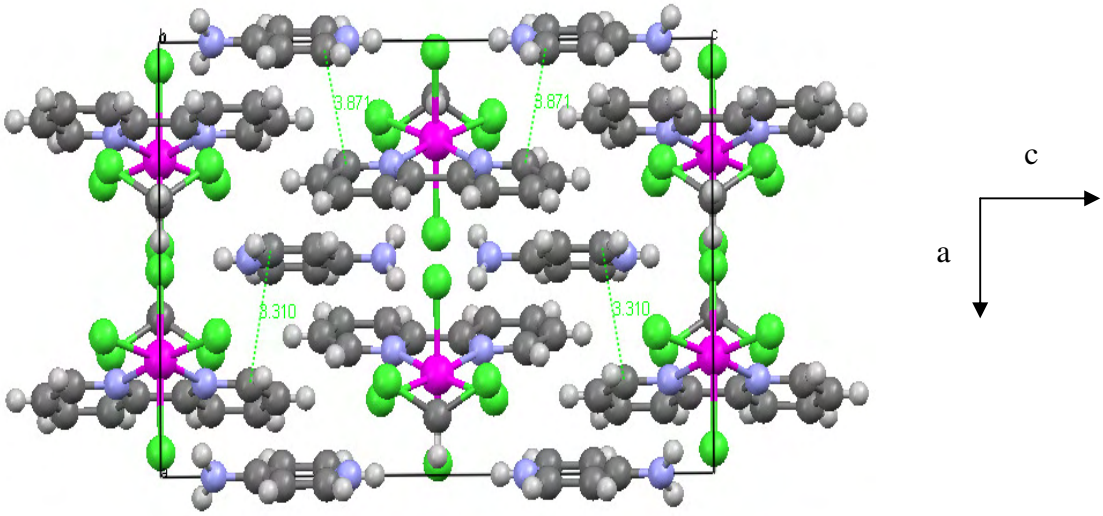

Figure 3.47 Staggered π–π interactions in the packing arrangement of [HpyNH$_2$][CrCl$_4$(bipy)]

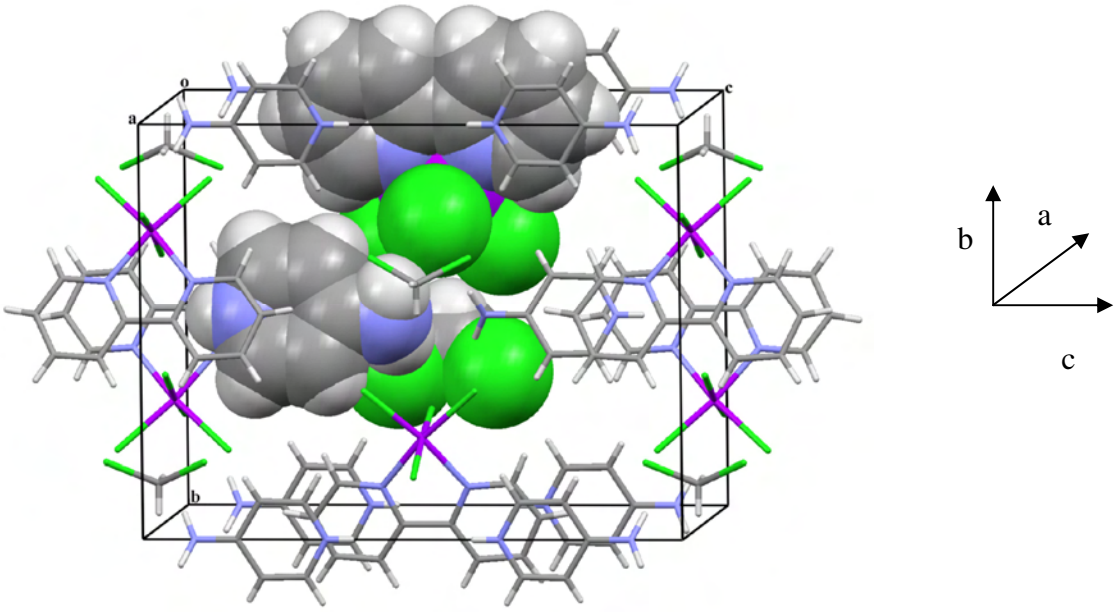

Figure 3.48 **Packing and space fill of $[HpyNH_2][CrCl_4(bipy)]$**

Table 3.23 **Crystal data and structure refinement for $[HpyNH_2][CrCl_4(bipy)]$**

Empirical formula	$C_{16}\ H_{17}\ Cl_6\ Cr\ N_4$	
Formula weight	530.04	
Temperature	293(2) K	
Wavelength	0.71073 Å	
Crystal system	Orthorhombic	
Space group	P n n m	
Unit cell dimensions	a = 10.4815(5) Å	α= 90º.
	b = 12.6236(6) Å	β= 90º.
	c = 16.4879(8) Å	γ = 90º.
Volume	2181.58(18) $Å^3$	
Z	4	
Density (calculated)	1.614 Mg/m^3	
Absorption coefficient	1.269 mm^{-1}	
F(000)	1 068	
Crystal size	0.32 x 0.26 x 0.15 mm^3	
Theta range for data collection	2.47 to 26.52º.	
Index ranges	-13<=h<=4, -14<=k<=15, -19<=l<=20	
Reflections collected	11 301	

Independent reflections	2 235 [R(int) = 0.0350]
Completeness to theta = 25.00º	99.9%
Absorption correction	Semi-empirical from equivalents
Max. and min. transmission	0.827 and 0.635
Refinement method	Full-matrix least-squares on F^2
Data / restraints / parameters	2 235 / 0 / 163
Goodness-of-fit on F^2	1.046
Final R indices [I>2σ(I)]	R1 = 0.0480, wR2 = 0.1327
R indices (all data)	R1 = 0.0543, wR2 = 0.1424
Extinction coefficient	0
Largest diff. peak and hole	0.693 and -1.079 e.Å^{-3}

3.8.4 $[CrCl_2(bipy)_2][Cl]\cdot H_2O$

The above two novel structures were obtained by the standard procedure involving the dissolution of precipitates in suitable solvents. This point is emphasised because a third structure was obtained but via a slightly unusual technique. A large excess of bipyridine dissolved in thf was added to a thf solution of $[CrCl_3(thf)_3]$ at room temperature (ratio of bipyridine to $[CrCl_3(thf)_3]$ was 10:1). The mixture was allowed to stand with no stirring of the solution. After about 60 seconds the solution turned green. After a number of days sizable crystals, light brown in colour, resulted. Their crystallographic analysis revealed the previously determined $[CrCl_2(bipy)_2]^+$ with Cl^- counter-ions. $[CrCl_2(bipy)_2][Cl]\cdot H_2O$ crystallises in an orthorhombic space group, Pbca, with two formula units in the asymmetrical unit. This contrasts with the triclinic unit cell reported for the corresponding dihydrate structure (no details of that structure were reported) [110]. Owing to the relatively low quality of the reflection intensity data and the severe disorder of the chloride anions and water molecules, the structural and geometrical parameters of the complex cations are of somewhat low precision. Regrettably, it was not possible to obtain any better crystals.

As expected, the complex cations have a *cis* arrangement of the chlorine ligands (see Figure 3.49). This arrangement and the bonding geometry of the cations are

comparable to those recently reported for the same complex cation in *cis* [Cr(2,2'–bipy)$_2$Cl$_2$](Cl)$_{0.38}$(PF$_6$)$_{0.62}$ [111].

The largest deviation from the octahedral coordination in [CrCl$_2$(bipy)$_2$][Cl] is the N(8)–Cr(2)–N(7) angle of 78.4(3)°, while all other *cis* X–Cr–Y bond angles are in the range 78.6(2) to 96.9(2)° (see Table 3.23).

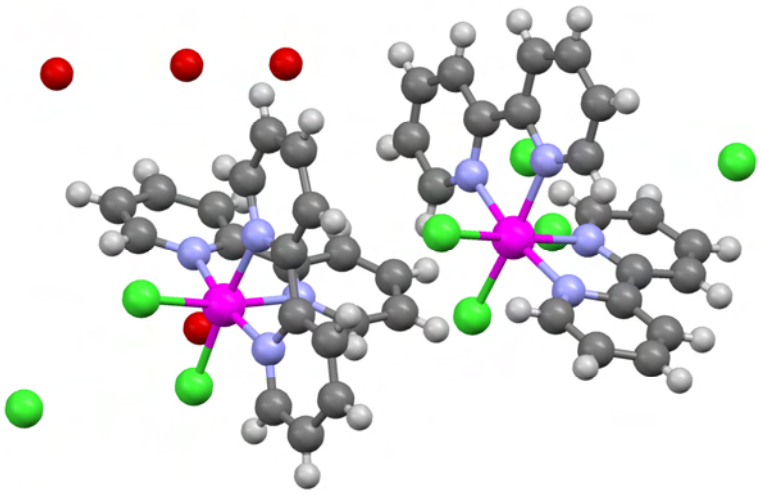

Figure 3.49 **Perspective drawing showing the two formula units of [CrCl$_2$(bipy)$_2$][Cl]·H$_2$O in the asymmetric unit**

The metal–ligand bond lengths are also very similar in the two structures (as would be expected), and only slight differences are observed in their bipyridine ring torsion angles. The greatest difference is observed between the equivalent N(3)–C(11)–C(16)–N(4) of this study and N(2)–C(6)–C(5)–N(1) from the literature, with a difference of 4.27°.

The major differences between the structures are with respect to structural and refinement data. These differences are highlighted in Table 3.24.

Table 3.24 Crystallographic differences between the two structures

Crystal data	$[CrCl_2(bipy)_2][Cl]\cdot H_2O$	$[CrCl_2(bipy)_2][PF_6]$ [111]
Crystal system	Orthorhombic	Monoclinic
Space group	Pbca	C2/c
Volume/non-H atoms	21.2 $Å^3$	17.2 $Å^3$
R-factor	8.75%	5.15%

As a consequence of the differing structural data and indeed the volumes/non-H atoms, it is not surprising that the packing arrangements are also different. Figures 3.50 and 3.51 illustrate the packing order and space fill arrangements of $[CrCl_2(bipy)_2][Cl]$.

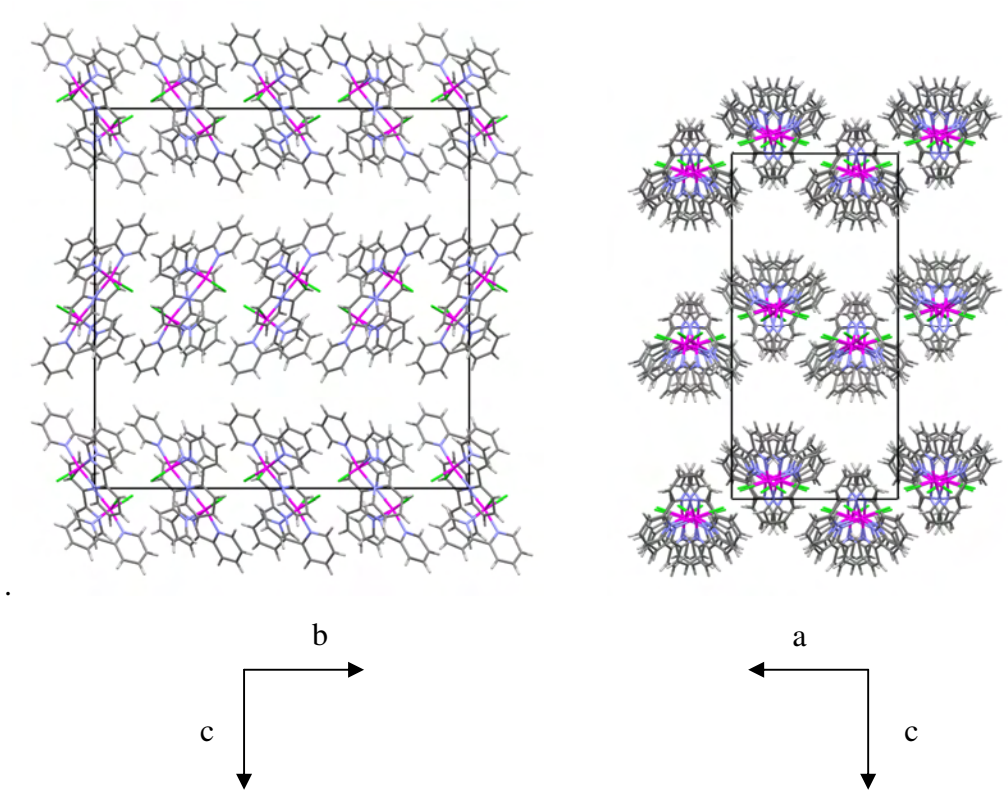

Figure 3.50 Packing arrangements for $[CrCl_2(bipy)_2][Cl]\cdot H_2O$

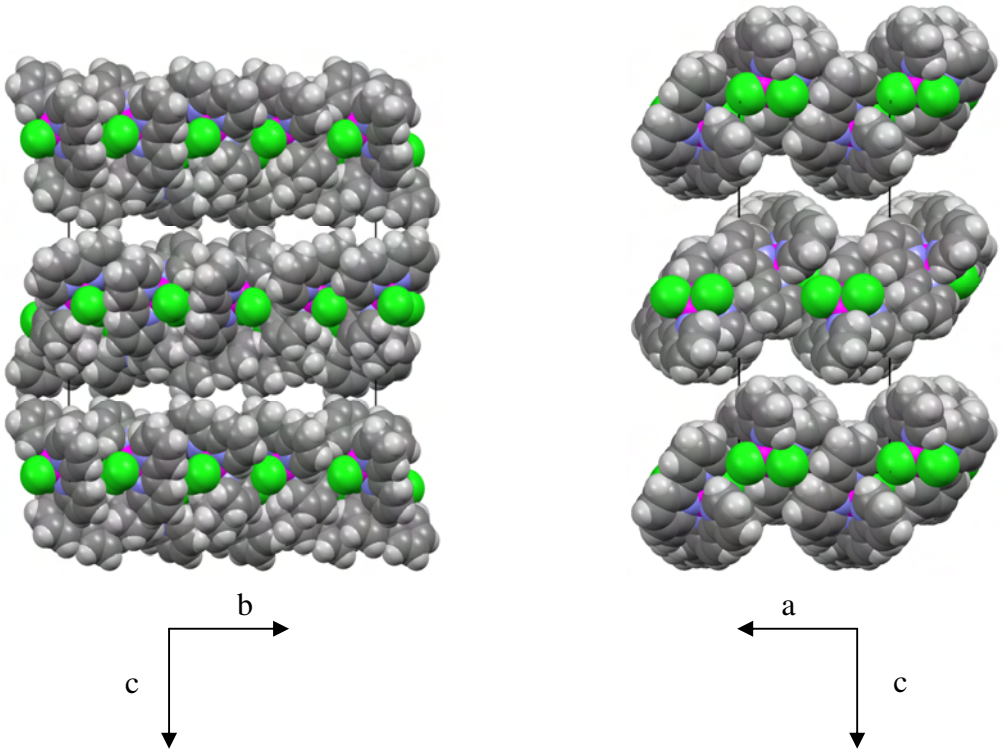

Figure 3.51 **Packing and space fill arrangements for $[CrCl_2(bipy)_2][Cl]\cdot H_2O$**

Table 3.25 **Bond lengths [Å] and angles [°] for $[CrCl_2(bipy)_2][Cl]\cdot H_2O$**

Cr(1)-N(1)	2.063(6)	Cr(1)-N(3)	2.068(5)
Cr(1)-N(2)	2.065(6)	Cr(1)-Cl(1)	2.285(2)
Cr(1)-N(4)	2.065(6)	Cr(1)-Cl(2)	2.2906(18)
N(1)-Cr(1)-N(2)	79.1(3)	N(8)-Cr(2)-N(7)	78.4(3)
N(1)-Cr(1)-N(4)	94.0(2)	N(6)-Cr(2)-N(7)	92.7(2)
N(1)-Cr(1)-N(3)	87.5(2)	N(8)-Cr(2)-N(5)	94.5(2)
N(2)-Cr(1)-N(3)	93.7(2)	N(6)-Cr(2)-N(5)	79.2(2)
N(4)-Cr(1)-N(3)	78.6(2)	N(7)-Cr(2)-N(5)	86.8(2)
N(2)-Cr(1)-Cl(1)	94.2(2)	N(8)-Cr(2)-Cl(3)	89.75(18)
N(4)-Cr(1)-Cl(1)	92.42(16)	N(6)-Cr(2)-Cl(3)	96.10(18)
N(3)-Cr(1)-Cl(1)	91.63(16)	N(7)-Cr(2)-Cl(3)	90.97(17)
N(1)-Cr(1)-Cl(2)	86.92(15)	N(8)-Cr(2)-Cl(4)	96.9(2)
N(2)-Cr(1)-Cl(2)	92.36(16)	N(6)-Cr(2)-Cl(4)	91.30(17)
N(4)-Cr(1)-Cl(2)	94.57(16)	N(5)-Cr(2)-Cl(4)	87.05(16)
Cl(1)-Cr(1)-Cl(2)	94.79(8)	Cl(3)-Cr(2)-Cl(4)	95.61(9)

N(1)-C(1)-C(6)-N(2)	3.9(10)	N(5)-C(21)-C(26)-N(6)	-2.8(8)
C(2)-C(1)-C(6)-C(7)	5.9(14)	C(22)-C(21)-C(26)-C(27)	-5.1(11)
N(3)-C(11)-C(16)-N(4)	0.4(8)	N(7)-C(31)-C(36)-N(8)	5.4(10)
C(12)-C(11)-C(16)-C(17)	-1.3(11)	C(32)-C(31)-C(36)-C(37)	6.3(13)

Table 3.26 Crystal data and structure refinement for $[CrCl_2(bipy)_2][Cl]\cdot H_2O$

Empirical formula	$C_{40}\ H_{32}\ Cl_6\ Cr_2\ N_8\ O_5$	
Formula weight	1 021.44	
Temperature	297(2) K	
Wavelength	0.71073 Å	
Crystal system	Orthorhombic	
Space group	P b c a	
Unit cell dimensions	a = 12.0476(8) Å	α = 90°.
	b = 29.148(2) Å	β = 90°.
	c = 29.449(2) Å	γ = 90°.
Volume	10 341.4(13) $Å^3$	
Z	8	
Density (calculated)	1.312 Mg/m^3	
Absorption coefficient	0.776 mm^{-1}	
F(000)	4 144	
Crystal size	0.46 x 0.20 x 0.02 mm^3	
Theta range for data collection	2.50 to 26.56°.	
Index ranges	-5<=h<=15, -35<=k<=36, -33<=l<=36	
Reflections collected	53 636	
Independent reflections	10 104 [R(int) = 0.0651]	
Completeness to theta = 25.00°	99.8%	
Absorption correction	Semi-empirical from equivalents	
Max. and min. transmission	0.985 and 0.712	
Refinement method	Full-matrix least-squares on F^2	
Data / restraints / parameters	10 104 / 0 / 568	
Goodness-of-fit on F^2	1.020	

Final R indices [I>2sigma(I)]	R1 = 0.0875, wR2 = 0.2656
R indices (all data)	R1 = 0.1712, wR2 = 0.3370

3.9 SYNTHETIC ROUTE CONCLUSIONS

When one combines all the evidence of this chapter, a mechanism similar to that of Chapter 2 is portrayed, with some interesting differences.

Direct ligand substitution is certainly a viable pathway to the formation of the neutral monomeric compounds. Unlike the immediate addition of the monodentate pyridine to all three available precursor sites, the addition of bipyridine allowed the isolation of an intermediate compound [$CrCl_3$(bipy)(thf)]. It would then be logical to assume that the secondary ligands simply displace and occupy the remaining site.

This same monomeric species could also have formed by the symmetrical cleavage of a dimeric intermediate, the existence of which is indirectly proven by the crystal structure of [$HpyNH_2$][$CrCl_4$(bipy)]; this had to have resulted from the asymmetrical cleavage of the same dimer. The detailed spectroscopic analysis suggests strongly that complexes of this study are monomeric and thus the addition of the secondary amine appears to break the bridging chloro bond in a symmetrical fashion to afford these compounds.

One cannot, however, ignore the isolation of the ionic complexes of which the structures [$HpyNH_2$][$CrCl_4$(bipy)] and [$CrCl_2(bipy)_2$][Cl]·H_2O were determined. Although not of the same compound, they importantly represent both the cationic and anionic Cr fragments that result from asymmetrical dimeric cleavage. It would appear that the cationic, coordinatively saturated fragment is stabilised by the coordination of a second bidentate bipyridine ligand.

As in Chapter 2, the reason why dimers such as these cleave symmetrically or asymmetrically is still unclear.

Figure 3.52 presents a summary of the routes to complex formation.

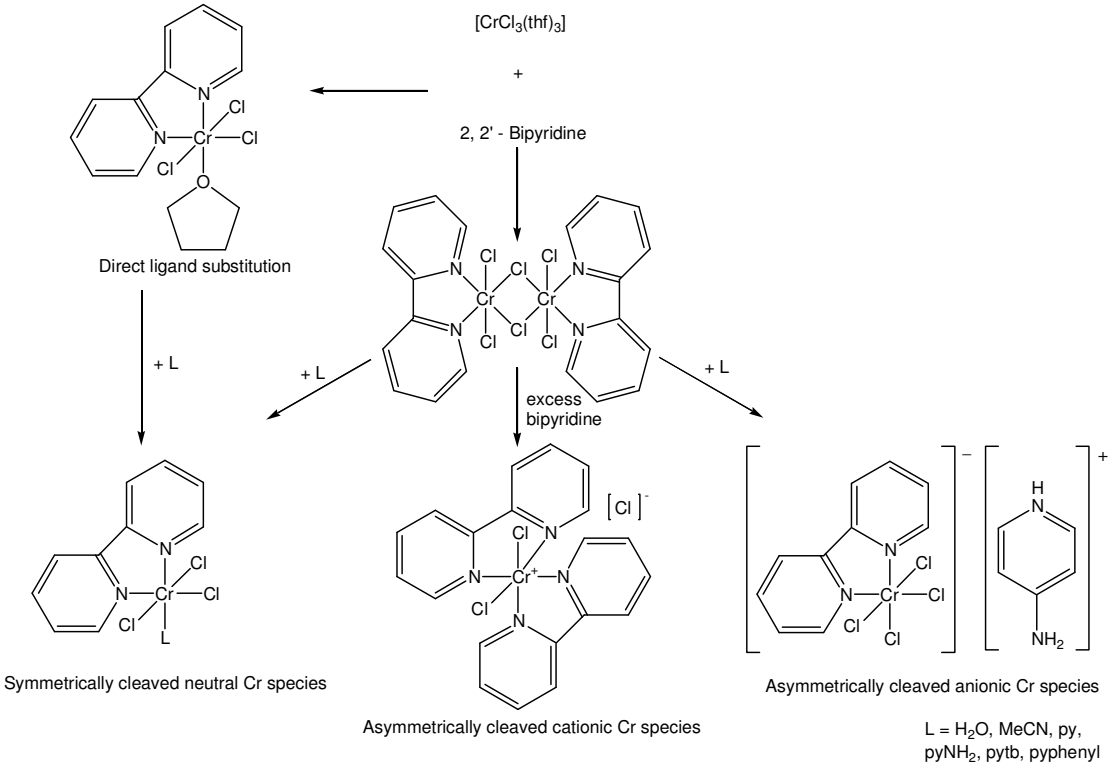

Figure 3.52 Proposed routes to complex formation

3.10 EXPERIMENTAL

3.10.1 SYNTHESIS OF [$CrCl_3$(bipy)(thf)] (9)

A Schlenk tube was charged with [$CrCl_3(thf)_3$] (0.31 g, 0.827 mmol) and thf (30 cm^3). Bipyridine (0.13 g, 0.827 mmol) was then added and the reaction mixture allowed to stir at room temperature. After *ca.* 2 hours the reaction colour was observed as a dark green solution with a light green precipitate starting to form. The reaction was left to stir overnight to ensure completion. The green supernatant solvent was removed via syringe after the crude product had been allowed to settle. The remaining precipitate was subsequently washed with Et_2O (3 x 20 cm^3), the supernatant removed and the final product dried under reduced pressure for 3 hours to afford an olive green solid **(9)** in good yield (0.27 g, 84%).

Repetition of this reaction using water-contaminated [$CrCl_3(thf)_3$] (resulting from the incomplete substitution of water by thf during synthesis from chromium hexahydrate), followed by dissolution in CH_3CN, yielded single crystals of **(16)**.

3.10.2 SYNTHESIS OF [$CrCl_3$(bipy)(CH_3CN)] (10)

A Schlenk tube was charged with [$CrCl_3$(bipy)(thf)] (0.23 g, 0.595 mmol) and CH_3CN (25 cm^3) (where CH_3CN acts as both solvent and N–donor ligand) and stirred overnight at room temperature. The supernatant was removed via syringe, the remaining residue washed with Et_2O (3 x 20 cm^3) and the product dried under reduced pressure for 3 hours. An olive green compound **(10)** was isolated as product (0.15 g, 71%).

3.10.3 SYNTHESIS OF [$CrCl_3$(bipy)(py)] (11)

A Schlenk tube was charged with [$CrCl_3$(bipy)(thf)] (0.21 g, 0.543 mmol) and pyridine (25 cm^3) and stirred at room temperature overnight. Again, the pyridine behaved as solvent and reagent. The supernatant was removed via syringe, and the residue washed with Et_2O (3 x 20 cm^3) and dried under reduced pressure for 3 hours to afford an olive green solid **(11)** as product (0.16 g, 76%).

3.10.4 SYNTHESIS OF [$CrCl_3$(bipy)($pyNH_2$)] (12)

A Schlenk tube was charged with [$CrCl_3(thf)_3$] (0.20 g, 0.534 mmol) and thf (30 cm^3). Bipyridine (0.08 g, 0.534 mmol) was then added and the reaction mixture was carefully monitored. After *ca.* 55 minutes, 4-amino pyridine (0.05 g, 0.534 mmol) was added. The reaction was allowed to stir overnight. The supernatant solvent was removed, the residue washed with Et_2O (3 x 20 cm^3) and the product dried under reduced pressure for 3 hours to afford an olive green solid **(12)** as product (0.15 g, 68%).

Crystals of [$HpyNH_2$][$CrCl_4$(bipy)]CH_2Cl_2 **(15)** were afforded by slow evaporation of [$CrCl_3$(bipy)($pyNH_2$)] in $ClCH_2CN$.

3.10.5 SYNTHESIS OF [$CrCl_3$(bipy)(pytb)] (13)

A Schlenk tube was charged with [$CrCl_3$(bipy)(thf)] (0.26 g, 0.672 mmol) and 4-tert butyl pyridine (20 cm^3) and stirred at room temperature overnight, with the 4-tert butyl pyridine acting as both solvent and reagent. The supernatant was removed, and the remaining residue washed with Et_2O (3 x 20 cm^3) and dried under reduced pressure for 3 hours. An olive green product **(13)** was isolated (0.19 g, 63%).

3.10.6 SYNTHESIS OF [$CrCl_3$(bipy)(pyphenyl)] (14)

A Schlenk tube was charged with [$CrCl_3$ $(thf)_3$] (0.20 g, 0.534 mmol) and thf (30 cm^3). Bipyridine (0.08 g, 0.534 mmol) was then added and the reaction mixture carefully monitored. After *ca.* 1 hour 4-phenyl pyridine (0.08 g, 0.534 mmol) was added and the reaction mixture stirred overnight at room temperature. The supernatant solvent was removed, the residue washed with Et_2O (3 x 20 cm^3) and the product dried under reduced pressure for 3 hours. An olive green product **(14)** was isolated (0.16 g, 64%).

3.10.7 SYNTHESIS OF [$CrCl_3$(bipy)(H_2O)] (16)

A Schlenk tube was charged with [$CrCl_3$(bipy)(thf)] (0.26 g, 0.672 mmol) and thf (30 cm^3). To the reaction 1 ml of distilled water was added. The reaction mixture was left to stir at room temperature overnight. The supernatant was removed via syringe and the product washed with Et_2O (3 x 20 cm^3) and then dried under reduced pressure for 3 hours. An olive green compound **(16)** was isolated as product in good yield (0.21 g, 95%).

3.10.8 SYNTHESIS OF [$CrCl_2(bipy)_2$][Cl]·H_2O (17)

A glass polytop was charged with [$CrCl_3(thf)_3$] (0.05 g, 0.133 mmol) and thf (5 cm^3). To the dissolved solution was added bipyridine (0.2 g, 1.33 mmol) which had been dissolved separately in thf (10 cm^3). The reaction was left to stand without stirring at room temperature. After a period of time large yellow-brown crystals of **(17)** formed.

Chapter 4

Chromium(III) Bidentate Phosphorus Chemistry

4.1 INTRODUCTION

The next class of compounds involved replacing the bidentate N–donor ligand, bipyridine, with a P–donor bidentate ligand, bis–diphenylphosphinoethane (dppe), while still maintaining the various substituted monodentate ligands as the secondary ligands.

The choice of dppe was based on the need to mimic the five–membered chelate ring that bipyridine formed when coordinated to the Cr(III) metal centre via substitution reactions of $[CrCl_3(thf)_3]$. The choice was also in keeping with known donor atoms that had been previously coordinated to Cr(III) to yield catalytically active species successfully [31].

Previously, Hermes and Girolami [112] synthesised the compound $[CrCl_3(dippe)(thf)]$, where dippe was diisopropylphosphinoethane. It was therefore of interest to exploit similar compounds with different steric and electronic properties as comparative studies could be undertaken. Also, by increasing the bulk of the ligand it was hoped to increase solubility and, in turn, increase the possibility of obtaining single crystals.

Furthermore, the addition of the substituted pyridines as secondary ligands had not been done previously.

Hermes and Girolami carried out ^1H NMR and IR analysis on their compound. However, the valuable IR data was not exploited in any detail and they simply documented a list of values with no band assignments. These values have, however, aided the detailed spectroscopic examination of the compounds of this study.

4.2 SYNTHESIS

Addition of one equivalent of dppe to an already dissolved one equivalent of $[CrCl_3(thf)_3]$ in thf afforded an immediate colour change from the characteristic deep precursor purple to a deep, dark blue. The reaction conditions of the previous classes were duplicated to ensure completion. As the substitution occurred so readily and remained in solution, the addition of the secondary pyridine ligands was straightforward. Unlike with the slowly coordinating bipyridine ligand, there was no concern about when to add the rapidly coordinating pyridine ligands so as to avoid them binding to all three of the metal sites before the bidentate dppe had done so. Upon the addition of the respective pyridine ligands, the solutions turned a notable blue-green colour which was perhaps expected as pyridine coordination to chromium results in an olive green-coloured reaction medium.

An interesting observation was the speed at which the addition of the dppe ligand to the chromium centre took place relative to its bipyridine counterpart. Although both appear to form stable five–membered chelate rings, the dppe coordinates immediately (formation of blue supernatant), while the bipyridine ligand, as previously discussed, only changes to its colour of coordination (green) and forms a precipitate after a fairly long period of time. The respective blue and green-coloured complexes were expected as they correlate well with the literature. It is simply an interesting observation considering that both P and N atoms coordinate via the same means – through their lone electron pair.

Although Hermes and Girolami [112] had no interest in the catalytic aspect of their compounds, nor in the mechanisms by which their compounds were formed (i.e. through possible dimeric intermediates), they were able to isolate a crystal structure with the dippe ligand and the analogous titanium precursor $[TiCl_3(thf)_3]$. They found the structure to be dimeric–$[TiCl_3(dippe)]_2$. As in this study, they were unable to isolate the corresponding chromium dimer and made no reference to a dimeric intermediate resulting in the formation of their monomer (i.e. they were suggesting the straightforward substitution of the thf molecules).

$$[CrCl_3(thf)_3] + dippe = [CrCl_3(dippe)(thf)] + 2\ thf$$

During the course of this study, while attempting to synthesise $[CrCl_3(dppe)(pyphenyl)]$ **(22)**, crystals large enough for the diffractometer were obtained. Once solved, it was interesting to find that the compound $[Hpyphenyl][CrCl_4(dppe)]$ **(23)** had formed. This was not completely unexpected as similar structures were obtained for both the pyridine and bipyridine classes of compound. Indeed, this result was once again a strong indication that dimeric intermediates do in fact exist within these systems and provide a plausible route for this and the N–ligand structures.

4.3 SYNTHETIC ROUTE TO PRODUCT FORMATION

The question of whether the precipitates of all the compounds formed within this class came from monomeric or dimeric intermediates was then posed.

Of particular interest was whether, like the monodentate and bidentate N–classes of ligands, there was vibrational evidence to suggest straightforward monomeric substitution of dppe with one remaining thf to give $[CrCl_3(dppe)(thf)]$ **(18)** or would the dimeric species form. Furthermore, would the addition of the respective secondary monodentate para-substituted pyridine derivatives yield the monomeric compounds via direct ligand substitution or symmetrical cleavage of the dimeric intermediate, or would this addition cause asymmetrical cleavage as seen by $[Hpyphenyl][CrCl_4(dppe)]$? A further reason for pursuing the various possible coordination pathways was the fact that the IR of the precipitate obtained from the reaction of $[CrCl_3(thf)_3]$, dppe and pyphenyl was different from that of the crystals of the same reaction. Figure 4.1 provides a summary of the routes to product formation.

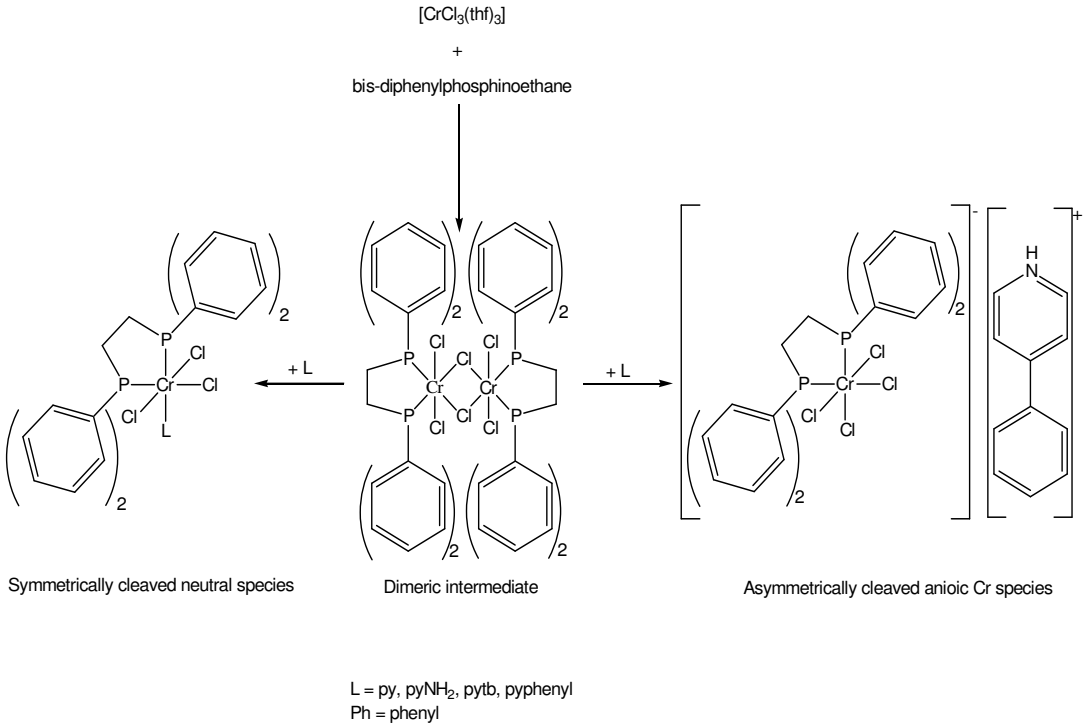

Figure 4.1 **Proposed routes to complex formation**

4.4 INFRARED AND RAMAN SPECTROSCOPY

Considering the obvious difficulty in obtaining single crystals of these compounds, spectroscopic techniques have proved extremely insightful as tools for characterising these compounds. In-depth IR (both MIR and FIR) and Raman analysis of these novel dppe–type compounds provides valuable information regarding coordination, structure, etc. – in particular when the analysis is complemented by the data from the other techniques used in this study.

As is widely recognised, a strong indication of the substitution of thf and subsequent coordination of dppe and the various pyridine derivatives to the metal centre is the shifting of free ligand vibrations to higher frequencies. The band assignments and the respective shifts will now be discussed.

As has been mentioned in connection with the analysis of the other classes of compound, the ability to obtain at least one single-crystal structure of a class of compounds and in turn to analyse the crystal's vibrational data has added a great deal to the confidence with which the vibrational assignments of all compounds within the class have been made. Note that no Raman spectra of either [$CrCl_3$(dppe)(pyphenyl)]

or [Hpyphenyl][$CrCl_4$(dppe)] were obtained as a result of sample fluorescence in the former and insufficient sample of the single-crystal material in the latter.

4.4.1 Region 3313–2863 cm^{-1}

Within this particular region there are a number of vibrations that are common to all the compounds. These include weak bands assigned to overtones that coincide with other metal–dppe complexes [113.]. They range from 3179 to 3130 cm^{-1} in the IR spectrum and from 3172 to 3142 cm^{-1} in the Raman spectrum. Although some of these modes are not visible in the IR, those that are appear at slightly stronger intensities than their Raman counterparts.

C–H bands pertaining to the phenyl (dppe) and heterocyclic (pyridine) rings were also observed in the complexes and can be equally assigned to either ring system as there is sufficient precedence in the literature for both [73, 74**,** 113]. They are present as two vibrations at ~3076 and ~3055 cm^{-1}. That being said, as there is no pyridine present in [$CrCl_3$(dppe)(thf)], its bands at 3076 cm^{-1} (weak in IR spectrum and absent in Raman spectrum) and 3055 cm^{-1} (medium in IR spectrum and strong in Raman spectrum) are related to phenyl C–H [113]. When compared with the corresponding free dppe vibrations, the bands appear to have shifted by 10 and 8 cm^{-1} respectively, which infers coordination. Although the pyridine-based complexes possess C–H vibrations at frequencies very similar to those of [$CrCl_3$(dppe)(thf)], it is nonetheless tempting to assign them all to phenyl C–Hs. This certainly does not imply the absence of pyridine C–Hs, but rather the dominance of phenyl C–Hs in this region. Figure 4.2 highlights the IR band shifts in [$CrCl_3$(dppe)(thf)] relative to free dppe.

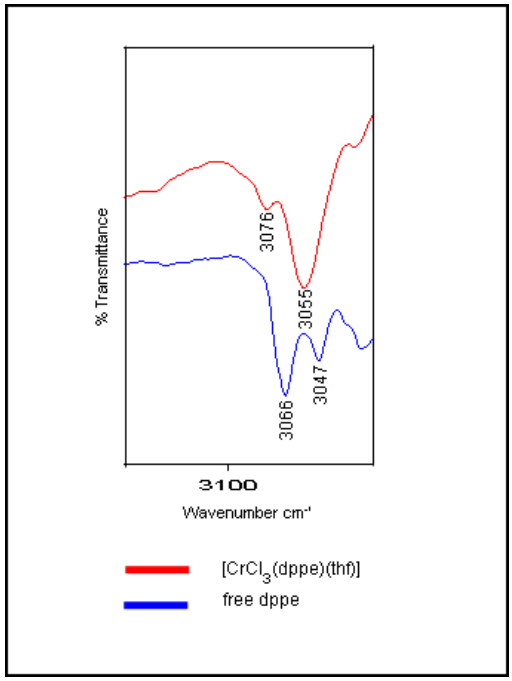

Figure 4.2 **IR spectra showing band shifts in [$CrCl_3$(dppe)(thf)] (red) relative to free dppe (blue)**

Pyridine-specific C–H modes are, however, observed in the IR spectra of [$CrCl_3$(dppe)(py)] **(19)** at 3101 cm^{-1} (shifted from 3083 cm^{-1} in the free ligand) [73, 74] and [$CrCl_3$(dppe)($pyNH_2$)] **(20)** at 3092 cm^{-1} (unshifted as expected) [96].

CH_2 modes that bridge the PP atoms of dppe are also common to more than half of the compounds. Both the CH_2 asymmetrical and symmetrical stretches are visible at ~2956 and ~2925 cm^{-1}, and both are considered to be weak vibrations, particularly in the IR spectra. However, as can be seen from the spectrum of free dppe in Figure 4.3, the mode at ~2926 cm^{-1} is considerably more prominent.

The fact that the band at ~2956 cm^{-1} is of very weak intensity proved to be advantageous when studying the spectrum of [$CrCl_3$(dppe)(pytb)] **(21)** as no ambiguity surrounds the strong vibration at 2964 cm^{-1}. It can therefore be confidently assigned to a CH_3 asymmetrical stretching mode [92, 113] and is shown in Figure 4.3. A close look at the figure also shows that the CH_2 symmetrical stretch at ~2925 cm^{-1} may be observed as a shoulder that has shifted to 2934 cm^{-1} in the complex.

Two other vibrations were observed solely in the spectrum of $[CrCl_3(dppe)(pytb)]$ at 2904 cm^{-1}(medium intensity) IR, 2908 cm^{-1}(medium intensity) Raman and 2869 cm^{-1} (medium intensity) IR, 2868 cm^{-1}(medium shoulder) Raman. They are duly assigned to CH_3 symmetrical stretches. Their minimal degree of shifting relative to the free pytb ligand corresponds to that of other metal–pytb complexes in the literature [92].

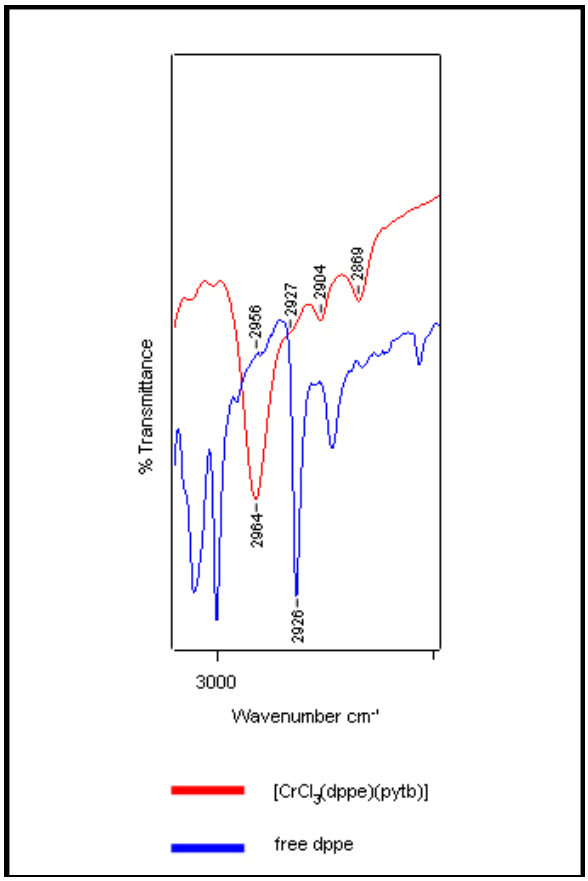

Figure 4.3 **IR spectra of $[CrCl_3(dppe)(pytb)]$ (red) and free dppe (blue)**

Other pyridine substituent bands that are assignable are those associated with the N–H vibrations of the $pyNH_2$ ligand and these are not subject to any ambiguity brought about by the overlap of other ligand vibrations. They are observed as strong IR vibrations at 3313 and 3206 cm^{-1} as highlighted in Figure 4.4, with only the latter visible as a weak vibration in the corresponding Raman spectrum [96].

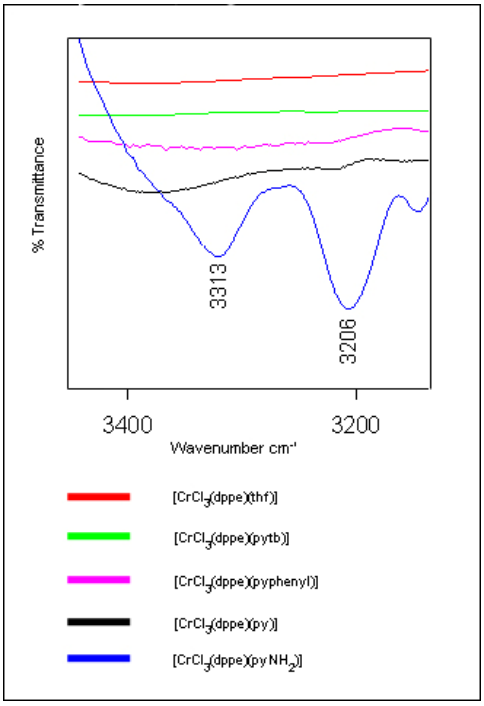

Figure 4.4 **N–H vibrations observed in the IR spectrum of [$CrCl_3$(dppe)($pyNH_2$)] (blue)**

As observed in the previous bipyridine ligand class of compounds, the presence and indeed absence of bands pertaining to the C–H vibrations of thf offer valuable insights into the mechanistic routes leading to compound formation. This essentially centres on the initial reaction involving the addition of dppe to [$CrCl_3(thf)_3$], whereby the presence of C–H thfs indicates direct monomeric ligand substitution, while their absence is indicative of dimeric formation. Unfortunately, the analysis is not as clear-cut as one had hoped owing to band superposition with dppe vibrations, coupled with the broad, shoulder-type nature of the bands in [$CrCl_3$(dppe)(thf)] in the IR spectrum (slightly more prominent in the Raman spectrum). However, as these modes are also present in the spectrum of [Hpyphenyl][$CrCl_4$(dppe)] which is known not to possess coordinated thf, one assumes that the thf modes are absent in [$CrCl_3$(dppe)(thf)]. See Figure 4.5. This is an early indication of dimer formation as opposed to the directly substituted monomeric species that is plausible for the bipyridine equivalent. Although seen to a greater extent in the following region, there is evidence to suggest that this dimeric species can be cleaved both symmetrically and asymmetrically as the compound [Hpyphenyl][$CrCl_4$(dppe)] possesses a strong characteristic pyridinium vibration (asymmetrical cleavage) at 3191 cm^{-1} [94] that is absent in the other complexes (symmetrical cleavage).

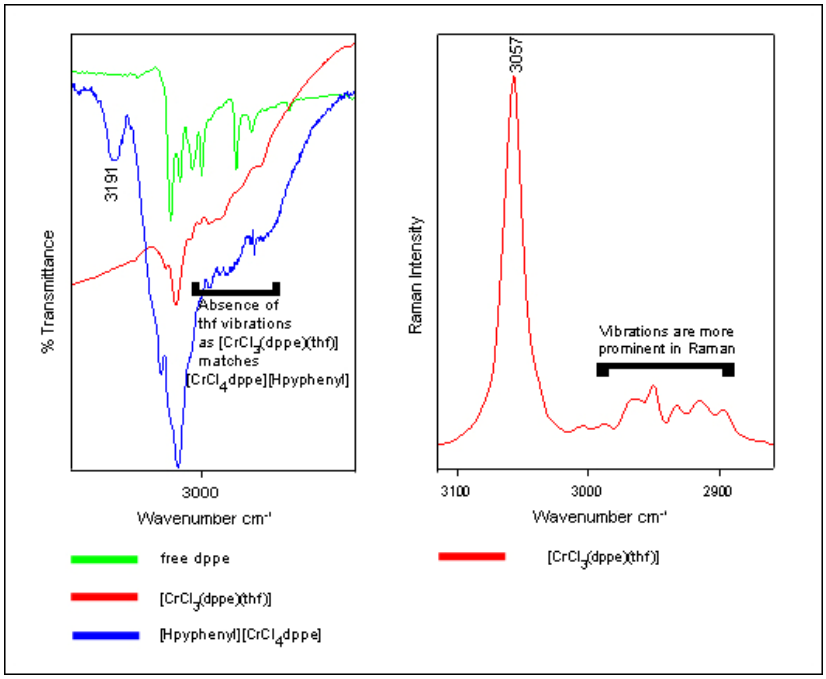

Figure 4.5 **Comparisons between IR spectra of [$CrCl_3$(dppe)(thf)] (red), [Hpyphenyl][$CrCl_4$(dppe)] (blue) and free dppe (green). Raman spectrum of [$CrCl_3$(dppe)(thf)]**

4.4.2 Region 1651 to 1045 cm^{-1}

This is an important region in the assignment of pyridinium vibrations, as well as giving indications of coordination (i.e. characteristic shifts).

The band at ~1632 cm^{-1} is a significant vibration. It is present as a medium to weak vibration in the compounds [$CrCl_3$(dppe)(py)], [$CrCl_3$(dppe)(pytb)] and [$CrCl_3$(dppe)(pyphenyl)], and as a very strong vibration in [Hpyphenyl][$CrCl_4$(dppe)]. Its absence in [$CrCl_3$(dppe)($pyNH_2$)] is more than likely due to it being masked by the strong, broad 1651 cm^{-1} vibration associated with N–H stretching [96]. It is assigned as a ring vibrational mode of pyridine [73, 74], which is reiterated by its absence in [$CrCl_3$(dppe)(thf)]. However, the intensity difference between [Hpyphenyl][$CrCl_4$(dppe)] and the others may be of importance as one cannot rule out the possibility that it is in fact an in-plane ring deformation of the pyridinium ion. This is characterised by a strong IR vibration at 1630 cm^{-1} as opposed to the weaker band that is indicative of pyridine [93].

Another band whose strength may very well be indicative of its assignment is that found between 1617 and 1605 cm^{-1} in all the complexes. Its presence as a medium to

strong vibration (particularly in the IR spectra) in the pyridine compounds correlates well to the shifting of free pyridine vibrations from ~1580 cm^{-1} upon coordination [73, 74]. Although also present in $[CrCl_3(dppe)(thf)]$ and $[Hpyphenyl][CrCl_4(dppe)]$, the vibration is notably weaker and can be assigned to C=C ring stretch of the phenyl ring [92,113].

A representative IR spectrum is shown in Figure 4.6 which highlights the differences in band intensity with respect to the vibrations at ~1630 and 1617 to 1605 cm^{-1} by comparing $[Hpyphenyl][CrCl_4(dppe)]$ and $[CrCl_3(dppe)(py)]$.

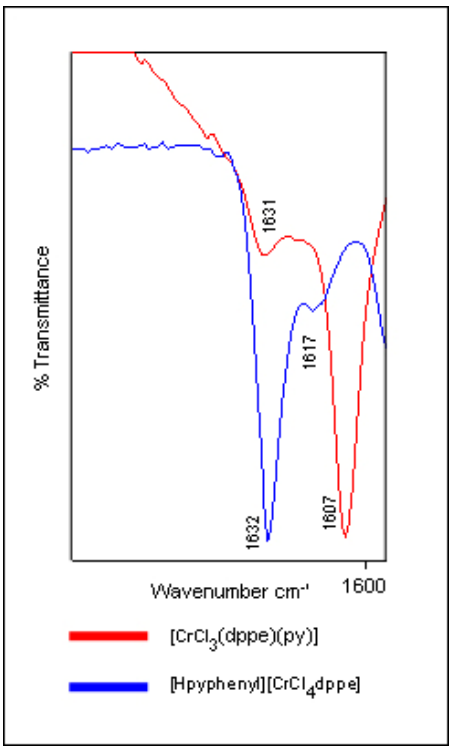

Figure 4.6 **Band intensity comparison between the IR spectra of $[CrCl_3(dppe)(py)]$ (red) and $[Hpyphenyl][CrCl_4(dppe)]$ (blue)**

Referring again to the topic of pyridinium vibrations, three further bands are observed only in $[Hpyphenyl][CrCl_4(dppe)]$ and are therefore assumed to be pyridinium-related. They include two medium-intensity bands at 1515 and 1212 cm^{-1}, as well as two weaker bands at 1495 and 1262 cm^{-1}. The literature proposes a number of other vibrations that are pyridinium-related, including 1530, 1480, 1327, 1250 and 1237 cm^{-1} [93, 94]. Unfortunately, these also coincide with dppe and pyridine vibrations and thus any definitive assignment either way is ambiguous.

With regard to C=C ring vibrations, one is able to assign the band at ~1587 cm^{-1} specifically to dppe C=C [92, 113] and that at ~1535 cm^{-1} to pyridine C=C [73, 74]. This is possible as the former in pyridine has shifted to the higher frequency upon coordination (already discussed), while the latter is absent in both free dppe and $[CrCl_3(dppe)(thf)]$. The only other C=C vibration is found at ~1574 cm^{-1} but is equally assignable to both aromatic systems.

Bands associated with the pyridine substituents are also visible in this region, with those expected to shift upon coordination doing so. The band at 1651 cm^{-1}, as mentioned previously, is identified as a characteristic N–H vibration from the $[CrCl_3(dppe)(pyNH_2)]$ compound that has shifted from 1645 cm^{-1} in the free ligand. There is also a weak C–NH_2 mode observed only in $[CrCl_3(dppe)(pyNH_2)]$ at 1258 cm^{-1} in the IR spectrum and at 1260 cm^{-1} in the Raman spectrum[96].

Bands indicative of the tertiary butyl group of $[CrCl_3(dppe)(pytb)]$ are also visible (Figure 4.7) and are assigned with relative confidence as they do not fall at frequencies where there is a possibility of overlap with other vibrations. Their coordinative shifts correlate well with those in the literature and are as shown in Table 4.1.

Table 4.1 pytb-specific vibrations

Free pytb / cm^{-1}		**$[CrCl_3(dppe)(pytb)]$ / cm^{-1}**		**Shift / cm^{-1}**	
IR	**RAMAN**	**IR**	**RAMAN**	**IR**	**RAMAN**
1494	1495	1500	1503	6	8
1457	1452	1462	1462	5	10

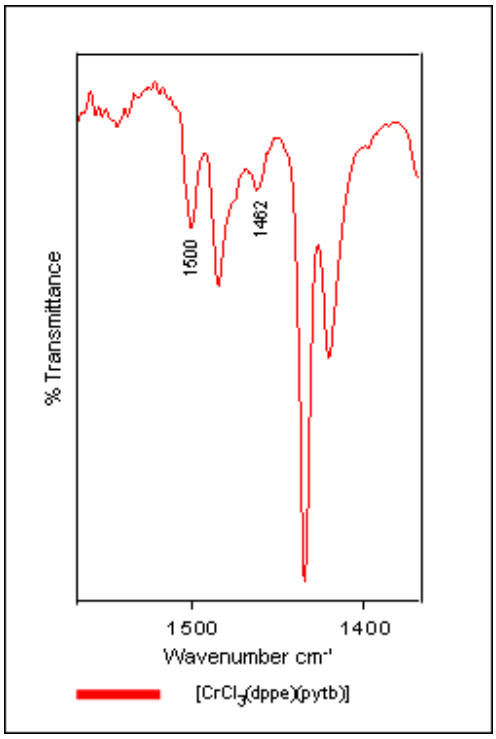

Figure 4.7 IR spectrum of [$CrCl_3$(dppe)(pytb)]-specific vibrations

As one might expect, the phenyl-specific vibrations associated with the pyphenyl ligand in [$CrCl_3$(dppe)(pyphenyl)] are equally assignable to dppe or pyridine ring vibrations.

The remaining bands in this region consist largely of C–H deformations (dppe) and C–H ring stretches (pyridines), with the majority remaining unshifted as is expected.

4.4.3 Region 1026– 519 cm^{-1}

As discussed in Chapters 2 and 3, and well documented in the literature, the band at 992 cm^{-1} in free unsubstituted pyridine shifts to 1015 cm^{-1} upon coordination to the metal centre in the IR spectrum. For the substituted pyridine compounds, the extent of this shift differs depends on the mass, nature and position of the substituent [75]. Although the dppe ligand possesses a band at a similar position to the expected shifts of the compounds, important assignments can still be made.

What is particularly interesting is that the shifts observed for the various pyridine compounds in this class follow the same trend as those for the monodentate and bidentate N–ligand systems. This takes on further importance when one considers that

crystal structures and subsequent IR spectra of coordinated unsubstituted and pytb compounds were obtained, making comparisons particularly meaningful. The dppe vibrations occur at 1026 and 999 cm^{-1} and, as shown in Figure 4.8 which compares both free dppe and $[CrCl_3(dppe)(thf)]$, they do not shift upon complexation. The same figure also shows the Raman spectrum of $[CrCl_3(dppe)(thf)]$ with both bands present at a strong intensity similar to that of the IR bands.

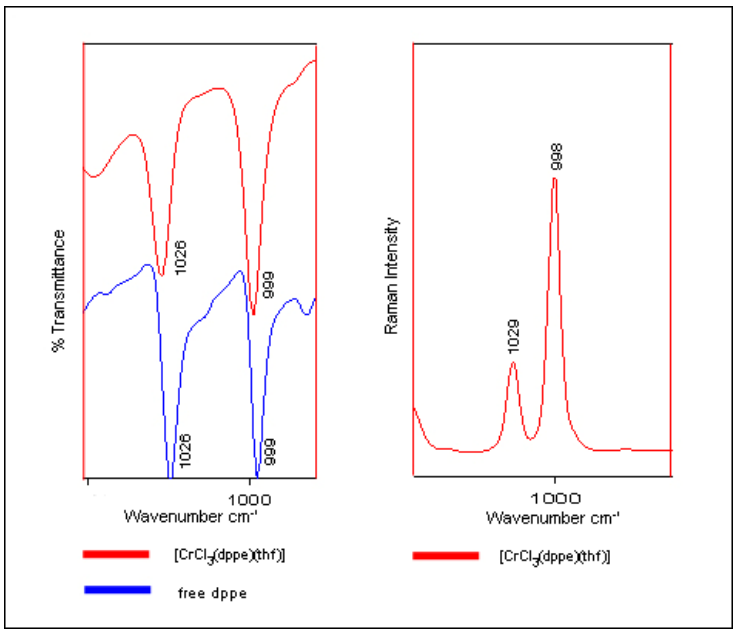

Figure 4.8 **IR and Raman spectra of $[CrCl_3(dppe)(thf)]$ (red) with the IR highlighting the lack of shifting relative to free dppe (blue)**

In $[CrCl_3(dppe)(py)]$ the 992 cm^{-1} band shifts to 1015 cm^{-1} so there is no problem with band overlap, particularly as the band at 1027 cm^{-1} is still visible (Figure 4.9).

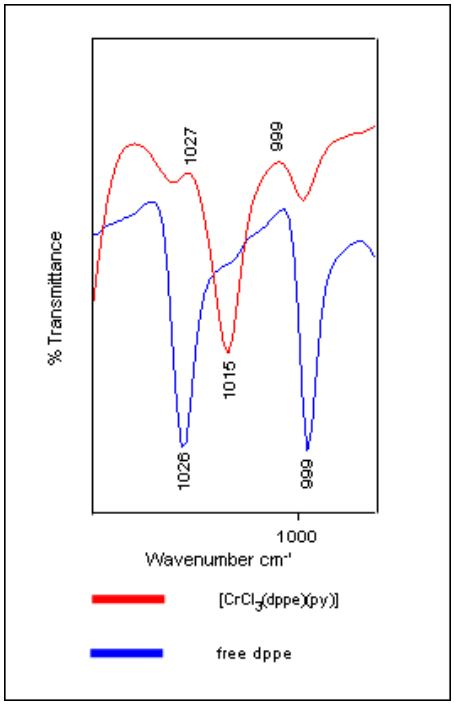

Figure 4.9 **Ring breathing shift in IR bands of [$CrCl_3$(dppe)(py)] (red)**

As expected, the pyNH_2 and pytb compounds, due to their increased mass, show larger shifts and are both found at 1027 cm^{-1}. They are assigned to the pyridine ring breathing shifts as opposed to the free dppe ligand as the free pyridine vibration in both spectra is absent. Therefore it is assumed that the dppe band is masked and not visible. Figure 4.10 shows the IR and Raman spectra.

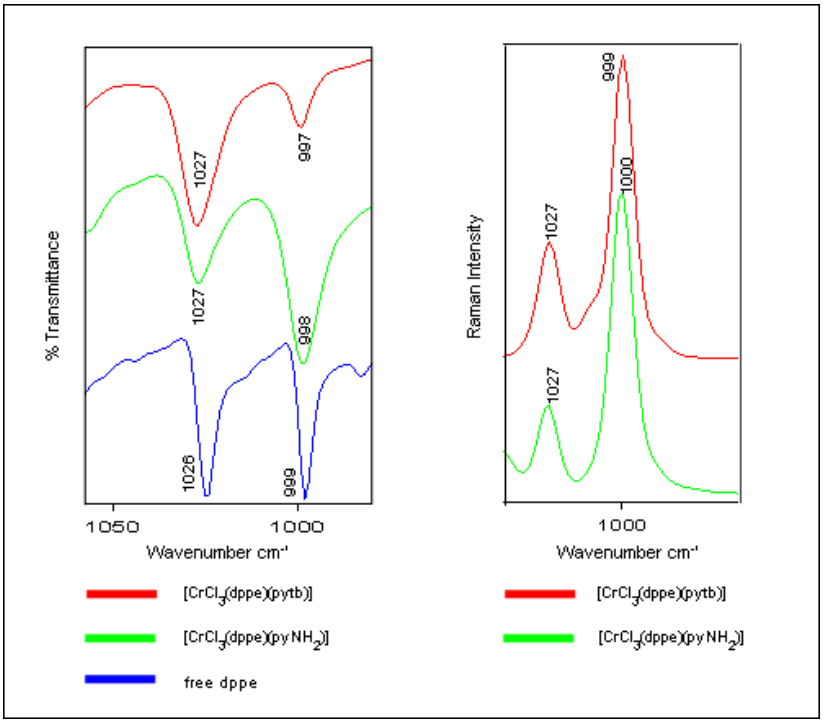

Figure 4.10 IR and Raman spectra of [$CrCl_3$(dppe)($pyNH_2$)] (green) and [$CrCl_3$(dppe)(pytb)] (red)

By following this increasing mass trend, one would expect the pyphenyl compound to show the greatest shift. In the previous N–compounds it was thought that the band at 1026 cm^{-1} was the shifted 992 cm^{-1} band, thus correlating with the expected trend. However, a band at 1011 cm^{-1} was also present and thus a degree of uncertainty arose in assignment. This ambiguity was cleared up by referring to the crystal structure and subsequent IR spectrum of [Hpyphenyl][$CrCl_4$(dppe)]. The band at 1026 cm^{-1} is present and that at 1011 cm^{-1} is absent. This suggests strongly that the 1026 cm^{-1} vibration is not the shifted 992 cm^{-1} band and it is instead assigned to the dppe ligand vibration [113] (Figure 4.11).

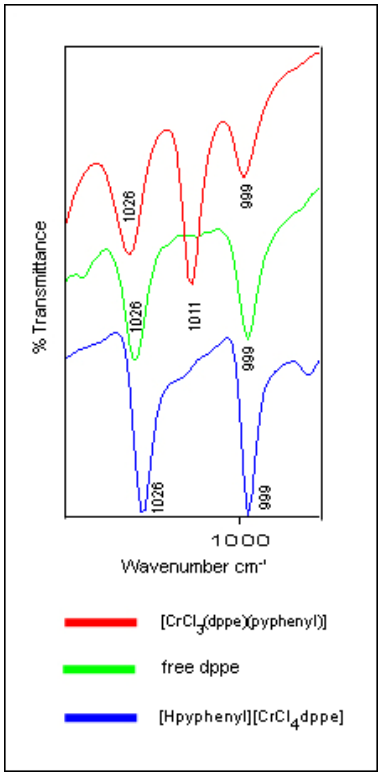

Figure 4.11 **Comparisons between IR spectra of [$CrCl_3$(dppe)(pyphenyl)] (red), [Hpyphenyl][$CrCl_4$(dppe)] (blue) and free dppe (green)**

It would seem that, perhaps somewhat surprisingly, due to its mass it is the 1011 cm^{-1} band that is assigned to the coordinated pyphenyl. Although the trend by mass is not followed, it serves to confirm that mass is not the only factor that determines the degree of shifting (see Table 4.2).

Table 4.2 **Shifting of the characteristic ring breathing vibration in [$CrCl_3$(dppe)(py)], [$CrCl_3$(dppe)($pyNH_2$)], [$CrCl_3$(dppe)(pytb)] and [$CrCl_3$(dppe)(pyphenyl)]**

Pyridine / cm^{-1}	[$CrCl_3$(dppe)(py)] / cm^{-1}	Shift / cm^{-1}
990	1015	25

$pyNH_2$ / cm^{-1}	[$CrCl_3$(dppe)($pyNH_2$)] / cm^{-1}	Shift / cm^{-1}
991	1027	36

Pytb / cm^{-1}	[$CrCl_3$(dppe)(pytb)] / cm^{-1}	Shift / cm^{-1}
995	1027	32

Pyphenyl / cm^{-1}	[$CrCl_3$(dppe)(pyphenyl)] / cm^{-1}	Shift / cm^{-1}
1001	1011	10

This result has further implications with regard to the nature of the products formed as what is implied by the above shifts is that the secondary amine ligands have indeed coordinated to the chromium centre. This results in neutral monomeric species, most probably from the symmetrical cleavage of the dimeric intermediate proposed from the results of region 3313 to 2863 cm^{-1}. The alternative would have been the asymmetrical cleavage of the dimer resulting in pyridinium-type compounds similar in nature to [Hpyphenyl][$CrCl_4$(dppe)] in which this specific pyridine shift is absent.

Yet further evidence of [Hpyphenyl][$CrCl_4$(dppe)] being the only pyH complex is the medium-intensity band at 819 cm^{-1} (see Figure 4.12) which is present only in [Hpyphenyl][$CrCl_4$(dppe)]. It is thus assumed to be associated with pyH.

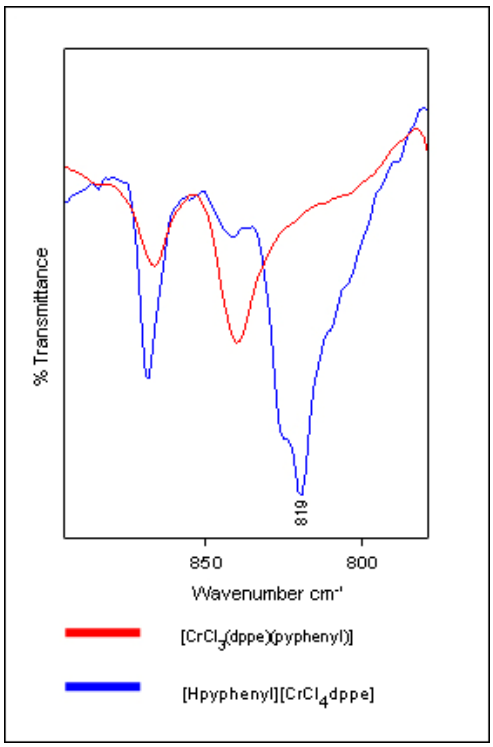

Figure 4.12 **IR spectra showing pyH-specific vibration in [Hpyphenyl][$CrCl_4$(dppe)] (blue) which is absent in [$CrCl_3$(dppe)(pyphenyl)] (red)**

Another pyridine vibration that characteristically shifts upon coordination is observed at 643 cm^{-1} in [$CrCl_3$(dppe)(py)], having shifted from 604 cm^{-1} in its free form [73, 74]. Unlike the shifting of the above-mentioned band at 992 cm^{-1}, this shift is indicative solely of unsubstituted coordinated pyridine, hence its absence in the other compounds.

Another vibration deserves mention as its very presence is indicative of dppe ligand coordination. It is observed at ~654 cm^{-1} in all the complexes and is assigned to P–C stretch of the five–membered chelate ring [113], hence its absence in free dppe.

A representation of the above data from all the compounds is given in Figure 4.13 which compares $[CrCl_3(dppe)(py)]$, $[CrCl_3(dppe)(pytb)]$, $[CrCl_3(dppe)(thf)]$ and free dppe.

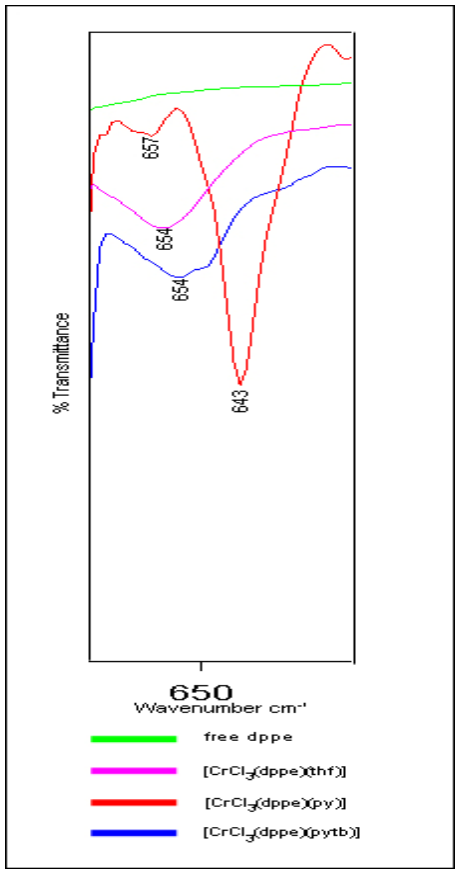

Figure 4.13 IR spectra of $[CrCl_3(dppe)(py)]$ (red), $[CrCl_3(dppe)(pytb)]$ (blue), $[CrCl_3(dppe)(thf)]$ (purple) and free dppe (green)

As expected, there are a considerable number of dppe-related vibrations in this region. Most are unshifted, except for that at 521 cm^{-1} which is indicative of in-plane quadrant ring stretch [113] and has notably shifted from the free ligand position of 505 cm^{-1}.

Within this region the presence of a band at ~856 cm^{-1} is perhaps the strongest indication of coordinated thf (C–O–C) [114]. It is, however, notably absent in the

complexes, including [$CrCl_3$(dppe)(thf)]. This is yet further evidence that this particular complex is the dimeric species as opposed to the directly substituted, monomeric [$CrCl_3$(dppe)(thf)] complex. This finding can be further confirmed by looking at the IR spectrum of a similar compound, [$CrCl_3$(dippe)(thf)], documented in the literature [112]. It has been characterised as a monomeric species and although not discussed as part of this study, its IR spectrum does possess a band at 856 cm^{-1} which in the light of this study confirms its monomeric status.

The remaining vibrations are specific to the pyridine substituent (Table 4.3). The majority pertain to the tertiary butyl group of [$CrCl_3$(dppe)(pytb)] at values that are expected upon coordination [92].

Table 4.3 pytb specific vibrations

Free pytb / cm^{-1}		**[$CrCl_3$(dppe)(pytb)] / cm^{-1}**		**Shift / cm^{-1}**	
IR	**RAMAN**	**IR**	**RAMAN**	**IR**	**RAMAN**
927	931	926	934	-1	3
711	710	729	729	18	19
569	572	571	564	2	-8

Unlike the other regions, there are two additional bands that can be confidently assigned to the phenyl substituent on the pyridine ring of pyphenyl. They are observed in the spectra of [$CrCl_3$(dppe)(pyphenyl)] and [Hpyphenyl][$CrCl_4$(dppe)] only, at ~912 and 625 cm^{-1} respectively, and correlate with the literature, with the latter shifting significantly from the free ligand position of 608 cm^{-1} [97].

4.4.4 Region 495-215 cm^{-1}

In addition to the characteristic metal–ligand vibrations found in this region, there are a further two bands that deserve comment. The first is a well-characterised IR vibration associated with coordinated unsubstituted pyridine at 444 cm^{-1} that has shifted from the free ligand position of 404 cm^{-1} [73, 74]. Note that a very weak vibration is visible at 435 cm^{-1} in the corresponding Raman spectrum.

The second relates to a tertiary butyl C–C–C deformation observed as a weak vibration at 399 cm^{-1} in both the IR and Raman spectra. According to the literature, it has shifted from a free ligand value of 392 cm^{-1} in the IR spectrum [92].

The metal–ligand vibrations of interest include Cr–P, Cr–Cl and Cr–N (py). The band at ~415 cm^{-1} in the spectra of all the complexes is tentatively assigned to a Cr–P vibration as although there is precedence in the literature for such an assignment involving other metals [114, 115], there is also the possibility that it is a dppe vibration shifted from 400 cm^{-1}. In either case it still infers dppe coordination.

In accordance with the IR data of the previous chapters, one expects the presence of three Cr–Cl vibrations between ~390 and ~300 cm^{-1} to be indicative of the *mer* monomer [80]. This is observed for all the pyridine-based complexes for which the IR bands are stronger than their Raman counterparts.

The $[CrCl_3(dppe)(thf)]$ compound deserves closer inspection. Although three weak vibrations are present in the Raman spectrum (indicating monomer), a more complex IR spectrum is observed with what appears to be four vibrations that fall within the so–called 'Cr–Cl range'. It is very difficult to confirm that these vibrations are a direct consequence of the formation of the dimeric species. What is, however, clear is that the vibrational pattern differs from that of all the other complexes in this class which all have strong precedence in the literature for their respective assignments. Importantly, it also differs from the spectrum of $[CrCl_3(dippe)(thf)]$ (two vibrations in this range) which, as stated earlier, was confirmed by Hermes and Girolami [112] to be monomeric (*cis* conformer [80]). Therefore by a process of elimination one of the very few remaining options is a dimeric species.

Another important vibration in the N–classes of compounds was that at 221 cm^{-1} which was confidently assigned to Cr–N (py) [41, 80, 81]. Unfortunately, due to the presence of Ph–P–Ph vibrations from the dppe ligand at a very similar frequency [113], overlap of bands was observed. Assignment was therefore ambiguous.

Figure 4.14 is a representation of the spectra from all the complexes, encompassing all details discussed above. The complexes include [$CrCl_3$(dppe)(thf)], [$CrCl_3$(dppe)(py)] and [$CrCl_3$(dppe)(pytb)].

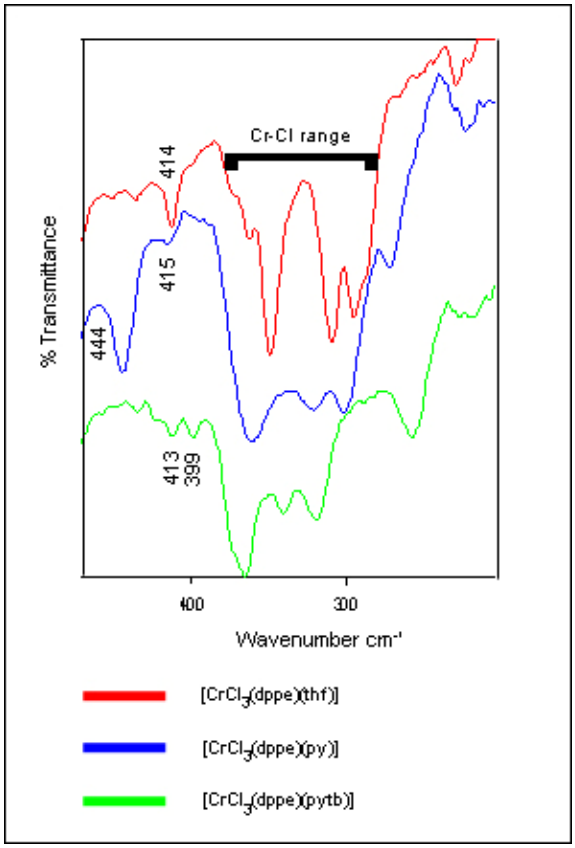

Figure 4.14 **FIR spectra of [$CrCl_3$(dppe)(thf)] (red), [$CrCl_3$(dppe)(py)] (blue) and [$CrCl_3$(dppe)(pytb)] (green)**

Finally, examination of the spectra of [$CrCl_3$(dppe)(pyphenyl)] and [Hpyphenyl][$CrCl_4$(dppe)] importantly confirm that they are not the same complex (Figure 4.15). [$CrCl_3$(dppe)(pyphenyl)] shows the bands indicative of the monomeric species, with two strong vibrations and one that is notably weaker (either way it is either the *cis* or *mer* conformer). [Hpyphenyl][$CrCl_4$(dppe)] possesses three strong vibrations with a further two weaker vibrations.

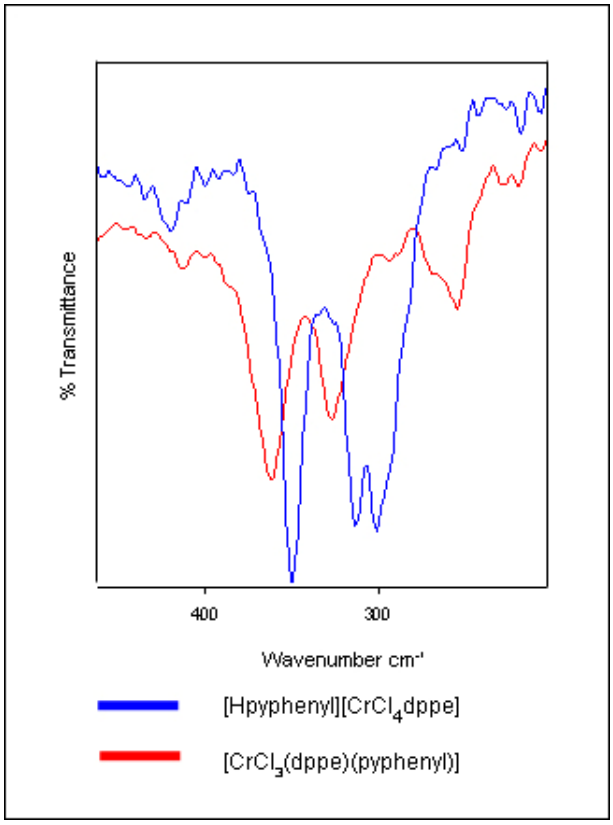

Figure 4.15 **FIR spectra of [$CrCl_3$(dppe)(pyphenyl)] (red) and [Hpyphenyl][$CrCl_4$(dppe)] (blue)**

In conclusion, the detailed vibrational study suggests that the complex initially suggested as [$CrCl_3$(dppe)(thf)], on the basis of the equivalent bipy structure, is [Cr(dppe)Cl_2(μ-Cl)]$_2$. The other compounds in this class show sufficient vibrational evidence to be monomeric in structure.

Table 4.4 **Vibrational assignments of $[CrCl_3(dppe)(thf)]$ (18), $[CrCl_3(dppe)(py)]$ (19), $[CrCl_3(dppe)(pyNH_2)]$ (20), $[CrCl_3(dppe)(pytb)]$ (21), $[CrCl_3(dppe)(pyphenyl)]$ (22) and [Hpyphenyl][$CrCl_4(dppe)$] (23)**

18		19		20		21		22	23	Assignment
IR / cm^{-1}	RAMAN / cm^{-1}	IR / cm^{-1}	RAMAN / cm^{-1}	IR / cm^{-1}	RAMAN / cm^{-1}	IR / cm^{-1}	RAMAN / cm^{-1}	IR / cm^{-1}	IR / cm^{-1}	
-	-	-	-	3313s	-	-	-	-	-	ν(NH_2) asym (76, 96)
-	-	-	-	3206s	3212w	-	-	-	-	ν(NH_2) sym (76, 96)
-	-	-	-	-	-	-	-	-	3191s	pyH
-	3172w	3157w	3167w	-	3169w	-	3169w	-	3179m	Overtone (113)
3141w	3145w	3133w	3140w	3143s	3142w	3141w	3141w	3136w	-	Overtone (113)
-	-	-	-	-	-	3130w	-	-	-	Overtone (113)
-	-	3101s/s	-	-	-	-	-	-	-	ν(CH) (py) (73, 74)
-	-	-	-	3092ssh	3092msh	-	-	-	-	ν(CH) ($pyNH_2$) (96)
3076w	-	-	3079s/s	-	-	3076ssh	3088sh	3076ssh	3086s	ν(CH) (dppe) (113)
3055m	3057s	3062s/s	3051s/s	3055s	3054s	3053s	3051s	3047s	3049s	ν(CH) (dppe) (113) / (py) (73, 74)

18		19		20		21		22	23	Assignment
3003w	3003w	3004ssh	3002w	3009sh	3003w	3003m	3002m	-		Combination (113)
2986m	2987w	-	-	2972s	2982w		-	2972s	2984s	Combination (113)
-	-	-	-	-	-	2964s	2965s	-	-	ν (CH_3) asym (92)
2956sh	2950m	2959w	2957w	-	2957m	-	-	-	2961w 2947w	ν (CH_2) asym (113)
2926sh, 2915sh	2932m, 2915m	2929w	2915w	-	2915m	2934sh	-	-	-	ν (CH_2) sym (113)
-	-	-	-	-	-	2904m	2908m	-	-	ν (CH_3) sym (92)
2878sh	2896m	2892ssh	2891w	-	2890m	-	-	2872s 2833s	2888s 2863s	Present in free dppe (unassigned)
-	-	-	-	-	-	2869m	2868msh	-		ν (CH_3) sym (92)
-	-	-	-	1651vs	1650m	-	-	-	-	δ (NH_2) (96)
-	-	1631m 1607s	1633w 1605m	-	-	1634m 1616s	1636w 1617w	1635w 1612s	1632s 1617w	ν_{ring} (py) (73, 74, 92, 97) / pyH (93, 94)
1617m	1617vw	-	-	-	-	-	-	-	-	unassigned
1587m	1587s	1584brsh	1585s	1587s	1585s	1586w	1585s	-	1590m	ν_{ring} (dppe) (113)

18		19		20		21		22	23	Assignment
1572m	1574m	1571w	1572m	1572sh	1573msh	1572w	1572msh	1568w	1577w	ν_{ring} (dppe) (113) / ν_{ring} (pyX) (73-75, 92, 96, 97)
-	-	1535m	1535vw	1529vs	1534m	1542w	1542vw	1539w	-	ν_{ring} (pyX) (73-75, 92, 96, 97)
-	-	-	-	-	-	-	-	-	1515m	PyH related
-	-	-	-	-	-	1500m	1503vw	-	-	ν_{ring} (pytb) (92)
-	-	-	-	-	-	-	-	-	1495w	PyH related
1485m	1487w	1485s	1487w	1484m	1486w	1485m	1484w	1480s	1482s	CH def + ν(semicircle) (113)
-	-	-	-	-	-	1462w	1462w	-	-	CH_3 asym def (92)
-	-	1445vs	-	-	-	-	-	-	-	ν_{ring} (py) (73, 74)
1435s	1434w	1432s	1437w	1434s	1435w	1434vs	1437m	1432s	1432s	CH def + ν(semicircle) (113)
1416m	1420w	1417w	1417w	1414w	1414w	1420s	1416w	1413m	1417m	Overtone(113) / CH_3 sym def (92) / ν_{ring} (97)

18		19		20		21		22	23	Assignment
-	-	-	-	1362w	-	1365w	-	-	1363m	ν_{ring} (96) / CH_3 asym def (92)
1334w	1337w	1333w	1333w	1336w	1333vw	1332w	1331w	1332w	1334w	δ (CH) def (113)
1314w	1312w	-	-	1314w	1306vw	1308w	1308vw	1310w	-	δ (CH) def (113) / ν_{ring} (pyphenyl) (97)
-	-	-	-	-	-	-	-	1288vw	1286m	ν_{ring} + ν(CH) (pyphenyl) (97)
1270w	1274w	1268w	1272w	1271w	1271w	1274m	1273w	-	-	CH_2 wag (113)
-	-	-	-	-	-	-	-	-	1262w	PyH related
-	-	-	-	1258w	1260w	-	-	-	-	ν (C-NH_2) (96)
-	-	1236w 1220m	- 1224w	1214w	-	1230m	1233w	1222m	1237w	ν_{ring} (73-75, 92, 96, 97)
-	-	-	-	-	-	-	-	-	1212m	PyH related
1190w 1160w	1195m 1163m	1196w 1155m	1197m 1158m	1197m 1158w	1194m 1159m	1190m 1157m	1191m 1159m	1188w 1155w	1189m 1156w	δ (CH) def (113)
1120wsh	1116msh	-	-	-	-	1121sh	1124w	-	-	ν (P-(C_6H_5)) (113)
1099m	1110m	1110m	1099m	1098m	1099m	1098s	1098m	1096m	1098m	Ring breathing (113)
1071w	1076vw	1069s	1073vw	1072w	-	1069s	1070m	1067m	1068m	δ (CH) def (113)

18		19		20		21		22	23	Assignment
-	-	1046m	1046w	1056w	1046m	-	-	1045m	-	ν_{ring} (73-75, 96, 97)
1026w	1029s	1027w	1028sh	-	-	-	-	1026m	1026m	δ (CH) def (113)
-	-	1015m	1018s	1027m	1027s	1027s	1027s	1011m	-	Ring breathing (pyX) (73, 74, 92, 96, 97)
999w	998vs	999w	998s	998m	1000s	997m	999s	999m	997m	Trigonal ring breathing (dppe) (113)
-	-	-	-	-	-	926w	934w	-	-	CH_3 rock (tb) (92)
-	-	-	-	-	-	-		912w	913w	ν (CH) pyphenyl (97)
868w	872w	864w	-	864w	-	867m	868vw	864m	868w	i.p o.p. def (113) / CH_3 rock (tb) (92) / CH py (73, 74, 92, 96, 97)
-	-	-	-	847sh	849s	843sh	842w	838m	841w	X-sens (96) / py breathing (92) / ν_{ring} (97)
827w	835w	823w	825w	825m	831sh	832s	827w	-	-	In phase γ(CH) def (113, 96, 92)
-	-	-	-	-	-	-	-	-	819m	PyH related

18		19		20		21		22	23	Assignment
-	-	758s	766w	-	765w	-	764w	764s	761s	γ(CH) (py) (73-75, 92, 96, 97)
741s	741vw	746s	746vw	742s	746vw	742s	-	742s	748s	In phase γ(CH) (dppe) (113)
-	-	-	-	-	-	-	-	-	737s	In phase γ(CH) (dppe) (113)
-	-	-	-	-	-	729m	729m	-	-	γ(CH) (pytb) (92)
-	-	-	-	-	-	-	-	-	708s	PyH related
693s	698m	694vs	700wsh	695s	-	691vs	-	691s	690s	CH_2 rock (113)
-	684m	679m	685m	-	683m	-	686m	-	-	γ (sextant ring) def (113)
-	-	-	-	-	-	668m	668m	-	-	ν (CC) (pytb) (92)
-	-	-	-	-	-	-	-	-	663w	PyH related
654w	665w	657vw	650w	645w	647m	653w	651w	654w	656m	ν (PC) (5-membered ring) (113)
-	-	-	-	-	-	-	-	-	648w	PyH related
-	-	643s	637w	-	-	-	-	-	-	ν_{ring} (py) (73, 74)
-	-	-	-	-	-	-	-	625m	626vw	Pyphenyl vib
613w	617m	616vw	617m	616w	617m	617w	617m	617w	617w	δ (quadrant ring) def (113)

18		19		20		21		22	23	Assignment
-	-	-	-	-	-	571m	564vw	-	-	Skeletal str (tb) (92)
-	-	-	-	-	-	-	-	-	550w	PyH related
-	-	-	-	-	-	546m	548vw	-	-	Rock (tb) (92)
521s	524m	520s	521w	525s	527m	522s	520w	523s	519s	δ (quadrant ring) def (113) / X-sens $pyNH_2$ (96)
495m	490vw	490sh	488vw	495s	491vw	494m	488vw	492s	497m 488m	δ (quadrant ring) def (113)
475sh	469vw	476m	473vw	-	475vw	474sh	474vw	-	-	unassigned
-	-	444m	435vw	-	-	-	-	-	-	ν_{ring} (py) (73, 74)
414m	413m	415w	-	413m	412m	413w	417w	413w	420w	Cr –P (114, 115)
-	-	-	-	-	-	399w	399w	-	-	CCC def (pytb) (92)
363m	370w	361m	367w	375w	370w	365m	367w	361s	349s	Cr – Cl (80)
									334w	Cr – Cl (80)
349m	344w	321m	341w	348m	337w	340m	336w	326s	326w	Cr – Cl (80)
308m	306w	301m	324w	309m	309w	319m	316w	293w	312s	Cr – Cl (80)
294m	-	-	-	-	-	-	-	-	300s	Cr – Cl (80)

18		19		20		21		22	23	Assignment
227w 220w	- 221w	229w 219w	222w 217w	222w 215w	227w -	226w 216w	228m -	225w 218w	224vw 216vw	Ph – P – Ph (113) Cr – N (py) (41, 80, 81)

ν = stretching, δ = in-plane bending, γ = out-of-plane bending, def = deformation, asym = asymmetrical, sym = symmetrical vs = very strong, s = strong, m= medium, w = weak, vw = very weak

4.5 COMPUTATIONAL STUDY

Computational analysis was carried out solely on [$CrCl_3$(dppe)(pytb)] on the basis of it being a sound representative model of all the complexes. Figures 4.16 and 4.17 illustrate the goodness of fit between the experimental MIR and Raman spectra and their respective calculated spectra. Unlike the analogous studies in the previous chapters, the FIR spectral comparison is also given (Figure 4.18) as this is the first compound of this study in which the solid-state effects do not hinder the observance of all three distinct Cr–Cl vibrations in the calculated spectrum. However, as one has now come to expect with these types of complex, the calculated vibrations are not pure Cr–Cl vibrations but are mixed with other modes.

These vibrations, along with a selection of other important frequencies, are presented in Tables 4.5 which show the excellent correlation and are thus further evidence to support the experimental deductions pertaining to ligand coordination.

At this stage, if any discrepancies in correlation have been observed, they have been associated largely with the metal–ligand vibrations. Therefore it was particularly satisfying to be able to confirm the Cr–P vibration by way of experimental–calculated correlations as it was initially a rather tentative assignment in the experimental analysis.

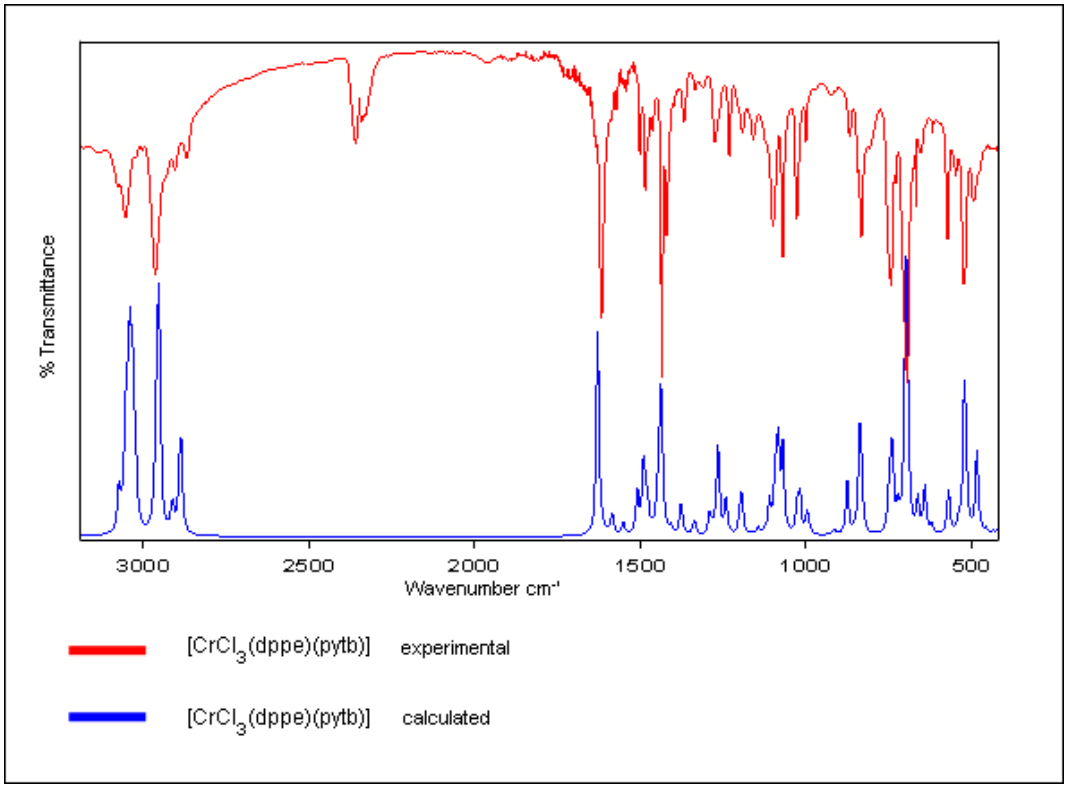

Figure 4.16 **Experimental (red) and calculated (blue) MIR spectra of [$CrCl_3$(dppe)(pytb)]**

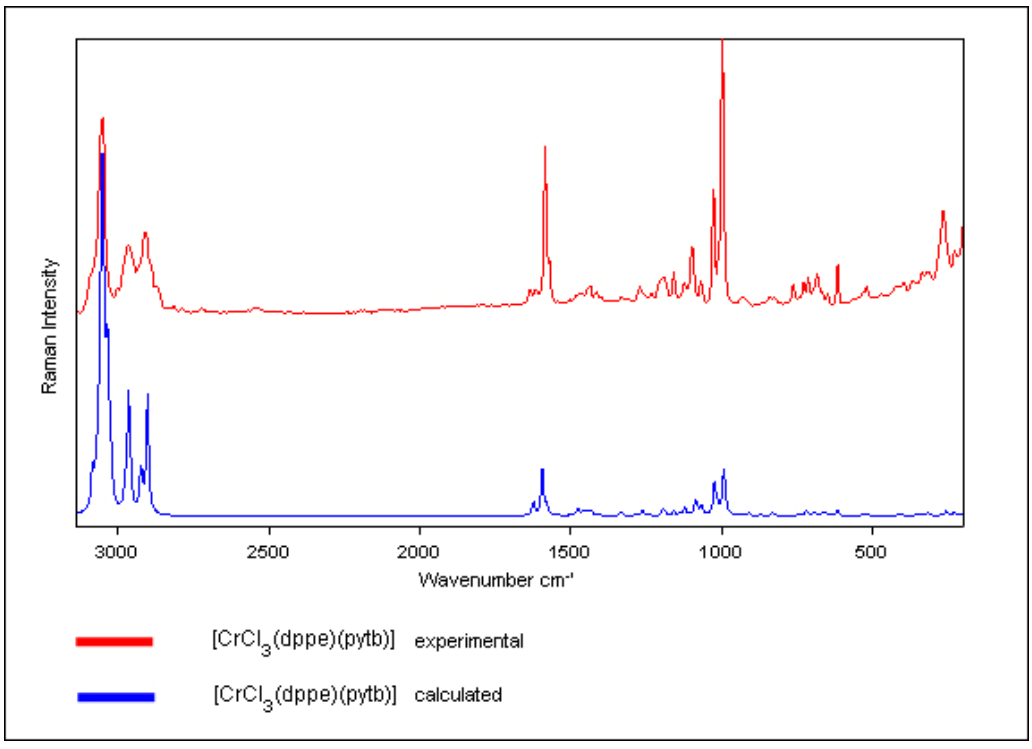

Figure 4.17 **Experimental (red) and calculated (blue) Raman spectra of [$CrCl_3$(dppe)(pytb)]**

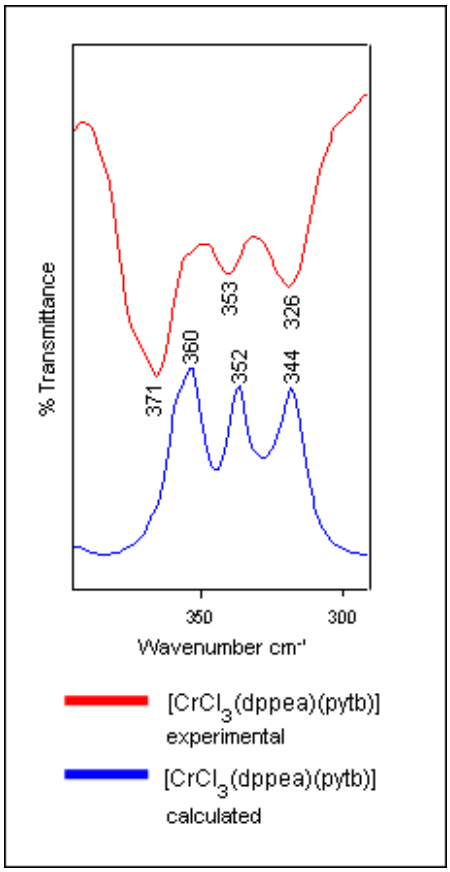

Figure 4.18 **Experimental (red) and calculated (blue) FIR spectra of [$CrCl_3$(dppe)(pytb)]**

Table 4.5 **Selected experimental and calculated IR and Raman band assignments for [$CrCl_3$(dppe)(pytb)]**

[$CrCl_3$(dppe)(pytb)] IR / cm^{-1}		[$CrCl_3$(dppe)(pytb)] Raman / cm^{-1}		Assignment	
Experimental	**Calculated**	**Experimental**	**Calculated**	**Experimental**	**Calculated**
2964	2957	2965	2967	$\nu(CH_3)$ asym	$\nu(CH_3)$ asym
2904	2891	2908	2901	$\nu(CH_3)$ sym	$\nu(CH_3)$ sym
1616	1628	1617	1624	ν_{ring} (py)	ν_{ring} (py)
1586	1585	1585	1596	ν_{ring} (dppe)	ν_{ring} (dppe)
1027	1023	1027	1021	Ring breathing (pytb)	Ring breathing (pytb)

997	997	999	995	Trigonal ring breathing (dppe)	Trigonal ring breathing (dppe)
653	660	651	660	ν (PC) (5-membered ring)	ν (PC) (5-membered ring)
413	416, 408	417	416, 407	Cr–P	Cr–P
365, 340, 319	358, 336, 317	367, 336, 316	358, 336, 318	Cr–Cl	Cr–Cl + tb breathing / tb rock / CH_3 twist
226, 219	240	228	239	Ph–P–Ph / Cr–N (py)	Cr–N (py)
-	232	-	232		Ph–P–Ph

Table 4.6 Scaling factors determined for [$CrCl_3$(dppe)(pytb)]

Region / cm^{-1}	IR	Raman
0 – 1861	0.980144	0.978311
2827 – 3424	0.953311	0.956743

The generation of the molecular orbitals associated with [$CrCl_3$(dppe)(pytb)] allows one to see that both the HOMO and LUMO orbitals are found around the chlorine atoms (Figure 4.19). Where differences arise is in the phenyl ring systems, where electrophilic attack is likely to take place on those rings that are found on the P–Cr–N axis, while attack by nucleophilic species will take place on the rings on the Cl–Cr–P axis.

HOMO **LUMO**

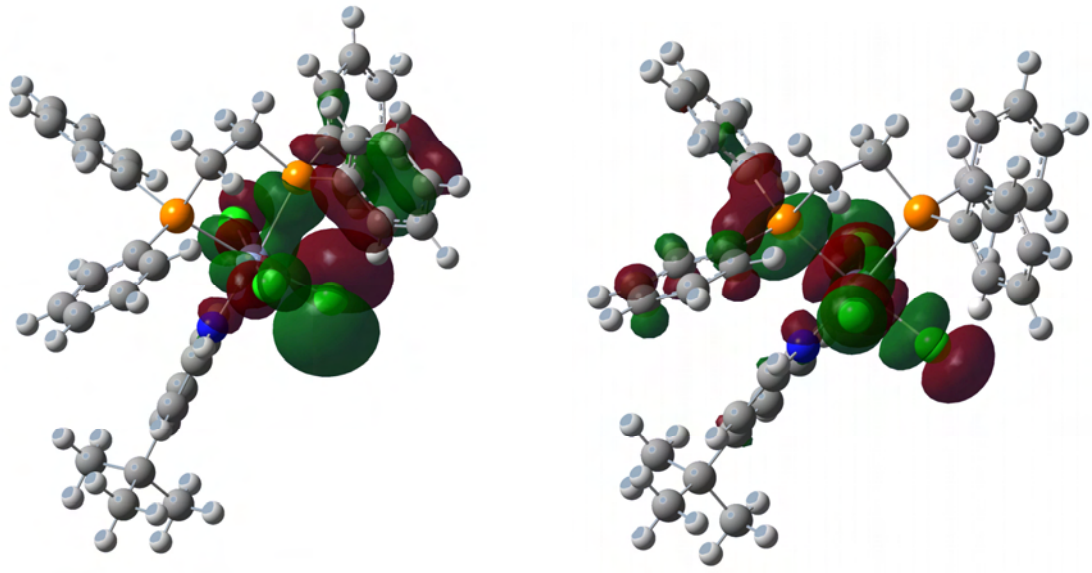

Figure 4.19 HOMO and LUMO orbitals of [$CrCl_3$(dppe)(pytb)]

4.6 NMR SPECTROSCOPY

As a result of the lack of aromaticity or conjugation associated directly with the coordinating phosphorus atoms, the substitution reaction resulting from the addition of dppe to [$CrCl_3(thf)_3$] was not followed by ^{1}H NMR spectroscopy as dppe ligand resonances were not expected to disappear upon coordination to the metal centre.

This was confirmed when the spectrum of the final product (see Figure 4.20) was recorded in DMSO-d_6 in which the aromatic protons are observed at 7.3 ppm and the CH_2 protons at 2.01 ppm.

On the basis of the deductions made in Chapter 3, the notable absence of thf resonances may suggest that this is a dimeric species, which would correlate with the deductions made in the corresponding IR and Raman spectral interpretation.

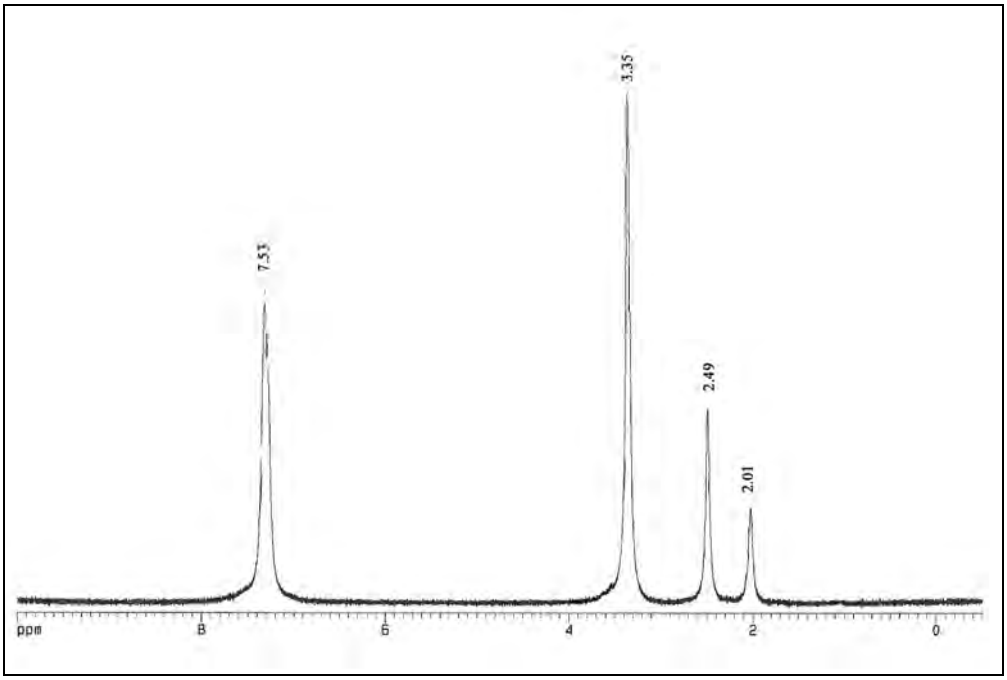

Figure 4.20 **^{1}H NMR spectrum of [$CrCl_3$(dppe)(thf)] final product in DMSO-d_6**

The presence of phosphorus in the ligand allowed ^{31}P NMR spectroscopy to be used. Spectra of both the free ligand and the [$CrCl_3(thf)_3$] plus dppe compound were recorded and a clear resonance shift of 5.25 ppm was observed upon coordination (Figures 4.21 and 4.22).

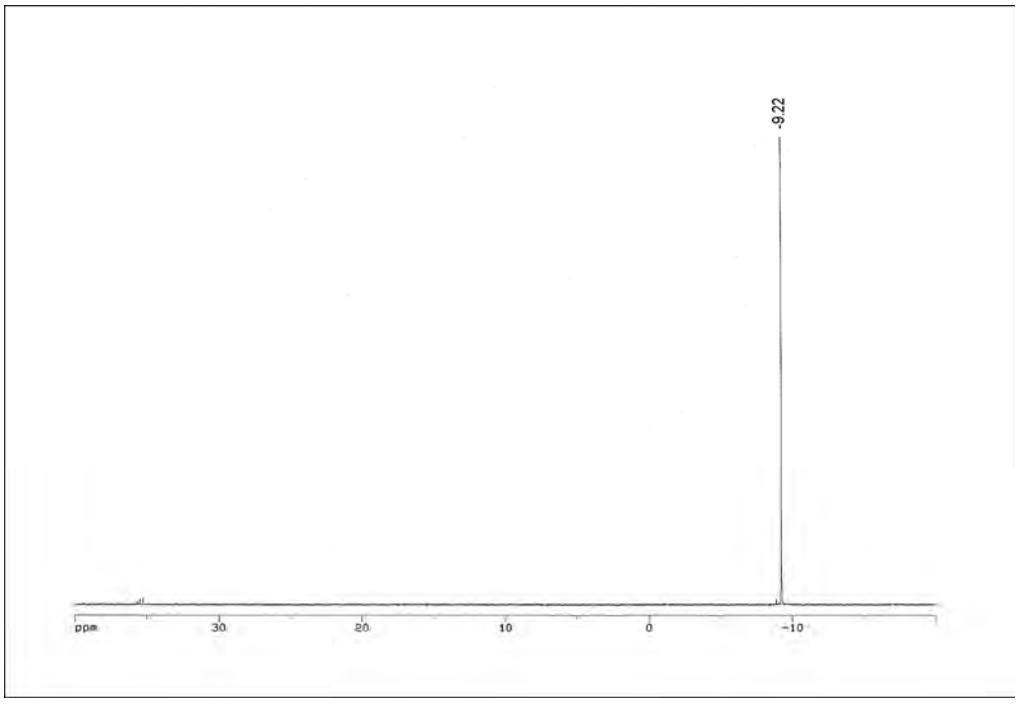

Figure 4.21 **^{31}P NMR spectrum of free dppe in DMSO-d_6**

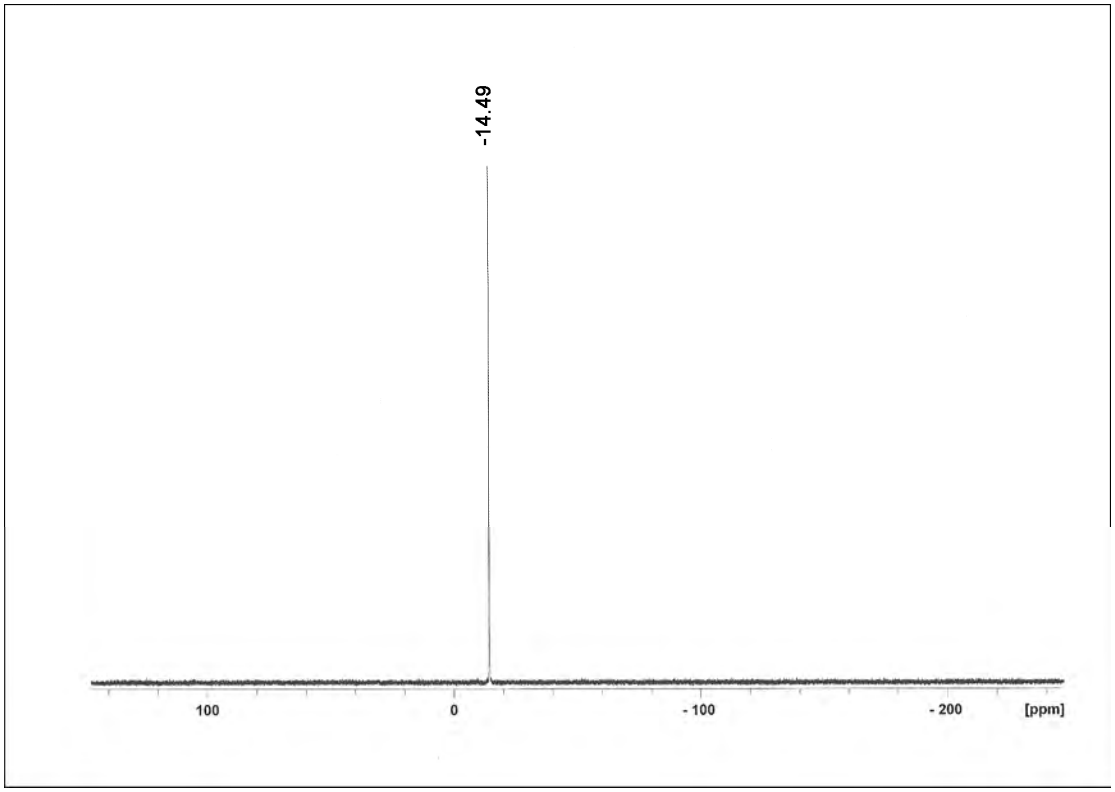

Figure 4.22 **^{31}P NMR spectrum of [$CrCl_3$(dppe)(thf)] in DMSO-d_6**

4.7 MASS SPECTROMETRY

As with the previous classes a selection of compounds were chosen for analysis. These included [$CrCl_3$(dppe)(thf)], [$CrCl_3$(dppe)($pyNH_2$)] and [$CrCl_3$(dppe)(pyphenyl)]. All three compounds showed good isotopic distribution patterns for the fragment that resulted from the loss of the respective monodentate ligands and a chlorine atom, i.e. $[M–thfCl]^+$, $[M–pyNH_2Cl]^+$ and $[M–pyphenylCl]^+$ (m/z = 520). This same fragment without a further chlorine atom was also observed for each of the compounds with similarly good distribution patterns ($[M–thf2Cl]^+$, $[M–pyNH_22Cl]^+$ and $[M–pyphenyl2Cl]^+$) (m/z = 485). These results are presented in Figure 4.23 The spectrum of [$CrCl_3$(dppe)(pyphenyl)] shown in Figure 4.24 also possessed an additional fragmentation pattern, $[M–Cl]^+$ (m/z = 675), which confirms its monomeric structure. Note that all of the above mentioned isotopic distribution patterns correlated well with those determined theoretically. It is plausible that the distribution patterns observed for [$CrCl_3$(dppe)(thf)] and [$CrCl_3$(dppe)($pyNH_2$)] could be fragments of a dimeric species. For the former compound this correlates well with the vibrational data, while the latter's vibrational spectra suggest the monomer. This structural deduction for [$CrCl_3$(dppe)($pyNH_2$)] is also based on the compound's

similarity to [$CrCl_3$(dppe)(pyphenyl)] in terms of the addition of a monodentate substituted pyridine ligand which yielded strong MS evidence for the monomer.

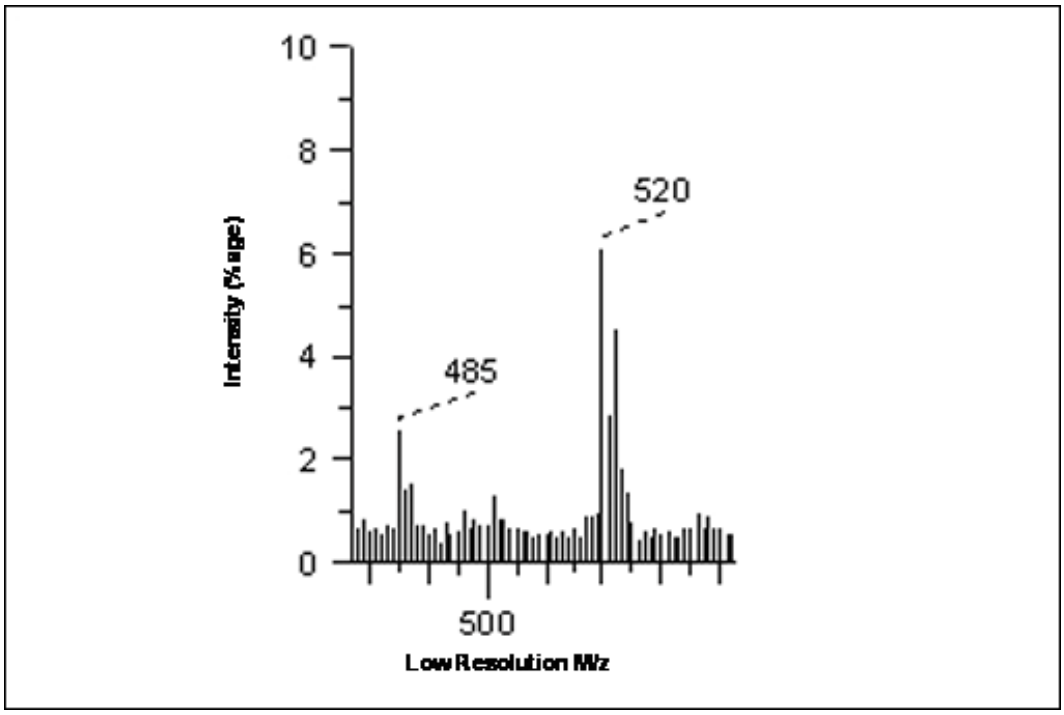

Figure 4.23 FAB-MS spectum showing paeks present in [$CrCl_3$(dppe)(thf)], [$CrCl_3$(dppe)($pyNH_2$)] and [$CrCl_3$(dppe)(pyphenyl)]

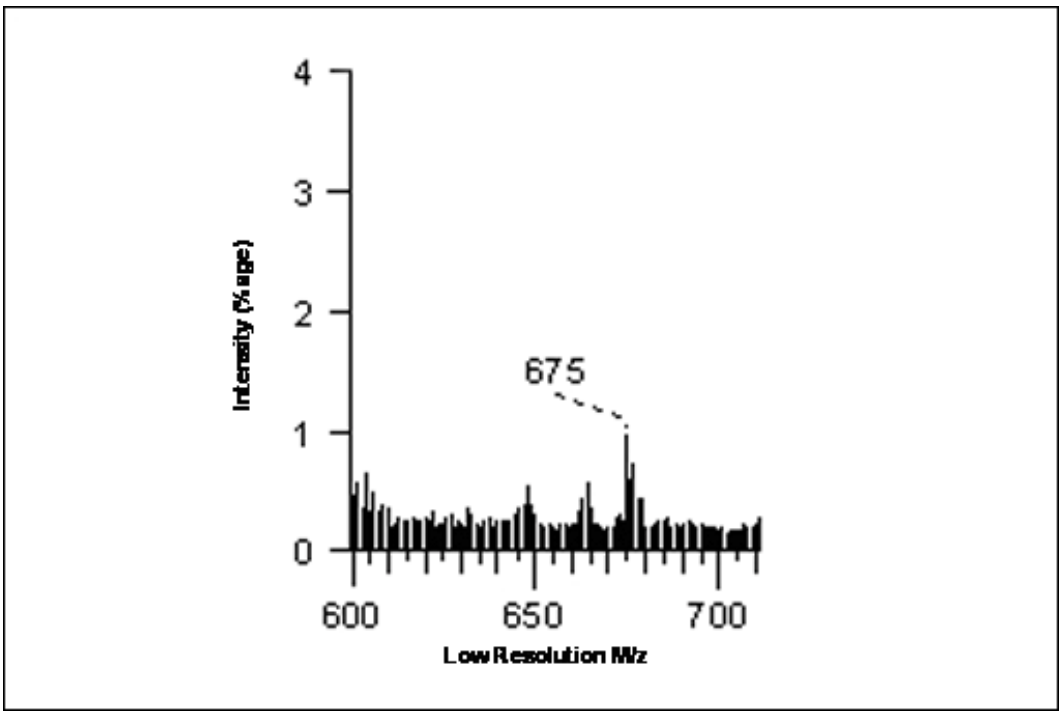

Figure 4.24 FAB-MS spectrum of [$CrCl_3$(dppe)(pyphenyl)]

4.8 X-RAY CRYSTALLOGRAPHY

4.8.1 [Hpyphenyl][$CrCl_4$(dppe)]

The molecular structure of [Hpyphenyl][$CrCl_4$(dppe)] is the only structure of a diphenylphosphinoethane–tetrachloro–chromium complex anion. Although the coordination geometry is similar to that of the tetra–n–propylammonium (*cis*–1,2–bis(diphenylphosphino) ethylene tetrachloro chromium(III) structure determined by Gray [99], there are significant structural differences arising from the reduction of the 'CC bridge' bond order, as well as from the novel counter-ion interactions that are absent in the 'Gray structure'.

Two formula units are observed in the asymmetrical unit of [Hpyphenyl][$CrCl_4$(dppe)] (Figure 4.25) as opposed to one formula unit in the Gray structure. The chromium atom is coordinated to four chlorine atoms and the two phosphorus atoms of the dppe ligand. The coordination is approximately octahedral, with the largest angle deviation being the P(3)–Cr(2)–Cl(8) (81.76(8)°). All other *cis* X–Cr–Y bond angles in the two formula units are in the range 81.93(7) to 96.27(8)°. These values are comparable to those found for the Gray structure.

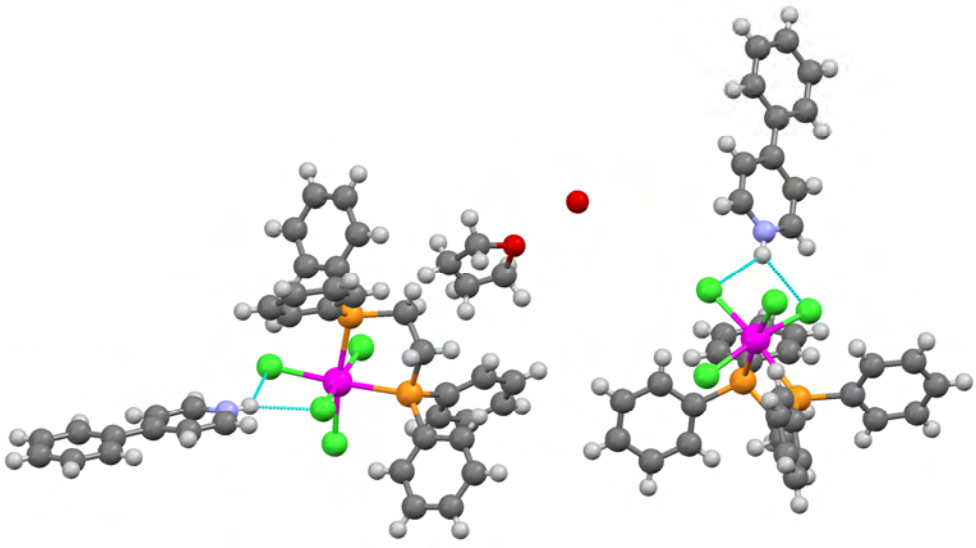

Figure 4.25 **Perspective drawing of the asymmetric unit of [Hpyphenyl][$CrCl_4$(dppe)] showing hydrogen bond interactions**

The metal–ligand bond lengths were also found to be very similar in the two structures (Table 4.7). The similarities continue with regard to both crystal system and space group as both crystallised in a triclinic space group, P–1.

The same cannot be said for the torsion angle comparisons. A large twist is observed for the P–C–C–P torsion angle of this study's structure (61.2(6)°) as opposed to the corresponding angle in the Gray structure, which twists 4.12° in the opposite direction. This feature makes any comparisons between the two structures' magnitudes of phenyl ring twisting awkward as there is no fixed P–C reference common to both structures. Suffice it to say that Figure 4.26 clearly shows that there are notable differences between the two.

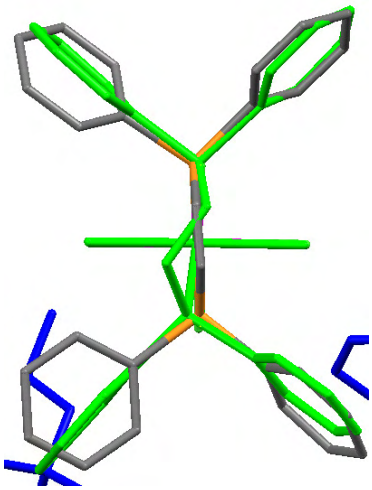

Figure 4.26 **P–C–C–P torsion angle comparison between [Hpyphenyl][$CrCl_4$(dppe)] and the Gray structure**

Table 4.7 **Bond lengths [Å] and angles [°] for [Hpyphenyl][$CrCl_4$(dppe)]**

Cr(1)-Cl(4)	2.310(2)	Cr(1)-Cl(2)	2.3450(19)
Cr(1)-Cl(3)	2.319(2)	Cr(1)-P(2)	2.492(2)
Cr(1)-Cl(1)	2.3401(19)	Cr(1)-P(1)	2.494(2)
Cl(4)-Cr(1)-Cl(1)	94.54(7)	Cl(8)-Cr(2)-Cl(6)	94.03(8)
Cl(3)-Cr(1)-Cl(1)	91.88(7)	Cl(6)-Cr(2)-Cl(7)	91.38(8)
Cl(4)-Cr(1)-Cl(2)	93.96(7)	Cl(8)-Cr(2)-Cl(5)	93.70(8)
Cl(3)-Cr(1)-Cl(2)	93.87(7)	Cl(6)-Cr(2)-Cl(5)	96.27(8)

Cl(1)-Cr(1)-Cl(2)	94.17(7)	Cl(7)-Cr(2)-Cl(5)	92.63(8)
Cl(4)-Cr(1)-P(2)	83.19(7)	Cl(8)-Cr(2)-P(3)	81.76(8)
Cl(3)-Cr(1)-P(2)	88.22(7)	Cl(6)-Cr(2)-P(3)	92.70(8)
Cl(1)-Cr(1)-P(2)	92.52(7)	Cl(7)-Cr(2)-P(3)	91.03(7)
Cl(4)-Cr(1)-P(1)	88.20(7)	Cl(8)-Cr(2)-P(4)	89.00(8)
Cl(3)-Cr(1)-P(1)	84.57(7)	Cl(7)-Cr(2)-P(4)	84.96(8)
Cl(2)-Cr(1)-P(1)	91.53(7)	Cl(5)-Cr(2)-P(4)	89.13(8)
P(2)-Cr(1)-P(1)	81.93(7)	P(3)-Cr(2)-P(4)	82.16(7)

P(1)-C(1)-C(2)-P(2)	59.8(7)	P(3)-C(3)-C(4)-P(4)	-61.2(6)
C(1)-P(1)-C(11)-C(12)	20.3(8)	C(3)-P(3)-C(71)-C(76)	33.6(8)
C(1)-P(1)-C(11)-C(16)	-164.6(6)	C(3)-P(3)-C(71)-C(72)	-145.8(7)
C(1)-P(1)-C(21)-C(26)	138.3(7)	C(3)-P(3)-C(81)-C(82)	178.2(7)
C(1)-P(1)-C(21)-C(22)	-46.8(8)	C(3)-P(3)-C(81)-C(86)	-5.2(9)
C(2)-P(2)-C(31)-C(32)	-171.2(6)	C(4)-P(4)-C(91)-C(92)	133.3(6)
C(2)-P(2)-C(31)-C(36)	11.5(7)	C(4)-P(4)-C(91)-C(96)	-47.8(7)
C(2)-P(2)-C(41)-C(42)	145.2(7)	C(4)-P(4)-C(101)-C(106)	157.1(6)
C(2)-P(2)-C(41)-C(46)	-36.3(9)	C(4)-P(4)-C(101)-C(102)	-22.7(7)

Although absent in the Gray structure, hydrogen bonding is present between the pyridinium N–H and the two closest chlorine atoms which are *cis* to each other Table 4.8). This is observed in both formula units in which N(1)–H(1) is hydrogen bonded to Cl(1) and Cl(3) and N(2)–H(2) is hydrogen bonded to Cl(5) and Cl(7). Figure 4.25 above illustrates the hydrogen bonding in one of the two formula units that are present in the asymmetrical unit.

Table 4.8 Hydrogen bonds for [Hpyphenyl][$CrCl_4$(dppe)] [Å and °]

D-H...A	d(D-H)	d(H...A)	d(D...A)	<(DHA)
N(1)-H(1)...Cl(1)	0.86	2.62	3.255(7)	131.9
N(1)-H(1)...Cl(3)	0.86	2.44	3.183(6)	145.1
N(2)-H(2)...Cl(5)	0.86	2.55	3.217(10)	134.8

N(2)-H(2)...Cl(7)	0.86	2.62	3.330(9)	140.0

The lattice packing of the structure is shown in Figure 4.27 and the crystal data in Table 4.9.

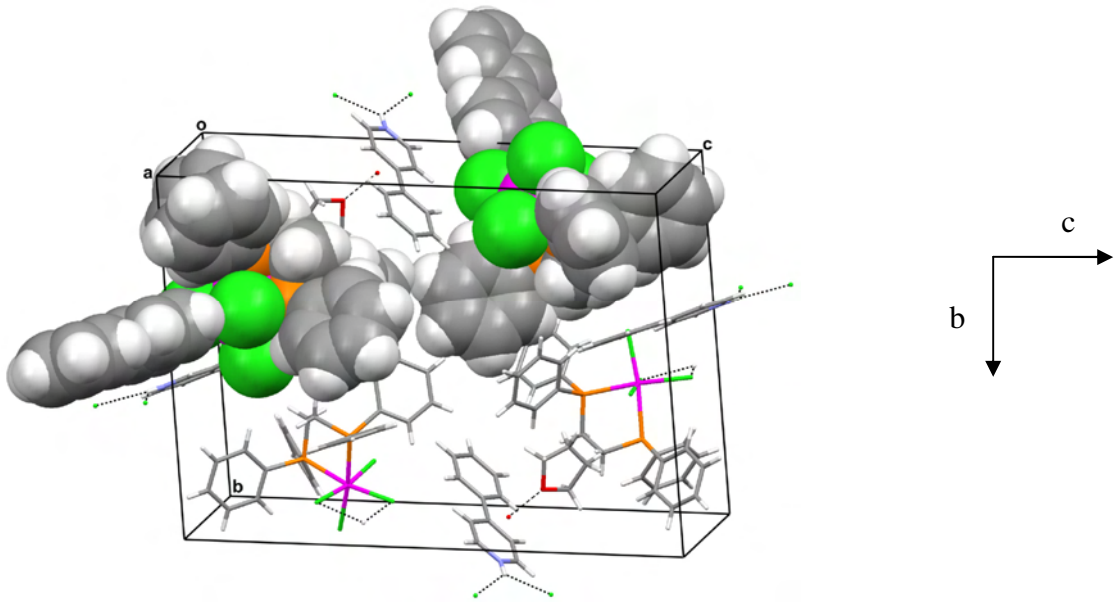

Figure 4.27 **Packing arrangement with space-filled component of [Hpyphenyl][$CrCl_4$(dppe)]**

Table 4.9 **Crystal data and structure refinement for [Hpyphenyl][$CrCl_4$(dppe)]**

Empirical formula	$C_{38.14}$ $H_{36.28}$ Cl_4 Cr N $O_{0.42}$ P_2	
Formula weight	771.10	
Temperature	293(2) K	
Wavelength	0.71073 Å	
Crystal system	Triclinic	
Space group	P 1	
Unit cell dimensions	a = 10.3411(16) Å	α= 86.581(3)°
	b = 16.328(3) Å	β= 85.538(3)°
	c = 22.859(3) Å	γ = 89.934(2)°
Volume	3 841.2(10) $Å^3$	
Z	4	
Density (calculated)	1.333 Mg/m^3	

Absorption coefficient	0.688 mm^{-1}
F(000)	1 590
Crystal size	0.22 x 0.08 x 0.08 mm^3
Theta range for data collection	2.56 to 26.53°
Index ranges	-12<=h<=11, -19<=k<=18, -28<=l<=11
Reflections collected	20 512
Independent reflections	13639 [R(int) = 0.0613]
Completeness to theta = 25.00°	96.7%
Absorption correction	Semi-empirical from equivalents
Max. and min. transmission	0.946 and 0.855
Refinement method	Full-matrix least-squares on F^2
Data / restraints / parameters	13 639 / 0 / 836
Goodness-of-fit on F^2	1.002
Final R indices [I>2σ(I)]	R1 = 0.0733, wR2 = 0.1836
R indices (all data)	R1 = 0.1599, wR2 = 0.2364
Extinction coefficient	0
Largest diff. peak and hole	0.819 and -0.669 e.$Å^{-3}$

4.9 EXPERIMENTAL

4.9.1 SYNTHESIS OF [$CrCl_3$(dppe)(thf)] / [Cr(dppe)Cl_2(μ-Cl)]$_2$ (18)

A Schlenk tube was charged with [$CrCl_3(thf)_3$] (0.28 g, 0.747 mmol) and thf (20 cm^3). The resulting dissolved purple solution turned a deep blue colour immediately upon addition of dppe (0.29 g, 0.747 mmol). The reaction was then allowed to stir at room temperature overnight to ensure completion. The volume of the final solution was then reduced, followed by the addition of Et_2O (20 cm^3), resulting in the formation of a light blue precipitate. The deep blue supernatant was removed via syringe and the residue dried under reduced pressure for 3 hours, which resulted in the isolation of a light blue precipitate **(18)** in good yield (monomer: 0.41 g, 87% / dimer: 0.41 g, 50%).

4.9.2 SYNTHESIS OF [$CrCl_3$(dppe)(py)] (19)

A Schlenk tube was charged with [$CrCl_3(thf)_3$] (0.31 g, 0.827 mmol) and thf (20 cm^3). Upon dissolution, dppe (0.33 g, 0.827 mmol) was added and the deep blue solution allowed to stir for a period of 10 minutes. At this point pyridine (0.06 cm^3, 0.827 mmol) was added, which afforded an immediate colour change to a blue-green solution. This reaction mixture was left to stir overnight at room temperature. Following the reduction of the final reaction solution, Et_2O (20 cm^3) addition allowed the formation a blue-green residue. After removal of the supernatant via syringe, the residue was washed with Et_2O (20 cm^3) and then allowed to dry under reduced pressure. The resulting precipitate **(19)** was present in good yield (0.41 g, 79%).

4.9.3 SYNTHESIS OF [$CrCl_3$(dppe)($pyNH_2$)] (20)

A Schlenk tube was charged with [$CrCl_3(thf)_3$] (0.27 g, 0.721 mmol) and thf (20 cm^3), followed 3 minutes later by the addition of dppe (0.28 g, 0.721 mmol) to yield a deep blue solution. Following a stirring period of ~10 minutes, $pyNH_2$ (0.06 g, 0.721 mmol) was added, yielding a lighter coloured supernatant coupled with a blue precipitate. To ensure completion the reaction mixture was stirred at room temperature overnight. The precipitate was then washed with Et_2O (20 cm^3) and dried under reduced pressure to afford a light blue precipitate **(20)** in good yield (0.33 g, 75%).

4.9.4 SYNTHESIS OF [$CrCl_3$(dppe)(pytb)] (21)

A Schlenk tube was charged with [$CrCl_3(thf)_3$] (0.30 g, 0.801 mmol) and thf (20 cm^3). Following the addition of dppe (0.32 g, 0.801 mmol), the ligand pytb (0.1 g, 0.801 mmol) was added to yield a blue-green reaction solution that was left to stir at room temperature overnight. The subsequent reduction of the solution, followed by the addition of Et_2O (20 cm^3), led to the formation of a blue-green precipitate. After removal of the supernatant via syringe, the residue was dried under reduced pressure for a period of 3 hours, which resulted in the isolation of a blue-green precipitate **(21)** in good yield (0.47 g, 85%).

4.9.5 SYNTHESIS OF [$CrCl_3$(dppe)(pyphenyl)] (22)

A Schlenk tube was charged with [$CrCl_3(thf)_3$] (0.27 g, 0.721 mmol) and thf (20 cm^3). Upon dissolution, dppe (0.28 g, 0.721 mmol) was added, followed 10 minutes later by pyphenyl (0.11 g, 0.721 mmol). The rich royal blue solution was stirred overnight at room temperature, followed by reduction and Et_2O (20 cm^3) addition to yield a blue-green precipitate. Removal of the supernatant via syringe and drying of the sample under reduced pressure for 3 hours allowed the isolation of a blue-green precipitate **(22)** in good yield (0.46 g, 90%).

Crystals of [Hpyphenyl][$CrCl_4$(dppe)] **(23)** were obtained from the rich royal blue reaction solution after a period of 3 weeks.

Chapter 5

Chromium(III) Bidentate Nitrogen / Phosphorus Mixed Ligand Chemistry

5.1 INTRODUCTION

Following the natural progression of the study of the novel complexes thus far, attention is now turned to the coordination of the bidentate ligands that encompass both phosphorus and nitrogen atoms within the same molecule. Such ligands possess the combination of donor atoms known to produce catalytically active species upon coordination to the $[CrCl_3(thf)_3]$ precursor [31]. One of the many intriguing properties of such ligands is that they combine both a soft phosphorus and a hard nitrogen donor atom. The fact that the phosphorus atom is a π–acceptor allows the stabilisation of a low oxidation state of a metal, while the σ–donor ability of the nitrogen is able to stabilise a higher oxidation state and the metal is therefore more susceptible to oxidative addition [116].

A variety of ligands were chosen and their coordination to the Cr(III) precursor allowed the formation and study of novel complexes with interesting properties. As well as steric and electronic differences, these ligands also differ in such a manner that they possess the ability to form chelate ring systems of various sizes once they have coordinated to the chromium centre via the respective P and N donor atoms.

A particularly intriguing aspect of the ligands with respect to chromium(III) chemistry was that to date no single crystal structures have been solved. A Cambridge Database search [117] was carried out in which chromium was selected first in any oxidation state and then specifically in the Cr^{3+} state. To encompass all possible structures, the bonds between the atoms, as well as the bridging atoms between the P and N donor atoms, were not specified. The structural frameworks that were searched are presented

in Figure 5.1. It is worth noting that regardless of the oxidation state of chromium, no complexes with PXN-type ligands have been solved to date.

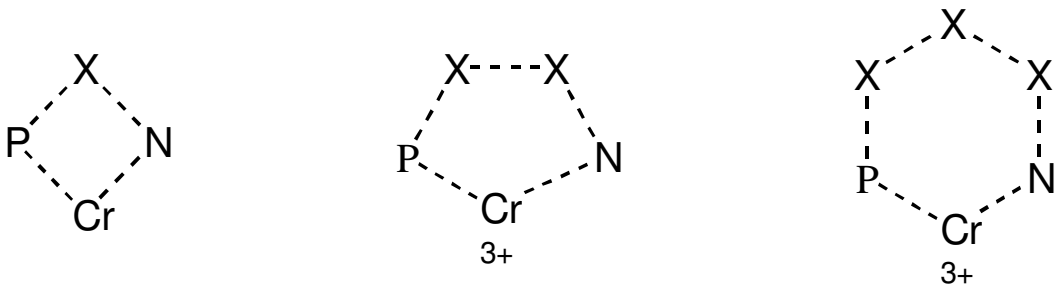

Cr	any oxidation state
Cr^{3+}	+3 oxidation state
X	any atom
------	any bond

Figure 5.1 Results of structural framework searches using Cambridge Database [118]

5.2 2-PYRIDYLDIPHENYLPHOSPHINE AND $[CrCl_3(thf)_3]$

The first ligand, 2–pyridyldiphenylphosphine (dpp), was a somewhat obvious choice as it combines the specific P and N ligand environments of the previous chapters, namely pyridine and diphenylphosphine. It was hoped that the presence of only one bridging atom between the P and N atoms would mimic the now highly regarded and catalytically active PNP ligand, which is known for its selectivity towards 1–octene catalysis. Of interest was whether a similar dimeric species formed upon coordination to $[CrCl_3(thf)_3]$, as isolated by Bollmann [34] in their PNP investigations, with a strained four-membered chelate ring could be replicated, with the electronic and steric differences between the two systems thus allowing for comparative studies.

It must be duly noted, however, that according to the literature this particular ligand has the potential to coordinate via a number of modes [116, 118]. It can act as a bridging ligand in both homo and hetero binuclear compounds, as a chelating ligand which forms a rigid, strained four–membered ring with the metal centre, as well as P and N monodentate ligands. In the latter two modes, due to the P atom being a weaker σ–donor and stronger π–acceptor, this ligand usually coordinates preferentially via the P atom.

5.2.1 SYNTHESIS

A series of reactions involving 2–pyridyldiphenylphosphine and $[CrCl_3(thf)_3]$ was undertaken. The addition of one molar equivalent of dpp to $[CrCl_3(thf)_3]$ dissolved in thf and stirred overnight at room temperature was expected to yield either a chelating-ring-type compound or coordination to Cr via either the P or N atom, with the literature findings making P donation more likely [116]. Somewhat surprisingly, no reaction took place. The reaction was then allowed to reflux for a number of days, but this too proved fruitless. thf was then replaced with DCM as solvent yet, somewhat frustratingly, this also failed to result in the ligand substitution reaction.

5.3 2-DIPHENYLPHOSPHINOETHYLAMINE AND $[CrCl_3(thf)_3]$

In the second of these heterodifunctional unsymmetrical bidentate ligands, 2-diphenylphosphinoethylamine (dppea), the number of bridging carbon atoms between the P and N donors increased to two. This allowed the formation of more stable five–membered chelate rings similar to those in the previous chapters, with the addition of the various substituted pyridines also being possible.

One notable difference from the first PN ligand of this study is that the electronic and steric properties of the nitrogen atom have been altered. Reasons include a willingness to incorporate variety into the systems, as well as the fact that it was a readily available ligand. However, the main reason is that in many respects this is a novel ligand. It is true that a number of researchers have previously incorporated this ligand into their respective systems, including europium-induced NMR studies [119], iridium-based asymmetrical C=O hydrogenation [120] and palladium-based Suzuki-Miyaura coupling [121]. However, to date no one has studied this ligand with respect to the chemistry surrounding tri- and tetramerisation catalysis. Furthermore, characterisation of any dppea complex thus far has been limited to elemental analysis and NMR spectroscopy, with the sum total of any IR studies being the mere mention of NH_2 and Pd–Cl vibrations. These were all good reasons for undertaking novel IR, Raman, computational and crystallographic studies.

5.3.1 SYNTHESIS

The addition of dppea to the $[CrCl_3(thf)_3]$ precursor led to the immediate formation of blue-green solutions. Unlike with the previous classes of compounds, one was acutely aware of carrying out these reactions on a smaller scale than usual due to the high cost of the ligand.

A direct result of the novel nature of this ligand was that no density information was provided by the manufacturer (Sigma Aldrich). This led to the required masses of the ligand for each experiment having to be determined with the aid of a weighing balance.

As in the dppe compounds, the fact that the coordination of this PN ligand appeared to be immediate (colour change), and that it yielded solutions and not immediate precipitates, removed any ambiguity as to when the pyridine ligands should be added. However, to ensure completion the ligand–$[CrCl_3(thf)_3]$ mixture was stirred at room temperature for about 10 minutes before the pyridines were added.

5.3.2 INFRARED AND RAMAN SPECTROSCOPY

All the IR discussions thus far have included comparative studies between the respective free ligand spectra and those observed upon coordination to the metal centre since many band shifts are indicative of coordination. To date the respective free ligand spectra have all been readily available from previously published literature. This, however, is not the case for dppea as its limited characterisation thus far has resulted in the absence of any IR and Raman data. This is thus the first detailed vibrational study carried out on this ligand system, both free and complexed.

As has been illustrated with the previous classes of compounds, the isolation of sufficient amounts of single-crystal material (for IR/Raman and X–ray structure determination) of at least one of the compounds within each grouping has aided the interpretation. However, although no crystal structure was isolated for this particular class of compounds, the IR assignments were not made with any less confidence than for the previous classes. The reason was that enough vibrational similarities to those compounds have already been analysed in this study, which thus allows comparisons to be drawn. In addition, there is ample literature data – perhaps not in terms of the

PN ligand directly, but with regard to the individual vibrations that make up this ligand, as well as the various pyridine ligands.

5.3.2.1 Region 3380–2867 cm^{-1}

This is a region of notable significance as the compounds possess a variety of characteristic N–H and C–H ligand vibrations.

Present in the IR spectra of all the compounds are the N–H vibrations associated with the dppea ligand. Their absence to a large extent in the corresponding Raman spectra is a result of a small amount of fluorescence that has affected some of the weaker vibrations in this region. The bands are therefore not definable from the broadness that is observed.

Deserving particular attention is the compound $[CrCl_3(dppea)(pyNH_2)]$ **(26)** as it possesses two different N–H environments. Although a degree of band superposition is expected, a closer examination shows the dominance of the $pyNH_2$ ligand environment as only two bands were observed – 3327 and 3198 cm^{-1}. This deduction resulted from comparative studies involving the $pyNH_2$-based compounds of the previous chapters $[CrCl_3(pyNH_2)_3]$, $[CrCl_3bipy(pyNH_2)]$ and $[CrCl_3(dppe)(pyNH_2)]$, as well as its dppea counterparts which included the free dppea ligand.

A representation of these observations is highlighted in Figure 5.2 which compares $[CrCl_3dppea(pyNH_2)]$ and $[CrCl_3(pyNH_2)_3]$.

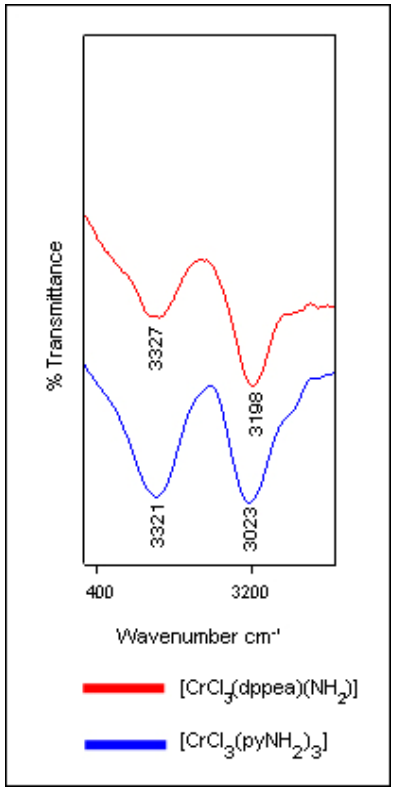

Figure 5.2 **IR spectra of N–H bands in [$CrCl_3$dppea($pyNH_2$)] (red) and [$CrCl_3(pyNH_2)_3$] (blue)**

The C–H environments observed include C–H ring vibrations. CH_2 modes that bridge the P and N donor atoms, and tertiary butyl C–H's associated with the para-substituted pyridine ligand, pytb. Also of interest are C–H vibrations indicative of thf as their presence or absence allows mechanistic and structural insights to be proposed.

Four vibrations are common to all the complexes. The first is observed as a strong vibration in both the IR and Raman spectra at ~3050 cm^{-1}. The fact that it is also present in [$CrCl_3$(dppea)(thf)] **(24)** suggests it is an unshifted C–H stretch associated with the phenyl rings of dppea. However, as the same unshifted vibration is observed in the literature of other metal–pyridine studies [73, 74, 92, 96, 97], one cannot assign with complete certainty.

The second vibration is at ~3003 cm^{-1} and corresponds to a combination mode that Benial [114] assigned to the similar ligand, dppe. Also common to dppe is the CH_2 asymmetrical stretch vibration at ~2962 cm^{-1} which has shifted from a free ligand

position of 2934 cm^{-1} that is indicative of coordination. The fourth band is observed as an unshifted free dppea vibration at ~2903 cm^{-1}. Although it is not present in the Cr-dppe compounds of this study, other metal–dppe studies in the literature assign it to a combination mode [113]. The problem of band superposition arises once again as the bands at ~2962 and ~2903 cm^{-1} are also indicative of the CH_3 stretching modes expected in the compound $[CrCl_3(dppea)(pytb)]$ **(27)**. Less ambiguous, however, are the other CH_3 symmetrical stretch vibrations that are observed at ~2928 cm^{-1} as a weak vibration (Raman spectrum only) and at 2868 cm^{-1} as a significantly stronger mode (both IR and Raman spectra). Both correlate with other metal–pytb vibrations, with the former at 2928 cm^{-1} having shifted from a free ligand position of 2920 cm^{-1} [92]. As all of the above vibrations are present in the IR and Raman spectra of $[CrCl_3(dppea)(pytb)]$, they have thus been chosen as representative spectra of what is observed in all the complexes (except for the tertiary butyl vibrations) and are presented in Figure 5.3.

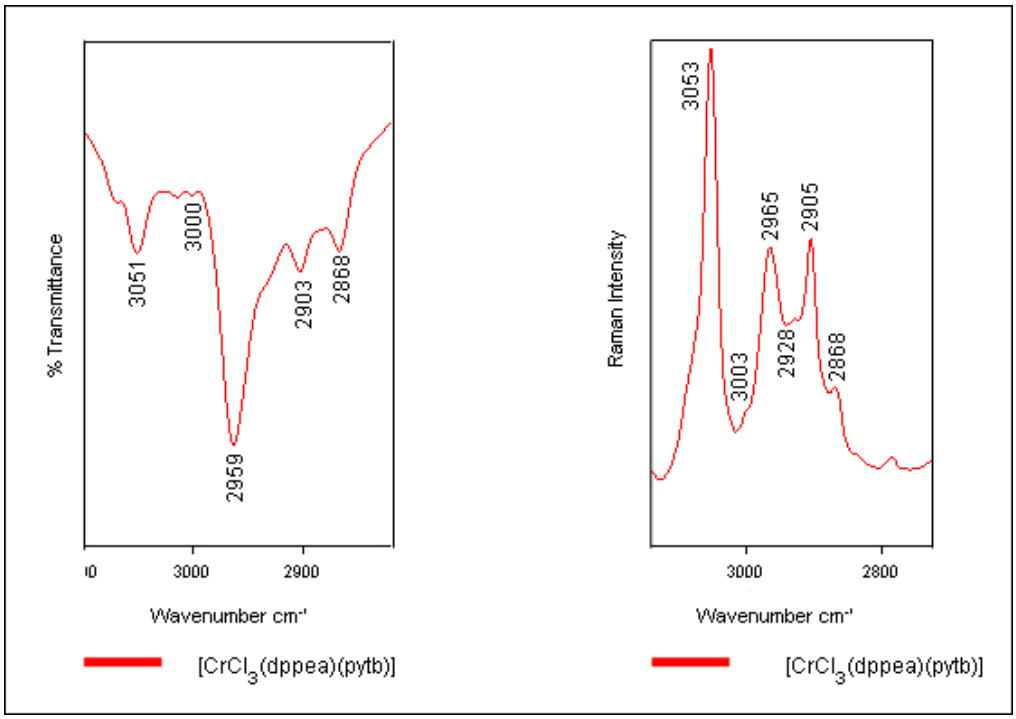

Figure 5.3 IR and Raman spectra of $[CrCl_3(dppea)(pytb)]$

Although not indicative of a specific substituent, the strong IR band at 3092 cm^{-1} is present only in $[CrCl_3(dppea)(pyNH_2)]$ and is associated with the C–H stretch vibration of $pyNH_2$, in correlation with the literature [96].

A further matter to be discussed with regard to this region is the presence or absence of thf C–H modes. They are expected on [$CrCl_3$(dppea)(thf)] only if direct ligand substitution has taken place. From comparative studies with [$CrCl_3$(bipy)(thf)] (which shows strong evidence of coordinated thf throughout its spectrum), it is clear that in this region there is no evidence of such vibrations. It is therefore duly noted that this is an early indication that this compound may in fact be a dimeric species.

Finally, as to the question of the presence of bands indicative of a pyridinium environment resulting from asymmetrical dimeric cleavage, the answer is negative with the absence of characteristic pyH vibrations at 2800 cm^{-1} [94], as well as the absence of those additional modes observed in the spectrum of [Hpyphenyl][$CrCl_4$(dppe)]. Although the literature-assigned pyH vibration at ~3200 cm^{-1} is observed in the spectra of all the compounds except for [$CrCl_3$(dppea)(thf)], it is deemed rather to be associated with N–H as throughout the rest of the spectra there is no further evidence of pyridinium formation.

5.3.2.2 Region 1652–1117 cm^{-1}

This is a region largely characteristic of C–H and C=C ring vibrations, with a relatively small degree of band superposition between the phenyl and pyridine environments observed. Also present in this region are bands associated with the para pyridine substituents, in particular CH_3 (tertiary butyl) and N–H (amino).

An expected phenomenon in line with similar vibrations in the dppe class is the distinct lack of shifting of the dppea ligand vibrations upon coordination, while the pyridine modes follow the same shift trends exhibited in all the previous chapters.

Furthermore, if any of the compounds have resulted from asymmetrical cleavage of a dimeric intermediate species, then characteristic pyridinium vibrations should be visible.

The majority of the dppea vibrations include C=C stretches, C–H twists and deformations, as well as ring breathing modes. Their assignments are relatively straightforward but special mention must be made of the two bands associated with C=C phenyl ring stretches at 1583 and 1568 cm^{-1} as the problematic overlap with

similar pyridine vibrations can to a certain extent be solved. Upon coordination to the chromium centre the former remains unshifted, while the latter shifts to a frequency of 1574 cm^{-1} [113]. These bands are visible in all the compounds in both the IR and Raman spectra, with that at 1583 cm^{-1} being noticeably stronger in the Raman. As has been observed in Chapter 4, both of these bands are observed in free pyridine. However, the opposite of the dppea band shifts is expected as upon coordination to the metal, 1583 cm^{-1} shifts to higher frequencies above 1600 cm^{-1}, while 1572 cm^{-1} remains unshifted [73, 74]. This is precisely what is seen in these novel compounds, which implies the coordination of the pyridine ligands to the metal. In terms of characterisation, the band at 1585 cm^{-1} is confidently assigned to a solely dppea ligand (C=C) [113], although ambiguity still surrounds the band at 1574 cm^{-1} (dppea/py). Table 5.1 presents the IR vibrations associated with coordinated pyridine while Figure 5.4 shows the IR and Raman spectra of $[CrCl_3(dppea)(py)]$ **(25)**.

Table 5.1 IR vibrations associated with coordinated pyridine

Free py	**$[CrCl_3(dppea)(py)]$ / cm^{-1}**	**$[CrCl_3(dppea)(pyNH_2)]$ / cm^{-1}**	**$[CrCl_3(dppea)(pytb)]$ / cm^{-1}**	**$[CrCl_3(dppea)(pyphenyl)]$ / cm^{-1}**
1599	1606	1618	1616	1615

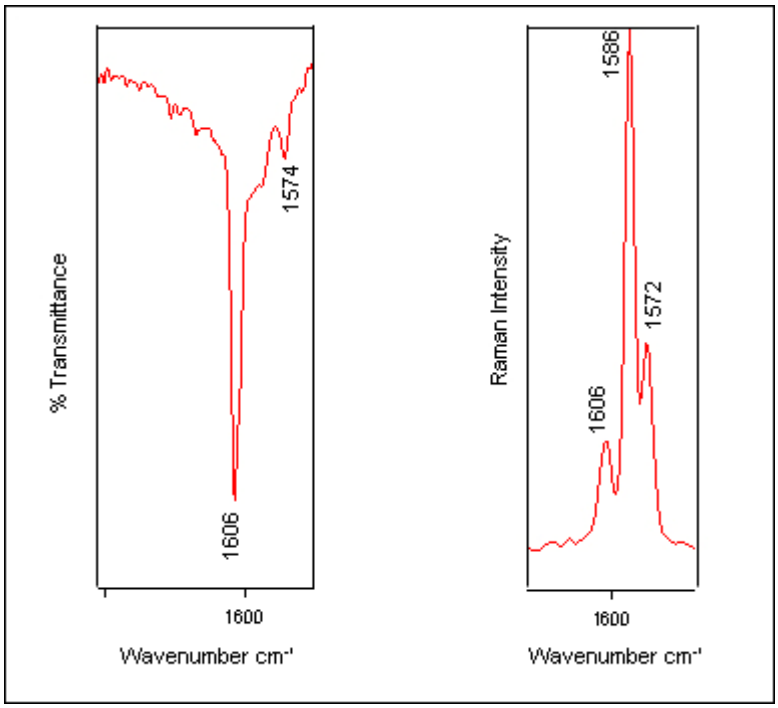

Figure 5.4 IR and Raman spectra of $[CrCl_3(dppea)(py)]$

Also worthy of mention is the fact that three vibrations are present in the IR and Raman spectra of all the compounds and notably absent in the dppe compounds. They are observed at 1461, 1379 and 1229 cm^{-1}. They are assumed to be dppea-specific vibrations which, in the light of the other types of vibration that surround them, are more than likely C–H modes.

The individual compounds are further discussed below, with the emphasis on the various pyridine-specific vibrations.

[$CrCl_3$(dppea)(py)]

The band observed as a strong IR vibration at 1447 cm^{-1} in [$CrCl_3$(dppea)(py)], and which is absent in the corresponding Raman spectrum, is a ring vibration that is characteristic of coordinated unsubstituted pyridine [73, 74]. It has shifted from a free ligand position of 1439 cm^{-1} and is unsurprisingly absent in the other compounds. Figure 5.5 compares [$CrCl_3$(dppea)(py)], [$CrCl_3$(dppea)(thf)] and free dppea to illustrate this additional band at 1447 cm^{-1}.

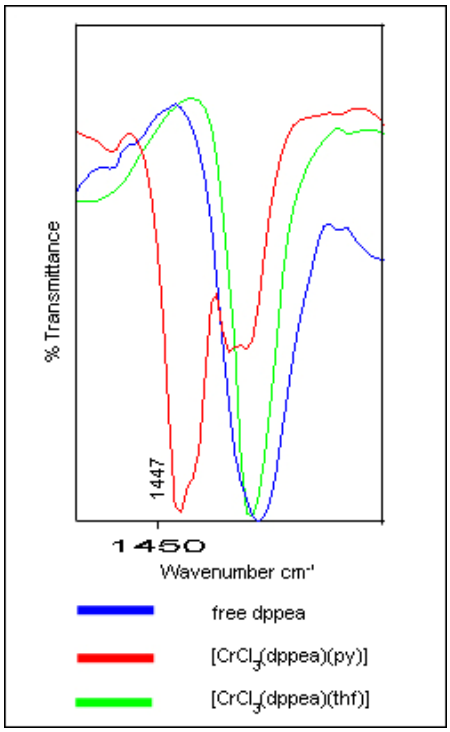

Figure 5.5 **Pyridine-specific vibration absent in [$CrCl_3$(dppea)(thf)] (green) and free dppea (blue)**

The only other vibration indicative of unsubstituted pyridine is that at 1221 cm^{-1} (C-H). However, it is not as specific as the previous band as it is also visible in $[CrCl_3(dppea)(pyNH_2)]$.

$[CrCl_3(dppea)(pyNH_2)]$

As well as the shared C–H vibration with $[CrCl_3(dppea)(py)]$, $[CrCl_3(dppea)(pyNH_2)]$ possesses two vibrations that are specific to the $pyNH_2$ ligand. They are both indicative of ring vibrations and, in direct correlation with aminopyridine literature [96], coordination is implied due to the free ligand shifts. Table 5.2 documents these shifts.

Table 5.2 IR vibrations associated with coordinated $pyNH_2$

Free $pyNH_2$ / cm^{-1}	$[CrCl_3(dppea)(pyNH_2)]$ / cm^{-1}	Shift / cm^{-1}
1508	1530	22
1333	1364	31

As one would expect, this compound also possesses bands that are characteristic of the amino substituent. These are present at 1652 cm^{-1} (N–H shifted from 1648 cm^{-1}) and 1281 cm^{-1} (C–NH_2 shifted from 1268 cm^{-1}) [96].

These IR vibrations are shown in Figure 5.6; the Raman spectrum is not shown as although the vibrations are present, the majority are weak and not as pronounced as their IR equivalents.

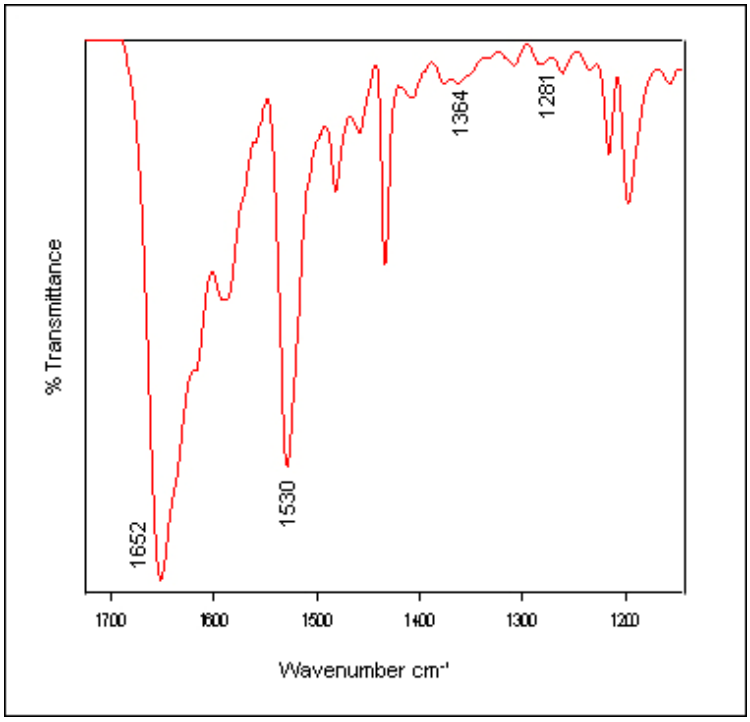

Figure 5.6 **IR spectrum of $pyNH_2$ vibrations observed in $[CrCl_3(dppea)(pyNH_2)]$**

$[CrCl_3(dppea)(pytb)]$

As well as the expected C–H and ring vibrations associated with the aromatic ring system, $[CrCl_3(dppea)(pytb)]$ also possesses a number of tertiary butyl-specific vibrations. These additional bands in the spectrum increase the likelihood of band superposition with the dppea ligand, which complicates their assignments.

The ring vibrations are observed at 1543 and 1501 cm^{-1}, with only the former being associated solely with pytb as the latter is also present in the spectrum of $[CrCl_3(dppea)(pyphenyl)]$ **(28)**. The latter has, however, shifted from a free ligand position of 1494 cm^{-1}, thus inferring coordination. Unfortunately, both the expected C–H specific vibrations are only tentatively assigned as they overlap with dppea vibrations. The same is true for the expected CH_3 asymmetrical and symmetrical deformations at 1462 (asym), 1368 (asym) and 1420 cm^{-1} (sym). The final weak band at 1201 cm^{-1} escaped ligand superposition and is confidently assigned to a C=C stretching mode that is specific to tb [92].

[$CrCl_3$(dppea)(pyphenyl)]

As was found in Chapter 4, it is rather difficult to differentiate between the phenyl rings attached to the phosphorus atoms and that which is substituted on the pyridine ring in the spectrum. Only the band at 1504 cm^{-1} is assignable and it is not pyphenyl-specific as it is also present in [$CrCl_3$(dppea)(pytb)].

Pyridinium vibrations

From a close inspection of all the spectra it is clear that there is a lack of evidence pertaining to pyridinium complex formation, a finding that is in agreement with the observations made in the region 3380 to 2861 cm^{-1}. Indeed, of the seven pyH vibrations that one would have expected to be present according to Mitchell [93], only three possibles are observed. These are 1480, 1158 and 1327 cm^{-1}. Apart from the fact that all three are present in the free dppea ligand and are assigned to C–H deformations, the band at 1327 cm^{-1} occurs at a weak intensity that is different from the strong intensity expected for pyH [94].

5.3.2.3 Region 1117–500 cm^{-1}

In direct correlation with the findings in the previous chapters, this particular region offers insights into the bond strengths and structural geometries that are, in addition to the fundamental assignments and coordinative shifts, common to all the regions.

Following the same trend as the previous region from 1652 to 1117 cm^{-1}, the majority of the bands that fall between these vibrational boundaries are ring and C–H vibrations. Overlap between the aromatic ligands is therefore unavoidable. However, a closer inspection of the nine vibrations that are common to the spectra of all the compounds shows that more than half are absent in the spectra of pyridine compounds, which signifies they are dppea phenyl ring-related vibrations. Furthermore, their lack of shifting upon coordination is not surprising, and indeed is expected, when comparisons are made with the findings in both the literature and the previous chapters of this thesis.

Bands absent in pyridine spectra:

- 1098 cm^{-1} ring breathing
- 999 cm^{-1} trigonal ring breathing
- 916 cm^{-1} C–H
- 508 cm^{-1} out of plane quadrant ring def

Bands present in pyridine spectra and thus indistinguishable:

- 1069 cm^{-1} in plane C–H def
- 739 cm^{-1} in plane out of phase C–H / ring
- 694 cm^{-1} CH_2 rock / ring

Figure 5.7 illustrates the presence and absence of these vibrations by comparing the IR spectra of the free ligands of pyridine, dppe and dppea.

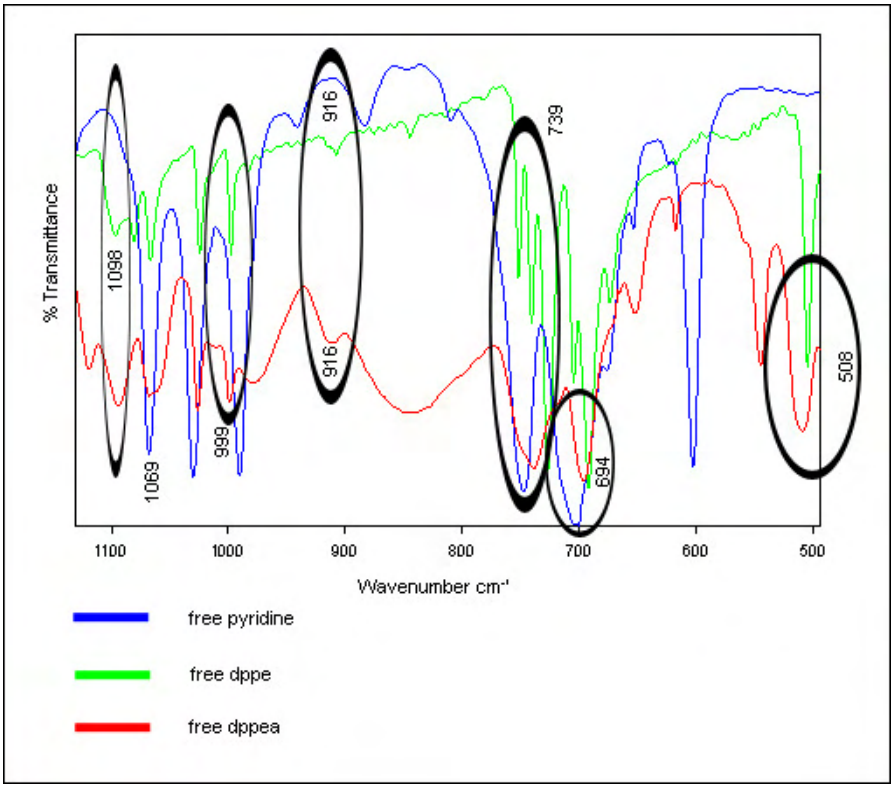

Figure 5.7 IR spectra of free pyridine (blue), free dppe (green) and free dppea (red)

An additional dppea-related vibration that deserves particular mention is that observed at ~666 cm^{-1} in all the compounds which, according to Benial [113], are indicative of a P–C stretching vibration resulting from the formation of the five-membered chelate

ring upon coordination. It is plausible that in these dppea compounds it has shifted from a free ligand position of 653 cm^{-1}.

In addition to these bands, there are a number of other vibrations that are present in the respective compounds which are indicative of the various pyridine derivatives. The shifts, and at times lack of shifts, relative to the free ligands compare very favourably with those in the literature and in previous chapters of this thesis.

The presence of strong IR bands at 757 and 641 cm^{-1} in $[CrCl_3(dppea)(py)]$ is indicative of coordinated pyridine ring vibrations that have shifted from free ligand values of 749 and 604 cm^{-1} respectively (Table 5.3 and Figure 5.8). The latter, in particular, has been common throughout the previously discussed unsubstituted pyridine compounds [73, 74].

Table 5.3 IR vibrations associated with coordinated pyridine

Free pyridine / cm^{-1}	$[CrCl_3(dppea)(py)]$ / cm^{-1}	Shift / cm^{-1}
749	757	8
604	641	37

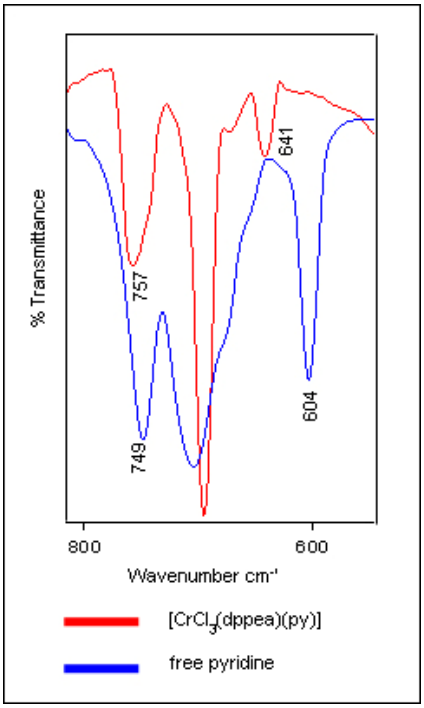

Figure 5.8 IR spectra comparison between $[CrCl_3(dppea)(py)]$ (red) and free pyridine (blue)

[$CrCl_3$(dppea)(pytb)] possesses two tertiary butyl-specific bands that are observed in the spectra as strong IR vibrations and weak Raman vibrations at 572 and 547 cm^{-1} (Table 5.4 and Figure 5.9). They are assigned to a skeletal stretch and a rocking mode respectively and according to the literature, a notable coordinative shift is observed only for the latter [92].

Table 5.4 IR vibrations associated with coordinated pytb

Free pytb / cm^{-1}	[$CrCl_3$(dppea)(pytb)] / cm^{-1}	Shift / cm^{-1}
569	572	3
534	547	13

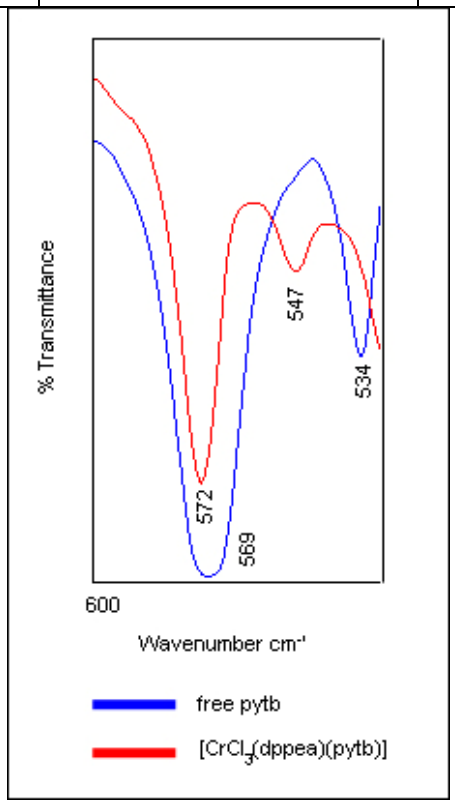

Figure 5.9 IR spectra comparison between [$CrCl_3$(dppea)(pytb)] (red) and free pytb (blue)

The compound [$CrCl_3$(dppea)(pyphenyl)] possesses ring vibrations that are indicative of the phenyl ring coordinated to the para-position of the pyridine (Table 5.5 and Figure 5.10) . Although one might expect these same bands in all the compounds due to the phenyl rings of the dppea ligand, this is not the case and their absence reinforces their py-phenyl assignments [97].

Table 5.5 IR vibrations associated with coordinated pyphenyl

Free pyphenyl / cm^{-1}	$[CrCl_3(dppea)(pyphenyl)]$ / cm^{-1}	Shift / cm^{-1}
762	765	3
561	561	0

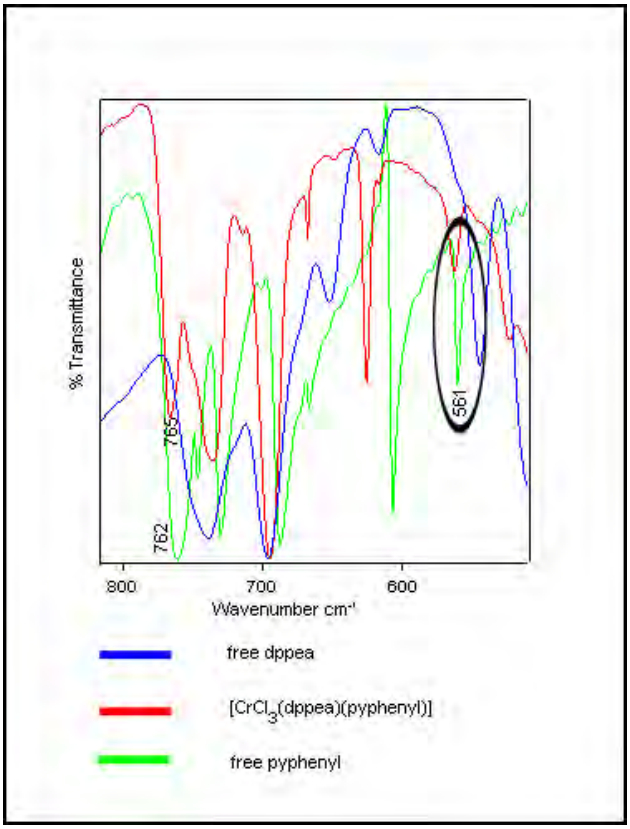

Figure 5.10 IR spectra comparison between $[CrCl_3(dppea)(pyphenyl)]$ (red) and free pyphenyl (green)

It should be noted that due to band superposition, it was not possible to assign any $pyNH_2$-specific vibrations with any degree of confidence.

Perhaps the most significant of all the bands indicating the coordination of pyridine and its substituted derivatives to the metal centre is that observed at 992 cm^{-1} in the free ligands, the reason being that the degrees of shifting are relative to the particular substituents [75].

The detailed theory surrounding these shifts has been documented in Chapter 2, yet what is more intriguing is that the shifts observed here are virtually identical to those of the previous chapters (Table 5.6 and Figure 5.11). This is significant in itself as the

coordination of some of these pyridine ligands was confirmed by crystal structure determinations.

Table 5.6 Shifting of the characteristic ring breathing vibration in [$CrCl_3$(dppea)(py)], [$CrCl_3$(dppea)($pyNH_2$)], [$CrCl_3$(dppea)(pytb)] and [$CrCl_3$(dppea)(pyphenyl)]

Pyridine / cm^{-1}	[$CrCl_3$(dppea)(py)] / cm^{-1}	Shift / cm^{-1}
990	1016	26

$pyNH_2$ / cm^{-1}	[$CrCl_3$(dppea)($pyNH_2$)] / cm^{-1}	Shift / cm^{-1}
991	1023	32

Pytb / cm^{-1}	[$CrCl_3$(dppea)(pytb)] / cm^{-1}	Shift / cm^{-1}
995	1027	32

Pyphenyl / cm^{-1}	[$CrCl_3$(dppea)(pyphenyl)] / cm^{-1}	Shift / cm^{-1}
1001	1012	11

The spectra of the complexes are given in Figure 5.23.

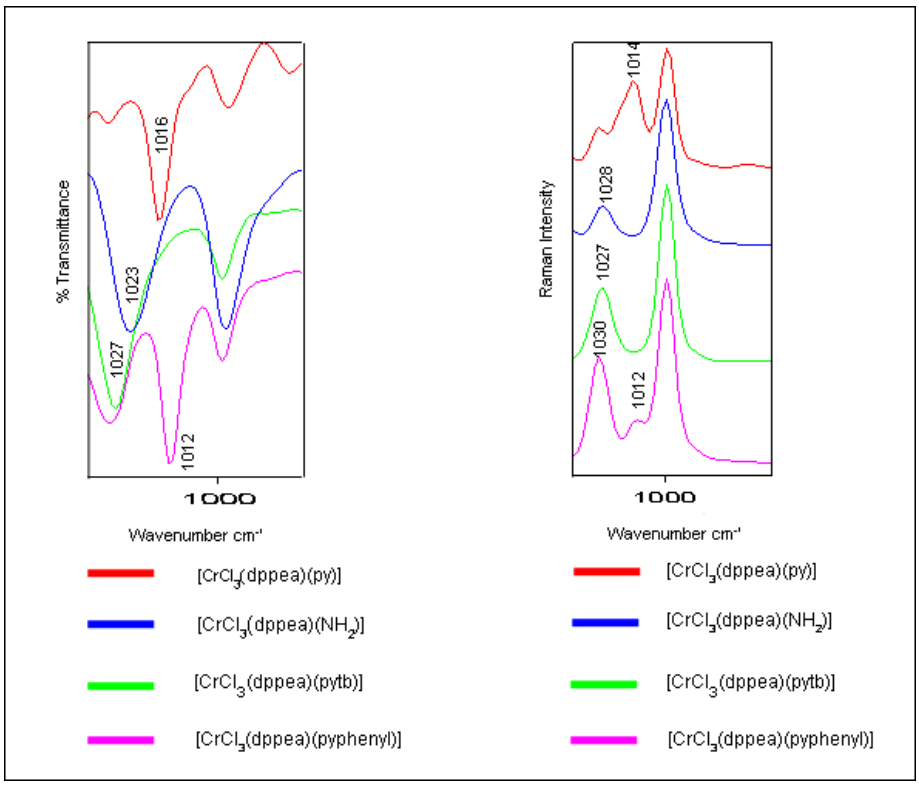

Figure 5.11 IR and Raman spectra of [$CrCl_3$(dppeay)(py)] (red), [$CrCl_3$(dppea)($pyNH_2$)] (blue), [$CrCl_3$(dppea)(pytb)] (green) and [$CrCl_3$(dppea)(pyphenyl)] (purple) showing shifting of the characteristic ring breathing vibration

Up to this point this regional IR study has focused mainly on the presence of bands, yet their absence can be just as informative. This is indeed the case for the [$CrCl_3$(dppea)(thf)] complex. The absence of the band at around 856 cm^{-1}, which is indicative of coordinated thf [77, 78], leads one to believe that this is in fact a dimeric species as opposed to the monomeric product resulting from direct ligand substitution. This is actually in accordance with the observation made regarding the region 3380 to 2861 cm^{-1} in which no thf C–H modes were found. When one then couples this finding with all the other analyses of these compounds, it is logical to assume that in each case the dimeric intermediate species is cleaved symmetrically by the addition of the amine ligand to yield monomeric products. This idea is supported by the absence of pyH vibrations which one would have expected if asymmetrical cleavage had taken place. As was the case in the previous region, those bands that could be related to pyH (1040 and 1000 cm^{-1}) are visible in the free dppea spectrum and are too intense to correlate with the literature expectations [93, 94].

5.3.2.4 Region 500–200 cm^{-1}

An FIR spectrum of the free dppea ligand was not obtainable due to the incompatibility between the need for instrumentation operated under vacuum and the liquid state of the sample since evaporation of sample would be problematic. This, however, did not hinder the analysis of the respective compounds' spectra to any great extent. Reasons include the fact that this is a region primarily synonymous with only metal–ligand vibrations, and that the spectrum of free dppe (which possesses many similar vibrational modes) was available. It should be noted that the MIR spectrum of the free dppea ligand extended to around 450 cm^{-1} so the higher frequency bands of the FIR spectra did permit free ligand comparisons.

The two vibrations at ~470 and ~450 cm^{-1} that are present in all the complexes are absent in the free ligand MIR spectrum. They are also notably absent in the free dppe spectrum. Thus, as assigned by Benial [113], it is logical to assume they are indicative of five–membered ring deformations that have resulted from P and N coordination to the chromium.

A final indication of unsubstituted pyridine coordination is also found in this region with the characteristic free pyridine vibration at 404 cm^{-1} having shifted to the expected coordination frequency of 438 cm^{-1} [73, 74].

The band at ~423 cm^{-1} in all the complexes is tentatively assigned to the Cr–P vibration, based on the similar assignment in the dppe class of compounds. While the corresponding dppe assignments could have been an out of plane quadrant ring deformation shifting from a value of 401 cm^{-1}, this is not the case for this dppea class as it possesses the band at 401 cm^{-1} in addition to that at 423 cm^{-1}.

With regard to bands associated with Cr–Cl vibrations, $[CrCl_3(dppea)(py)]$, $[CrCl_3(dppea)(pytb)]$ and $[CrCl_3(dppea)(pyphenyl)]$ appear to possess the three bands indicative of the monomeric *mer* arrangement [80]. This leaves $[CrCl_3(dppea)(thf)]$ and $[CrCl_3(dppea)(pyNH_2)]$ in which only two bands are observed. What this implies is one of two possibilities: either the *cis* arrangement or dimer formation. On the basis of all the previous evidence from the other regions for these two compounds, it is logical to suggest that $[CrCl_3(dppea)(pyNH_2)]$ adopts the *cis* orientation and that the $[CrCl_3(dppea)(thf)]$ is in fact a dimeric species.

Of the remaining bands, those at ~284 and 269 cm^{-1} are assumed to be dppea-related vibrations as they are absent in dppe as well as in pyridine and its derivatives.

The band at 243 cm^{-1} in all the complexes is assigned to the Cr–N vibration resulting from the coordinating dppea ligand. This is based on the absence of such a band in free dppe and indeed in its Cr-based complexes, but perhaps more important is that a similar assignment was made for the Cr–N (bipy) mode of the bipyridine compounds in Chapter 3 [79].

Unfortunately, the Cr–N (py) band at around 220 cm^{-1} was affected by band superposition as the Ph–P–Ph vibration of the dppea ligand occurs at around the same frequency. Unlike with the dppe compounds, differentiation between the two could not be made as even in the $[CrCl_3(dppea)(thf)]$ compound the band was split to give values of 218 and 214 cm^{-1}.

The IR and Raman spectra of $[CrCl_3(dppea)(py)]$ (Figure 5.12) were chosen as representative spectra of all the compounds to illustrate the vibrations that are common to all. In addition, this particular IR spectrum also shows the vibration associated with unsubstituted pyridine coordination at 438 cm^{-1}.

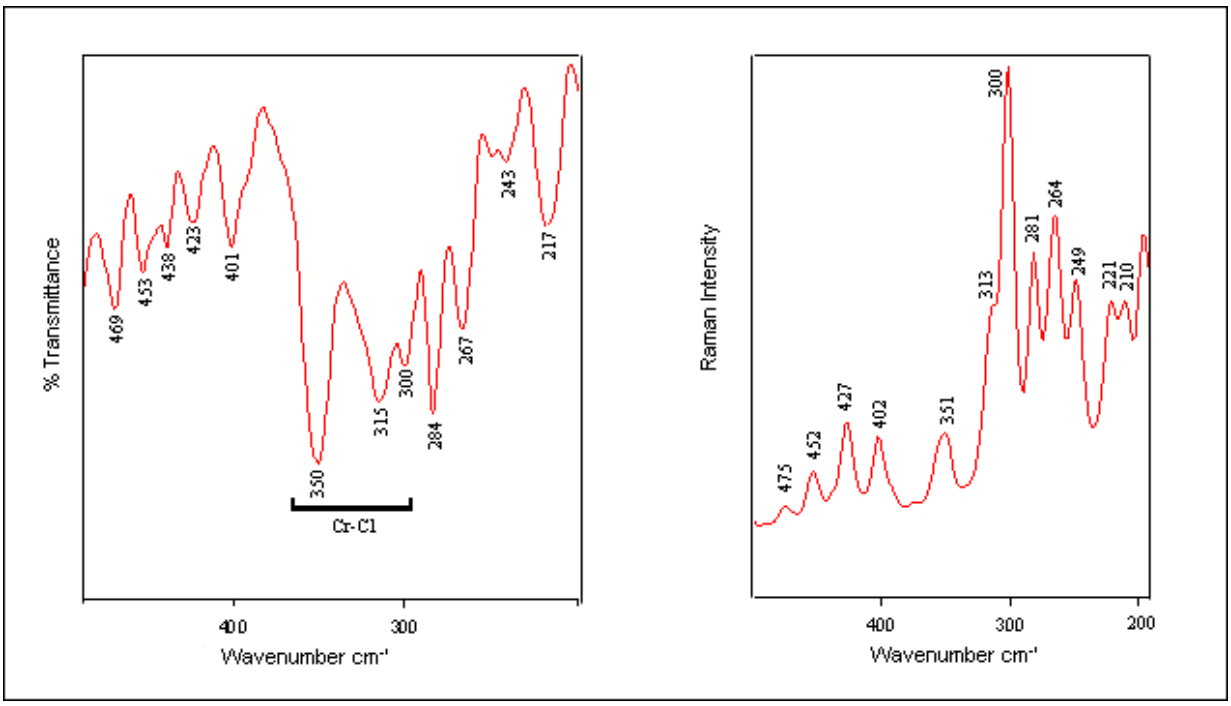

Figure 5.12 FIR and Raman spectra of $[CrCl_3(dppea)(py)]$

Table 5.7 **Vibrational assignments of [$CrCl_3$(dppea)(thf)] (24), [$CrCl_3$(dppea)(py)] (25), [$CrCl_3$(dppea)($pyNH_2$)] (26), [$CrCl_3$(dppea)(pytb)] (27) and [$CrCl_3$(dppea)(pyphenyl)] (28)**

24		25		26		27		28		
IR / cm^{-1}	**R / cm^{-1}**	**IR / cm^{-1}**	**R / cm^{-1}**	**IR / cm^{-1}**	**R / cm^{-1}**	**IR / cm^{-1}**	**R / cm^{-1}**	**IR / cm^{-1}**	**R / cm^{-1}**	**Assignment**
3365s	-	-	-	-	-	3372s,	-	3380s	-	ν (NH) asym (dppea) (76)
-	-	-	-	3327s	-	-	-	-	-	ν(NH) asym ($pyNH_2$) (76, 96)
3291s/sh	-	-	-	-	-	-	-	3298w	-	ν(NH) (dppea) sym (dppea) (76)
-	-	3242s	3243w	-	-	3236sh	-	-	-	ν(NH) (dppea)
-	-	3211s	3210w	3198s	-	3202w	-	3195sh	-	ν(NH) sym (76) / overtone / pyH
-	3169w	-	-	-	3168w	-	3168w	-	3166w	ν(NH) sym (76) / Overtone (113)
-	3140w	3134s	3135m	-	3139w	-	3141w	-	3138w	Overtone (113)
-	-	-	-	-	-	-	-	3114s	-	unassigned
-	-	-	-	3092s	3089sh	-	-	-	-	ν (CH) ($pyNH_2$) (96)
-	-	3075s	3071s	-	-	3067sh	-	3069sh	-	ν (CH) (dppe) (113) / (py) (73)
3051s	3054s	3050s	3056s	3047sh	3054s	3051s,	3053s	3047s	3055s	ν (CH) (dppe) (113) / (py) (73, 74, 92, 96, 97)
-	3001w	3002w	3002w	-	3003w	3000w	3003msh	-	3004w	Combination (113)
-	-	2974m	2987w	-	-	-	-	-	-	unassigned
2964s	2959m	2962sh, 2951w	2962m, 2945m	2965s	2957m	2959s	2965s	2959sh	2961m	ν (CH_2) asym (113)/ ν (CH_3) asym (92)
-	-	-	-	-	-	-	2928s, 2924s	-	-	ν (CH_3) sym (92)
2900ssh	2909m	-	2910m	-	2909m	2903s	-	2907sh	2911m	Combination (113)/ ν (CH_3) sym (92)
-	-	2889w	2888m	-	-	-	-	-	-	unassigned
-	-	-	-	-	-	2868s	2867m	-	-	ν (CH_3) sym (92)
-	-	-	-	1652s	1644m	-	-	-	-	δ (NH_2) (96)
-	-	1606s	1606m	1618s/sh	1616w	1616s	1618m	1615s	1615s	ν_{ring} (py) (73, 74, 92, 96,

24		25		26		27		28		
										97)
-	-	-	-	-	-	-	-	-	1598s	ν_{ring} (py) (97)
1583m	1585s	1588w	1586s	1590m	1585s	1585m/sh	1585s	1585m	1587s	ν_{ring} (dppe) (113)
1574m	1573msh	1572w	1572m	1572sh	1572msh	1570sh	1572msh	-	1573msh	ν_{ring} (dppe) (113) / ν_{ring} (py) (73, 74, 92, 96, 97)
-	-	-	-	-	-	1543w	1547vw	-	-	ν_{ring} (pytb) (92)
-	-	-	-	1530s	1533m	-	-	-	-	ν_{ring} (96)
-	-	-	-	-	-	1501m	1499vw	1504w	1513m	ν_{ring} (py) (92) (97)
1481s	1484w	1485m	1486w	1482m	1485vw	1482m	1483w	1482s	1485vw	CH def + ν(semicircle) (113)
1461m	1461w	1459w	1458w	1458w	1460vw	1462m	1463m	1462w	1462vw	Dppea vib / CH_3 asym def (92)
-	-	1447s	-	-	-	-	-	-	-	Py ring (73, 74)
1432s	1435w	1435s	1437w	1434m	1435w	1434s	1443m	1432s	1432vw	CH def + ν(semicircle) (113)
1410w	1411w	1408w	1407vw	1408w	1414w	1420s	1396vw	1416s	1416vw	Overtone(113) / CH_3 sym def (92) / ν_{ring} (97)
1379w	1379w	-	-	1376w	1375vw	1368m	1375vw	1378w	1379w	Dppea vib
-	-	-	-	1364w	-	-	-	-	-	ν_{ring} (96)
1329w	1331w	1338w	1335vw			1330w	1331w	1332w	1332w	δ (CH) def (113)
1309w	1308w	1316w	1316w	1308w	1308vw	1307w	1306w	1308w	1293s	CH_2 twist(113)
-	-	1278w	1281w	1281w	-	-	-	-	-	unassigned
1260w	1273w	-	-	1261w	1269w	1272m	1274w	1260w	-	unassigned
1229w	1232w	1237m	-	1233w		1230m	1232m	1226s	1229m	Dppea vib
	-	1221m	1220m	1215m	1217w	-	-	-	-	δ (CH) (73, 74, 92)
-	-	-	-	-	-	1201w	1201m	-	-	ν (CC) (pytb) (92)
1186w	1188m	1187w	1188m	1197m	1189w	1188w	1188m	1188w	1188m	δ (CH) def (113)
1158w	1159m	1155w	1157m	1157w	1159w	1157w	1156m	1156w	1159m	δ (CH) def (113)
1117m	-	1127m	1129w	1123w	1128vw	1125m	1126m	1118m	1130w	ν (P-C(C_6H_5)) (113)
1098s	1099m	1104m	1101m	1099	1098m	1096m	1097m	1100m	1099m	Ring breathing (113)
1069m	1071vw	1068s	1069w	1071vw	-	1067s	1069m	1070s	1072m	δ (CH) def (113)
1043m	-	1046m	1046m	1055w	1047m	-	-	-	-	ν_{ring} (63, 64, 113))

24		25		26		27		28		
1026m	1027s	1030w	1029s	-	-	-	-	1030m	1030s	δ (CH) def (113)
-	-	1016m	1014s	1023m	1028m	1027s	1027s	1012m	1012m	Ring breathing (pyX) (73-75, 92, 96, 97)
1000m	999s	998w	999s	999m	999s	998m	999s	998m	999s	Trigonal ring breathing (113)
957w	956vw	962m	962w	957w	-	958m	954w	956m	-	Dppea vib
916w	920w	923w	920w	919w	924vw	925w	929m	920m	919w	Dppea vib
-	-	-	-	-	848s	843m	844w	837m	843w	ν_{ring} breathing (py) (92) / X-sens (96) / δ_{ring} (97)
819sh/m	824vw	823m	822w	827m	-	831s	-	-	-	In phase γ(CH) def (92, 96, 113)
803m	795vw	-	-	807sh/m	-	-	-	-	-	unassigned
-	-	784s	-	-	-	-	-	-	-	Py vib
-	-	-	-	-	-	-	-	765s	762m	$\delta_{ring} + \nu_{ring}$ (97)
-	-	757s	756w	-	-	-	-	-	-	γ (CH) (73, 74)
739s	741w	746s	-	743s	750vw	739s	732m	735s	734vw	In phase γ(CH) (dppe) (113)
694s	685m	695s	693w	697s	684w	697s	684m	693s	684m	CH_2 rock (113)
-	673sh	668w	666m	-	667w	668w	668m	667w	667m	ν (PC) (5 membered ring) (113)
-	-	-	650m	-	-	-	-	-	-	δ_{ring} (73, 74)
-	-	641m	641vw	-	-	-	-	-	-	ν_{ring} (py) (73, 74)
-	617m	617w	617m	-	617m	616w	617m	625s	618m	δ (quadrant ring) def (dppea) (113)
-	-	-	-	-	-	572s	570w	-	-	Skeletal str (tb) (92)
-	-	-	-	-	-	-	-	561m	563w	δ_{ring} (97)
-	-	-	-	-	-	547m	549w	-	-	Rock (tb) (92)
522s	523w	522s	524w	524s	527m	524m	526w	523s	524w	δ (quadrant ring) def (dppea) (113)
508s	506vw	505s	506vw	500s	505w	509s	505w	505s	504vw	γ (quadrant ring) def (113)
471w	471w	469w	475w	473w	471vw	474w	465w	471w	470vw	5 membered ring def
449w	446w	453w	452w	453w	446vw	449w	-	448w	446w	5 membered ring def

24		**25**		**26**		**27**		**28**		
-	-	438w	-	-		-	-	-	-	γ_{ring} (py)(73, 74)
421w	419w	423w	427w	421w	415m	427w	432w	422w	431vw	Cr-P ? (114, 115)
400w	397w	401w	402w	402w	-	400w	396w	397w	405m	γ (quadrant ring) str (113)
339w	357w	350w	351w	350w	350w	373w	358br	360w	362w	Cr-Cl (80)
313w	314w	315w	313msh	316w	313sh	350w	336br	336w	-	Cr-Cl (80)
-	-	300w	300s	-	-	319w	320m	315w	319m	Cr-Cl (80)
287w	293m	284w	281m	287w	296m	295w	297m	283w	293m	Dppea specific
269w	260m	267w	264m	269w	275msh	273w	271m	271w	263m	Dppea specific
243w	br (fluor)	242w	249m	243w	254m	243w	258m	240w	-	Cr-N (NH_2) (79)
218w	br (fluor)	217w	221m	218w	-	220w	-	221w	-	Ph-P-Ph (114) / Cr-N (41, 80, 81)
214w	br (fluor)	-	210m	214w	208msh	215w	207m	-	-	Ph-P-Ph (114) / Cr-N (py) (41, 80, 81)

ν = stretching, δ = in-plane bending, γ = out-of-plane bending, def = deformation, asym = asymmetrical, sym = symmetrical vs = very strong, s = strong, m= medium, w = weak, vw = very weak, br (fluor) = broad due to fluorescence

5.3.3 COMPUTATIONAL STUDY

In keeping with the selection of [$CrCl_3$(dppe)(pytb)] in Chapter 4, the analogous dppea complex, [$CrCl_3$(dppea)(pytb)], was also selected as being representative of the other complexes in its class.

As has been the case throughout this study, excellent correlation between the experimental and calculated spectra, which are presented in Figures 5.13 and 5.14, is again observed. However, unlike [$CrCl_3$(dppe)(pytb)], and in common with all the other computationally studied complexes, no FIR spectrum is shown owing to the problems associated with solid-state effects that limit the number of distinct Cr–Cl modes observed in the actual spectrum.

A selection of important vibrations, which through their experimental-calculated correlations confirm previous experimental indications of coordination, is presented in Tables 5.8 and 5.9.

Also to be found in the table is an example of vibrations that, on the basis of a combination of comparative and literature studies, have been loosely assigned as dppea-specific vibrations. However, the successful correlation of the calculated results has allowed these bands to be assigned to specific vibrations as in the case of the mode at ~950 cm^{-1} which is a CH_2–NH_2 vibration.

While the Cr–P vibration is confirmed at a slightly higher frequency than its dppe counterpart, the remaining metal ligand vibrations are for the most part difficult to correlate due to the mixing modes.

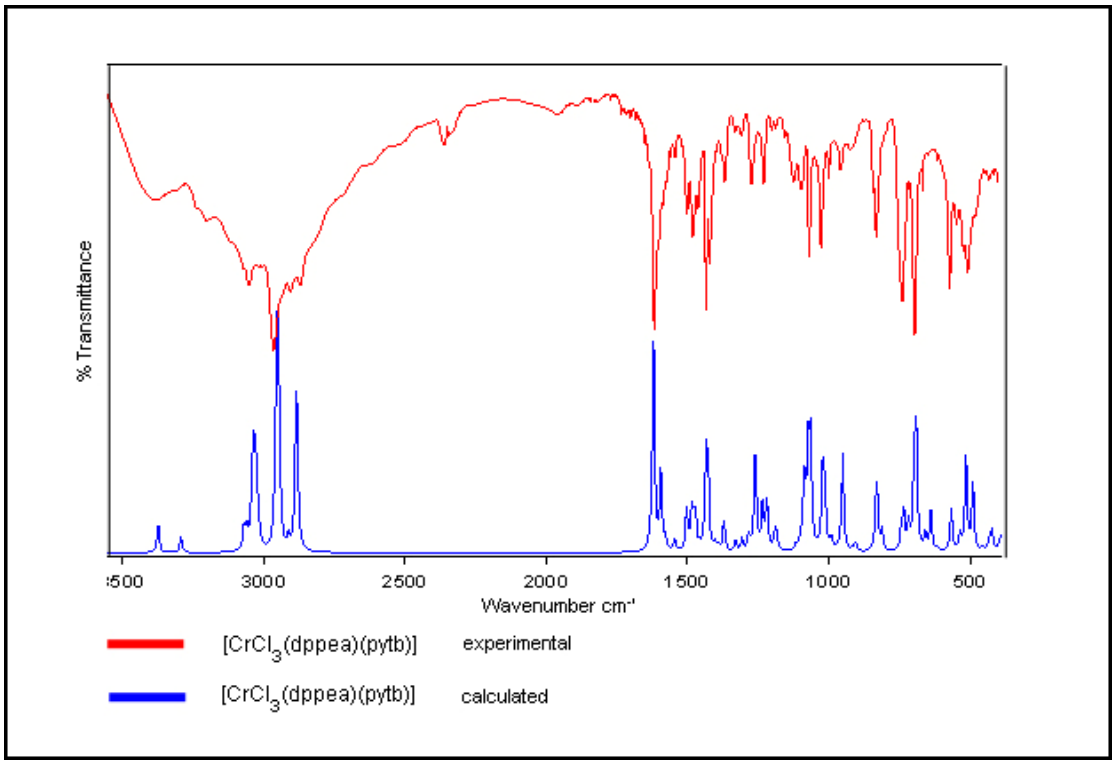

Figure 5.13 **Experimental (red) and calculated (blue) MIR spectra of [$CrCl_3$(dppea)(pytb)]**

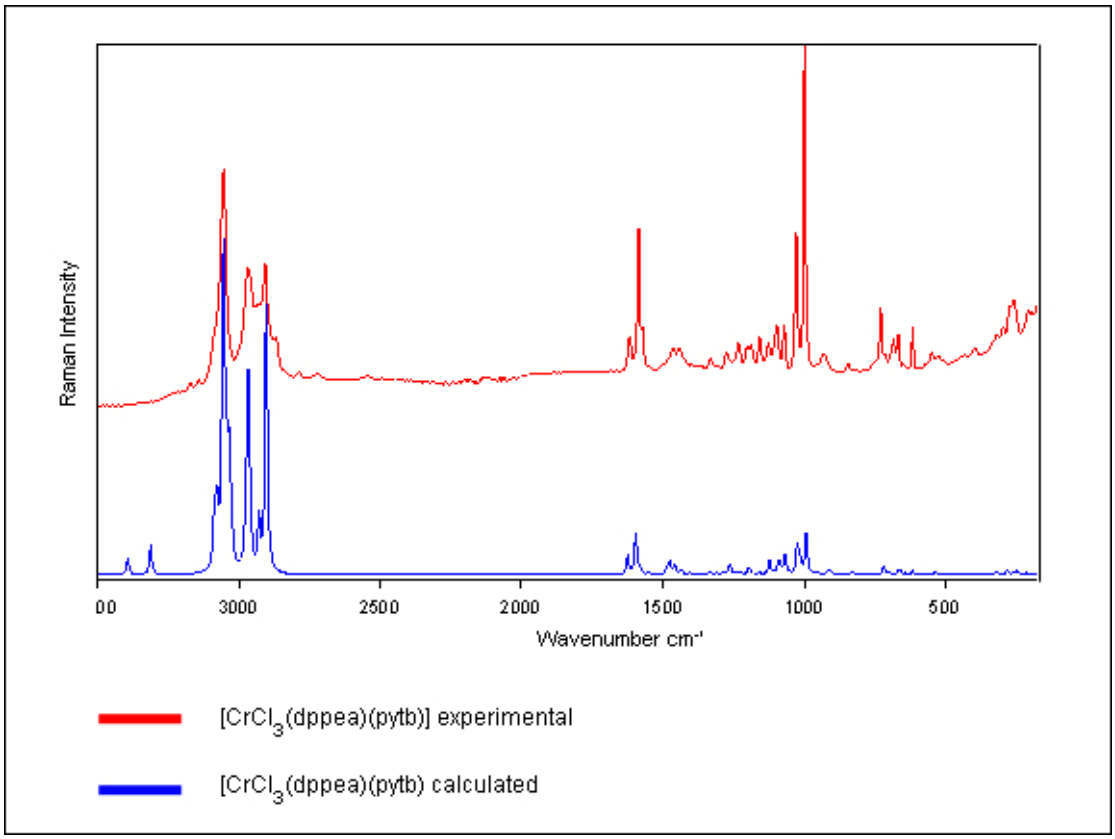

Figure 5.14 **Experimental (red) and calculated (blue) Raman spectra of [$CrCl_3$(dppea)(pytb)]**

Table 5.8 **Selected experimental and calculated IR and Raman band assignments for [$CrCl_3$(dppea)(pytb)]**

[$CrCl_3$(dppea)(pytb)] IR / cm^{-1}		[$CrCl_3$(dppea)(pytb)] Raman / cm^{-1}		Assignment	
Experimental	**Calculated**	**Experimental**	**Calculated**	**Experimental**	**Calculated**
3372	3371	-	3391	ν (NH) asym	ν (NH) asym
1616	1618	1618	1624	ν_{ring} (py)	ν_{ring} (py)
1585	1592	1585	1596	ν_{ring} (dppea)	ν_{ring} (dppea)
1027	1018	1027	1021	Ring breathing (pytb)	Ring breathing (pytb)
998	993	999	993	Trigonal ring breathing (dppea)	Trigonal ring breathing (dppea)
958	952	954	953	dppea specific	CH_2–NH_2 (dppea)
668	674	668	659	ν (PC) (5-membered ring)	ν (PC) (5- membered ring)
427	432	432	433	Cr–P	Cr–P
-	422		423	-	Cr–N (NH_2) + P-C(C_6H_5)
373, 350, 319	380, 369, 336, 315	358, 336, 320	380, 370, 337, 315	Cr–Cl	Cr–Cl + Cr–N (NH_2)/ pytb rock
-	259		260	-	Cr–N (py) + CH_3 twist
243	243	258	244	Cr–N (NH_2)	Cr–Cl + Cr–N (NH_2)
220, 215	-	207	-	Ph–P–Ph / Cr–N (py)	-

Table 5.9 Scaling factors determined for [$CrCl_3$(dppea)(pytb)]

Region / cm^{-1}	IR	Raman
0 – 1860	0.975824	0.978314
2827 – 3745	0.951054	0.956602

The HOMO and LUMO orbitals that were generated by computational means (Figure 5.15) illustrate that while attack by electrophiles is likely to take place around the chlorine atoms only, nucleophilic attack is possible at the trans chlorine atoms as well as at the pyrindine and phenyl rings that are trans to each other.

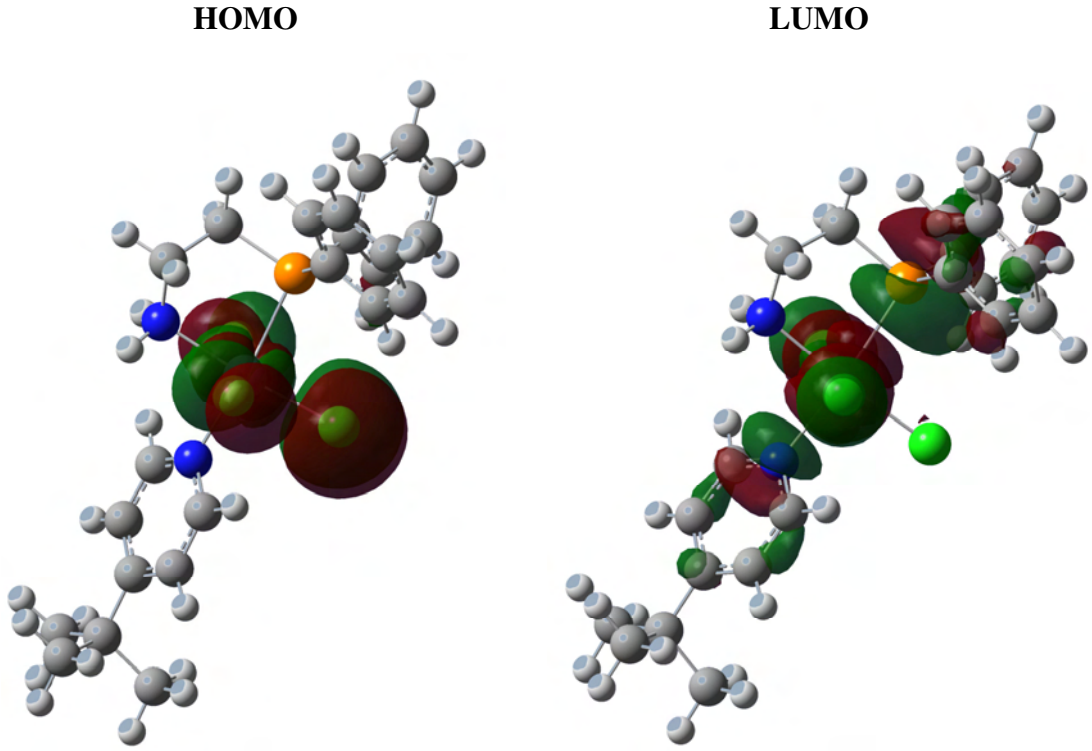

Figure 5.15 HOMO and LUMO orbitals of [$CrCl_3$(dppea)(pytb)]]

5.3.4 MASS SPECTROMETRY

[$CrCl_3$(dppea)(pytb)] and [$CrCl_3$(dppea)(pyphenyl)] were selected for FAB-MS analysis. These structures were confirmed by the isotopic distribution pattern $[M–Cl]^+$ (m/z = 486), (m/z = 506) which was observed in the respective spectra and shown in Figures 5.16 and 5.17. Both patterns corresponded well with the theoretically generated equivalents.

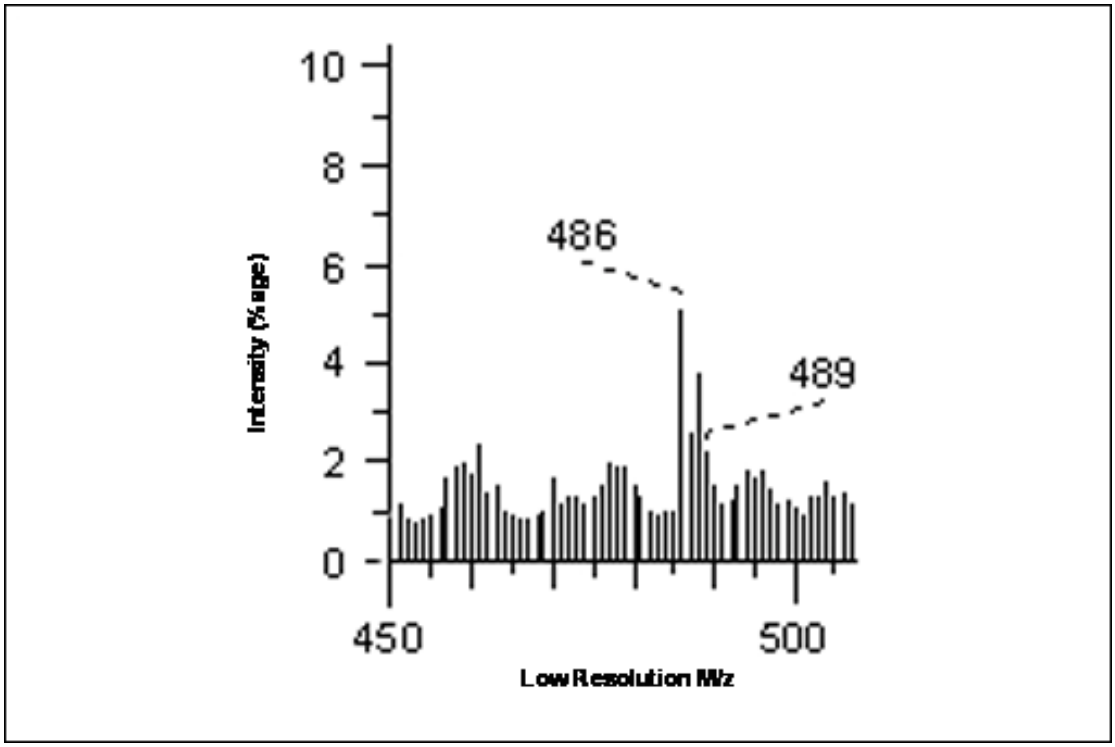

Figure 5.16 **FAB-MS spectrum of [$CrCl_3$(dppea)(pytb)]**

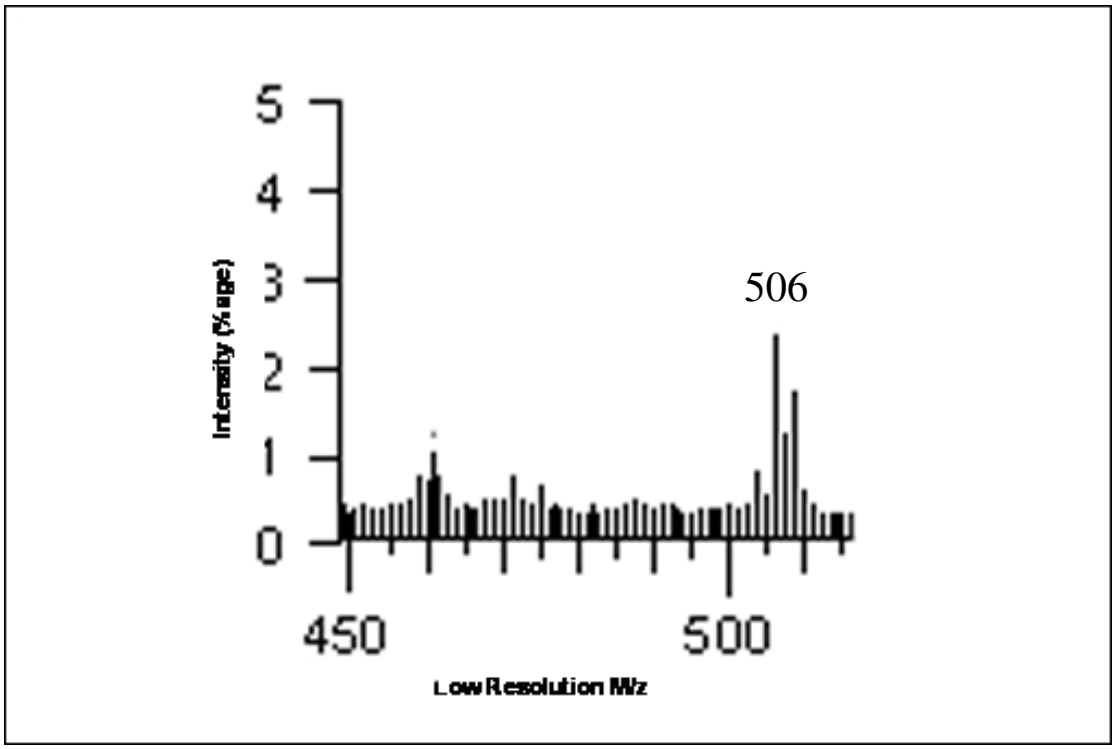

Figure 5.17 **FAB-MS spectrum of [$CrCl_3$(dppea)(pyphenyl)]**

5.4 EXPERIMENTAL

5.4.1 SYNTHESIS OF [$CrCl_3$(dppea)(thf)] / [Cr(dppea)Cl_2(μ-Cl)]$_2$ (24)

A Schlenk tube was charged with [$CrCl_3(thf)_3$] (0.1 g, 0.267 mmol) and thf (20 cm^3). The addition of dppea (0.06 g, 0.267 mmol) resulted in an immediate colour change with the reaction mixture being observed as a blue-green solution. To ensure completion it was allowed to stir overnight at room temperature. Following the reduction of volume and the addition of Et_2O (20 cm^3), a blue-green precipitate was visible. Removal of the supernatant via syringe and addition of Et_2O (3 x 20 cm^3) was then followed by drying of the residue under reduced pressure. After a period of 3 hours a blue-green precipitate **(24)** was isolated in good yield (monomer: 0.1 g, 81% / dimer: 0.1 g, 48%)

5.4.2 SYNTHESIS OF [$CrCl_3$(dppea)(py)] (25)

Following the charging of a Schlenk tube with [$CrCl_3(thf)_3$] (0.1 g, 0.267 mmol) and thf (20 cm^3), dppea was added, followed 10 minutes later by pyridine. The resulting blue-green solution was left to stir at room temperature overnight. The volume was then reduced and upon addition of Et_2O (20 cm^3) a blue precipitate was observed. The supernatant was removed via syringe and the residue washed with Et_2O (3 x 20 cm^3) and dried under reduced pressure to result in a light blue precipitate **(25)** isolated in good yield (0.9 g, 73%)

5.4.3 SYNTHESIS OF [$CrCl_3$(dppea)($pyNH_2$)] (26)

A Schlenk tube was charged with [$CrCl_3(thf)_3$] (0.1 g, 0.267 mmol) and thf (20 cm^3). The blue-green solution resulting from the subsequent addition of dppea turned more of a light blue colour with the formation of a precipitate once $pyNH_2$ had been added after 10 minutes. After it had been stirred at room temperature overnight to ensure completion of the reaction, the supernatant was removed via syringe and the light blue residue washed with Et_2O (3 x 20 cm^3), followed by drying under reduced pressure. The result was a light blue precipitate **(26)** in good yield (0.11 g, 85%).

5.4.4 SYNTHESIS OF [$CrCl_3$(dppea)(pytb)] (27)

A Schlenk tube was charged with [$CrCl_3(thf)_3$] (0.1 g, 0.267 mmol) and thf (20 cm^3). Dppea was then added and the blue-green solution stirred at room temperature for 10 minutes. Following the addition of pytb, the solution remained blue-green and it was allowed to stir overnight at room temperature. Reduction of volume and addition of Et_2O (20 cm^3) resulted in a blue-green precipitate. Removal of the supernatant via syringe and addition of Et_2O (3 x 20 cm^3) allowed the residue to be dried under reduced pressure, resulting in the isolation of a blue-green precipitate **(27)** in good yield (0.11 g, 78%).

5.4.5 SYNTHESIS OF [$CrCl_3$(dppea)(pyphenyl)] (28)

Upon dissolution of [$CrCl_3(thf)_3$] (0.1 g, 0.267 mmol) in thf (20 cm^3) within a Schlenk tube, dppea was added, followed 10 minutes later by pyphenyl. To ensure completion of the reaction, the blue-green solution was stirred at room temperature overnight. The volume was then reduced and Et_2O (20 cm^3) added. The precipitate that resulted was washed with Et_2O (3 x 20 cm^3) and dried under reduced pressure for 3 hours. A blue-green precipitate **(28)** was isolated in good yield (0.12 g, 83%).

Chapter 6

Future work and Conclusions

6.1 FUTURE WORK

Future work could be directed towards the synthesis, isolation and investigation of the C–C coupling reactions of dimeric (chloro-bridged) Cr(III) complexes and cation Cr(III) complexes with labile ligands. Such studies would aid the greater understanding of oligomerisation reactions with Cr(III) catalysts.

From the wide variety of ligands that could be employed, it may be of interest to consider those that would lead to bimetallic complexes upon coordination to $[CrCl_3(thf)_3]$. An example of such a ligand is ((RP)–1–[(1S)–1–aminoethyl)–2–(diphenylphosphino)ferrocene) which would lead to a Fe–Cr system. This would also be a direct progression from the ligands of this study with respect to the Ph_2P and NH_2 donor environments, with the added interest of incorporating a six–membered chelate ring.

From an extensive literature search only one reference was found to this specific ligand, with the focus on the Ru(II)-catalysed asymmetrical hydrogenation of ketones [122] (Figure 6.1). This therefore opens the door to structural and spectroscopic studies similar to those carried out in this study, as well as to investigations into catalytic activity. The literature also revealed that although novel, the formation of the six-membered chelate ring with chromium is a plausible expectation as such systems have been solved crystallographically with similar ligands and metals, including tungsten, palladium and ruthenium [123, 124, 125].

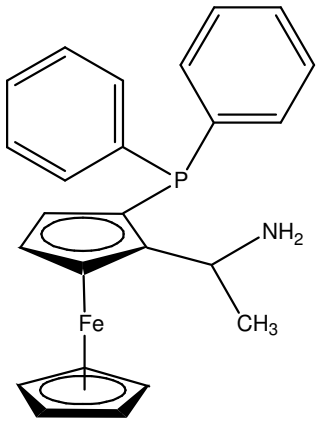

Figure 6.1 **((RP)–1–[(1S)–1–aminoethyl)–2–(diphenylphosphino)ferrocene)**

6.2 CONCLUSION

This project succeeded in fulfilling its core objective which was to enhance the fundamental knowledge of Cr(III) compounds via detailed structural and spectroscopic techniques. It is, however, noted that further analytical techniques must be applied before the structures are defined with absolute certainty. What proved to be particularly interesting was that all the techniques used complemented each other extremely well and thus the findings of an individual technique could assist or add weight to the findings of another.

IR and Raman spectroscopy proved to be extremely useful as analytical tools for providing evidence of ligand coordination. Furthermore, they offered insights into both the molecular geometry of the compounds and the synthetic routes via which the products were formed. Ligand coordination was based on vibrational shifts relative to the respective free ligands and these shifts correlated very well indeed with similar vibrations found in the literature. Additional evidence of ligand coordination was found in the FIR region where metal–ligand vibrations were observed. Once again the previous literature assisted in these assignments. The FIR region also led to deductions regarding the molecular geometry of the compounds, whereby the number of Cr–Cl vibrations related to either the *cis* or *mer* arrangements. Synthetic route deductions were based principally on the crystallographic findings of this study. However, by studying the IR and Raman spectra of these structures it was possible to add weight to these pathway proposals even when structures were not available.

A direct complement to the IR and Raman spectroscopic analysis was the generation of the corresponding theoretical spectra by means of DFT calculations. This proved to be highly successful as excellent correlations between the experimental and calculated spectra were observed. The generation of HOMO and LUMO orbitals of the compounds by computational means also proved successful as sites of potential electrophilic and nucleophilic attack were determined. Of interest was that while electrophilic attack consistently occurred at the *mer* arranged chlorine atoms, regardless of the ligand environment, sites of nucleophilic attack were determined by geometry-related factors. These were particularly prevalent in the monodentate pyridine complexes of Chapter 2, in which nucleophilic attack was expected only at the pyridine ring system *trans* to a chlorine atom. A further conclusion drawn from the generation of these frontier orbitals was that the sterically and electronically different substituted pyridine ligands did not play a role in altering the region of nucleophilic attack.

The use of NMR spectroscopy to study paramagnetic systems is ordinarily avoided. However, this study proved that information associated with ligand coordination and the determination of reaction times can be obtained from such a practice. Regardless of the inability to conduct kinetic studies, for reasons discussed in this study, NMR spectroscopy was successfully incorporated into this study of paramagnetic systems.

The number of single crystal structures that were determined was a considerable achievement considering that the isolated precipitates were so highly insoluble. All eight structures provided novel insights with regard to bond lengths, bond angles, packing arrangements, etc. They were also instrumental in the proposal of synthetic routes to compound formation as it was clear that dimeric intermediates existed which offered alternative pathways to the initially expected route of direct ligand substitution.

The results of the FAB-MS provided additional confirmation of compound identities by way of identifiable fragmentation patterns. In addition the presence of chlorine atoms in the compounds allowed for the successful comparison of isotopic distribution patterns between the experimental results and those generated theoretically.

With regard the proposed synthetic pathways to product formation discussed throughout the thesis, one is able to conclude that based on the information available in literature as well as the vibrational and structural data presented in this study, product formation via dimerisation is plausible.

REFERENCES

1. G. P. Chiusoli, P. Maitlis (Eds). Metal-catalysis in Industrial Organic Processes. RSC Publishing (2006).
2. C. Masters. Homogeneous Transition-metal Catalysis – A Gentle Art. Chapman and Hall (1981).
3. J. M. Thomas, K. I. Zamaraev (Eds). Perspectives in Catalysis. Blackwell Scientific (1992).
4. J. T. Dixon, M. J. Green, F. M. Hess, D. H. Morgan, J. Organomet. Chem. 689 (2004) 3641.
5. M. J. Overett, K. Blann, A. Bollmann, J. T. Dixon, D. Haasbroek, E. Killian, H. Maumela, D. S. McGuinness, D. H. Morgan, J. Am. Chem. Soc. 127 (2005) 10723.
6. W. K. Reagan, Symp. Prepr. Conv. Light Olefins, Div. Pet. Chem., Am. Chem. Soc. 34 (1989) 583.
7. W. K. Reagan, European Patent 0417477 (Phillips Petroleum Company) March 20 (1991).
8. R. M. Manyik, W. E. Walker, T. P. Wilson, US 3300458 (Union Carbide Corporation, January 24 (1967).
9. R. M. Manyik, W. E. Walker, T. P. Wilson, J. Catal. 47 (1977) 197.
10. E. Derat, P. Bouquant, J. Bertus, S. Szymoniak, J. Humbel, J. Organomet. Chem. 664 (2002) 268.
11. M. Wang, Y. Shen, M. Qian, R. Li, J. He, J. Organomet. Chem. 599 (2000) 143.
12. R. Santi, A. M. Romano, M. Grande, A. Sommazzi, F. Masi, A. Proto, WO 01/68572 (Enichem S. P. A) 20 September (2001).
13. S. Murtuza, S. B. Harkins, G. S. Long, A. Sen, J. Am. Chem. Soc. 122 (2000) 1867.
14. C. Andes, S. B. Harkins, S. Murtuza, K. Oyler, A. Sen, J. Am. Chem. Soc. 123 (2001) 7423.
15. C. Pellecchia, D. Pappalardo, G. Gruter, Macromolecules 32 (1999) 4491.

16. (a) P. J. W. Deckers, B. Hessen, J. H. Teuben, Organometallics 21 (2002) 5122. (b) P. J. W. Deckers, B. Hessen, J. H. Teuben, Angew. Chem. Int. Ed. 40(2) (2001) 2516. (c) P. J. W. Deckers, B. Hessen, J. H. Teuben, WO 02/066404 (Stichting Dutch Polymer Institute), 29 August 2002. (d) P. J. W. Deckers, B. Hessen, WO 02/066405 (Stichting Dutch Polymer Institute), 29 August 2002.
17. T. Aoyama, H. Mimura, T. Yamamoto, M. Oguri, Y. Koie, Japanese Patent 09176299 (Tosoh Corpoation) 8 July 1997.
18. H. Mahomed, A. Bollmann, J. Dixon, V. Gokul, L. Griesel, C. Grove, F. Hess, H. Maumela and L. Pepler, Appl. Catal. A. 255 (2003) 355.
19. J. J. C., Grove, H. A. Mahomed, L. Griesel. WO 03/004158 (Sasol Technolgy (Pty) Ltd), 27 June 2002.
20. T. Aoshima, T. Urata. Japanese Patent 11181016 (Mitshubishi Chemical Industries), 6 July 1999.
21. D. C. Commereuc, R. M. Drochon, C. Saussine. US Patent 6031145 (Institut Francais du Petrole, 17 June 1998.
22. D. C. Commereuc, R. M. Drochon, C. Saussine. European Patent 1110930 (Institut Francais du Petrole), 27 June 2001.
23. D. H. Morgan, J. J. C. Grove, B. C. B. Bezuidenhout, S. L. Schwikkard. WO 02/083306 (Sasol Technology (Pty) Ltd), 12 April 2001.
24. D. H. Morgan, S. L. Schwikkard, J. T. Dixon, J. J. Nair, R. Hunter, Adv. Synth. Catal. 345 (2003) 939.
25. R. D. Kohn, M. Haufe, S. Mihan, D. Lilge, Chem. Commun. (2000) 1927.
26. R. D. Kohn, M. Haufe, G. Kociak-Kohn, S. Grimm, P. Wasserscheid, W. Keim, Angew. Chem. Int. Ed. 39(23) (2000) 4337.
27. P. Wasserscheid, S. Grimm, R. Kohn, M. Haufe, Adv. Synth. Catal. 343(8) (2001) 814.
28. D. F. Wass, Dalton Trans. (2007) 816.
29. T. Agapie, S.J. Schofer, J. A. Labinger, J. E. Bercaw. J. Am. Chem. Soc. 126 (2004) 1304.

30. (a) S. J. Schofer, M. W. Day, L. M. Henling, J. A. Labinger, J. E. Bercaw, Organometallics 25 (2006) 2743; (b) T. Agapie, M. W. Day, L. M. Henling, J. A. Labinger, J. E.Bercaw, Organometallics 25 (2006) 2733.
31. D. S. McGuinness, P. Wasserscheid, W. Keim, C. Hu, U. Englert, J. T. Dixon, J. J. C. Grove, Chem. Commun. (2003) 334.
32. D. S. McGuinness, P. Wasserscheid, W. Keim, D. H. Morgan, J. T. Dixon, A. Bollmann, H. Maumela, F. M. Hess, U. Englert, J. Am. Chem. Soc. 125 (2003) 5272.
33. D. McGuinness, P. Wasserscheid, D. H. Morgan, J. T. Dixon, Organometallics 24 (2005) 552.
34. A. Bollmann, K. Blann, J. T. Dixon, F. M. Hess, E. Killian, H. Maumela, D. S. McGuinness, D. H. Morgan, A. Neveling, S. Otto, M. J. Overett, A. M. Z. Slawin, P. Wasserscheid, S. Kuhlmann, J. Am. Chem. Soc. 126 (2004) 14712.
35. A. Jabri, P. Crewdson, S. Gambarotta, I. Korobkov, R. Duchateau, Organometallics 25 (2006) 715.
36. A. J. Rucklidge, D. S. McGuinness, R. T Tooze, A. M. Z Slawin, J. D. A. Pelletier, M. J. Hanton, P. B. Webb, Organometallics 26 (2007) 2782.
37. K. A. Kreisel, G. P. A. Yap, K. H. Theopold, Organometallics 25 (2006) 4670.
38. P. R. Elowe, C. McCann, P. G. Pringle, S. K. Spitzmesser, J. E. Bercaw, Organometallics 25 (2006) 5255.
39. A. Jabri, C. Temple, P. Crewdson, S. Gambarotta, I. Korobkov, R. Duchateau, J. Am. Chem. Soc. 128 (2006) 9238.
40. C. Temple, A. Jabri, P. Crewdson, S. Gambarotta, I. Korobkov, R. Duchateau, Angew. Chem., Int. Ed. 45 (2006) 7050.
41. D. H. Brown, R. T. Richardson, J. Inorg. Nucl. Chem. 35 (1973) 755.
42. D. S. McGuinness, J. A. Suttil, M.G. Gardiner, N. W. Davies, Organometallics 27(16) (2008) 4238.
43. www.oci.unizh.ch/service/cx/Crystal_Growth.pdf, page 4 (accessed April 2006)
44. www.hamptonresearch.com/support/pdf101/CG101HDC.pdf (accessed June 2006)
45. www.cem.msu.edu/~cem472/ramanir.pdf (accessed February 2008)

46. http://161.58.205.25/Raman_Spectroscopy/rtr-ramantutorial.php?ss=800 (accessed February 2008)
47. C. N. Banwell, E. M. McCash. Fundamentals of Molecular Spectroscopy, 4th ed. McGraw-Hill (1994).
48. R. K. Harris. Nuclear Magnetic Resonance Spectroscopy: A Physiochemical View. Wiley (1986).
49. P. J. Hore. Nuclear Magnetic Resonance. Oxford University Press (1995).
50. H. Friebolin. Basic One and Two-Dimensional NMR Spectroscopy. (Transl. by J. Becconsall), 2nd ed. Weinheim; Basel (Switzerland); Cambridge; New York, NY: VCH (1993).
51. Y. Tantirungrotechai, K. Phanasant, S. Roddecha, P. Surawatanwong, V. Sutthikhum, J. Limtrakul, J. Mol. Struct., Theochem. 760 (2006) 189.
52. www.wpi.edu/Academics/Depts/Chemistry/Courses/CH2670/infrared, page 15 (accessed March 2008).
53. Introduction to FT-Raman Spectroscopy, FT-Raman Users Manual. pp 7-18.
54. SMART (Version 5.054), SAINT (Version 6.45), SADABS (Version 2.10) and SHELXTS/SHELXTL (Version 6.12), Bruker AXS Inc., Madison, WI, USA, (2001).
55. SHELXS-97 and SHELXL-97, G. M. Sheldrick, University of Göttingen, Germany, (1997).
56. L. J. Faruggia, J. Appl. Crystallogr. 30 (1997) 565.
57. Mercury (Version 1.4.2) Cambridge Crystallographic Data Centre, (2007). URL: http://www.ccdc.cam.ac.uk.
58. POV-Ray for Windows (Version 3.6), Persistence of Vision Raytracer Pty. Ltd., Victoria, Australia, (2004). URL: http://www.povray.org.
59. Gaussian03, Revision D.01. Frisch M. J., Trucks G. W., Schlegel H. B., Scuseria G. E., Robb M. A., Cheeseman J. R., Montgomery J. A., Vreven T., Kudin K. N., Burant J. C., Millam J. M., Iyengar S. S., Tomasi J., Barone V., Mennucci B., Cossi M., Scalmani G., Rega N., Petersson G. A., Nakatsuji H., Hada M., Ehara M., Toyota K., Fukuda R., Hasegawa J., Ishida M., Nakajima T., Honda Y., Kitao O., Nakai H., Klene M., Li X., Knox J. E., Hratchian H. P., Cross J. B., Bakken

V., Adamo C., Jaramillo J., Gomperts R., Stratmann R. E., Yazyev O., Austin A. J., Cammi R., Pomelli C., Ochterski J. W., Ayala P. Y., Morokuma K., Voth G. A., Salvador P., Dannenberg J. J., Zakrzewski V. G., Dapprich S., Daniels A. D., Strain M. C., Farkas O., Malick D. K., Rabuck A. D., Raghavachari K., Foresman J. B., Ortiz J. V., Cui Q., Baboul A. G., Clifford S., Cioslowski J., Stefanov B. B., Liu G., Liashenko A., Piskorz P., Komamori I., Martin R. L., Fox D. J., Keith T., Al-Laham M. A., Peng C. Y., Nanayakkara A., Challacombe M., Gill P. M. W., Johnson B., Chen W., Wong M. W., Gonzalez C., Pople J.A. (2004) http://www.gaussian.com

60. Linux Enterprise Server version 9.3.
61. Æ. Frisch, M. J. Frisch, G. W. Trucks. Gaussian 03 User's Reference, Gaussian Inc., Wallingford, CT 06492, U.S.A. (info@gaussian.com).
62. D. Hirst, A Computational Approach to Chemistry. Blackwell Scientific Publications (1990).
63. J. Kohanoff, Electronic Structure Calculations for Solids and Molecules. Theory and Computational Methods. Cambridge University Press (2006).
64. J. B. Foresman, *Æ.* Frisch. Exploring Chemistry with Electronic Structure Methods, 2nd ed. Pittsburgh, PA: Gaussian Inc.
65. J. W. Ochterski, Vibrational Analysis in Gaussian, (1999) (www.gaussian.com)
66. J. C. Fettinger, S. P. Mattamana, R. Poli, R. D. Rogers, Organometallics, 15(20) (1996) 4211.
67. O. Swang, R. Blom, J. Organomet. Chem. 561 (1998) 29.
68. I. Cacelli, D. Webster Keogh, R. Poli, A. Rizzo, J. Phys. Chem. A 101 (1997) 9801.
69. G. M. Badger. The Chemistry of Heterocyclic Compounds. New York and London: Academic Press (1961).
70. L. A. Paquette, W. A. Benjamin. Modern Heterocyclic Chemistry. Reading, MA: INC (1968).
71. J. C. Taft, M. M. Jones, Inorg. Synth. 7 (1963) 132.
72. R. J. Gritter, A. W. Godfrey, J. Am. Chem. Soc. 86(21) (1964) 4724.
73. D. A. Thornton, Coord. Chem. Rev. 104(2) (1990) 251.

74. S. Akyuz, A. B. Dempster, R. L. Morehouse, J. Mol. Struct. 17 (1973) 105.
75. A. Topacli, S. Bayari, Spectrochim. Acta Part A 57 (2001) 1385.
76. D. Lin-Vien, N. B. Colthup, W. G. Flateley, J. G. Grasselli. The Handbook of Infrared and Raman Characteristic Frequencies of Organic Molecules. Boston, MA: Academic Press (1991).
77. J. Shamir, Inorg. Chim. Acta, 156 (1989) 163.
78. P. Boudjouk, J. –H. So, Inorg. Synth. 29 (1992) 108
79. D. A. Edwards, S. C. Jennison, Trans. Metal Chem. 6 (1981) 235.
80. R. J. H. Clarke, C. S. Williams, Inorg. Chem. 4 (1965) 350.
81. D. M. Adams, Metal-Ligand Vibrations. London: Edward Arnold (1996).
82. G. W. A. Fowles, P. T. Greene, T. E. Lester, J. Nucl. Chem. 29 (1967) 2365.
83. S. A. Howard, K. I. Hardcastle, J. Crystallogr. Spectr. Res. 15(6) (1985) 643.
84. J. V. Brenčič, B. Čeh, T. Zlebnik, Vestn. Slov. Kem. Drus. (1990) 9.
85. F. A. Cotton, R. L. Luck, Acta Cryst. C47 (1991) 1069.
86. C. K. Prout, P. D. P. Thomas, Eur. Cryst. Meeting (1977) 221.
87. T. C. Jao, I. Scott, D. Steele, J. Mol. Spectr. 92 (1982) 1.
88. J. A. Broomhead, J. Evans, W. D. Grumley, M. Sterns, J. Chem. Soc., Dalton Trans. (1977), 173.
89. G. Durgaprasad, D. N. Sathyanarayana, C. C. Patel, Bull. Chem. Soc. Jpn. 44 (1971) 316.
90. D. B. Powell, A. Woollins, Spectrochim. Acta, 41A(9) (1985) 1023.
91. A. Finch, I. J. Hyams, D. Steele, J. Mol. Spectr. 16 (1965) 103.
92. S. Yurdakul, M. Bahat, J. Mol. Struct. 412 (1997) 97.
93. P. C. H. Mitchell, J. Inorg. Nucl. Chem. 21(3-4) (1961) 382.
94. N. S. Gill, R. H. Nuttall. D. E. Scaife, D. W. A. Sharp, J. Inorg. Nucl. Chem. 18 (1961) 79.
95. D. L. Cummings, J. L. Wood, J. Mol. Struct. 17 (1973) 257.
96. Y. Buyukmurat, S. Akyuz, J. Mol. Struct. 651 (2003) 533.
97. S. Bayari, A. Topacli, A. Aydinli, Spectrosc. Lett. 27(9) (1994) 1083.
98. P. Carmona, M. Molina, R. Escobar, Spectrochim. Acta 49A(1) (1993) 1.

99. L. R. Gray, A. L. Hale, W. Levason, F. P. McCullough, M. Webster, J. Chem. Soc., Dalton Trans. (1983) 2573.
100. N. F. Brennan, B. Blom, S. Lotz, P .H. van Rooyen, M. Landman, D. C. Liles, M. J. Green, Inorg. Chim. Acta 361 (2008) 3042.
101. B. Modec, J. V. Brencic, G. Giester, J. Chem. Cryst. 30(5) (2000) 345.
102. C. Kaes, Chem. Rev. 100 (2000) 3553.
103. H. Franz, K. J. Schiedeknecht, J. Organomet. Chem. 5 (1966) 454.
104. E. Spinner, J. Chem. Soc. (1963) 3860.
105. B. Šopotrajanov, V. Stefov, M. Žugić, V. M. Petruševski, J. Mol. Struct. 482-483 (1999) 109.
106. V. Stefov, V. M. Petruševski, B. Šoptrajanov, J. Mol. Struct. 293 (1993) 97.
107. M. F. Farona, J. G. Grasselli, B. L. Ross, Spectrochim Acta, 23A (1967) 1875.
108. K. Namba, J. Wang, S. Cui, Y. Kishi, Org. Lett. 7 (2005) 5421.
109. C. Redshaw, G. Wilkinson, B. Hussain-Bates, M. B. Hursthouse, J. Chem. Soc. Dalton Trans. (1992) 1803.
110. P. Andersen, J. Josephsen, Acta Chem. Scand. 25 (1971) 3255.
111. T. Kar, M. –S. Liao, S. Biswas, S. Sarkar, K. Dey, G. P. A. Yap, K. Kreisel, Spectrochim. Acta, Part A 65 (2006) 882.
112. A. R. Hermes, G. S. Girolami, Inorg. Chem. 29 (1990) 313.
113. A. M. F. Benial, V. Ramakrishnan, R. Murugesan, Spectrochim. Acta Part A 58 (2002) 1703.
114. G. B. Deacon, J. H. S. Green, J. Chem. Soc. Chem. Commun. (London) 18 (1966) 629.
115. M. A. Bennett, R. J. H. Clark, D. J. Goodwin, Inorg. Chem. 6(9) (1967) 1625.
116. K. Wadja-Hermanowicz, Z. Ciunik, A. Kochel, Inorg. Chem. 45(8) (2006) 3369.
117. Cambridge Crystallographic Data Centre, (2007). URL: http://www.ccdc.cam.ac.uk.
118. Z-Z Zhang, H. Cheng, Coord. Chem. Rev. 147 (1996) 1.
119. R. C. Taylor, D. B. Walters, Tetrahedron Lett. 1 (1972) 63.
120. L. Dahlenburg, R. Goetz, Eur. J. Inorg. Chem. 4 (2004) 888.
121. P. R. Kumar, S. Upreti, A. K. Singh, Polyhedron 27(6) (2008) 1610.

122. W. Chen, W. Mbafor, S. M. Roberts, J. Whittall, Tetrahedron: Asym. 17 (2006) 1161.

123. T-J Kim, Y-H Kim, E-J Kim, S-H Oh, H-S Kim, J-H Jeong, Bull. Kor. Chem. Soc. 15 (1994) 379.

124. F. H. van Steen, J. A. Kanters, Acta Cryst. C42 (1986) 547.

125. C. Nilewski, M. Neumann, L. Tebben, R. Frohlich, G. Kehr, G. Erker, Synth. (2006) 2191.

APPENDIX 1 : ADDITIONAL CRYSTALLOGRAPHIC DATA

$[CrCl_3(py)_3]$

Table A.1 **Atomic coordinates (x 10^4) and equivalent isotropic displacement parameters ($Å^2$x 10^3) for $[CrCl_3(py)_3]$. U(eq) is defined as one-third of the trace of the orthogonalized U^{ij} tensor**

	x	y	z	U(eq)
Cr(1)	0	8137(1)	2500	30(1)
Cl(1)	572(1)	8198(1)	4675(1)	44(1)
Cl(2)	0	5993(1)	2500	44(1)
N(1)	1096(1)	8135(1)	2527(1)	37(1)
C(1)	1653(1)	7383(2)	3317(2)	45(1)
C(2)	2360(1)	7262(2)	3311(2)	58(1)
C(3)	2504(1)	7936(2)	2472(2)	67(1)
C(4)	1945(1)	8733(2)	1676(2)	63(1)
C(5)	1250(1)	8810(2)	1723(2)	48(1)
N(2)	0	10082(2)	2500	39(1)
C(6)	642(1)	10718(2)	3221(2)	52(1)
C(7)	661(2)	11989(2)	3228(3)	72(1)
C(8)	0	12632(3)	2500	83(1)
N(3)	2230(1)	5471(2)	189(2)	94(1)
C(9)	1717(1)	5385(2)	390(2)	63(1)
C(10)	1065(2)	5262(3)	656(3)	73(1)

Table A.2 Bond lengths [Å] and angles [°] for $[CrCl_3(py)_3]$

Cr(1)-N(2)	2.1037(17)	C(10)-H(10C)	0.87(4)
Cr(1)-N(1)#1	2.1040(13)	N(2)-Cr(1)-N(1)#1	90.06(3)
Cr(1)-N(1)	2.1040(13)	N(2)-Cr(1)-N(1)	90.06(3)
Cr(1)-Cl(2)	2.3196(6)	N(1)#1-Cr(1)-N(1)	179.88(6)
Cr(1)-Cl(1)#1	2.3304(4)	N(2)-Cr(1)-Cl(2)	180.0
Cr(1)-Cl(1)	2.3304(4)	N(1)#1-Cr(1)-Cl(2)	89.94(3)
N(1)-C(1)	1.344(2)	N(1)-Cr(1)-Cl(2)	89.94(3)
N(1)-C(5)	1.344(2)	N(2)-Cr(1)-Cl(1)#1	88.386(11)
C(1)-C(2)	1.376(2)	N(1)#1-Cr(1)-Cl(1)#1	90.64(4)
C(1)-H(1)	0.93(2)	N(1)-Cr(1)-Cl(1)#1	89.36(4)
C(2)-C(3)	1.367(3)	Cl(2)-Cr(1)-Cl(1)#1	91.614(11)
C(2)-H(2)	0.89(2)	N(2)-Cr(1)-Cl(1)	88.386(11)
C(3)-C(4)	1.378(3)	N(1)#1-Cr(1)-Cl(1)	89.36(4)
C(3)-H(3)	0.88(3)	N(1)-Cr(1)-Cl(1)	90.64(4)
C(4)-C(5)	1.373(3)	Cl(2)-Cr(1)-Cl(1)	91.614(11)
C(4)-H(4)	0.91(2)	Cl(1)#1-Cr(1)-Cl(1)	176.77(2)
C(5)-H(5)	0.98(2)	C(1)-N(1)-C(5)	117.90(14)
N(2)-C(6)	1.342(2)	C(1)-N(1)-Cr(1)	119.78(10)
N(2)-C(6)#1	1.342(2)	C(5)-N(1)-Cr(1)	122.18(11)
C(6)-C(7)	1.375(3)	N(1)-C(1)-C(2)	122.70(17)
C(6)-H(6)	0.952(18)	N(1)-C(1)-H(1)	116.5(12)
C(7)-C(8)	1.370(3)	C(2)-C(1)-H(1)	120.8(12)
C(7)-H(7)	0.89(2)	C(3)-C(2)-C(1)	118.86(19)
C(8)-C(7)#1	1.370(3)	C(3)-C(2)-H(2)	120.0(15)
C(8)-H(8)	1.03(5)	C(1)-C(2)-H(2)	121.0(15)
N(3)-C(9)	1.123(3)	C(2)-C(3)-C(4)	119.12(18)
C(9)-C(10)	1.439(3)	C(2)-C(3)-H(3)	117.8(16)
C(10)-H(10A)	1.00(3)	C(4)-C(3)-H(3)	123.0(16)
C(10)-H(10B)	0.91(3)	C(5)-C(4)-C(3)	119.29(19)

C(5)-C(4)-H(4)	117.8(14)	C(8)-C(7)-H(7)	124.6(17)
C(3)-C(4)-H(4)	122.9(14)	C(6)-C(7)-H(7)	116.1(17)
N(1)-C(5)-C(4)	122.10(18)	C(7)#1-C(8)-C(7)	119.0(3)
N(1)-C(5)-H(5)	113.9(11)	C(7)#1-C(8)-H(8)	120.48(14)
C(4)-C(5)-H(5)	123.9(11)	C(7)-C(8)-H(8)	120.48(14)
C(6)-N(2)-C(6)#1	118.2(2)	N(3)-C(9)-C(10)	179.4(3)
C(6)-N(2)-Cr(1)	120.90(10)	C(9)-C(10)-H(10A)	111.5(15)
C(6)#1-N(2)-Cr(1)	120.90(10)	C(9)-C(10)-H(10B)	107.0(19)
N(2)-C(6)-C(7)	122.1(2)	H(10A)-C(10)-H(10B)	108(3)
N(2)-C(6)-H(6)	117.8(11)	C(9)-C(10)-H(10C)	104(2)
C(7)-C(6)-H(6)	120.1(11)	H(10A)-C(10)-H(10C)	123(3)
C(8)-C(7)-C(6)	119.3(2)	H(10B)-C(10)-H(10C)	102(3)

Symmetry transformations used to generate equivalent atoms:

#1 -x,y,-z+1/2

Table A.3 **Anisotropic displacement parameters ($Å^2 x\ 10^3$) for $[CrCl_3(py)_3]$. The anisotropic displacement factor exponent takes the form: $-2p^2[h^2a^{*2}U^{11} + ... + 2\ h\ k\ a^*\ b^*\ U^{12}]$**

	U^{11}	U^{22}	U^{33}	U^{23}	U^{13}	U^{12}
Cr(1)	30(1)	27(1)	31(1)	0	12(1)	0
Cl(1)	43(1)	52(1)	33(1)	0(1)	13(1)	5(1)
Cl(2)	53(1)	27(1)	55(1)	0	26(1)	0
N(1)	35(1)	37(1)	38(1)	-1(1)	17(1)	-1(1)
C(1)	39(1)	46(1)	47(1)	-3(1)	16(1)	5(1)
C(2)	38(1)	65(1)	64(1)	-14(1)	16(1)	8(1)
C(3)	41(1)	88(2)	78(1)	-27(1)	33(1)	-9(1)
C(4)	58(1)	80(1)	63(1)	-11(1)	38(1)	-21(1)
C(5)	46(1)	52(1)	48(1)	-1(1)	23(1)	-7(1)

N(2)	44(1)	29(1)	45(1)	0	20(1)	0
C(6)	61(1)	41(1)	57(1)	-9(1)	28(1)	-11(1)
C(7)	104(2)	44(1)	79(2)	-18(1)	51(1)	-28(1)
C(8)	144(3)	33(1)	90(2)	0	68(2)	0
N(3)	102(2)	95(2)	117(2)	-1(1)	78(2)	-6(1)
C(9)	73(1)	57(1)	68(1)	-6(1)	38(1)	-3(1)
C(10)	70(1)	79(2)	80(2)	-22(1)	42(1)	-11(1)

Table A.4 **Hydrogen coordinates (x 10^4) and isotropic displacement parameters ($Å^2$x 10^3) for $[CrCl_3(py)_3]$**

	x	y	z	U(eq)
H(1)	1537(12)	6932(16)	3869(19)	50(5)
H(2)	2730(14)	6790(20)	3870(20)	68(7)
H(3)	2951(14)	7820(20)	2450(20)	79(7)
H(4)	2011(12)	9210(20)	1110(20)	70(6)
H(5)	815(11)	9320(18)	1158(18)	52(5)
H(6)	1095(10)	10261(17)	3731(17)	47(5)
H(7)	1117(14)	12340(30)	3720(20)	78(7)
H(8)	0	13580(50)	2500	116(14)
H(10A)	759(16)	4500(30)	270(30)	90(8)
H(10B)	1255(17)	5190(30)	1500(30)	107(10)
H(10C)	860(20)	6000(40)	520(30)	128(13)

Table A.5 Torsion angles [°] for $[CrCl_3(py)_3]$

N(2)-Cr(1)-N(1)-C(1)	134.20(11)	Cr(1)-N(1)-C(5)-C(4)	-174.73(13)
Cl(2)-Cr(1)-N(1)-C(1)	-45.80(11)	C(3)-C(4)-C(5)-N(1)	0.4(3)
Cl(1)#1-Cr(1)-N(1)-C(1)	-137.42(11)	N(1)#1-Cr(1)-N(2)-C(6)	138.73(9)
Cl(1)-Cr(1)-N(1)-C(1)	45.81(11)	N(1)-Cr(1)-N(2)-C(6)	-41.27(9)
N(2)-Cr(1)-N(1)-C(5)	-50.02(12)	Cl(1)#1-Cr(1)-N(2)-C(6)	-130.63(9)
Cl(2)-Cr(1)-N(1)-C(5)	129.98(12)	Cl(1)-Cr(1)-N(2)-C(6)	49.37(9)
Cl(1)#1-Cr(1)-N(1)-C(5)	38.36(12)	N(1)#1-Cr(1)-N(2)-C(6)#1	-41.27(9)
Cl(1)-Cr(1)-N(1)-C(5)	-138.41(12)	N(1)-Cr(1)-N(2)-C(6)#1	138.73(9)
C(5)-N(1)-C(1)-C(2)	-1.5(2)	Cl(1)#1-Cr(1)-N(2)-C(6)#1	49.37(9)
Cr(1)-N(1)-C(1)-C(2)	174.50(13)	Cl(1)-Cr(1)-N(2)-C(6)#1	-130.63(9)
N(1)-C(1)-C(2)-C(3)	0.3(3)	C(6)#1-N(2)-C(6)-C(7)	-0.78(15)
C(1)-C(2)-C(3)-C(4)	1.3(3)	Cr(1)-N(2)-C(6)-C(7)	179.22(15)
C(2)-C(3)-C(4)-C(5)	-1.6(3)	N(2)-C(6)-C(7)-C(8)	1.5(3)
C(1)-N(1)-C(5)-C(4)	1.1(2)	C(6)-C(7)-C(8)-C(7)#1	-0.7(3)

Symmetry transformations used to generate equivalent atoms:

#1 -x,y,-z+1/2

[Hpy][$CrCl_4(py)_2$]

Table A.6 **Atomic coordinates (x 10^4) and equivalent isotropic displacement parameters ($Å^2$x 10^3) for [Hpy][$CrCl_4(py)_2$]. U(eq) is defined as one-third of the trace of the orthogonalised U^{ij} tensor**

	x	y	z	U(eq)
Cr(1)	1842(1)	975(1)	2533(1)	36(1)
Cl(1)	1013(1)	1234(1)	372(1)	50(1)
Cl(2)	4224(1)	1552(1)	2392(1)	50(1)
Cl(3)	2614(1)	709(1)	4707(1)	53(1)
Cl(4)	-556(1)	401(1)	2705(1)	50(1)
N(1)	3099(3)	233(1)	1848(2)	39(1)
C(1)	2425(3)	-117(1)	900(3)	48(1)
C(2)	3234(4)	-595(1)	402(3)	56(1)
C(3)	4802(4)	-722(1)	881(3)	55(1)
C(4)	5499(4)	-378(1)	1865(3)	57(1)
C(5)	4629(3)	97(1)	2318(3)	49(1)
N(2)	561(3)	1720(1)	3209(2)	45(1)
C(6)	1253(4)	2087(1)	4111(3)	55(1)
C(7)	459(5)	2587(1)	4543(4)	69(1)
C(8)	-1089(5)	2711(1)	4052(4)	76(1)
C(9)	-1811(4)	2339(1)	3123(4)	75(1)
C(10)	-955(4)	1849(1)	2728(3)	59(1)
N(3)	1370(5)	-769(2)	3807(3)	74(1)
C(11)	636(5)	-1138(2)	2974(4)	82(1)
C(12)	1239(5)	-1684(2)	2815(4)	81(1)
C(13)	2617(5)	-1847(2)	3521(4)	78(1)
C(14)	3368(5)	-1456(2)	4376(4)	90(1)
C(15)	2703(6)	-907(2)	4485(4)	83(1)

Table A.7 **Bond lengths [Å] and angles [°] for [Hpy][$CrCl_4(py)_2$]**

Cr(1)-N(1)	2.097(2)	N(3)-C(15)	1.290(5)
Cr(1)-N(2)	2.109(2)	N(3)-C(11)	1.309(5)
Cr(1)-Cl(2)	2.3387(8)	N(3)-H(3N)	0.89(5)
Cr(1)-Cl(1)	2.3398(8)	C(11)-C(12)	1.336(5)
Cr(1)-Cl(3)	2.3451(8)	C(11)-H(11)	0.9300
Cr(1)-Cl(4)	2.3490(8)	C(12)-C(13)	1.347(5)
N(1)-C(1)	1.339(3)	C(12)-H(12)	0.9300
N(1)-C(5)	1.341(3)	C(13)-C(14)	1.362(5)
C(1)-C(2)	1.372(4)	C(13)-H(13)	0.9300
C(1)-H(1)	0.9300	C(14)-C(15)	1.356(6)
C(2)-C(3)	1.369(4)	C(14)-H(14)	0.9300
C(2)-H(2)	0.9300	C(15)-H(15)	0.9300
C(3)-C(4)	1.365(4)		
C(3)-H(3)	0.9300	N(1)-Cr(1)-N(2)	179.49(9)
C(4)-C(5)	1.374(4)	N(1)-Cr(1)-Cl(2)	90.36(6)
C(4)-H(4)	0.9300	N(2)-Cr(1)-Cl(2)	89.95(6)
C(5)-H(5)	0.9300	N(1)-Cr(1)-Cl(1)	90.43(6)
N(2)-C(10)	1.331(4)	N(2)-Cr(1)-Cl(1)	89.17(7)
N(2)-C(6)	1.337(3)	Cl(2)-Cr(1)-Cl(1)	90.05(3)
C(6)-C(7)	1.380(4)	N(1)-Cr(1)-Cl(3)	89.99(6)
C(6)-H(6)	0.9300	N(2)-Cr(1)-Cl(3)	90.41(7)
C(7)-C(8)	1.355(5)	Cl(2)-Cr(1)-Cl(3)	91.12(3)
C(7)-H(7)	0.9300	Cl(1)-Cr(1)-Cl(3)	178.75(3)
C(8)-C(9)	1.372(5)	N(1)-Cr(1)-Cl(4)	90.23(6)
C(8)-H(8)	0.9300	N(2)-Cr(1)-Cl(4)	89.46(6)
C(9)-C(10)	1.375(4)	Cl(2)-Cr(1)-Cl(4)	179.16(3)
C(9)-H(9)	0.9300	Cl(1)-Cr(1)-Cl(4)	90.54(3)
C(10)-H(10)	0.9300	Cl(3)-Cr(1)-Cl(4)	88.28(3)

C(1)-N(1)-C(5)	117.2(2)	C(7)-C(8)-C(9)	118.8(3)
C(1)-N(1)-Cr(1)	121.46(18)	C(7)-C(8)-H(8)	120.6
C(5)-N(1)-Cr(1)	121.31(18)	C(9)-C(8)-H(8)	120.6
N(1)-C(1)-C(2)	122.9(3)	C(8)-C(9)-C(10)	119.2(3)
N(1)-C(1)-H(1)	118.5	C(8)-C(9)-H(9)	120.4
C(2)-C(1)-H(1)	118.5	C(10)-C(9)-H(9)	120.4
C(3)-C(2)-C(1)	119.1(3)	N(2)-C(10)-C(9)	122.6(3)
C(3)-C(2)-H(2)	120.5	N(2)-C(10)-H(10)	118.7
C(1)-C(2)-H(2)	120.5	C(9)-C(10)-H(10)	118.7
C(4)-C(3)-C(2)	118.9(3)	C(15)-N(3)-C(11)	122.2(4)
C(4)-C(3)-H(3)	120.6	C(15)-N(3)-H(3N)	120(4)
C(2)-C(3)-H(3)	120.6	C(11)-N(3)-H(3N)	117(4)
C(3)-C(4)-C(5)	119.3(3)	N(3)-C(11)-C(12)	120.4(4)
C(3)-C(4)-H(4)	120.4	N(3)-C(11)-H(11)	119.8
C(5)-C(4)-H(4)	120.4	C(12)-C(11)-H(11)	119.8
N(1)-C(5)-C(4)	122.6(3)	C(11)-C(12)-C(13)	119.1(4)
N(1)-C(5)-H(5)	118.7	C(11)-C(12)-H(12)	120.5
C(4)-C(5)-H(5)	118.7	C(13)-C(12)-H(12)	120.5
C(10)-N(2)-C(6)	117.5(2)	C(12)-C(13)-C(14)	119.6(4)
C(10)-N(2)-Cr(1)	121.01(19)	C(12)-C(13)-H(13)	120.2
C(6)-N(2)-Cr(1)	121.4(2)	C(14)-C(13)-H(13)	120.2
N(2)-C(6)-C(7)	122.5(3)	C(15)-C(14)-C(13)	118.5(4)
N(2)-C(6)-H(6)	118.7	C(15)-C(14)-H(14)	120.8
C(7)-C(6)-H(6)	118.7	C(13)-C(14)-H(14)	120.8
C(8)-C(7)-C(6)	119.3(3)	N(3)-C(15)-C(14)	120.1(4)
C(8)-C(7)-H(7)	120.3	N(3)-C(15)-H(15)	119.9
C(6)-C(7)-H(7)	120.3	C(14)-C(15)-H(15)	119.9

Table A.8 **Anisotropic displacement parameters ($Å^2 x\ 10^3$) for $[Hpy][CrCl_4(py)_2]$. The anisotropic displacement factor exponent takes the form: $-2p^2[h^2a^{*2}U^{11} + ... + 2\ h\ k\ a^*\ b^*\ U^{12}]$**

	U^{11}	U^{22}	U^{33}	U^{23}	U^{13}	U^{12}
Cr(1)	35(1)	36(1)	38(1)	-1(1)	3(1)	-3(1)
Cl(1)	47(1)	59(1)	45(1)	7(1)	-3(1)	-3(1)
Cl(2)	44(1)	51(1)	56(1)	1(1)	2(1)	-14(1)
Cl(3)	62(1)	58(1)	39(1)	3(1)	2(1)	0(1)
Cl(4)	39(1)	44(1)	66(1)	-1(1)	9(1)	-6(1)
N(1)	35(1)	41(1)	40(1)	-1(1)	2(1)	-2(1)
C(1)	41(2)	48(2)	54(2)	-10(1)	0(1)	-3(1)
C(2)	60(2)	46(2)	62(2)	-13(1)	5(2)	-4(1)
C(3)	58(2)	39(2)	69(2)	-1(1)	17(2)	6(1)
C(4)	42(2)	57(2)	71(2)	1(2)	4(2)	11(1)
C(5)	41(2)	52(2)	54(2)	-4(1)	-2(1)	-1(1)
N(2)	48(1)	39(1)	49(1)	-4(1)	9(1)	-3(1)
C(6)	62(2)	49(2)	55(2)	-9(1)	3(2)	0(1)
C(7)	77(3)	54(2)	76(2)	-21(2)	19(2)	-6(2)
C(8)	73(2)	44(2)	114(3)	-18(2)	34(2)	2(2)
C(9)	52(2)	51(2)	124(3)	-14(2)	14(2)	8(2)
C(10)	46(2)	47(2)	83(2)	-12(2)	2(2)	3(1)
N(3)	93(3)	63(2)	68(2)	3(2)	19(2)	14(2)
C(11)	64(2)	98(3)	82(3)	9(2)	-10(2)	5(2)
C(12)	90(3)	73(2)	78(3)	-14(2)	-5(2)	-23(2)
C(13)	95(3)	58(2)	82(3)	2(2)	14(2)	14(2)
C(14)	72(3)	100(3)	94(3)	7(2)	-21(2)	7(2)
C(15)	105(3)	76(3)	67(2)	-12(2)	-8(2)	-22(2)

Table A.9 **Hydrogen coordinates (x 10^4) and isotropic displacement parameters (Å^{2}x 10^3) for [Hpy][$CrCl_4(py)_2$]**

	x	y	z	U(eq)
H(1)	1362	-32	565	57
H(2)	2723	-829	-253	67
H(3)	5384	-1038	543	65
H(4)	6550	-463	2224	68
H(5)	5120	333	2977	59
H(6)	2310	2003	4461	66
H(7)	980	2835	5164	82
H(8)	-1651	3042	4340	91
H(9)	-2868	2417	2765	90
H(10)	-1454	1598	2101	70
H(3N)	1010(70)	-390(20)	3790(50)	89
H(11)	-312	-1020	2489	98
H(12)	715	-1947	2226	97
H(13)	3052	-2226	3424	94
H(14)	4317	-1562	4875	108
H(15)	3209	-630	5050	100

Table A.10 Torsion angles [°] for [Hpy][$CrCl_4(py)_2$]

Cl(2)-Cr(1)-N(1)-C(1)	-133.5(2)	Cl(4)-Cr(1)-N(2)-C(10)	-45.6(2)
Cl(1)-Cr(1)-N(1)-C(1)	-43.4(2)	Cl(2)-Cr(1)-N(2)-C(6)	-43.4(2)
Cl(3)-Cr(1)-N(1)-C(1)	135.4(2)	Cl(1)-Cr(1)-N(2)-C(6)	-133.5(2)
Cl(4)-Cr(1)-N(1)-C(1)	47.1(2)	Cl(3)-Cr(1)-N(2)-C(6)	47.7(2)
Cl(2)-Cr(1)-N(1)-C(5)	44.9(2)	Cl(4)-Cr(1)-N(2)-C(6)	136.0(2)
Cl(1)-Cr(1)-N(1)-C(5)	134.9(2)	C(10)-N(2)-C(6)-C(7)	-0.3(4)
Cl(3)-Cr(1)-N(1)-C(5)	-46.3(2)	Cr(1)-N(2)-C(6)-C(7)	178.2(2)
Cl(4)-Cr(1)-N(1)-C(5)	-134.5(2)	N(2)-C(6)-C(7)-C(8)	0.7(5)
C(5)-N(1)-C(1)-C(2)	-0.5(4)	C(6)-C(7)-C(8)-C(9)	-0.9(6)
Cr(1)-N(1)-C(1)-C(2)	177.9(2)	C(7)-C(8)-C(9)-C(10)	0.7(6)
N(1)-C(1)-C(2)-C(3)	-0.4(5)	C(6)-N(2)-C(10)-C(9)	0.0(5)
C(1)-C(2)-C(3)-C(4)	1.6(5)	Cr(1)-N(2)-C(10)-C(9)	-178.4(3)
C(2)-C(3)-C(4)-C(5)	-1.9(4)	C(8)-C(9)-C(10)-N(2)	-0.2(6)
C(1)-N(1)-C(5)-C(4)	0.1(4)	C(15)-N(3)-C(11)-C(12)	1.2(6)
Cr(1)-N(1)-C(5)-C(4)	-178.3(2)	N(3)-C(11)-C(12)-C(13)	-0.3(6)
C(3)-C(4)-C(5)-N(1)	1.1(5)	C(11)-C(12)-C(13)-C(14)	-0.1(6)
Cl(2)-Cr(1)-N(2)-C(10)	135.0(2)	C(12)-C(13)-C(14)-C(15)	-0.4(6)
Cl(1)-Cr(1)-N(2)-C(10)	44.9(2)	C(11)-N(3)-C(15)-C(14)	-1.8(6)
Cl(3)-Cr(1)-N(2)-C(10)	-133.9(2)	C(13)-C(14)-C(15)-N(3)	1.3(6)

Table A.11 Hydrogen bonds for [Hpy][$CrCl_4(py)_2$] [Å and °]

D-H...A	d(D-H)	d(H...A)	d(D...A)	<(DHA)
N(3)-H(3N)...Cl(4)	0.89(5)	2.43(5)	3.235(4)	150(5)
N(3)-H(3N)...Cl(3)	0.89(5)	2.94(5)	3.586(4)	131(4)

$[CrCl_3(py)_2(DMF)]$

Table A.12 **Atomic coordinates (x 10^4) and equivalent isotropic displacement parameters ($Å^2$x 10^3) for $[CrCl_3(py)_2(DMF)]$. U(eq) is defined as one-third of the trace of the orthogonalised U^{ij} tensor**

	x	y	z	U(eq)
Cr(1)	3856(1)	9243(1)	3357(1)	34(1)
Cl(1)	3988(1)	10037(1)	1097(1)	51(1)
Cl(2)	2058(1)	8139(1)	2288(1)	47(1)
Cl(3)	5605(1)	10338(1)	4523(1)	54(1)
N(1)	2108(3)	10180(2)	3978(3)	40(1)
C(1)	2092(4)	11171(3)	3715(4)	51(1)
C(2)	960(5)	11789(3)	4101(4)	62(1)
C(3)	-222(5)	11385(4)	4795(4)	67(1)
C(4)	-236(4)	10377(4)	5080(4)	60(1)
C(5)	943(4)	9795(3)	4653(4)	49(1)
N(2)	5604(3)	8252(2)	2890(2)	39(1)
C(6)	5425(4)	7259(3)	2972(3)	45(1)
C(7)	6491(5)	6580(3)	2586(4)	64(1)
C(8)	7797(5)	6934(4)	2119(4)	72(1)
C(9)	8025(4)	7949(4)	2033(4)	64(1)
C(10)	6903(4)	8578(3)	2425(3)	51(1)
O(1)	3685(2)	8522(2)	5281(2)	44(1)
N(3)	4421(3)	8025(2)	7596(3)	44(1)
C(11)	4693(4)	8393(3)	6327(3)	42(1)
C(12)	2939(5)	7703(5)	7924(5)	94(2)
C(13)	5620(5)	7871(3)	8776(4)	60(1)
O(2)	839(5)	3826(3)	2134(4)	93(1)
N(4)	1039(4)	5140(3)	594(3)	56(1)
C(14)	355(6)	4351(3)	1113(4)	69(1)
C(15)	2507(5)	5459(3)	1202(5)	69(1)
C(16)	362(6)	5697(4)	-639(5)	84(1)

Table A.13 **Bond lengths [Å] and angles [°] for $[CrCl_3(py)_2(DMF)]$**

Cr(1)-O(1)	2.003(2)	N(3)-C(13)	1.465(4)
Cr(1)-N(1)	2.102(3)	C(11)-H(11)	0.9300
Cr(1)-N(2)	2.106(3)	C(12)-H(12A)	0.9600
Cr(1)-Cl(1)	2.3120(9)	C(12)-H(12B)	0.9600
Cr(1)-Cl(3)	2.3268(9)	C(12)-H(12C)	0.9600
Cr(1)-Cl(2)	2.3277(9)	C(13)-H(13A)	0.9600
N(1)-C(1)	1.343(5)	C(13)-H(13B)	0.9600
N(1)-C(5)	1.343(4)	C(13)-H(13C)	0.9600
C(1)-C(2)	1.365(6)	O(2)-C(14)	1.212(5)
C(1)-H(1)	0.9300	N(4)-C(14)	1.318(5)
C(2)-C(3)	1.373(6)	N(4)-C(16)	1.434(5)
C(2)-H(2)	0.9300	N(4)-C(15)	1.442(5)
C(3)-C(4)	1.367(7)	C(14)-H(14)	0.9300
C(3)-H(3)	0.9300	C(15)-H(15A)	0.9600
C(4)-C(5)	1.382(5)	C(15)-H(15B)	0.9600
C(4)-H(4)	0.9300	C(15)-H(15C)	0.9600
C(5)-H(5)	0.9300	C(16)-H(16A)	0.9600
N(2)-C(10)	1.331(4)	C(16)-H(16B)	0.9600
N(2)-C(6)	1.336(5)	C(16)-H(16C)	0.9600
C(6)-C(7)	1.374(5)		
C(6)-H(6)	0.9300	O(1)-Cr(1)-N(1)	86.98(10)
C(7)-C(8)	1.350(7)	O(1)-Cr(1)-N(2)	88.77(10)
C(7)-H(7)	0.9300	N(1)-Cr(1)-N(2)	175.74(10)
C(8)-C(9)	1.370(8)	O(1)-Cr(1)-Cl(1)	177.96(7)
C(8)-H(8)	0.9300	N(1)-Cr(1)-Cl(1)	92.93(7)
C(9)-C(10)	1.370(6)	N(2)-Cr(1)-Cl(1)	91.33(7)
C(9)-H(9)	0.9300	O(1)-Cr(1)-Cl(3)	89.91(7)
C(10)-H(10)	0.9300	N(1)-Cr(1)-Cl(3)	89.32(8)
O(1)-C(11)	1.265(4)	N(2)-Cr(1)-Cl(3)	90.36(8)
N(3)-C(11)	1.287(4)	Cl(1)-Cr(1)-Cl(3)	92.12(4)
N(3)-C(12)	1.437(5)	O(1)-Cr(1)-Cl(2)	87.90(7)

N(1)-Cr(1)-Cl(2)	89.34(8)	C(9)-C(8)-H(8)	120.1
N(2)-Cr(1)-Cl(2)	90.83(8)	C(10)-C(9)-C(8)	118.4(4)
Cl(1)-Cr(1)-Cl(2)	90.06(3)	C(10)-C(9)-H(9)	120.8
Cl(3)-Cr(1)-Cl(2)	177.49(4)	C(8)-C(9)-H(9)	120.8
C(1)-N(1)-C(5)	117.2(3)	N(2)-C(10)-C(9)	123.2(4)
C(1)-N(1)-Cr(1)	122.4(2)	N(2)-C(10)-H(10)	118.4
C(5)-N(1)-Cr(1)	120.3(2)	C(9)-C(10)-H(10)	118.4
N(1)-C(1)-C(2)	123.1(4)	C(11)-O(1)-Cr(1)	128.2(2)
N(1)-C(1)-H(1)	118.4	C(11)-N(3)-C(12)	122.3(3)
C(2)-C(1)-H(1)	118.4	C(11)-N(3)-C(13)	121.9(3)
C(1)-C(2)-C(3)	119.0(4)	C(12)-N(3)-C(13)	115.8(3)
C(1)-C(2)-H(2)	120.5	O(1)-C(11)-N(3)	123.2(3)
C(3)-C(2)-H(2)	120.5	O(1)-C(11)-H(11)	118.4
C(4)-C(3)-C(2)	119.3(4)	N(3)-C(11)-H(11)	118.4
C(4)-C(3)-H(3)	120.4	N(3)-C(12)-H(12A)	109.5
C(2)-C(3)-H(3)	120.4	N(3)-C(12)-H(12B)	109.5
C(3)-C(4)-C(5)	118.7(4)	H(12A)-C(12)-H(12B)	109.5
C(3)-C(4)-H(4)	120.6	N(3)-C(12)-H(12C)	109.5
C(5)-C(4)-H(4)	120.6	H(12A)-C(12)-H(12C)	109.5
N(1)-C(5)-C(4)	122.7(4)	H(12B)-C(12)-H(12C)	109.5
N(1)-C(5)-H(5)	118.7	N(3)-C(13)-H(13A)	109.5
C(4)-C(5)-H(5)	118.7	N(3)-C(13)-H(13B)	109.5
C(10)-N(2)-C(6)	116.8(3)	H(13A)-C(13)-H(13B)	109.5
C(10)-N(2)-Cr(1)	122.0(2)	N(3)-C(13)-H(13C)	109.5
C(6)-N(2)-Cr(1)	121.1(2)	H(13A)-C(13)-H(13C)	109.5
N(2)-C(6)-C(7)	123.4(4)	H(13B)-C(13)-H(13C)	109.5
N(2)-C(6)-H(6)	118.3	C(14)-N(4)-C(16)	120.8(4)
C(7)-C(6)-H(6)	118.3	C(14)-N(4)-C(15)	121.9(4)
C(8)-C(7)-C(6)	118.4(4)	C(16)-N(4)-C(15)	117.3(4)
C(8)-C(7)-H(7)	120.8	O(2)-C(14)-N(4)	125.8(5)
C(6)-C(7)-H(7)	120.8	O(2)-C(14)-H(14)	117.1
C(7)-C(8)-C(9)	119.8(4)	N(4)-C(14)-H(14)	117.1
C(7)-C(8)-H(8)	120.1	N(4)-C(15)-H(15A)	109.5

N(4)-C(15)-H(15B)	109.5	N(4)-C(16)-H(16B)	109.5
H(15A)-C(15)-H(15B)	109.5	H(16A)-C(16)-H(16B)	109.5
N(4)-C(15)-H(15C)	109.5	N(4)-C(16)-H(16C)	109.5
H(15A)-C(15)-H(15C)	109.5	H(16A)-C(16)-H(16C)	109.5
H(15B)-C(15)-H(15C)	109.5	H(16B)-C(16)-H(16C)	109.5
N(4)-C(16)-H(16A)	109.5		

Table A.14 **Anisotropic displacement parameters ($Å^2 x\ 10^3$) for $[CrCl_3(py)_2(DMF)]$. The anisotropic displacement factor exponent takes the form: $-2p^2[h^2a^{*2}U^{11} + ... + 2\ h\ k\ a^*\ b^*\ U^{12}]$**

	U^{11}	U^{22}	U^{33}	U^{23}	U^{13}	U^{12}
Cr(1)	31(1)	38(1)	32(1)	3(1)	4(1)	0(1)
Cl(1)	62(1)	52(1)	41(1)	12(1)	15(1)	7(1)
Cl(2)	36(1)	49(1)	54(1)	-4(1)	-3(1)	-4(1)
Cl(3)	47(1)	56(1)	59(1)	-11(1)	2(1)	-12(1)
N(1)	39(1)	44(2)	39(1)	3(1)	6(1)	4(1)
C(1)	60(2)	50(2)	41(2)	4(2)	7(2)	6(2)
C(2)	78(3)	54(2)	54(2)	0(2)	2(2)	26(2)
C(3)	65(3)	86(3)	49(2)	-3(2)	5(2)	34(3)
C(4)	47(2)	82(3)	51(2)	5(2)	12(2)	17(2)
C(5)	44(2)	58(2)	47(2)	8(2)	10(2)	6(2)
N(2)	33(1)	50(2)	34(1)	3(1)	2(1)	2(1)
C(6)	40(2)	52(2)	43(2)	6(2)	2(1)	9(2)
C(7)	74(3)	64(3)	53(2)	1(2)	1(2)	25(2)
C(8)	59(3)	106(4)	50(2)	9(2)	9(2)	45(3)
C(9)	38(2)	98(4)	56(2)	9(2)	10(2)	14(2)
C(10)	36(2)	68(3)	48(2)	7(2)	6(1)	0(2)
O(1)	38(1)	58(1)	35(1)	8(1)	2(1)	2(1)
N(3)	48(2)	53(2)	31(1)	1(1)	1(1)	-1(1)
C(11)	42(2)	46(2)	39(2)	3(1)	3(1)	6(2)

C(12)	67(3)	165(6)	50(2)	27(3)	10(2)	-24(3)
C(13)	73(3)	62(2)	44(2)	5(2)	-10(2)	9(2)
O(2)	122(3)	70(2)	90(2)	21(2)	22(2)	0(2)
N(4)	60(2)	59(2)	48(2)	1(1)	3(1)	-10(2)
C(14)	88(3)	64(3)	57(2)	-1(2)	14(2)	-13(3)
C(15)	65(3)	61(3)	80(3)	-6(2)	-1(2)	-5(2)
C(16)	86(3)	101(4)	63(3)	20(3)	4(2)	-4(3)

Table A.15 **Hydrogen coordinates (x 10^4) and isotropic displacement parameters (Å^{2}x 10^3) for $[CrCl_3(py)_2(DMF)]$**

	x	y	z	U(eq)
H(1)	2890	11451	3247	61
H(2)	989	12472	3897	75
H(3)	-1004	11792	5068	80
H(4)	-1024	10090	5553	72
H(5)	929	9109	4841	59
H(6)	4532	7014	3309	54
H(7)	6317	5894	2644	76
H(8)	8540	6491	1856	86
H(9)	8921	8204	1717	76
H(10)	7056	9266	2363	61
H(11)	5680	8572	6170	51
H(12A)	2196	8055	7298	141
H(12B)	2791	7844	8944	141
H(12C)	2841	6995	7750	141
H(13A)	5722	7167	8985	90
H(13B)	5368	8218	9654	90
H(13C)	6554	8126	8462	90
H(14)	-583	4183	655	83

H(15A)	2737	5139	2143	104
H(15B)	2509	6174	1332	104
H(15C)	3253	5277	535	104
H(16A)	-640	5450	-889	125
H(16B)	956	5620	-1476	125
H(16C)	315	6394	-378	125

Table A.16 Torsion angles [°] for [$CrCl_3(py)_2(DMF)$]

O(1)-Cr(1)-N(1)-C(1)	140.8(2)	Cl(1)-Cr(1)-N(2)-C(6)	-126.2(2)
Cl(1)-Cr(1)-N(1)-C(1)	-41.2(2)	Cl(3)-Cr(1)-N(2)-C(6)	141.7(2)
Cl(3)-Cr(1)-N(1)-C(1)	50.9(2)	Cl(2)-Cr(1)-N(2)-C(6)	-36.1(2)
Cl(2)-Cr(1)-N(1)-C(1)	-131.3(2)	C(10)-N(2)-C(6)-C(7)	-1.0(5)
O(1)-Cr(1)-N(1)-C(5)	-39.7(2)	Cr(1)-N(2)-C(6)-C(7)	175.6(3)
Cl(1)-Cr(1)-N(1)-C(5)	138.2(2)	N(2)-C(6)-C(7)-C(8)	1.0(5)
Cl(3)-Cr(1)-N(1)-C(5)	-129.7(2)	C(6)-C(7)-C(8)-C(9)	-0.4(6)
Cl(2)-Cr(1)-N(1)-C(5)	48.2(2)	C(7)-C(8)-C(9)-C(10)	-0.2(6)
C(5)-N(1)-C(1)-C(2)	0.0(5)	C(6)-N(2)-C(10)-C(9)	0.3(5)
Cr(1)-N(1)-C(1)-C(2)	179.5(3)	Cr(1)-N(2)-C(10)-C(9)	-176.2(3)
N(1)-C(1)-C(2)-C(3)	0.2(6)	C(8)-C(9)-C(10)-N(2)	0.3(5)
C(1)-C(2)-C(3)-C(4)	-0.1(6)	N(1)-Cr(1)-O(1)-C(11)	-121.5(3)
C(2)-C(3)-C(4)-C(5)	-0.2(6)	N(2)-Cr(1)-O(1)-C(11)	58.1(3)
C(1)-N(1)-C(5)-C(4)	-0.3(5)	Cl(3)-Cr(1)-O(1)-C(11)	-32.2(3)
Cr(1)-N(1)-C(5)-C(4)	-179.8(3)	Cl(2)-Cr(1)-O(1)-C(11)	149.0(3)
C(3)-C(4)-C(5)-N(1)	0.4(6)	Cr(1)-O(1)-C(11)-N(3)	171.1(3)
O(1)-Cr(1)-N(2)-C(10)	-131.9(2)	C(12)-N(3)-C(11)-O(1)	1.7(6)
Cl(1)-Cr(1)-N(2)-C(10)	50.2(2)	C(13)-N(3)-C(11)-O(1)	179.0(3)
Cl(3)-Cr(1)-N(2)-C(10)	-42.0(2)	C(16)-N(4)-C(14)-O(2)	179.1(5)
Cl(2)-Cr(1)-N(2)-C(10)	140.2(2)	C(15)-N(4)-C(14)-O(2)	1.1(7)
O(1)-Cr(1)-N(2)-C(6)	51.8(2)		

[$CrCl_3(pytb)_3$]

Table A.17 **Atomic coordinates (x 10^4) and equivalent isotropic displacement parameters ($Å^2$x 10^3) for [$CrCl_3(pytb)_3$]. U(eq) is defined as one-third of the trace of the orthogonalised U^{ij} tensor**

	x	y	z	U(eq)
Cr(1)	8089(1)	511(1)	3464(1)	47(1)
Cl(1)	7480(1)	89(1)	2524(1)	64(1)
Cl(2)	8604(1)	930(1)	2390(1)	84(1)
Cl(3)	8641(1)	897(1)	4523(1)	68(1)
N(1)	8288(1)	4(1)	3358(2)	51(1)
C(1)	8734(1)	127(1)	3339(3)	71(1)
C(2)	8885(1)	-187(1)	3282(3)	80(1)
C(3)	8578(1)	-655(1)	3255(2)	60(1)
C(4)	8115(1)	-782(1)	3281(2)	62(1)
C(5)	7988(1)	-449(1)	3326(2)	55(1)
C(6)	8745(1)	-1007(1)	3211(3)	77(1)
C(7)	8949(2)	-1012(2)	4085(3)	108(2)
C(8)	8350(2)	-1493(2)	3011(4)	111(2)
C(9)	9111(2)	-866(2)	2505(3)	99(2)
N(11)	7633(1)	109(1)	4467(1)	46(1)
C(11)	7745(1)	-121(1)	5034(2)	51(1)
C(12)	7456(1)	-391(1)	5673(2)	54(1)
C(13)	7030(1)	-422(1)	5800(2)	48(1)
C(14)	6923(1)	-173(1)	5230(2)	55(1)
C(15)	7219(1)	73(1)	4575(2)	54(1)
C(16)	6717(1)	-696(1)	6536(2)	69(1)
C(17)	6984(2)	-450(2)	7373(3)	141(2)
C(18)	6277(2)	-679(2)	6561(3)	121(2)
C(19)	6632(2)	-1177(2)	6541(5)	165(3)

N(21)	7876(1)	1008(1)	3541(1)	49(1)
C(21)	7787(1)	1153(1)	4278(2)	57(1)
C(22)	7604(1)	1440(1)	4317(2)	59(1)
C(23)	7508(1)	1608(1)	3576(2)	51(1)
C(24)	7619(1)	1471(1)	2821(2)	56(1)
C(25)	7792(1)	1175(1)	2827(2)	57(1)
C(26)	7309(1)	1933(1)	3609(2)	64(1)
C(27)	7688(2)	2400(2)	3879(6)	193(4)
C(28)	7112(2)	1961(2)	2752(3)	135(2)
C(29)	6913(2)	1757(2)	4242(3)	105(2)
O(31)	4990(4)	191(3)	270(6)	128(3)
C(31)	5777(10)	279(11)	220(30)	188(16)
C(32)	5520(20)	188(19)	703(18)	290(30)
C(33)	4730(11)	-79(12)	-160(30)	260(20)
C(34)	4412(19)	-133(16)	-100(20)	230(20)
C(41)	7101(18)	3670(30)	3810(40)	380(30)
C(42)	7020(30)	3630(30)	2980(40)	390(30)

Table A.18 **Bond lengths [Å] and angles [°] for $[CrCl_3(pytb)_3]$**

Cr(1)-N(1)	2.105(2)	C(1)-H(1)	0.9300
Cr(1)-N(21)	2.105(2)	C(2)-C(3)	1.375(5)
Cr(1)-N(11)	2.130(2)	C(2)-H(2)	0.9300
Cr(1)-Cl(2)	2.3056(9)	C(3)-C(4)	1.379(4)
Cr(1)-Cl(1)	2.3248(9)	C(3)-C(6)	1.530(5)
Cr(1)-Cl(3)	2.3263(9)	C(4)-C(5)	1.375(4)
N(1)-C(5)	1.332(4)	C(4)-H(4)	0.9300
N(1)-C(1)	1.332(4)	C(5)-H(5)	0.9300
C(1)-C(2)	1.368(5)	C(6)-C(8)	1.525(6)

C(6)-C(7)	1.532(6)	C(19)-H(19A)	0.9600
C(6)-C(9)	1.534(5)	C(19)-H(19B)	0.9600
C(7)-H(7A)	0.9600	C(19)-H(19C)	0.9600
C(7)-H(7B)	0.9600	N(21)-C(25)	1.338(4)
C(7)-H(7C)	0.9600	N(21)-C(21)	1.341(4)
C(8)-H(8A)	0.9600	C(21)-C(22)	1.369(4)
C(8)-H(8B)	0.9600	C(21)-H(21)	0.9300
C(8)-H(8C)	0.9600	C(22)-C(23)	1.391(4)
C(9)-H(9A)	0.9600	C(22)-H(22)	0.9300
C(9)-H(9B)	0.9600	C(23)-C(24)	1.381(4)
C(9)-H(9C)	0.9600	C(23)-C(26)	1.528(4)
N(11)-C(15)	1.331(4)	C(24)-C(25)	1.370(4)
N(11)-C(11)	1.342(4)	C(24)-H(24)	0.9300
C(11)-C(12)	1.369(4)	C(25)-H(25)	0.9300
C(11)-H(11)	0.9300	C(26)-C(27)	1.493(6)
C(12)-C(13)	1.386(4)	C(26)-C(29)	1.513(5)
C(12)-H(12)	0.9300	C(26)-C(28)	1.517(6)
C(13)-C(14)	1.380(4)	C(27)-H(27A)	0.9600
C(13)-C(16)	1.516(4)	C(27)-H(27B)	0.9600
C(14)-C(15)	1.374(4)	C(27)-H(27C)	0.9600
C(14)-H(14)	0.9300	C(28)-H(28A)	0.9600
C(15)-H(15)	0.9300	C(28)-H(28B)	0.9600
C(16)-C(19)	1.480(6)	C(28)-H(28C)	0.9600
C(16)-C(18)	1.497(6)	C(29)-H(29A)	0.9600
C(16)-C(17)	1.564(7)	C(29)-H(29B)	0.9600
C(17)-H(17A)	0.9600	C(29)-H(29C)	0.9600
C(17)-H(17B)	0.9600	O(31)-C(33)	1.11(3)
C(17)-H(17C)	0.9600	O(31)-C(32)	1.90(5)
C(18)-H(18A)	0.9600	C(31)-C(32)	1.07(5)
C(18)-H(18B)	0.9600	C(31)-H(31A)	0.9600
C(18)-H(18C)	0.9600	C(31)-H(31B)	0.9600

C(31)-H(31C)	0.9600	C(2)-C(1)-H(1)	118.4
C(32)-H(32A)	0.9700	C(1)-C(2)-C(3)	121.4(3)
C(32)-H(32B)	0.9700	C(1)-C(2)-H(2)	119.3
C(33)-C(34)	0.99(4)	C(3)-C(2)-H(2)	119.3
C(33)-H(33A)	0.9700	C(2)-C(3)-C(4)	115.5(3)
C(33)-H(33B)	0.9700	C(2)-C(3)-C(6)	121.5(3)
C(34)-H(34A)	0.9600	C(4)-C(3)-C(6)	123.1(3)
C(34)-H(34B)	0.9600	C(5)-C(4)-C(3)	120.2(3)
C(34)-H(34C)	0.9600	C(5)-C(4)-H(4)	119.9
C(41)-C(42)#1	1.18(7)	C(3)-C(4)-H(4)	119.9
C(41)-C(42)#2	1.29(7)	N(1)-C(5)-C(4)	123.9(3)
N(1)-Cr(1)-N(21)	178.27(10)	N(1)-C(5)-H(5)	118.0
N(1)-Cr(1)-N(11)	88.03(9)	C(4)-C(5)-H(5)	118.0
N(21)-Cr(1)-N(11)	92.08(9)	C(8)-C(6)-C(3)	111.8(3)
N(1)-Cr(1)-Cl(2)	89.49(7)	C(8)-C(6)-C(7)	108.8(4)
N(21)-Cr(1)-Cl(2)	90.44(7)	C(3)-C(6)-C(7)	107.6(3)
N(11)-Cr(1)-Cl(2)	177.30(7)	C(8)-C(6)-C(9)	108.0(4)
N(1)-Cr(1)-Cl(1)	89.70(7)	C(3)-C(6)-C(9)	109.7(3)
N(21)-Cr(1)-Cl(1)	88.57(7)	C(7)-C(6)-C(9)	111.0(4)
N(11)-Cr(1)-Cl(1)	87.32(7)	C(6)-C(7)-H(7A)	109.5
Cl(2)-Cr(1)-Cl(1)	93.73(4)	C(6)-C(7)-H(7B)	109.5
N(1)-Cr(1)-Cl(3)	91.18(7)	H(7A)-C(7)-H(7B)	109.5
N(21)-Cr(1)-Cl(3)	90.55(7)	C(6)-C(7)-H(7C)	109.5
N(11)-Cr(1)-Cl(3)	86.58(7)	H(7A)-C(7)-H(7C)	109.5
Cl(2)-Cr(1)-Cl(3)	92.41(4)	H(7B)-C(7)-H(7C)	109.5
Cl(1)-Cr(1)-Cl(3)	173.80(4)	C(6)-C(8)-H(8A)	109.5
C(5)-N(1)-C(1)	115.8(3)	C(6)-C(8)-H(8B)	109.5
C(5)-N(1)-Cr(1)	123.7(2)	H(8A)-C(8)-H(8B)	109.5
C(1)-N(1)-Cr(1)	120.5(2)	C(6)-C(8)-H(8C)	109.5
N(1)-C(1)-C(2)	123.2(3)	H(8A)-C(8)-H(8C)	109.5
N(1)-C(1)-H(1)	118.4	H(8B)-C(8)-H(8C)	109.5

C(6)-C(9)-H(9A)	109.5	C(16)-C(17)-H(17B)	109.5
C(6)-C(9)-H(9B)	109.5	H(17A)-C(17)-H(17B)	109.5
H(9A)-C(9)-H(9B)	109.5	C(16)-C(17)-H(17C)	109.5
C(6)-C(9)-H(9C)	109.5	H(17A)-C(17)-H(17C)	109.5
H(9A)-C(9)-H(9C)	109.5	H(17B)-C(17)-H(17C)	109.5
H(9B)-C(9)-H(9C)	109.5	C(16)-C(18)-H(18A)	109.5
C(15)-N(11)-C(11)	115.9(2)	C(16)-C(18)-H(18B)	109.5
C(15)-N(11)-Cr(1)	122.07(19)	H(18A)-C(18)-H(18B)	109.5
C(11)-N(11)-Cr(1)	122.06(18)	C(16)-C(18)-H(18C)	109.5
N(11)-C(11)-C(12)	123.6(3)	H(18A)-C(18)-H(18C)	109.5
N(11)-C(11)-H(11)	118.2	H(18B)-C(18)-H(18C)	109.5
C(12)-C(11)-H(11)	118.2	C(16)-C(19)-H(19A)	109.5
C(11)-C(12)-C(13)	120.7(3)	C(16)-C(19)-H(19B)	109.5
C(11)-C(12)-H(12)	119.7	H(19A)-C(19)-H(19B)	109.5
C(13)-C(12)-H(12)	119.7	C(16)-C(19)-H(19C)	109.5
C(14)-C(13)-C(12)	115.2(3)	H(19A)-C(19)-H(19C)	109.5
C(14)-C(13)-C(16)	123.2(3)	H(19B)-C(19)-H(19C)	109.5
C(12)-C(13)-C(16)	121.5(3)	C(25)-N(21)-C(21)	116.0(3)
C(15)-C(14)-C(13)	121.1(3)	C(25)-N(21)-Cr(1)	120.1(2)
C(15)-C(14)-H(14)	119.4	C(21)-N(21)-Cr(1)	123.7(2)
C(13)-C(14)-H(14)	119.4	N(21)-C(21)-C(22)	123.1(3)
N(11)-C(15)-C(14)	123.4(3)	N(21)-C(21)-H(21)	118.4
N(11)-C(15)-H(15)	118.3	C(22)-C(21)-H(21)	118.4
C(14)-C(15)-H(15)	118.3	C(21)-C(22)-C(23)	121.1(3)
C(19)-C(16)-C(18)	112.3(4)	C(21)-C(22)-H(22)	119.5
C(19)-C(16)-C(13)	111.0(3)	C(23)-C(22)-H(22)	119.5
C(18)-C(16)-C(13)	112.8(3)	C(24)-C(23)-C(22)	115.3(3)
C(19)-C(16)-C(17)	108.4(5)	C(24)-C(23)-C(26)	123.1(3)
C(18)-C(16)-C(17)	105.5(4)	C(22)-C(23)-C(26)	121.6(3)
C(13)-C(16)-C(17)	106.3(3)	C(25)-C(24)-C(23)	120.7(3)
C(16)-C(17)-H(17A)	109.5	C(25)-C(24)-H(24)	119.7

C(23)-C(24)-H(24)	119.7	C(33)-O(31)-C(32)	124(2)
N(21)-C(25)-C(24)	123.8(3)	C(32)-C(31)-H(31A)	109.5
N(21)-C(25)-H(25)	118.1	C(32)-C(31)-H(31B)	109.5
C(24)-C(25)-H(25)	118.1	H(31A)-C(31)-H(31B)	109.5
C(27)-C(26)-C(29)	109.8(5)	C(32)-C(31)-H(31C)	109.5
C(27)-C(26)-C(28)	110.7(5)	H(31A)-C(31)-H(31C)	109.5
C(29)-C(26)-C(28)	106.4(4)	H(31B)-C(31)-H(31C)	109.5
C(27)-C(26)-C(23)	107.7(3)	C(31)-C(32)-O(31)	111(3)
C(29)-C(26)-C(23)	110.6(3)	C(31)-C(32)-H(32A)	109.4
C(28)-C(26)-C(23)	111.6(3)	O(31)-C(32)-H(32A)	109.4
C(26)-C(27)-H(27A)	109.5	C(31)-C(32)-H(32B)	109.4
C(26)-C(27)-H(27B)	109.5	O(31)-C(32)-H(32B)	109.4
H(27A)-C(27)-H(27B)	109.5	H(32A)-C(32)-H(32B)	108.0
C(26)-C(27)-H(27C)	109.5	C(34)-C(33)-O(31)	115(3)
H(27A)-C(27)-H(27C)	109.5	C(34)-C(33)-H(33A)	108.6
H(27B)-C(27)-H(27C)	109.5	O(31)-C(33)-H(33A)	108.6
C(26)-C(28)-H(28A)	109.5	C(34)-C(33)-H(33B)	108.6
C(26)-C(28)-H(28B)	109.5	O(31)-C(33)-H(33B)	108.6
H(28A)-C(28)-H(28B)	109.5	H(33A)-C(33)-H(33B)	107.6
C(26)-C(28)-H(28C)	109.5	C(33)-C(34)-H(34A)	109.5
H(28A)-C(28)-H(28C)	109.5	C(33)-C(34)-H(34B)	109.5
H(28B)-C(28)-H(28C)	109.5	H(34A)-C(34)-H(34B)	109.5
C(26)-C(29)-H(29A)	109.5	C(33)-C(34)-H(34C)	109.5
C(26)-C(29)-H(29B)	109.5	H(34A)-C(34)-H(34C)	109.5
H(29A)-C(29)-H(29B)	109.5	H(34B)-C(34)-H(34C)	109.5
C(26)-C(29)-H(29C)	109.5	C(42)#1-C(41)-C(42)#2	101(6)
H(29A)-C(29)-H(29C)	109.5	C(41)#2-C(42)-C(41)#1	134(9)
H(29B)-C(29)-H(29C)	109.5		

Symmetry transformations used to generate equivalent atoms:

#1 y+1/3,-x+y+2/3,-z+2/3 #2 x-y+1/3,x-1/3,-z+2/3

Table A.19 **Anisotropic displacement parameters ($Å^2 x\ 10^3$) for $[CrCl_3(pytb)_3]$. The anisotropic displacement factor exponent takes the form: $-2p^2[h^2a^{*2}U^{11} + ... + 2\ h\ k\ a^*\ b^*\ U^{12}]$**

	U^{11}	U^{22}	U^{33}	U^{23}	U^{13}	U^{12}
Cr(1)	45(1)	48(1)	47(1)	5(1)	5(1)	23(1)
Cl(1)	74(1)	70(1)	56(1)	-10(1)	-16(1)	43(1)
Cl(2)	93(1)	81(1)	87(1)	34(1)	45(1)	49(1)
Cl(3)	53(1)	59(1)	83(1)	-5(1)	-14(1)	21(1)
N(1)	42(1)	54(2)	58(1)	4(1)	8(1)	24(1)
C(1)	44(2)	55(2)	107(3)	9(2)	12(2)	20(2)
C(2)	47(2)	76(3)	121(3)	9(2)	14(2)	33(2)
C(3)	62(2)	69(2)	63(2)	14(2)	14(2)	43(2)
C(4)	63(2)	50(2)	74(2)	8(2)	13(2)	29(2)
C(5)	44(2)	57(2)	64(2)	2(2)	5(1)	26(2)
C(6)	86(3)	88(3)	83(2)	23(2)	18(2)	63(2)
C(7)	141(4)	139(4)	95(3)	25(3)	8(3)	108(4)
C(8)	122(4)	82(3)	153(5)	19(3)	24(3)	70(3)
C(9)	112(4)	126(4)	100(3)	22(3)	34(3)	91(3)
N(11)	40(1)	52(1)	47(1)	2(1)	0(1)	23(1)
C(11)	44(2)	64(2)	51(2)	4(1)	1(1)	32(2)
C(12)	62(2)	59(2)	50(2)	6(1)	1(1)	37(2)
C(13)	51(2)	41(2)	54(2)	-1(1)	6(1)	24(1)
C(14)	46(2)	59(2)	67(2)	11(2)	9(1)	32(2)
C(15)	48(2)	56(2)	64(2)	12(1)	1(1)	30(2)
C(16)	68(2)	63(2)	79(2)	21(2)	27(2)	35(2)
C(17)	150(5)	160(5)	65(3)	19(3)	31(3)	42(4)
C(18)	105(4)	135(4)	136(4)	54(4)	70(3)	69(3)
C(19)	183(6)	64(3)	248(8)	69(4)	132(6)	61(4)
N(21)	53(1)	46(1)	45(1)	3(1)	2(1)	23(1)

C(21)	69(2)	58(2)	43(2)	5(1)	1(1)	32(2)
C(22)	75(2)	58(2)	49(2)	3(1)	8(2)	37(2)
C(23)	46(2)	44(2)	56(2)	6(1)	4(1)	18(1)
C(24)	67(2)	57(2)	46(2)	7(1)	-2(1)	33(2)
C(25)	72(2)	61(2)	42(2)	-1(1)	1(1)	36(2)
C(26)	67(2)	58(2)	72(2)	9(2)	8(2)	36(2)
C(27)	111(4)	60(3)	418(14)	-43(5)	-47(6)	50(3)
C(28)	192(6)	219(7)	92(3)	37(4)	23(4)	176(6)
C(29)	120(4)	137(4)	97(3)	29(3)	35(3)	95(4)
O(31)	170(9)	125(7)	112(6)	8(5)	0(6)	91(7)
C(31)	119(13)	210(20)	200(30)	80(20)	-32(15)	60(13)
C(32)	520(70)	350(50)	140(20)	150(30)	160(40)	330(50)
C(33)	160(20)	250(30)	390(50)	-200(30)	10(20)	100(20)
C(34)	320(70)	280(40)	160(20)	-80(30)	-30(30)	210(50)
C(41)	410(60)	400(90)	410(80)	220(60)	230(50)	260(60)
C(42)	510(90)	360(70)	370(60)	240(60)	290(60)	260(50)

Table A.20 **Hydrogen coordinates (x 10^4) and isotropic displacement parameters ($Å^2$x 10^3) for $[CrCl_3(pytb)_3]$**

	x	y	z	U(eq)
H(1)	8954	440	3366	85
H(2)	9201	-80	3262	96
H(4)	7889	-1094	3269	74
H(5)	7673	-546	3335	66
H(7A)	9229	-723	4176	162
H(7B)	9016	-1261	4104	162
H(7C)	8729	-1057	4524	162

H(8A)	8110	-1583	3430	166
H(8B)	8464	-1707	3024	166
H(8C)	8228	-1497	2454	166
H(9A)	8992	-816	1981	148
H(9B)	9183	-1109	2424	148
H(9C)	9386	-586	2667	148
H(11)	8035	-95	4989	61
H(12)	7546	-557	6026	64
H(14)	6647	-171	5291	66
H(15)	7126	221	4186	65
H(17A)	6776	-566	7850	211
H(17B)	7106	-122	7321	211
H(17C)	7234	-510	7460	211
H(18A)	6095	-829	6063	181
H(18B)	6349	-361	6572	181
H(18C)	6104	-834	7065	181
H(19A)	6483	-1328	6017	248
H(19B)	6435	-1343	7014	248
H(19C)	6921	-1172	6594	248
H(21)	7852	1054	4788	68
H(22)	7542	1525	4846	71
H(24)	7575	1581	2304	67
H(25)	7855	1085	2305	68
H(27A)	7565	2603	3962	289
H(27B)	7923	2524	3444	289
H(27C)	7822	2372	4404	289
H(28A)	6897	1654	2555	203
H(28B)	7359	2112	2346	203
H(28C)	6954	2135	2812	203
H(29A)	7022	1736	4798	157
H(29B)	6670	1457	4067	157

H(29C)	6796	1968	4262	157
H(31A)	5662	44	-216	282
H(31B)	6053	306	466	282
H(31C)	5848	571	-32	282
H(32A)	5649	406	1173	350
H(32B)	5429	-119	921	350
H(33A)	4830	10	-748	316
H(33B)	4726	-368	-54	316
H(34A)	4414	96	274	340
H(34B)	4215	-436	133	340
H(34C)	4296	-112	-651	340

Table A.21 Torsion angles [°] for $[CrCl_3(pytb)_3]$

N(11)-Cr(1)-N(1)-C(5)	47.5(2)	Cr(1)-N(1)-C(5)-C(4)	-178.1(2)
Cl(2)-Cr(1)-N(1)-C(5)	-133.5(2)	C(3)-C(4)-C(5)-N(1)	-0.9(5)
Cl(1)-Cr(1)-N(1)-C(5)	-39.8(2)	C(2)-C(3)-C(6)-C(8)	-168.8(4)
Cl(3)-Cr(1)-N(1)-C(5)	134.1(2)	C(4)-C(3)-C(6)-C(8)	12.1(5)
N(11)-Cr(1)-N(1)-C(1)	-130.8(3)	C(2)-C(3)-C(6)-C(7)	71.8(5)
Cl(2)-Cr(1)-N(1)-C(1)	48.1(3)	C(4)-C(3)-C(6)-C(7)	-107.3(4)
Cl(1)-Cr(1)-N(1)-C(1)	141.9(3)	C(2)-C(3)-C(6)-C(9)	-49.1(5)
Cl(3)-Cr(1)-N(1)-C(1)	-44.3(3)	C(4)-C(3)-C(6)-C(9)	131.8(4)
C(5)-N(1)-C(1)-C(2)	0.7(5)	N(1)-Cr(1)-N(11)-C(15)	-143.5(2)
Cr(1)-N(1)-C(1)-C(2)	179.1(3)	N(21)-Cr(1)-N(11)-C(15)	34.8(2)
N(1)-C(1)-C(2)-C(3)	-1.1(7)	Cl(1)-Cr(1)-N(11)-C(15)	-53.7(2)
C(1)-C(2)-C(3)-C(4)	0.5(6)	Cl(3)-Cr(1)-N(11)-C(15)	125.2(2)
C(1)-C(2)-C(3)-C(6)	-178.7(4)	N(1)-Cr(1)-N(11)-C(11)	36.9(2)
C(2)-C(3)-C(4)-C(5)	0.4(5)	N(21)-Cr(1)-N(11)-C(11)	-144.9(2)
C(6)-C(3)-C(4)-C(5)	179.6(3)	Cl(1)-Cr(1)-N(11)-C(11)	126.7(2)
C(1)-N(1)-C(5)-C(4)	0.3(5)	Cl(3)-Cr(1)-N(11)-C(11)	-54.4(2)

C(15)-N(11)-C(11)-C(12)	2.0(4)	N(11)-Cr(1)-N(21)-C(21)	39.0(2)
Cr(1)-N(11)-C(11)-C(12)	-178.3(2)	Cl(2)-Cr(1)-N(21)-C(21)	-140.0(2)
N(11)-C(11)-C(12)-C(13)	-3.6(5)	Cl(1)-Cr(1)-N(21)-C(21)	126.3(2)
C(11)-C(12)-C(13)-C(14)	1.5(4)	Cl(3)-Cr(1)-N(21)-C(21)	-47.5(2)
C(11)-C(12)-C(13)-C(16)	-176.3(3)	C(25)-N(21)-C(21)-C(22)	2.5(5)
C(12)-C(13)-C(14)-C(15)	1.9(5)	Cr(1)-N(21)-C(21)-C(22)	-173.2(2)
C(16)-C(13)-C(14)-C(15)	179.7(3)	N(21)-C(21)-C(22)-C(23)	-1.4(5)
C(11)-N(11)-C(15)-C(14)	1.6(4)	C(21)-C(22)-C(23)-C(24)	-1.1(5)
Cr(1)-N(11)-C(15)-C(14)	-178.1(2)	C(21)-C(22)-C(23)-C(26)	-179.4(3)
C(13)-C(14)-C(15)-N(11)	-3.7(5)	C(22)-C(23)-C(24)-C(25)	2.6(5)
C(14)-C(13)-C(16)-C(19)	128.8(5)	C(26)-C(23)-C(24)-C(25)	-179.2(3)
C(12)-C(13)-C(16)-C(19)	-53.6(5)	C(21)-N(21)-C(25)-C(24)	-1.0(5)
C(14)-C(13)-C(16)-C(18)	1.7(5)	Cr(1)-N(21)-C(25)-C(24)	174.9(3)
C(12)-C(13)-C(16)-C(18)	179.3(4)	C(23)-C(24)-C(25)-N(21)	-1.6(5)
C(14)-C(13)-C(16)-C(17)	-113.5(4)	C(24)-C(23)-C(26)-C(27)	-104.0(5)
C(12)-C(13)-C(16)-C(17)	64.2(4)	C(22)-C(23)-C(26)-C(27)	74.2(5)
N(11)-Cr(1)-N(21)-C(25)	-136.5(2)	C(24)-C(23)-C(26)-C(29)	136.0(4)
Cl(2)-Cr(1)-N(21)-C(25)	44.5(2)	C(22)-C(23)-C(26)-C(29)	-45.9(5)
Cl(1)-Cr(1)-N(21)-C(25)	-49.2(2)	C(24)-C(23)-C(26)-C(28)	17.8(5)
Cl(3)-Cr(1)-N(21)-C(25)	136.9(2)	C(22)-C(23)-C(26)-C(28)	-164.1(4)

Symmetry transformations used to generate equivalent atoms:

#1 y+1/3,-x+y+2/3,-z+2/3 #2 x-y+1/3,x-1/3,-z+2/3

[$CrCl_3(bipy)(H_2O)$]

Table A.22 **Atomic coordinates (x 10^4) and equivalent isotropic displacement parameters ($Å^2$x 10^3) for [$CrCl_3(bipy)(H_2O)$]. U(eq) is defined as one-third of the trace of the orthogonalised U^{ij} tensor**

	x	y	z	U(eq)
Cr(1)	8853(1)	1809(1)	8330(1)	34(1)
Cl(1)	9614(1)	1872(1)	9761(1)	51(1)
Cl(2)	8148(1)	1943(1)	6740(1)	44(1)
Cl(3)	8699(1)	-360(1)	8875(1)	57(1)
N(1)	8973(1)	3795(2)	8041(2)	36(1)
N(2)	8460(1)	2637(2)	9782(2)	36(1)
C(1)	8733(1)	4622(3)	8802(3)	40(1)
C(2)	8810(1)	5977(3)	8774(3)	49(1)
C(3)	9132(1)	6471(3)	7918(4)	58(1)
C(4)	9368(1)	5619(3)	7126(3)	54(1)
C(5)	9284(1)	4277(3)	7222(3)	46(1)
C(6)	8412(1)	3967(3)	9704(3)	39(1)
C(7)	8092(1)	4634(3)	10455(3)	50(1)
C(8)	7838(1)	3935(3)	11342(3)	55(1)
C(9)	7907(1)	2605(3)	11469(3)	52(1)
C(10)	8216(1)	1970(3)	10664(3)	43(1)
O(1)	9231(1)	1302(2)	6791(2)	46(1)
O(2)	10000	-352(3)	7500	49(1)

Table A.23 Bond lengths [Å] and angles [°] for [$CrCl_3$(bipy)(H_2O)]

Cr(1)-O(1)	2.003(2)	O(2)-H(2A)	0.84(3)
Cr(1)-N(1)	2.059(2)	O(1)-Cr(1)-N(1)	92.28(9)
Cr(1)-N(2)	2.066(2)	O(1)-Cr(1)-N(2)	170.71(9)
Cr(1)-Cl(3)	2.3083(8)	N(1)-Cr(1)-N(2)	78.79(9)
Cr(1)-Cl(2)	2.3114(8)	O(1)-Cr(1)-Cl(3)	93.31(7)
Cr(1)-Cl(1)	2.3435(8)	N(1)-Cr(1)-Cl(3)	174.10(6)
N(1)-C(5)	1.331(4)	N(2)-Cr(1)-Cl(3)	95.70(7)
N(1)-C(1)	1.345(3)	O(1)-Cr(1)-Cl(2)	87.50(7)
N(2)-C(10)	1.341(3)	N(1)-Cr(1)-Cl(2)	88.83(6)
N(2)-C(6)	1.353(4)	N(2)-Cr(1)-Cl(2)	89.74(6)
C(1)-C(2)	1.386(4)	Cl(3)-Cr(1)-Cl(2)	93.26(3)
C(1)-C(6)	1.476(4)	O(1)-Cr(1)-Cl(1)	88.28(7)
C(2)-C(3)	1.382(5)	N(1)-Cr(1)-Cl(1)	85.16(6)
C(2)-H(2)	0.9300	N(2)-Cr(1)-Cl(1)	93.46(6)
C(3)-C(4)	1.374(5)	Cl(3)-Cr(1)-Cl(1)	93.16(3)
C(3)-H(3)	0.9300	Cl(2)-Cr(1)-Cl(1)	172.51(3)
C(4)-C(5)	1.381(4)	C(5)-N(1)-C(1)	119.9(2)
C(4)-H(4)	0.9300	C(5)-N(1)-Cr(1)	124.3(2)
C(5)-H(5)	0.9300	C(1)-N(1)-Cr(1)	115.63(18)
C(6)-C(7)	1.384(4)	C(10)-N(2)-C(6)	119.0(2)
C(7)-C(8)	1.376(5)	C(10)-N(2)-Cr(1)	125.93(19)
C(7)-H(7)	0.9300	C(6)-N(2)-Cr(1)	114.66(17)
C(8)-C(9)	1.361(5)	N(1)-C(1)-C(2)	121.3(3)
C(8)-H(8)	0.9300	N(1)-C(1)-C(6)	114.9(2)
C(9)-C(10)	1.382(4)	C(2)-C(1)-C(6)	123.8(3)
C(9)-H(9)	0.9300	C(3)-C(2)-C(1)	118.5(3)
C(10)-H(10)	0.9300	C(3)-C(2)-H(2)	120.8
O(1)-H(1A)	0.80(3)	C(1)-C(2)-H(2)	120.8
O(1)-H(1B)	0.72(4)	C(4)-C(3)-C(2)	119.8(3)

C(4)-C(3)-H(3)	120.1	C(6)-C(7)-H(7)	120.4
C(2)-C(3)-H(3)	120.1	C(9)-C(8)-C(7)	119.4(3)
C(3)-C(4)-C(5)	119.0(3)	C(9)-C(8)-H(8)	120.3
C(3)-C(4)-H(4)	120.5	C(7)-C(8)-H(8)	120.3
C(5)-C(4)-H(4)	120.5	C(8)-C(9)-C(10)	119.5(3)
N(1)-C(5)-C(4)	121.6(3)	C(8)-C(9)-H(9)	120.2
N(1)-C(5)-H(5)	119.2	C(10)-C(9)-H(9)	120.2
C(4)-C(5)-H(5)	119.2	N(2)-C(10)-C(9)	121.6(3)
N(2)-C(6)-C(7)	121.0(3)	N(2)-C(10)-H(10)	119.2
N(2)-C(6)-C(1)	114.9(2)	C(9)-C(10)-H(10)	119.2
C(7)-C(6)-C(1)	124.1(3)	Cr(1)-O(1)-H(1A)	122(2)
C(8)-C(7)-C(6)	119.3(3)	Cr(1)-O(1)-H(1B)	111(3)
C(8)-C(7)-H(7)	120.4	H(1A)-O(1)-H(1B)	111(4)

Table A.24 **Anisotropic displacement parameters ($Å^2 x\ 10^3$) for $[CrCl_3(bipy)(H_2O)]$. The anisotropic displacement factor exponent takes the form: $-2p^2[h^2a^{*2}U^{11} + ... + 2\ h\ k\ a^*\ b^*\ U^{12}]$**

	U^{11}	U^{22}	U^{33}	U^{23}	U^{13}	U^{12}
Cr(1)	46(1)	28(1)	28(1)	0(1)	5(1)	5(1)
Cl(1)	59(1)	53(1)	38(1)	-4(1)	-6(1)	17(1)
Cl(2)	46(1)	46(1)	38(1)	-2(1)	3(1)	1(1)
Cl(3)	98(1)	29(1)	43(1)	3(1)	8(1)	0(1)
N(1)	42(1)	32(1)	34(1)	4(1)	1(1)	1(1)
N(2)	44(1)	34(1)	32(1)	-2(1)	3(1)	2(1)
C(1)	45(2)	32(1)	39(1)	0(1)	-7(1)	3(1)
C(2)	58(2)	30(1)	55(2)	0(1)	-6(1)	2(1)
C(3)	61(2)	36(2)	71(2)	12(2)	-13(2)	-6(1)
C(4)	49(2)	52(2)	58(2)	21(2)	-5(1)	-10(1)

C(5)	42(2)	49(2)	46(2)	9(1)	0(1)	1(1)
C(6)	43(1)	36(1)	36(1)	-7(1)	-1(1)	2(1)
C(7)	52(2)	43(2)	53(2)	-16(1)	0(1)	5(1)
C(8)	46(2)	67(2)	52(2)	-21(2)	10(1)	3(2)
C(9)	49(2)	66(2)	41(2)	-7(1)	9(1)	-7(2)
C(10)	47(2)	46(2)	36(2)	-2(1)	4(1)	-4(1)
O(1)	50(1)	50(1)	36(1)	-7(1)	4(1)	10(1)
O(2)	62(2)	44(2)	39(2)	0	4(1)	0

Table A.25 **Hydrogen coordinates (x 10^4) and isotropic displacement parameters ($Å^2$x 10^3) for [$CrCl_3$(bipy)(H_2O)]**

	x	y	z	U(eq)
H(2)	8648	6541	9319	58
H(3)	9188	7376	7878	69
H(4)	9581	5941	6536	65
H(5)	9448	3696	6701	55
H(7)	8050	5544	10362	59
H(8)	7620	4368	11850	66
H(9)	7748	2127	12093	62
H(10)	8254	1057	10736	52
H(1A)	9095(12)	1030(30)	6080(40)	55
H(1B)	9441(13)	890(40)	7030(40)	55
H(2A)	9985(13)	-870(30)	6830(30)	59

Table A.26 Torsion angles [°] for [$CrCl_3(bipy)(H_2O)$]

O(1)-Cr(1)-N(1)-C(5)	-10.0(2)	Cr(1)-N(1)-C(1)-C(6)	-1.3(3)
N(2)-Cr(1)-N(1)-C(5)	172.6(2)	N(1)-C(1)-C(2)-C(3)	1.5(4)
Cl(3)-Cr(1)-N(1)-C(5)	151.6(6)	C(6)-C(1)-C(2)-C(3)	177.9(3)
Cl(2)-Cr(1)-N(1)-C(5)	-97.5(2)	C(1)-C(2)-C(3)-C(4)	-0.3(4)
Cl(1)-Cr(1)-N(1)-C(5)	78.1(2)	C(2)-C(3)-C(4)-C(5)	-1.0(5)
O(1)-Cr(1)-N(1)-C(1)	173.47(18)	C(1)-N(1)-C(5)-C(4)	-0.1(4)
N(2)-Cr(1)-N(1)-C(1)	-3.95(18)	Cr(1)-N(1)-C(5)-C(4)	-176.5(2)
Cl(3)-Cr(1)-N(1)-C(1)	-24.9(8)	C(3)-C(4)-C(5)-N(1)	1.3(4)
Cl(2)-Cr(1)-N(1)-C(1)	86.02(17)	C(10)-N(2)-C(6)-C(7)	-4.0(4)
Cl(1)-Cr(1)-N(1)-C(1)	-98.46(18)	Cr(1)-N(2)-C(6)-C(7)	169.3(2)
O(1)-Cr(1)-N(2)-C(10)	165.6(5)	C(10)-N(2)-C(6)-C(1)	174.4(2)
N(1)-Cr(1)-N(2)-C(10)	-178.3(2)	Cr(1)-N(2)-C(6)-C(1)	-12.3(3)
Cl(3)-Cr(1)-N(2)-C(10)	-0.4(2)	N(1)-C(1)-C(6)-N(2)	9.0(3)
Cl(2)-Cr(1)-N(2)-C(10)	92.9(2)	C(2)-C(1)-C(6)-N(2)	-167.6(2)
Cl(1)-Cr(1)-N(2)-C(10)	-93.9(2)	N(1)-C(1)-C(6)-C(7)	-172.6(2)
O(1)-Cr(1)-N(2)-C(6)	-7.2(7)	C(2)-C(1)-C(6)-C(7)	10.8(4)
N(1)-Cr(1)-N(2)-C(6)	8.99(18)	N(2)-C(6)-C(7)-C(8)	3.0(4)
Cl(3)-Cr(1)-N(2)-C(6)	-173.12(17)	C(1)-C(6)-C(7)-C(8)	-175.2(3)
Cl(2)-Cr(1)-N(2)-C(6)	-79.87(17)	C(6)-C(7)-C(8)-C(9)	0.4(4)
Cl(1)-Cr(1)-N(2)-C(6)	93.35(17)	C(7)-C(8)-C(9)-C(10)	-2.7(5)
C(5)-N(1)-C(1)-C(2)	-1.3(4)	C(6)-N(2)-C(10)-C(9)	1.6(4)
Cr(1)-N(1)-C(1)-C(2)	175.4(2)	Cr(1)-N(2)-C(10)-C(9)	-170.9(2)
C(5)-N(1)-C(1)-C(6)	-178.0(2)	C(8)-C(9)-C(10)-N(2)	1.8(4)

Table A.27 Hydrogen bonds for [$CrCl_3$(bipy)(H_2O)] [Å and °]

D-H...A	d(D-H)	d(H...A)	d(D...A)	<(DHA)
O(1)-H(1B)...O(2)	0.72(4)	1.98(4)	2.690(3)	173(4)
O(1)-H(1A)...Cl(3)#1	0.80(3)	2.40(4)	3.192(2)	176(3)
O(2)-H(2A)...Cl(1)#1	0.84(3)	2.39(3)	3.1671(17)	156(3)

Symmetry transformations used to generate equivalent atoms:

#1 x,-y,z-1/2

[$HpyNH_2$][$CrCl_4$(bipy)]

Table A.28 **Atomic coordinates (x 10^4) and equivalent isotropic displacement parameters ($Å^2$x 10^3) for [$HpyNH_2$][$CrCl_4$(bipy)]. U(eq) is defined as one-third of the trace of the orthogonalised U^{ij} tensor**

	x	y	z	U(eq)
Cr(1)	2303(1)	2244(1)	5000	33(1)
Cl(1)	4444(1)	2771(1)	5000	46(1)
Cl(2)	255(1)	1482(1)	5000	40(1)
Cl(3)	1754(1)	3416(1)	3976(1)	50(1)
N(1)	2854(2)	1042(2)	4203(2)	36(1)
C(1)	3152(3)	109(2)	4551(2)	36(1)
C(2)	3473(3)	-767(3)	4094(2)	49(1)
C(3)	3490(4)	-691(3)	3260(2)	55(1)
C(4)	3209(4)	266(3)	2907(2)	53(1)
C(5)	2896(3)	1115(3)	3387(2)	43(1)
N(2)	5000	5000	1603(3)	53(1)
C(6)	4807(4)	4087(3)	1999(2)	53(1)
C(7)	4794(4)	4061(3)	2814(2)	55(1)
C(8)	5000	5000	3254(3)	60(1)
N(3)	5000	5000	4043(3)	125(4)
Cl(4)	2165(3)	6616(2)	4095(2)	166(1)
C(9)	1356(6)	6046(5)	5000	65(2)

Table A.29 Bond lengths [Å] and angles [°] for $[HpyNH_2][CrCl_4(bipy)]$

Cr(1)-N(1)	2.088(3)	C(9)-H(9A)	0.90(7)
Cr(1)-N(1)#1	2.088(3)	C(9)-H(9B)	0.97(7)
Cr(1)-Cl(3)#1	2.3172(9)		
Cr(1)-Cl(3)	2.3172(9)	N(1)-Cr(1)-N(1)#1	78.02(14)
Cr(1)-Cl(1)	2.3415(13)	N(1)-Cr(1)-Cl(3)#1	172.25(7)
Cr(1)-Cl(2)	2.3515(12)	N(1)#1-Cr(1)-Cl(3)#1	94.23(7)
N(1)-C(1)	1.347(4)	N(1)-Cr(1)-Cl(3)	94.23(7)
N(1)-C(5)	1.348(4)	N(1)#1-Cr(1)-Cl(3)	172.25(7)
C(1)-C(2)	1.381(4)	Cl(3)#1-Cr(1)-Cl(3)	93.52(5)
C(1)-C(1)#1	1.479(6)	N(1)-Cr(1)-Cl(1)	86.63(7)
C(2)-C(3)	1.378(5)	N(1)#1-Cr(1)-Cl(1)	86.63(7)
C(2)-H(2)	0.94(4)	Cl(3)#1-Cr(1)-Cl(1)	93.22(4)
C(3)-C(4)	1.374(6)	Cl(3)-Cr(1)-Cl(1)	93.22(4)
C(3)-H(3)	0.94(4)	N(1)-Cr(1)-Cl(2)	87.46(7)
C(4)-C(5)	1.372(5)	N(1)#1-Cr(1)-Cl(2)	87.46(7)
C(4)-H(4)	0.88(5)	Cl(3)#1-Cr(1)-Cl(2)	91.99(4)
C(5)-H(5)	0.93(4)	Cl(3)-Cr(1)-Cl(2)	91.99(4)
N(2)-C(6)#2	1.340(4)	Cl(1)-Cr(1)-Cl(2)	172.39(5)
N(2)-C(6)	1.340(4)	C(1)-N(1)-C(5)	118.5(3)
N(2)-H(2N)	0.76(7)	C(1)-N(1)-Cr(1)	115.5(2)
C(6)-C(7)	1.344(5)	C(5)-N(1)-Cr(1)	126.0(2)
C(6)-H(6)	0.94(4)	N(1)-C(1)-C(2)	121.6(3)
C(7)-C(8)	1.406(4)	N(1)-C(1)-C(1)#1	115.26(16)
C(7)-H(7)	0.80(4)	C(2)-C(1)-C(1)#1	123.1(2)
C(8)-N(3)	1.300(7)	C(3)-C(2)-C(1)	119.5(3)
C(8)-C(7)#2	1.406(4)	C(3)-C(2)-H(2)	123(3)
N(3)-H(3N)	0.96(7)	C(1)-C(2)-H(2)	118(3)
Cl(4)-C(9)	1.861(5)	C(4)-C(3)-C(2)	118.8(3)
C(9)-Cl(4)#1	1.861(5)	C(4)-C(3)-H(3)	120(2)

C(2)-C(3)-H(3)	121(2)	C(6)-C(7)-C(8)	119.6(4)
C(5)-C(4)-C(3)	119.6(3)	C(6)-C(7)-H(7)	122(3)
C(5)-C(4)-H(4)	116(3)	C(8)-C(7)-H(7)	119(3)
C(3)-C(4)-H(4)	124(3)	N(3)-C(8)-C(7)	121.1(2)
N(1)-C(5)-C(4)	122.1(3)	N(3)-C(8)-C(7)#2	121.1(2)
N(1)-C(5)-H(5)	118(2)	C(7)-C(8)-C(7)#2	117.9(5)
C(4)-C(5)-H(5)	120(2)	C(8)-N(3)-H(3N)	112(4)
C(6)#2-N(2)-C(6)	121.7(5)	Cl(4)#1-C(9)-Cl(4)	106.6(3)
C(6)#2-N(2)-H(2N)	119.2(2)	Cl(4)#1-C(9)-H(9A)	109(2)
C(6)-N(2)-H(2N)	119.2(2)	Cl(4)-C(9)-H(9A)	109(2)
N(2)-C(6)-C(7)	120.6(4)	Cl(4)#1-C(9)-H(9B)	115(2)
N(2)-C(6)-H(6)	120(2)	Cl(4)-C(9)-H(9B)	115(2)
C(7)-C(6)-H(6)	119(2)	H(9A)-C(9)-H(9B)	102(6)

Symmetry transformations used to generate equivalent atoms:

#1 x, y, -z+1 #2 -x+1, -y+1, z

Table A.30 **Anisotropic displacement parameters ($Å^2 x\ 10^3$) for $[HpyNH_2][CrCl_4(bipy)]$. The anisotropic displacement factor exponent takes the form: $-2p^2[h^2a^{*2}U^{11} + ... + 2\ h\ k\ a^*\ b^*\ U^{12}]$**

	U^{11}	U^{22}	U^{33}	U^{23}	U^{13}	U^{12}
Cr(1)	39(1)	25(1)	35(1)	0	0	2(1)
Cl(1)	42(1)	34(1)	63(1)	0	0	-3(1)
Cl(2)	44(1)	38(1)	39(1)	0	0	-2(1)
Cl(3)	62(1)	39(1)	50(1)	14(1)	3(1)	8(1)
N(1)	39(1)	32(1)	36(1)	0(1)	0(1)	0(1)
C(1)	36(1)	31(1)	41(2)	-2(1)	0(1)	-1(1)
C(2)	55(2)	32(2)	59(2)	-10(2)	-4(2)	6(1)
C(3)	60(2)	50(2)	54(2)	-21(2)	-2(2)	8(2)

C(4)	54(2)	65(2)	40(2)	-9(2)	2(2)	-1(2)
C(5)	49(2)	44(2)	37(2)	1(1)	2(1)	3(1)
N(2)	53(2)	70(3)	36(2)	0	0	2(2)
C(6)	53(2)	57(2)	49(2)	-11(2)	0(2)	-2(2)
C(7)	74(2)	44(2)	47(2)	-2(2)	4(2)	-10(2)
C(8)	97(4)	46(3)	36(2)	0	0	-12(3)
N(3)	281(12)	54(3)	39(3)	0	0	-37(5)
Cl(4)	157(2)	126(2)	217(3)	-73(2)	11(2)	-15(1)
C(9)	55(3)	43(3)	97(5)	0	0	-4(2)

Table A.31 **Hydrogen coordinates (x 10^4) and isotropic displacement parameters ($Å^2$x 10^3) for $[HpyNH_2][CrCl_4(bipy)]$**

	x	y	z	U(eq)
H(2)	3620(40)	-1400(30)	4370(30)	60(11)
H(3)	3710(40)	-1280(30)	2940(20)	55(10)
H(4)	3210(40)	380(40)	2380(30)	70(13)
H(5)	2740(30)	1770(30)	3150(20)	42(9)
H(2N)	5000	5000	1140(40)	56(17)
H(6)	4690(40)	3450(30)	1710(30)	53(11)
H(7)	4650(40)	3520(30)	3060(30)	58(12)
H(3N)	5490(70)	4430(60)	4260(40)	150
H(9A)	1460(70)	5340(60)	5000	78
H(9B)	430(70)	6120(50)	5000	78

Table A.32 Torsion angles [°] for [HpyNH$_2$][CrCl$_4$(bipy)]

N(1)#1-Cr(1)-N(1)-C(1)	6.0(2)
Cl(1)-Cr(1)-N(1)-C(1)	93.3(2)
Cl(2)-Cr(1)-N(1)-C(1)	-81.9(2)
N(1)#1-Cr(1)-N(1)-C(5)	-176.1(2)
Cl(3)-Cr(1)-N(1)-C(5)	4.1(3)
Cl(1)-Cr(1)-N(1)-C(5)	-88.8(3)
Cl(2)-Cr(1)-N(1)-C(5)	95.9(3)
C(5)-N(1)-C(1)-C(2)	-1.2(4)
Cr(1)-N(1)-C(1)-C(2)	176.8(2)
C(5)-N(1)-C(1)-C(1)#1	176.8(2)
Cr(1)-N(1)-C(1)-C(1)#1	-5.2(2)
N(1)-C(1)-C(2)-C(3)	0.0(5)
C(1)#1-C(1)-C(2)-C(3)	-177.8(3)
C(1)-C(2)-C(3)-C(4)	1.2(6)
C(2)-C(3)-C(4)-C(5)	-1.2(6)
C(1)-N(1)-C(5)-C(4)	1.2(5)
Cr(1)-N(1)-C(5)-C(4)	-176.6(3)
C(3)-C(4)-C(5)-N(1)	0.0(6)
C(6)#2-N(2)-C(6)-C(7)	0.4(3)
N(2)-C(6)-C(7)-C(8)	-0.7(6)
C(6)-C(7)-C(8)-N(3)	-179.6(3)
C(6)-C(7)-C(8)-C(7)#2	0.4(3)

Symmetry transformations used to generate equivalent atoms:

#1 x, y, -z+1 #2 -x+1, -y+1, z

Table A.33 Hydrogen bonds for $[HpyNH_2][CrCl_4(bipy)]$ [Å and º]

D-H...A	d(D-H)	d(H...A)	d(D...A)	<(DHA)
N(2)-H(2N)...Cl(2)#3	0.76(7)	2.67(5)	3.250(4)	134.9(10)
N(3)-H(3N)...Cl(1)	0.96(7)	2.66(8)	3.278(3)	123(6)
N(3)-H(3N)...Cl(4)#2	0.96(7)	2.80(7)	3.605(3)	142(6)

Symmetry transformations used to generate equivalent atoms:

#1 x ,y, -z+1 #2 -x+1, -y+1, z #3 x+1/2, -y+1/2, -z+1/2

$[CrCl_2(bipy)_2][Cl]\cdot H_2O$

Table A.34 **Atomic coordinates (x 10^4) and equivalent isotropic displacement parameters ($Å^2$x 10^3) for $[CrCl_2(bipy)_2][Cl]\cdot H_2O$. U(eq) is defined as one-third of the trace of the orthogonalised U^{ij} tensor**

	x	y	z	U(eq)
Cr(1)	2223(1)	416(1)	533(1)	73(1)
Cl(1)	3202(1)	995(1)	197(1)	97(1)
Cl(2)	541(1)	644(1)	249(1)	86(1)
N(1)	1359(4)	-65(2)	907(2)	77(1)
N(2)	1979(5)	770(2)	1132(2)	87(2)
N(3)	3665(4)	105(2)	759(2)	80(2)
N(4)	2554(4)	-32(2)	7(2)	73(1)
C(1)	983(7)	90(3)	1307(3)	95(2)
C(2)	277(9)	-177(4)	1577(3)	131(3)
C(3)	-40(10)	-597(4)	1408(4)	143(4)
C(4)	371(8)	-763(3)	1020(3)	114(3)
C(5)	1079(6)	-485(3)	767(3)	89(2)
C(6)	1356(7)	547(3)	1441(3)	96(2)
C(7)	1150(9)	759(5)	1859(4)	147(4)
C(8)	1555(12)	1184(5)	1955(4)	148(4)
C(9)	2189(9)	1391(4)	1663(4)	128(4)
C(10)	2378(7)	1186(3)	1232(3)	106(3)
C(11)	4081(5)	-229(2)	478(2)	76(2)
C(12)	5021(6)	-475(3)	605(3)	96(2)
C(13)	5538(7)	-375(4)	1001(4)	116(3)
C(14)	5147(7)	-30(3)	1284(3)	112(3)
C(15)	4198(7)	205(3)	1148(3)	106(2)
C(16)	3463(5)	-306(2)	62(2)	75(2)

C(17)	3748(7)	-627(2)	-260(3)	93(2)
C(18)	3130(8)	-677(3)	-637(3)	103(2)
C(19)	2228(7)	-398(3)	-697(3)	103(2)
C(20)	1956(6)	-82(3)	-367(3)	91(2)
Cr(2)	2036(1)	2963(1)	537(1)	79(1)
Cl(3)	3180(2)	3482(1)	194(1)	102(1)
Cl(4)	416(2)	3305(1)	311(1)	100(1)
N(5)	1063(5)	2446(2)	811(2)	79(1)
N(6)	1972(4)	2518(2)	7(2)	80(2)
N(7)	3384(5)	2632(2)	825(2)	83(2)
N(8)	2201(5)	3307(2)	1133(2)	89(2)
C(21)	847(6)	2098(2)	525(3)	82(2)
C(22)	146(7)	1743(3)	649(3)	97(2)
C(23)	-359(7)	1760(3)	1078(4)	110(3)
C(24)	-108(7)	2109(3)	1364(3)	107(2)
C(25)	586(7)	2452(3)	1218(3)	99(2)
C(26)	1378(5)	2128(2)	74(2)	78(2)
C(27)	1292(7)	1789(3)	-254(3)	105(2)
C(28)	1834(9)	1841(4)	-659(3)	120(3)
C(29)	2405(8)	2241(4)	-734(3)	116(3)
C(30)	2465(7)	2565(3)	-391(3)	102(2)
C(31)	3653(6)	2783(3)	1227(3)	90(2)
C(32)	4532(9)	2553(4)	1474(3)	131(3)
C(33)	5067(9)	2207(4)	1287(5)	142(4)
C(34)	4786(8)	2060(4)	865(4)	127(3)
C(35)	3927(6)	2281(3)	631(3)	100(2)
C(36)	3036(7)	3174(3)	1396(3)	94(2)
C(37)	3287(9)	3406(4)	1803(3)	129(3)
C(38)	2659(13)	3784(5)	1912(4)	148(4)
C(39)	1823(12)	3927(4)	1642(4)	145(4)
C(40)	1610(9)	3670(3)	1254(3)	120(3)

Cl(5)	8871(13)	120(5)	2664(3)	293(6)
Cl(6)	4814(13)	980(5)	1997(5)	380(10)
Cl(7)	7750(20)	6179(10)	1740(5)	530(20)
Cl(8)	9180(20)	1837(8)	2547(6)	486(16)
O(1)	252(18)	2982(10)	2305(5)	468(18)
O(2)	7390(30)	8686(12)	1741(6)	630(30)
O(3)	50(30)	4107(19)	2471(9)	1040(60)
O(4)	1480(40)	2393(8)	2445(8)	660(40)
O(5)	7960(20)	4680(10)	2130(8)	548(19)

Table A.35 Bond lengths [Å] and angles [°] for $[CrCl_2(bipy)_2][Cl]\cdot H_2O$

Cr(1)-N(1)	2.063(6)	C(2)-H(2)	0.9300
Cr(1)-N(2)	2.065(6)	C(3)-C(4)	1.335(13)
Cr(1)-N(4)	2.065(6)	C(3)-H(3)	0.9300
Cr(1)-N(3)	2.068(5)	C(4)-C(5)	1.391(10)
Cr(1)-Cl(1)	2.285(2)	C(4)-H(4)	0.9300
Cr(1)-Cl(2)	2.2906(18)	C(5)-H(5)	0.9300
N(1)-C(5)	1.336(8)	C(6)-C(7)	1.401(12)
N(1)-C(1)	1.342(9)	C(7)-C(8)	1.359(15)
N(2)-C(10)	1.337(9)	C(7)-H(7)	0.9300
N(2)-C(6)	1.345(10)	C(8)-C(9)	1.298(14)
N(3)-C(15)	1.346(9)	C(8)-H(8)	0.9300
N(3)-C(11)	1.372(8)	C(9)-C(10)	1.423(12)
N(4)-C(20)	1.324(9)	C(9)-H(9)	0.9300
N(4)-C(16)	1.365(8)	C(10)-H(10)	0.9300
C(1)-C(2)	1.401(12)	C(11)-C(12)	1.393(10)
C(1)-C(6)	1.459(11)	C(11)-C(16)	1.450(9)
C(2)-C(3)	1.375(13)	C(12)-C(13)	1.356(12)

C(12)-H(12)	0.9300	C(22)-H(22)	0.9300
C(13)-C(14)	1.389(12)	C(23)-C(24)	1.355(12)
C(13)-H(13)	0.9300	C(23)-H(23)	0.9300
C(14)-C(15)	1.392(11)	C(24)-C(25)	1.374(11)
C(14)-H(14)	0.9300	C(24)-H(24)	0.9300
C(15)-H(15)	0.9300	C(25)-H(25)	0.9300
C(16)-C(17)	1.376(9)	C(26)-C(27)	1.386(10)
C(17)-C(18)	1.344(11)	C(27)-C(28)	1.370(12)
C(17)-H(17)	0.9300	C(27)-H(27)	0.9300
C(18)-C(19)	1.369(12)	C(28)-C(29)	1.370(13)
C(18)-H(18)	0.9300	C(28)-H(28)	0.9300
C(19)-C(20)	1.378(11)	C(29)-C(30)	1.385(11)
C(19)-H(19)	0.9300	C(29)-H(29)	0.9300
C(20)-H(20)	0.9300	C(30)-H(30)	0.9300
Cr(2)-N(8)	2.030(6)	C(31)-C(36)	1.448(11)
Cr(2)-N(6)	2.031(6)	C(31)-C(32)	1.449(12)
Cr(2)-N(7)	2.072(6)	C(32)-C(33)	1.320(14)
Cr(2)-N(5)	2.075(6)	C(32)-H(32)	0.9300
Cr(2)-Cl(3)	2.281(2)	C(33)-C(34)	1.356(14)
Cr(2)-Cl(4)	2.290(2)	C(33)-H(33)	0.9300
N(5)-C(25)	1.328(9)	C(34)-C(35)	1.401(12)
N(5)-C(21)	1.344(8)	C(34)-H(34)	0.9300
N(6)-C(30)	1.321(9)	C(35)-H(35)	0.9300
N(6)-C(26)	1.357(9)	C(36)-C(37)	1.410(12)
N(7)-C(31)	1.305(9)	C(37)-C(38)	1.373(15)
N(7)-C(35)	1.342(9)	C(37)-H(37)	0.9300
N(8)-C(40)	1.324(10)	C(38)-C(39)	1.350(16)
N(8)-C(36)	1.328(10)	C(38)-H(38)	0.9300
C(21)-C(22)	1.385(10)	C(39)-C(40)	1.390(13)
C(21)-C(26)	1.476(10)	C(39)-H(39)	0.9300
C(22)-C(23)	1.402(12)	C(40)-H(40)	0.9300

		C(3)-C(2)-C(1)	117.3(9)
N(1)-Cr(1)-N(2)	79.1(3)	C(3)-C(2)-H(2)	121.3
N(1)-Cr(1)-N(4)	94.0(2)	C(1)-C(2)-H(2)	121.4
N(2)-Cr(1)-N(4)	170.0(2)	C(4)-C(3)-C(2)	121.9(9)
N(1)-Cr(1)-N(3)	87.5(2)	C(4)-C(3)-H(3)	119.0
N(2)-Cr(1)-N(3)	93.7(2)	C(2)-C(3)-H(3)	119.0
N(4)-Cr(1)-N(3)	78.6(2)	C(3)-C(4)-C(5)	118.3(9)
N(1)-Cr(1)-Cl(1)	173.21(18)	C(3)-C(4)-H(4)	120.8
N(2)-Cr(1)-Cl(1)	94.2(2)	C(5)-C(4)-H(4)	120.9
N(4)-Cr(1)-Cl(1)	92.42(16)	N(1)-C(5)-C(4)	121.6(8)
N(3)-Cr(1)-Cl(1)	91.63(16)	N(1)-C(5)-H(5)	119.2
N(1)-Cr(1)-Cl(2)	86.92(15)	C(4)-C(5)-H(5)	119.2
N(2)-Cr(1)-Cl(2)	92.36(16)	N(2)-C(6)-C(7)	118.7(9)
N(4)-Cr(1)-Cl(2)	94.57(16)	N(2)-C(6)-C(1)	115.4(7)
N(3)-Cr(1)-Cl(2)	170.85(18)	C(7)-C(6)-C(1)	125.8(9)
Cl(1)-Cr(1)-Cl(2)	94.79(8)	C(8)-C(7)-C(6)	121.3(11)
C(5)-N(1)-C(1)	119.6(6)	C(8)-C(7)-H(7)	119.2
C(5)-N(1)-Cr(1)	125.9(5)	C(6)-C(7)-H(7)	119.4
C(1)-N(1)-Cr(1)	114.2(5)	C(9)-C(8)-C(7)	119.8(11)
C(10)-N(2)-C(6)	119.3(7)	C(9)-C(8)-H(8)	120.0
C(10)-N(2)-Cr(1)	126.1(6)	C(7)-C(8)-H(8)	120.2
C(6)-N(2)-Cr(1)	114.6(5)	C(8)-C(9)-C(10)	119.3(11)
C(15)-N(3)-C(11)	119.6(6)	C(8)-C(9)-H(9)	120.5
C(15)-N(3)-Cr(1)	125.4(5)	C(10)-C(9)-H(9)	120.2
C(11)-N(3)-Cr(1)	115.0(4)	N(2)-C(10)-C(9)	121.3(9)
C(20)-N(4)-C(16)	118.2(6)	N(2)-C(10)-H(10)	119.3
C(20)-N(4)-Cr(1)	126.0(5)	C(9)-C(10)-H(10)	119.4
C(16)-N(4)-Cr(1)	115.8(5)	N(3)-C(11)-C(12)	120.1(7)
N(1)-C(1)-C(2)	121.0(8)	N(3)-C(11)-C(16)	115.6(6)
N(1)-C(1)-C(6)	116.1(7)	C(12)-C(11)-C(16)	124.3(7)
C(2)-C(1)-C(6)	122.9(8)	C(13)-C(12)-C(11)	119.6(8)

C(13)-C(12)-H(12)	120.2	N(7)-Cr(2)-N(5)	86.8(2)
C(11)-C(12)-H(12)	120.2	N(8)-Cr(2)-Cl(3)	89.75(18)
C(12)-C(13)-C(14)	121.1(8)	N(6)-Cr(2)-Cl(3)	96.10(18)
C(12)-C(13)-H(13)	119.5	N(7)-Cr(2)-Cl(3)	90.97(17)
C(14)-C(13)-H(13)	119.4	N(5)-Cr(2)-Cl(3)	174.70(18)
C(15)-C(14)-C(13)	117.6(8)	N(8)-Cr(2)-Cl(4)	96.9(2)
C(15)-C(14)-H(14)	121.2	N(6)-Cr(2)-Cl(4)	91.30(17)
C(13)-C(14)-H(14)	121.2	N(7)-Cr(2)-Cl(4)	171.92(18)
N(3)-C(15)-C(14)	122.0(8)	N(5)-Cr(2)-Cl(4)	87.05(16)
N(3)-C(15)-H(15)	119.0	Cl(3)-Cr(2)-Cl(4)	95.61(9)
C(14)-C(15)-H(15)	119.0	C(25)-N(5)-C(21)	119.6(7)
N(4)-C(16)-C(17)	121.0(7)	C(25)-N(5)-Cr(2)	125.8(5)
N(4)-C(16)-C(11)	114.9(6)	C(21)-N(5)-Cr(2)	114.4(5)
C(17)-C(16)-C(11)	124.0(7)	C(30)-N(6)-C(26)	116.9(7)
C(18)-C(17)-C(16)	120.3(8)	C(30)-N(6)-Cr(2)	126.8(5)
C(18)-C(17)-H(17)	119.8	C(26)-N(6)-Cr(2)	116.3(5)
C(16)-C(17)-H(17)	119.9	C(31)-N(7)-C(35)	121.6(7)
C(17)-C(18)-C(19)	118.8(7)	C(31)-N(7)-Cr(2)	114.1(5)
C(17)-C(18)-H(18)	120.6	C(35)-N(7)-Cr(2)	124.2(5)
C(19)-C(18)-H(18)	120.6	C(40)-N(8)-C(36)	118.9(7)
C(18)-C(19)-C(20)	119.7(8)	C(40)-N(8)-Cr(2)	125.1(6)
C(18)-C(19)-H(19)	120.2	C(36)-N(8)-Cr(2)	115.7(5)
C(20)-C(19)-H(19)	120.1	N(5)-C(21)-C(22)	121.0(7)
N(4)-C(20)-C(19)	122.0(7)	N(5)-C(21)-C(26)	115.8(6)
N(4)-C(20)-H(20)	119.0	C(22)-C(21)-C(26)	123.2(7)
C(19)-C(20)-H(20)	119.0	C(21)-C(22)-C(23)	118.5(8)
N(8)-Cr(2)-N(6)	169.4(3)	C(21)-C(22)-H(22)	120.8
N(8)-Cr(2)-N(7)	78.4(3)	C(23)-C(22)-H(22)	120.8
N(6)-Cr(2)-N(7)	92.7(2)	C(24)-C(23)-C(22)	119.4(8)
N(8)-Cr(2)-N(5)	94.5(2)	C(24)-C(23)-H(23)	120.3
N(6)-Cr(2)-N(5)	79.2(2)	C(22)-C(23)-H(23)	120.3

C(23)-C(24)-C(25)	119.1(9)	C(31)-C(32)-H(32)	119.9
C(23)-C(24)-H(24)	120.4	C(32)-C(33)-C(34)	120.2(10)
C(25)-C(24)-H(24)	120.4	C(32)-C(33)-H(33)	119.9
N(5)-C(25)-C(24)	122.3(8)	C(34)-C(33)-H(33)	119.9
N(5)-C(25)-H(25)	118.8	C(33)-C(34)-C(35)	119.3(10)
C(24)-C(25)-H(25)	118.8	C(33)-C(34)-H(34)	120.3
N(6)-C(26)-C(27)	122.4(7)	C(35)-C(34)-H(34)	120.3
N(6)-C(26)-C(21)	114.2(6)	N(7)-C(35)-C(34)	120.0(9)
C(27)-C(26)-C(21)	123.4(7)	N(7)-C(35)-H(35)	120.0
C(28)-C(27)-C(26)	119.5(8)	C(34)-C(35)-H(35)	120.0
C(28)-C(27)-H(27)	120.3	N(8)-C(36)-C(37)	121.2(9)
C(26)-C(27)-H(27)	120.3	N(8)-C(36)-C(31)	114.8(7)
C(27)-C(28)-C(29)	118.2(9)	C(37)-C(36)-C(31)	124.0(9)
C(27)-C(28)-H(28)	120.9	C(38)-C(37)-C(36)	117.7(10)
C(29)-C(28)-H(28)	120.9	C(38)-C(37)-H(37)	121.1
C(28)-C(29)-C(30)	119.4(9)	C(36)-C(37)-H(37)	121.1
C(28)-C(29)-H(29)	120.3	C(39)-C(38)-C(37)	121.4(10)
C(30)-C(29)-H(29)	120.4	C(39)-C(38)-H(38)	119.3
N(6)-C(30)-C(29)	123.5(8)	C(37)-C(38)-H(38)	119.3
N(6)-C(30)-H(30)	118.3	C(38)-C(39)-C(40)	117.1(11)
C(29)-C(30)-H(30)	118.2	C(38)-C(39)-H(39)	121.5
N(7)-C(31)-C(36)	116.7(7)	C(40)-C(39)-H(39)	121.4
N(7)-C(31)-C(32)	118.7(8)	N(8)-C(40)-C(39)	123.5(10)
C(36)-C(31)-C(32)	124.5(8)	N(8)-C(40)-H(40)	118.1
C(33)-C(32)-C(31)	120.0(10)	C(39)-C(40)-H(40)	118.4
C(33)-C(32)-H(32)	120.0		

Table A.36 **Anisotropic displacement parameters ($Å^2 x\ 10^3$) for $[CrCl_2(bipy)_2][Cl]\cdot H_2O$. The anisotropic displacement factor exponent takes the form: $-2p^2[h^2a^{*2}U^{11} + ... + 2\ h\ k\ a^*\ b^*\ U^{12}]$**

	U^{11}	U^{22}	U^{33}	U^{23}	U^{13}	U^{12}
Cr(1)	57(1)	76(1)	87(1)	-6(1)	0(1)	2(1)
Cl(1)	72(1)	88(1)	129(2)	6(1)	9(1)	-7(1)
Cl(2)	62(1)	81(1)	114(1)	-7(1)	-8(1)	5(1)
N(1)	66(3)	84(4)	80(4)	-3(3)	6(3)	5(3)
N(2)	73(3)	88(4)	99(4)	-19(4)	-7(3)	8(3)
N(3)	65(3)	92(4)	83(4)	-1(3)	-8(3)	0(3)
N(4)	63(3)	81(3)	76(3)	2(3)	4(3)	-3(3)
C(1)	95(5)	100(6)	89(5)	-1(5)	7(4)	4(4)
C(2)	161(9)	128(8)	105(7)	-5(6)	39(6)	-7(7)
C(3)	153(9)	144(9)	134(8)	1(8)	60(7)	-30(8)
C(4)	122(6)	99(6)	122(7)	25(5)	12(6)	-10(5)
C(5)	78(4)	96(5)	94(5)	4(4)	2(4)	-5(4)
C(6)	97(5)	109(6)	81(5)	-14(5)	6(4)	10(5)
C(7)	151(9)	180(12)	109(8)	-22(8)	30(6)	14(9)
C(8)	195(12)	131(10)	118(9)	-39(8)	21(8)	8(9)
C(9)	125(8)	120(8)	140(9)	-56(7)	-32(7)	21(6)
C(10)	86(5)	97(6)	135(7)	-20(5)	-12(5)	2(4)
C(11)	63(4)	66(4)	100(5)	7(4)	4(4)	5(3)
C(12)	77(4)	82(5)	128(7)	16(5)	11(5)	17(4)
C(13)	74(5)	133(8)	140(8)	40(7)	-12(5)	13(5)
C(14)	81(5)	135(7)	120(7)	15(6)	-27(5)	13(5)
C(15)	89(5)	125(6)	103(6)	-10(5)	-10(5)	5(5)
C(16)	65(4)	66(4)	92(5)	5(4)	16(3)	-2(3)
C(17)	98(5)	75(5)	105(6)	-4(4)	23(5)	10(4)
C(18)	113(6)	92(6)	103(6)	-30(5)	17(5)	2(5)
C(19)	93(5)	122(7)	96(6)	-20(5)	-1(4)	-13(5)

C(20)	71(4)	102(6)	100(6)	-14(5)	8(4)	0(4)
Cr(2)	84(1)	75(1)	79(1)	-2(1)	-8(1)	-3(1)
Cl(3)	112(1)	94(1)	99(1)	4(1)	-3(1)	-23(1)
Cl(4)	98(1)	87(1)	114(2)	4(1)	-19(1)	8(1)
N(5)	85(4)	76(4)	74(4)	-3(3)	-2(3)	6(3)
N(6)	80(3)	92(4)	69(4)	-1(3)	-3(3)	-2(3)
N(7)	82(4)	89(4)	79(4)	2(3)	-9(3)	-5(3)
N(8)	100(4)	78(4)	89(4)	-3(3)	-14(4)	-1(3)
C(21)	74(4)	71(4)	102(6)	2(4)	-9(4)	11(3)
C(22)	88(5)	79(5)	124(7)	2(5)	-7(5)	2(4)
C(23)	98(6)	97(6)	135(8)	5(6)	11(6)	-11(5)
C(24)	110(6)	110(6)	100(6)	15(5)	16(5)	-11(5)
C(25)	105(6)	88(5)	102(6)	2(5)	3(5)	6(5)
C(26)	71(4)	75(4)	88(5)	1(4)	-6(4)	5(3)
C(27)	108(6)	88(5)	120(7)	-20(5)	-1(5)	-7(5)
C(28)	129(7)	130(8)	102(7)	-30(6)	5(6)	-17(6)
C(29)	110(6)	152(8)	87(6)	-11(6)	10(5)	-11(6)
C(30)	102(5)	118(7)	87(5)	-8(5)	1(5)	-20(5)
C(31)	88(5)	107(6)	76(5)	7(4)	-3(4)	-8(4)
C(32)	119(7)	180(10)	96(7)	15(7)	-16(6)	2(7)
C(33)	103(7)	178(11)	144(10)	28(9)	-15(7)	34(7)
C(34)	97(6)	130(8)	154(10)	21(7)	-12(6)	11(6)
C(35)	84(5)	104(6)	112(6)	-1(5)	1(4)	12(4)
C(36)	101(5)	107(6)	75(5)	-6(4)	1(4)	-15(5)
C(37)	119(7)	182(10)	87(6)	-18(7)	-10(5)	-8(7)
C(38)	190(12)	169(11)	87(7)	-47(7)	10(8)	-22(10)
C(39)	203(12)	124(8)	109(8)	-35(7)	3(8)	14(8)
C(40)	156(8)	103(6)	100(7)	-13(5)	-11(6)	15(6)
Cl(5)	335(15)	391(16)	153(7)	0(9)	23(8)	29(13)
Cl(6)	363(16)	369(17)	409(18)	-189(15)	-235(15)	124(15)
Cl(7)	560(30)	840(50)	208(11)	-163(19)	-121(16)	380(30)

Cl(8)	560(30)	610(30)	283(15)	143(18)	230(20)	100(30)
O(1)	430(30)	740(40)	234(15)	-210(20)	189(17)	-310(30)
O(2)	880(50)	780(60)	230(15)	-40(20)	210(30)	-460(50)
O(3)	720(50)	1880(120)	500(30)	-770(60)	520(40)	-880(70)
O(4)	1210(100)	390(20)	380(30)	-260(20)	180(40)	-300(40)
O(5)	490(40)	620(40)	540(30)	170(30)	300(30)	-40(30)

Table A.37 **Hydrogen coordinates (x 10^4) and isotropic displacement parameters (Å^{2}x 10^3) for $[CrCl_2(bipy)_2][Cl]\cdot H_2O$**

	x	y	z	U(eq)
H(2)	33	-75	1859	157
H(3)	-556	-771	1568	172
H(4)	189	-1056	921	137
H(5)	1364	-595	495	107
H(7)	727	607	2076	176
H(8)	1378	1326	2228	177
H(9)	2517	1670	1736	154
H(10)	2787	1344	1014	127
H(12)	5293	-707	418	115
H(13)	6165	-541	1086	139
H(14)	5506	42	1555	134
H(15)	3923	439	1332	127
H(17)	4371	-810	-217	111
H(18)	3311	-897	-853	123
H(19)	1801	-421	-959	124
H(20)	1333	102	-409	109
H(22)	12	1499	453	116

H(23)	-861	1534	1165	132
H(24)	-402	2115	1656	128
H(25)	727	2698	1411	118
H(27)	870	1528	-199	126
H(28)	1815	1612	-878	144
H(29)	2750	2293	-1011	140
H(30)	2874	2831	-444	123
H(32)	4720	2650	1765	158
H(33)	5638	2062	1444	170
H(34)	5159	1815	733	152
H(35)	3734	2185	340	120
H(37)	3858	3307	1992	155
H(38)	2814	3944	2178	178
H(39)	1408	4186	1713	174
H(40)	1020	3757	1070	144

Table A.38 Torsion angles [°] for $[CrCl_2(bipy)_2][Cl]\cdot H_2O$

N(2)-Cr(1)-N(1)-C(5)	-179.7(6)	N(4)-Cr(1)-N(2)-C(10)	128.5(13)
N(4)-Cr(1)-N(1)-C(5)	-7.1(6)	N(3)-Cr(1)-N(2)-C(10)	89.0(6)
N(3)-Cr(1)-N(1)-C(5)	-85.5(6)	Cl(1)-Cr(1)-N(2)-C(10)	-2.9(6)
Cl(1)-Cr(1)-N(1)-C(5)	-167.9(11)	Cl(2)-Cr(1)-N(2)-C(10)	-97.9(6)
Cl(2)-Cr(1)-N(1)-C(5)	87.3(5)	N(1)-Cr(1)-N(2)-C(6)	-4.2(5)
N(2)-Cr(1)-N(1)-C(1)	6.3(5)	N(4)-Cr(1)-N(2)-C(6)	-51.5(15)
N(4)-Cr(1)-N(1)-C(1)	179.0(5)	N(3)-Cr(1)-N(2)-C(6)	-90.9(5)
N(3)-Cr(1)-N(1)-C(1)	100.6(5)	Cl(1)-Cr(1)-N(2)-C(6)	177.2(5)
Cl(1)-Cr(1)-N(1)-C(1)	18.1(17)	Cl(2)-Cr(1)-N(2)-C(6)	82.2(5)
Cl(2)-Cr(1)-N(1)-C(1)	-86.7(5)	N(1)-Cr(1)-N(3)-C(15)	-87.0(6)
N(1)-Cr(1)-N(2)-C(10)	175.7(6)	N(2)-Cr(1)-N(3)-C(15)	-8.1(6)

N(4)-Cr(1)-N(3)-C(15)	178.4(6)	C(10)-N(2)-C(6)-C(1)	-178.3(7)
Cl(1)-Cr(1)-N(3)-C(15)	86.2(6)	Cr(1)-N(2)-C(6)-C(1)	1.6(8)
Cl(2)-Cr(1)-N(3)-C(15)	-139.2(10)	N(1)-C(1)-C(6)-N(2)	3.9(10)
N(1)-Cr(1)-N(3)-C(11)	92.7(5)	C(2)-C(1)-C(6)-N(2)	-176.3(8)
N(2)-Cr(1)-N(3)-C(11)	171.6(5)	N(1)-C(1)-C(6)-C(7)	-174.0(8)
N(4)-Cr(1)-N(3)-C(11)	-1.9(4)	C(2)-C(1)-C(6)-C(7)	5.9(14)
Cl(1)-Cr(1)-N(3)-C(11)	-94.0(4)	N(2)-C(6)-C(7)-C(8)	0.7(15)
Cl(2)-Cr(1)-N(3)-C(11)	40.5(14)	C(1)-C(6)-C(7)-C(8)	178.5(10)
N(1)-Cr(1)-N(4)-C(20)	93.8(6)	C(6)-C(7)-C(8)-C(9)	-3(2)
N(2)-Cr(1)-N(4)-C(20)	140.2(12)	C(7)-C(8)-C(9)-C(10)	5.1(19)
N(3)-Cr(1)-N(4)-C(20)	-179.5(6)	C(6)-N(2)-C(10)-C(9)	2.2(11)
Cl(1)-Cr(1)-N(4)-C(20)	-88.4(6)	Cr(1)-N(2)-C(10)-C(9)	-177.7(6)
Cl(2)-Cr(1)-N(4)-C(20)	6.6(6)	C(8)-C(9)-C(10)-N(2)	-4.7(15)
N(1)-Cr(1)-N(4)-C(16)	-84.5(4)	C(15)-N(3)-C(11)-C(12)	2.6(10)
N(2)-Cr(1)-N(4)-C(16)	-38.2(15)	Cr(1)-N(3)-C(11)-C(12)	-177.1(5)
N(3)-Cr(1)-N(4)-C(16)	2.1(4)	C(15)-N(3)-C(11)-C(16)	-178.8(6)
Cl(1)-Cr(1)-N(4)-C(16)	93.3(4)	Cr(1)-N(3)-C(11)-C(16)	1.4(7)
Cl(2)-Cr(1)-N(4)-C(16)	-171.7(4)	N(3)-C(11)-C(12)-C(13)	-1.6(11)
C(5)-N(1)-C(1)-C(2)	-1.6(11)	C(16)-C(11)-C(12)-C(13)	180.0(7)
Cr(1)-N(1)-C(1)-C(2)	172.7(7)	C(11)-C(12)-C(13)-C(14)	-0.1(13)
C(5)-N(1)-C(1)-C(6)	178.2(6)	C(12)-C(13)-C(14)-C(15)	0.8(13)
Cr(1)-N(1)-C(1)-C(6)	-7.5(9)	C(11)-N(3)-C(15)-C(14)	-2.0(12)
N(1)-C(1)-C(2)-C(3)	-2.0(15)	Cr(1)-N(3)-C(15)-C(14)	177.8(6)
C(6)-C(1)-C(2)-C(3)	178.2(10)	C(13)-C(14)-C(15)-N(3)	0.2(13)
C(1)-C(2)-C(3)-C(4)	5.2(18)	C(20)-N(4)-C(16)-C(17)	-0.4(9)
C(2)-C(3)-C(4)-C(5)	-4.7(17)	Cr(1)-N(4)-C(16)-C(17)	178.1(5)
C(1)-N(1)-C(5)-C(4)	2.3(11)	C(20)-N(4)-C(16)-C(11)	179.5(6)
Cr(1)-N(1)-C(5)-C(4)	-171.4(6)	Cr(1)-N(4)-C(16)-C(11)	-2.0(7)
C(3)-C(4)-C(5)-N(1)	0.8(13)	N(3)-C(11)-C(16)-N(4)	0.4(8)
C(10)-N(2)-C(6)-C(7)	-0.3(11)	C(12)-C(11)-C(16)-N(4)	178.9(6)
Cr(1)-N(2)-C(6)-C(7)	179.7(7)	N(3)-C(11)-C(16)-C(17)	-179.7(6)

C(12)-C(11)-C(16)-C(17)	-1.3(11)	Cl(3)-Cr(2)-N(7)-C(31)	91.2(5)
N(4)-C(16)-C(17)-C(18)	-0.1(11)	Cl(4)-Cr(2)-N(7)-C(31)	-53.3(16)
C(11)-C(16)-C(17)-C(18)	180.0(7)	N(8)-Cr(2)-N(7)-C(35)	179.7(6)
C(16)-C(17)-C(18)-C(19)	1.2(12)	N(6)-Cr(2)-N(7)-C(35)	5.4(6)
C(17)-C(18)-C(19)-C(20)	-1.8(13)	N(5)-Cr(2)-N(7)-C(35)	84.5(6)
C(16)-N(4)-C(20)-C(19)	-0.2(10)	Cl(3)-Cr(2)-N(7)-C(35)	-90.7(6)
Cr(1)-N(4)-C(20)-C(19)	-178.5(6)	Cl(4)-Cr(2)-N(7)-C(35)	124.7(13)
C(18)-C(19)-C(20)-N(4)	1.3(13)	N(6)-Cr(2)-N(8)-C(40)	-151.9(13)
N(8)-Cr(2)-N(5)-C(25)	12.5(6)	N(7)-Cr(2)-N(8)-C(40)	175.3(7)
N(6)-Cr(2)-N(5)-C(25)	-176.1(6)	N(5)-Cr(2)-N(8)-C(40)	-98.9(7)
N(7)-Cr(2)-N(5)-C(25)	90.6(6)	Cl(3)-Cr(2)-N(8)-C(40)	84.3(7)
Cl(3)-Cr(2)-N(5)-C(25)	155.5(16)	Cl(4)-Cr(2)-N(8)-C(40)	-11.3(7)
Cl(4)-Cr(2)-N(5)-C(25)	-84.2(6)	N(6)-Cr(2)-N(8)-C(36)	34.1(17)
N(8)-Cr(2)-N(5)-C(21)	-173.1(5)	N(7)-Cr(2)-N(8)-C(36)	1.3(5)
N(6)-Cr(2)-N(5)-C(21)	-1.7(5)	N(5)-Cr(2)-N(8)-C(36)	87.1(6)
N(7)-Cr(2)-N(5)-C(21)	-95.0(5)	Cl(3)-Cr(2)-N(8)-C(36)	-89.7(5)
Cl(3)-Cr(2)-N(5)-C(21)	-30(2)	Cl(4)-Cr(2)-N(8)-C(36)	174.6(5)
Cl(4)-Cr(2)-N(5)-C(21)	90.2(4)	C(25)-N(5)-C(21)-C(22)	-0.8(10)
N(8)-Cr(2)-N(6)-C(30)	-124.4(14)	Cr(2)-N(5)-C(21)-C(22)	-175.5(5)
N(7)-Cr(2)-N(6)-C(30)	-92.3(6)	C(25)-N(5)-C(21)-C(26)	177.6(6)
N(5)-Cr(2)-N(6)-C(30)	-178.5(7)	Cr(2)-N(5)-C(21)-C(26)	2.9(7)
Cl(3)-Cr(2)-N(6)-C(30)	-1.0(6)	N(5)-C(21)-C(22)-C(23)	1.5(11)
Cl(4)-Cr(2)-N(6)-C(30)	94.7(6)	C(26)-C(21)-C(22)-C(23)	-176.8(7)
N(8)-Cr(2)-N(6)-C(26)	54.3(15)	C(21)-C(22)-C(23)-C(24)	-3.1(12)
N(7)-Cr(2)-N(6)-C(26)	86.3(5)	C(22)-C(23)-C(24)-C(25)	3.8(13)
N(5)-Cr(2)-N(6)-C(26)	0.1(5)	C(21)-N(5)-C(25)-C(24)	1.5(11)
Cl(3)-Cr(2)-N(6)-C(26)	177.6(4)	Cr(2)-N(5)-C(25)-C(24)	175.6(6)
Cl(4)-Cr(2)-N(6)-C(26)	-86.6(5)	C(23)-C(24)-C(25)-N(5)	-3.1(13)
N(8)-Cr(2)-N(7)-C(31)	1.7(5)	C(30)-N(6)-C(26)-C(27)	0.7(10)
N(6)-Cr(2)-N(7)-C(31)	-172.6(5)	Cr(2)-N(6)-C(26)-C(27)	-178.0(6)
N(5)-Cr(2)-N(7)-C(31)	-93.6(5)	C(30)-N(6)-C(26)-C(21)	-179.9(6)

Cr(2)-N(6)-C(26)-C(21)	1.3(7)	C(32)-C(33)-C(34)-C(35)	0.3(17)
N(5)-C(21)-C(26)-N(6)	-2.8(8)	C(31)-N(7)-C(35)-C(34)	1.9(11)
C(22)-C(21)-C(26)-N(6)	175.6(6)	Cr(2)-N(7)-C(35)-C(34)	-175.9(6)
N(5)-C(21)-C(26)-C(27)	176.5(7)	C(33)-C(34)-C(35)-N(7)	-0.7(14)
C(22)-C(21)-C(26)-C(27)	-5.1(11)	C(40)-N(8)-C(36)-C(37)	1.2(12)
N(6)-C(26)-C(27)-C(28)	0.9(12)	Cr(2)-N(8)-C(36)-C(37)	175.6(7)
C(21)-C(26)-C(27)-C(28)	-178.4(8)	C(40)-N(8)-C(36)-C(31)	-178.2(7)
C(26)-C(27)-C(28)-C(29)	-2.9(14)	Cr(2)-N(8)-C(36)-C(31)	-3.8(9)
C(27)-C(28)-C(29)-C(30)	3.4(15)	N(7)-C(31)-C(36)-N(8)	5.4(10)
C(26)-N(6)-C(30)-C(29)	-0.3(12)	C(32)-C(31)-C(36)-N(8)	-174.4(8)
Cr(2)-N(6)-C(30)-C(29)	178.4(7)	N(7)-C(31)-C(36)-C(37)	-174.0(8)
C(28)-C(29)-C(30)-N(6)	-1.8(15)	C(32)-C(31)-C(36)-C(37)	6.3(13)
C(35)-N(7)-C(31)-C(36)	177.7(7)	N(8)-C(36)-C(37)-C(38)	-1.9(14)
Cr(2)-N(7)-C(31)-C(36)	-4.2(8)	C(31)-C(36)-C(37)-C(38)	177.4(9)
C(35)-N(7)-C(31)-C(32)	-2.5(11)	C(36)-C(37)-C(38)-C(39)	0.6(18)
Cr(2)-N(7)-C(31)-C(32)	175.6(6)	C(37)-C(38)-C(39)-C(40)	1.4(19)
N(7)-C(31)-C(32)-C(33)	2.0(14)	C(36)-N(8)-C(40)-C(39)	1.0(14)
C(36)-C(31)-C(32)-C(33)	-178.2(9)	Cr(2)-N(8)-C(40)-C(39)	-172.9(8)
C(31)-C(32)-C(33)-C(34)	-0.9(17)	C(38)-C(39)-C(40)-N(8)	-2.3(17)

[Hpyphenyl][$CrCl_4$(dppe)]

Table A.39 **Atomic coordinates (x 10^4) and equivalent isotropic displacement parameters ($Å^2$x 10^3) for [Hpyphenyl][$CrCl_4$(dppe)]. U(eq) is defined as one-third of the trace of the orthogonalised U^{ij} tensor**

	x	y	z	U(eq)
Cr(1)	8697(1)	3680(1)	1508(1)	39(1)
Cl(1)	9169(2)	3834(1)	489(1)	52(1)
Cl(2)	8754(2)	5093(1)	1638(1)	53(1)
Cl(3)	10867(2)	3491(1)	1668(1)	50(1)
Cl(4)	6477(2)	3647(1)	1453(1)	52(1)
P(1)	8318(2)	3361(1)	2589(1)	47(1)
P(2)	8482(2)	2162(1)	1490(1)	49(1)
C(1)	8434(9)	2247(5)	2683(3)	71(2)
C(2)	7763(9)	1839(5)	2231(3)	71(2)
C(11)	6797(7)	3669(5)	2942(3)	57(2)
C(12)	6111(9)	3182(7)	3368(4)	100(3)
C(13)	4965(12)	3506(10)	3661(5)	130(5)
C(14)	4569(12)	4271(12)	3512(6)	135(6)
C(15)	5243(11)	4743(8)	3107(5)	103(4)
C(16)	6353(8)	4447(6)	2813(4)	76(3)
C(21)	9424(7)	3711(5)	3102(3)	58(2)
C(22)	9396(9)	3370(7)	3672(4)	99(3)
C(23)	10194(12)	3664(9)	4070(4)	120(4)
C(24)	10975(10)	4328(8)	3917(5)	106(4)
C(25)	11037(9)	4683(6)	3362(4)	82(3)
C(26)	10244(8)	4357(5)	2962(3)	65(2)
C(31)	9954(7)	1568(4)	1367(3)	55(2)
C(32)	10751(8)	1778(5)	880(4)	73(2)

C(33)	11860(10)	1325(7)	729(5)	101(3)
C(34)	12131(10)	663(7)	1100(6)	105(4)
C(35)	11347(10)	461(6)	1599(5)	100(3)
C(36)	10247(8)	898(5)	1736(4)	72(2)
C(41)	7403(7)	1704(4)	1003(4)	56(2)
C(42)	7151(9)	2091(6)	489(4)	84(3)
C(43)	6378(11)	1721(7)	101(4)	101(3)
C(44)	5870(12)	973(8)	248(7)	126(5)
C(45)	6123(15)	598(8)	752(7)	157(6)
C(46)	6868(12)	950(6)	1154(5)	116(4)
N(1)	12323(7)	3906(4)	407(3)	67(2)
C(52)	13471(9)	3679(5)	577(3)	72(2)
C(53)	14563(8)	3767(5)	201(3)	68(2)
C(54)	14484(6)	4099(4)	-368(3)	46(2)
C(55)	13269(7)	4343(5)	-515(4)	66(2)
C(56)	12198(8)	4232(5)	-130(4)	72(2)
C(57)	15631(7)	4216(4)	-784(3)	51(2)
C(58)	16864(7)	4048(5)	-612(3)	58(2)
C(59)	17945(8)	4149(5)	-1014(4)	71(2)
C(60)	17813(9)	4433(5)	-1562(4)	75(2)
C(61)	16585(10)	4631(6)	-1742(4)	81(3)
C(62)	15503(7)	4523(5)	-1354(3)	63(2)
Cr(2)	1659(1)	1461(1)	6796(1)	50(1)
Cl(5)	1047(2)	1130(1)	5864(1)	75(1)
Cl(6)	2332(2)	150(1)	7088(1)	71(1)
Cl(7)	-415(2)	1209(1)	7239(1)	64(1)
Cl(8)	3714(2)	1891(1)	6437(1)	64(1)
P(3)	2346(2)	2056(1)	7704(1)	49(1)
P(4)	860(2)	2891(1)	6600(1)	49(1)
C(3)	2245(7)	3169(4)	7550(3)	51(2)
C(4)	961(7)	3385(4)	7292(3)	51(2)

C(71)	3990(7)	1894(4)	7924(3)	55(2)
C(72)	4691(10)	1198(6)	7789(4)	94(3)
C(73)	5915(10)	1088(7)	7964(5)	107(4)
C(74)	6490(10)	1619(7)	8275(4)	90(3)
C(75)	5849(10)	2327(7)	8389(5)	102(3)
C(76)	4607(9)	2449(5)	8223(4)	86(3)
C(81)	1341(7)	1836(5)	8389(3)	58(2)
C(82)	1224(11)	1035(5)	8592(4)	95(3)
C(83)	516(12)	817(6)	9119(4)	111(4)
C(84)	-97(10)	1388(7)	9438(4)	95(3)
C(85)	17(11)	2186(7)	9233(4)	114(4)
C(86)	755(10)	2423(6)	8723(3)	92(3)
C(91)	-790(7)	3084(4)	6415(3)	55(2)
C(92)	-1077(8)	3361(5)	5861(4)	67(2)
C(93)	-2357(10)	3495(6)	5721(5)	87(3)
C(94)	-3350(10)	3361(6)	6142(6)	96(3)
C(95)	-3081(9)	3098(6)	6699(5)	87(3)
C(96)	-1831(8)	2942(5)	6833(4)	71(2)
C(101)	1824(7)	3522(4)	6049(3)	51(2)
C(102)	2087(8)	4346(5)	6121(4)	72(2)
C(103)	2821(10)	4806(6)	5692(4)	93(3)
C(104)	3307(9)	4448(7)	5190(4)	91(3)
C(105)	3031(10)	3643(7)	5121(4)	91(3)
C(106)	2314(9)	3177(5)	5543(3)	79(3)
N(2)	-1916(9)	532(5)	6124(4)	102(3)
C(112)	-1662(12)	-8(8)	5717(5)	122(4)
C(113)	-2663(11)	-435(7)	5520(5)	107(4)
C(114)	-3910(9)	-338(5)	5751(4)	69(2)
C(115)	-4121(10)	241(6)	6163(4)	91(3)
C(116)	-3126(12)	658(7)	6340(5)	106(4)
C(117)	-5003(9)	-817(5)	5560(3)	67(2)

C(118)	-4796(10)	-1382(6)	5135(4)	90(3)
C(119)	-5789(13)	-1839(7)	4966(5)	116(4)
C(120)	-7037(12)	-1742(7)	5205(5)	103(3)
C(121)	-7272(11)	-1177(8)	5621(5)	106(3)
C(122)	-6251(11)	-729(6)	5796(4)	95(3)
O(1S)	2758(17)	1391(11)	2992(8)	162(6)
C(1S)	3850(20)	1284(13)	2586(10)	125(7)
C(2S)	3780(20)	2019(13)	2182(9)	114(6)
C(3S)	3410(20)	2523(15)	2469(11)	134(8)
C(4S)	2600(20)	2244(14)	2897(10)	133(8)
O(2S)	90(20)	925(15)	3463(11)	102(8)

Table A.40 Bond lengths [Å] and angles [°] for [Hpyphenyl][$CrCl_4$(dppe)]

Cr(1)-Cl(4)	2.310(2)	C(2)-H(2A)	0.9700
Cr(1)-Cl(3)	2.319(2)	C(2)-H(2B)	0.9700
Cr(1)-Cl(1)	2.3401(19)	C(11)-C(12)	1.372(11)
Cr(1)-Cl(2)	2.3450(19)	C(11)-C(16)	1.374(11)
Cr(1)-P(2)	2.492(2)	C(12)-C(13)	1.432(14)
Cr(1)-P(1)	2.494(2)	C(12)-H(12)	0.9300
P(1)-C(11)	1.797(7)	C(13)-C(14)	1.347(17)
P(1)-C(21)	1.817(8)	C(13)-H(13)	0.9300
P(1)-C(1)	1.824(8)	C(14)-C(15)	1.323(17)
P(2)-C(31)	1.817(7)	C(14)-H(14)	0.9300
P(2)-C(41)	1.828(8)	C(15)-C(16)	1.386(12)
P(2)-C(2)	1.843(8)	C(15)-H(15)	0.9300
C(1)-C(2)	1.480(11)	C(16)-H(16)	0.9300
C(1)-H(1A)	0.9700	C(21)-C(26)	1.361(11)
C(1)-H(1B)	0.9700	C(21)-C(22)	1.385(11)

C(22)-C(23)	1.382(13)	N(1)-C(52)	1.323(10)
C(22)-H(22)	0.9300	N(1)-C(56)	1.325(9)
C(23)-C(24)	1.364(15)	N(1)-H(1)	0.8600
C(23)-H(23)	0.9300	C(52)-C(53)	1.366(10)
C(24)-C(25)	1.360(13)	C(52)-H(52)	0.9300
C(24)-H(24)	0.9300	C(53)-C(54)	1.387(9)
C(25)-C(26)	1.402(11)	C(53)-H(53)	0.9300
C(25)-H(25)	0.9300	C(54)-C(55)	1.379(9)
C(26)-H(26)	0.9300	C(54)-C(57)	1.467(9)
C(31)-C(32)	1.360(11)	C(55)-C(56)	1.364(10)
C(31)-C(36)	1.389(10)	C(55)-H(55)	0.9300
C(32)-C(33)	1.395(12)	C(56)-H(56)	0.9300
C(32)-H(32)	0.9300	C(57)-C(58)	1.384(9)
C(33)-C(34)	1.376(14)	C(57)-C(62)	1.386(10)
C(33)-H(33)	0.9300	C(58)-C(59)	1.393(10)
C(34)-C(35)	1.371(14)	C(58)-H(58)	0.9300
C(34)-H(34)	0.9300	C(59)-C(60)	1.328(11)
C(35)-C(36)	1.368(11)	C(59)-H(59)	0.9300
C(35)-H(35)	0.9300	C(60)-C(61)	1.396(11)
C(36)-H(36)	0.9300	C(60)-H(60)	0.9300
C(41)-C(42)	1.343(11)	C(61)-C(62)	1.376(11)
C(41)-C(46)	1.364(12)	C(61)-H(61)	0.9300
C(42)-C(43)	1.402(12)	C(62)-H(62)	0.9300
C(42)-H(42)	0.9300	Cr(2)-Cl(8)	2.312(2)
C(43)-C(44)	1.343(14)	Cr(2)-Cl(6)	2.326(2)
C(43)-H(43)	0.9300	Cr(2)-Cl(7)	2.326(2)
C(44)-C(45)	1.316(16)	Cr(2)-Cl(5)	2.361(2)
C(44)-H(44)	0.9300	Cr(2)-P(3)	2.496(2)
C(45)-C(46)	1.395(15)	Cr(2)-P(4)	2.502(2)
C(45)-H(45)	0.9300	P(3)-C(71)	1.825(8)
C(46)-H(46)	0.9300	P(3)-C(81)	1.827(7)

P(3)-C(3)	1.835(7)	C(91)-C(92)	1.372(10)
P(4)-C(91)	1.813(8)	C(91)-C(96)	1.393(10)
P(4)-C(101)	1.815(7)	C(92)-C(93)	1.399(11)
P(4)-C(4)	1.829(6)	C(92)-H(92)	0.9300
C(3)-C(4)	1.528(9)	C(93)-C(94)	1.359(13)
C(3)-H(3A)	0.9700	C(93)-H(93)	0.9300
C(3)-H(3B)	0.9700	C(94)-C(95)	1.370(13)
C(4)-H(4A)	0.9700	C(94)-H(94)	0.9300
C(4)-H(4B)	0.9700	C(95)-C(96)	1.371(11)
C(71)-C(76)	1.358(10)	C(95)-H(95)	0.9300
C(71)-C(72)	1.383(10)	C(96)-H(96)	0.9300
C(72)-C(73)	1.364(12)	C(101)-C(106)	1.376(10)
C(72)-H(72)	0.9300	C(101)-C(102)	1.394(10)
C(73)-C(74)	1.323(13)	C(102)-C(103)	1.379(11)
C(73)-H(73)	0.9300	C(102)-H(102)	0.9300
C(74)-C(75)	1.360(12)	C(103)-C(104)	1.378(13)
C(74)-H(74)	0.9300	C(103)-H(103)	0.9300
C(75)-C(76)	1.377(12)	C(104)-C(105)	1.368(13)
C(75)-H(75)	0.9300	C(104)-H(104)	0.9300
C(76)-H(76)	0.9300	C(105)-C(106)	1.365(11)
C(81)-C(82)	1.363(11)	C(105)-H(105)	0.9300
C(81)-C(86)	1.372(10)	C(106)-H(106)	0.9300
C(82)-C(83)	1.386(12)	N(2)-C(116)	1.330(12)
C(82)-H(82)	0.9300	N(2)-C(112)	1.330(12)
C(83)-C(84)	1.346(13)	N(2)-H(2)	0.8600
C(83)-H(83)	0.9300	C(112)-C(113)	1.367(14)
C(84)-C(85)	1.359(13)	C(112)-H(112)	0.9300
C(84)-H(84)	0.9300	C(113)-C(114)	1.367(12)
C(85)-C(86)	1.379(12)	C(113)-H(113)	0.9300
C(85)-H(85)	0.9300	C(114)-C(115)	1.379(11)
C(86)-H(86)	0.9300	C(114)-C(117)	1.483(12)

C(115)-C(116)	1.337(13)	Cl(4)-Cr(1)-Cl(2)	93.96(7)
C(115)-H(115)	0.9300	Cl(3)-Cr(1)-Cl(2)	93.87(7)
C(116)-H(116)	0.9300	Cl(1)-Cr(1)-Cl(2)	94.17(7)
C(117)-C(122)	1.370(12)	Cl(4)-Cr(1)-P(2)	83.19(7)
C(117)-C(118)	1.383(11)	Cl(3)-Cr(1)-P(2)	88.22(7)
C(118)-C(119)	1.364(13)	Cl(1)-Cr(1)-P(2)	92.52(7)
C(118)-H(118)	0.9300	Cl(2)-Cr(1)-P(2)	172.92(8)
C(119)-C(120)	1.375(14)	Cl(4)-Cr(1)-P(1)	88.20(7)
C(119)-H(119)	0.9300	Cl(3)-Cr(1)-P(1)	84.57(7)
C(120)-C(121)	1.371(14)	Cl(1)-Cr(1)-P(1)	173.48(8)
C(120)-H(120)	0.9300	Cl(2)-Cr(1)-P(1)	91.53(7)
C(121)-C(122)	1.383(13)	P(2)-Cr(1)-P(1)	81.93(7)
C(121)-H(121)	0.9300	C(11)-P(1)-C(21)	100.1(3)
C(122)-H(122)	0.9300	C(11)-P(1)-C(1)	108.2(4)
O(1S)-C(4S)	1.41(2)	C(21)-P(1)-C(1)	102.9(4)
O(1S)-C(1S)	1.42(2)	C(11)-P(1)-Cr(1)	117.6(3)
C(1S)-C(2S)	1.47(2)	C(21)-P(1)-Cr(1)	121.7(3)
C(1S)-H(1SA)	0.9700	C(1)-P(1)-Cr(1)	105.0(2)
C(1S)-H(1SB)	0.9700	C(31)-P(2)-C(41)	102.0(3)
C(2S)-C(3S)	1.13(2)	C(31)-P(2)-C(2)	106.9(4)
C(2S)-H(2SA)	0.9700	C(41)-P(2)-C(2)	103.4(4)
C(2S)-H(2SB)	0.9700	C(31)-P(2)-Cr(1)	117.9(3)
C(3S)-C(4S)	1.30(3)	C(41)-P(2)-Cr(1)	120.9(2)
C(3S)-H(3SA)	0.9700	C(2)-P(2)-Cr(1)	104.2(3)
C(3S)-H(3SB)	0.9700	C(2)-C(1)-P(1)	111.4(6)
C(4S)-H(4SA)	0.9700	C(2)-C(1)-H(1A)	109.3
C(4S)-H(4SB)	0.9700	P(1)-C(1)-H(1A)	109.3
		C(2)-C(1)-H(1B)	109.3
Cl(4)-Cr(1)-Cl(3)	169.48(8)	P(1)-C(1)-H(1B)	109.3
Cl(4)-Cr(1)-Cl(1)	94.54(7)	H(1A)-C(1)-H(1B)	108.0
Cl(3)-Cr(1)-Cl(1)	91.88(7)	C(1)-C(2)-P(2)	110.4(6)

C(1)-C(2)-H(2A)	109.6	C(22)-C(23)-H(23)	119.8
P(2)-C(2)-H(2A)	109.6	C(25)-C(24)-C(23)	120.8(10)
C(1)-C(2)-H(2B)	109.6	C(25)-C(24)-H(24)	119.6
P(2)-C(2)-H(2B)	109.6	C(23)-C(24)-H(24)	119.6
H(2A)-C(2)-H(2B)	108.1	C(24)-C(25)-C(26)	117.6(10)
C(12)-C(11)-C(16)	118.6(8)	C(24)-C(25)-H(25)	121.2
C(12)-C(11)-P(1)	122.7(7)	C(26)-C(25)-H(25)	121.2
C(16)-C(11)-P(1)	118.5(6)	C(21)-C(26)-C(25)	123.5(8)
C(11)-C(12)-C(13)	118.8(11)	C(21)-C(26)-H(26)	118.3
C(11)-C(12)-H(12)	120.6	C(25)-C(26)-H(26)	118.3
C(13)-C(12)-H(12)	120.6	C(32)-C(31)-C(36)	120.2(7)
C(14)-C(13)-C(12)	120.0(12)	C(32)-C(31)-P(2)	117.6(6)
C(14)-C(13)-H(13)	120.0	C(36)-C(31)-P(2)	122.2(6)
C(12)-C(13)-H(13)	120.0	C(31)-C(32)-C(33)	121.6(9)
C(15)-C(14)-C(13)	121.0(12)	C(31)-C(32)-H(32)	119.2
C(15)-C(14)-H(14)	119.5	C(33)-C(32)-H(32)	119.2
C(13)-C(14)-H(14)	119.5	C(34)-C(33)-C(32)	117.3(10)
C(14)-C(15)-C(16)	120.4(12)	C(34)-C(33)-H(33)	121.4
C(14)-C(15)-H(15)	119.8	C(32)-C(33)-H(33)	121.4
C(16)-C(15)-H(15)	119.8	C(35)-C(34)-C(33)	121.3(9)
C(11)-C(16)-C(15)	121.1(10)	C(35)-C(34)-H(34)	119.3
C(11)-C(16)-H(16)	119.4	C(33)-C(34)-H(34)	119.3
C(15)-C(16)-H(16)	119.4	C(36)-C(35)-C(34)	120.9(9)
C(26)-C(21)-C(22)	116.8(8)	C(36)-C(35)-H(35)	119.5
C(26)-C(21)-P(1)	122.0(6)	C(34)-C(35)-H(35)	119.5
C(22)-C(21)-P(1)	121.0(7)	C(35)-C(36)-C(31)	118.6(9)
C(23)-C(22)-C(21)	120.9(10)	C(35)-C(36)-H(36)	120.7
C(23)-C(22)-H(22)	119.5	C(31)-C(36)-H(36)	120.7
C(21)-C(22)-H(22)	119.5	C(42)-C(41)-C(46)	119.3(8)
C(24)-C(23)-C(22)	120.3(10)	C(42)-C(41)-P(2)	120.9(6)
C(24)-C(23)-H(23)	119.8	C(46)-C(41)-P(2)	119.8(7)

C(41)-C(42)-C(43)	120.9(9)	N(1)-C(56)-H(56)	120.1
C(41)-C(42)-H(42)	119.6	C(55)-C(56)-H(56)	120.1
C(43)-C(42)-H(42)	119.6	C(58)-C(57)-C(62)	118.5(7)
C(44)-C(43)-C(42)	119.6(10)	C(58)-C(57)-C(54)	121.1(6)
C(44)-C(43)-H(43)	120.2	C(62)-C(57)-C(54)	120.3(7)
C(42)-C(43)-H(43)	120.2	C(57)-C(58)-C(59)	120.7(7)
C(45)-C(44)-C(43)	119.1(11)	C(57)-C(58)-H(58)	119.7
C(45)-C(44)-H(44)	120.4	C(59)-C(58)-H(58)	119.7
C(43)-C(44)-H(44)	120.4	C(60)-C(59)-C(58)	120.4(8)
C(44)-C(45)-C(46)	123.1(11)	C(60)-C(59)-H(59)	119.8
C(44)-C(45)-H(45)	118.4	C(58)-C(59)-H(59)	119.8
C(46)-C(45)-H(45)	118.4	C(59)-C(60)-C(61)	120.1(8)
C(41)-C(46)-C(45)	117.9(10)	C(59)-C(60)-H(60)	119.9
C(41)-C(46)-H(46)	121.0	C(61)-C(60)-H(60)	119.9
C(45)-C(46)-H(46)	121.0	C(62)-C(61)-C(60)	120.3(8)
C(52)-N(1)-C(56)	121.1(7)	C(62)-C(61)-H(61)	119.8
C(52)-N(1)-H(1)	119.5	C(60)-C(61)-H(61)	119.8
C(56)-N(1)-H(1)	119.5	C(61)-C(62)-C(57)	119.9(7)
N(1)-C(52)-C(53)	121.0(7)	C(61)-C(62)-H(62)	120.1
N(1)-C(52)-H(52)	119.5	C(57)-C(62)-H(62)	120.1
C(53)-C(52)-H(52)	119.5	Cl(8)-Cr(2)-Cl(6)	94.03(8)
C(52)-C(53)-C(54)	120.3(7)	Cl(8)-Cr(2)-Cl(7)	171.18(8)
C(52)-C(53)-H(53)	119.9	Cl(6)-Cr(2)-Cl(7)	91.38(8)
C(54)-C(53)-H(53)	119.9	Cl(8)-Cr(2)-Cl(5)	93.70(8)
C(55)-C(54)-C(53)	116.2(7)	Cl(6)-Cr(2)-Cl(5)	96.27(8)
C(55)-C(54)-C(57)	121.6(6)	Cl(7)-Cr(2)-Cl(5)	92.63(8)
C(53)-C(54)-C(57)	122.2(6)	Cl(8)-Cr(2)-P(3)	81.76(8)
C(56)-C(55)-C(54)	121.7(7)	Cl(6)-Cr(2)-P(3)	92.70(8)
C(56)-C(55)-H(55)	119.1	Cl(7)-Cr(2)-P(3)	91.03(7)
C(54)-C(55)-H(55)	119.1	Cl(5)-Cr(2)-P(3)	170.22(8)
N(1)-C(56)-C(55)	119.7(8)	Cl(8)-Cr(2)-P(4)	89.00(8)

Cl(6)-Cr(2)-P(4)	173.62(8)	C(73)-C(72)-C(71)	120.8(9)
Cl(7)-Cr(2)-P(4)	84.96(8)	C(73)-C(72)-H(72)	119.6
Cl(5)-Cr(2)-P(4)	89.13(8)	C(71)-C(72)-H(72)	119.6
P(3)-Cr(2)-P(4)	82.16(7)	C(74)-C(73)-C(72)	123.0(9)
C(71)-P(3)-C(81)	103.1(3)	C(74)-C(73)-H(73)	118.5
C(71)-P(3)-C(3)	104.2(3)	C(72)-C(73)-H(73)	118.5
C(81)-P(3)-C(3)	105.6(3)	C(73)-C(74)-C(75)	117.5(9)
C(71)-P(3)-Cr(2)	120.2(2)	C(73)-C(74)-H(74)	121.3
C(81)-P(3)-Cr(2)	117.8(3)	C(75)-C(74)-H(74)	121.3
C(3)-P(3)-Cr(2)	104.3(2)	C(74)-C(75)-C(76)	120.6(9)
C(91)-P(4)-C(101)	103.3(3)	C(74)-C(75)-H(75)	119.7
C(91)-P(4)-C(4)	103.9(3)	C(76)-C(75)-H(75)	119.7
C(101)-P(4)-C(4)	105.9(3)	C(71)-C(76)-C(75)	122.2(8)
C(91)-P(4)-Cr(2)	121.2(2)	C(71)-C(76)-H(76)	118.9
C(101)-P(4)-Cr(2)	116.0(2)	C(75)-C(76)-H(76)	118.9
C(4)-P(4)-Cr(2)	105.0(2)	C(82)-C(81)-C(86)	118.2(7)
C(4)-C(3)-P(3)	109.9(5)	C(82)-C(81)-P(3)	117.3(6)
C(4)-C(3)-H(3A)	109.7	C(86)-C(81)-P(3)	124.4(6)
P(3)-C(3)-H(3A)	109.7	C(81)-C(82)-C(83)	121.0(8)
C(4)-C(3)-H(3B)	109.7	C(81)-C(82)-H(82)	119.5
P(3)-C(3)-H(3B)	109.7	C(83)-C(82)-H(82)	119.5
H(3A)-C(3)-H(3B)	108.2	C(84)-C(83)-C(82)	120.9(9)
C(3)-C(4)-P(4)	109.9(4)	C(84)-C(83)-H(83)	119.5
C(3)-C(4)-H(4A)	109.7	C(82)-C(83)-H(83)	119.5
P(4)-C(4)-H(4A)	109.7	C(83)-C(84)-C(85)	118.0(9)
C(3)-C(4)-H(4B)	109.7	C(83)-C(84)-H(84)	121.0
P(4)-C(4)-H(4B)	109.7	C(85)-C(84)-H(84)	121.0
H(4A)-C(4)-H(4B)	108.2	C(84)-C(85)-C(86)	122.3(9)
C(76)-C(71)-C(72)	115.8(8)	C(84)-C(85)-H(85)	118.9
C(76)-C(71)-P(3)	122.2(6)	C(86)-C(85)-H(85)	118.9
C(72)-C(71)-P(3)	121.9(6)	C(81)-C(86)-C(85)	119.5(9)

C(81)-C(86)-H(86)	120.3	C(103)-C(104)-H(104)	120.4
C(85)-C(86)-H(86)	120.3	C(106)-C(105)-C(104)	121.7(9)
C(92)-C(91)-C(96)	117.1(8)	C(106)-C(105)-H(105)	119.2
C(92)-C(91)-P(4)	122.2(6)	C(104)-C(105)-H(105)	119.2
C(96)-C(91)-P(4)	120.7(6)	C(105)-C(106)-C(101)	119.9(8)
C(91)-C(92)-C(93)	121.6(9)	C(105)-C(106)-H(106)	120.0
C(91)-C(92)-H(92)	119.2	C(101)-C(106)-H(106)	120.0
C(93)-C(92)-H(92)	119.2	C(116)-N(2)-C(112)	120.8(10)
C(94)-C(93)-C(92)	119.9(9)	C(116)-N(2)-H(2)	119.6
C(94)-C(93)-H(93)	120.0	C(112)-N(2)-H(2)	119.6
C(92)-C(93)-H(93)	120.0	N(2)-C(112)-C(113)	119.3(11)
C(93)-C(94)-C(95)	119.3(9)	N(2)-C(112)-H(112)	120.4
C(93)-C(94)-H(94)	120.4	C(113)-C(112)-H(112)	120.4
C(95)-C(94)-H(94)	120.4	C(112)-C(113)-C(114)	121.1(9)
C(94)-C(95)-C(96)	121.0(10)	C(112)-C(113)-H(113)	119.5
C(94)-C(95)-H(95)	119.5	C(114)-C(113)-H(113)	119.5
C(96)-C(95)-H(95)	119.5	C(113)-C(114)-C(115)	117.2(9)
C(95)-C(96)-C(91)	121.1(8)	C(113)-C(114)-C(117)	122.0(8)
C(95)-C(96)-H(96)	119.5	C(115)-C(114)-C(117)	120.8(8)
C(91)-C(96)-H(96)	119.5	C(116)-C(115)-C(114)	120.3(10)
C(106)-C(101)-C(102)	118.9(7)	C(116)-C(115)-H(115)	119.8
C(106)-C(101)-P(4)	119.0(6)	C(114)-C(115)-H(115)	119.8
C(102)-C(101)-P(4)	122.1(6)	N(2)-C(116)-C(115)	121.3(10)
C(103)-C(102)-C(101)	120.4(8)	N(2)-C(116)-H(116)	119.4
C(103)-C(102)-H(102)	119.8	C(115)-C(116)-H(116)	119.4
C(101)-C(102)-H(102)	119.8	C(122)-C(117)-C(118)	117.1(9)
C(104)-C(103)-C(102)	119.8(9)	C(122)-C(117)-C(114)	122.1(8)
C(104)-C(103)-H(103)	120.1	C(118)-C(117)-C(114)	120.8(8)
C(102)-C(103)-H(103)	120.1	C(119)-C(118)-C(117)	121.4(10)
C(105)-C(104)-C(103)	119.2(8)	C(119)-C(118)-H(118)	119.3
C(105)-C(104)-H(104)	120.4	C(117)-C(118)-H(118)	119.3

C(118)-C(119)-C(120)	120.9(10)	C(1S)-C(2S)-H(2SA)	110.7
C(118)-C(119)-H(119)	119.6	C(4S)-C(2S)-H(2SA)	141.6
C(120)-C(119)-H(119)	119.6	C(3S)-C(2S)-H(2SB)	110.7
C(121)-C(120)-C(119)	118.9(11)	C(1S)-C(2S)-H(2SB)	110.7
C(121)-C(120)-H(120)	120.5	C(4S)-C(2S)-H(2SB)	104.0
C(119)-C(120)-H(120)	120.5	H(2SA)-C(2S)-H(2SB)	108.8
C(120)-C(121)-C(122)	119.5(10)	C(2S)-C(3S)-C(4S)	112(3)
C(120)-C(121)-H(121)	120.3	C(2S)-C(3S)-H(3SA)	109.3
C(122)-C(121)-H(121)	120.3	C(4S)-C(3S)-H(3SA)	109.3
C(117)-C(122)-C(121)	122.2(9)	C(2S)-C(3S)-H(3SB)	109.3
C(117)-C(122)-H(122)	118.9	C(4S)-C(3S)-H(3SB)	109.3
C(121)-C(122)-H(122)	118.9	H(3SA)-C(3S)-H(3SB)	107.9
C(4S)-O(1S)-C(1S)	98.9(18)	C(3S)-C(4S)-O(1S)	110(2)
O(1S)-C(1S)-C(2S)	102.1(17)	O(1S)-C(4S)-C(2S)	80.1(14)
O(1S)-C(1S)-H(1SA)	111.4	C(3S)-C(4S)-H(4SA)	109.7
C(2S)-C(1S)-H(1SA)	111.4	O(1S)-C(4S)-H(4SA)	109.7
O(1S)-C(1S)-H(1SB)	111.4	C(2S)-C(4S)-H(4SA)	112.3
C(2S)-C(1S)-H(1SB)	111.4	C(3S)-C(4S)-H(4SB)	109.7
H(1SA)-C(1S)-H(1SB)	109.2	O(1S)-C(4S)-H(4SB)	109.7
C(3S)-C(2S)-C(1S)	105(2)	C(2S)-C(4S)-H(4SB)	131.8
C(1S)-C(2S)-C(4S)	74.2(14)	H(4SA)-C(4S)-H(4SB)	108.2
C(3S)-C(2S)-H(2SA)	110.7		

Table A.41 **Anisotropic displacement parameters ($Å^2 x\ 10^3$) for [Hpyphenyl][$CrCl_4$(dppe)]. The anisotropic displacement factor exponent takes the form:**

$2p^2[h^2a^{*2}U^{11} + ... + 2\ h\ k\ a^*\ b^*\ U^{12}]$

	U^{11}	U^{22}	U^{33}	U^{23}	U^{13}	U^{12}
Cr(1)	44(1)	37(1)	36(1)	-6(1)	-3(1)	5(1)
Cl(1)	58(1)	60(1)	38(1)	-2(1)	-3(1)	3(1)
Cl(2)	66(1)	38(1)	57(1)	-11(1)	-13(1)	6(1)
Cl(3)	45(1)	58(1)	47(1)	-6(1)	-2(1)	7(1)
Cl(4)	44(1)	58(1)	54(1)	-10(1)	-8(1)	6(1)
P(1)	50(1)	53(1)	36(1)	-6(1)	0(1)	6(1)
P(2)	62(1)	38(1)	48(1)	-8(1)	-3(1)	4(1)
C(1)	105(7)	61(5)	42(4)	12(4)	9(4)	13(5)
C(2)	92(6)	57(5)	62(5)	-7(4)	12(5)	-7(4)
C(11)	56(5)	78(6)	38(4)	-18(4)	3(3)	3(4)
C(12)	72(7)	138(9)	85(7)	3(7)	25(6)	3(6)
C(13)	90(9)	202(15)	91(8)	-13(9)	48(7)	-11(9)
C(14)	74(8)	243(19)	90(9)	-34(11)	7(7)	55(10)
C(15)	89(8)	157(11)	69(6)	-33(7)	-16(6)	43(7)
C(16)	64(6)	104(7)	62(5)	-23(5)	1(4)	29(5)
C(21)	51(5)	76(6)	46(4)	-9(4)	-1(4)	8(4)
C(22)	85(7)	163(10)	49(5)	21(6)	-16(5)	-29(7)
C(23)	115(10)	193(13)	51(6)	21(7)	-31(6)	-16(9)
C(24)	80(8)	168(12)	78(8)	-44(8)	-25(6)	10(7)
C(25)	85(7)	91(7)	74(6)	-21(5)	-25(5)	3(5)
C(26)	73(6)	69(5)	57(5)	-22(4)	-17(4)	18(5)
C(31)	57(5)	50(4)	59(5)	-14(4)	-11(4)	5(4)
C(32)	76(6)	68(6)	76(6)	-18(5)	-8(5)	20(5)
C(33)	88(8)	104(8)	110(8)	-24(7)	13(6)	20(6)
C(34)	85(8)	81(7)	146(10)	-13(7)	15(7)	35(6)

C(35)	72(7)	83(7)	140(10)	23(7)	1(7)	20(5)
C(36)	63(6)	60(5)	92(6)	6(5)	-10(5)	17(4)
C(41)	58(5)	37(4)	74(5)	-12(4)	-8(4)	5(3)
C(42)	111(8)	75(6)	70(6)	-11(5)	-23(5)	-18(5)
C(43)	144(10)	90(8)	78(7)	-27(6)	-42(6)	-17(7)
C(44)	138(11)	95(9)	160(13)	-42(9)	-74(10)	-19(8)
C(45)	208(16)	85(9)	188(15)	6(9)	-99(13)	-64(9)
C(46)	150(10)	72(7)	132(10)	9(6)	-65(8)	-31(7)
N(1)	61(5)	70(5)	65(4)	-1(4)	19(4)	-1(4)
C(52)	75(6)	91(7)	48(5)	1(4)	2(4)	10(5)
C(53)	64(5)	90(6)	48(5)	9(4)	-2(4)	17(4)
C(54)	41(4)	47(4)	52(4)	-8(3)	-7(3)	3(3)
C(55)	56(5)	78(6)	62(5)	11(4)	-2(4)	-7(4)
C(56)	53(5)	79(6)	81(6)	17(5)	-1(5)	3(4)
C(57)	53(5)	50(4)	52(4)	-11(3)	-4(4)	-2(3)
C(58)	48(5)	70(5)	57(5)	2(4)	-7(4)	4(4)
C(59)	47(5)	89(6)	78(6)	-5(5)	-5(4)	-5(4)
C(60)	64(6)	89(7)	72(6)	-16(5)	9(5)	-9(5)
C(61)	93(7)	94(7)	54(5)	4(5)	3(5)	6(6)
C(62)	50(5)	87(6)	51(5)	0(4)	3(4)	12(4)
Cr(2)	66(1)	41(1)	41(1)	-10(1)	5(1)	6(1)
Cl(5)	98(2)	77(1)	51(1)	-23(1)	2(1)	-4(1)
Cl(6)	105(2)	40(1)	64(1)	-5(1)	9(1)	12(1)
Cl(7)	70(1)	67(1)	55(1)	-10(1)	6(1)	-4(1)
Cl(8)	62(1)	64(1)	62(1)	-3(1)	10(1)	10(1)
P(3)	64(1)	41(1)	43(1)	-10(1)	-1(1)	11(1)
P(4)	61(1)	46(1)	40(1)	-7(1)	0(1)	8(1)
C(3)	68(5)	40(4)	44(4)	-8(3)	-4(4)	4(3)
C(4)	64(5)	47(4)	42(4)	-11(3)	-3(3)	13(4)
C(71)	66(5)	51(5)	47(4)	-6(3)	-3(4)	13(4)
C(72)	102(8)	78(6)	111(8)	-34(6)	-51(6)	37(6)

C(73)	102(8)	104(8)	126(9)	-46(7)	-47(7)	51(7)
C(74)	84(7)	95(8)	97(7)	-16(6)	-35(6)	22(6)
C(75)	95(8)	96(8)	123(9)	-36(7)	-49(7)	11(6)
C(76)	90(7)	64(6)	112(8)	-42(5)	-38(6)	14(5)
C(81)	74(5)	60(5)	41(4)	-5(4)	0(4)	3(4)
C(82)	156(10)	50(5)	74(6)	-16(5)	37(6)	3(6)
C(83)	177(11)	74(7)	74(7)	-1(5)	30(7)	-17(7)
C(84)	131(9)	94(8)	54(5)	-5(5)	29(6)	-9(7)
C(85)	159(11)	102(9)	73(7)	-19(6)	43(7)	29(8)
C(86)	149(9)	68(6)	52(5)	-4(4)	33(6)	29(6)
C(91)	62(5)	52(4)	51(4)	-6(4)	-2(4)	7(4)
C(92)	76(6)	67(5)	59(5)	-11(4)	-9(4)	0(4)
C(93)	88(8)	98(8)	82(7)	-11(6)	-36(6)	19(6)
C(94)	72(7)	86(7)	137(10)	-46(7)	-35(7)	16(6)
C(95)	69(7)	97(7)	96(8)	-24(6)	-1(6)	12(5)
C(96)	68(6)	72(6)	74(6)	-12(4)	-11(5)	11(4)
C(101)	62(5)	51(5)	40(4)	-1(3)	-6(3)	9(4)
C(102)	80(6)	74(6)	62(5)	-10(4)	3(4)	-16(5)
C(103)	119(8)	85(7)	74(6)	-1(5)	9(6)	-43(6)
C(104)	87(7)	107(9)	73(7)	32(6)	2(5)	-22(6)
C(105)	121(8)	89(7)	55(5)	14(5)	23(5)	19(6)
C(106)	123(8)	57(5)	53(5)	2(4)	20(5)	15(5)
N(2)	92(7)	97(6)	122(7)	-29(6)	-31(6)	-6(5)
C(112)	100(9)	148(11)	122(9)	-67(9)	7(7)	-6(8)
C(113)	96(8)	117(9)	111(8)	-64(7)	7(7)	-5(7)
C(114)	79(6)	72(6)	59(5)	-18(4)	-7(5)	3(5)
C(115)	95(7)	84(7)	102(7)	-50(6)	-22(6)	12(6)
C(116)	114(10)	95(8)	116(9)	-48(7)	-24(8)	6(7)
C(117)	85(6)	65(5)	54(5)	-14(4)	-1(4)	10(5)
C(118)	101(8)	78(7)	92(7)	-38(5)	12(6)	10(6)
C(119)	132(11)	97(8)	123(10)	-56(7)	-1(8)	-19(8)

C(120)	121(10)	94(8)	93(8)	-17(6)	-4(7)	-31(7)
C(121)	84(8)	132(10)	100(8)	-16(7)	12(6)	-12(7)
C(122)	103(8)	101(8)	82(7)	-42(6)	10(6)	3(6)

Table A.42 **Hydrogen coordinates (x 10^4) and isotropic displacement parameters (Å^{2}x 10^3) for [Hpyphenyl][$CrCl_4$(dppe)]**

	x	y	z	U(eq)
H(1A)	9341	2089	2658	85
H(1B)	8052	2065	3070	85
H(2A)	6850	1981	2263	85
H(2B)	7834	1249	2294	85
H(12)	6386	2652	3464	120
H(13)	4494	3188	3954	156
H(14)	3809	4471	3696	162
H(15)	4971	5276	3020	124
H(16)	6804	4781	2522	92
H(22)	8833	2937	3789	119
H(23)	10199	3409	4445	144
H(24)	11471	4540	4195	128
H(25)	11585	5126	3251	98
H(26)	10281	4594	2581	78
H(32)	10553	2234	641	87
H(33)	12394	1465	392	121
H(34)	12859	347	1011	126
H(35)	11567	20	1848	120
H(36)	9707	751	2070	86
H(42)	7494	2611	390	101

H(43)	6217	1991	-255	121
H(44)	5346	724	-3	151
H(45)	5789	73	844	188
H(46)	6997	680	1515	139
H(1)	11648	3840	649	80
H(52)	13536	3457	958	86
H(53)	15362	3603	328	82
H(55)	13176	4591	-886	79
H(56)	11384	4385	-244	87
H(58)	16971	3867	-226	70
H(59)	18765	4015	-897	86
H(60)	18539	4501	-1827	90
H(61)	16498	4837	-2125	98
H(62)	14687	4656	-1476	76
H(3A)	2308	3447	7910	61
H(3B)	2962	3352	7274	61
H(4A)	899	3976	7223	61
H(4B)	245	3203	7568	61
H(72)	4324	801	7578	112
H(73)	6365	619	7859	128
H(74)	7302	1512	8410	108
H(75)	6252	2731	8580	122
H(76)	4177	2929	8320	103
H(82)	1625	629	8375	114
H(83)	463	268	9253	133
H(84)	-583	1242	9788	114
H(85)	-418	2585	9445	136
H(86)	855	2976	8606	110
H(92)	-404	3461	5571	81
H(93)	-2528	3675	5342	105
H(94)	-4203	3447	6052	115

H(95)	-3755	3024	6991	104
H(96)	-1675	2738	7210	85
H(102)	1766	4586	6461	86
H(103)	2988	5356	5741	112
H(104)	3816	4752	4901	109
H(105)	3340	3406	4777	109
H(106)	2156	2627	5490	95
H(2)	-1289	802	6248	122
H(112)	-813	-95	5568	146
H(113)	-2492	-797	5225	128
H(115)	-4960	341	6319	109
H(116)	-3282	1045	6620	127
H(118)	-3962	-1451	4962	108
H(119)	-5620	-2222	4684	139
H(120)	-7710	-2055	5088	123
H(121)	-8111	-1096	5784	127
H(122)	-6417	-355	6084	114
H(1SA)	3770	785	2381	150
H(1SB)	4649	1270	2780	150
H(2SA)	4632	2157	1993	137
H(2SB)	3193	1929	1881	137
H(3SA)	2985	2938	2231	161
H(3SB)	4138	2781	2630	161
H(4SA)	1717	2361	2800	160
H(4SB)	2749	2514	3252	160

Table A.43 Torsion angles [°] for [Hpyphenyl][$CrCl_4$(dppe)]

Cl(4)-Cr(1)-P(1)-C(11)	-26.7(3)	C(41)-P(2)-C(2)-C(1)	-173.0(6)
Cl(3)-Cr(1)-P(1)-C(11)	161.0(3)	Cr(1)-P(2)-C(2)-C(1)	-45.8(6)
Cl(2)-Cr(1)-P(1)-C(11)	67.2(3)	C(21)-P(1)-C(11)-C(12)	-87.0(8)
P(2)-Cr(1)-P(1)-C(11)	-110.0(3)	C(1)-P(1)-C(11)-C(12)	20.3(8)
Cl(4)-Cr(1)-P(1)-C(21)	-150.4(3)	Cr(1)-P(1)-C(11)-C(12)	139.0(7)
Cl(3)-Cr(1)-P(1)-C(21)	37.3(3)	C(21)-P(1)-C(11)-C(16)	88.1(7)
Cl(2)-Cr(1)-P(1)-C(21)	-56.5(3)	C(1)-P(1)-C(11)-C(16)	-164.6(6)
P(2)-Cr(1)-P(1)-C(21)	126.3(3)	Cr(1)-P(1)-C(11)-C(16)	-46.0(7)
Cl(4)-Cr(1)-P(1)-C(1)	93.7(3)	C(16)-C(11)-C(12)-C(13)	-0.3(14)
Cl(3)-Cr(1)-P(1)-C(1)	-78.6(3)	P(1)-C(11)-C(12)-C(13)	174.8(8)
Cl(2)-Cr(1)-P(1)-C(1)	-172.4(3)	C(11)-C(12)-C(13)-C(14)	0.8(19)
P(2)-Cr(1)-P(1)-C(1)	10.3(3)	C(12)-C(13)-C(14)-C(15)	-2(2)
Cl(4)-Cr(1)-P(2)-C(31)	167.4(3)	C(13)-C(14)-C(15)-C(16)	2(2)
Cl(3)-Cr(1)-P(2)-C(31)	-18.7(3)	C(12)-C(11)-C(16)-C(15)	0.7(13)
Cl(1)-Cr(1)-P(2)-C(31)	73.1(3)	P(1)-C(11)-C(16)-C(15)	-174.6(7)
P(1)-Cr(1)-P(2)-C(31)	-103.4(3)	C(14)-C(15)-C(16)-C(11)	-1.6(15)
Cl(4)-Cr(1)-P(2)-C(41)	41.2(3)	C(11)-P(1)-C(21)-C(26)	-110.2(7)
Cl(3)-Cr(1)-P(2)-C(41)	-144.9(3)	C(1)-P(1)-C(21)-C(26)	138.3(7)
Cl(1)-Cr(1)-P(2)-C(41)	-53.1(3)	Cr(1)-P(1)-C(21)-C(26)	21.3(8)
P(1)-Cr(1)-P(2)-C(41)	130.4(3)	C(11)-P(1)-C(21)-C(22)	64.8(8)
Cl(4)-Cr(1)-P(2)-C(2)	-74.3(3)	C(1)-P(1)-C(21)-C(22)	-46.8(8)
Cl(3)-Cr(1)-P(2)-C(2)	99.6(3)	Cr(1)-P(1)-C(21)-C(22)	-163.7(7)
Cl(1)-Cr(1)-P(2)-C(2)	-168.6(3)	C(26)-C(21)-C(22)-C(23)	-1.6(15)
P(1)-Cr(1)-P(2)-C(2)	14.8(3)	P(1)-C(21)-C(22)-C(23)	-176.8(9)
C(11)-P(1)-C(1)-C(2)	84.0(6)	C(21)-C(22)-C(23)-C(24)	3.6(19)
C(21)-P(1)-C(1)-C(2)	-170.7(6)	C(22)-C(23)-C(24)-C(25)	-3.7(19)
Cr(1)-P(1)-C(1)-C(2)	-42.4(6)	C(23)-C(24)-C(25)-C(26)	1.8(16)
P(1)-C(1)-C(2)-P(2)	59.8(7)	C(22)-C(21)-C(26)-C(25)	-0.3(12)
C(31)-P(2)-C(2)-C(1)	79.8(6)	P(1)-C(21)-C(26)-C(25)	174.9(6)

C(24)-C(25)-C(26)-C(21)	0.2(13)	C(52)-C(53)-C(54)-C(55)	1.5(12)
C(41)-P(2)-C(31)-C(32)	80.6(7)	C(52)-C(53)-C(54)-C(57)	179.1(7)
C(2)-P(2)-C(31)-C(32)	-171.2(6)	C(53)-C(54)-C(55)-C(56)	-2.7(12)
Cr(1)-P(2)-C(31)-C(32)	-54.4(7)	C(57)-C(54)-C(55)-C(56)	179.7(7)
C(41)-P(2)-C(31)-C(36)	-96.7(7)	C(52)-N(1)-C(56)-C(55)	-0.5(13)
C(2)-P(2)-C(31)-C(36)	11.5(7)	C(54)-C(55)-C(56)-N(1)	2.3(13)
Cr(1)-P(2)-C(31)-C(36)	128.3(6)	C(55)-C(54)-C(57)-C(58)	173.1(7)
C(36)-C(31)-C(32)-C(33)	1.4(13)	C(53)-C(54)-C(57)-C(58)	-4.3(11)
P(2)-C(31)-C(32)-C(33)	-176.0(7)	C(55)-C(54)-C(57)-C(62)	-4.8(11)
C(31)-C(32)-C(33)-C(34)	-1.2(15)	C(53)-C(54)-C(57)-C(62)	177.8(7)
C(32)-C(33)-C(34)-C(35)	-0.5(17)	C(62)-C(57)-C(58)-C(59)	-3.1(11)
C(33)-C(34)-C(35)-C(36)	1.9(18)	C(54)-C(57)-C(58)-C(59)	178.9(7)
C(34)-C(35)-C(36)-C(31)	-1.6(16)	C(57)-C(58)-C(59)-C(60)	2.3(13)
C(32)-C(31)-C(36)-C(35)	0.0(13)	C(58)-C(59)-C(60)-C(61)	-0.3(13)
P(2)-C(31)-C(36)-C(35)	177.2(7)	C(59)-C(60)-C(61)-C(62)	-0.8(14)
C(31)-P(2)-C(41)-C(42)	-103.9(7)	C(60)-C(61)-C(62)-C(57)	-0.1(13)
C(2)-P(2)-C(41)-C(42)	145.2(7)	C(58)-C(57)-C(62)-C(61)	2.0(11)
Cr(1)-P(2)-C(41)-C(42)	29.3(8)	C(54)-C(57)-C(62)-C(61)	180.0(7)
C(31)-P(2)-C(41)-C(46)	74.5(9)	Cl(8)-Cr(2)-P(3)-C(71)	-41.0(3)
C(2)-P(2)-C(41)-C(46)	-36.3(9)	Cl(6)-Cr(2)-P(3)-C(71)	52.7(3)
Cr(1)-P(2)-C(41)-C(46)	-152.3(7)	Cl(7)-Cr(2)-P(3)-C(71)	144.1(3)
C(46)-C(41)-C(42)-C(43)	-1.8(15)	P(4)-Cr(2)-P(3)-C(71)	-131.1(3)
P(2)-C(41)-C(42)-C(43)	176.6(8)	Cl(8)-Cr(2)-P(3)-C(81)	-168.2(3)
C(41)-C(42)-C(43)-C(44)	0.8(17)	Cl(6)-Cr(2)-P(3)-C(81)	-74.5(3)
C(42)-C(43)-C(44)-C(45)	-1(2)	Cl(7)-Cr(2)-P(3)-C(81)	16.9(3)
C(43)-C(44)-C(45)-C(46)	2(3)	P(4)-Cr(2)-P(3)-C(81)	101.7(3)
C(42)-C(41)-C(46)-C(45)	2.8(17)	Cl(8)-Cr(2)-P(3)-C(3)	75.2(2)
P(2)-C(41)-C(46)-C(45)	-175.6(10)	Cl(6)-Cr(2)-P(3)-C(3)	168.8(2)
C(44)-C(45)-C(46)-C(41)	-3(2)	Cl(7)-Cr(2)-P(3)-C(3)	-99.7(2)
C(56)-N(1)-C(52)-C(53)	-0.7(13)	P(4)-Cr(2)-P(3)-C(3)	-15.0(2)
N(1)-C(52)-C(53)-C(54)	0.1(13)	Cl(8)-Cr(2)-P(4)-C(91)	149.6(3)

Cl(7)-Cr(2)-P(4)-C(91)	-36.8(3)	C(74)-C(75)-C(76)-C(71)	-2.5(17)
Cl(5)-Cr(2)-P(4)-C(91)	55.9(3)	C(71)-P(3)-C(81)-C(82)	-72.7(8)
P(3)-Cr(2)-P(4)-C(91)	-128.6(3)	C(3)-P(3)-C(81)-C(82)	178.2(7)
Cl(8)-Cr(2)-P(4)-C(101)	23.0(3)	Cr(2)-P(3)-C(81)-C(82)	62.3(8)
Cl(7)-Cr(2)-P(4)-C(101)	-163.5(3)	C(71)-P(3)-C(81)-C(86)	103.9(8)
Cl(5)-Cr(2)-P(4)-C(101)	-70.7(3)	C(3)-P(3)-C(81)-C(86)	-5.2(9)
P(3)-Cr(2)-P(4)-C(101)	104.8(3)	Cr(2)-P(3)-C(81)-C(86)	-121.1(7)
Cl(8)-Cr(2)-P(4)-C(4)	-93.4(3)	C(86)-C(81)-C(82)-C(83)	0.9(16)
Cl(7)-Cr(2)-P(4)-C(4)	80.1(3)	P(3)-C(81)-C(82)-C(83)	177.8(9)
Cl(5)-Cr(2)-P(4)-C(4)	172.8(3)	C(81)-C(82)-C(83)-C(84)	1.3(19)
P(3)-Cr(2)-P(4)-C(4)	-11.6(3)	C(82)-C(83)-C(84)-C(85)	-1.0(18)
C(71)-P(3)-C(3)-C(4)	173.5(5)	C(83)-C(84)-C(85)-C(86)	-1.5(19)
C(81)-P(3)-C(3)-C(4)	-78.2(5)	C(82)-C(81)-C(86)-C(85)	-3.3(15)
Cr(2)-P(3)-C(3)-C(4)	46.6(5)	P(3)-C(81)-C(86)-C(85)	-179.9(8)
P(3)-C(3)-C(4)-P(4)	-61.2(6)	C(84)-C(85)-C(86)-C(81)	3.7(18)
C(91)-P(4)-C(4)-C(3)	171.9(5)	C(101)-P(4)-C(91)-C(92)	22.9(7)
C(101)-P(4)-C(4)-C(3)	-79.6(5)	C(4)-P(4)-C(91)-C(92)	133.3(6)
Cr(2)-P(4)-C(4)-C(3)	43.6(5)	Cr(2)-P(4)-C(91)-C(92)	-109.3(6)
C(81)-P(3)-C(71)-C(76)	-76.6(8)	C(101)-P(4)-C(91)-C(96)	-158.2(6)
C(3)-P(3)-C(71)-C(76)	33.6(8)	C(4)-P(4)-C(91)-C(96)	-47.8(7)
Cr(2)-P(3)-C(71)-C(76)	149.8(7)	Cr(2)-P(4)-C(91)-C(96)	69.6(7)
C(81)-P(3)-C(71)-C(72)	104.0(8)	C(96)-C(91)-C(92)-C(93)	0.0(12)
C(3)-P(3)-C(71)-C(72)	-145.8(7)	P(4)-C(91)-C(92)-C(93)	178.9(6)
Cr(2)-P(3)-C(71)-C(72)	-29.6(8)	C(91)-C(92)-C(93)-C(94)	0.9(14)
C(76)-C(71)-C(72)-C(73)	1.2(15)	C(92)-C(93)-C(94)-C(95)	0.2(15)
P(3)-C(71)-C(72)-C(73)	-179.4(8)	C(93)-C(94)-C(95)-C(96)	-2.2(15)
C(71)-C(72)-C(73)-C(74)	1.3(18)	C(94)-C(95)-C(96)-C(91)	3.2(14)
C(72)-C(73)-C(74)-C(75)	-4.3(18)	C(92)-C(91)-C(96)-C(95)	-2.0(12)
C(73)-C(74)-C(75)-C(76)	4.9(18)	P(4)-C(91)-C(96)-C(95)	179.1(6)
C(72)-C(71)-C(76)-C(75)	-0.6(14)	C(91)-P(4)-C(101)-C(106)	-93.9(7)
P(3)-C(71)-C(76)-C(75)	-180.0(8)	C(4)-P(4)-C(101)-C(106)	157.1(6)

Cr(2)-P(4)-C(101)-C(106) 41.2(7)	C(115)-C(114)-C(117)-C(122)-2.3(14)
C(91)-P(4)-C(101)-C(102) 86.3(7)	C(113)-C(114)-C(117)-C(118)-0.3(14)
C(4)-P(4)-C(101)-C(102) -22.7(7)	C(115)-C(114)-C(117)-C(118)178.3(9)
Cr(2)-P(4)-C(101)-C(102) -138.6(6)	C(122)-C(117)-C(118)-C(119)-0.9(15)
C(106)-C(101)-C(102)-C(103) 0.3(13)	C(114)-C(117)-C(118)-C(119)178.5(10)
P(4)-C(101)-C(102)-C(103)-179.9(7)	C(117)-C(118)-C(119)-C(120) 1.2(18)
C(101)-C(102)-C(103)-C(104)-0.5(15)	C(118)-C(119)-C(120)-C(121)-0.1(19)
C(102)-C(103)-C(104)-C(105) 1.2(16)	C(119)-C(120)-C(121)-C(122)-1.0(17)
C(103)-C(104)-C(105)-C(106)-1.7(16)	C(118)-C(117)-C(122)-C(121)-0.3(15)
C(104)-C(105)-C(106)-C(101) 1.5(15)	C(114)-C(117)-C(122)-C(121)-179.7(9)
C(102)-C(101)-C(106)-C(105)-0.8(13)	C(120)-C(121)-C(122)-C(117) 1.3(17)
P(4)-C(101)-C(106)-C(105) 179.4(7)	C(4S)-O(1S)-C(1S)-C(2S) -21(2)
C(116)-N(2)-C(112)-C(113) 0.1(19)	O(1S)-C(1S)-C(2S)-C(3S) 35(3)
N(2)-C(112)-C(113)-C(114) -3(2)	O(1S)-C(1S)-C(2S)-C(4S) 15.0(16)
C(112)-C(113)-C(114)-C(115) 3.7(17)	C(1S)-C(2S)-C(3S)-C(4S) -34(3)
C(112)-C(113)-C(114)-C(117)-177.7(10)	C(2S)-C(3S)-C(4S)-O(1S) 20(3)
C(113)-C(114)-C(115)-C(116)-2.6(15)	C(1S)-O(1S)-C(4S)-C(3S) 5(3)
C(117)-C(114)-C(115)-C(116)178.8(10)	C(1S)-O(1S)-C(4S)-C(2S) 15.2(15)
C(112)-N(2)-C(116)-C(115) 1.0(18)	C(1S)-C(2S)-C(4S)-C(3S) 146(3)
C(114)-C(115)-C(116)-N(2) 0.3(17)	C(3S)-C(2S)-C(4S)-O(1S) -161(3)
C(113)-C(114)-C(117)-C(122)179.1(10)	C(1S)-C(2S)-C(4S)-O(1S) -15.0(16)

Table A.44 Hydrogen bonds for [Hpyphenyl][$CrCl_4$(dppe)] [Å and °]

D-H...A	d(D-H)	d(H...A)	d(D...A)	<(DHA)
N(1)-H(1)...Cl(1)	0.86	2.62	3.255(7)	131.9
N(1)-H(1)...Cl(3)	0.86	2.44	3.183(6)	145.1
N(2)-H(2)...Cl(5)	0.86	2.55	3.217(10)	134.8
N(2)-H(2)...Cl(7)	0.86	2.62	3.330(9)	140.0

APPENDIX 2 : CALCULATED MS DISTRIBUTION PATTERNS

DISTRIBUTION OF ISOTOPES CALCULATED BY 'ISOFORM' PROGRAM FOR
Formula : CrCl2C15H15N3
Factor : 100 Nominal MW = 359 Exact MW = 359.00479 Average MW = 360.21

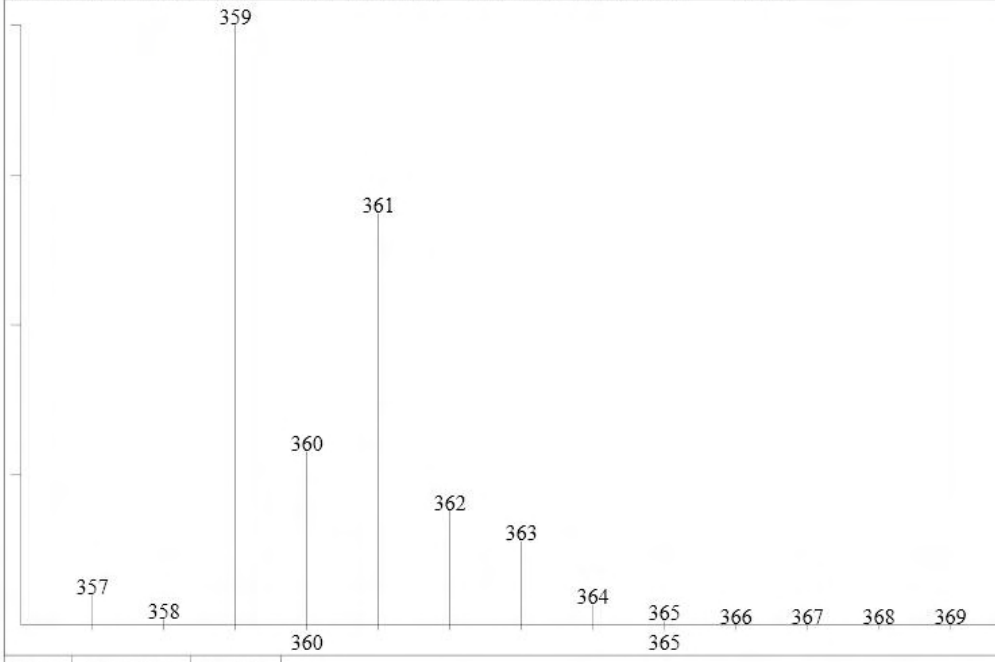

Mass	Abundance	*Factor
357	4.95391	4.95
358	0.89096	0.89
359	100.00000	100.00
360	28.90886	28.91
361	68.60853	68.61
362	18.95201	18.95
363	13.90177	13.90
364	3.37117	3.37
365	0.66502	0.67
366	0.07687	0.08
367	0.00551	0.01
368	0.00027	0.00
369	0.00001	0.00

Figure B1 Calculated isotopic distribution pattern for $[CrCl_2(py)_3]$

DISTRIBUTION OF ISOTOPES CALCULATED BY 'ISOFORM' PROGRAM FOR
Formula : CrC15H15N3
Factor : 100 Nominal MW = 289 Exact MW = 289.06708 Average MW = 289.30

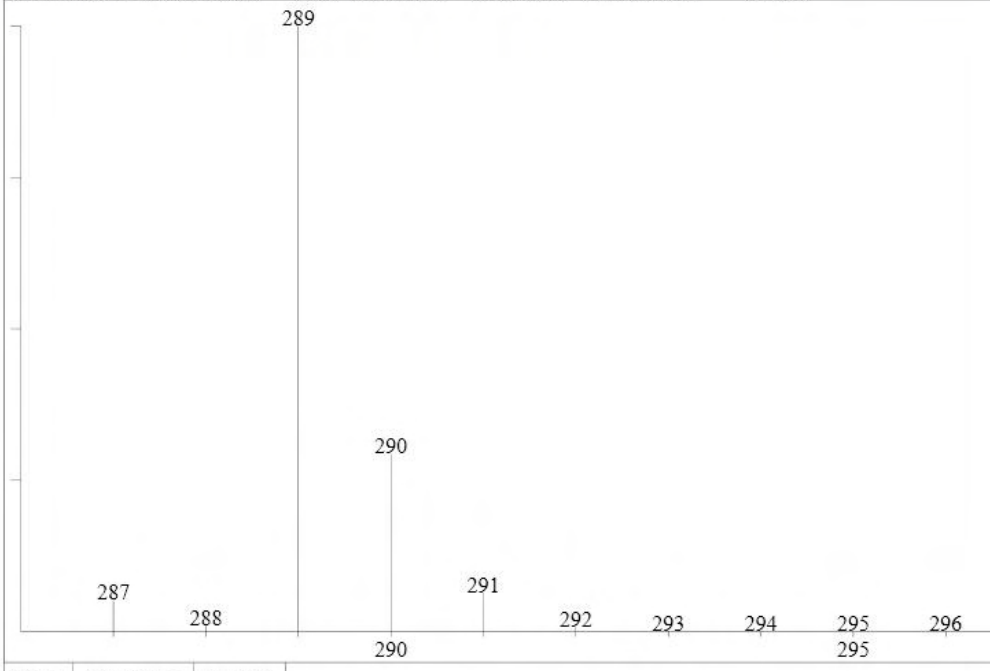

Mass	Abundance	*Factor
287	5.11601	5.12
288	0.92011	0.92
289	100.00000	100.00
290	29.26631	29.27
291	6.37031	6.37
292	0.75932	0.76
293	0.05501	0.06
294	0.00269	0.00
295	0.00010	0.00
296	0.00000	0.00

Figure B2 Calculated distribution pattern for $[Cr(py)_3]$

DISTRIBUTION OF ISOTOPES CALCULATED BY 'ISOFORM' PROGRAM FOR
Formula : CrCl3C33H27N3
Factor : 100 Nominal MW = 622 Exact MW = 622.06757 Average MW = 623.96

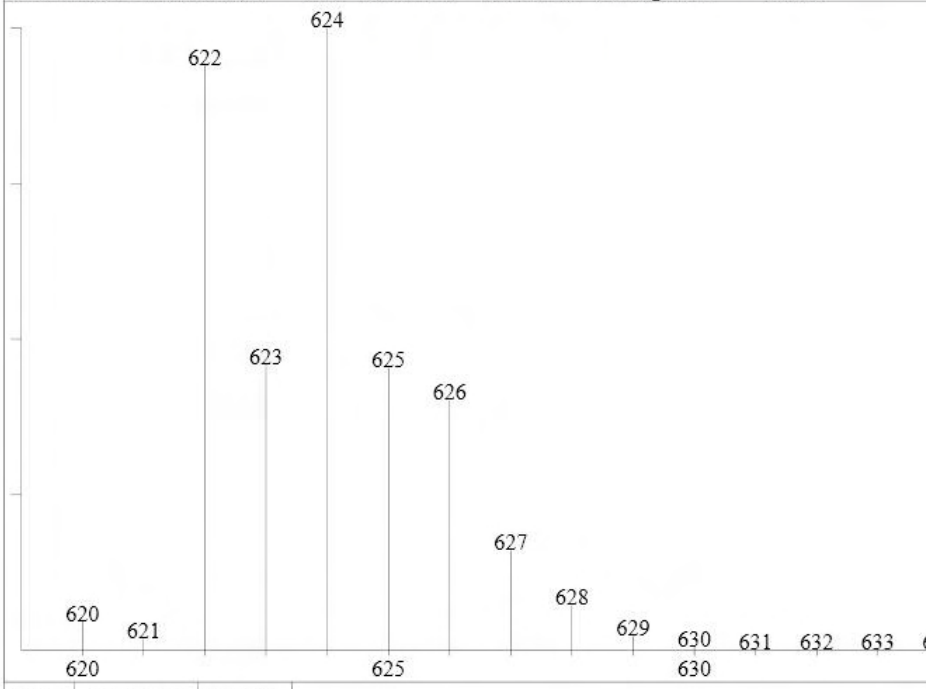

Mass	Abundance	*Factor
620	4.56889	4.57
621	1.74280	1.74
622	93.94258	93.94
623	45.83363	45.83
624	100.00000	100.00
625	45.33328	45.33
626	40.11766	40.12
627	15.97106	15.97
628	7.13687	7.14
629	2.22202	2.22
630	0.51818	0.52
631	0.08985	0.09
632	0.01159	0.01
633	0.00114	0.00

Figure B3 Calculated isotopic distribution pattern for [$CrCl_3$(pyphenyl)$_3$]

DISTRIBUTION OF ISOTOPES CALCULATED BY 'ISOFORM' PROGRAM FOR
Formula : CrCl2C33H27N3
Factor : 100 Nominal MW = 587 Exact MW = 587.09869 Average MW = 588.50

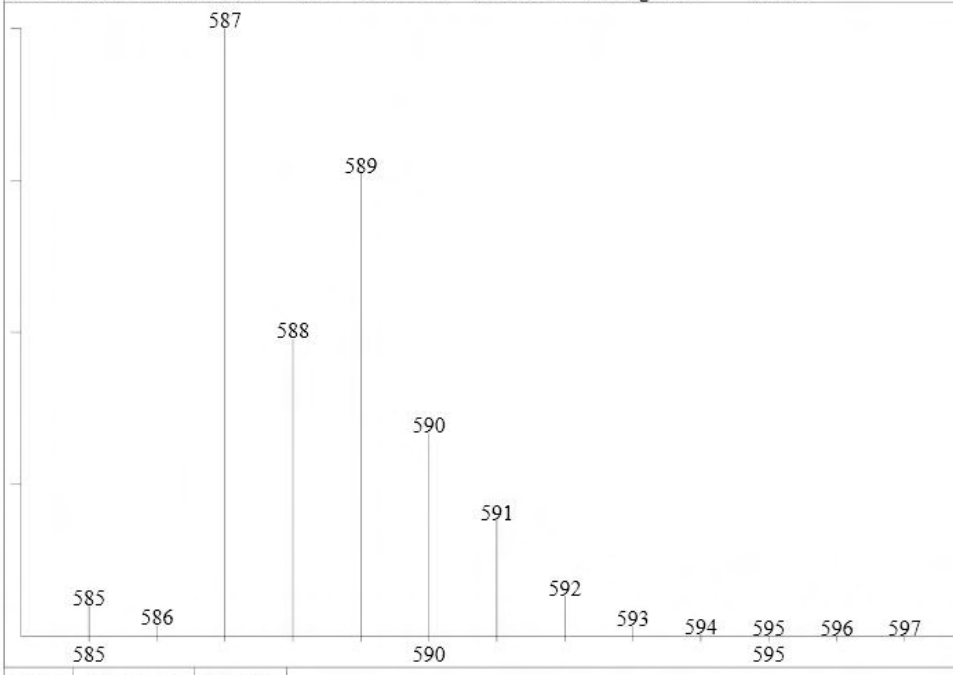

Mass	Abundance	*Factor
585	4.94033	4.94
586	1.88449	1.88
587	100.00000	100.00
588	48.95714	48.96
589	76.14979	76.15
590	33.36229	33.36
591	19.02644	19.03
592	6.60021	6.60
593	1.63242	1.63
594	0.29192	0.29
595	0.03826	0.04
596	0.00380	0.00
597	0.00029	0.00

Figure B4 Calculated isotopic distribution pattern for [$CrCl_2$(pyphenyl)$_3$]

DISTRIBUTION OF ISOTOPES CALCULATED BY 'ISOFORM' PROGRAM FOR
Formula : CrCl2C22H18N2
Factor : 100 Nominal MW = 432 Exact MW = 432.02518 Average MW = 433.30

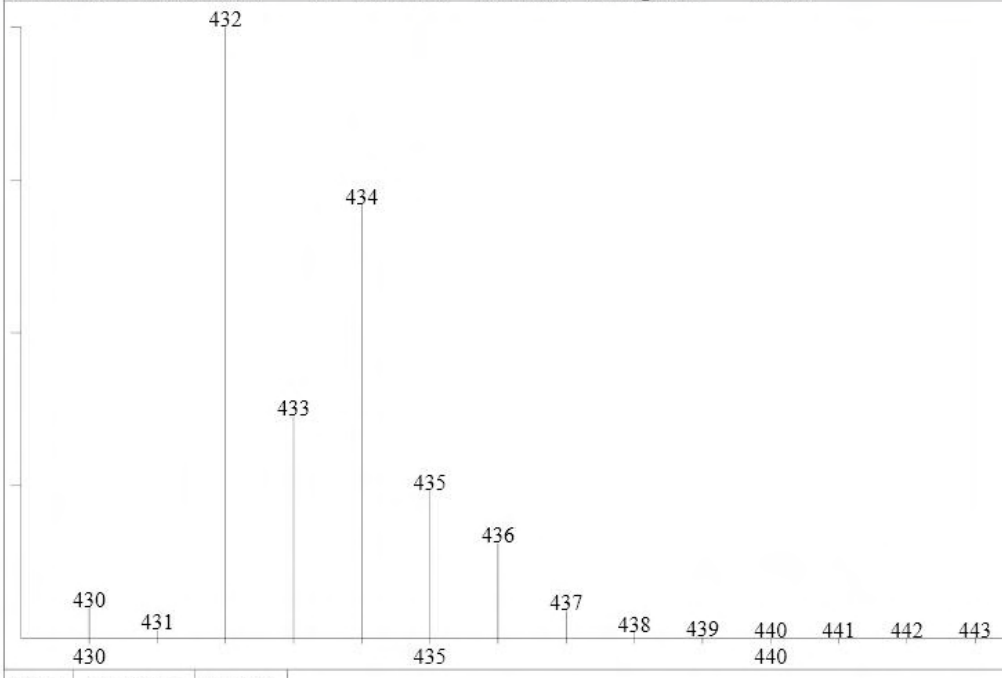

Mass	Abundance	*Factor
430	4.95005	4.95
431	1.25880	1.26
432	100.00000	100.00
433	36.32783	36.33
434	70.94023	70.94
435	24.11300	24.11
436	15.46292	15.46
437	4.44995	4.45
438	0.94869	0.95
439	0.13475	0.13
440	0.01292	0.01
441	0.00089	0.00
442	0.00005	0.00
443	0.00000	0.00

Figure B5 Calculated isotopic distribution pattern for [$CrCl_2$(pyphenyl)$_2$]

DISTRIBUTION OF ISOTOPES CALCULATED BY 'ISOFORM' PROGRAM FOR
Formula : CrClC22H18N2
Factor : 100 Nominal MW = 397 Exact MW = 397.05630 Average MW = 397.85

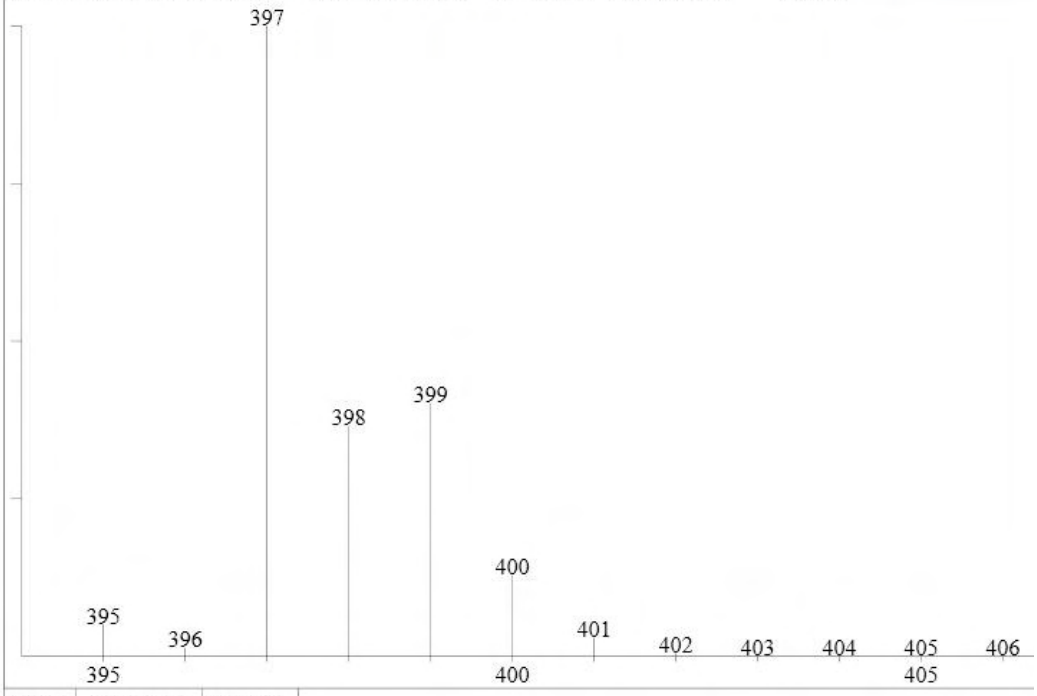

Mass	Abundance	*Factor
395	5.02967	5.03
396	1.27905	1.28
397	100.00000	100.00
398	36.50312	36.50
399	40.10129	40.10
400	12.82716	12.83
401	2.88725	2.89
402	0.41940	0.42
403	0.04060	0.04
404	0.00280	0.00
405	0.00014	0.00
406	0.00001	0.00

Figure B6 Calculated isotopic distribution pattern for [CrCl(pyphenyl)$_2$]

DISTRIBUTION OF ISOTOPES CALCULATED BY 'ISOFORM' PROGRAM FOR
Formula : CrCl2C10H8N2
Factor : 100 Nominal MW = 278 Exact MW = 277.94693 Average MW = 279.09

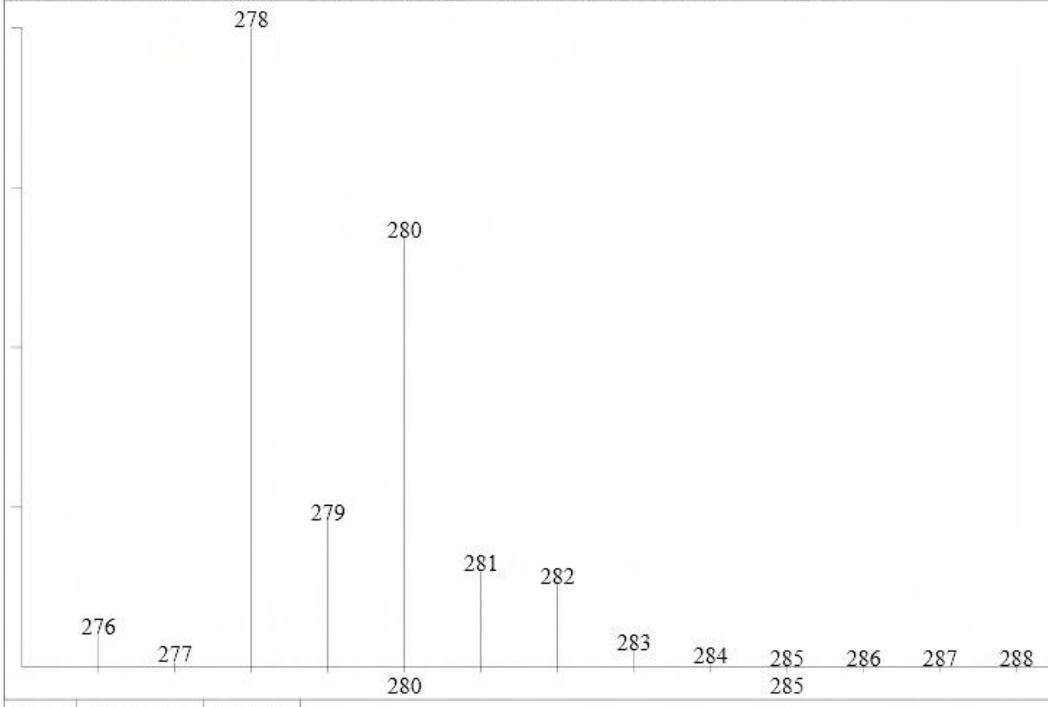

Mass	Abundance	*Factor
276	4.95605	4.96
277	0.59274	0.59
278	100.00000	100.00
279	22.89535	22.90
280	67.10867	67.11
281	14.88057	14.88
282	12.91008	12.91
283	2.57114	2.57
284	0.49073	0.49
285	0.04322	0.04
286	0.00212	0.00
287	0.00007	0.00
288	0.00000	0.00

Figure B7 Calculated isotopic distribution pattern for [$CrCl_2$(bipy)]

DISTRIBUTION OF ISOTOPES CALCULATED BY 'ISOFORM' PROGRAM FOR
Formula : CrClC10H8N2
Factor : 100 Nominal MW = 243 Exact MW = 242.97810 Average MW = 243.64

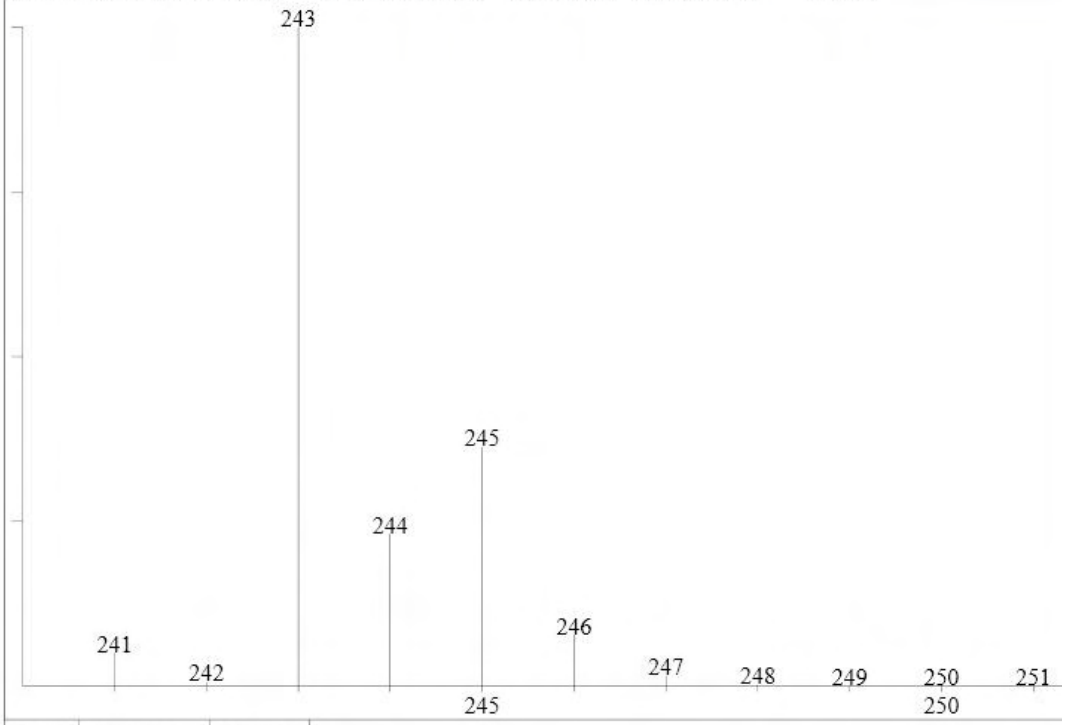

Mass	Abundance	*Factor
241	5.03586	5.04
242	0.60229	0.60
243	100.00000	100.00
244	23.07146	23.07
245	36.20943	36.21
246	7.74196	7.74
247	1.53822	1.54
248	0.13667	0.14
249	0.00671	0.01
250	0.00021	0.00
251	0.00000	0.00

Figure B8 Calculated isotopic distribution pattern for [CrCl(bipy)]

DISTRIBUTION OF ISOTOPES CALCULATED BY 'ISOFORM' PROGRAM FOR
Formula : CrCl2C10H10N2O
Factor : 100 Nominal MW = 296 Exact MW = 295.95749 Average MW = 297.11

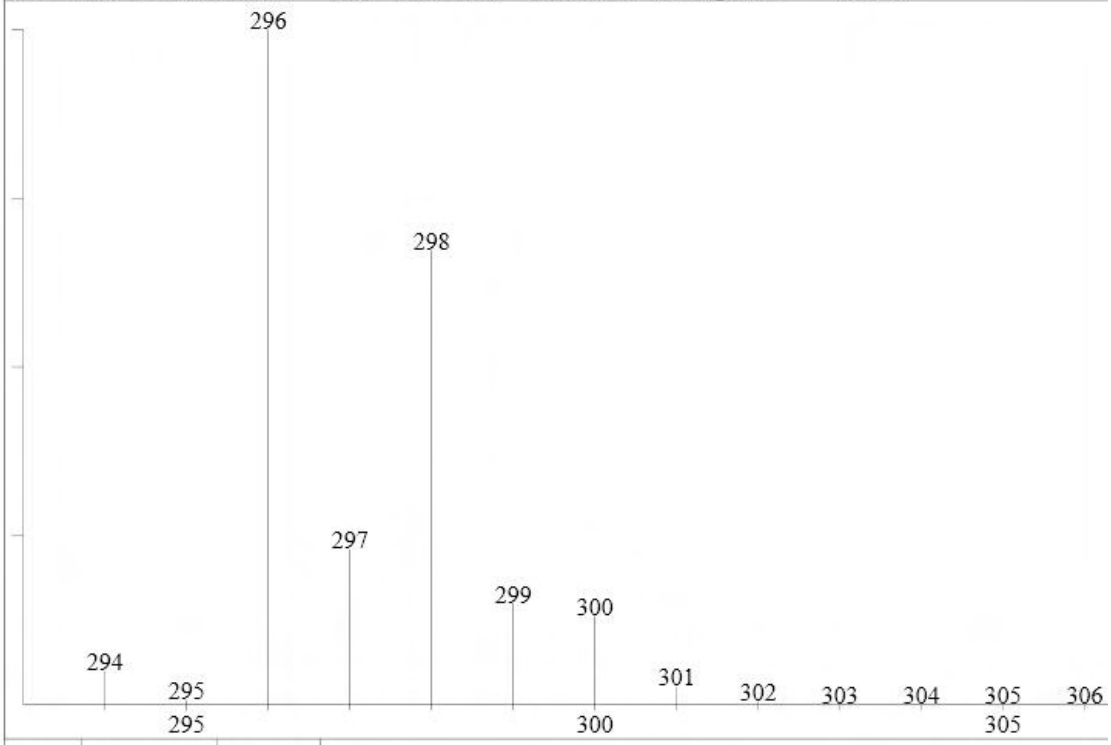

Mass	Abundance	*Factor
294	4.95553	4.96
295	0.59611	0.60
296	100.00000	100.00
297	22.96326	22.96
298	67.31802	67.32
299	14.97135	14.97
300	13.05357	13.05
301	2.60966	2.61
302	0.51834	0.52
303	0.04872	0.05
304	0.00313	0.00
305	0.00015	0.00
306	0.00001	0.00

Figure B9 Calculated isotopic distribution pattern for [$CrCl_2$(bipy)(H_2O)]

DISTRIBUTION OF ISOTOPES CALCULATED BY 'ISOFORM' PROGRAM FOR
Formula : CrCl2C21H17N3
Factor : 100 Nominal MW = 433 Exact MW = 433.02045 Average MW = 434.29

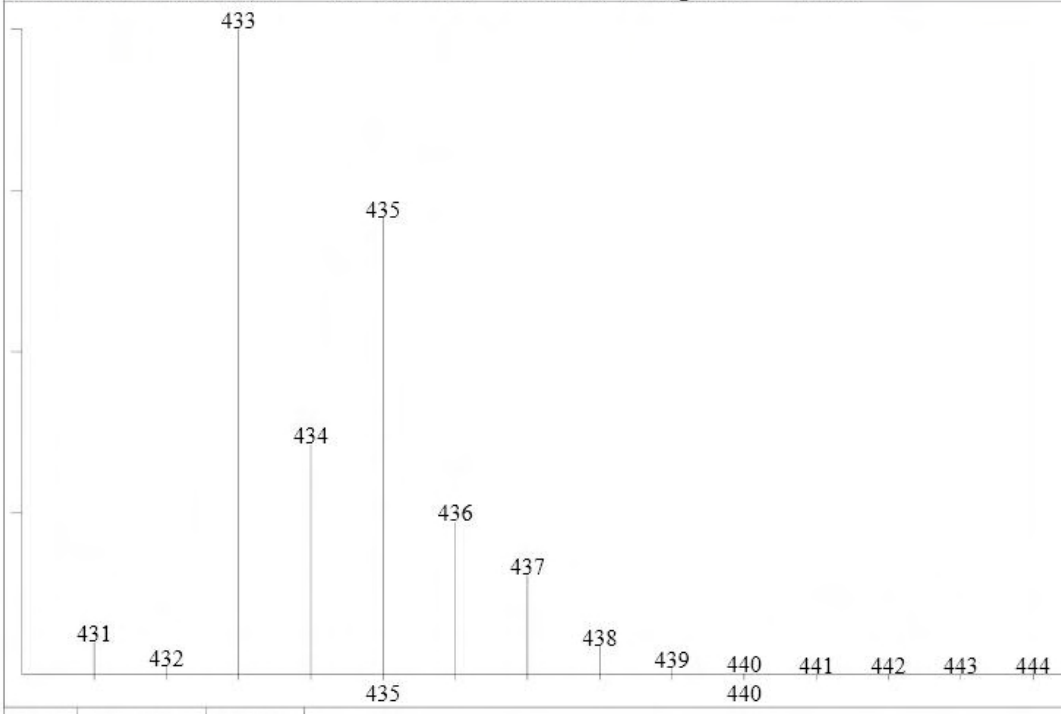

Mass	Abundance	*Factor
431	4.95050	4.95
432	1.22154	1.22
433	100.00000	100.00
434	35.57617	35.58
435	70.68070	70.68
436	23.58248	23.58
437	15.28814	15.29
438	4.33554	4.34
439	0.91644	0.92
440	0.12796	0.13
441	0.01198	0.01
442	0.00080	0.00
443	0.00004	0.00
444	0.00000	0.00

Figure B10 Calculated isotopic distribution pattern for [$CrCl_2$(bipy)(pyphenyl)]

DISTRIBUTION OF ISOTOPES CALCULATED BY 'ISOFORM' PROGRAM FOR
Formula : CrCl2C26H24P2
Factor : 100 Nominal MW = 520 Exact MW = 520.01355 Average MW = 521.33

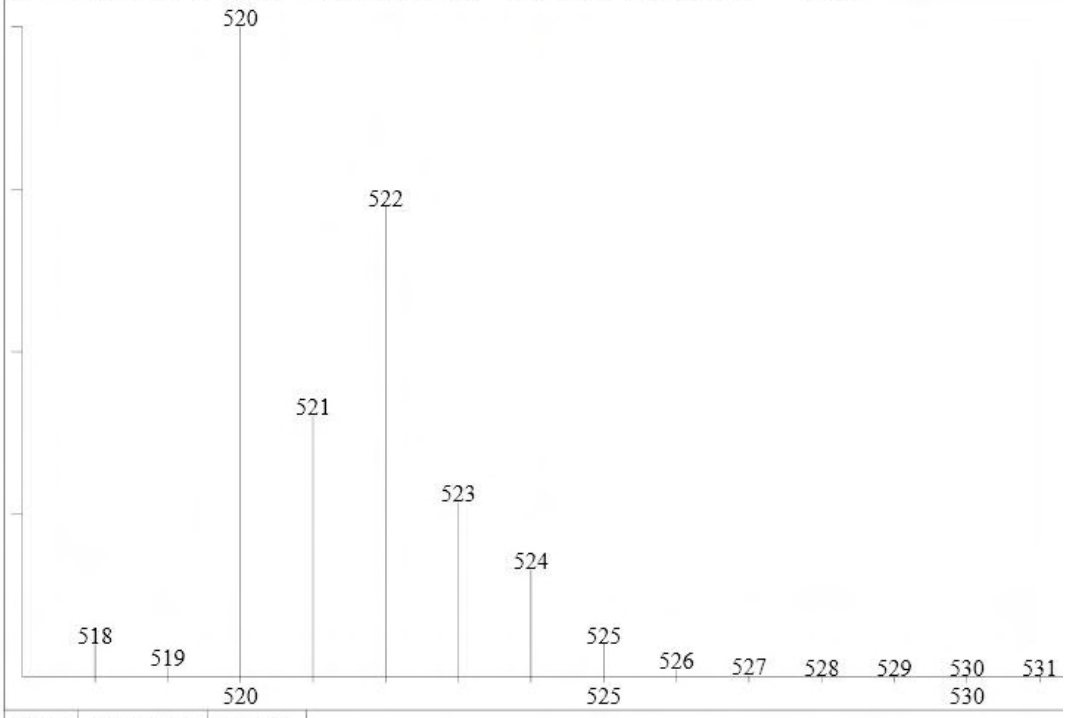

Mass	Abundance	*Factor
518	4.94757	4.95
519	1.44568	1.45
520	100.00000	100.00
521	40.09836	40.10
522	72.32935	72.33
523	26.80604	26.81
524	16.40310	16.40
525	5.04531	5.05
526	1.12433	1.12
527	0.17281	0.17
528	0.01849	0.02
529	0.00144	0.00
530	0.00009	0.00
531	0.00000	0.00

Figure B11 Calculated isotopic distribution pattern for [$CrCl_2$(dppe)]

DISTRIBUTION OF ISOTOPES CALCULATED BY 'ISOFORM' PROGRAM FOR
Formula : CrClC26H24P2
Factor : 100 Nominal MW = 485 Exact MW = 485.04468 Average MW = 485.87

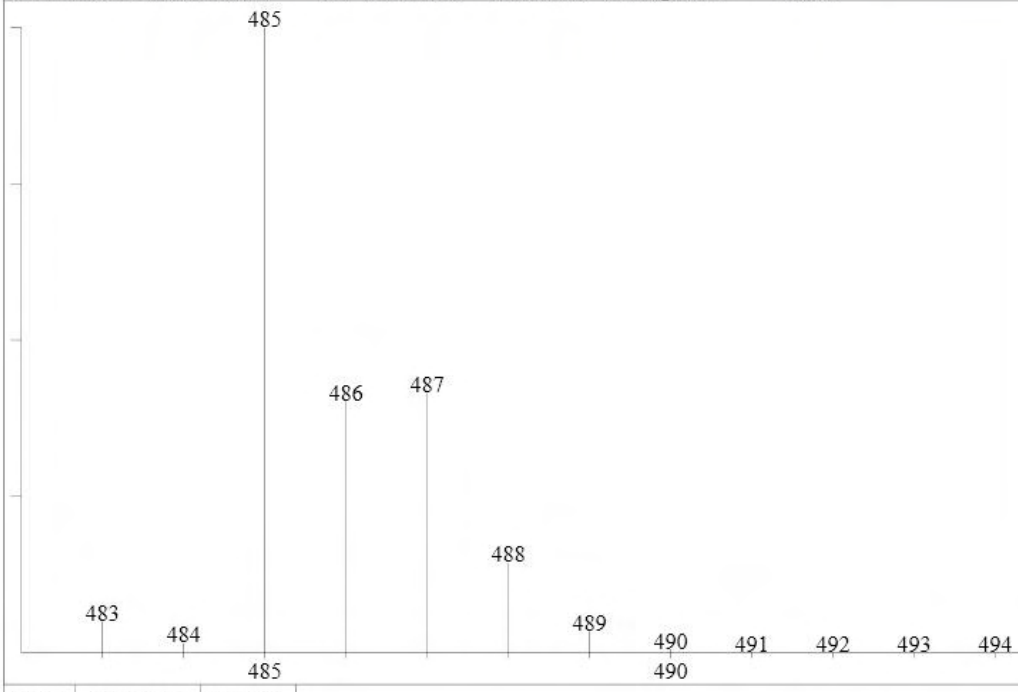

Mass	Abundance	*Factor
483	5.02711	5.03
484	1.46892	1.47
485	100.00000	100.00
486	40.27325	40.27
487	41.51217	41.51
488	14.35761	14.36
489	3.39121	3.39
490	0.53486	0.53
491	0.05790	0.06
492	0.00454	0.00
493	0.00027	0.00
494	0.00001	0.00

Figure B12 Calculated isotopic distribution pattern for [CrCl(dppe)]

DISTRIBUTION OF ISOTOPES CALCULATED BY 'ISOFORM' PROGRAM FOR
Formula : CrCl2C37H33NP2
Factor : 100 Nominal MW = 675 Exact MW = 675.08698 Average MW = 676.53

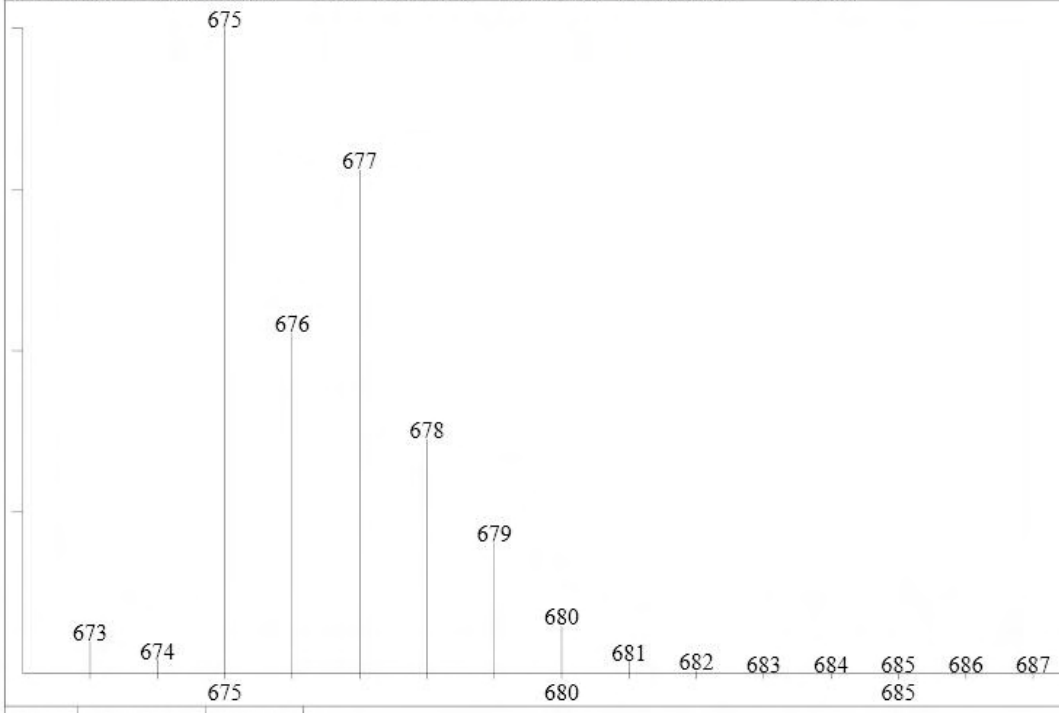

Mass	Abundance	*Factor
673	4.93669	4.94
674	2.07020	2.07
675	100.00000	100.00
676	52.70916	52.71
677	77.99624	78.00
678	36.24558	36.25
679	20.31294	20.31
680	7.33225	7.33
681	1.89048	1.89
682	0.35676	0.36
683	0.05009	0.05
684	0.00539	0.01
685	0.00046	0.00
686	0.00003	0.00
687	0.00000	0.00

Figure B13 Calculated isotopic distribution pattern for [$CrCl_2$(dppe)(pyphenyl)]

DISTRIBUTION OF ISOTOPES CALCULATED BY 'ISOFORM' PROGRAM FOR
Formula : CrCl2C23H29N2P
Factor : 100 Nominal MW = 486 Exact MW = 486.08502 Average MW = 487.37

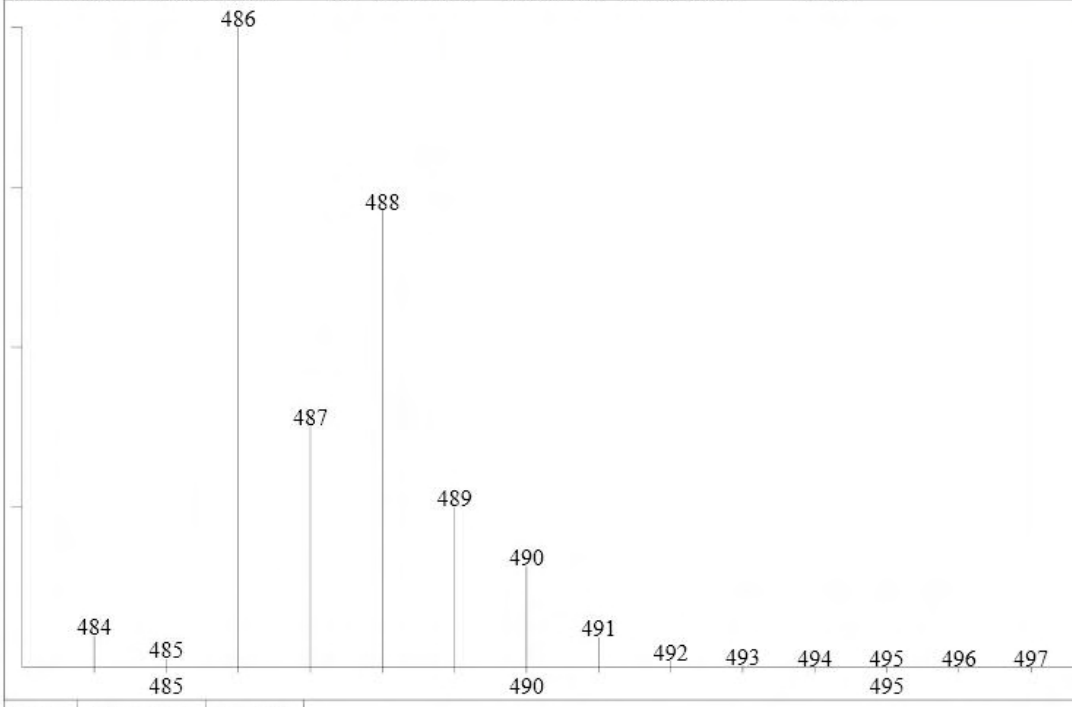

Mass	Abundance	*Factor
484	4.94925	4.95
485	1.32170	1.32
486	100.00000	100.00
487	37.59678	37.60
488	71.39383	71.39
489	25.01416	25.01
490	15.76921	15.77
491	4.64682	4.65
492	1.00556	1.01
493	0.14691	0.15
494	0.01466	0.01
495	0.00105	0.00
496	0.00006	0.00
497	0.00000	0.00

Figure B14 Calculated isotopic distribution pattern for [$CrCl_2$(dppea)(pytb)]

DISTRIBUTION OF ISOTOPES CALCULATED BY 'ISOFORM' PROGRAM FOR
Formula : CrCl2C25H25N2P
Factor : 100 Nominal MW = 506 Exact MW = 506.05371 Average MW = 507.36

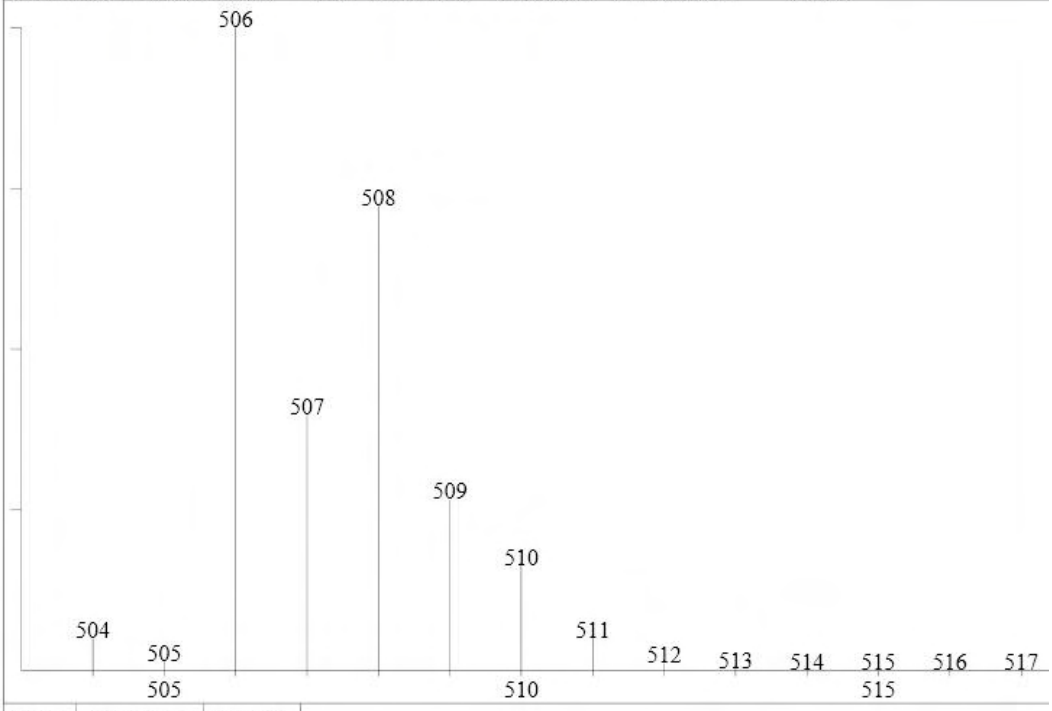

Mass	Abundance	*Factor
504	4.94781	4.95
505	1.42819	1.43
506	100.00000	100.00
507	39.74537	39.75
508	72.19593	72.20
509	26.55268	26.55
510	16.31263	16.31
511	4.98874	4.99
512	1.10735	1.11
513	0.16910	0.17
514	0.01793	0.02
515	0.00139	0.00
516	0.00008	0.00
517	0.00000	0.00

Figure B15 Calculated isotopic distribution pattern for [$CrCl_2$(dppea)(pyphenyl)]